**DOT/FAA/TC-21/27**

Federal Aviation Administration
William J. Hughes Technical Center
Aviation Research Division
Atlantic City International Airport
New Jersey 08405

# Bonded Repairs to Composite Wing Panel Structure: Phase 3—Bonded Repair Size Limits Study for Solid Laminates with Full-Depth and Partial-Depth Scarf Configurations

July 2021

Final report

U.S. Department of Transportation
**Federal Aviation Administration**

## NOTICE



This report is available at the Federal Aviation Administration William J. Hughes Technical Center's Full-Text Technical Reports page: actlibrary.tc.faa.gov in Adobe Acrobat portable document format (PDF).

**Form DOT F 1700.7** (8-72) Reproduction of completed page authorized

| 1. Report No. | 2. Government Accession No. | 3. Recipient's Catalog No. |
|---|---|---|
| DOT/FAA/TC-21/27 | | |

| 4. Title and Subtitle | 5. Report Date |
|---|---|
| Bonded Repairs to Composite Wing Panel Structure: Phase 3—Bonded Repair Size Limits Study for Solid Laminates with Full-Depth and Partial-Depth Scarf Configurations | July 2021 |
| | 6. Performing Organization Code |

| 7. Author(s) | 8. Performing Organization Report No. |
|---|---|
| Ryan J. Neel[1], Reewanshu Chadha[2], John G. Bakuckas, Jr.[3], Michael Fleming[4], John Z. Lin[4], Erick Espinar-Mick[5]<br><br>[1]Federal Aviation Administration (FAA-Drexel Fellow)<br>[2]Federal Aviation Administration (Diakon Solutions, LLC)<br>[3]Federal Aviation Administration<br>[4]Boeing Research & Technology<br>[5]Boeing Commercial Airplane | |

| 9. Performing Organization Name and Address | 10. Work Unit No. (TRAIS) |
|---|---|
| William J. Hughes Technical Center<br>Aviation Research Division<br>Structures and Materials Section<br>Atlantic City International Airport, NJ 08405 | 11. Contract or Grant No. |

| 12. Sponsoring Agency Name and Address | 13. Type of Report and Period Covered |
|---|---|
| U.S. Department of Transportation<br>Federal Aviation Administration<br>Transport Standards Branch<br>Airframe & Cabin Safety Section, AIR-675<br>2200 South 216th Street<br>Des Moines, Washington 98198 | 14. Sponsoring Agency Code<br>AIR-675 |

15. Supplementary Notes

The FAA William J. Hughes Technical Center Aviation Research Division COR was John G. Bakuckas, Jr.

16. Abstract

In a collaborative effort, the Federal Aviation Administration (FAA) and The Boeing Company are assessing bonded repair technologies of composite panels representative of transport airplane wing structures through test and analysis using the FAA's Aircraft Beam Structural Test (ABST) fixture. Emphasis has been placed on investigating methods and tools used to conduct analysis and predict structural performance of bonded repairs and those used to monitor and evaluate repair quality over the life of the part. This project is carried out in a phased approach where phase 1 was fixture development and verification. Phase 2 was the initial baseline testing that verified the analysis models and provided an initial reference point for inspection and monitoring systems used to detect and track damage formation. This report discusses the recent third-phase efforts to support bonded repair size limit (BRSL) studies and methods used to predict the limit-load residual strength for a failed scarfed repair in solid composite laminates with full-depth and partial-depth scarf configurations. Scarfs were inserted in carbon-fiber-reinforced polymer (CFRP) panels having an 18-ply quasi-isotropic layup. The panels were attached as top-side components (e.g., skins) of a cantilevered, 24-inch-wide by 40-inch-long wingbox structure. These panels were subjected to constant-moment loads tested either quasi-statically loaded to failure or subjected to fatigue before loading them to failure. The applied fatigue loading conditions simulated highest operational strain levels for transport-category wing panels for 165,000 cycles, which is approximately equal to three design service goals (DSGs). The test and analysis results revealed a significant benefit of partial-depth scarfs over full-depth scarfs. In addition, there was no debit in strength due to fatigue in both type of panels tested. For both full-depth and partial-depth scarf configurations, the methods under development for BRSL residual strength predictions correlated well with test results. Follow-on efforts are focused on panels with double-sided scarf configurations, which will be documented in a companion technical note.

| 17. Key Words | 18. Distribution Statement |
|---|---|
| Bonded repair size limits, Full-depth scarf, Partial-depth scarf, Scarf repairs, Carbon fiber reinforced polymer, Nondestructive inspection, Test, Analysis, Digital image correlation, Thermography | This document is available to the U.S. public through the National Technical Information Service (NTIS), Springfield, Virginia 22161. This document is also available from the Federal Aviation Administration William J. Hughes Technical Center at actlibrary.tc.faa.gov. |

| 19. Security Classif. (of this report) | 20. Security Classif. (of this page) | 21. No. of Pages | 22. Price |
|---|---|---|---|
| Unclassified | Unclassified | 319 | |

# Contents

## Figures

## Tables

## Acronyms

| Acronym | Definition |
|---|---|
| ABST | Aircraft Beam Structural Test |
| BRSL | Bonded repair size limit |
| CFRP | Carbon-fiber-reinforced polymer |
| DIC | Digital image correlation |
| DSG | Design service goal |
| DSO | Design service objective (used interchangeably with DSG) |
| FAA | Federal Aviation Administration |
| FEM | Finite element model |
| NDI | Nondestructive inspection |
| NFOV | Narrow field of view |
| PFA | Progressive failure analysis |
| SHM | Structural health monitoring |
| SL | Service load |
| WFOV | Wide field of view |

## Executive summary

In a collaborative effort, the Federal Aviation Administration (FAA) and The Boeing Company are assessing bonded repair technologies of composite panels representative of transport airplane wing structures through test and analysis using the FAA's Aircraft Beam Structural Test (ABST) fixture. Emphasis has been placed on investigating methods and tools used to conduct analysis and predict structural performance of bonded repairs and those used to monitor and evaluate repair quality over the life of the part. This project is carried out in a phased approach where phase 1 was fixture development and verification. Phase 2 was the initial baseline testing that verified the analysis models and provided an initial reference point for inspection and monitoring systems used to detect and track damage formation. This report discusses the recent third-phase efforts to support bonded repair size limit (BRSL) studies and methods used to predict the limit-load residual strength for a failed scarfed repair in solid composite laminates with full-depth and partial-depth scarf configurations. Scarfs were inserted in carbon-fiber-reinforced polymer (CFRP) panels having an 18-ply quasi-isotropic layup. The panels were attached as top-side components (e.g., skins) of a cantilevered, 24-in-wide by 40-in-long wingbox structure. These panels were subjected to constant-moment loads tested either quasi-statically loaded to failure or subjected to fatigue before loading them to failure. The applied fatigue-loading conditions simulated highest operational strain levels for transport-category wing panels for 165,000 cycles, which is approximately equal to three design service goals (DSGs). The test and analysis results revealed a significant benefit of partial-depth scarfs over full-depth scarfs. In addition, there was no debit in strength due to fatigue in both type of panels tested. For both full-depth and partial-depth scarf configurations, the methods under development for BRSL residual strength predictions correlated well with test results. Follow-on efforts are focused on panels with double-sided scarf configurations, which will be documented in a companion technical report.

# 1 Introduction

Although the effectiveness of adhesive-bonded repair patches has been demonstrated to maintain aging military fleets worldwide (Baker, Rose, & Jones, 2003), challenges remain with respect to commercial aircraft applications. One such challenge pertains to the integrity of the bond between the repair patch and the damaged structure, which depends on numerous installation parameters. Errors during installation, including exposure of the repair patch to a humid environment, improper surface preparation, contamination of the bond line, insufficient control of the curing temperature, and loss of vacuum pressure, can lead to a reduction in bond-line strength. Furthermore, bond integrity, especially weak bonds, cannot be detected by existing non-destructive inspection (NDI) techniques. Consequently, the Federal Aviation Administration (FAA) issued a policy statement regarding bonded repair size limits (BRSL) to primary structure (Federal Aviation Administration, 2014). According to this BRSL policy statement, "All critical structures must have a repair size limit no larger than a size that maintains limit load residual strength capability with the repair completely failed or failed within arresting design structures." To expand the size limits of a given bonded repair patch, repair designs must have structural substantiation based on either tests or analysis supported by tests. Additional data sets are required to qualify bonded material and process compatibilities, to demonstrate proof of structure, and to establish reliable inspection procedures.

In a multiyear, multiphase research program, the FAA and The Boeing Company are working in partnership to gain better insight into the fatigue and damage tolerance performance of adhesive-bonded repairs and to help address issues cited in the FAA policy statement above. Current efforts focus on testing and analysing bonded repairs to representative composite wing panels using the Aircraft Beam Structural Test (ABST) fixture (Chadha, Bakuckas Jr., Fleming, Lin, & Korkosz, 2019), a new structural test capability at the FAA William J. Hughes Technical Center. The program objectives are to characterize the fatigue and damage tolerance performance of bonded repairs subjected to a simulated service load (SL) and to evaluate the limit-load capability of a typical composite wing panel of transport category aircraft with a failed repair. In addition, methods and tools used for the performance analysis and for evaluating and monitoring repair integrity are being assessed.

This program was conducted in a phased approach, where phase 1 (Chadha, Bakuckas Jr., Fleming, Lin, & Korkosz, 2019) was the development of the ABST fixture, and phase 2 (Neel, et al., 2020) characterized the material response of composite panels in unnotched pristine and open-hole configurations under constant moment loading. This baseline information provided verification of the test fixture loading, validation of analysis models, and an initial reference point for NDI and structural health monitoring (SHM) systems. In general, the baseline panels were subjected to fatigue-loading conditions that produce highest operational strain levels for transport-category wing panels for 165,000 cycles, which is approximately equal to three design service goals (DSGs). The fatigue-loading conditions used did not consider scatter. Per AC-25.571-1D , a DSG is defined as "The period of time (in flight cycles or flight hours, or both) established at design and/or certification during which the airplane structure is reasonably free from significant cracking" (Federal Aviation Administration, 2011). For the unnotched panel (panel 1), structural integrity was maintained through testing with no signs of damage in the test section. Measured strains in the test section were relatively constant and remained unchanged during fatigue. For the open-hole panel (panel 2), strain surveys revealed excellent correlation between test and analysis. Strain concentrations measured using strain gages and a digital image correlation (DIC) system matched finite element analysis results. The details of phase 2 results were published in a previous FAA technical report (Neel, et al., 2020).

Phase 3 of this program more directly supports the FAA BRSL policy issued to address concerns of not being able to detect weak bonds that result in failure. BRSL analysis methods for sizing bonded repairs to critical solid laminates and honeycomb panels are needed. Tests validated such analysis methods to determine allowable repair sizes within the requirements of BRSL policy. Test information will be useful because of the ABST fixture's ability to produce effects of boundary conditions and load redistribution that can be understood and incorporated into the analysis models and tool. Data from the analysis methods and tools can also be used to develop design curves. The first part of phase 3 was the limit-load characterization for partial- and full-depth scarf configurations for solid laminates under tension produced by constant moment. A total of four panels (panels 3–6) were tested in phase 3, and the results are reported in this document. The benefit gained in the residual-strength limit-load capability of a partial-depth scarf was revealed in these tests. In addition, analytical models currently under development to accurately predict the strain levels associated with scarfs with failed repair were demonstrated. The second part of phase 3 will address the challenges with double-sided scarf configurations, and the findings will be documented in a companion technical report.

Future work will study fatigue and residual strength aspects for more configurations and loading for both solid laminates and honeycomb panels. In addition, compression-loading tests and analyses are considered in the long-term planning of this program.

# 2 Experimental procedures

A description of the experimental procedures used in this program, including the test fixture, panels, applied loads, and the inspection and monitoring methods, are outlined in sections 2.1 through 2.4.

## 2.1 Test fixture description

The FAA conducted tests using the ABST fixture (Chadha, Bakuckas Jr., Fleming, Lin, & Korkosz, 2019) located at the FAA William J. Hughes Technical Center. The FAA developed this new structural test capability in collaboration with The Boeing Company (herein referred to as Boeing) as part of this program. The fixture is capable of applying major modes of loading to panels representative of a typical wing or stabilizer components (see Figure 1).

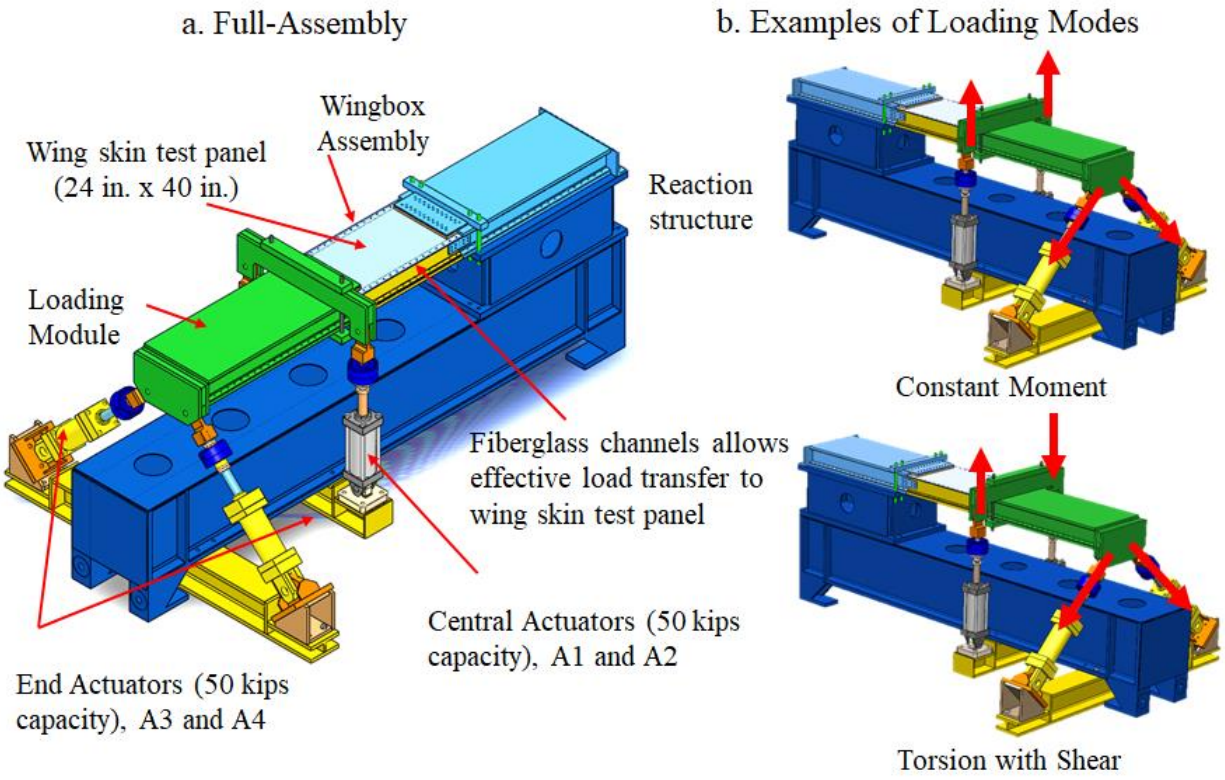


Figure 1. The ABST fixture and subcomponents (a) and examples of fixture loading modes (b)

The ABST fixture is self-reacting and integrates mechanical, hydraulic, control, and data-acquisition systems. The mechanical system consists of a load module, wingbox assembly, and reaction structure. The wingbox assembly consists of the test panel (24 in. wide and 40 in. long), two pultruded fiberglass channels, and a lower steel plate. The entire wingbox assembly is mounted on one end to the load module and on the other to the reaction structure. The fiberglass channels allow for efficient load transfer to the test panels. Loads are applied via the loading module using four hydraulic actuators (50-Kips capacity and 12-in. stroke) powered by a 60-gallons/minute hydraulic power unit (HPU), controlled by an MTS FlexTest® 100 system. Two central vertical actuators (A1 and A2) and two end actuators (A3 and A4) mounted at a 45° angle provide a multitude of individual loading modes, including constant moment, torsion, cantilever shear, and horizontal bending, which can be combined to yield complex loading configurations. In the current test program, only constant moment loading is applied to the panels. An MTS FlexDAC™ 20 data acquisition system provides 64 channels to collect strain gages and displacement sensors data. A detailed, component-by-component description of the ABST fixture and supporting systems within the FAA's Structures and Materials Laboratory is provided in a separate report (Chadha, Bakuckas Jr., Fleming, Lin, & Korkosz, 2019).

## 2.2 Test specimen descriptions

The test articles fabricated by Boeing were flat, composite, solid laminate panels (24 in. wide, 40 in. long, and 0.135 in. thick) representing typical carbon fiber-reinforced polymer (CFRP) skin in outboard wing panels approaching wing tips. An 18-ply panel was considered having a quasi-isotropic layup, $[\pm 45°_{fabric}/\text{-}45°/90°/45°/0°/\text{-}45°/90°/45°/0°]_s$. Panels were fabricated with a high-modulus carbon/epoxy prepreg material, a typical material used by Boeing for the composite primary structure of commercial applications. These panels had holes machined to match the fixture attachment points. The 24-in.-long ends of the panel were reinforced with doublers (end tabs) for load introduction into the test article. These end tabs were made from the same material and layup as the test panel and included a taper region with ratios of 30:1.

During this phase, four 18-ply solid laminate panels were tested. Panels 3 and 5 were tested with failed (cavity) partial (half)-depth scarfs and panels 4 and 6 were tested with failed (cavity) full-depth scarfs. Figure 2 shows the geometry of the two partial-depth scarf panels on the left and two full-depth scarf panels on the right. The scarfs in the partial-depth panels were only half the depth, with 3-in. inner diameters and 6.7-in. outer diameters. The scarfs in the full-depth panels were through-the-thickness, with 3-in. inner diameters and 10.7-in. outer diameters. Scarf ratio for both full-depth and partial-depth scarfs was 30:1. Detailed schematic of the scarfs and the plies layup for partial- and full-depth scarf panels are shown in Figure 3 and Figure 4, respectively. Appendix A provides the detailed drawings of all the panels.

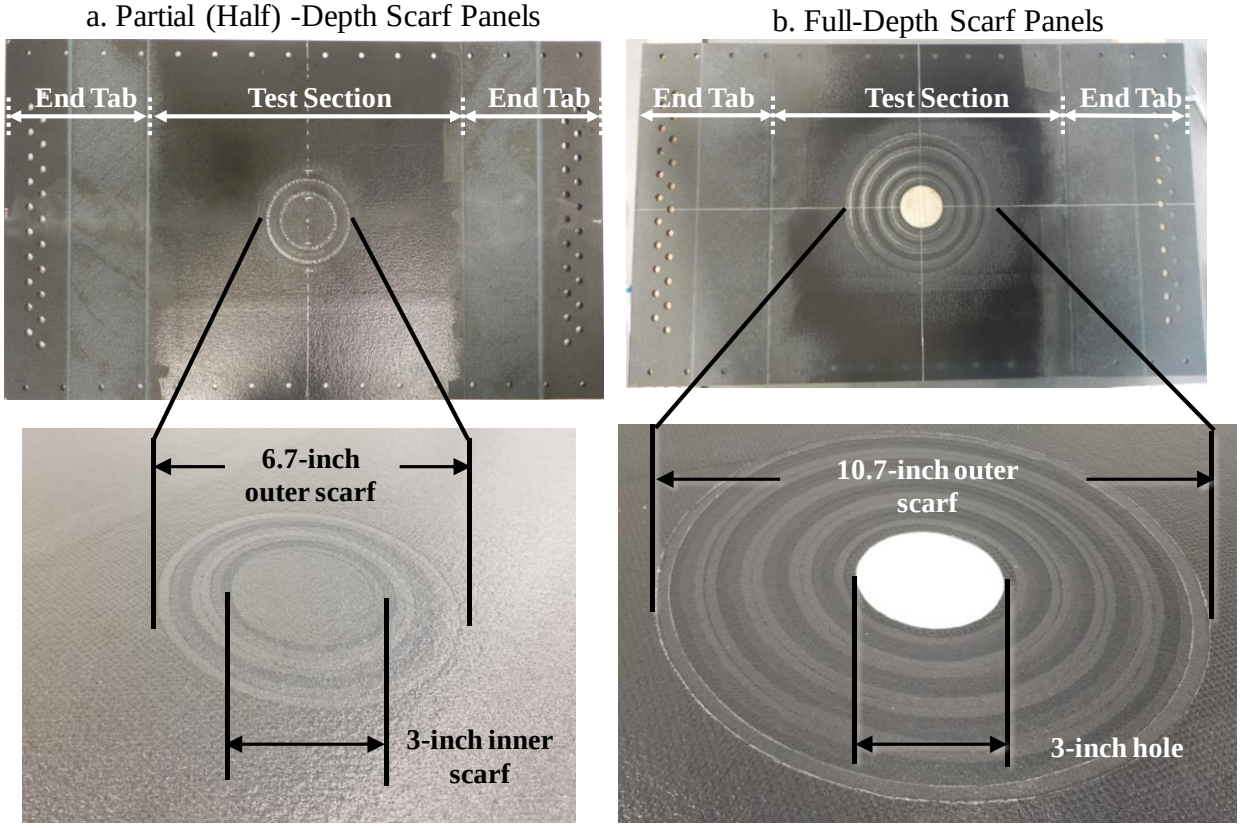


Figure 2. Partial- (a) and full-depth (b) scarf panels

## 2.3 Applied load and test matrix

The applied test loads used in this study represent compression, tension, and shear, or the strains usually experienced by a composite wing panel of a typical transport-category aircraft (Figure 3 and Figure 4). Three loading types were considered:

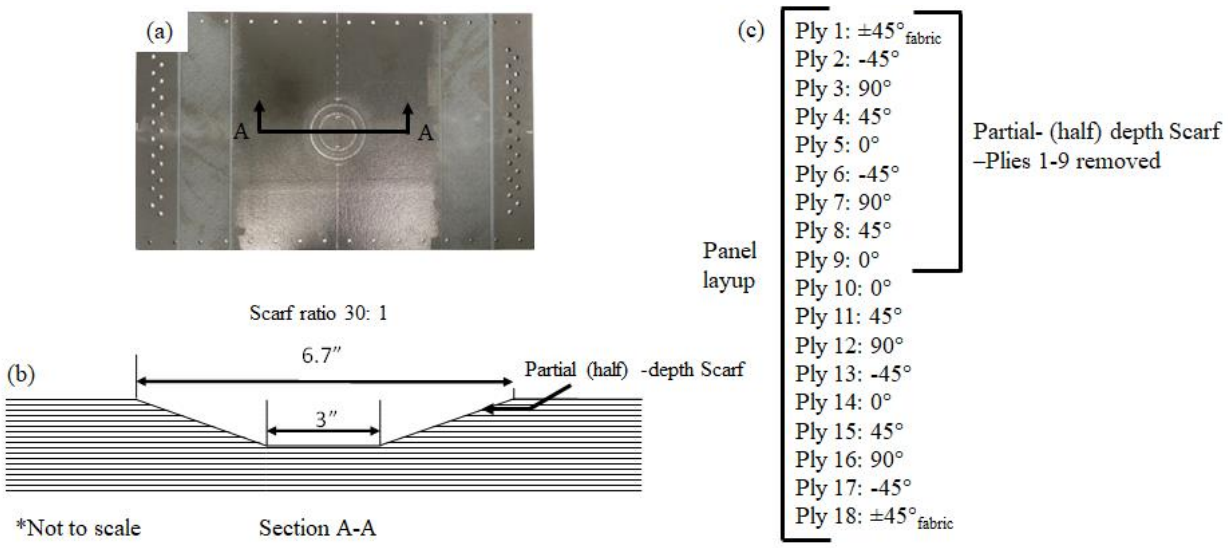


Figure 3. Details of partial-depth scarf panels (panels 3 and 5)

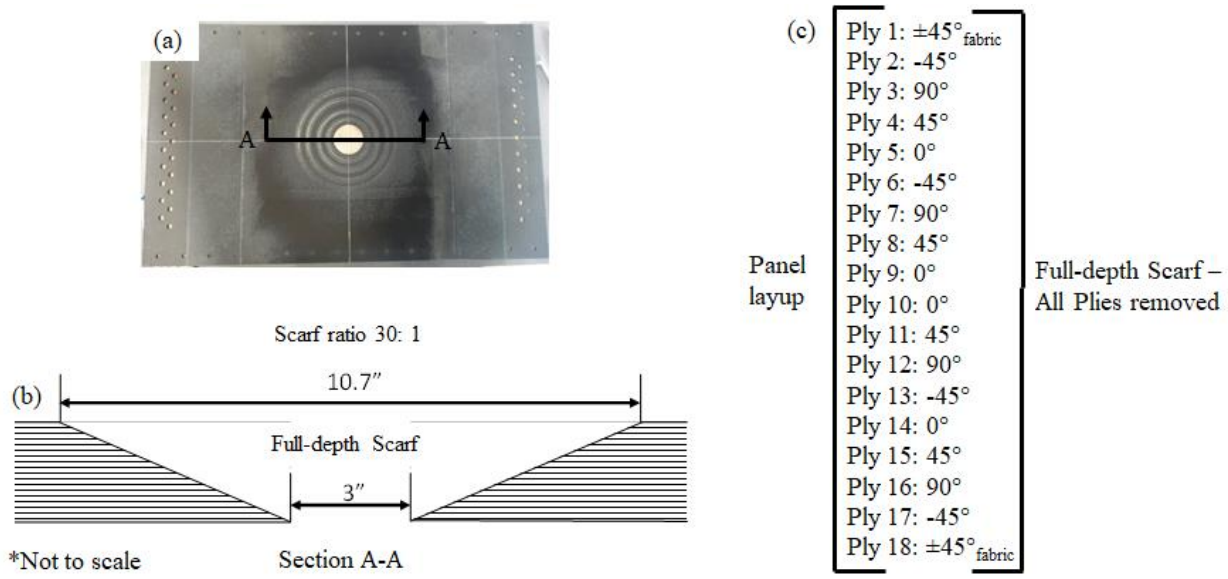


Figure 4. Details of full-depth scarf panels (panels 4 and 6)

1. Strain survey loads applied quasi-statically to a percentage of the SL conditions (typically 75%–100% of the SL conditions) to ensure proper load introduction into the panel.
2. Fatigue loads simulating SL conditions considered the highest operational strain levels that could occur during a flight cycle, conservatively estimated to be 37% of the ultimate load conditions. Elevated fatigue loads were used to induce damage growth (40%–60% of the ultimate load conditions). Fatigue loading conditions did not consider scatter.
3. Ultimate loads applied quasi-statically based on notched allowable coupons or barely visible impact damage load conditions.

A summary of these load configurations and the corresponding strain values is provided in Table 1. The tests covered in this report were for tensile loading conditions only.

Table 1. Strain levels used in program

| **Test Description** | **Load Type** | **Strains (με)** |
|---|---|---|
| | | **Tension** |
| Strain survey—75%–100% of the simulated service loads (SL) strain conditions | Static | 1,660 – 2,200 |
| Fatigue—simulated SL conditions (37% of ultimate strains) | Cyclic (R = 0.1) | 2,200 |
| Fatigue—elevated loads to induce damage growth (40 - 60% of ultimate strain) | Cyclic (R = 0.1) | 2,400 – 3,600 |
| Residual strength (ultimate strains)—typical design ultimate loads of notched allowables | Static | 6,000 |

The sequence of applied loads used for each test panel are shown in Table 2. Panels 3 and 4 were first subjected to strain surveys and then loaded quasi-statically up to failure to determine the baseline residual strength of both scarf configurations. Panel 5 was also subjected to strain surveys and then to three fatigue-loading intervals to determine the effect of fatigue damage on post-fatigue residual strength. The three fatigue-loading intervals were 1) apply service load conditions for 3 DSG i.e., 165,000 cycles; 2) increase the load to 60% of ultimate strength to promote delamination growth to a size of 0.25 in.; and 3) apply SL conditions for additional 3 DSGs to see if delamination growth continued to occur. After completing the fatigue-loading intervals, panel 5 was loaded quasi-statically up to failure to determine the post-fatigue residual strength. Similarly, panel 6 was subjected to strain surveys and then fatigue-loaded for 165,000 cycles before being subjected to failure to measure post-fatigue residual strength. The test data will be used to evaluate the benefit in residual strength limit-load capability that a partial-depth scarf offers and to validate an analytical model that predicts the strain levels associated with scarf depth.

Table 2. Summary of applied loads

| **Panel #** | **Test Panel** | **Load Type** | | **Moment ($lb_f$-ft)** | **Actuator 1 & 2 ($lb_f$)** | **Actuator 3 & 4 ($lb_f$)** | **Target Strain (με)** |
|---|---|---|---|---|---|---|---|
| 3 | Partial-depth scarf panel-1 | Baseline strain survey (82% of fatigue) | | 30,157 | -3,583 | 5,067 | 1,800 |
| | | | Predicted critical loads | 169,318 | -20,117 | 28,445 | 9,000 |

| Panel # | Test Panel | Load Type | | Moment ($lb_f$-ft) | Actuator 1 & 2 ($lb_f$) | Actuator 3 & 4 ($lb_f$) | Target Strain (με) |
|---|---|---|---|---|---|---|---|
| | | Residual strength test | Measured baseline failure loads | 168,611 | -20,033 | 28,123 | 7,718 at 152,260 $lb_f$-ft |
| 4 | Full-depth scarf panel-1 | Baseline strain survey (75% of fatigue) | | 25,629 | -3,045 | 4,307 | 1,660 |
| | | Residual strength test | Predicted critical loads | 95,698 | -11,370 | 16,078 | 5,491 |
| | | | Measured baseline failure loads | 81,068 | -9,632 | 13,620 | 5,163 |
| 5 | Partial-depth scarf panel-2 | Baseline strain survey (100% of fatigue) | | 38,581 | -4,584 | 6,483 | 2,200 |
| | | Fatigue at service load strain level (165,000 cycles) | | 38,581 | -4,584 | 6,483 | 2,200 |
| | | Fatigue at elevated load strain level (4,500 cycles) | | 65,579 | -7,792 | 11,019 | 3,600 |
| | | Additional fatigue at service load strain level (165,000 cycles) | | 38,581 | -4,584 | 6,483 | 2,200 |
| | | Post-fatigue residual strength test | Predicted critical loads | 169,318 | -20,117 | 28,445 | 9,000 |
| | | | Measured failure loads | 167,273 | -19,874 | 28,095 | 8,392 |
| 6 | Full-depth scarf panel-2 | Baseline strain survey (100% of fatigue) | | 36,441 | -4,330 | 6,122 | 2,200 |
| | | Fatigue at service load strain level (165,000 Cycles) | | 36,441 | -4,330 | 6,122 | 2,200 |
| | | Post-fatigue residual strength test | Predicted critical loads | 95,698 | -11,370 | 16,078 | 5,491 |
| | | | Measured failure loads | 84,520 | -10,042 | 14,201 | 4,944 |

The applied actuator loads used for each test panel shown in Table 2 were first predetermined from finite element analysis to provide constant target strains under a tensile-bending moment. Slight adjustments in the actuator loads were made during the test until the target strains were obtained. Fatigue loading was conducted at $R = 0.1$ and a frequency of 0.5 Hz. All testing was done under laboratory ambient conditions.

## 2.4 Inspection and deformation monitoring methods

Several methods were used to monitor the deformation of the specimens throughout the duration of the tests. Displacement sensors installed on the load application assembly were used to monitor the horizontal and vertical deflections of the cantilevered wingbox. Strain gages installed in the internal and external surfaces of the panel as well as DIC systems positioned above the wingbox were used to monitor strains and displacements. The strain gage map and two DIC fields of view for all four panels are shown in Figure 5 and Figure 6, respectively. Detailed descriptions of these instruments are provided in (Neel et al., 2020). DIC systems were used to monitor two field of views, a narrow field of view (NFOV) and a wide field of view (WFOV). The NFOV was approximately 5 in. by 5 in. and was used to resolve high strains at the center of the scarf. The WFOV was approximately 11 in. by 11 in. and was used to measure global strains in the vicinity of the scarf.

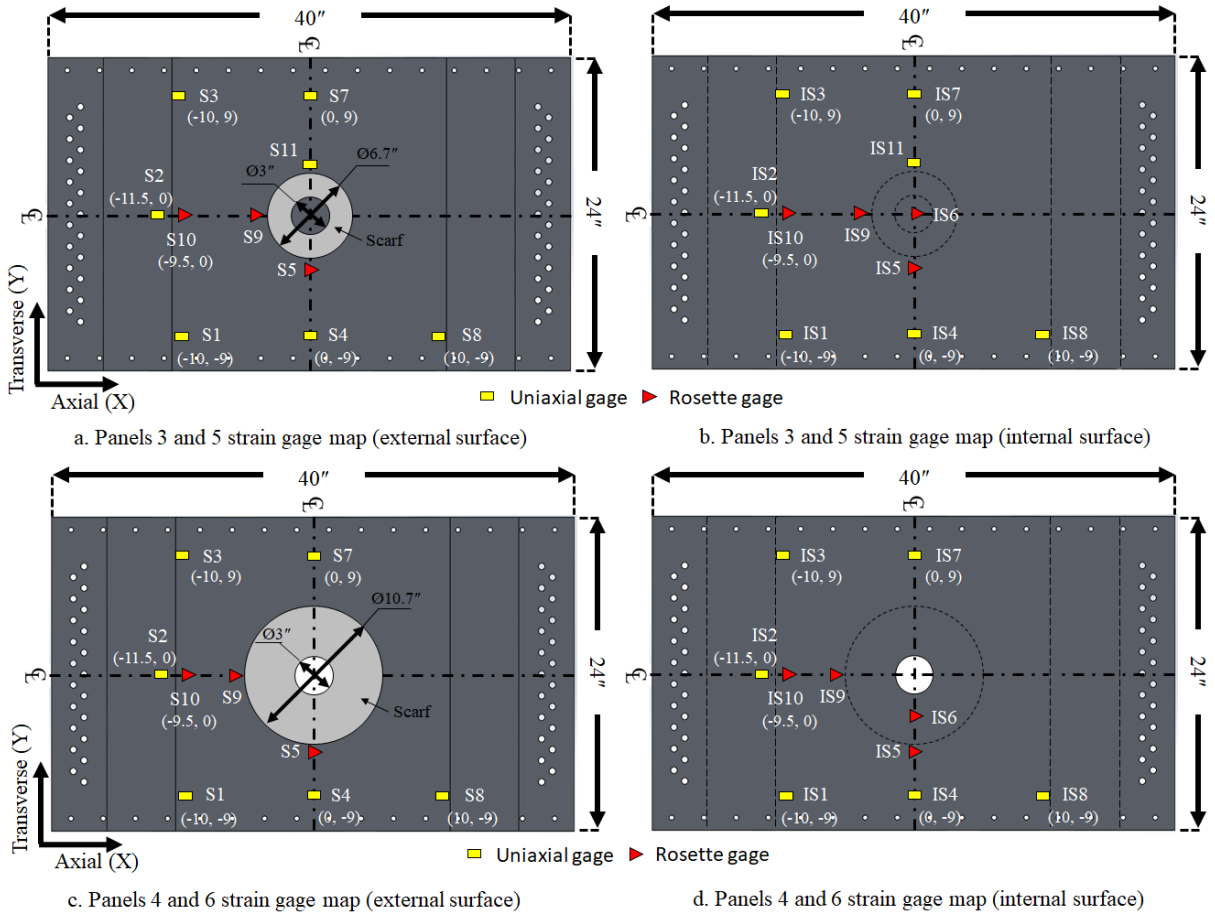


a. Panels 3 and 5 strain gage map (external surface)

b. Panels 3 and 5 strain gage map (internal surface)

c. Panels 4 and 6 strain gage map (external surface)

d. Panels 4 and 6 strain gage map (internal surface)

Figure 5. Strain gage maps for panels 3–6

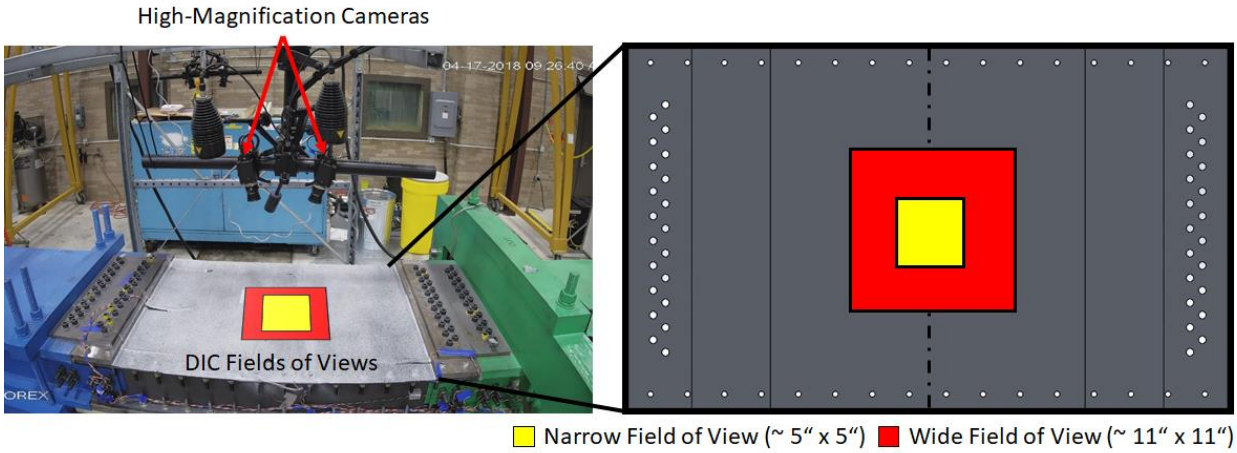


Figure 6. Typical setup of a DIC system and two fields of view during the tests

During the test, several methods were used to monitor the initiation and growth of damage within the CFRP specimens. For visual detection, several camera systems with varying magnifications were used to monitor the specimens. For detection of nonvisual damage, flash thermography, phased array ultrasonic, and pulse-echo ultrasonic methods were used. For real-time damage detection, an acoustic emission system was used.

# 3 Analytical procedures

Boeing conducted the analysis in support of this program, as outlined in sections 3.1 and 3.2

## 3.1 Finite element analysis

Finite element models (FEM) of the test fixture and test panels were created to simulate the loading of the panel prior to actual testing and provided predictions of: (1) actuator loads that the ABST fixture should apply to provide appropriate target strains; (2) stress and strain fields; (3) damage initiation and growth in the composite panel, and (4) ultimate load and residual strength. An example of a full-depth scarf panel model under strain survey loading is shown in Figure 7.

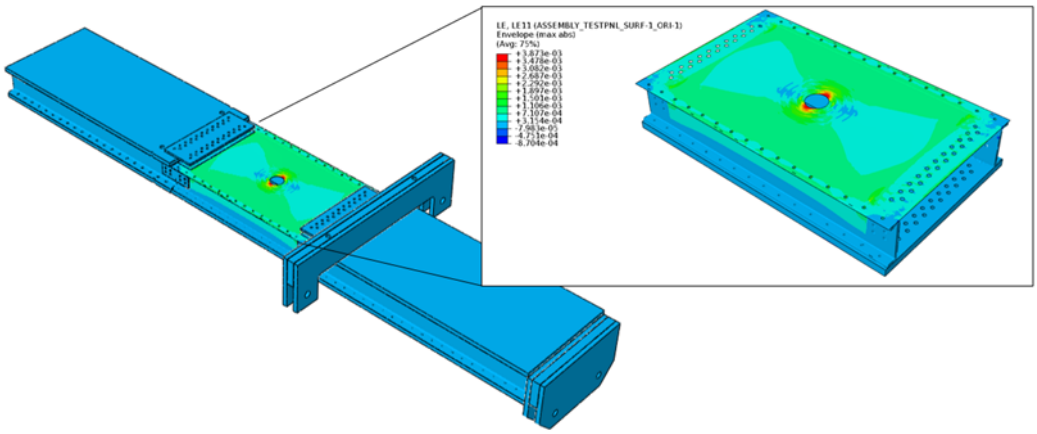


Figure 7. Full-depth scarf panel FEM with axial strain contour under 11,783 $lb_f$-ft

An advanced progressive failure analysis (PFA) approach was used to predict the ultimate load levels for various damaged panels in this test program. The current approach implements the Hashin in-plane failure criteria and the PFA input properties were derived from analysis and tests for the specific materials, processes and design practices. Figure 8 shows the matrix and fiber tensile failure index contours at ultimate load for a 30:1 scarf panel (only the damaged regions were shown).

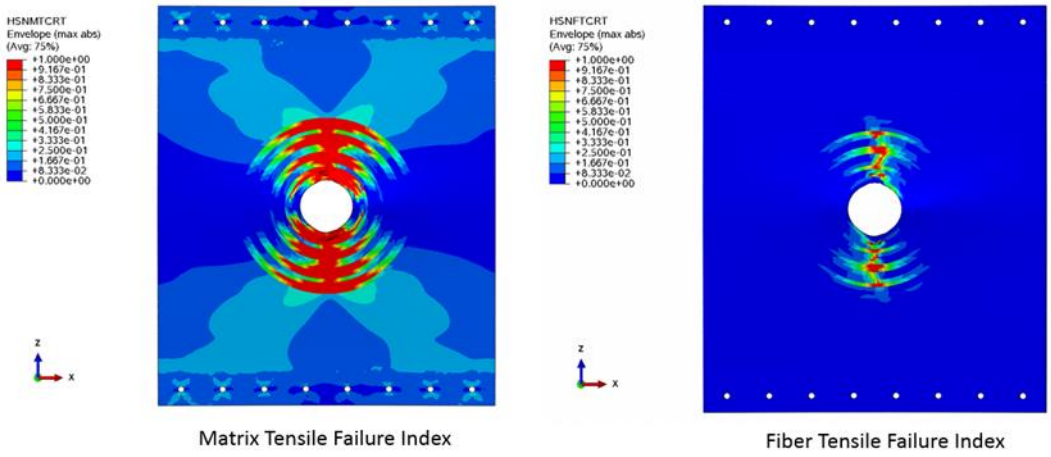


(a) Full-depth scarf panel at failure

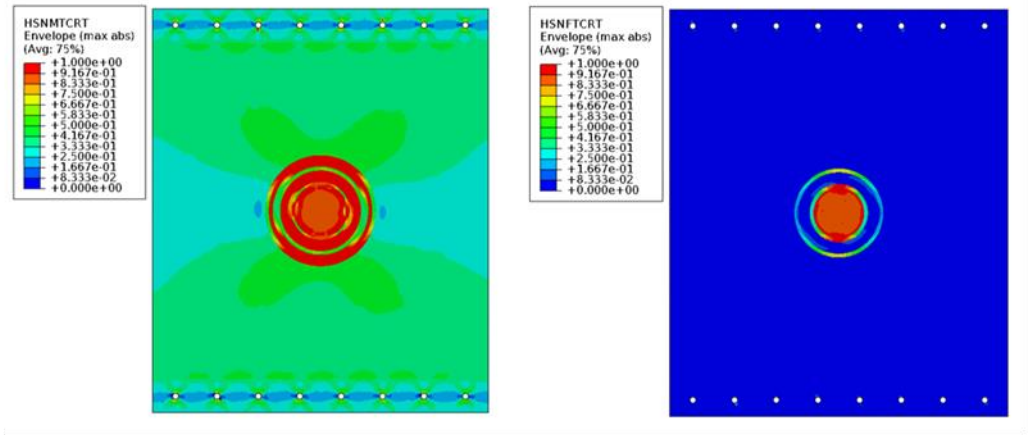


(b) Partial-depth scarf panel at failure

Figure 8. The PFA approach to predict residual strength

## 3.2 BRSL semi-analytical method development and verification

The development and verification of a rapid-executing BRSL analysis method is being undertaken to predict the limit-load residual strength for a failed scarf repair in solid composite laminates and honeycomb panels. It is based on the classic strain concentration factor $K_{d0}$ approach modified by a geometry factor $K_{sr}$, as shown in Figure 9, under tensile loading. Testing will support improved analysis methods to better represent the actual damage within the requirements of BRSL policy. The initial focus of this phase has been the limit-load characterization for partial- and full-depth scarf configurations for solid laminates under tension produced by constant moment. From the open-hole panel testing, the characteristic length parameter $d_0$ was found to be 0.05 inch based on equation (4) in Figure 9.

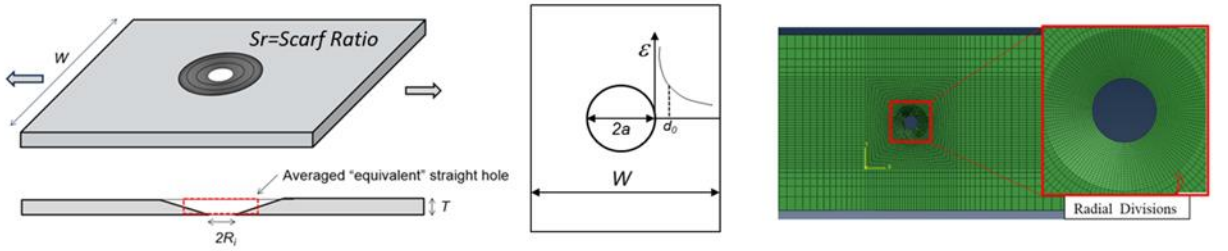


| | |
|---|---|
| (1)Strain Concentration Factor (SCF) | $K_t = K_{d0}(K_{Sr})$ |
| (2) Scarf Factor | $K_{Sr} = 1 + function(\frac{T}{Ri}, \frac{Ri}{W}, Sr)$ |
| (3) Predicted failure strain | $\varepsilon_{scarf} = {}^{\varepsilon_{unt}}/_{YK_t}$ *Y is a configuration dependent load redistribution factor* |
| (4) Strain Concentration Factor for Straight Hole ($d_0$: Characteristic Length) | $K_{d0} = \frac{1}{2}C_w\left\{2 + \left(\frac{a}{a+d_0}\right)^2 + 3\left(\frac{a}{a+d_0}\right)^4 - (K_T^\infty - 3)\left[5\left(\frac{a}{a+d_0}\right)^6 - 7\left(\frac{a}{a+d_0}\right)^8\right]\right\}$ |
| (5) Edge Factor | $C_w = \left\{\frac{3(1-2a/W)}{2+(1-2a/W)^3} + \frac{1}{2}\left(\frac{2a}{W}M\right)^6 (K_T^\infty - 3)\left[1 - \left(\frac{2a}{W}M\right)^2\right]\right\}^{-1}$ |
| (6)Edge Factor Term M | $M^2 = \frac{\sqrt{1 - 8\left[\frac{3(1-2a/W)}{2+(1-2a/W)^3} - 1\right]} - 1}{2(2a/W)^2}$ |
| (7) SCF for an infinitely large orthotropic plate | $K_T^\infty = 1 + \sqrt{2\left(\sqrt{\frac{E_x}{E_y}} - \nu_{xy}\right) + \frac{E_x}{G_{xy}}}$ |

Figure 9. Engineering approach based on $K_t$ to predict residual strength

Because of the significant change in skin stiffness implied in the fully disbonded full-scarf scenario, it is expected that loads will redistribute toward stiffening elements within the same panel, as well as to neighboring panels. A load redistribution factor can be calculated based on the product of modulus and cross-sectional area (EA) for each component, by comparison between the intact and failed configuration magnitudes. The first step is to define the effective width that will remain constant for the total load calculation. Then, the adjacent stiffeners and half the adjacent bay's skin are identified (Figure 10). Assuming strain compatibility, total load is apportioned according to extensional stiffness of each component (adjacent bay, stiffeners, scarf bay).

PTOTAL is assumed to remain constant. Component loads are calculated for both intact panel and failed scarf configurations. PI3 and PF3 are the segment axial load for the bay presenting a scarf cutout. PTOTAL and all geometry and material inputs are known values. The values for the intact configuration can be determined by solving the set of corresponding equations. The values for the failed configuration can be determined in a similar fashion, after determining the unknown value φ. The load redistribution factor Y for the failed bay is PF3/PI3.

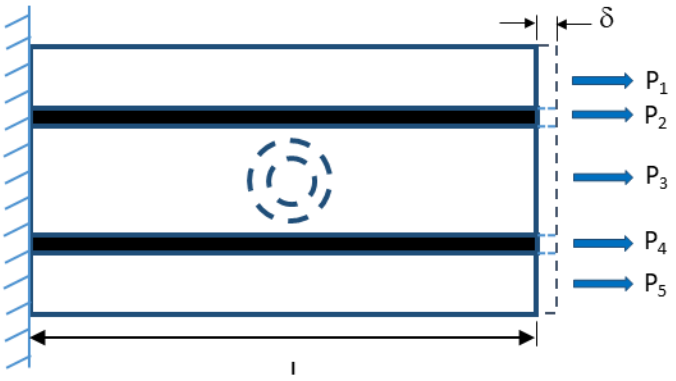


**Intact**

$P_{TOTAL} = P_{I1} + P_{I2} + P_{I3} + P_{I4} + P_{I5}$

$\delta_I = \delta_{I1} = \delta_{I2} = \delta_{I3} = \delta_{I4} = \delta_{I5}$

$\delta_{I1} = P_{I1} L / A_1 E_1$

$\delta_{I2} = P_{I2} L / A_2 E_2$

$\delta_{I3} = P_{I3} L / A_3 E_3$

$\delta_{I4} = P_{I4} L / A_4 E_4$

$\delta_{I5} = P_{I5} L / A_5 E_5$

**Failed Scarf**

$P_{TOTAL} = P_{F1} + P_{F2} + P_{F3} + P_{F4} + P_{F5}$

$\delta_F = \delta_{F1} = \delta_{F2} = \delta_{F3} = \delta_{F4} = \delta_{F5}$

$\delta_{F1} = P_{F1} L / A_1 E_1$

$\delta_{F2} = P_{F2} L / A_2 E_2$

$\delta_{F4} = P_{F4} L / A_4 E_4$

$\delta_{F5} = P_{F5} L / A_5 E_5$

$\delta_{F3} = P_{F3} (L-2R_o) / A_3 E_3 + 2P_{F3} \varphi / t_3 E_3$

Figure 10. Calculating load distribution factor Y

# 4 Results and discussion

Tests and analyses were performed to determine the fatigue and damage tolerance performance of CFRP panels representative of wing structure of typical transport category aircraft. Typical results described below are focused on the BRSL study of the solid laminate CFRP panels having partial (half)-depth scarfs (panels 3 and 5), and full-depth scarfs (panels 4 and 6).

## 4.1 Panel 3, partial-depth scarf

Panel 3 was first subjected to a baseline strain survey followed by quasi-statically loading to failure as summarized in sections 4.1.1 and 4.1.2.

### 4.1.1 Baseline strain surveys

Figure 11 shows the baseline strain survey results for panel 3, where loads were applied to yield far-field target strain of 1800 με. Strain concentrations at the partial-depth scarf were measured using DIC and strain gages. Figure 11a shows the location of strain gages and the DIC field of view. Figure 11b and Figure 11c shows the axial strains measured via DIC and comparison of strain gage results and analysis predictions respectively. In addition, the axial strains measured via DIC along the section from 6 o'clock position to 12 o'clock position and strain gage S-11 are compared to the analysis predictions (Figure 11b and Figure 11d). The test results had excellent agreement with the finite element analysis predictions (Figure 11d). Detailed strain survey results are provided in appendix B.

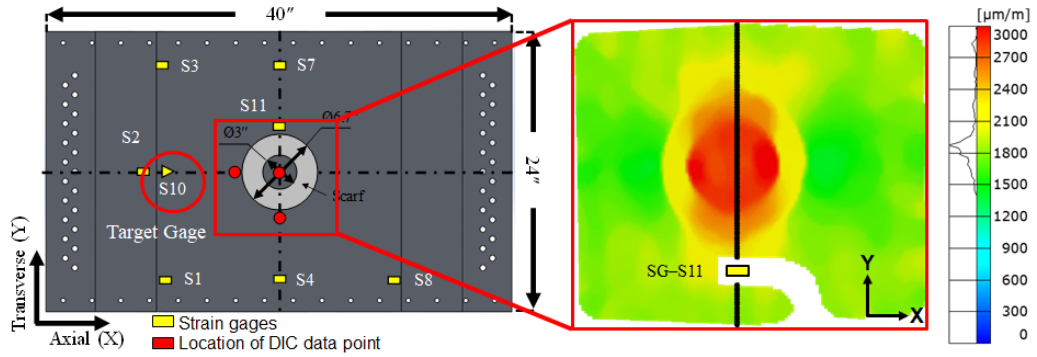


a. Partial-depth scarf configuration and location of strain gages

b. Axial strains measured via DIC

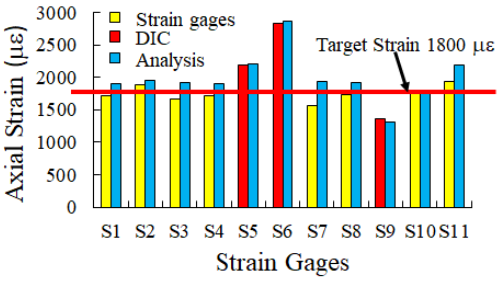


c. Test and analyses correlation

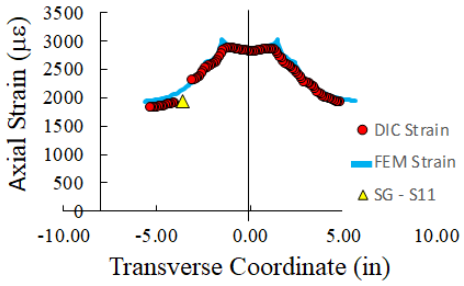


d. Axial strains along the Y-coordinate passing through the center

Figure 11. Baseline strain survey results for panel 3, partial- depth scarf panel

### 4.1.2 Residual strength test

After the initial strain survey, panel 3 was subjected to a residual strength test. Results are shown in Figure 12. The panel was loaded quasi-statically in a saw-tooth profile (sinusoidal loading), increasing the load level up to failure based on percentages of the predicted critical strength of 169,318 ft-$lb_f$ calculated by PFA. During loading, damage formation was monitored visually using high-magnification cameras and DIC. After each load increment, the panel was inspected using a thermography system. Damage was first detected visually at 60% load level in the form of edge delamination (ply #9, middle $0^o$ ply) along the scarf inner-edge at the 3 o'clock position. The edge delamination continued to grow circumferentially while loading to 80% load level. In addition, a delamination initiated in the fifth ply (first $0^o$ ply from the panel external surface). At 90% load level, extensive damage occurred where the entire scarf region in the 3 o'clock position delaminated. Final failure through the net section of the panel occurred at an applied moment of 168,611ft-$lb_f$, which was within 1% of the predicted value. As soon as the $0^o$ plies delaminated, the load was transferred to the 12 o'clock and 6 o'clock positions and the panel failed catastrophically along the net section. Both DIC and thermography successfully captured the damage progression. The strain gage data collected during residual strength test is provided in appendix C.

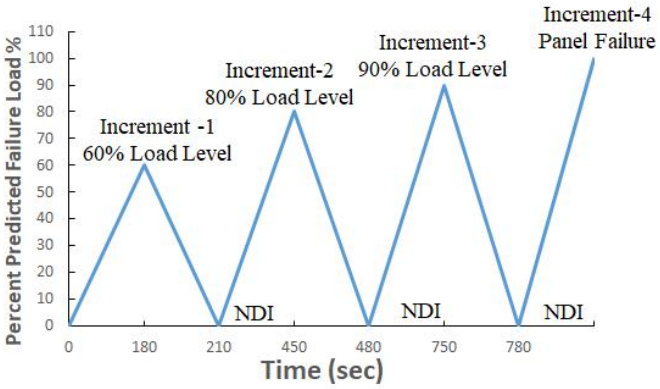


a. Residual strength load profile

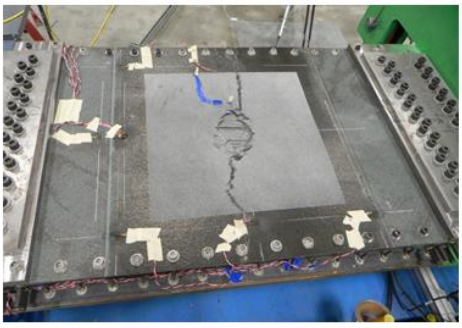

b. Net section failure of panel 3

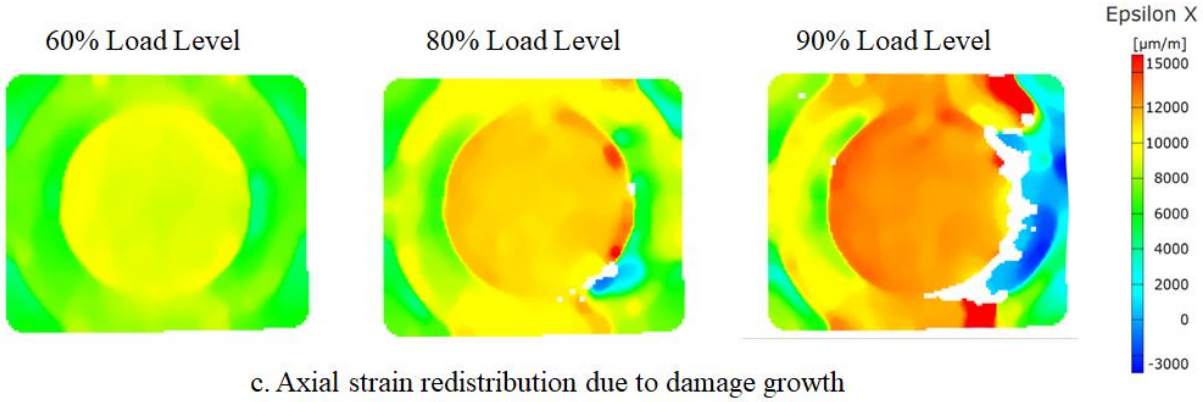


c. Axial strain redistribution due to damage growth

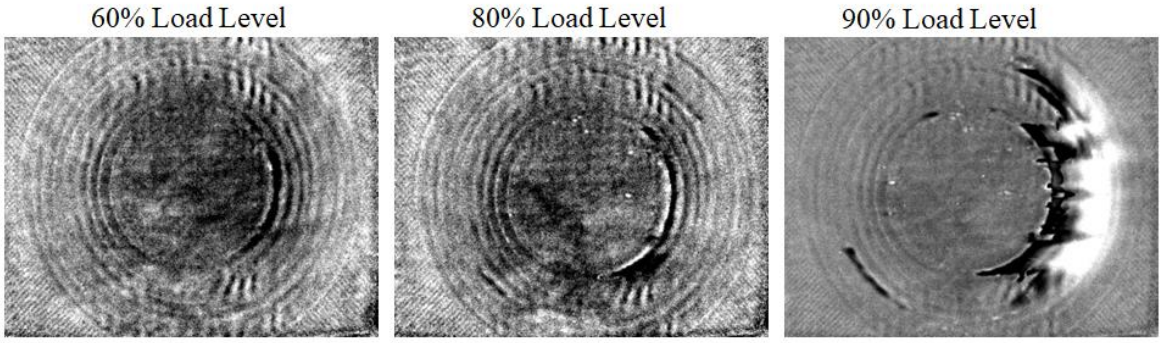


d. Indications of delamination on the edge of the scarf

Figure 12. Residual strength test results for panel 3, partial-depth scarf panel

## 4.2 Panel 5, partial-depth scarf

Panel 5 was the second panel with partial-depth scarf. For this panel, a baseline strain survey was conducted, followed by three intervals of fatigue, and a final post-fatigue residual strength test as outlined in sections 4.2.1–4.2.5.

### 4.2.1 Baseline strain surveys

First, a baseline strain survey was conducted on panel 5 to verify proper panel installation, alignment, and loading. The strain results for panel 5 and for panel 3 were similar. The results showed that panels 3 and 5 with identical construction had similar response to the same loading conditions and thus were used for comparative studies.

### 4.2.2 Fatigue at SL strain level

Next, panel 5 was subjected to 165,000 fatigue cycles (3 DSGs) at SL conditions and R=0.1. No strain redistribution was observed during the fatigue cycles as shown by strain gage and DIC results in Figure 13b and Figure 13c. During the tests, the panel was also inspected using several NDI techniques. Although there were few spots of possible local delamination, the sizes of these possible indications were too small to provide any conclusive results, as shown in Figure 13d. Overall, the scarf was able to sustain 3 DSGs without any damage formation or growth.

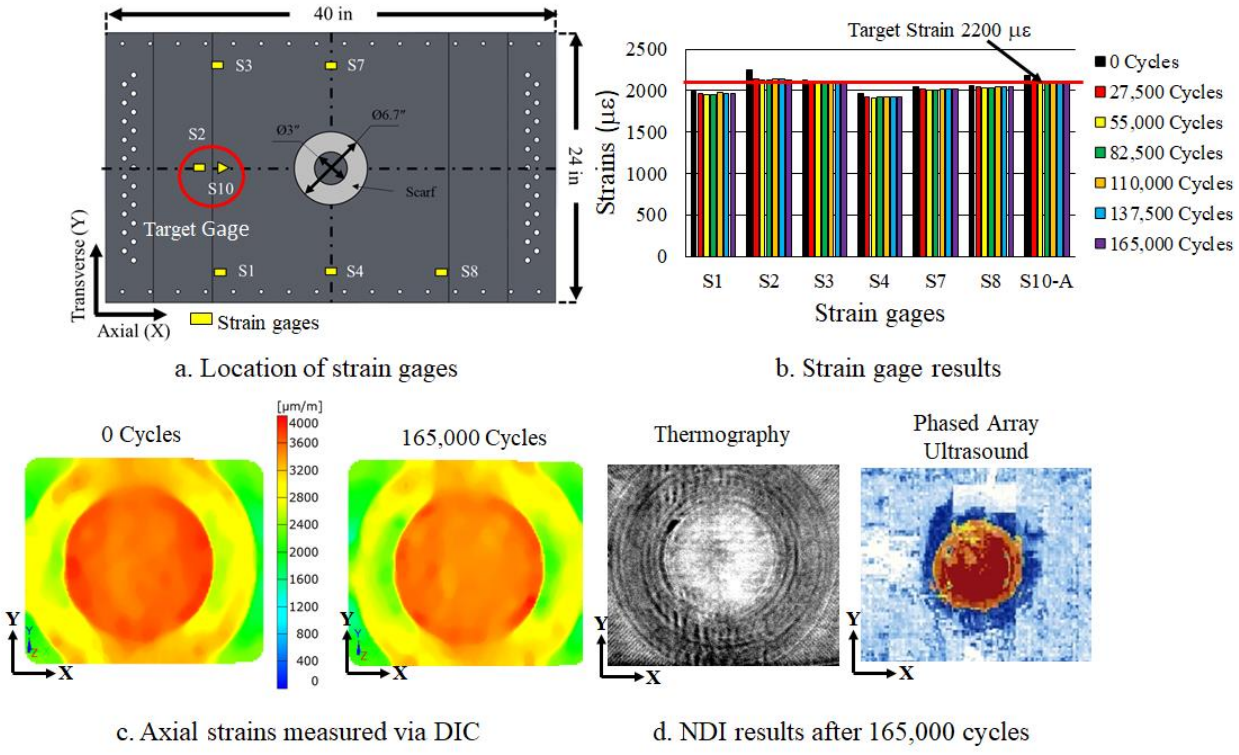


Figure 13. Panel 5 results during fatigue at SL strain level

### 4.2.3 Fatigue at elevated load strain level

In the next sequence of testing, the fatigue load levels were increased to the target maximum far-field strain of 3,600 με and R=0.1. The goal was to induce naturally occurring delaminations in the scarf. The first delamination was detected very early during the fatigue loading (about 1,000 fatigue cycles) along the scarf inner-edge at the 9 o'clock position in ply #9 (middle 0º ply of the panel). Later, another delamination appeared in the symmetrically opposite 3 o'clock position in the same ply #9 (0º ply). Once the 9 o'clock position delamination (largest delamination) grew to 0.25 inches in the radial direction, the elevated load level fatigue test was terminated at 4,500 cycles. The NDI results during this step are shown in Figure 14.

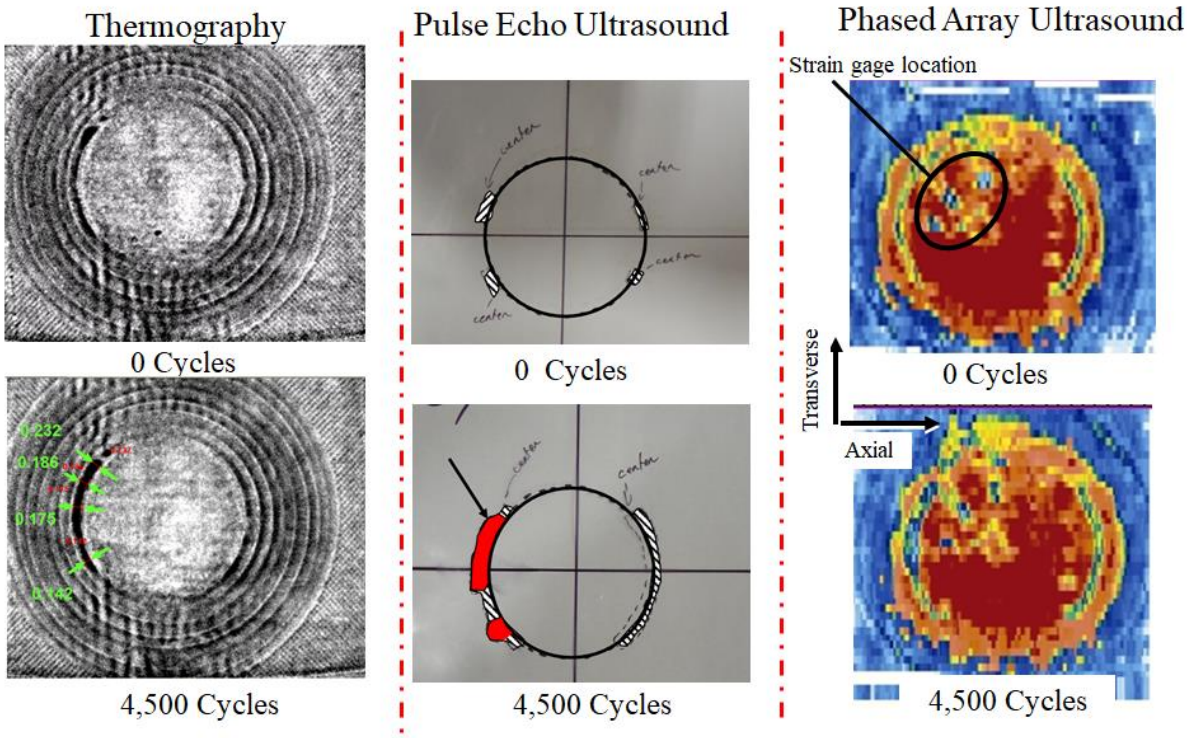


Figure 14. Panel 5 NDI results during fatigue at elevated load strain level

### 4.2.4 Additional fatigue at SL strain level

After fatigue at the elevated load strain level, panel 5 was subjected to an additional 165,000 fatigue cycles (3 DSGs) at lower-level SL conditions and R=0.1. The goal of this test was to monitor the growth of the delamination (developed during fatigue at elevated load strain level), when the panel is subjected to the SL strain levels. All the strain gages and DICs showed no strain redistribution, and NDI techniques showed no growth in delaminations, as shown in Figure 15.

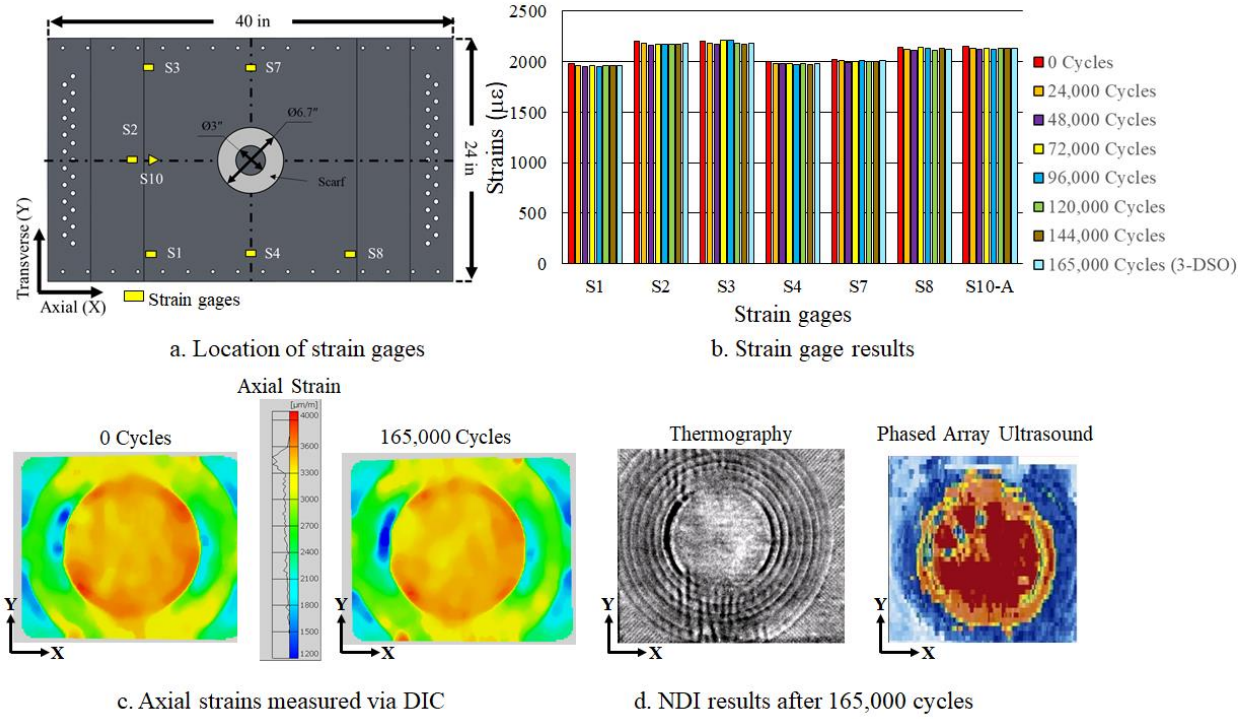


Figure 15. Panel 5 results during additional fatigue at SL strain level

### 4.2.5 Post-fatigue residual strength test

The goal of this step was to subject panel 5 to failure and measure the residual strength of this panel. Similar to panel 3, panel 5 was loaded quasi-statically in a saw-tooth profile, increasing the load level up to failure based on percentages of the predicted critical strength of 169,318 ft-$lb_f$ calculated by PFA. The delamination developed during fatigue at elevated load strain level continued to grow circumferentially and a new delamination initiated and grew in the fifth ply (first 0º ply from the panel external surface). At 90% load level, extensive damage occurred where the entire scarf region in the 9 o'clock position delaminated. Final failure through the net section of the panel occurred at an applied moment of 167,273 ft-$lb_f$, which was within 1% of the predicted value. Figure 16 shows a comparison of thermography results during 60%, 80% and 90% load level for panels 3 and 5. As shown in the figure, the damage growth in panel 5 was identical to panel 3. For panel 3, the major damage was in 9'o clock position and for panel 5, it was 3 o'clock position. This can be expected because both 3 o'clock and 9 o'clock positions experience the same load due to constant moment loading.

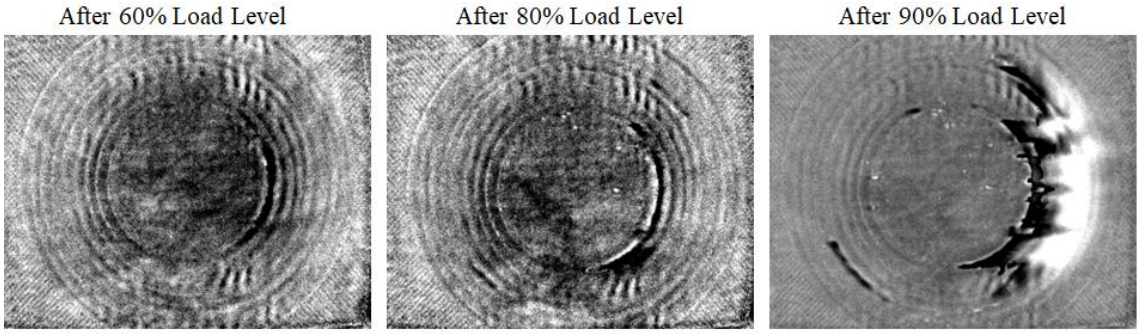


a. Thermography results for panel 3

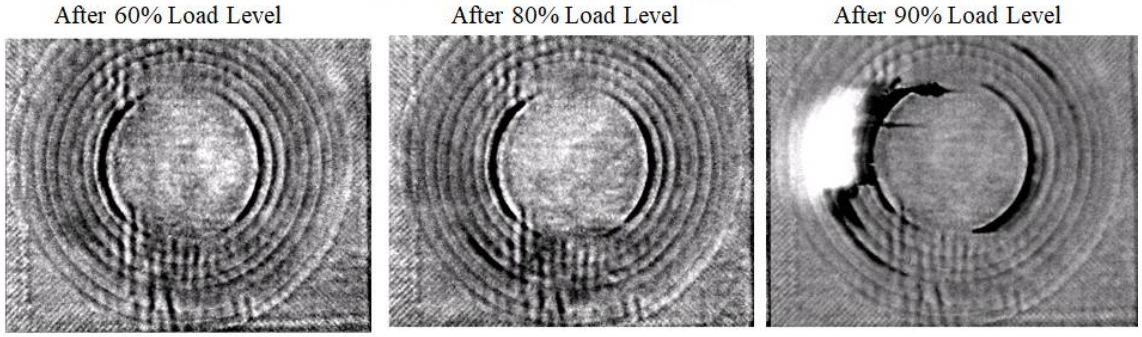


b. Thermography results for panel 5

Figure 16. Thermography results for panel 3 (a) and panel 5 (b) during residual strength tests

Summarizing the major results for panel 5, no damage developed when subjected to 3 DSGs under SL conditions (2,200 με far-field strains, R=0.1). Delamination was induced when the loads were increased to 60% higher (3,600 με) than the SL strains. This naturally induced delamination showed no indications of growth when the panel was subjected to another 3 DSGs under SL conditions. During the residual strength test, the panel failed at 167,273 ft-$lb_f$, which was almost equal to panel 3's 168,611ft-$lb_f$ failure loads indicating no degradation in the strength of the panel 5 due to fatigue loading for 6 DSGs. In addition, all the delaminations in the scarf that developed during the fatigue test at the elevated load levels were local and had no effect on the overall strength of the panel. Appendices D–H provides the detailed DIC, visual, thermography, phased array, and pulse-echo results at each sequence of testing for panels 3 and 5.

## 4.3 Panel 4, full-depth scarf

Panel 4 was first subjected to a baseline strain survey followed by quasi-statically loading to failure as summarized below.

### 4.3.1 Baseline strain surveys

Figure 17 shows the baseline strain survey results for panel 4, where loads were applied to yield far-field target strain of 1767 με. As shown in the figure, the strain gage S-10 was significantly lower than the target strain due the bending caused by the presence of a large scarf. Thus, the average of strain gages S-1 and S-3 was considered for target strains. It is clear that for both external and internal gages, there was good agreement between the test results and the analysis predictions.

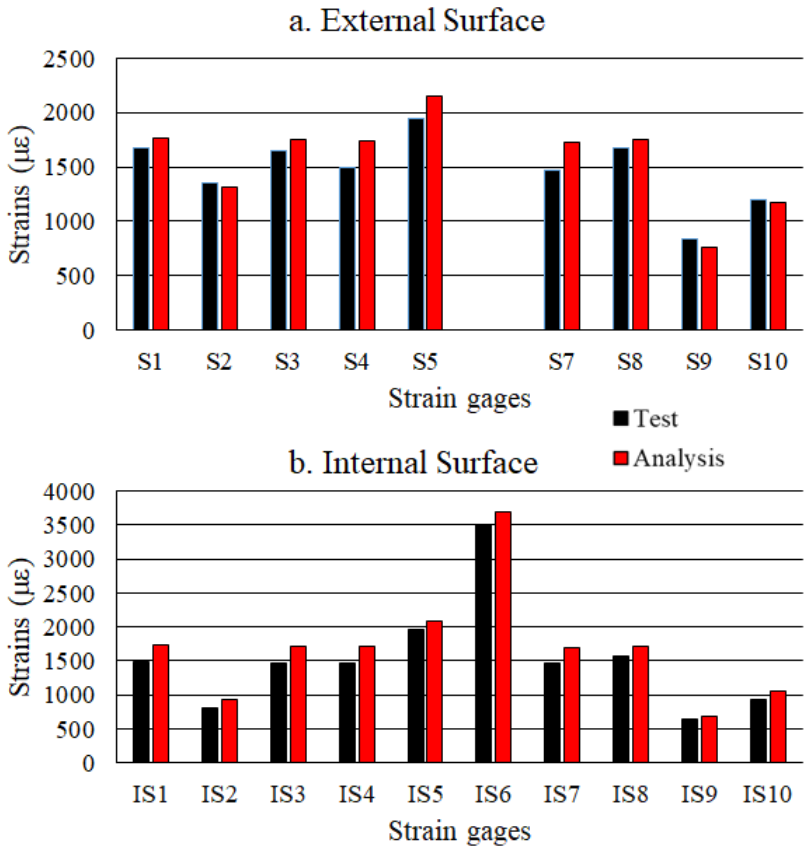


Figure 17. Baseline strain survey results for panel 4

### 4.3.2 Residual strength test

After the initial strain survey, panel 4 was subjected to a residual strength test, where it was loaded quasi-statically in a saw-tooth profile, increasing the applied moment to failure based on percentages of the predicted critical strength of 95,698 ft-$lb_f$ (see Figure 18). First visual indication of the damage appeared at 60% load level in the form of cracking at the inner scarf edge at the 6 o'clock position. On increased load, damage progressed through the net section up to the middle 0° plies (plies #9 and10). Delamination was then observed as shown; for example, at 70% load level. Progressive damage growth occurred in the 12 o'clock position through the entire net section of the scarf region during 80% load increment. At the 6 o'clock position, damage was still contained within the scarf. Final failure occurred at 85% of the predicted strength through the net section of the panel, which occurred at an applied moment of 81,068 ft-$lb_f$.

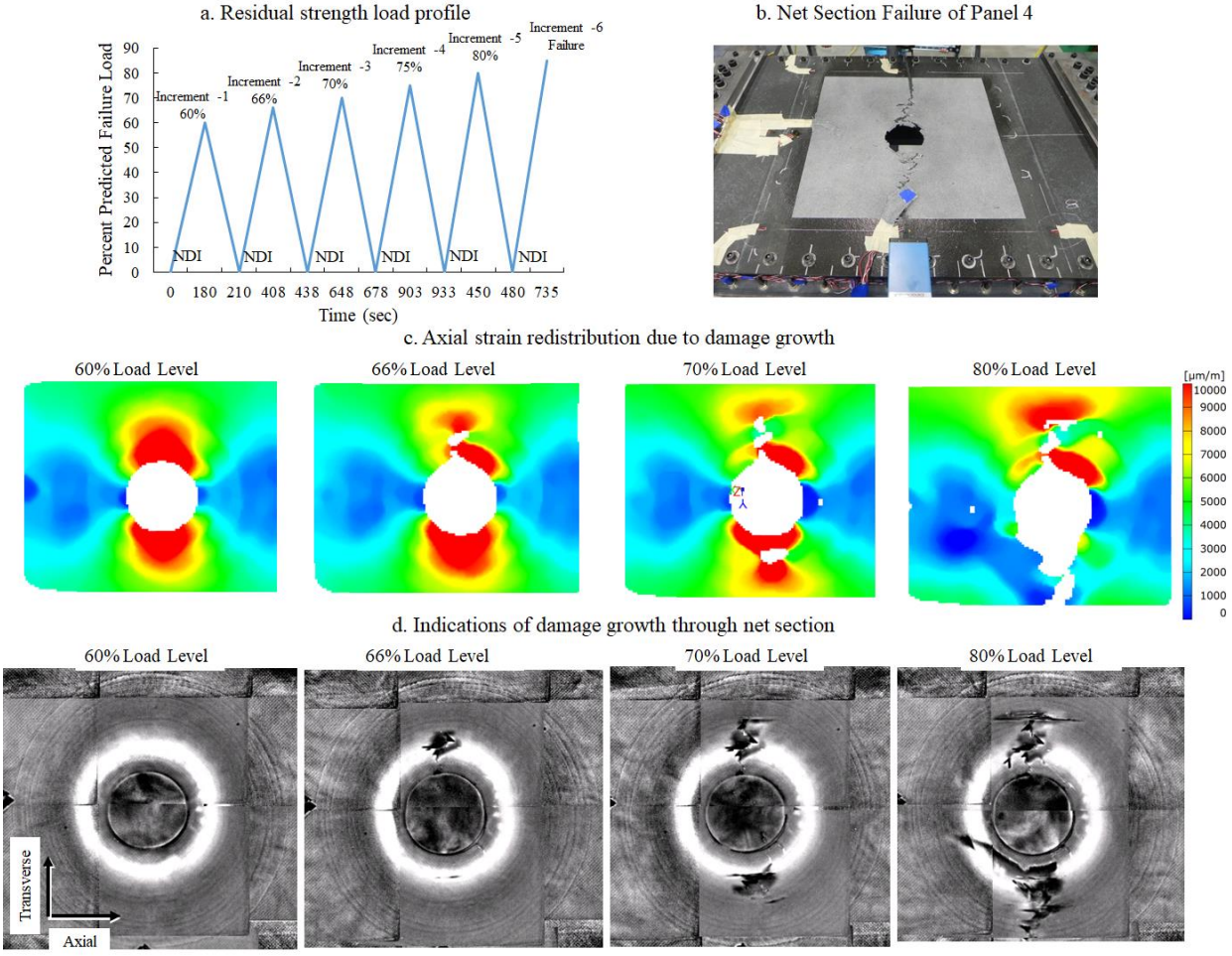


Figure 18. Panel 4 (full-depth scarf panel) results during residual strength test

## 4.4 Panel 6, full-depth scarf

Panel 6 was the second panel with full-depth scarf. For this panel, a baseline strain survey was first conducted, followed by fatigue test to one DSG (165,000 fatigue cycles), and then a final post-fatigue residual strength test. Results for each panel are summarized in sections 4.4.1–4.4.3.

### 4.4.1 Baseline strain surveys

Like other panels, panel 6 was first subjected to baseline strain surveys. The strain results were compared to panel 4, and the results showed that the two full-depth scarf panels with identical construction had similar responses to the same loading conditions. Thus, both panels were used for comparative studies.

### 4.4.2 Fatigue at service load strain level

Next, panel 6 was subjected to 165,000 fatigue cycles (3 DSGs) at SL conditions with R=0.1. The first local delamination in the scarf appeared at 2,000 fatigue cycles in ply #14 (first 0º ply from the internal surface of the panel) at the 12 o'clock position. Both flash thermography and DIC were able to detect the delamination, as shown in Figure 19c and Figure 19d. With the progress in fatigue cycles, another delamination appeared in the scarf at 6 o'clock position in the same ply #14 (0º ply). In addition, there were few small delamination indications in plies #9 and #10 (middle 0º plies), both at 6 o'clock and 12 o'clock positions. By the end of the third DSG, the delamination in ply #14 (0º ply) grew to 1.866 in. and 1 in. long at the 12 o'clock and 6 o'clock positions, respectively, as shown in Figure 20. The growth in the other delamination was significantly smaller. All the delamination occurrences were localized and did not cause any strain redistribution in the panel, as shown by constant far-field strains measured by the strain gages (see Figure 19b).

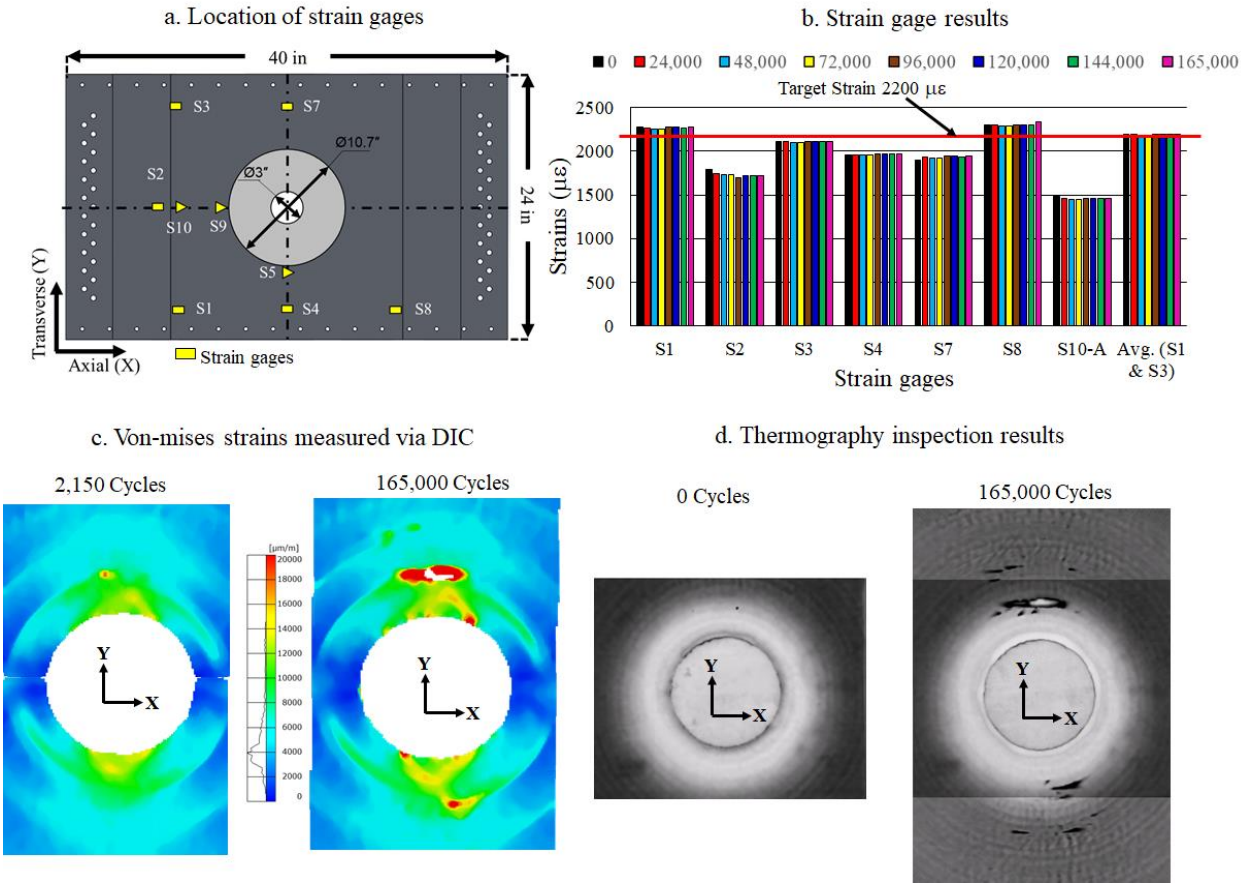


Figure 19. Panel 6 results during fatigue at service load strain level

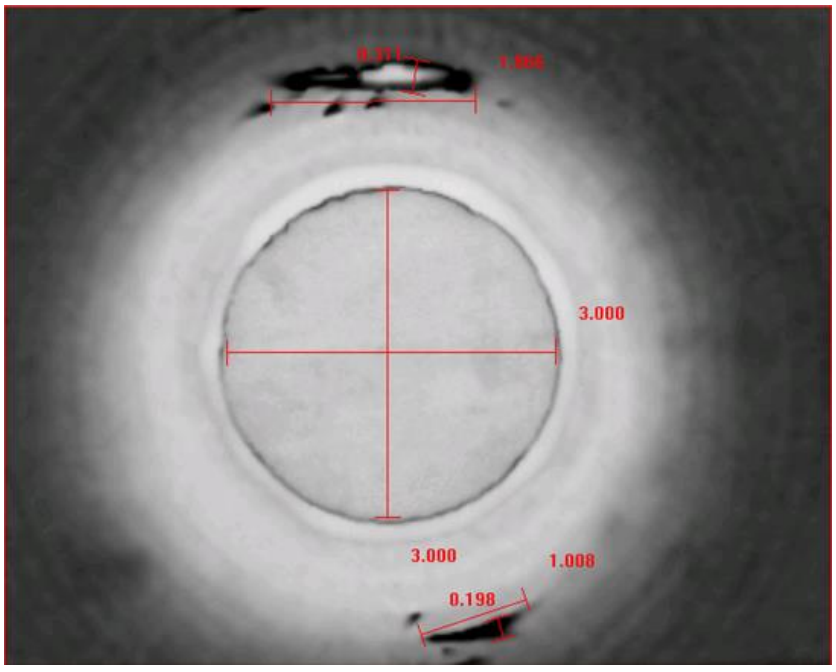


Figure 20. Panel 6 thermography image showing delaminations

### 4.4.3 Post-fatigue residual strength test

After the panel was subjected to 3 DSGs, it was loaded up to failure to measure the residual strength. Like panel 4, the residual strength test for panel 6 was conducted by quasi-statically loading the panel in a saw-tooth profile, increasing the load level up to failure based on percentages of the predicted critical strength of 95,698 ft-lb$_f$ (see Figure 18a). With the increase in loading, the delamination that developed during fatigue, started growing both in circumferential and radial direction, as shown in Figure 21b.

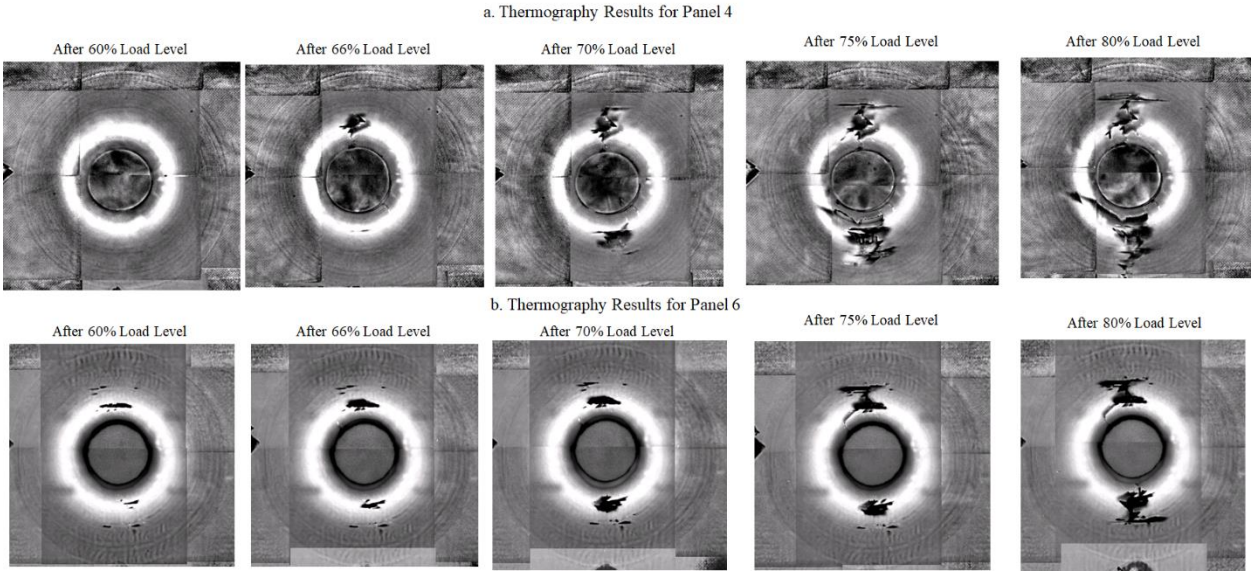


Figure 21. Flash thermography results for panels 4 and 6 during residual strength test

At the 70% load level, the damage also started emanating from the hole edge in the net section. In the next increment (75%), the damage grew from ply #14 (first 0º ply) to ply #10 (second 0º ply) both in 6 o'clock and 12 o'clock positions. At the 80% load level, both the damages in 6 o'clock and 12 o'clock positions have extended from the edge of the hole to the ply #10 (second 0º ply) and the second 0º ply is still carrying the load. At last load increment, the second 0º ply could not bear the load any longer, and the damage progressed through the net section to the transverse edges of the panel, breaking the panel into two parts. The panel failed catastrophically at 84,520 ft-lb$_f$, which was within 5% of panel 4 failure load, indicating that the delamination developed during fatigue test had no effect on the residual strength of the panel. For comparison purposes, the thermography images after each load increment for both panels 4 and 6 are shown in Figure 21. Appendices D–H provides the detailed DIC, visual, thermography, phased array, and pulse-echo results at every test step for panels 4 and 6.

The residual strength of all four panels is summarized in Figure 22.

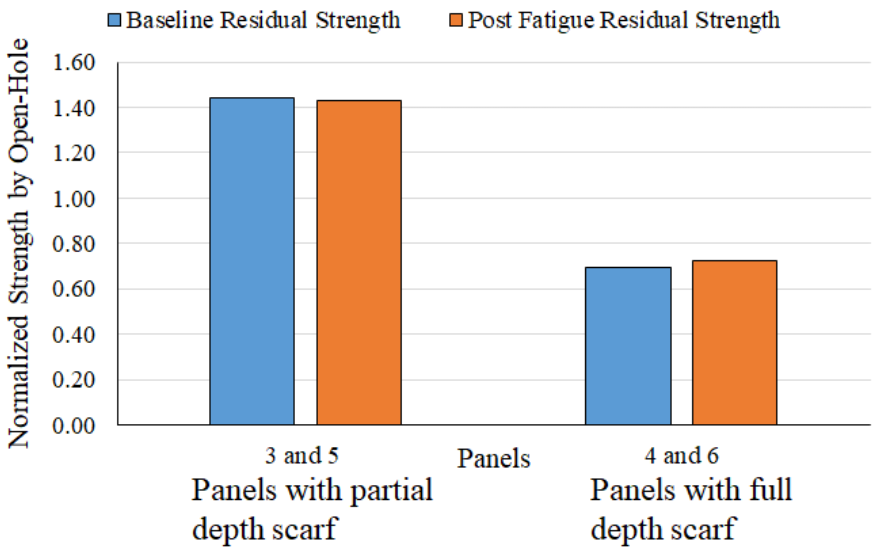


Figure 22. Comparison of strength for all four panels

Their strength is normalized by the strength of the open-hole panel (panel 2) tested during phase 2 (Neel et al., 2020). A comparison of panels 3 and 5 showed that subjecting the panel with the partial-depth scarf to 6 DSGs did not cause any reduction in the residual strength. Similar results were shown in panels 4 and 6, where there was no debit in strength of the panel with the full-depth scarf due to 3 DSGs. In addition, the strength of panels with partial-depth scarfs was almost twice the strength of the panels with full-depth scarfs, indicating the benefit of removing partial plies as compared to all the plies.

## 4.5 Test and analysis correlations

The effect of notched geometry on the ultimate strength of the solid laminates tested in this program is summarized in Figure 23.

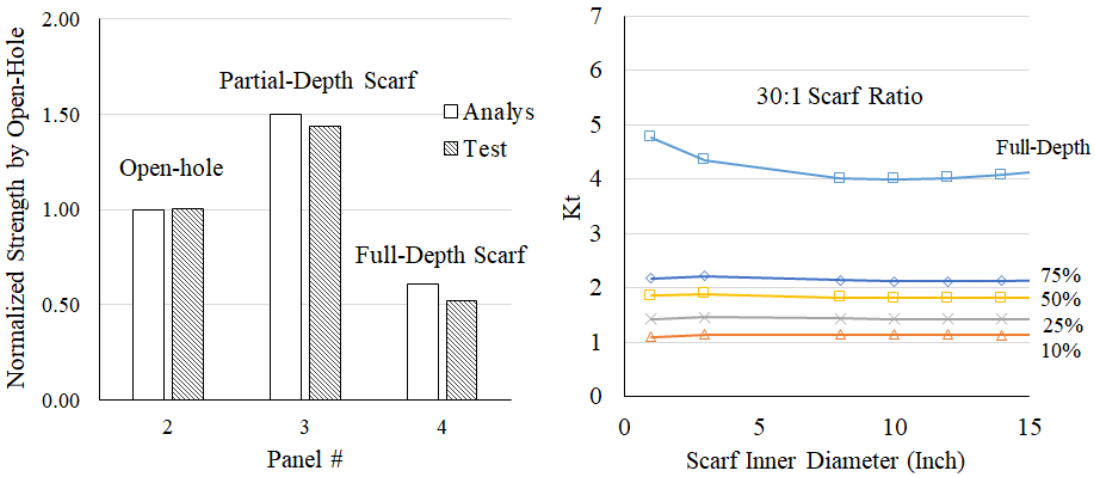


a. Effect of notch geometry on strength

b. Predicted trend showing reduction $K_t$ as scarf depth decreases.

Figure 23. Benefits of partial-depth scarf

As shown, good agreement was obtained between the test and stress concentration factor ($K_t$)-based analysis. The ultimate strains measured in panel 3 containing a partial-depth scarf were the highest, as expected, followed by panel 2 with the center hole (Neel et al., 2020), and then panel 4 containing the full-depth scarf. The benefit gained in the residual-strength limit-load capability of the failed partial-depth scarf is evident because it was much higher than the open-hole panel. In addition, analytical models currently under development to accurately predict the strain levels associated with failed repair depth are demonstrated. Model predictions show reduction of the $K_t$, as the scarf depth decreases.

The effect of load redistribution caused by the presence of a large cut-out within a panel, such as the case for a full-depth scarf, is a significant component that will be investigated during a future phase. It is expected that some sort of load mitigation can be assumed due to loads being redistributed toward stiffening elements within the same panel and to neighboring panels. Multi-bay test articles, which include stiffening elements, will be used for such study.

# 5 Summary and conclusions

In a joint effort, the FAA and Boeing are addressing safety and structural integrity issues of bonded repair technology. Recent efforts have focused on bonded repairs to composite panels representative of typical transport aircraft wing structure. The program objectives are to characterize the fatigue and damage tolerance performance of bonded repairs subjected to simulated service load and to evaluate the limit-load capability of typical composite wing panels with a failed repair. Emphasis has been placed on investigating the methods and tools used for predicting structural performance of repairs and as those used to evaluate and monitor repair integrity over the life of the part.

A phased approach is being undertaken in the multiyear effort. The initial baseline testing (phase 2) of this program characterized the material response of composite panels in the unnotched pristine and open-hole configurations under constant moment loading. This verified the test-fixture loading, validated analysis models, and provided an initial reference point for NDI and SHM systems.

The third phase of this program more directly supports the FAA BRSL policy issued to address concerns of not being able to detect weak bonds that result in failure. Testing of partial depth and full-depth scarf configurations for solid laminates was used to verify BRSL analysis methods where the focus was on characterizing the limit-load capability for these scarf configurations. The benefit gained in the residual-strength limit-load capability of a failed partial-depth scarf was revealed and documented in this technical note. For both partial- and full-depth scarf configurations, there was no debit in strength due to 3 DSGs. In addition, analytical models currently under development to accurately predict the strain levels associated with failed repair depth were demonstrated. Good agreement was obtained between test and analysis in terms of residual strength using both engineering $K_t$-based and finite element-based PFA approaches.

The next sequence of phase 3 is focused on double-sided scarf configurations for solid laminates under constant-moment tensile loading and the results will be published in a forthcoming companion technical note. Future work will consider fatigue and residual strength aspects for more configurations and loading for both solid laminates and honeycomb panels. In addition, compression loading tests and analyses are considered in the long-term planning of this program.

# 6 References

Baker, A. A., Rose, L., & Jones, R. (Eds.). (2003). *Advances in the bonded composite repair of metallic aircraft structure* (Vol. 1). Elsevier.

Chadha, R., Bakuckas Jr., J. G., Fleming, M., Lin, J., & Korkosz, G. (2019). *Airframe beam structural test (ABST) fixture—capabilities description and user manual.* DOT/FAA/TC-TN19/7.

Federal Aviation Administration. (2011, January 13). *Damage tolerance and fatigue evaluation of structure.* Advisory Circular AC 25.571-1D. Retrieved from https://www.faa.gov/documentLibrary/media/Advisory_Circular/AC_25_571-1D_.pdf

Federal Aviation Administration. (2014). *Bonded repair size limits.* FAA Policy Statement No. PS-AIR-20-130-01, U.S. Department of Transportation.

Neel, R. J., Chadha, R., Bakuckas Jr., J. G., Fleming, M., Lin, J., & Espinar-Mick, E. (2020). *Bonded repairs to composite wing panel structure: phase 2, baseline testing.* Submitted for publication.

# A Specimen engineering drawings

This appendix presents detailed drawings of the partial- and full-depth scarf panels. Detailed drawings of panels 3–6 are provided in Figure A 1 to Figure A 4, respectively.

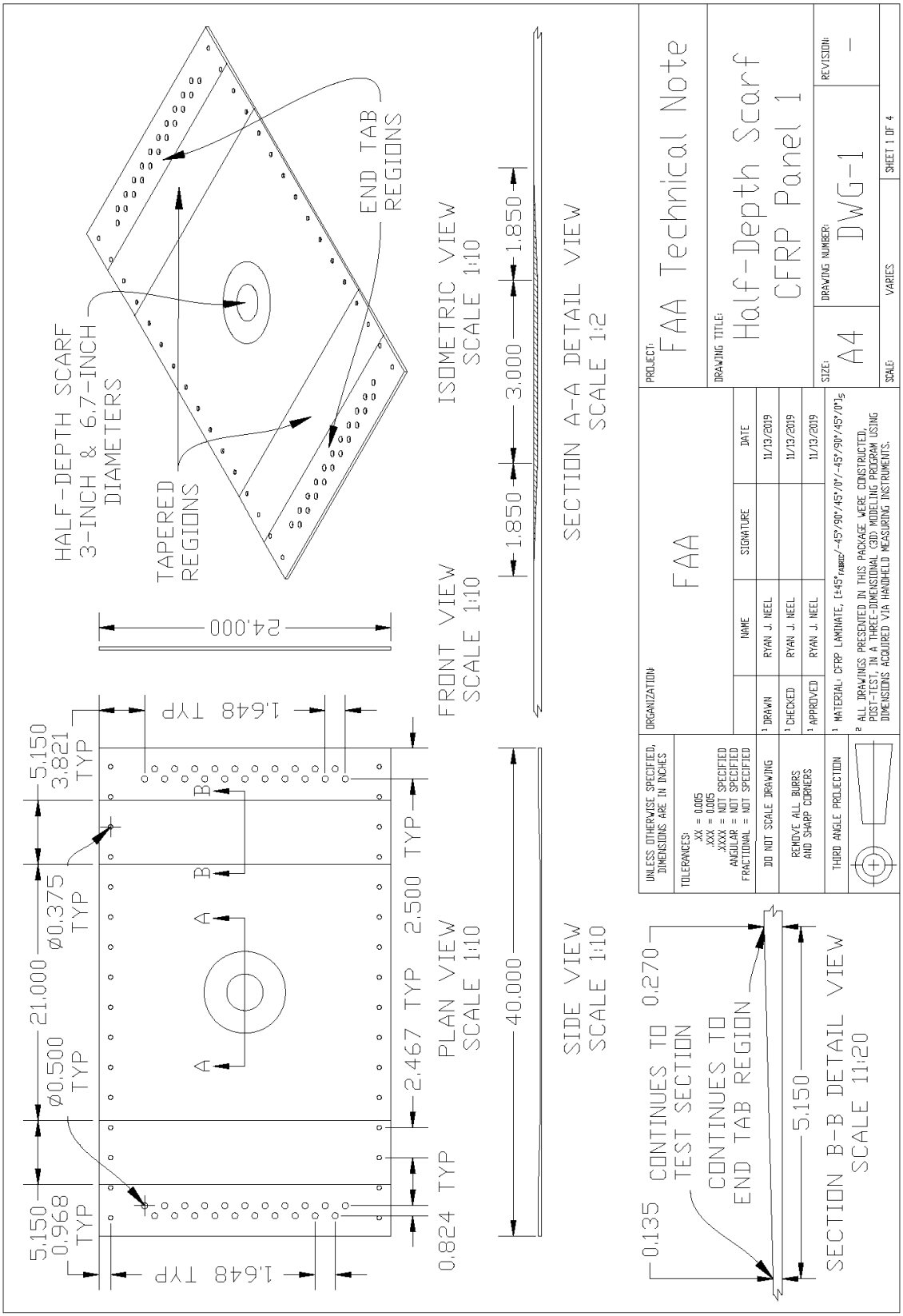


Figure A 1. Drawing of panel 3 (partial-depth scarf)

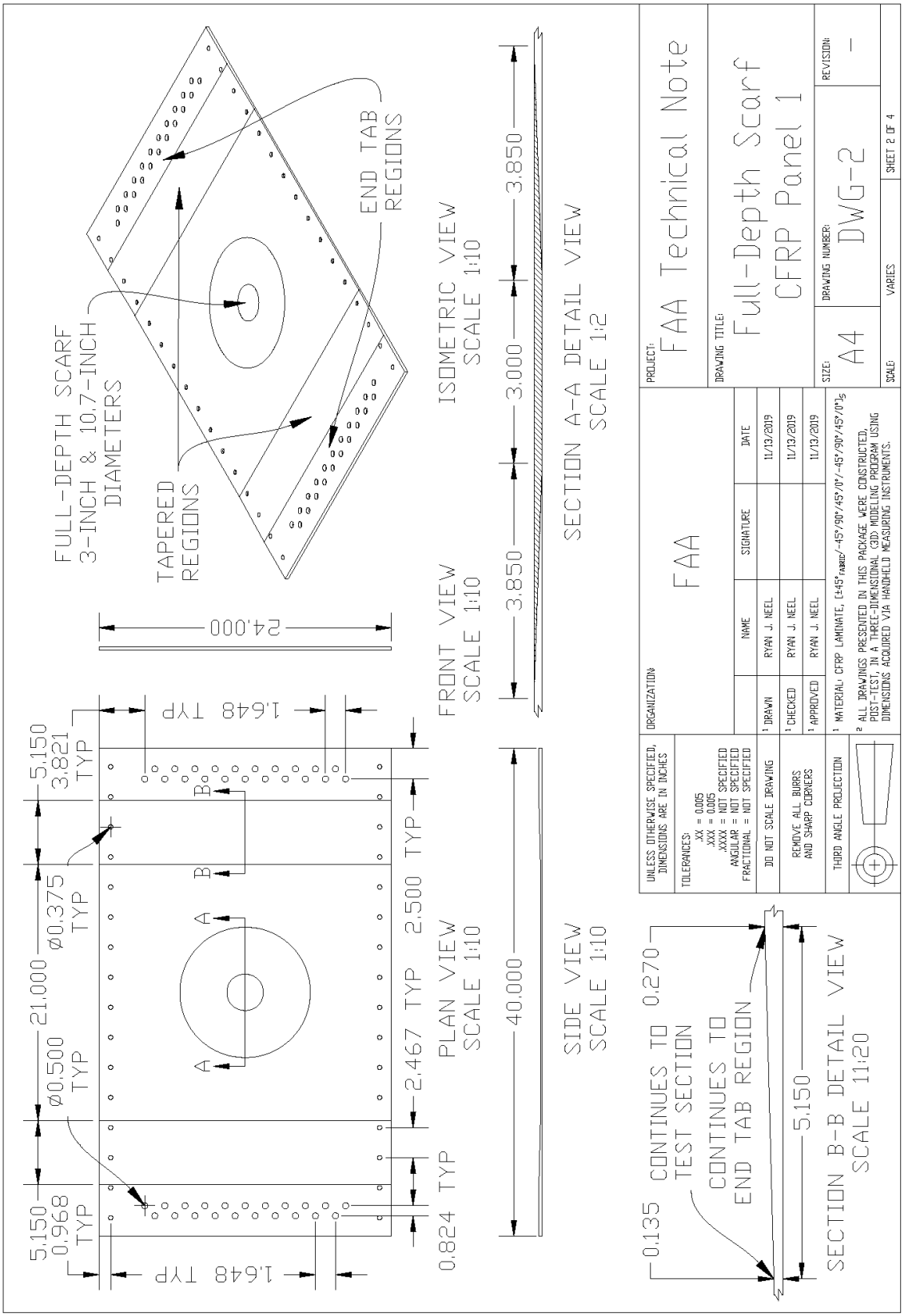


Figure A 2. Drawing of panel 4 (full-depth scarf)

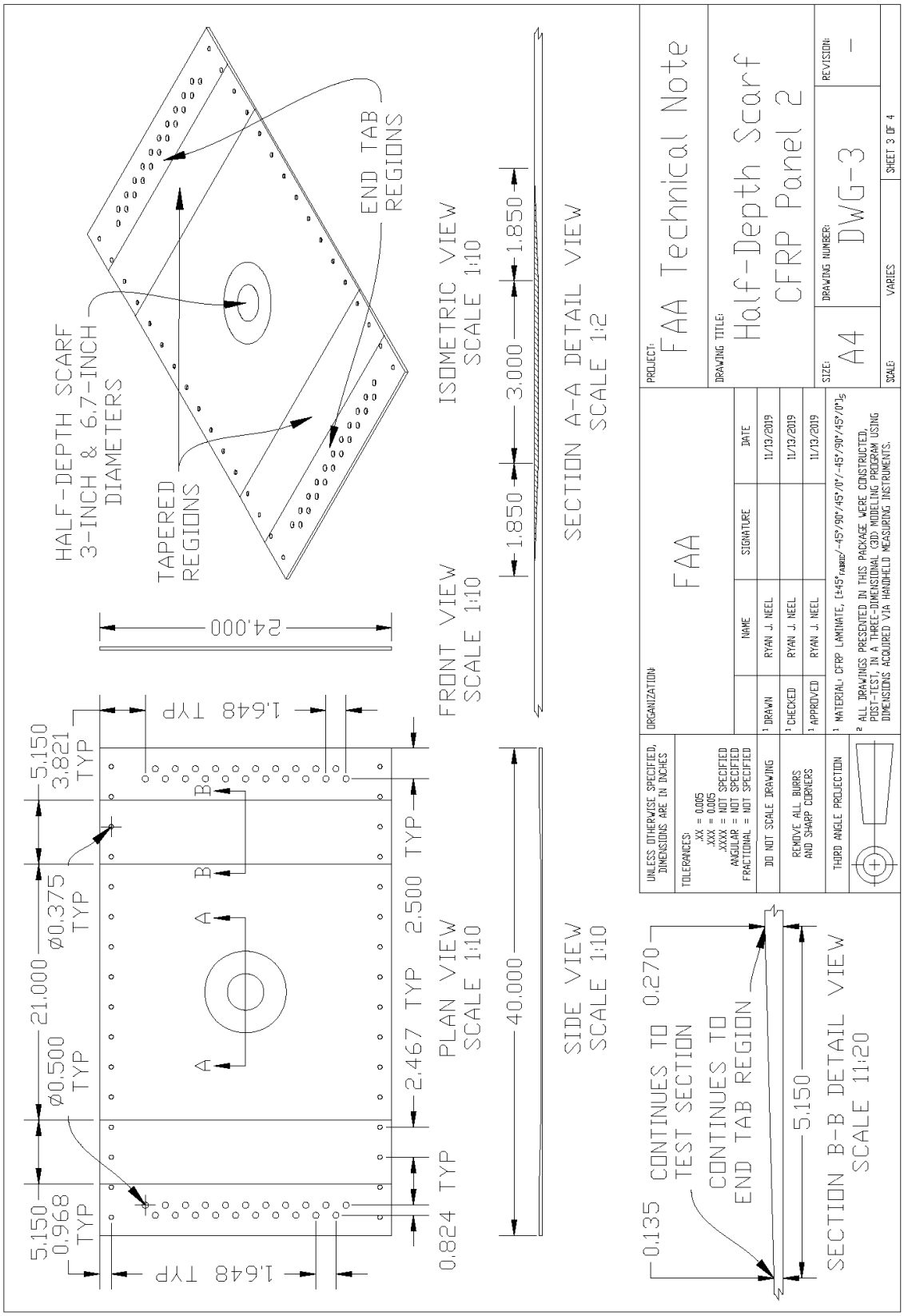


Figure A 3. Drawing of panel 5 (partial-depth scarf)

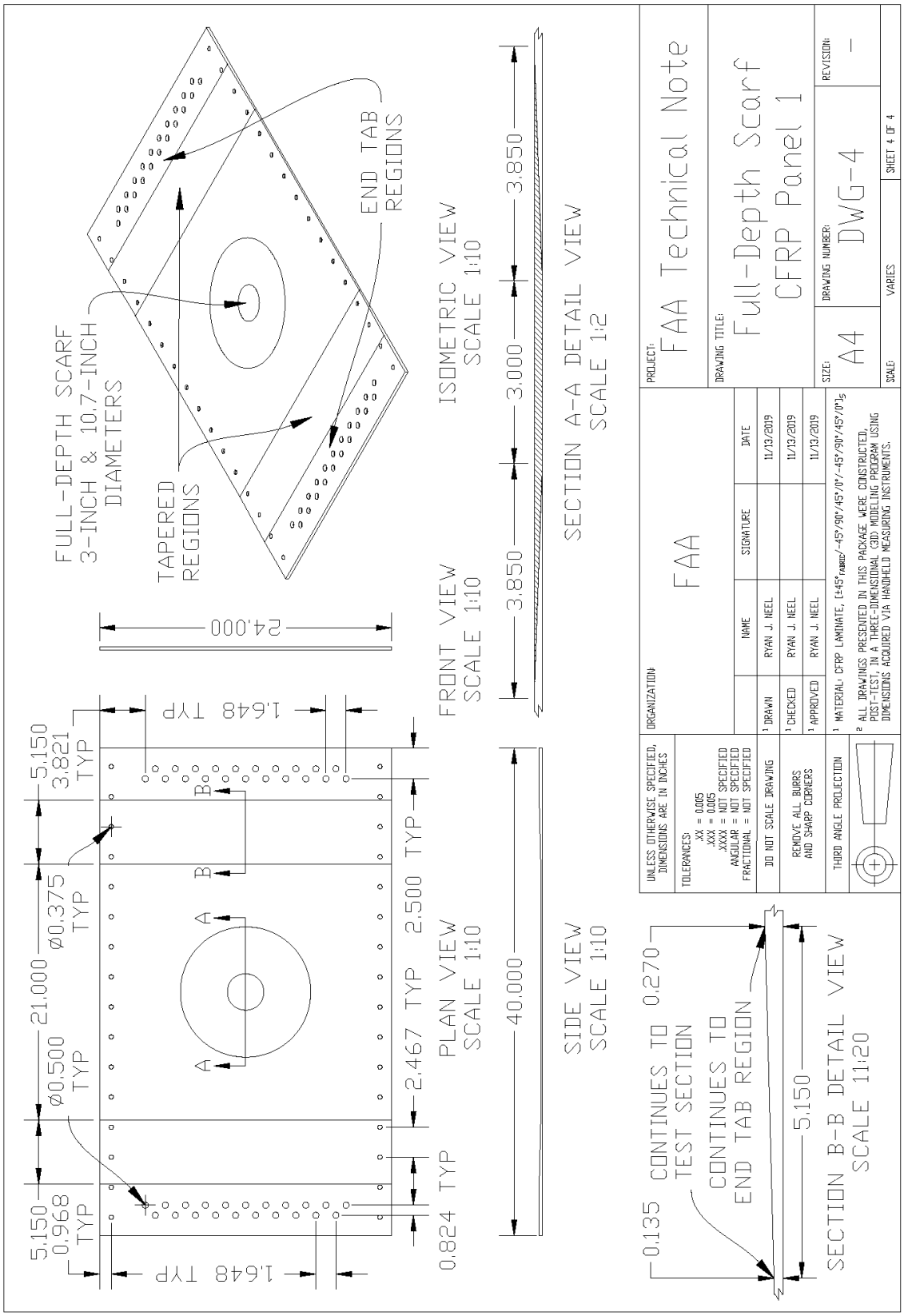


Figure A 4. Drawing of panel 6 (full-depth scarf)

# B Strain and displacement during strain surveys

This appendix presents the results of strain gages and displacement transducers captured during quasi-static loading of the partial-depth scarf panels (panels 3 and 5) and full-depth scarf panels (panels 4 and 6). The location and nomenclature for displacement sensors and strain gages for both the panels are shown in Figure B 1 and Figure B 2, respectively. For panel 3, baseline strain survey results are shown in Figure B 3 and Figure B 4. For panel 5, results during fatigue at SL strain level, fatigue at elevated load strain level, and additional fatigue at SL strain level are shown in Figure B 5–Figure B 10, Figure B 11–Figure B 24, Figure B 25–Figure B 38 and Figure B 39–Figure B 58, respectively. Baseline strain survey results for panel 4 are provided in Figure B 59 and Figure B 60. Baseline strain survey and fatigue at SL load strain level results for panel 6 are shown in Figure B 61–Figure B 62 and Figure B 63–Figure B 92, respectively.

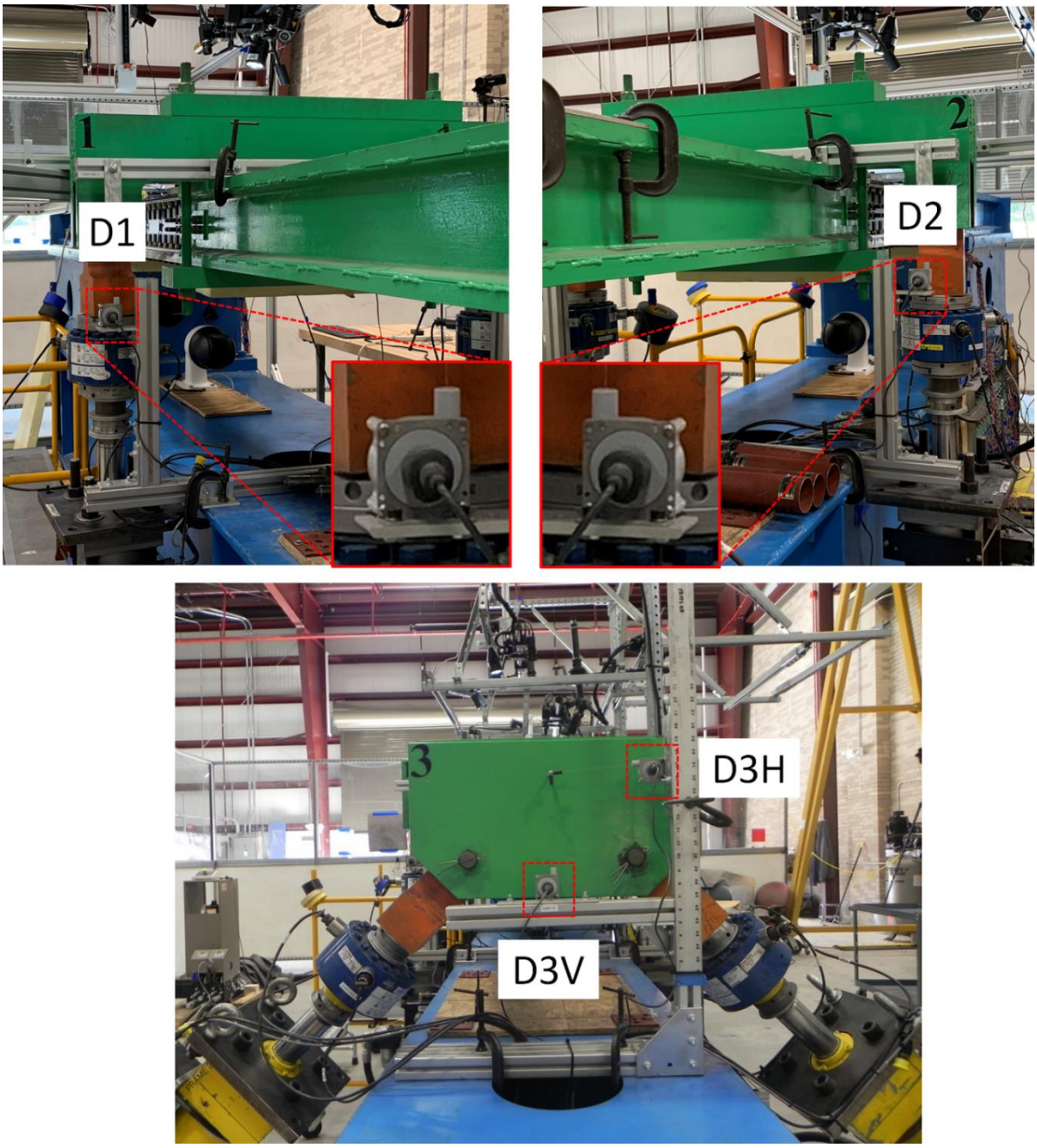


Figure B 1. Displacement transducer positions

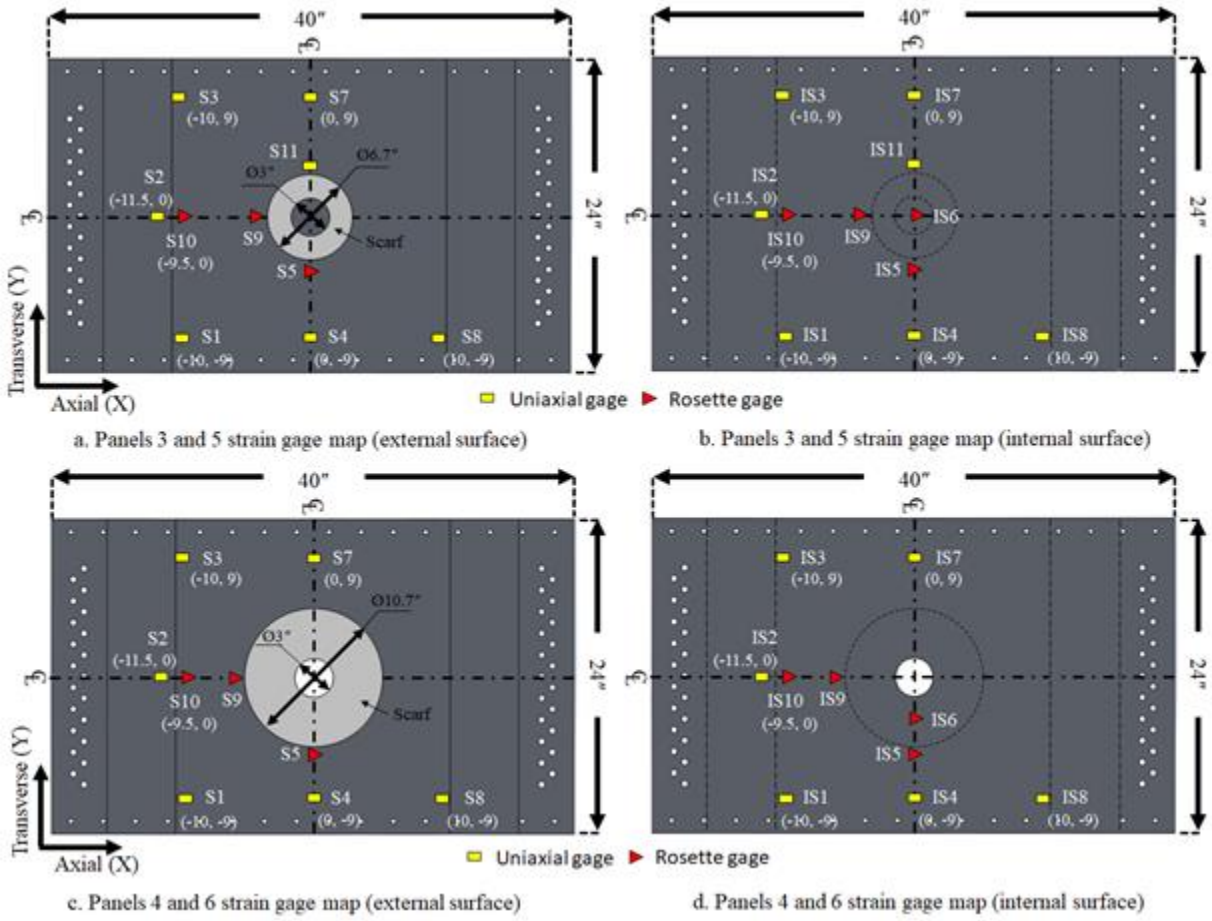


a. Panels 3 and 5 strain gage map (external surface)

b. Panels 3 and 5 strain gage map (internal surface)

c. Panels 4 and 6 strain gage map (external surface)

d. Panels 4 and 6 strain gage map (internal surface)

Figure B 2. External and internal surface strain gages layout for panels 3–6

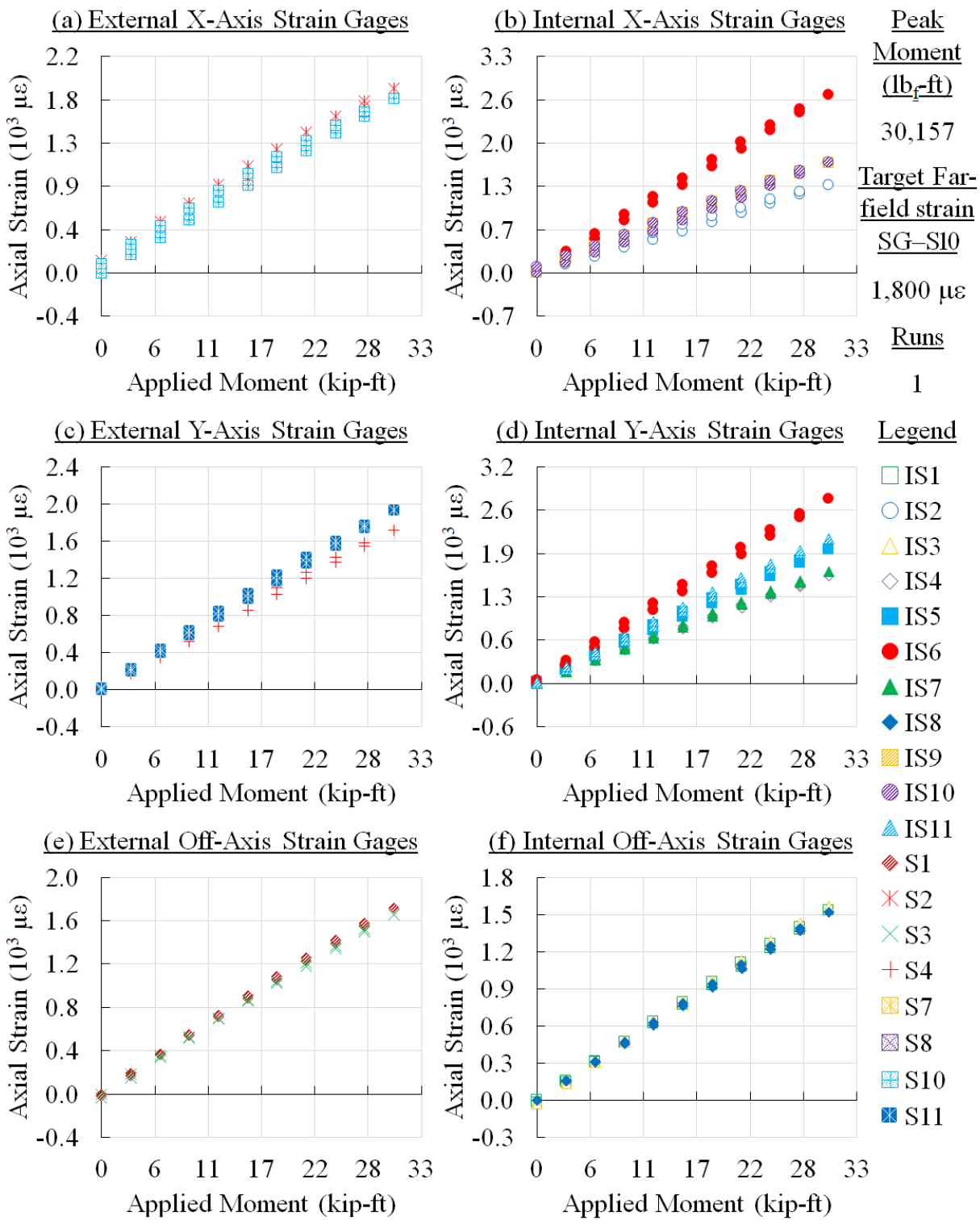


Figure B 3. Panel 3: baseline strain survey (axial strain)

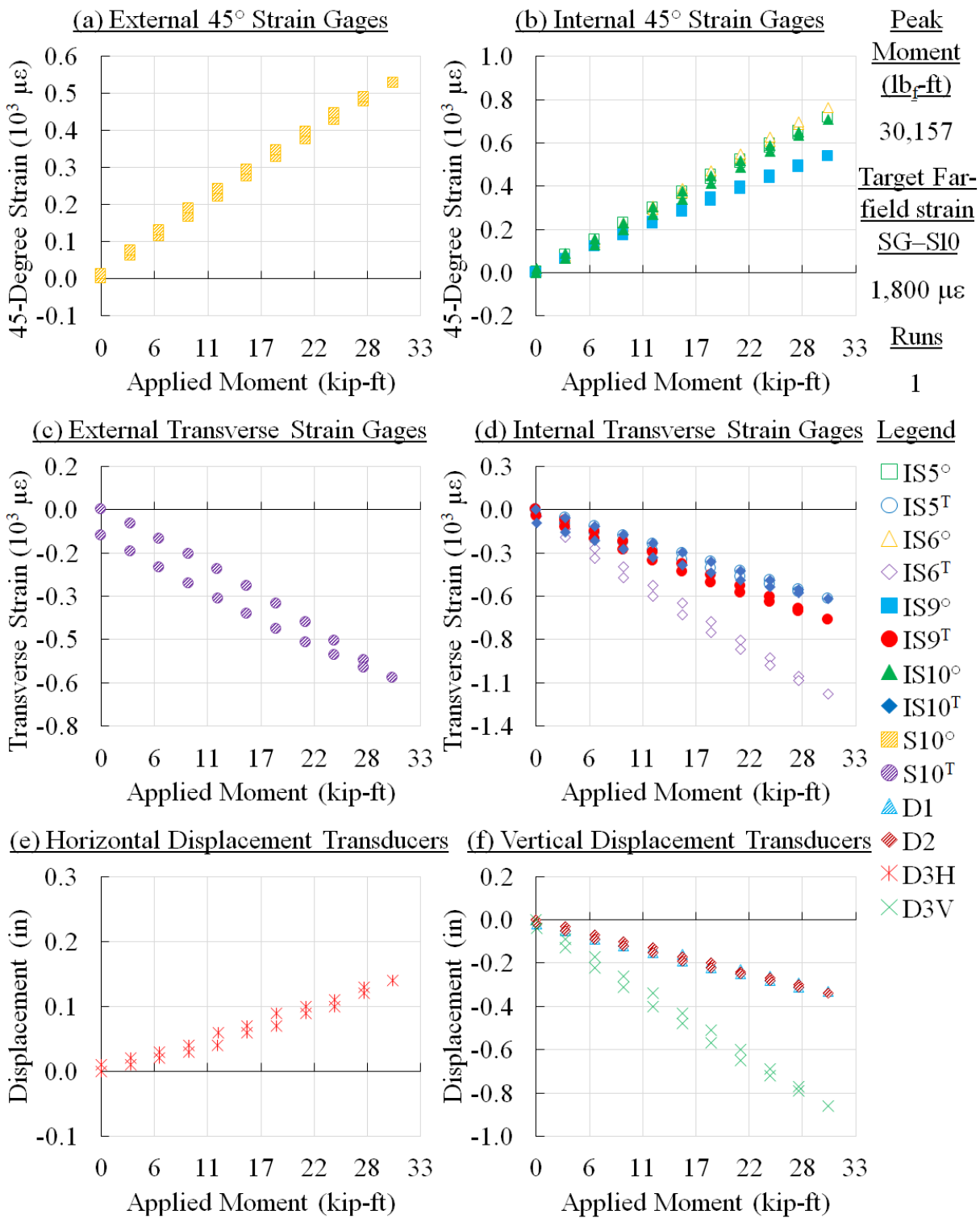


Figure B 4. Panel 3: baseline strain survey (other strain and displacement)

**CFRP Panel 5 – Partial (Half)-Depth Scarf 2, Step 1: Baseline Strain Survey Results**

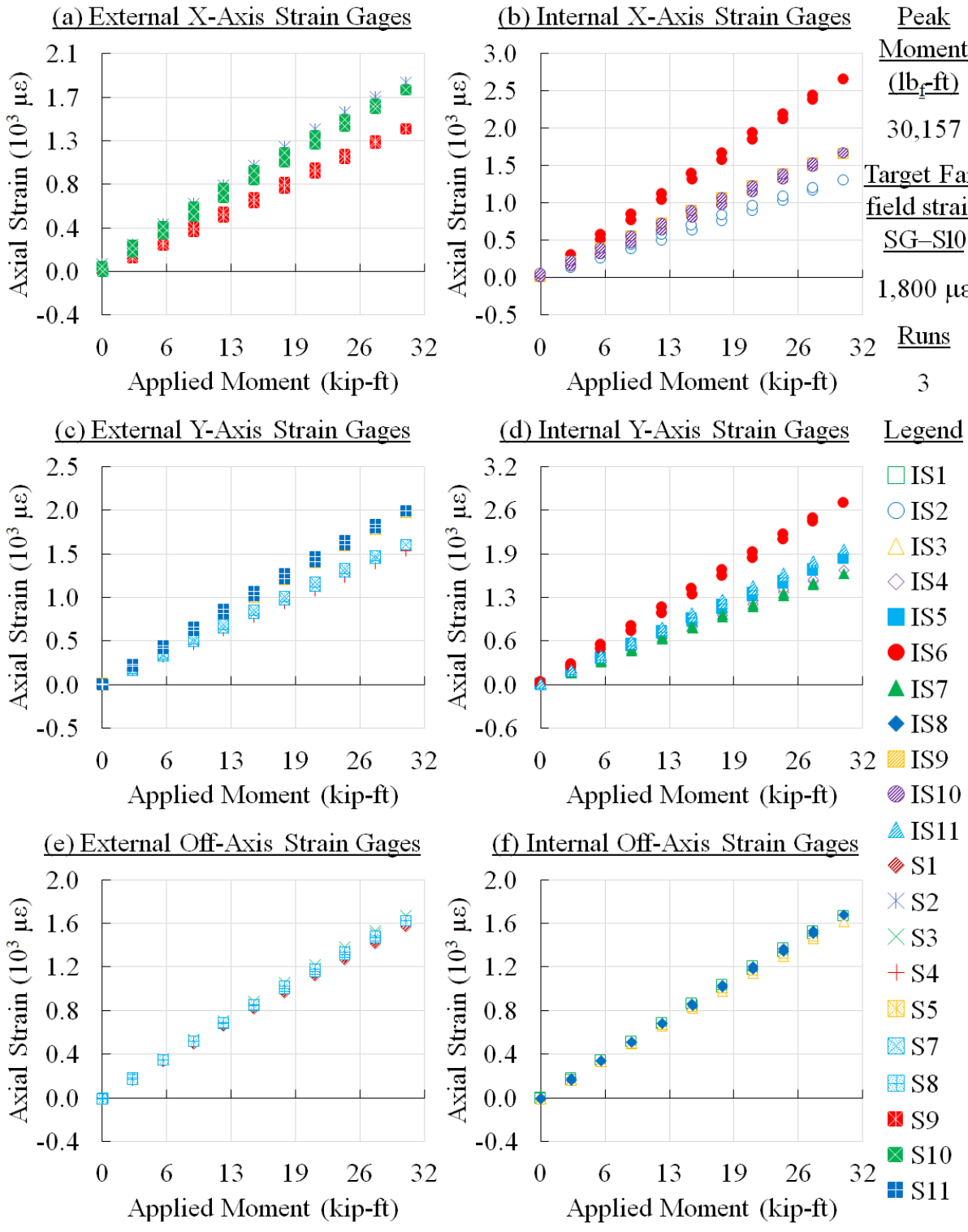


Figure B 5. Panel 5: baseline strain survey (axial strain)

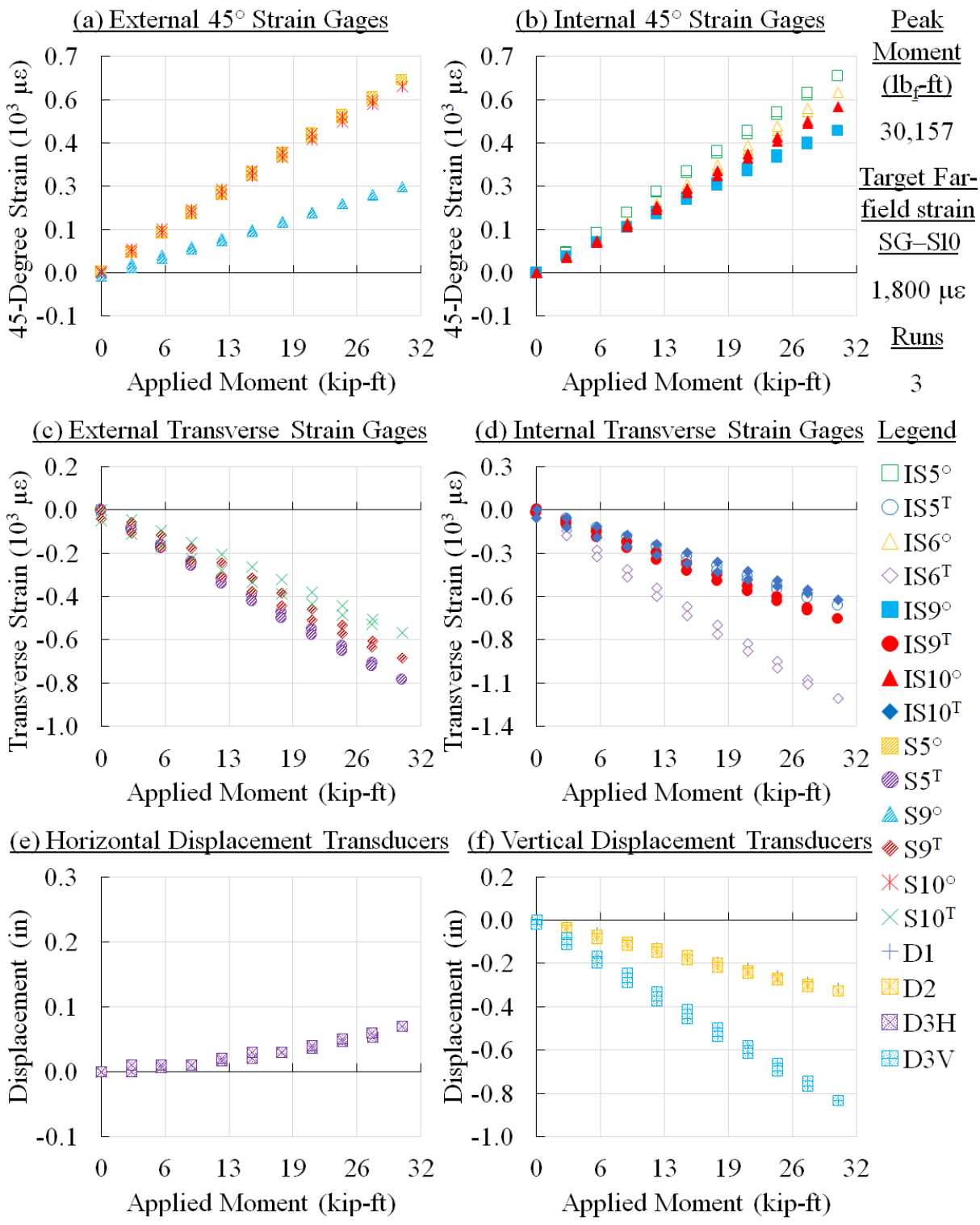


Figure B 6. Panel 5: baseline strain survey (other strain and displacement)

**CFRP Panel 5 – Partial (Half)-Depth Scarf 2, Step 1: Baseline Strain Survey Results**

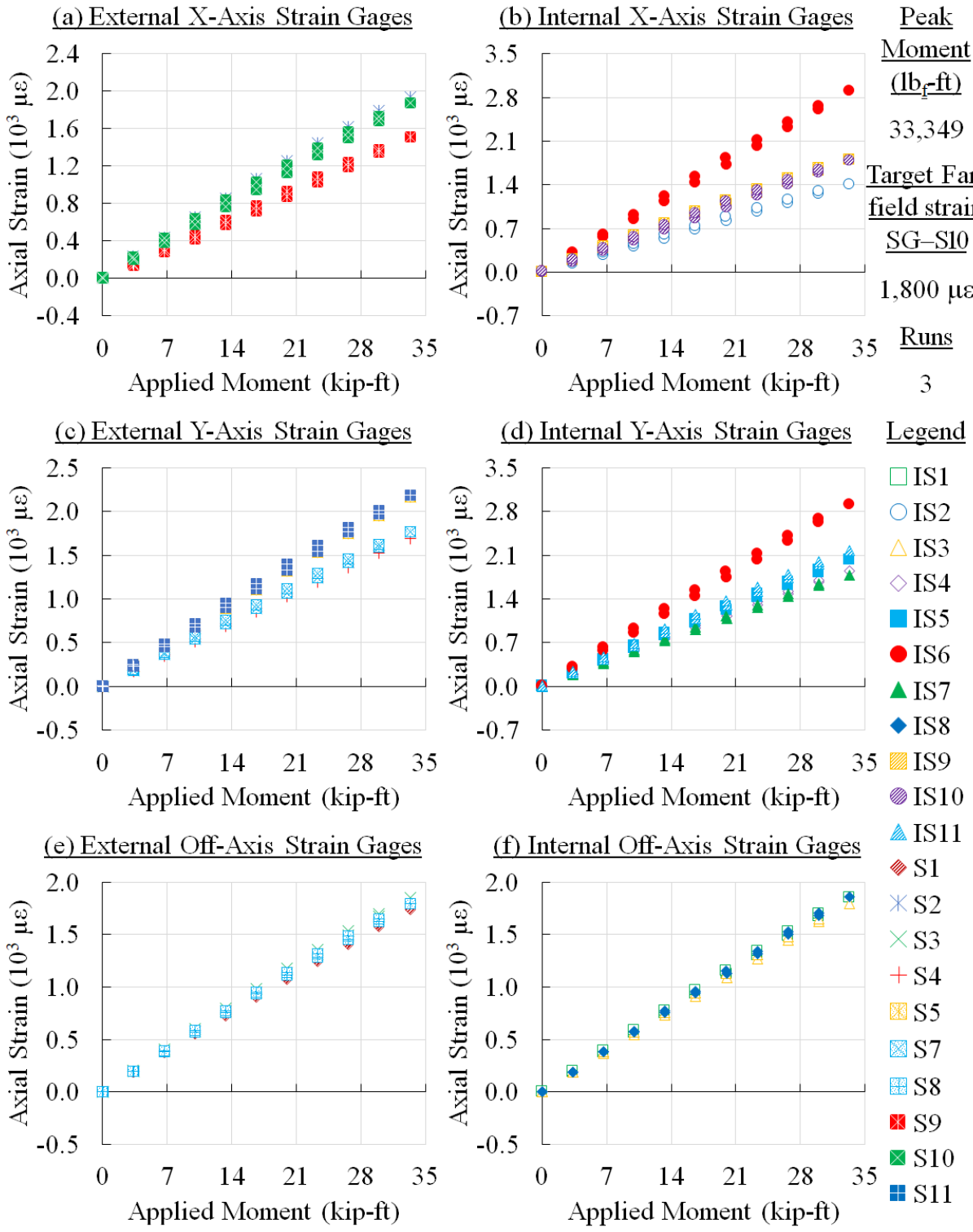


Figure B 7. Panel 5: baseline strain survey (axial strain)

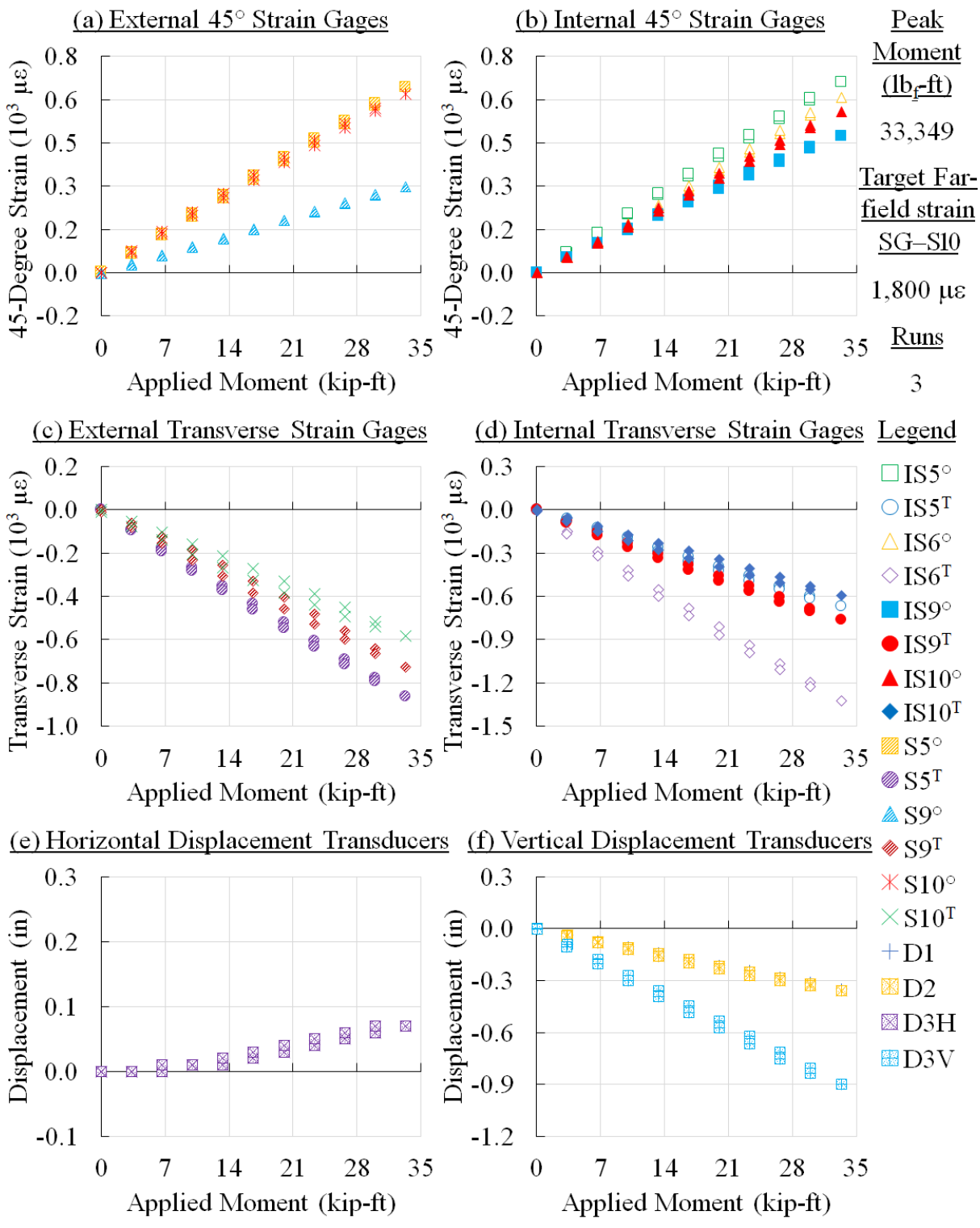


Figure B 8. Panel 5: baseline strain survey (other strain and displacement)

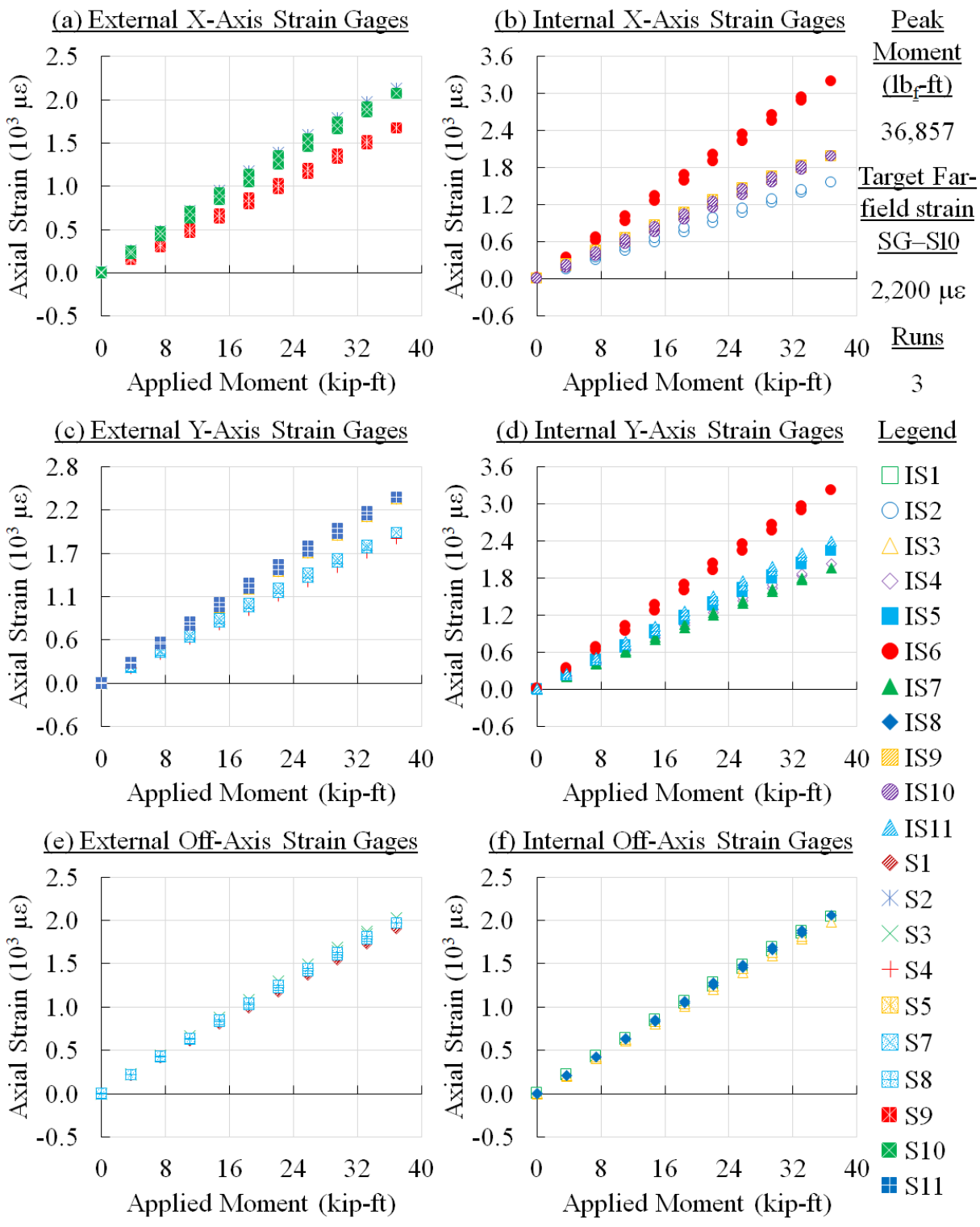


Figure B 9. Panel 5: baseline strain survey (axial strain)

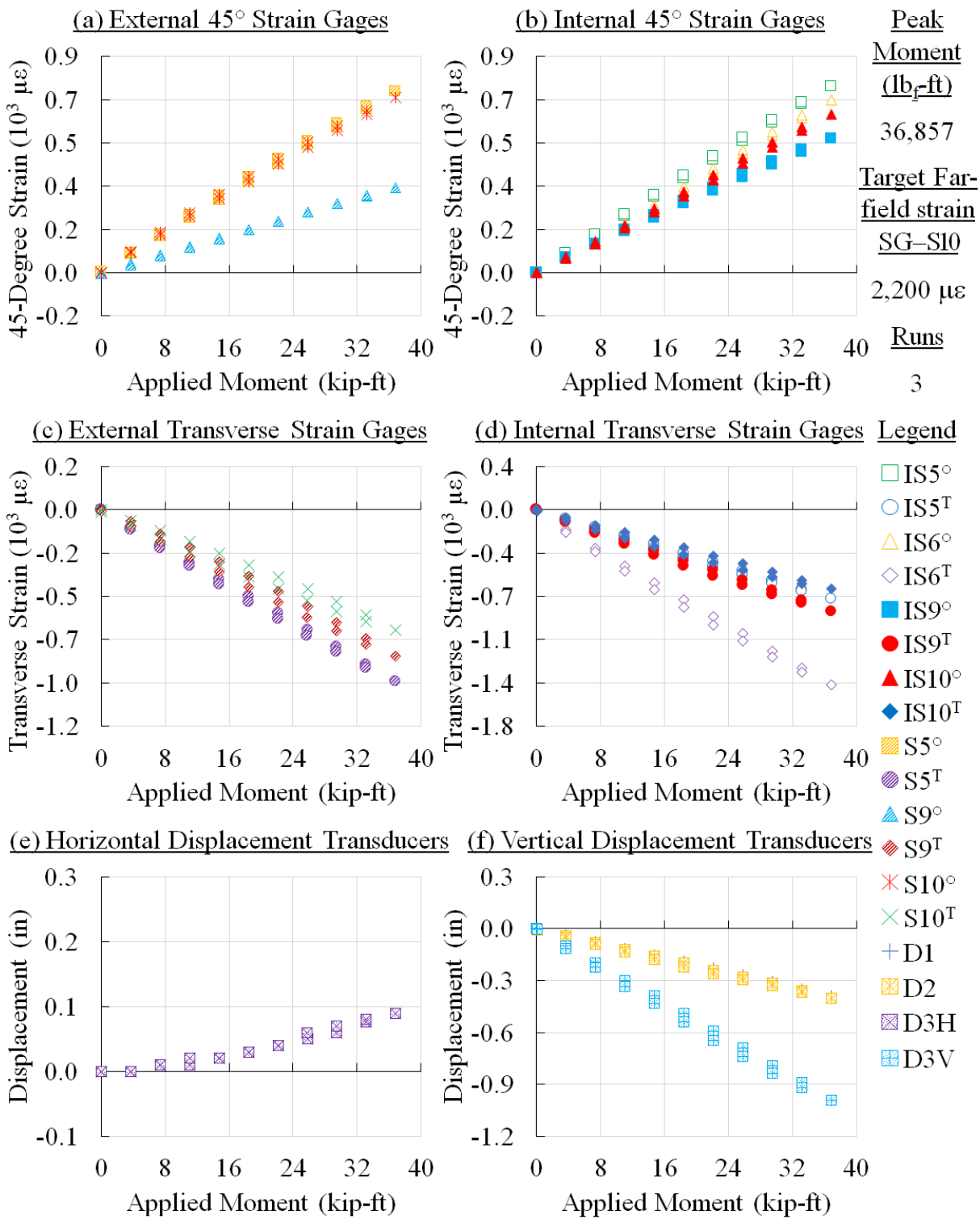


Figure B 10. Panel 5: baseline strain survey (other strain and displacement)

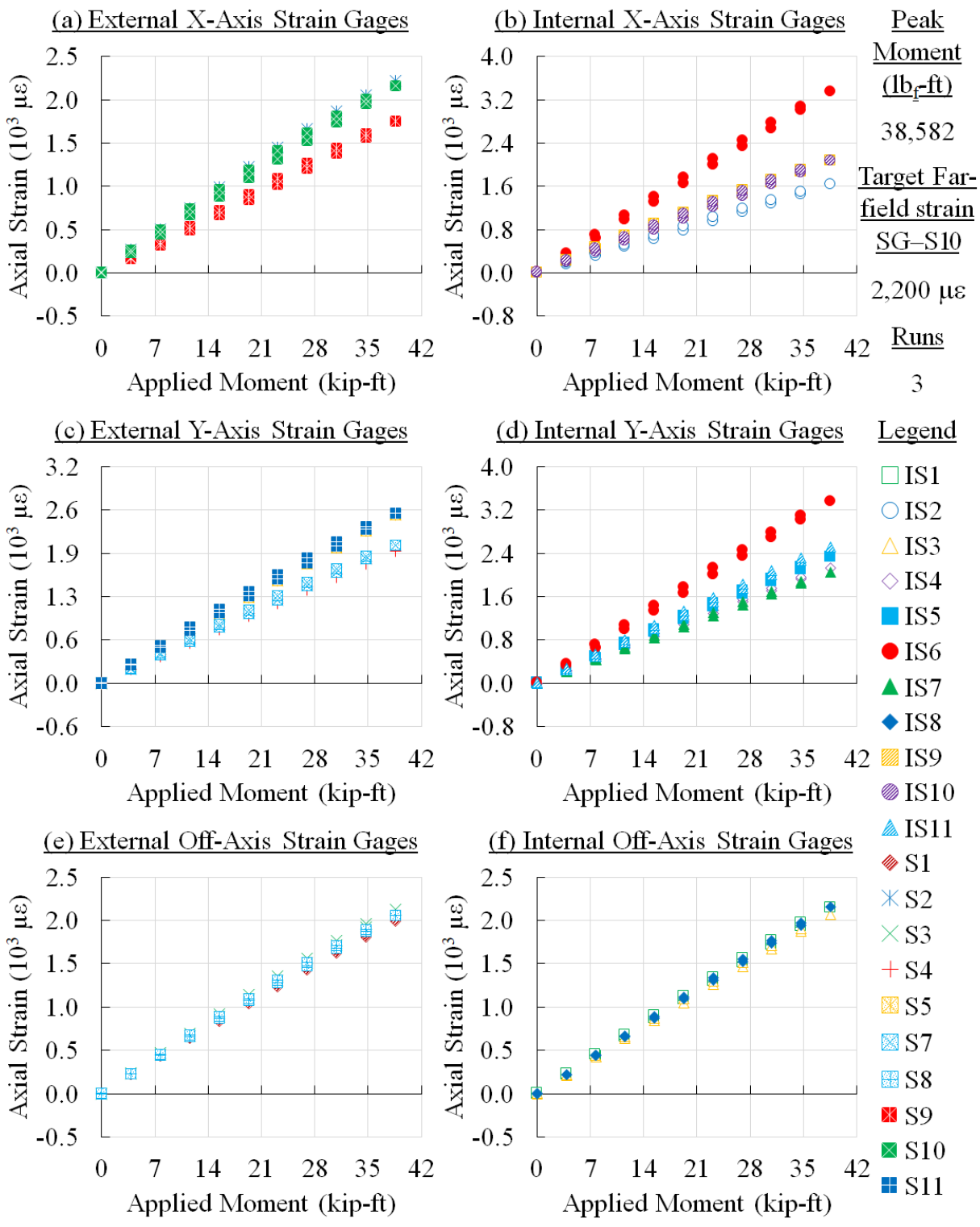


Figure B 11. Panel 5 (fatigue at SL strain level): strain survey at 0 cycles (axial strain)

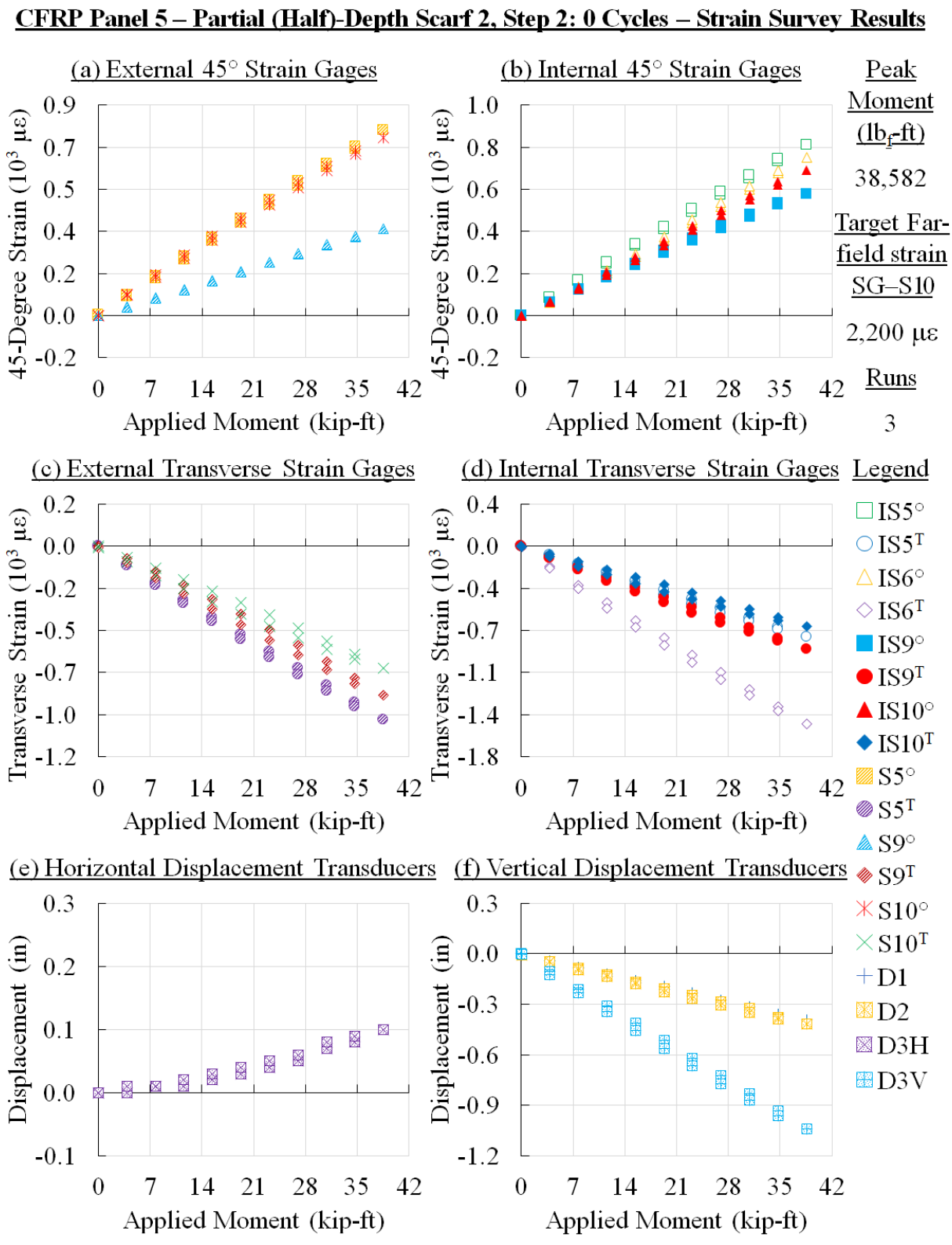


Figure B 12. Panel 5 (fatigue at SL strain level): strain survey at 0 cycles (other strain and displacement)

**CFRP Panel 5 – Partial (Half)-Depth Scarf 2, Step 2: 27,500 Cycles – Strain Survey Results**

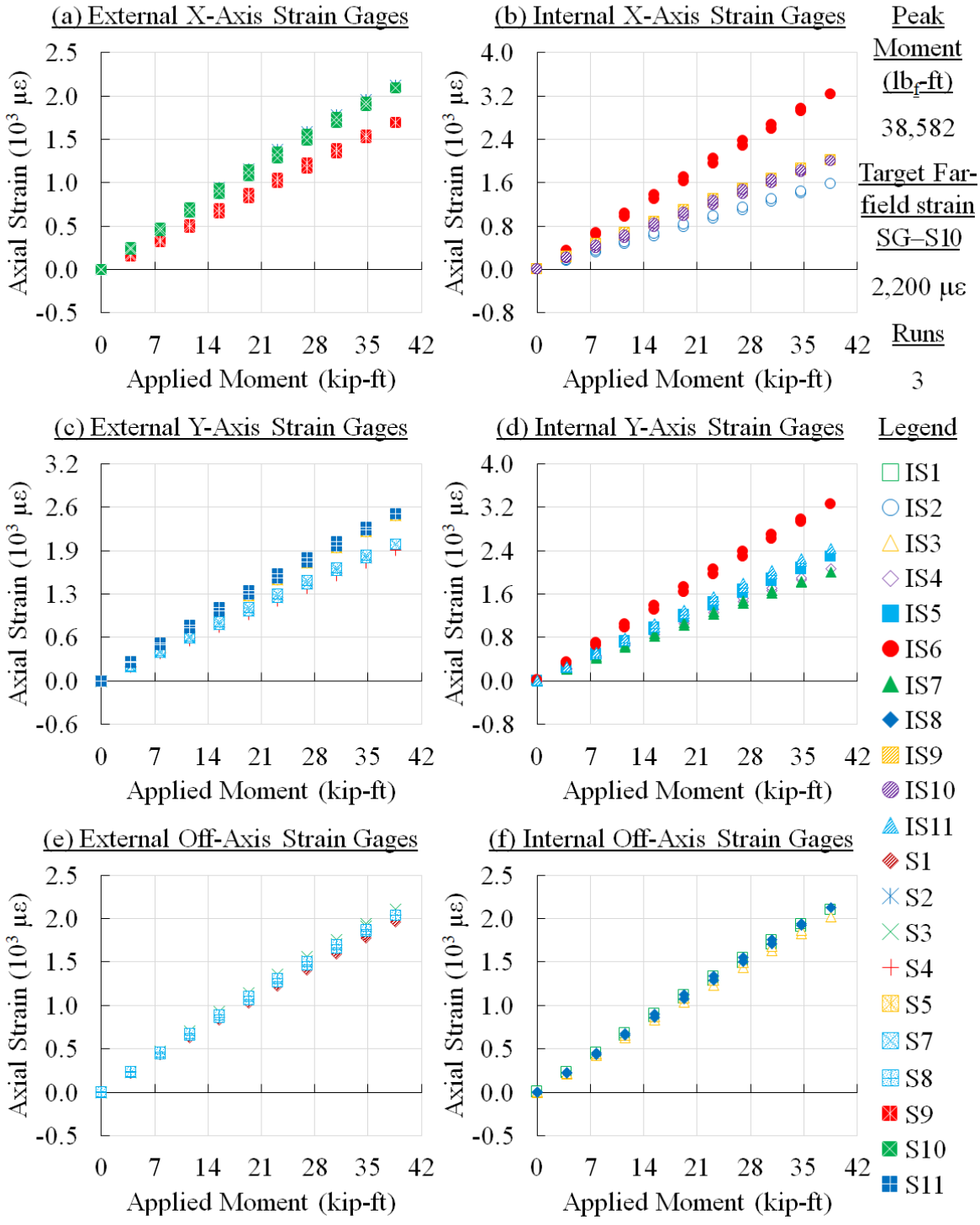


Figure B 13. Panel 5 (fatigue at SL strain level): strain survey at 27,500 cycles (axial strain)

**CFRP Panel 5 – Partial (Half)-Depth Scarf 2, Step 2: 27,500 Cycles – Strain Survey Results**

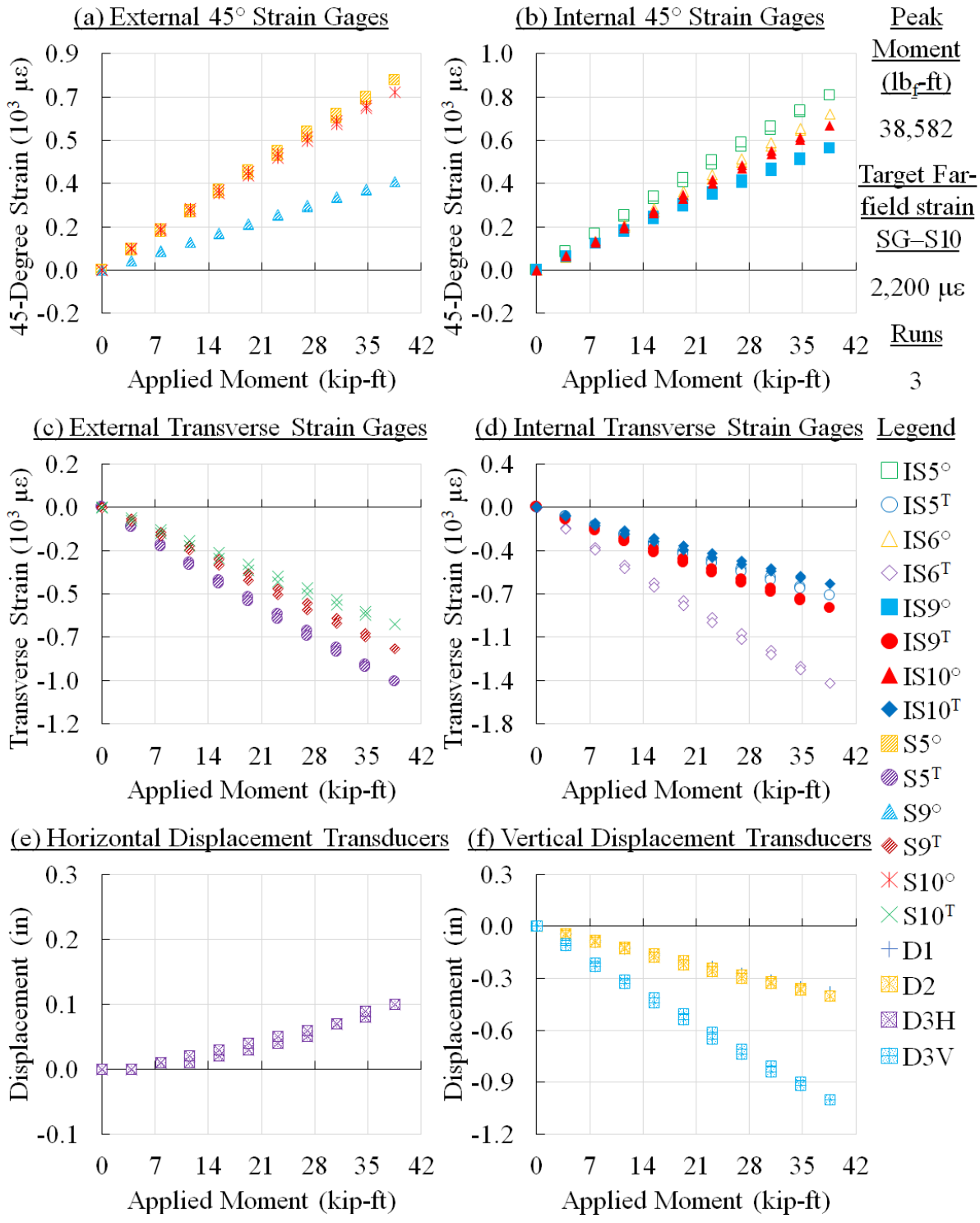


Figure B 14. Panel 5 (fatigue at SL strain level): strain survey at 27,500 cycles (other strain and displacement)

**CFRP Panel 5 – Partial (Half)-Depth Scarf 2, Step 2: 55,000 Cycles – Strain Survey Results**

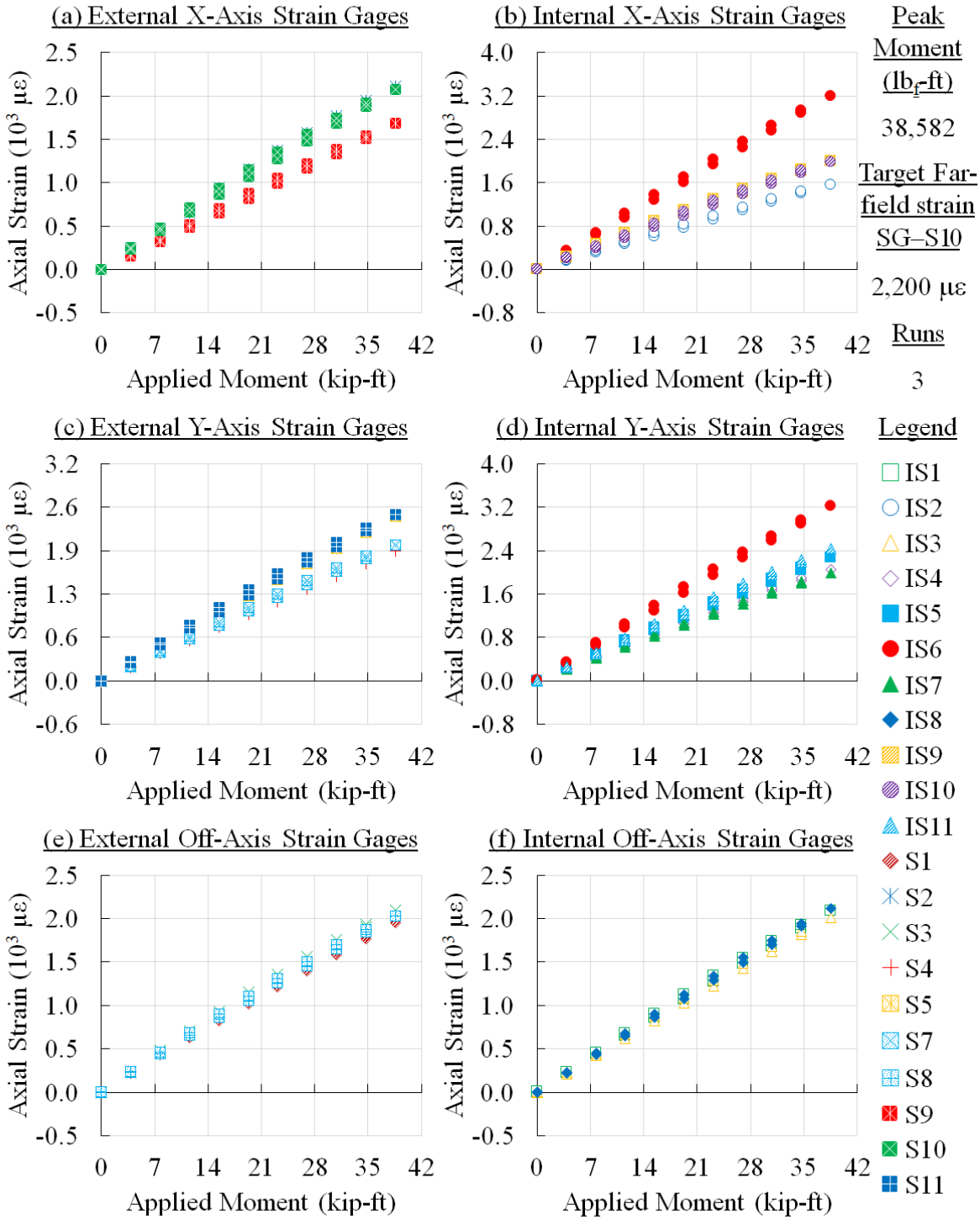


Figure B 15. Panel 5 (fatigue at SL strain level): strain survey at 55,000 cycles (axial strain)

**CFRP Panel 5 – Partial (Half)-Depth Scarf 2, Step 2: 55,000 Cycles – Strain Survey Results**

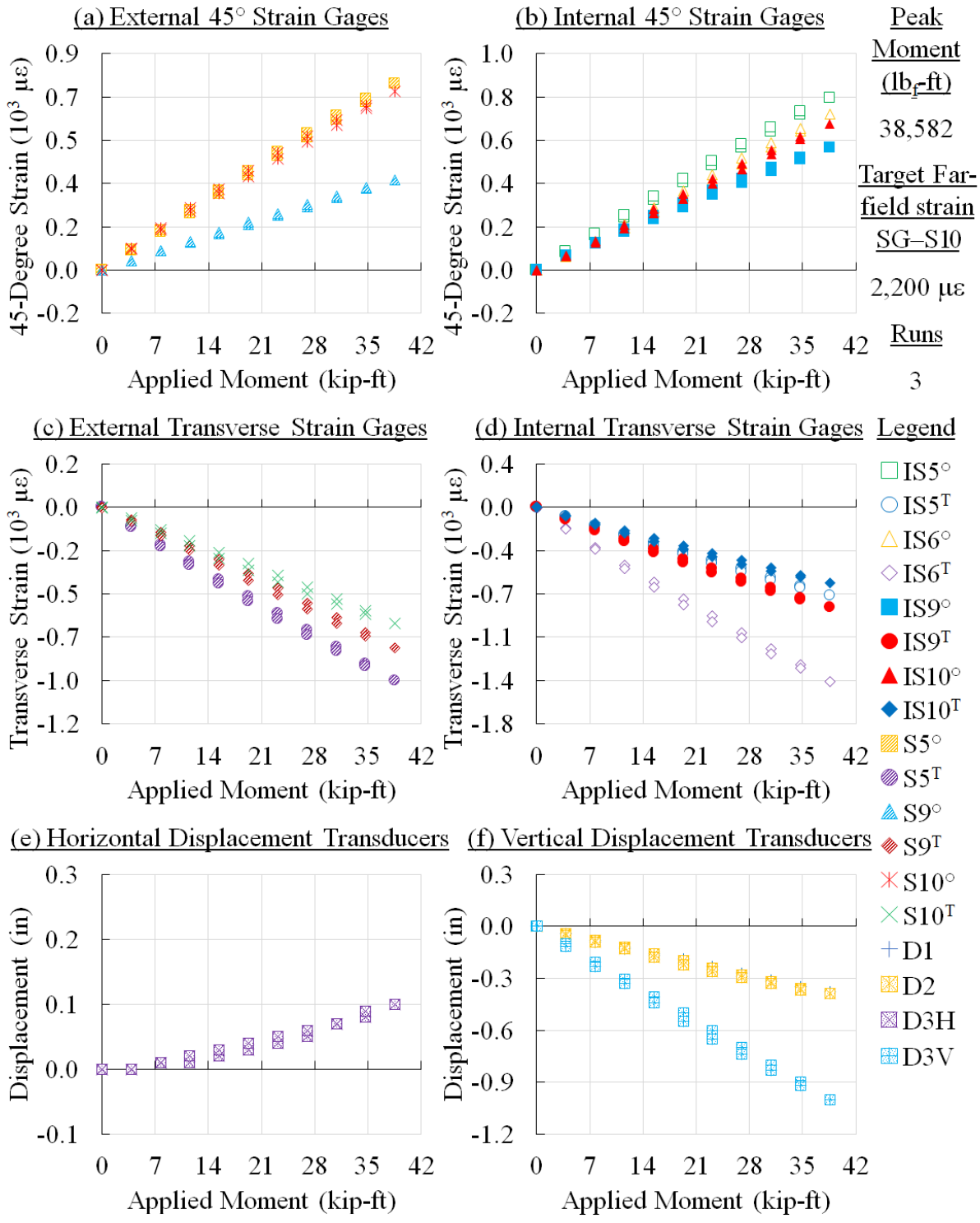


Figure B 16. Panel 5 (fatigue at SL strain level): strain survey at 55,000 cycles (other strain and displacement)

**CFRP Panel 5 – Partial (Half)-Depth Scarf 2, Step 2: 82,500 Cycles – Strain Survey Results**

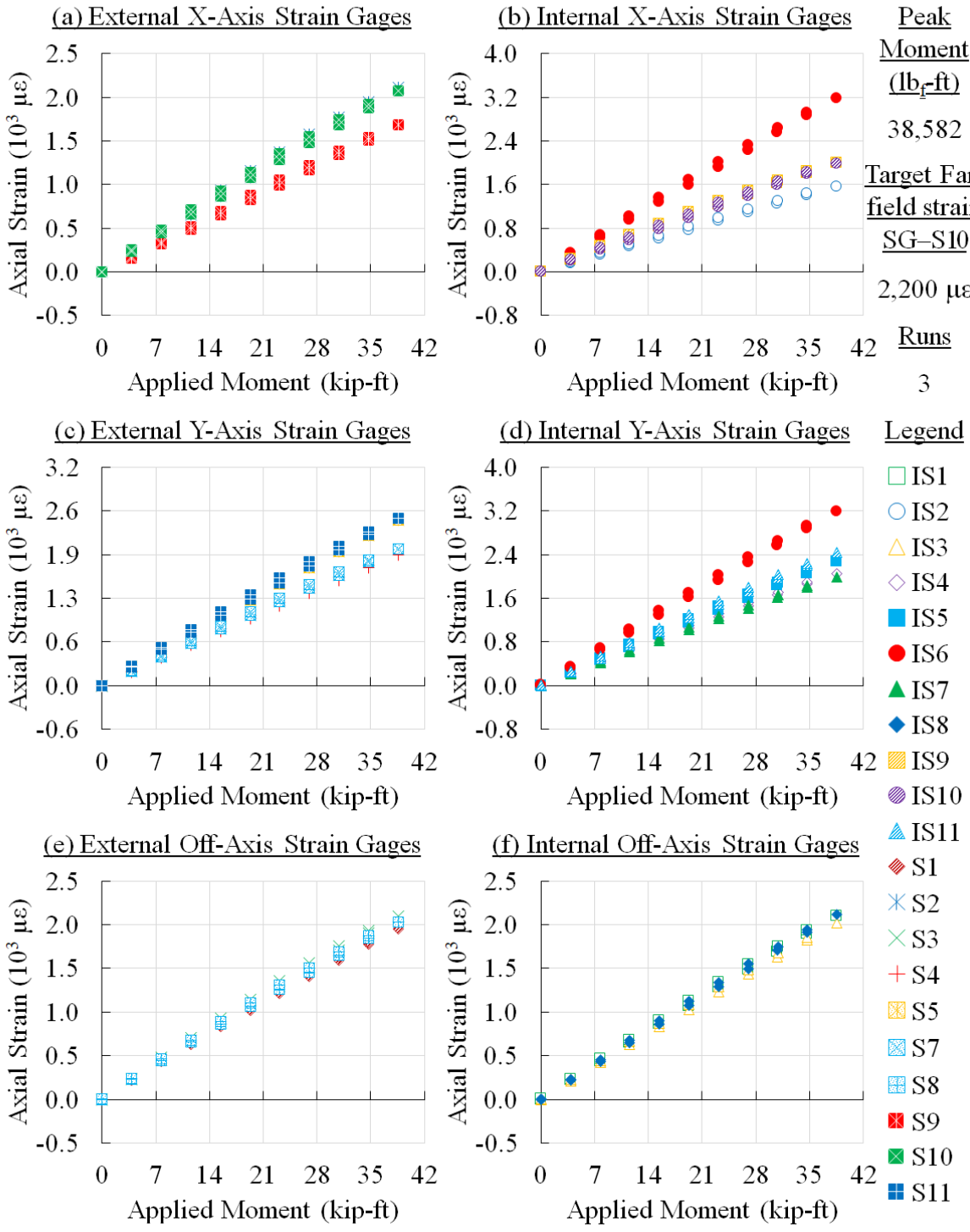


Figure B 17. Panel 5 (fatigue at SL strain level): strain survey at 82,500 cycles (axial strain)

**CFRP Panel 5 – Partial (Half)-Depth Scarf 2, Step 2: 82,500 Cycles – Strain Survey Results**

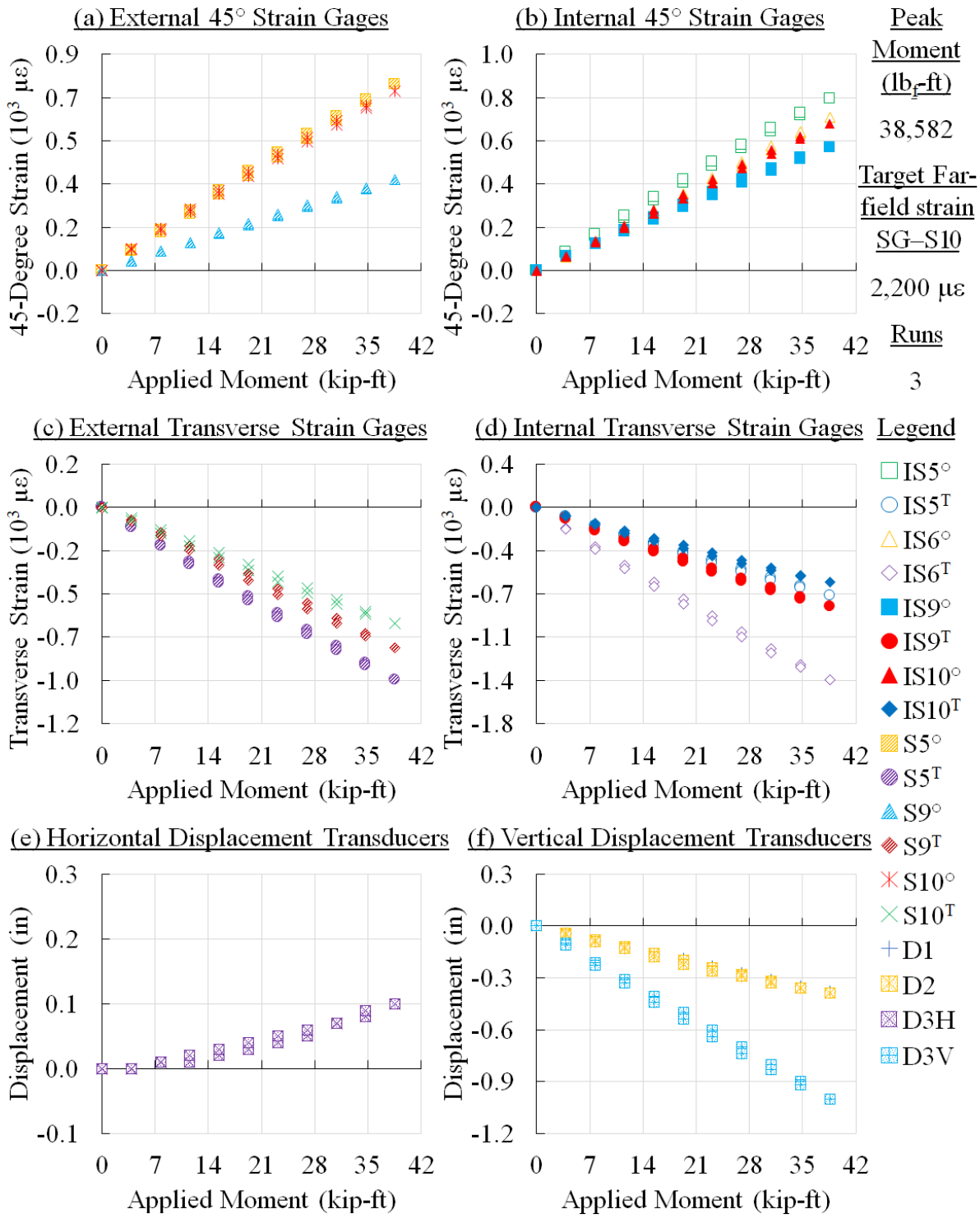


Figure B 18. Panel 5 (fatigue at SL strain level): strain survey at 82,500 cycles (other strain and displacement)

**CFRP Panel 5 – Partial (Half)-Depth Scarf 2, Step 2: 110,000 Cycles – Strain Survey Results**

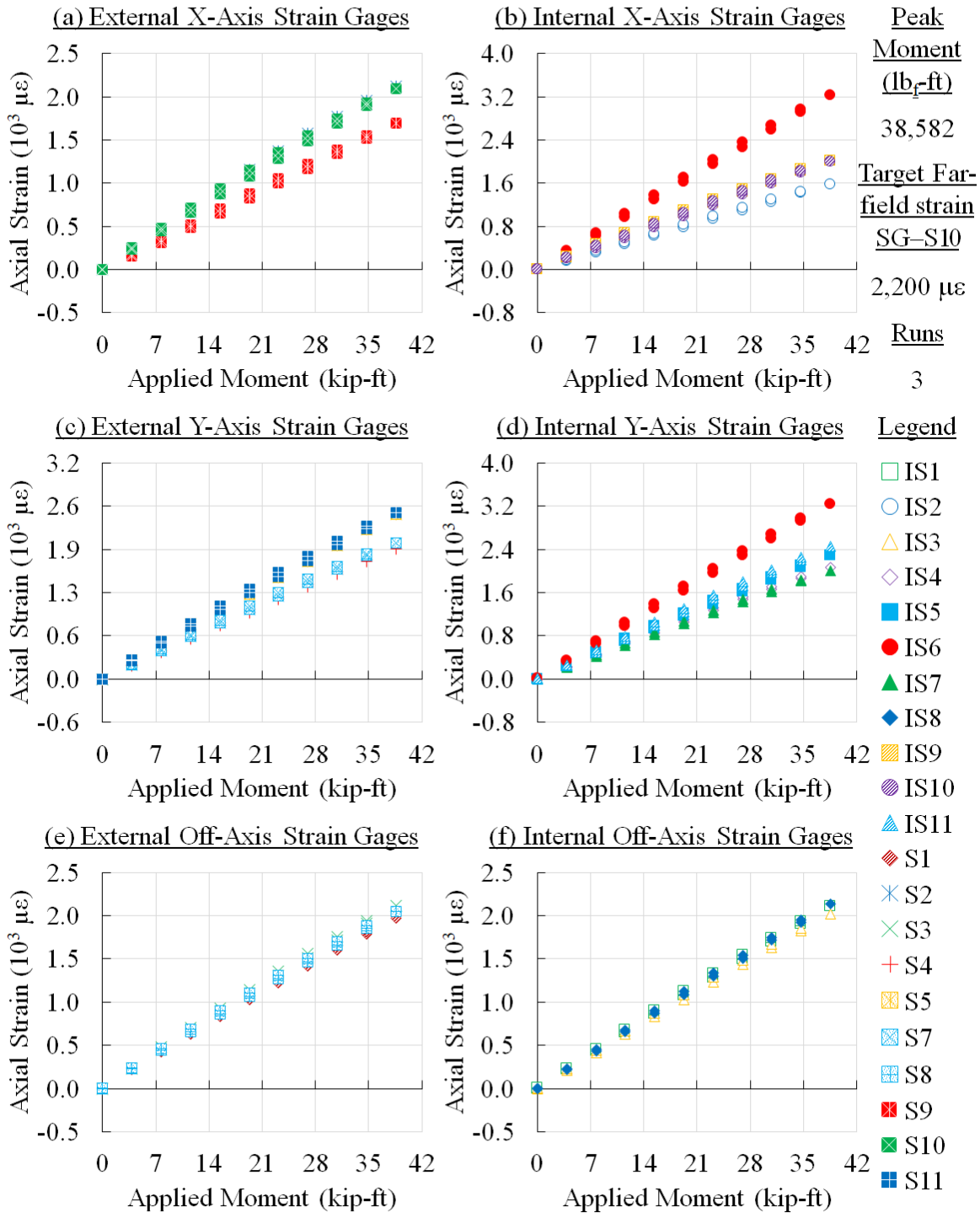


Figure B 19. Panel 5 (fatigue at SL strain level): strain survey at 110,000 cycles (axial strain)

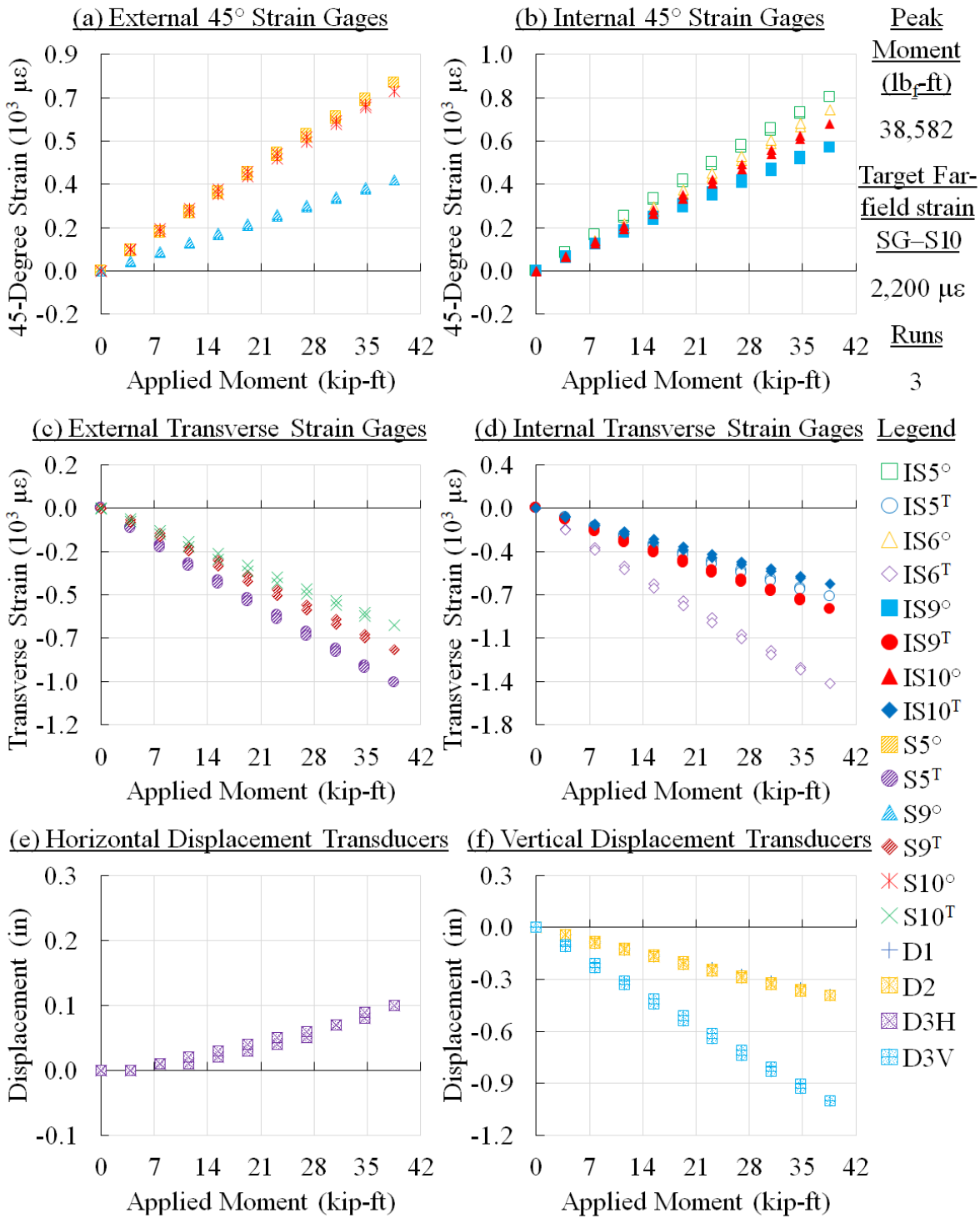


Figure B 20. Panel 5 (fatigue at SL strain level): strain survey at 110,000 cycles (other strain and displacement)

**CFRP Panel 5 – Partial (Half)-Depth Scarf 2, Step 2: 137,500 Cycles – Strain Survey Results**

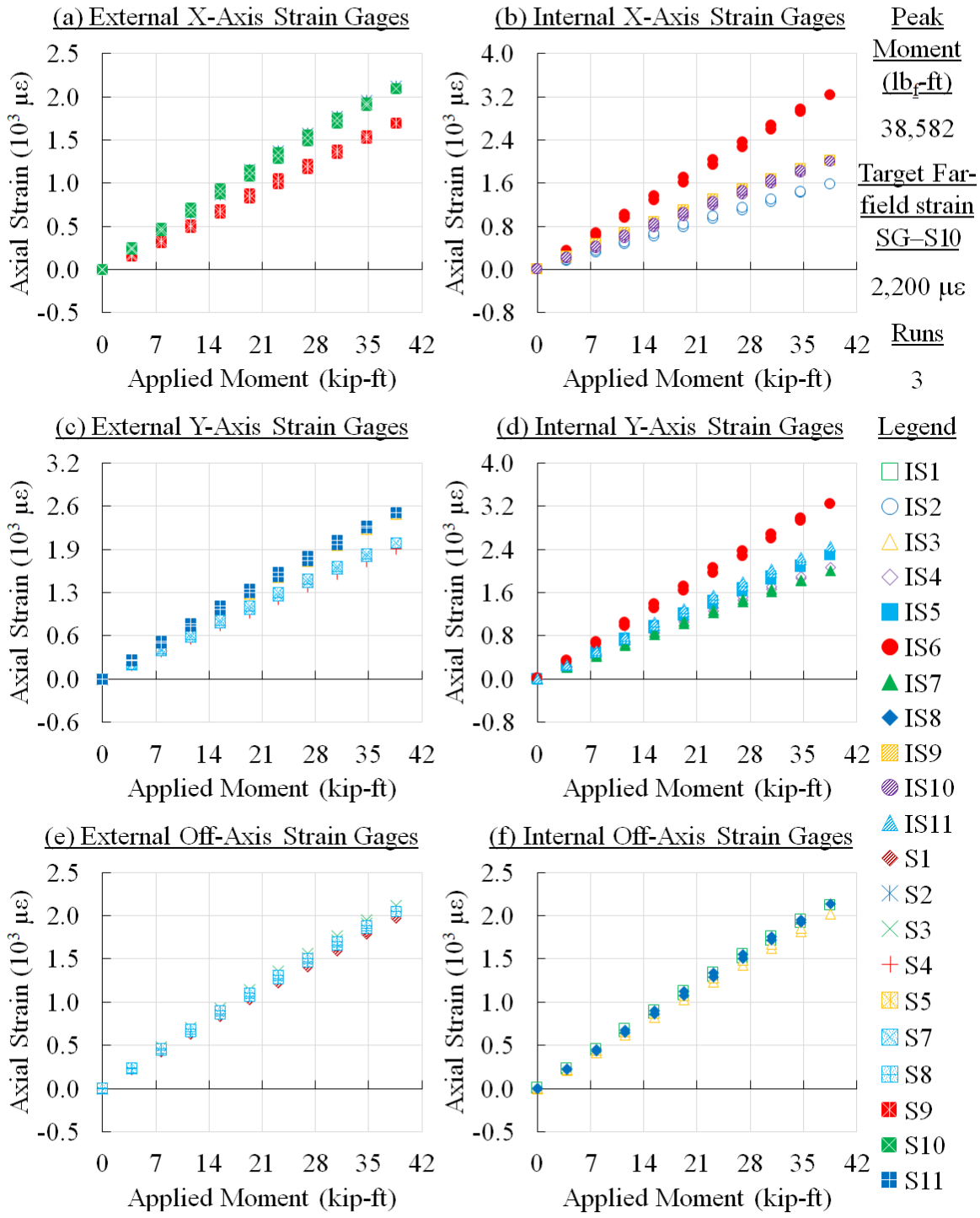


Figure B 21. Panel 5 (fatigue at SL strain level): strain survey at 137,500 cycles (axial strain)

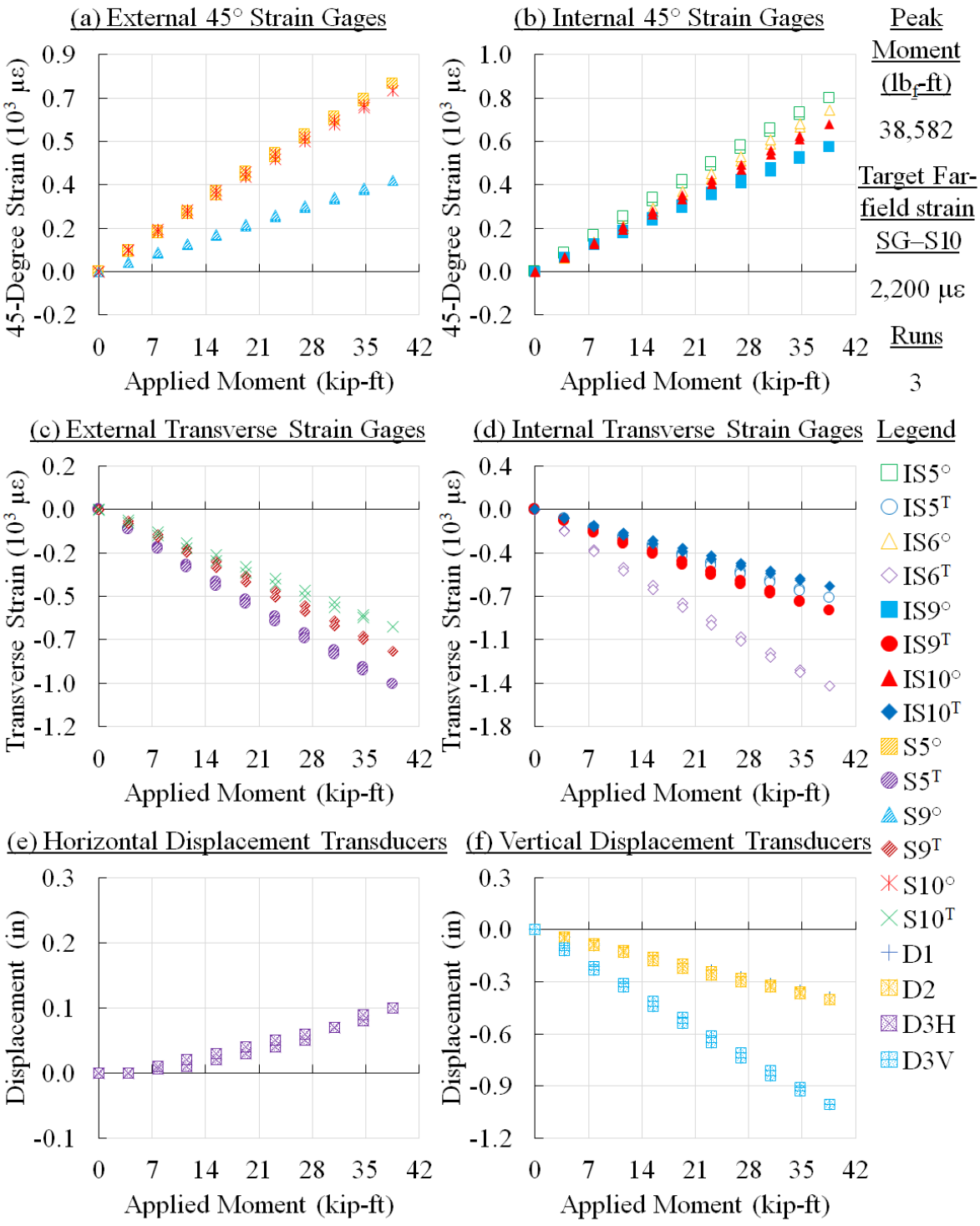


Figure B 22. Panel 5 (fatigue at SL strain level): strain survey at 137,500 cycles (other strain and displacement)

**CFRP Panel 5 – Partial (Half)-Depth Scarf 2, Step 2: 165,000 Cycles – Strain Survey Results**

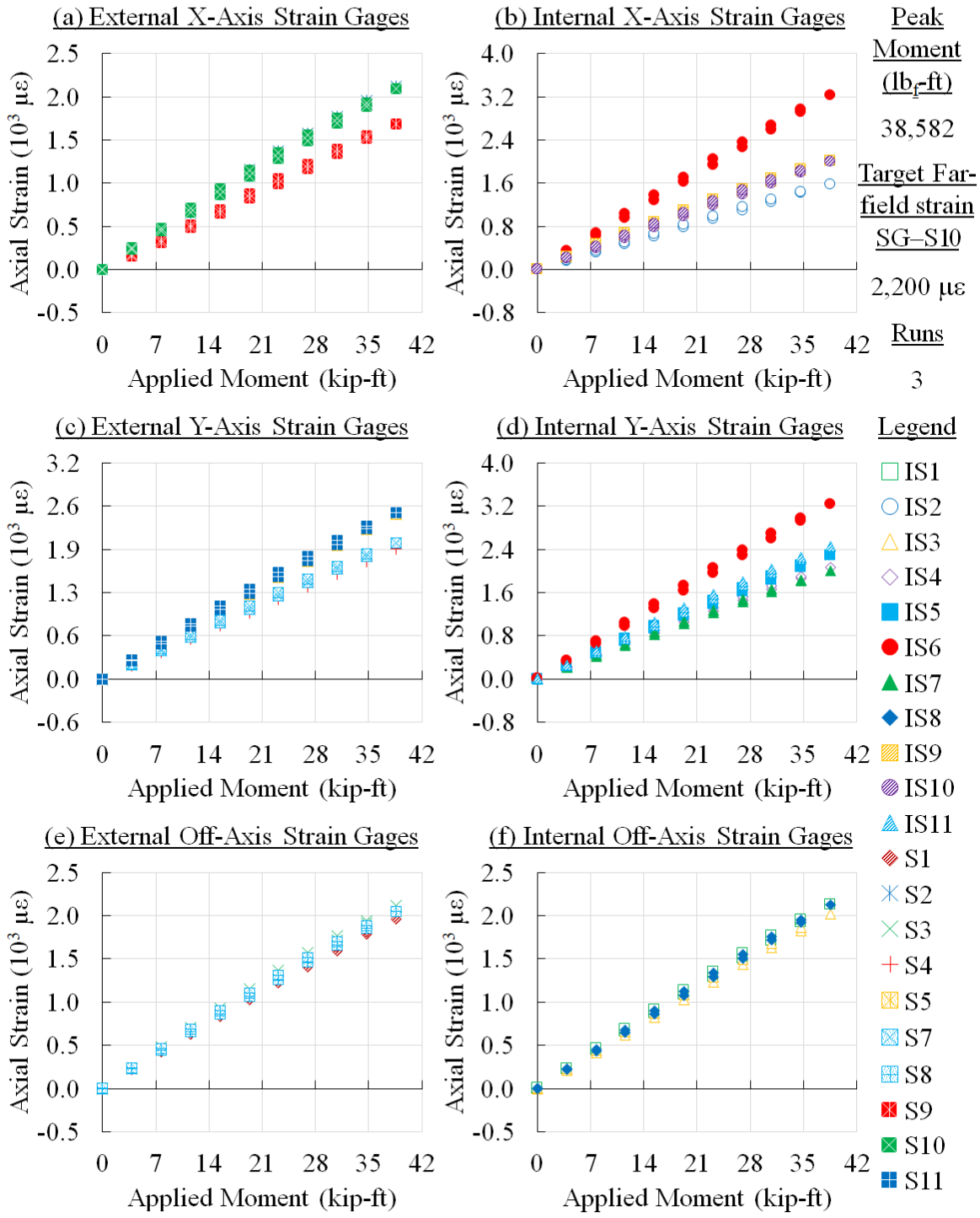


Figure B 23. Panel 5 (fatigue at SL strain level): strain survey at 165,000 cycles (axial strain)

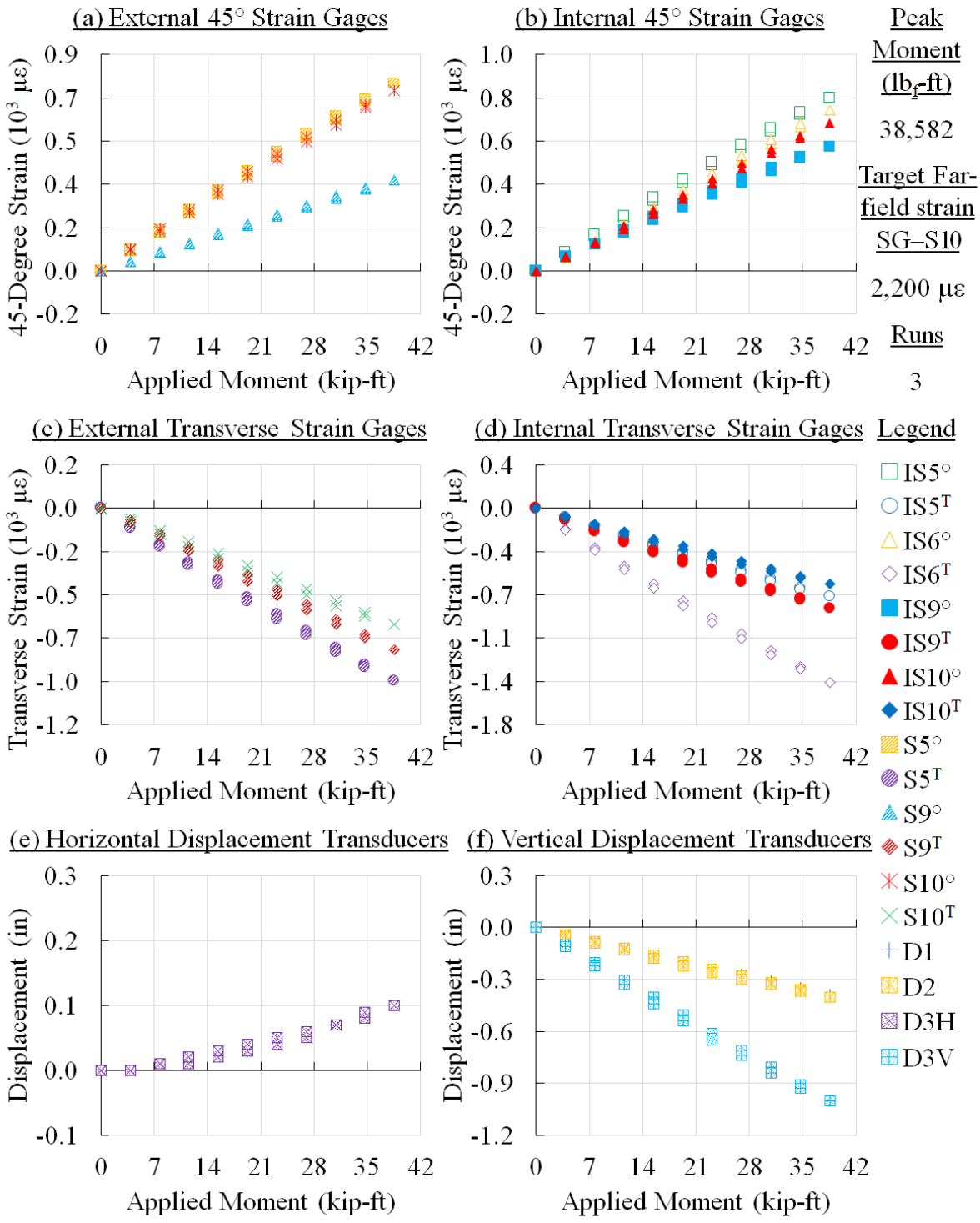


Figure B 24. Panel 5 (fatigue at SL strain level): strain survey at 165,000 cycles (other strain and displacement)

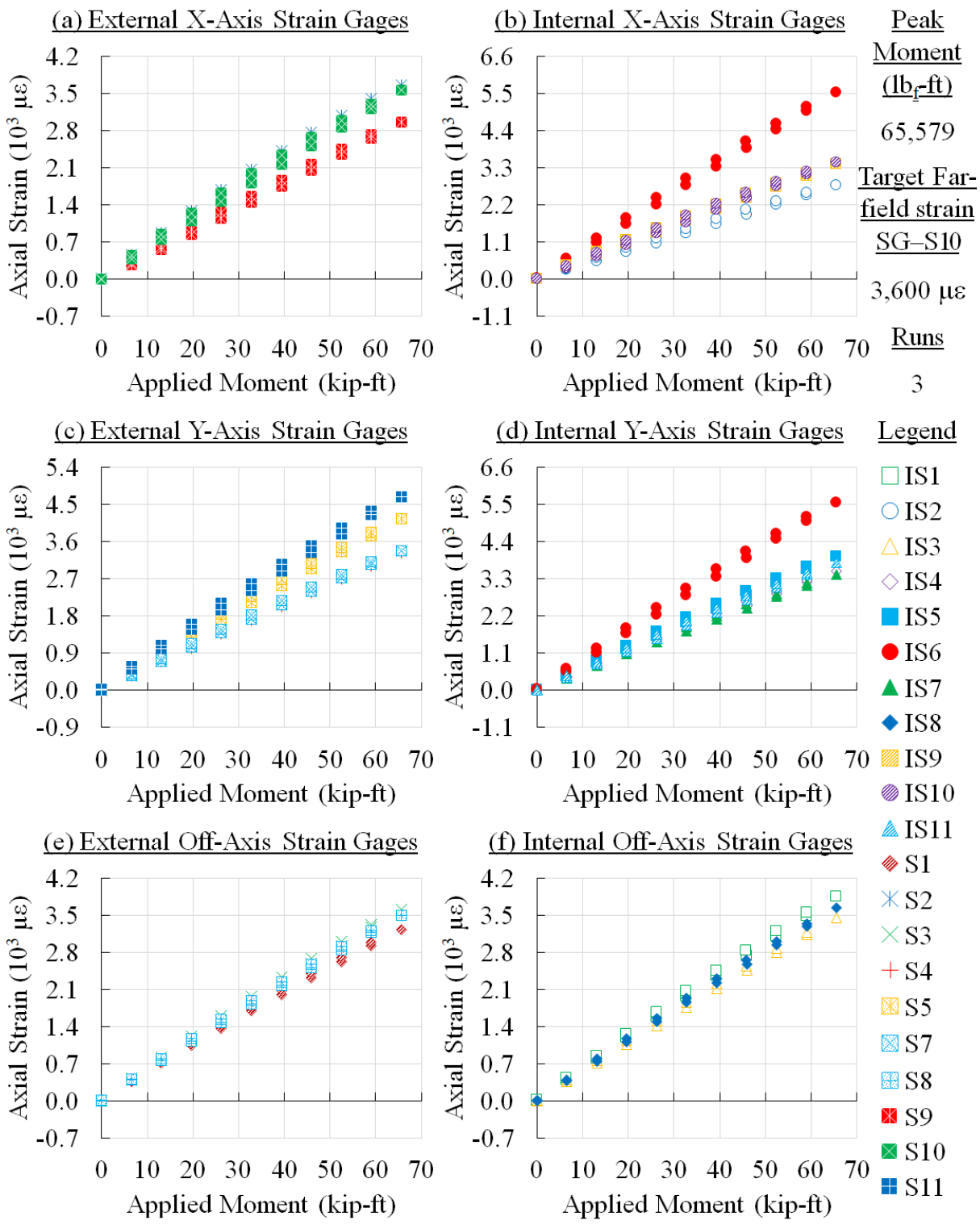


Figure B 25. Panel 5 (fatigue at elevated load strain level): strain survey at 0 cycles (axial strain)

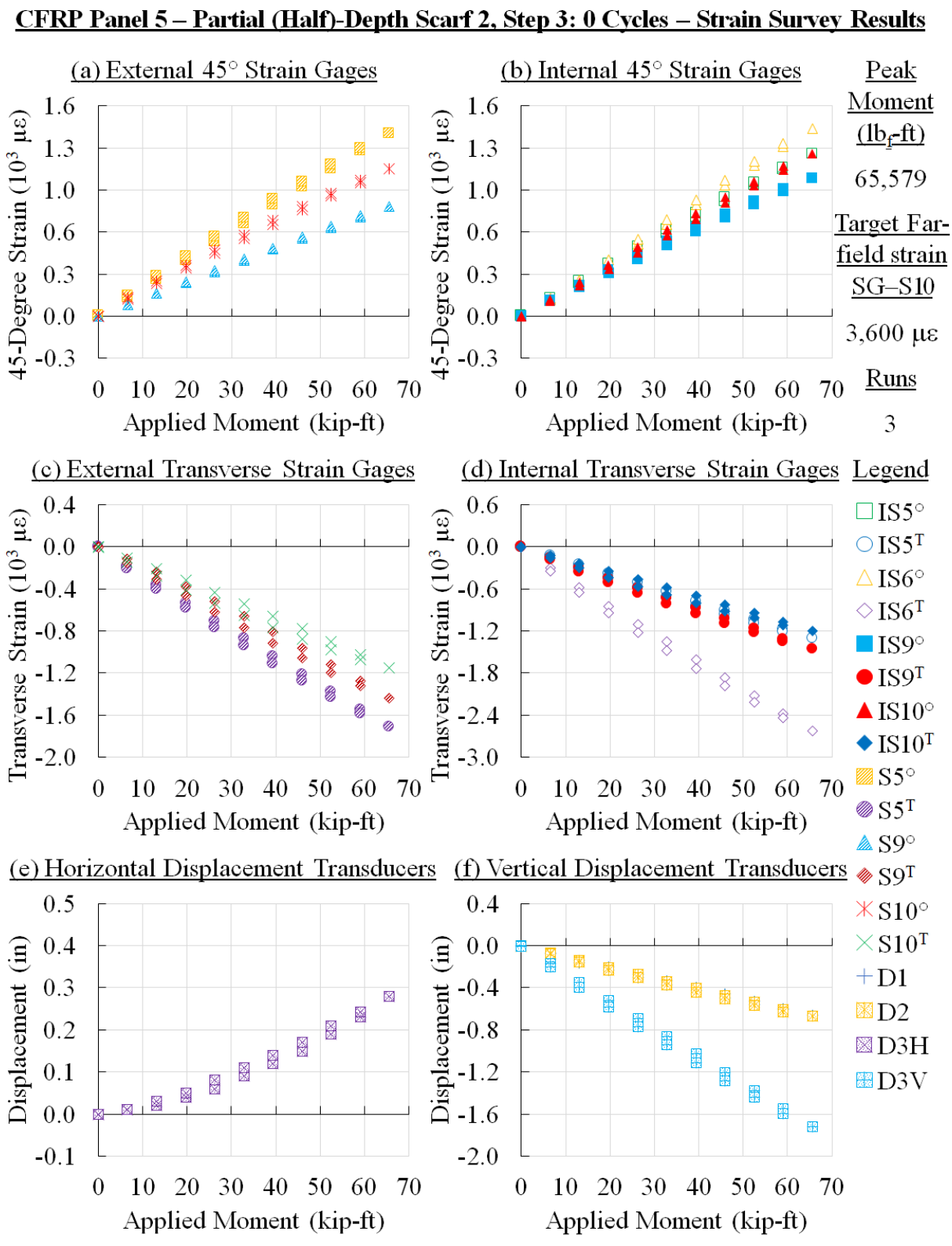


Figure B 26. Panel 5 (fatigue at elevated load strain level): strain survey at 0 cycles (other strain and displacement)

**CFRP Panel 5 – Partial (Half)-Depth Scarf 2, Step 3: 1,800 Cycles – Strain Survey Results**

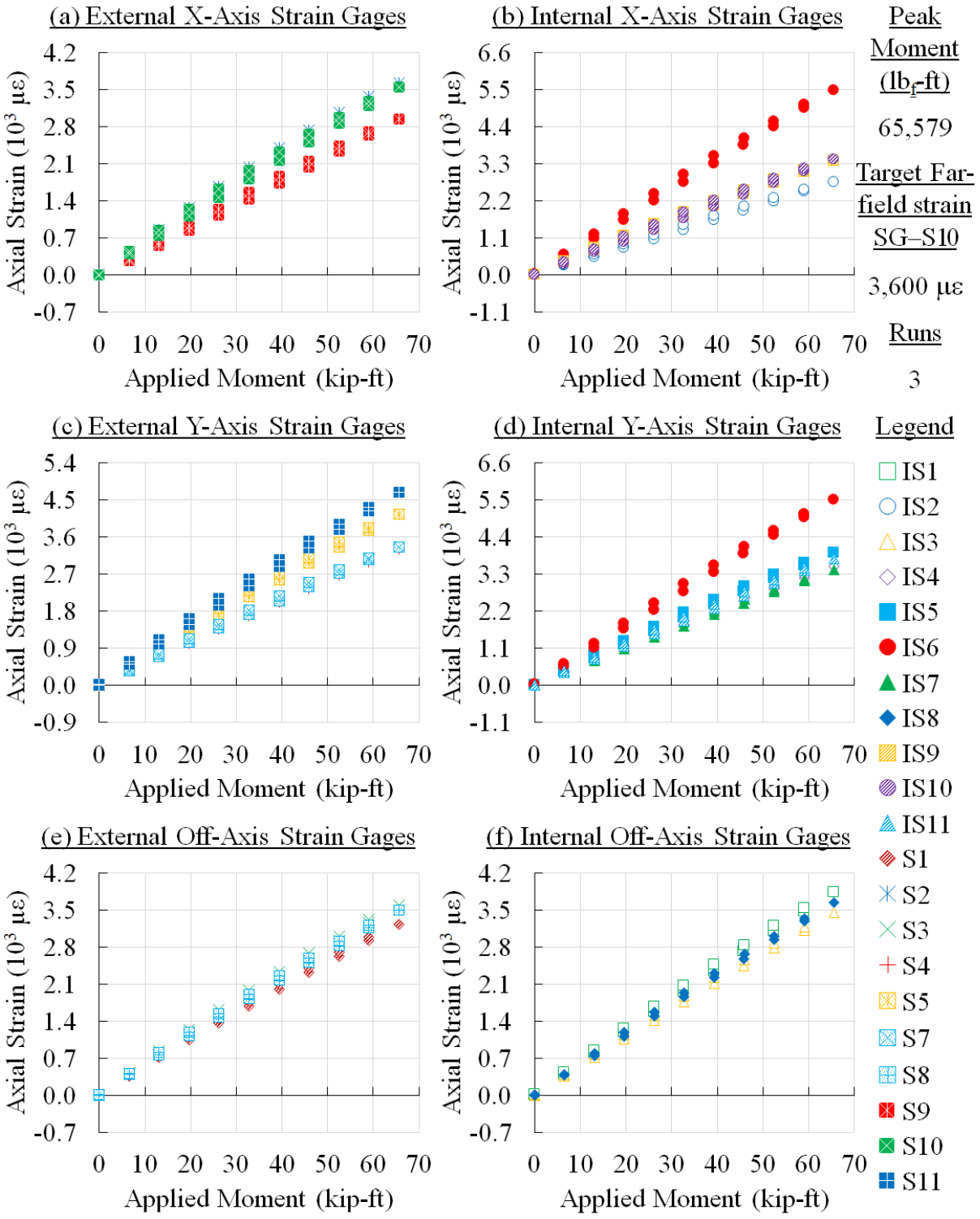


Figure B 27. Panel 5 (fatigue at elevated load strain level): strain survey at 1,800 cycles (axial strain)

**CFRP Panel 5 – Partial (Half)-Depth Scarf 2, Step 3: 1,800 Cycles – Strain Survey Results**

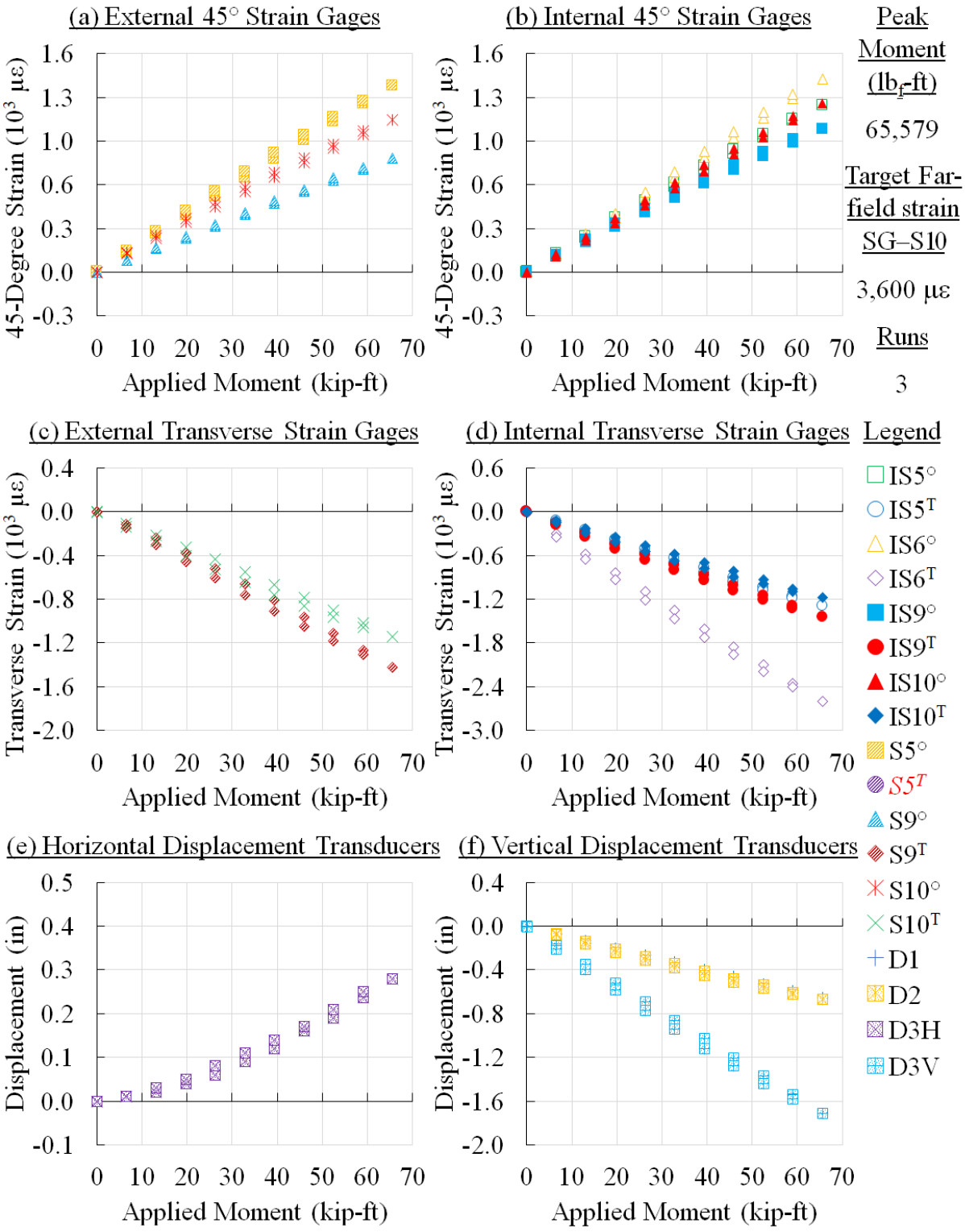


Figure B 28. Panel 5 (fatigue at elevated load strain level): strain survey at 1,800 cycles (other strain and displacement)

**CFRP Panel 5 – Partial (Half)-Depth Scarf 2, Step 3: 2,500 Cycles – Strain Survey Results**

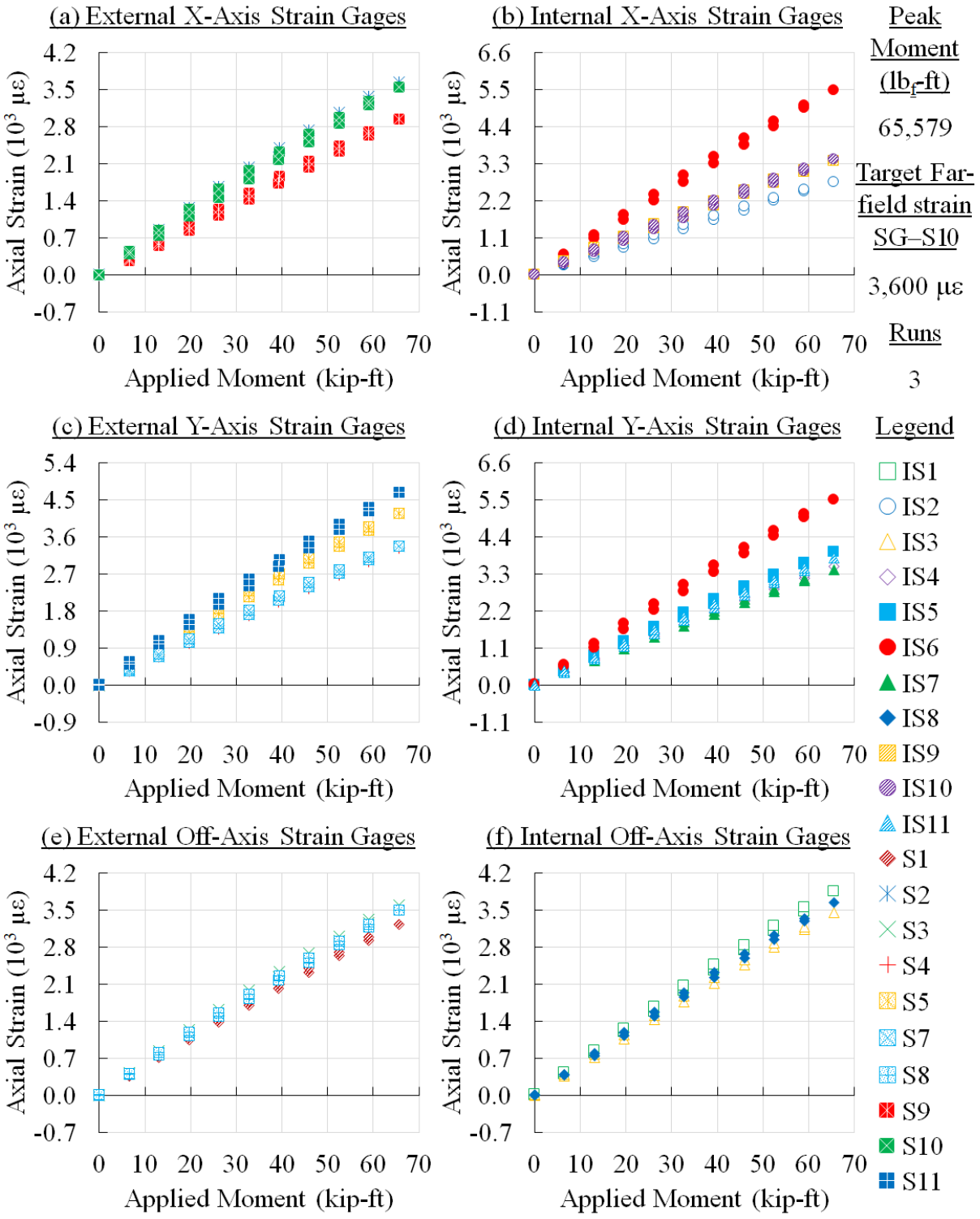


Figure B 29. Panel 5 (fatigue at elevated load strain level): strain survey at 2,500 cycles (axial strain)

**CFRP Panel 5 – Partial (Half)-Depth Scarf 2, Step 3: 2,500 Cycles – Strain Survey Results**

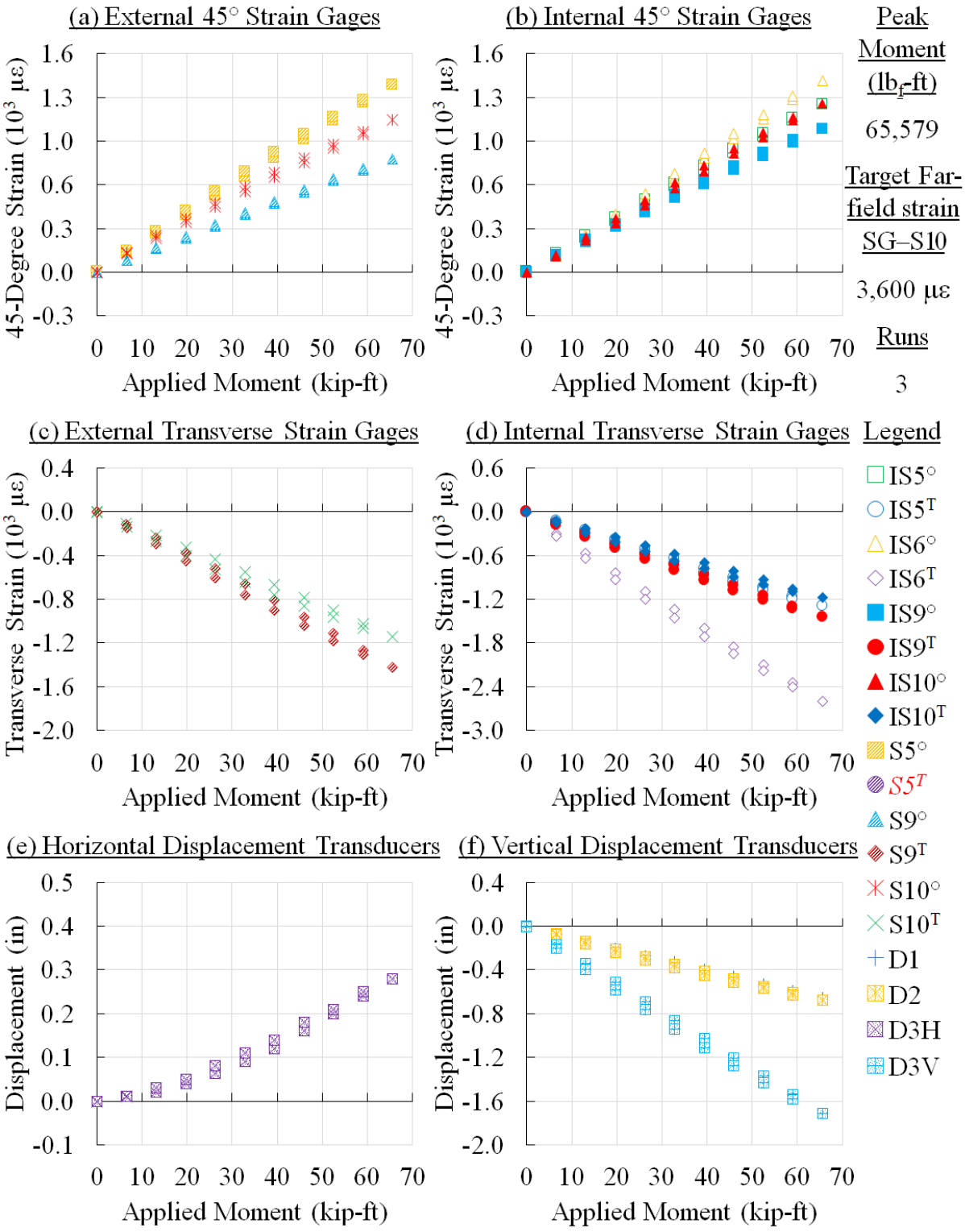


Figure B 30. Panel 5 (fatigue at elevated load strain level): strain survey at 2,500 cycles (other strain and displacement)

**CFRP Panel 5 – Partial (Half)-Depth Scarf 2, Step 3: 3,000 Cycles – Strain Survey Results**

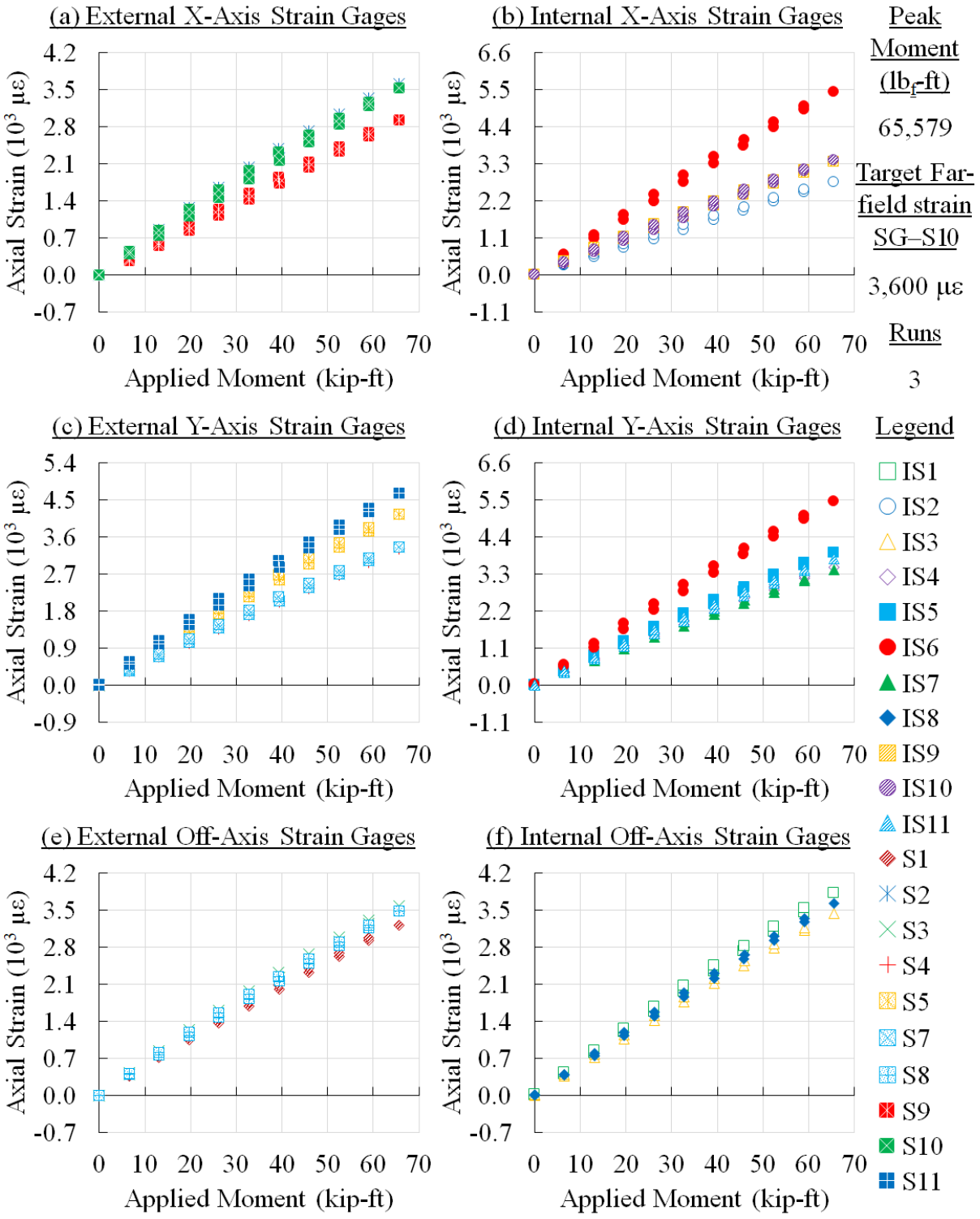


Figure B 31. Panel 5 (fatigue at elevated load strain level): strain survey at 3,000 cycles (axial strain)

**CFRP Panel 5 – Partial (Half)-Depth Scarf 2, Step 3: 3,000 Cycles – Strain Survey Results**

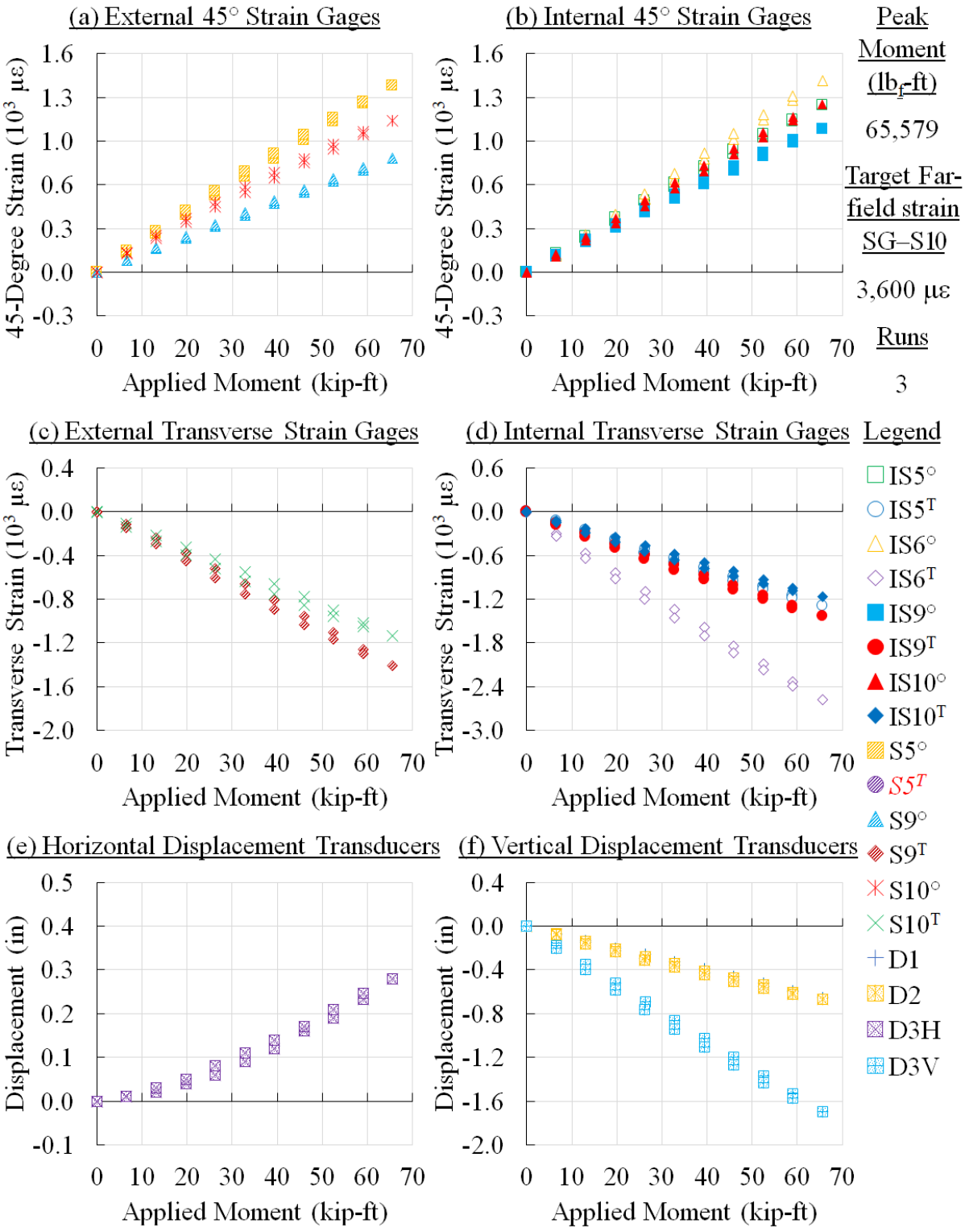


Figure B 32. Panel 5 (fatigue at elevated load strain level): strain survey at 3,000 cycles (other strain and displacement)

**CFRP Panel 5 – Partial (Half)-Depth Scarf 2, Step 3: 3,500 Cycles – Strain Survey Results**

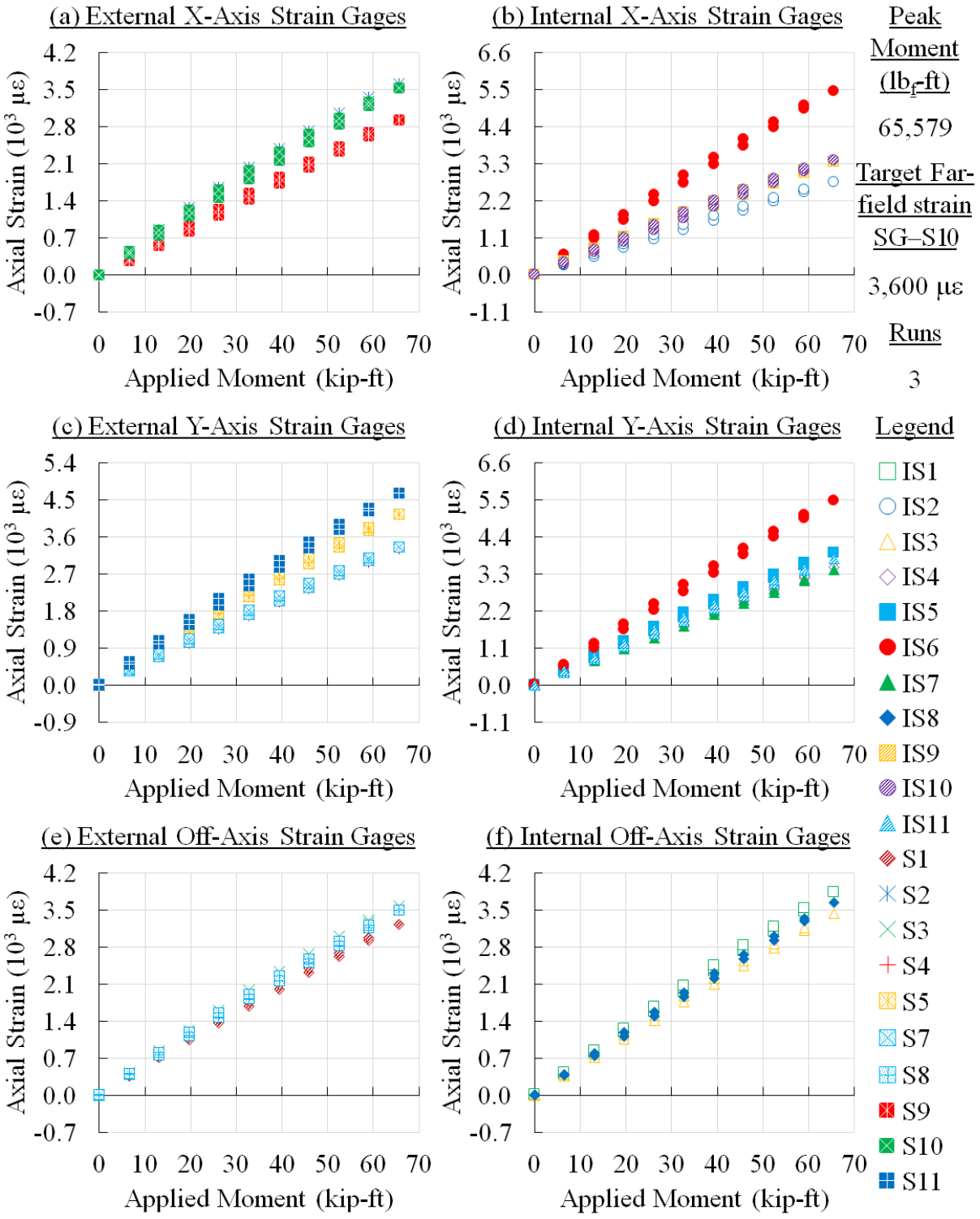


Figure B 33. Panel 5 (fatigue at elevated load strain level): strain survey at 3,500 cycles (axial strain)

**CFRP Panel 5 – Partial (Half)-Depth Scarf 2, Step 3: 3,500 Cycles – Strain Survey Results**

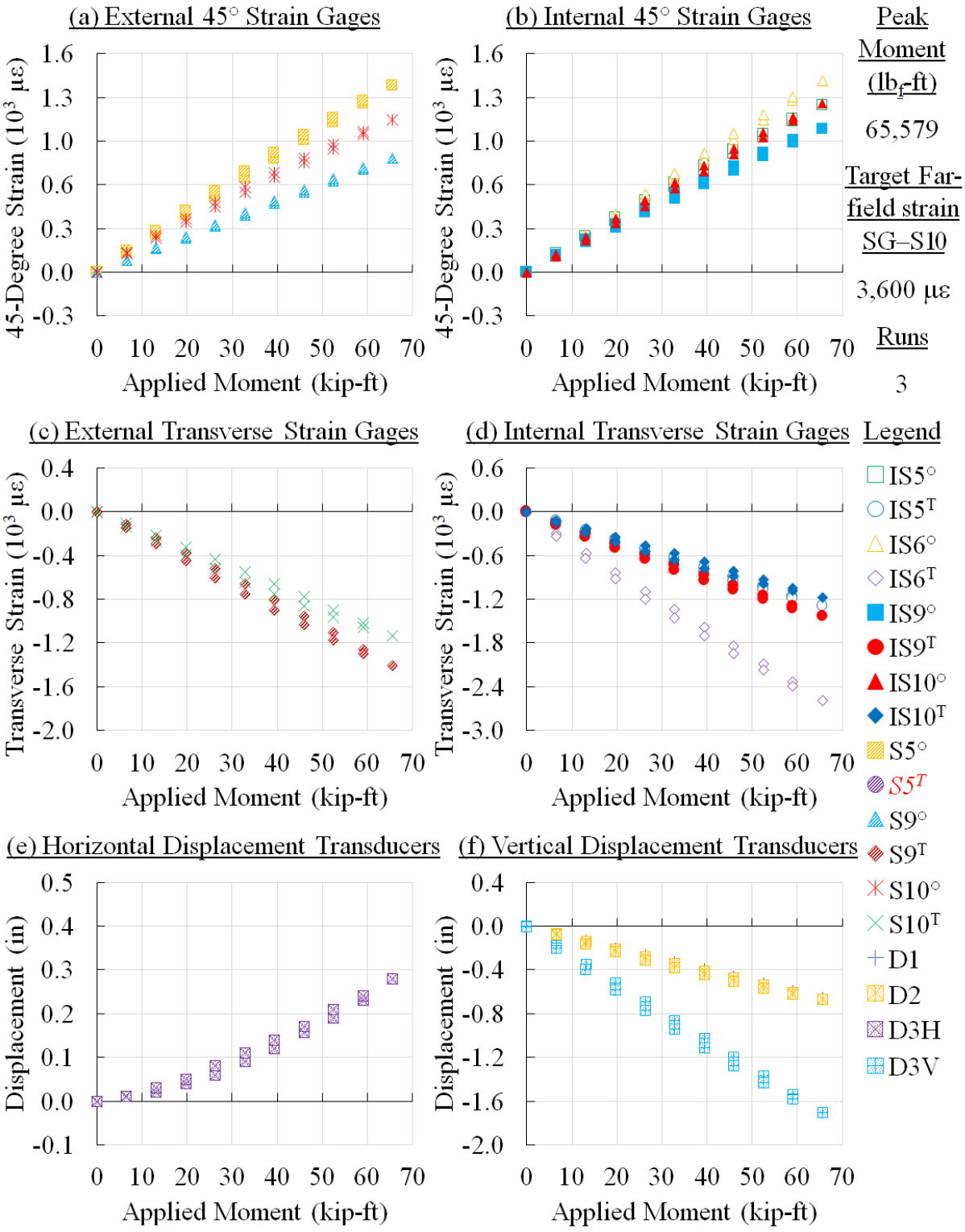


Figure B 34. Panel 5 (fatigue at elevated load strain level): strain survey at 3,500 cycles (other strain and displacement)

**CFRP Panel 5 – Partial (Half)-Depth Scarf 2, Step 3: 4,000 Cycles – Strain Survey Results**

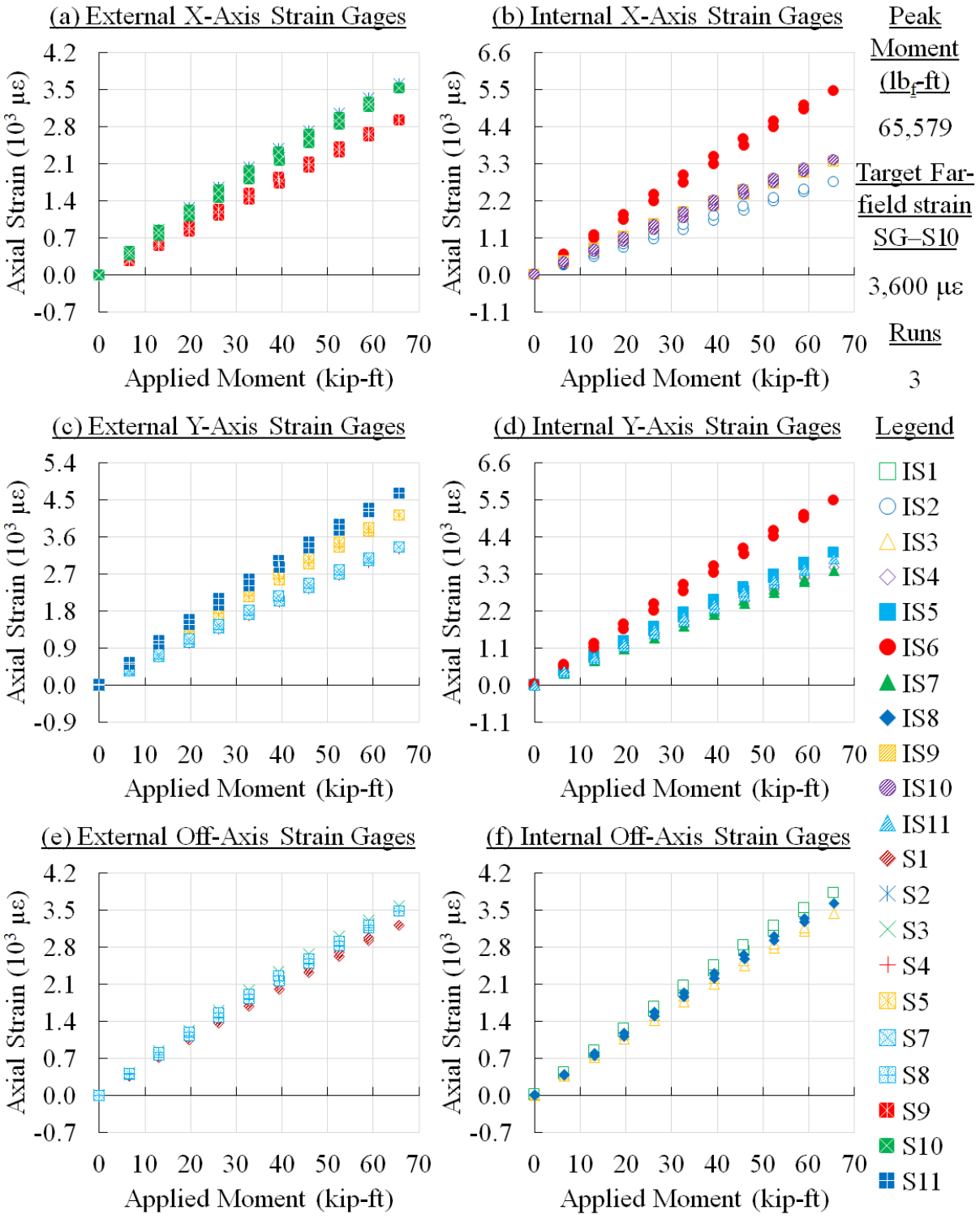


Figure B 35. Panel 5 (fatigue at elevated load strain level): strain survey at 4,000 cycles (axial strain)

**CFRP Panel 5 – Partial (Half)-Depth Scarf 2, Step 3: 4,000 Cycles – Strain Survey Results**

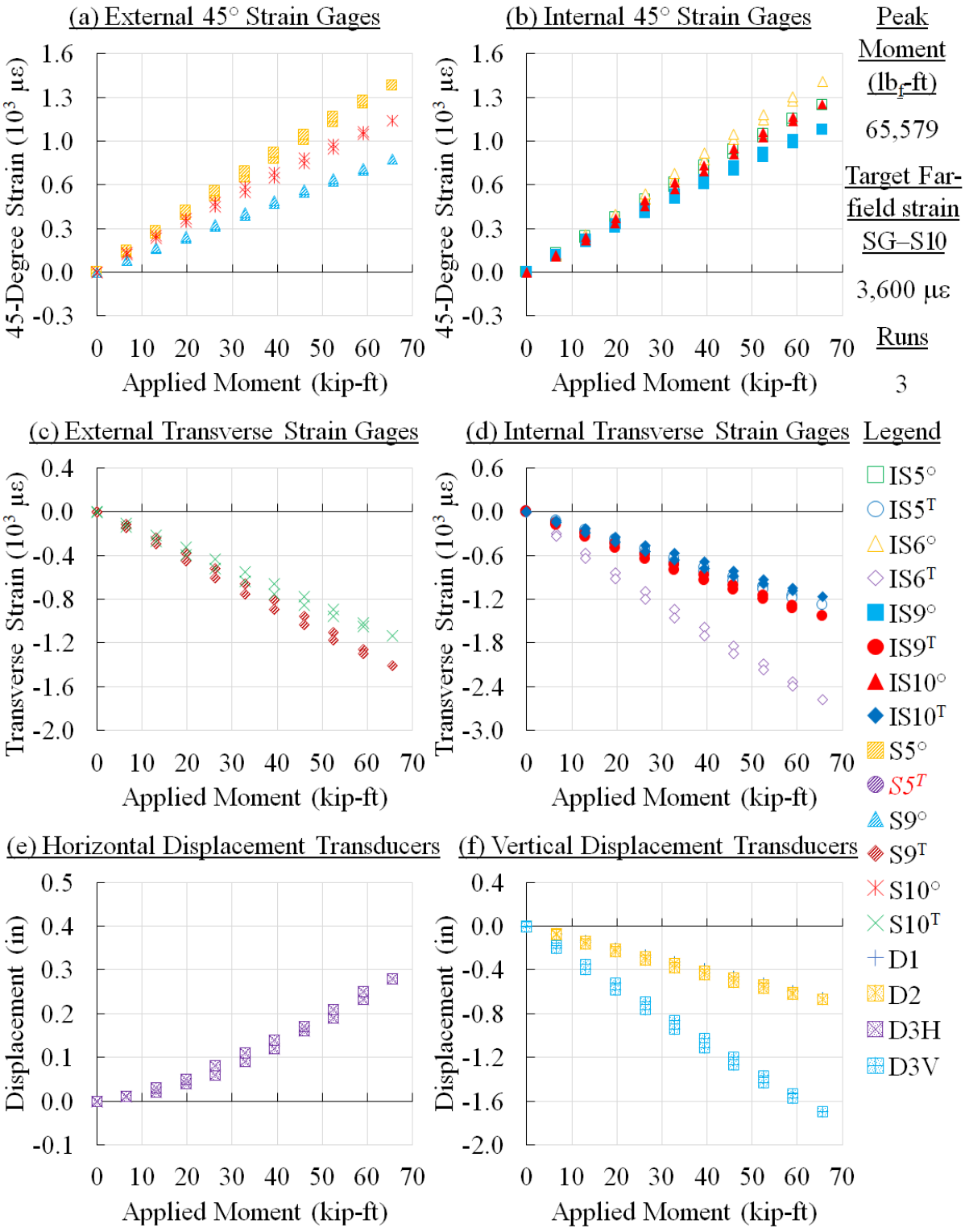


Figure B 36. Panel 5 (fatigue at elevated load strain level): strain survey at 4,000 cycles (other strain and displacement)

**CFRP Panel 5 – Partial (Half)-Depth Scarf 2, Step 3: 4,500 Cycles – Strain Survey Results**

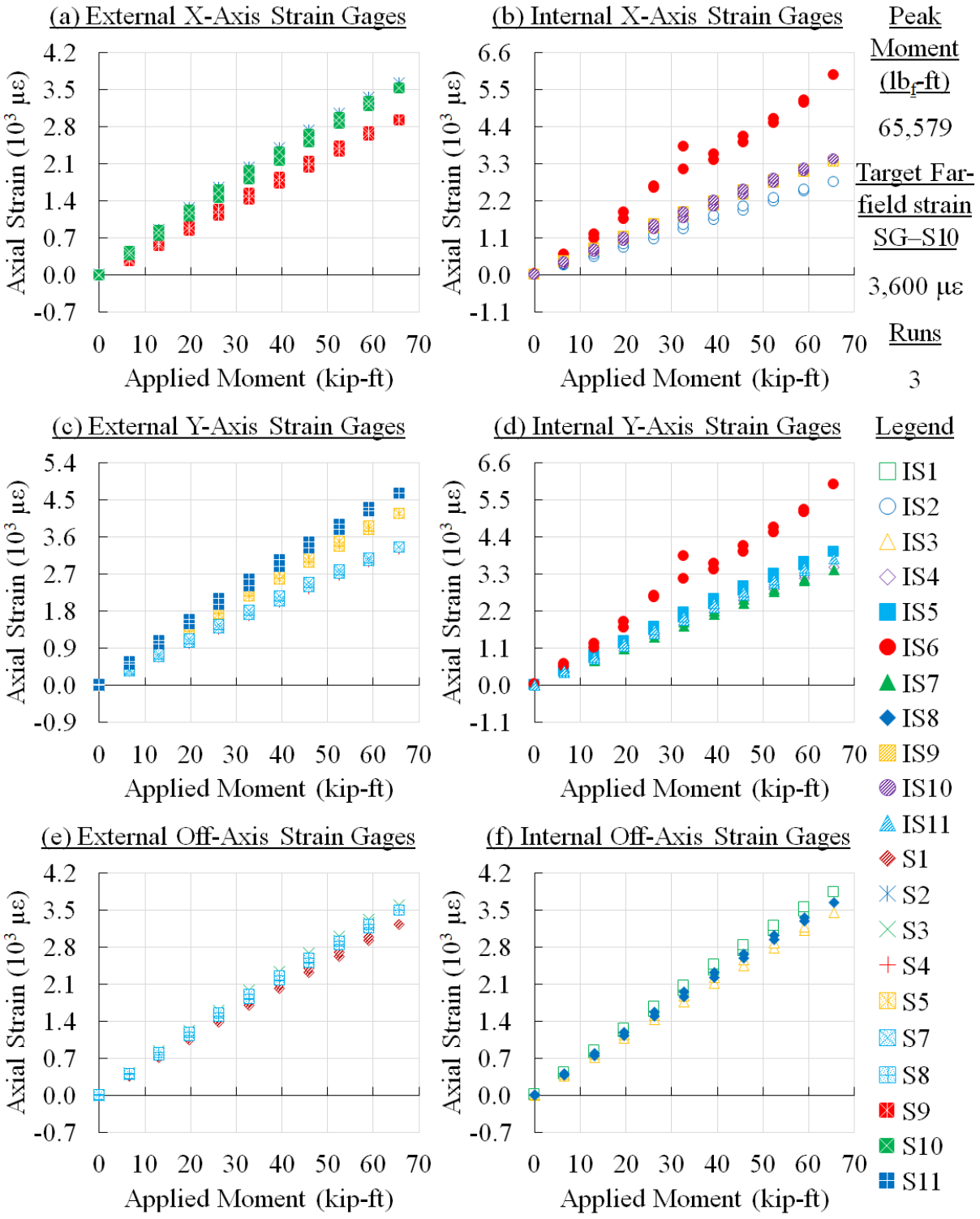


Figure B 37. Panel 5 (fatigue at elevated load strain level): strain survey at 4,500 cycles (axial strain)

**CFRP Panel 5 – Partial (Half)-Depth Scarf 2, Step 3: 4,500 Cycles – Strain Survey Results**

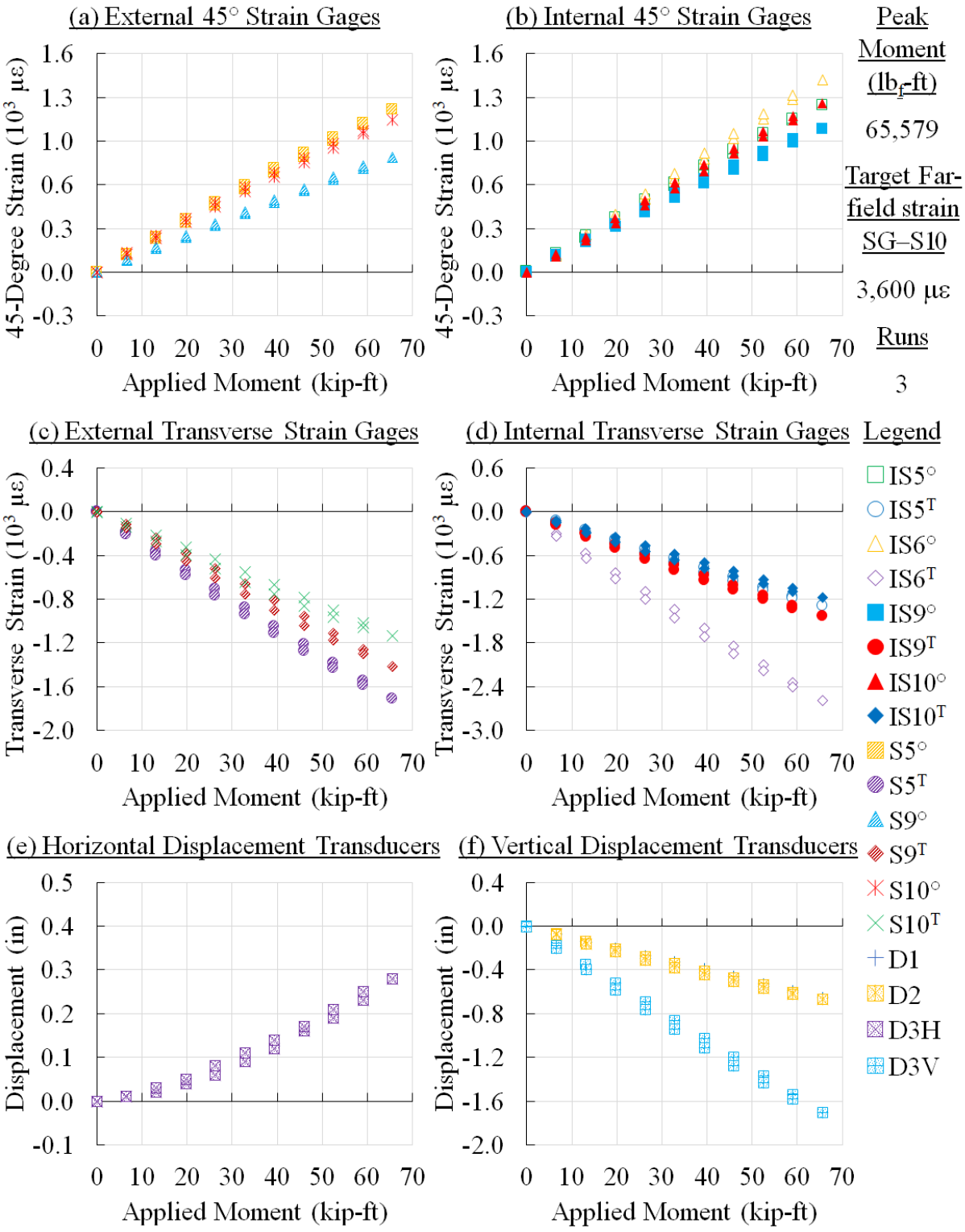


Figure B 38. Panel 5 (fatigue at elevated load strain level): strain survey at 4,500 cycles (other strain and displacement)

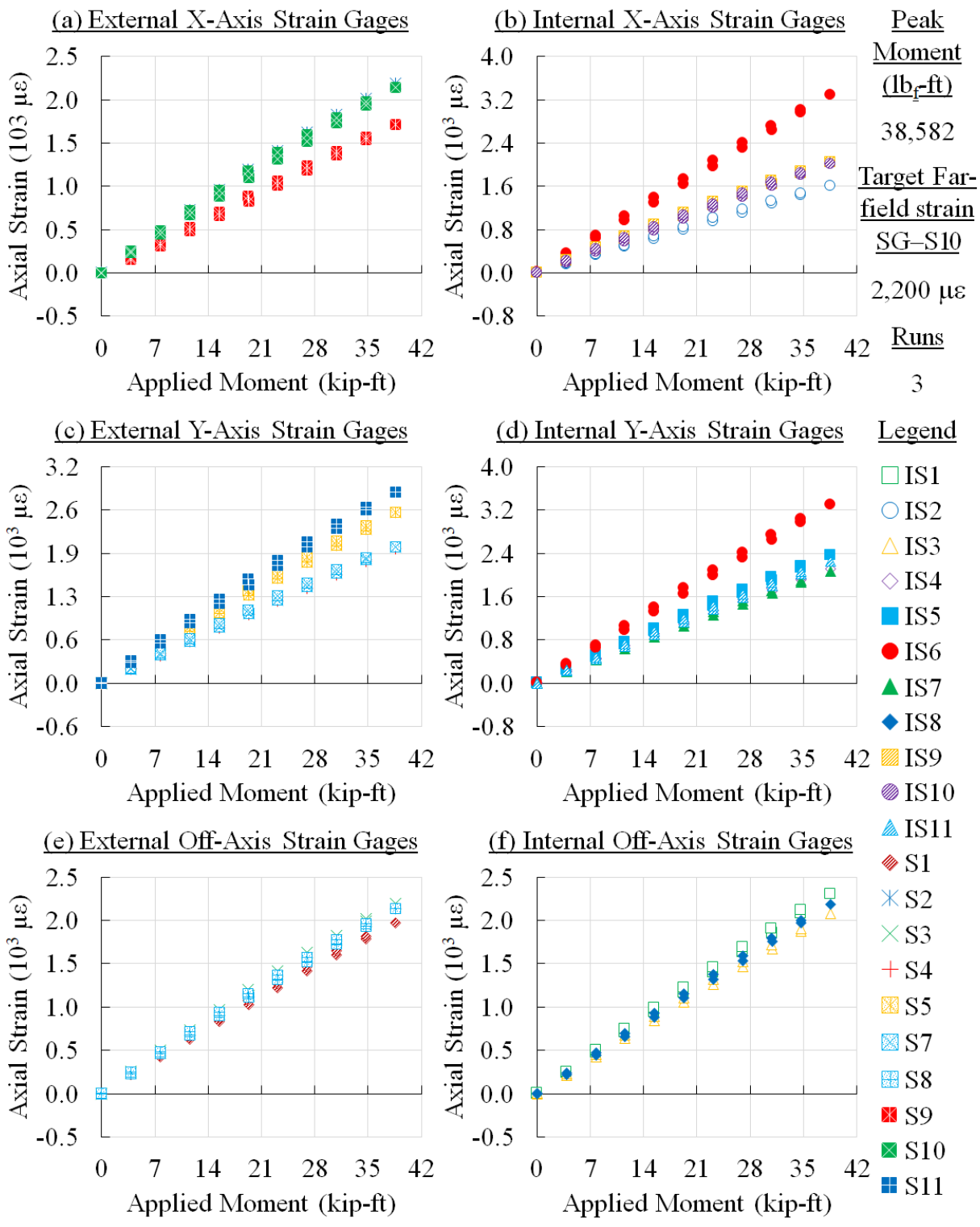


Figure B 39. Panel 5 (additional fatigue at SL strain level): strain survey at 0 cycles (axial strain)

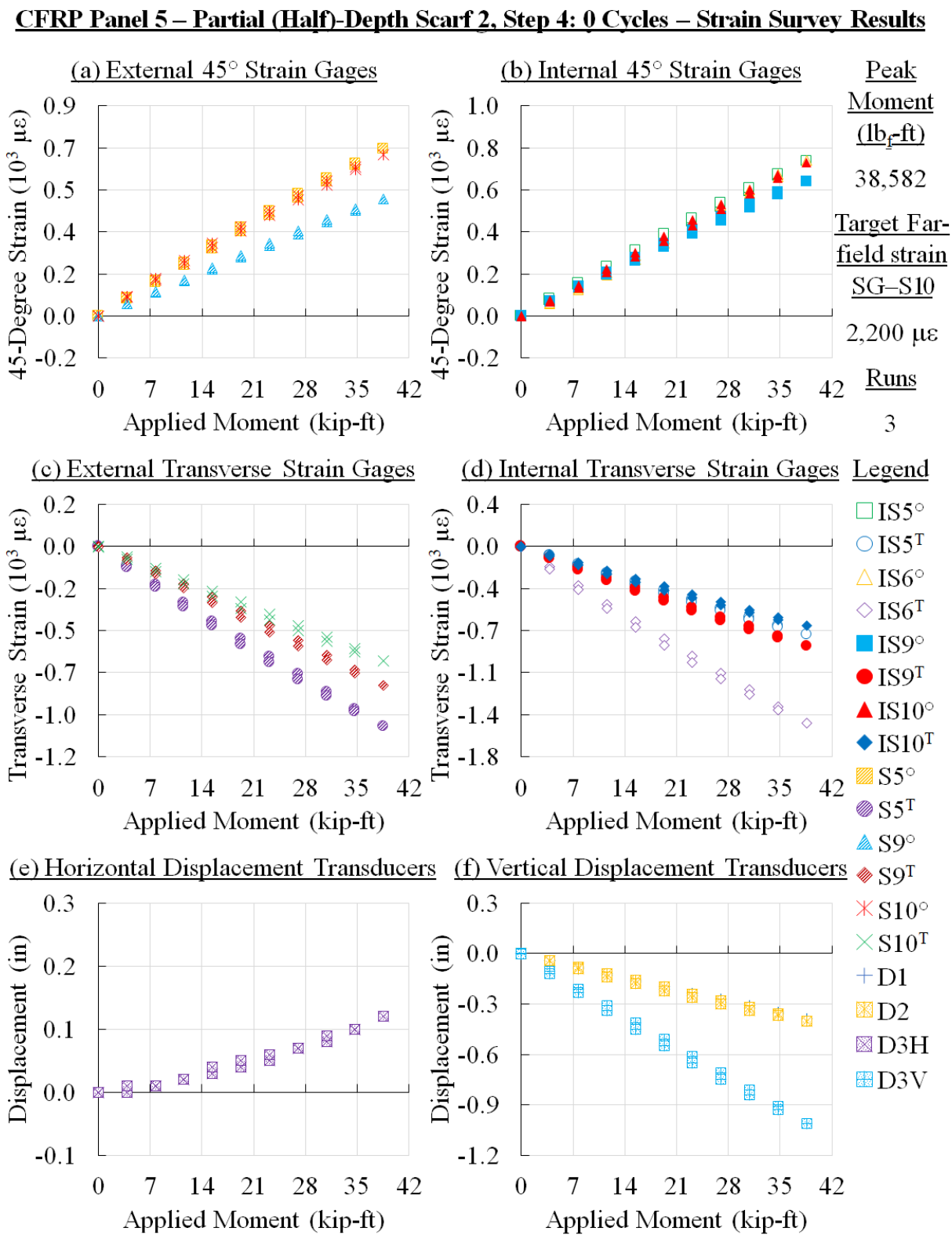


Figure B 40. Panel 5 (additional fatigue at SL strain level): strain survey at 0 cycles (other strain and displacement)

**CFRP Panel 5 – Partial (Half)-Depth Scarf 2, Step 4: 12,000 Cycles – Strain Survey Results**

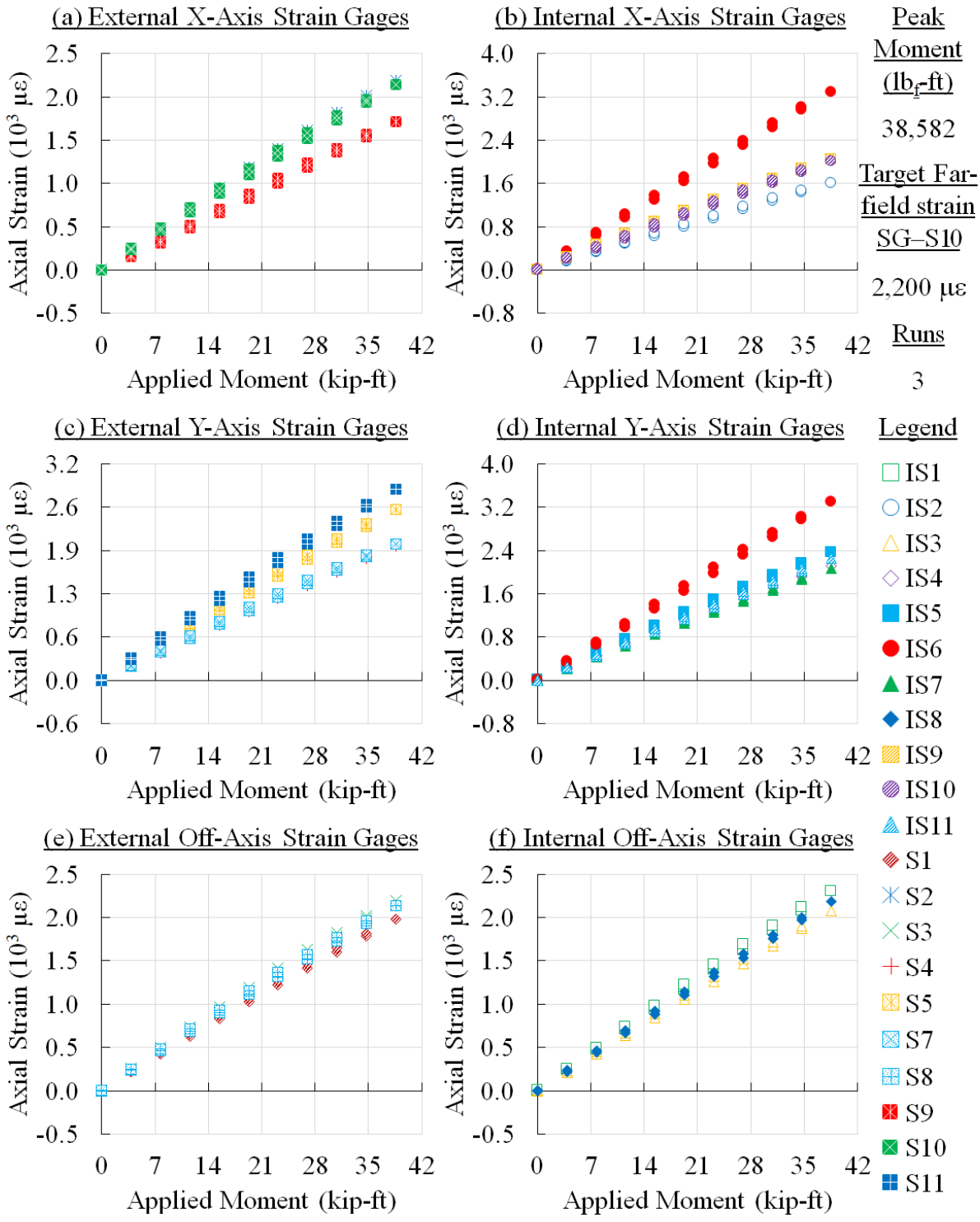


Figure B 41. Panel 5 (additional fatigue at SL strain level): strain survey at 12,000 cycles (axial strain)

**CFRP Panel 5 – Partial (Half)-Depth Scarf 2, Step 4: 12,000 Cycles – Strain Survey Results**

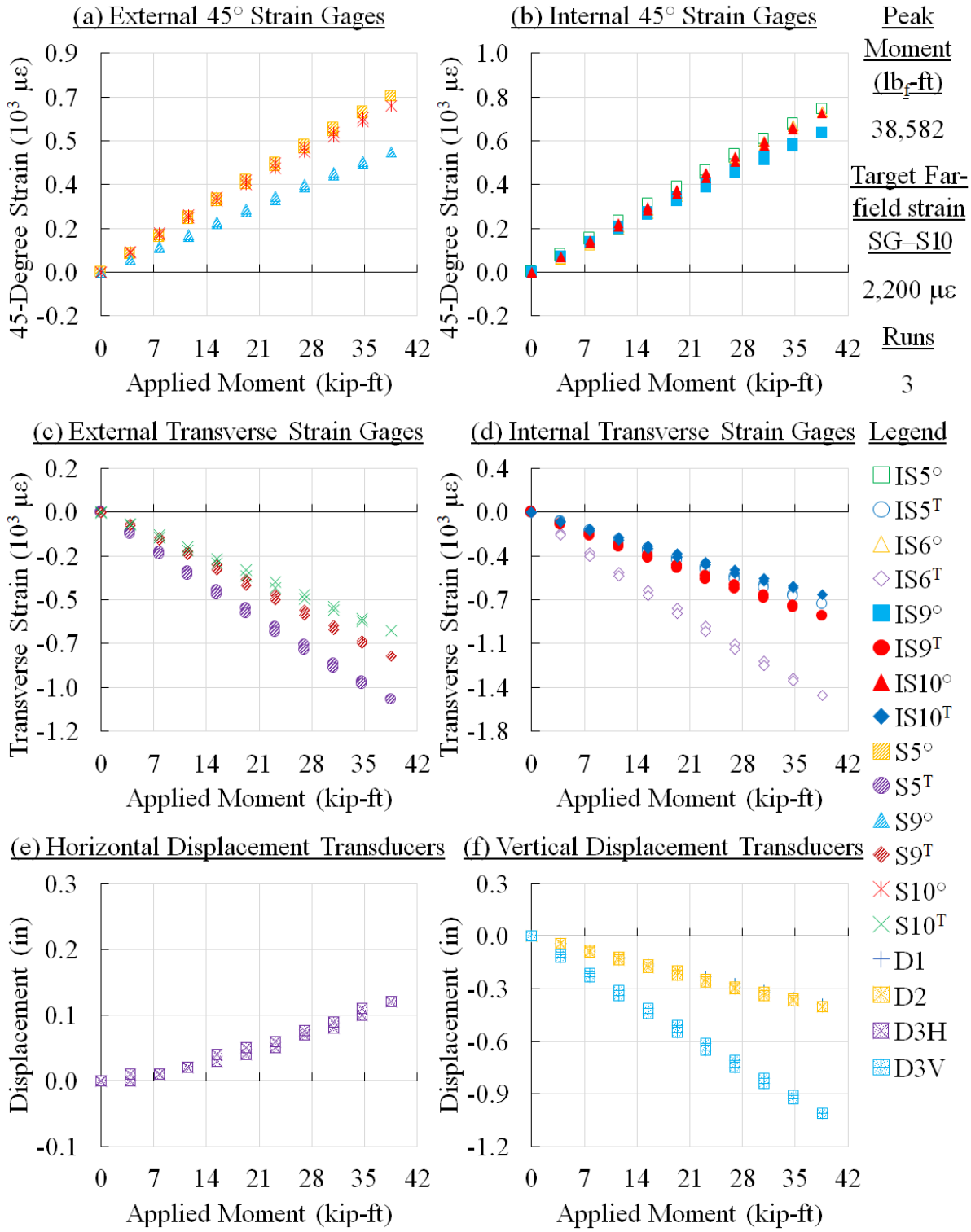


Figure B 42. Panel 5 (additional fatigue at SL strain level): strain survey at 12,000 cycles (other strain and displacement)

**CFRP Panel 5 – Partial (Half)-Depth Scarf 2, Step 4: 24,000 Cycles – Strain Survey Results**

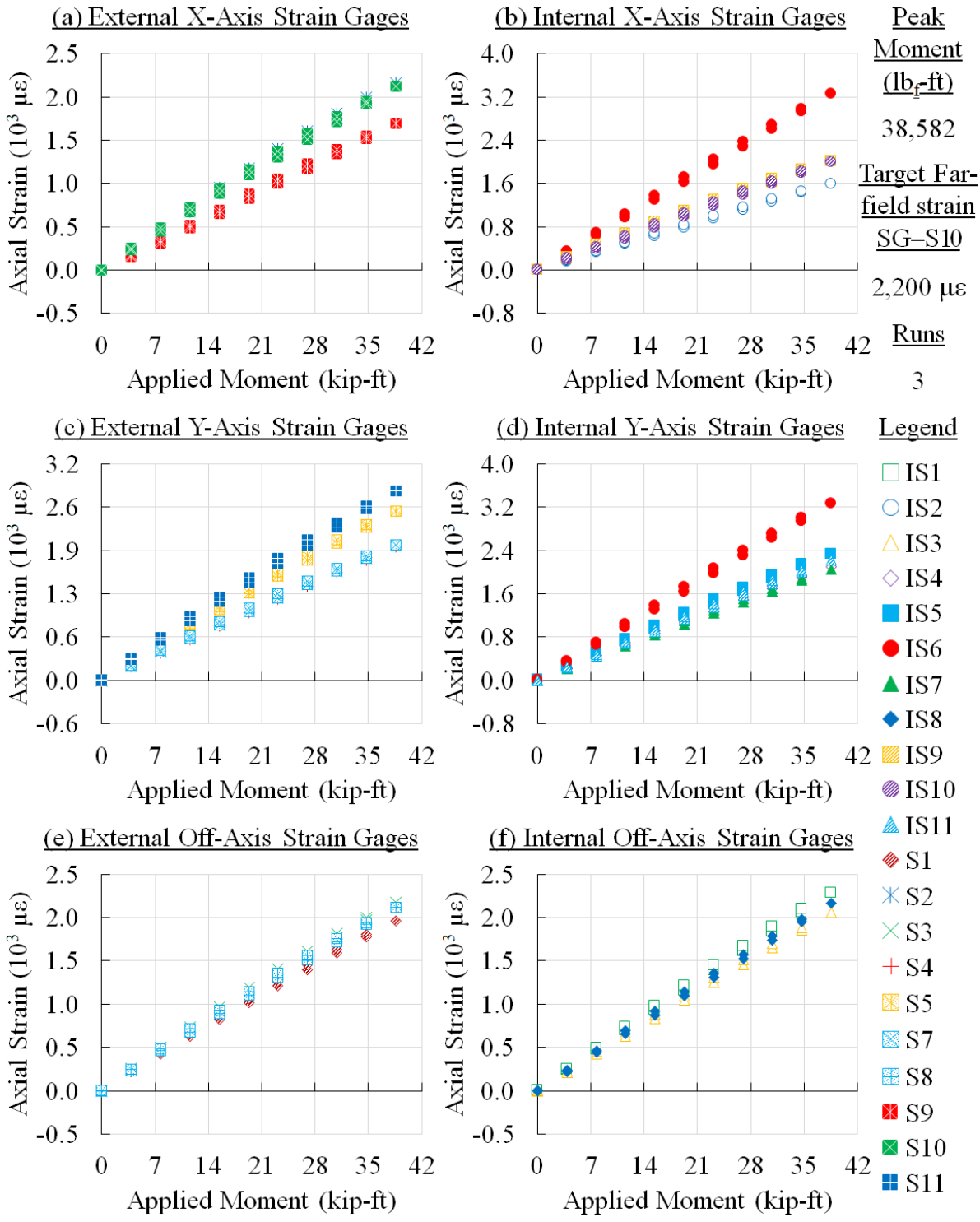


Figure B 43. Panel 5 (additional fatigue at SL strain level): strain survey at 24,000 cycles (axial strain)

**CFRP Panel 5 – Partial (Half)-Depth Scarf 2, Step 4: 24,000 Cycles – Strain Survey Results**

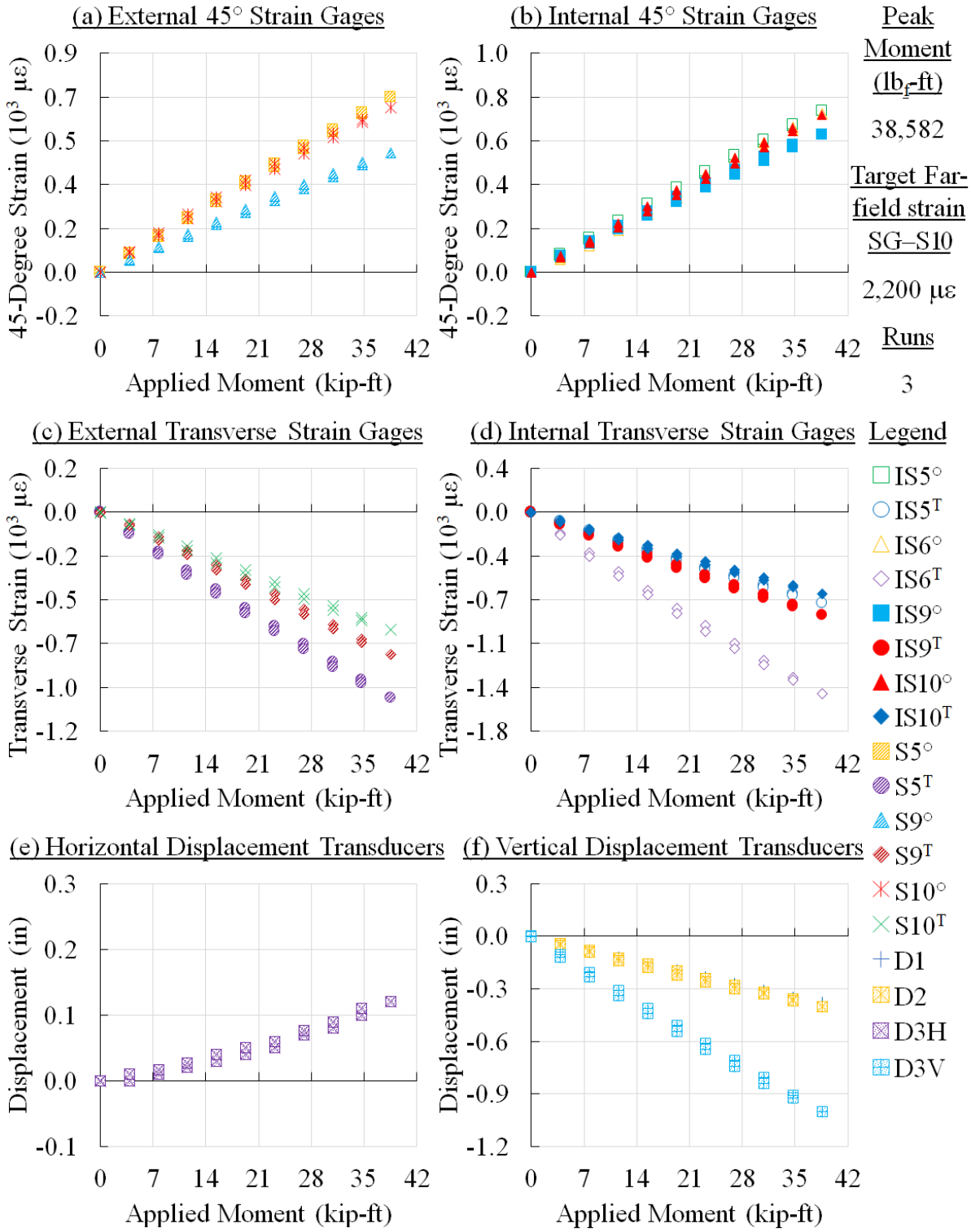


Figure B 44. Panel 5 (additional fatigue at SL strain level): strain survey at 24,000 cycles (other strain and displacement)

**CFRP Panel 5 – Partial (Half)-Depth Scarf 2, Step 4: 36,000 Cycles – Strain Survey Results**

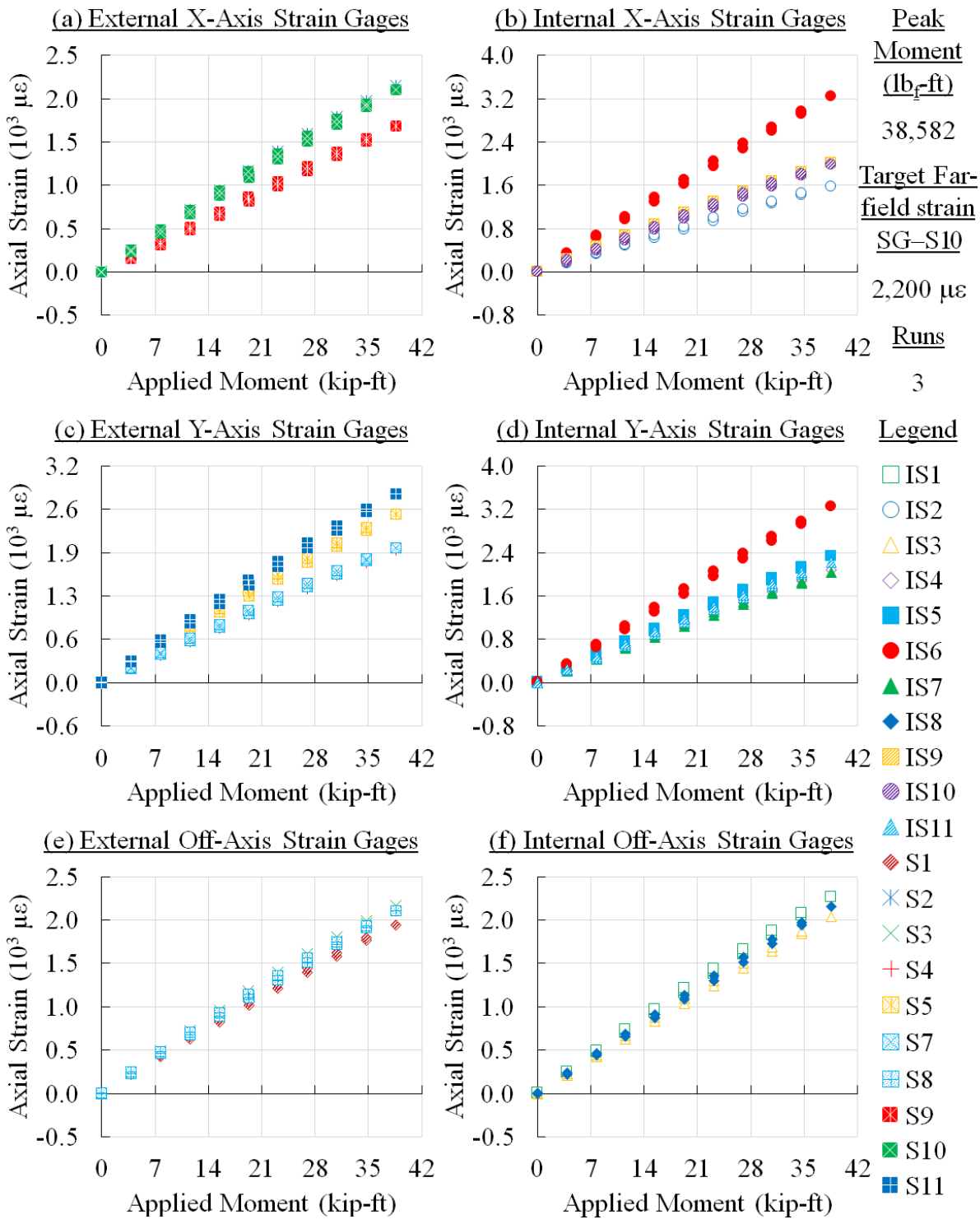


Figure B 45. Panel 5 (additional fatigue at SL strain level): strain survey at 36,000 cycles (axial strain)

**CFRP Panel 5 – Partial (Half)-Depth Scarf 2, Step 4: 36,000 Cycles – Strain Survey Results**

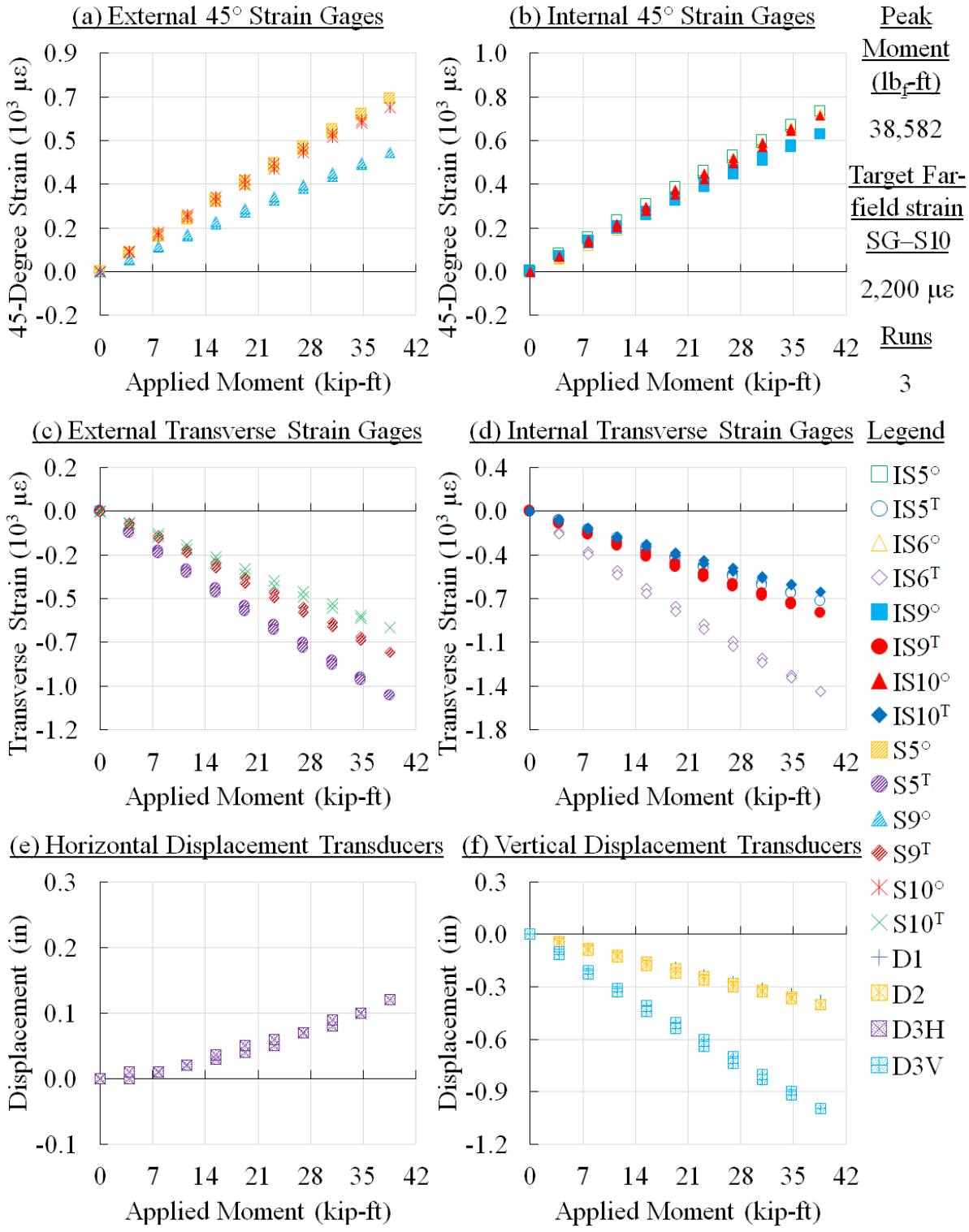


Figure B 46. Panel 5 (additional fatigue at SL strain level): strain survey at 36,000 cycles (other strain and displacement)

**CFRP Panel 5 – Partial (Half)-Depth Scarf 2, Step 4: 48,000 Cycles – Strain Survey Results**

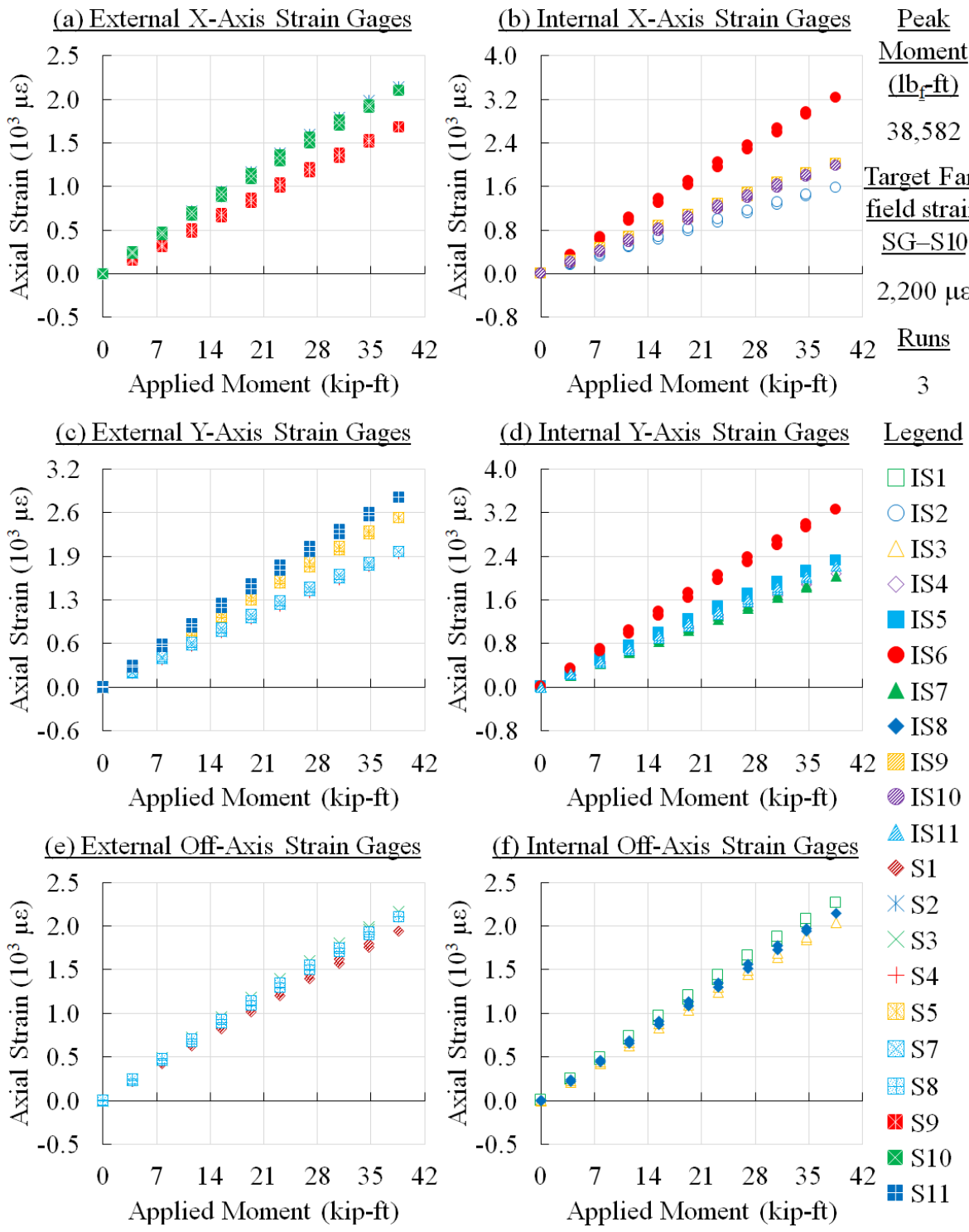


Figure B 47. Panel 5 (additional fatigue at SL strain level): strain survey at 48,000 cycles (axial strain)

**CFRP Panel 5 – Partial (Half)-Depth Scarf 2, Step 4: 48,000 Cycles – Strain Survey Results**

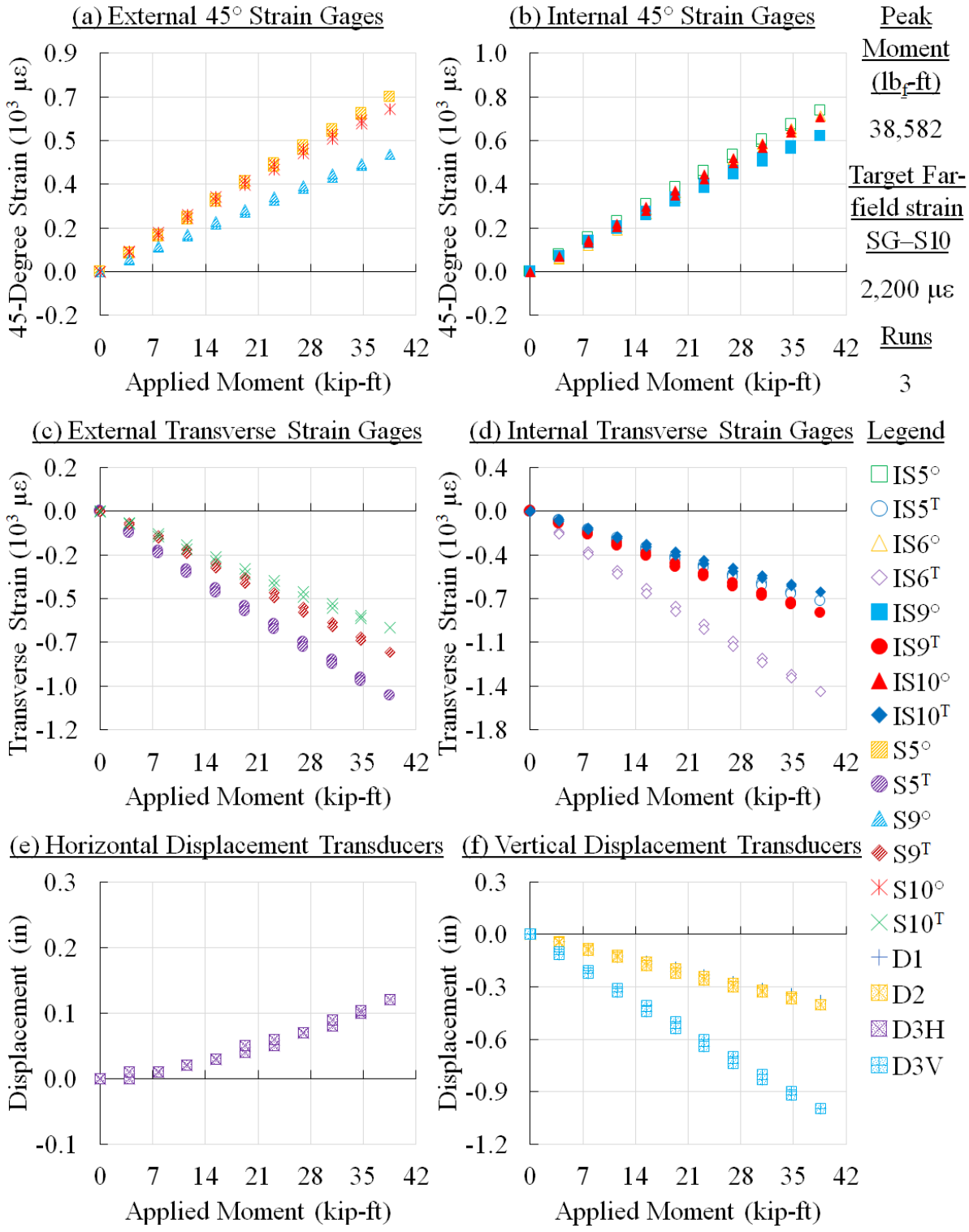


Figure B 48. Panel 5 (additional fatigue at SL strain level): strain survey at 48,000 cycles (other strain and displacement)

**CFRP Panel 5 – Partial (Half)-Depth Scarf 2, Step 4: 72,000 Cycles – Strain Survey Results**

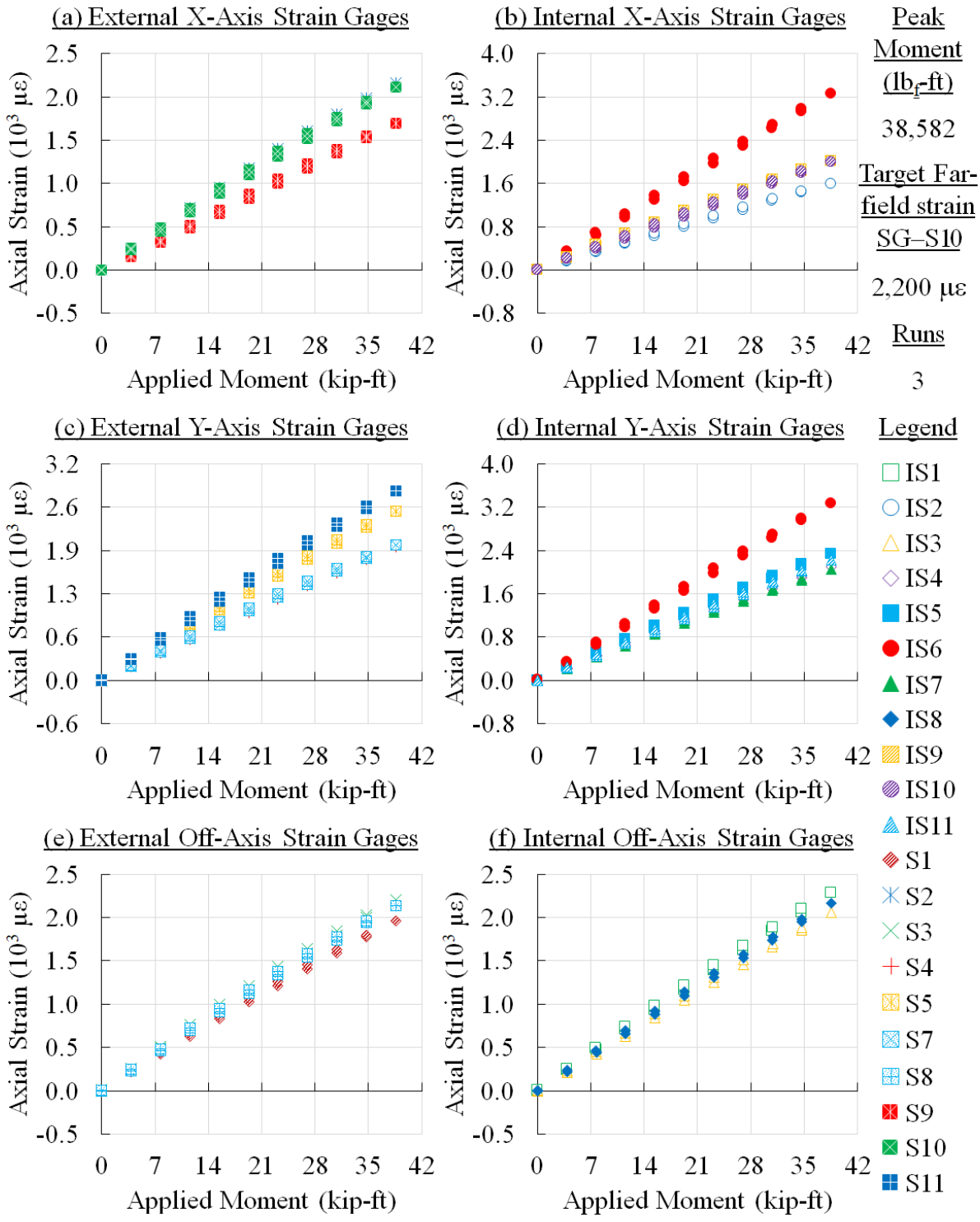


Figure B 49. Panel 5 (additional fatigue at SL strain level): strain survey at 72,000 cycles (axial strain)

**CFRP Panel 5 – Partial (Half)-Depth Scarf 2, Step 4: 72,000 Cycles – Strain Survey Results**

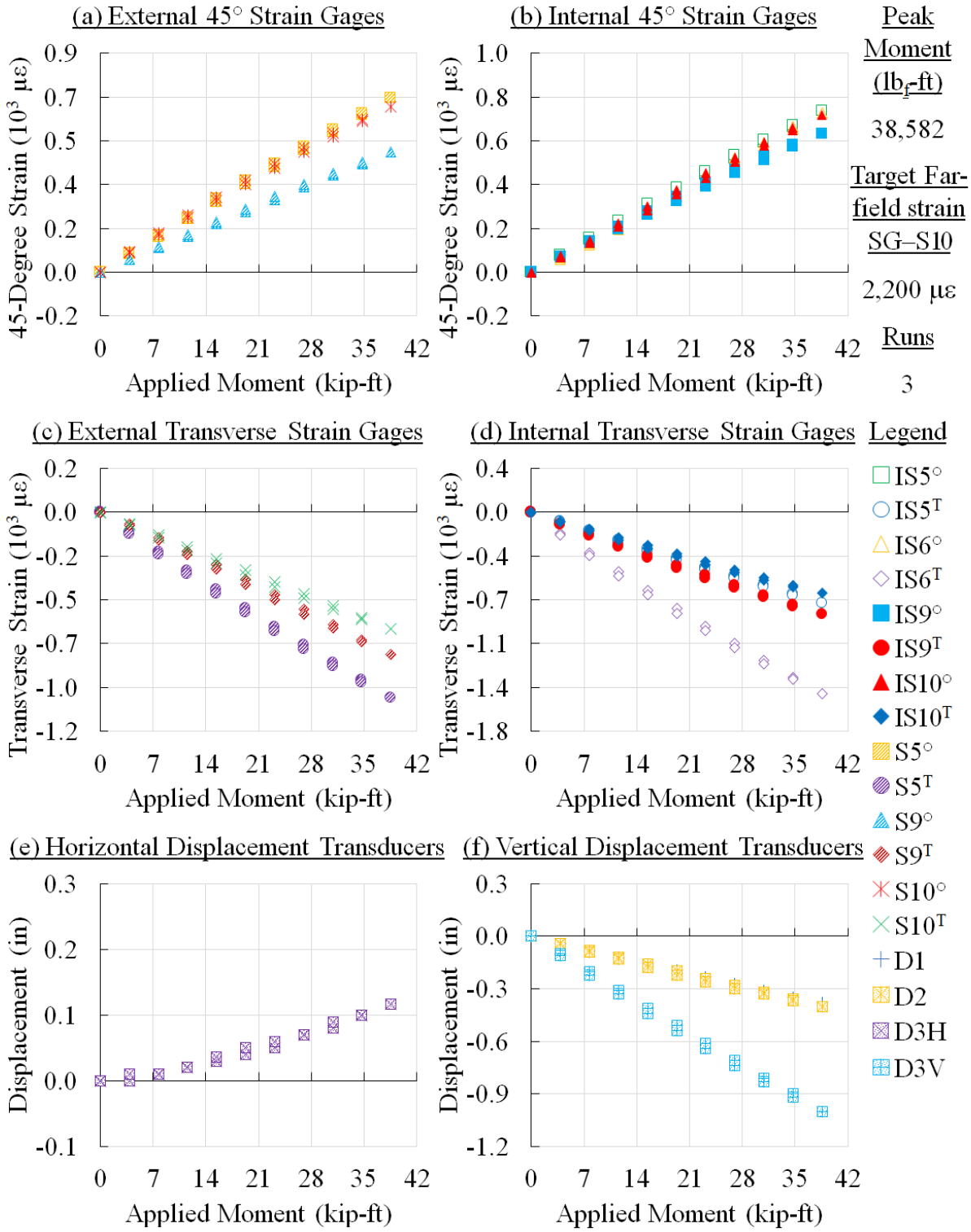


Figure B 50. Panel 5 (additional fatigue at SL strain level): strain survey at 72,000 cycles (other strain and displacement)

**CFRP Panel 5 – Partial (Half)-Depth Scarf 2, Step 4: 96,000 Cycles – Strain Survey Results**

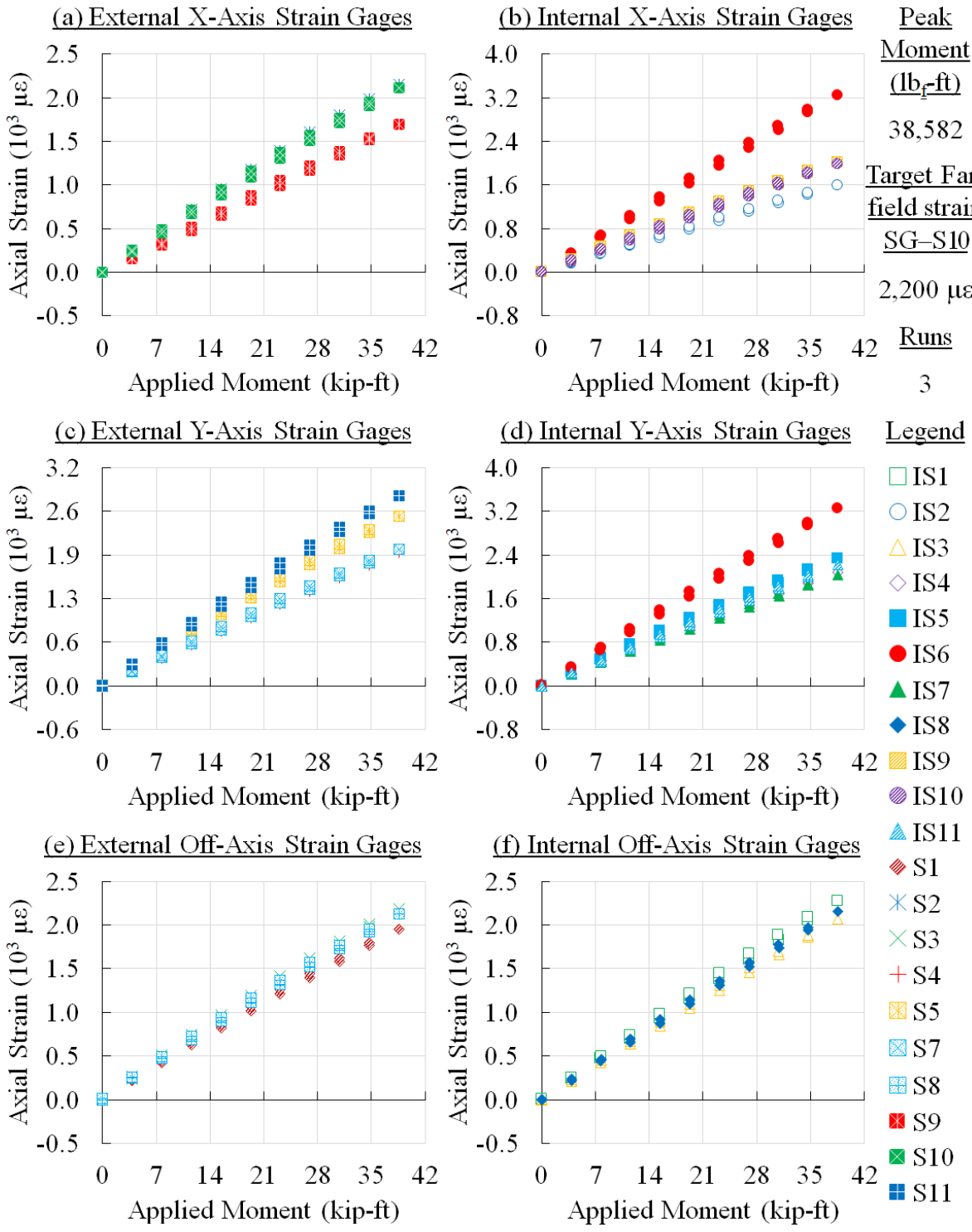


Figure B 51. Panel 5 (additional fatigue at SL strain level): strain survey at 96,000 cycles (axial strain)

**CFRP Panel 5 – Partial (Half)-Depth Scarf 2, Step 4: 96,000 Cycles – Strain Survey Results**

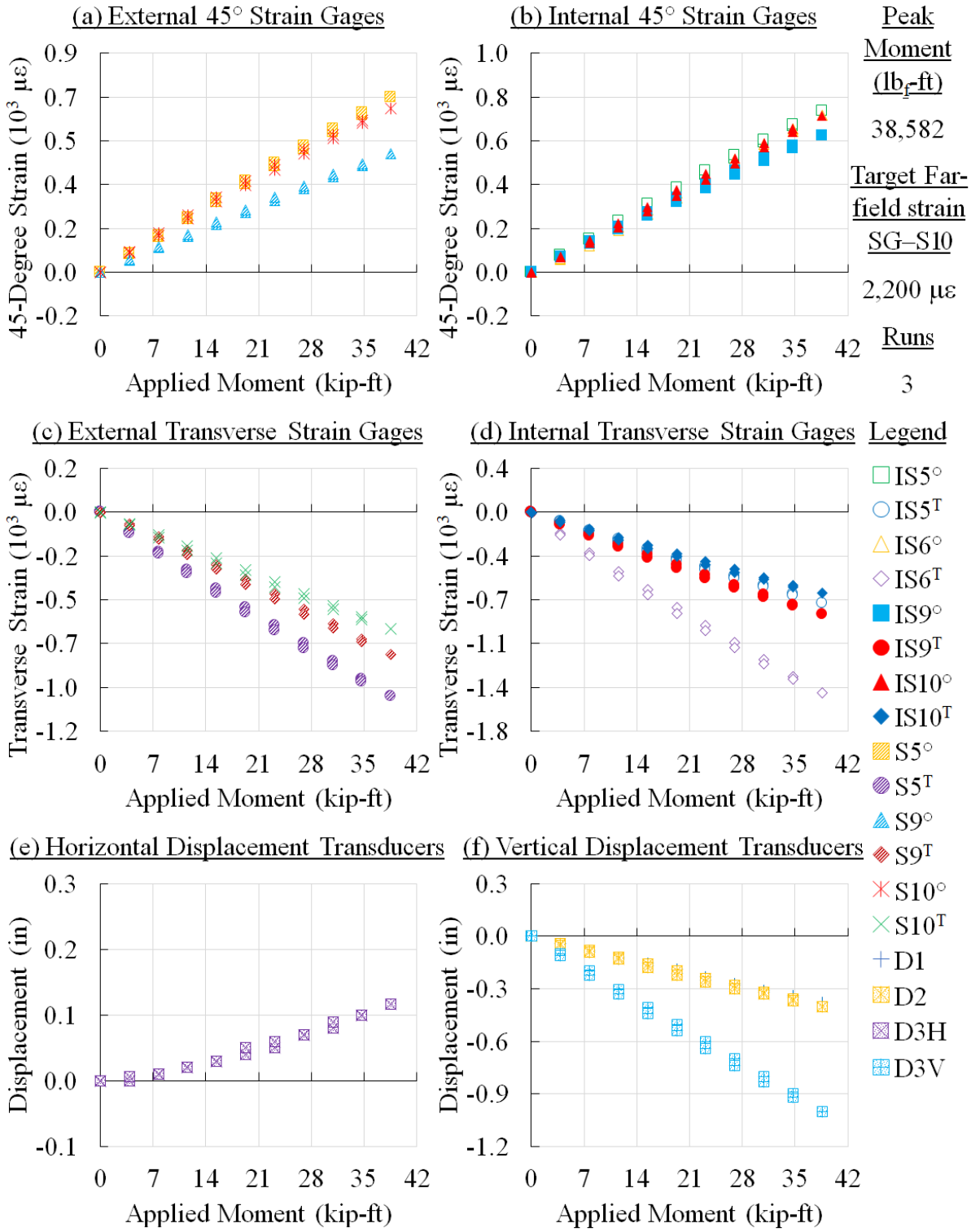


Figure B 52. Panel 5 (additional fatigue at SL strain level): strain survey at 96,000 cycles (other strain and displacement)

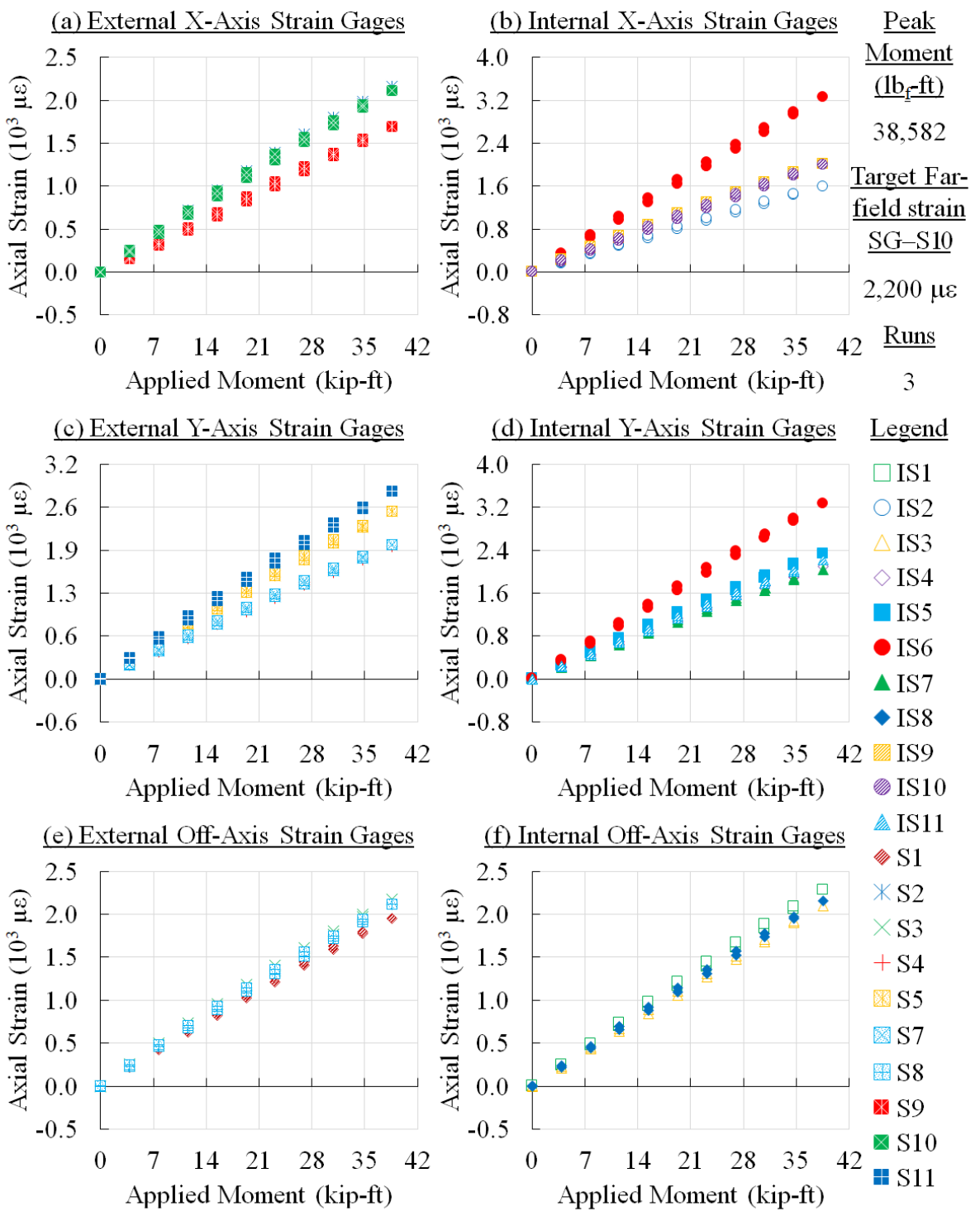


Figure B 53. Panel 5 (additional fatigue at SL strain level): strain survey at 120,000 cycles (axial strain)

**CFRP Panel 5 – Partial (Half)-Depth Scarf 2, Step 4: 120,000 Cycles – Strain Survey Results**

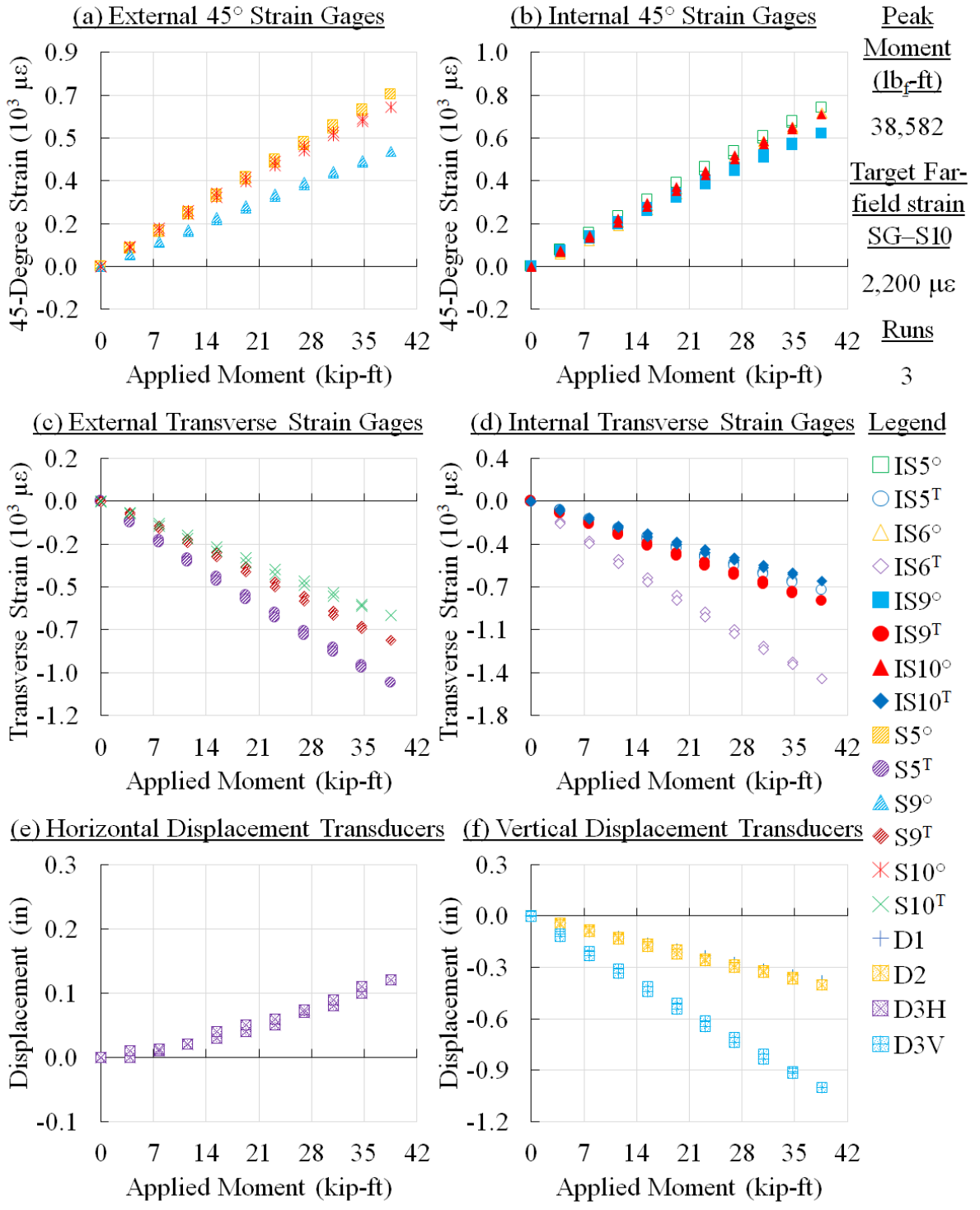


Figure B 54. Panel 5 (additional fatigue at SL strain level): strain survey at 120,000 cycles (other strain and displacement)

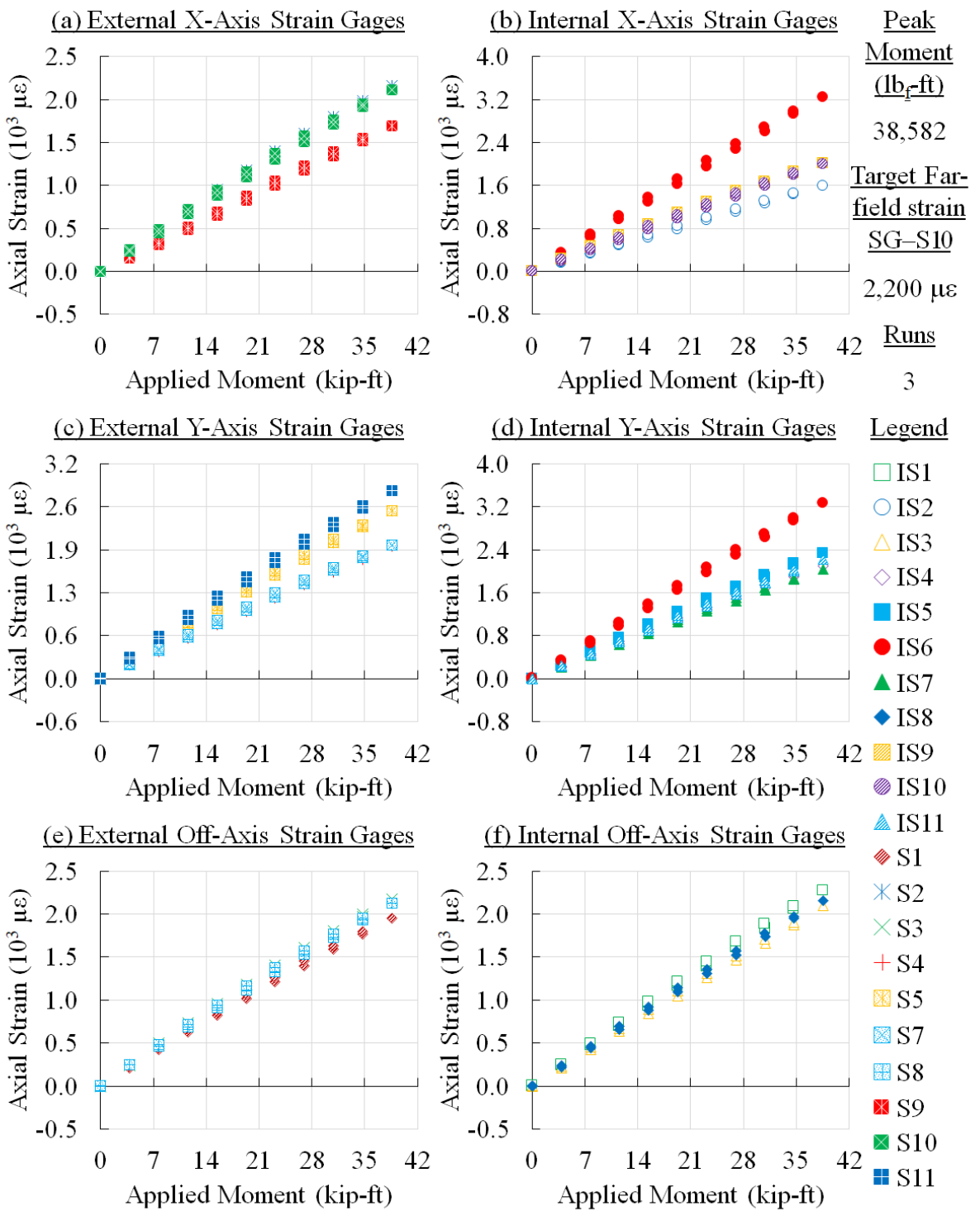


Figure B 55. Panel 5 (additional fatigue at SL strain level): strain survey at 144,000 cycles (axial strain)

**CFRP Panel 5 – Partial (Half)-Depth Scarf 2, Step 4: 144,000 Cycles – Strain Survey Results**

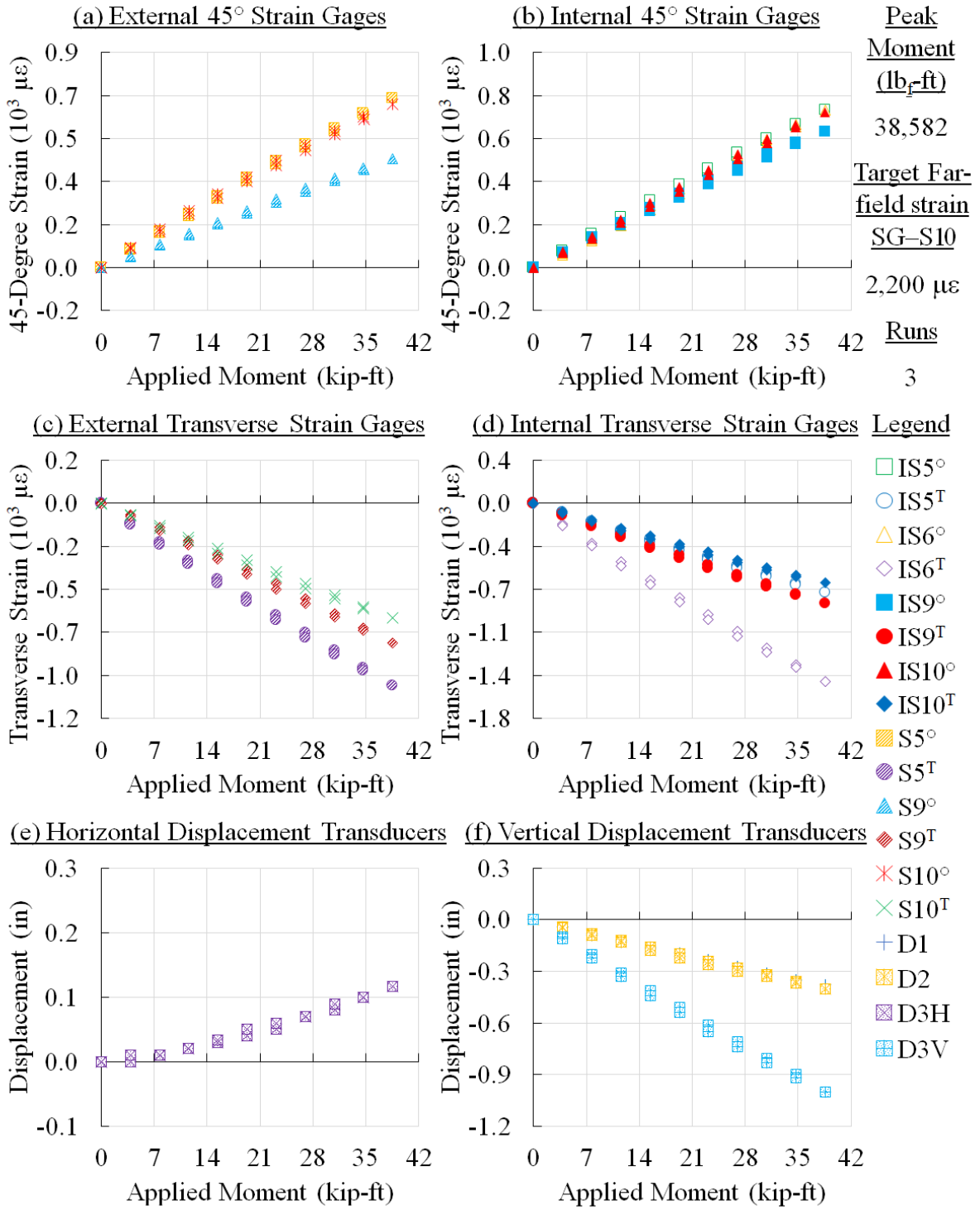


Figure B 56. Panel 5 (additional fatigue at SL strain level): strain survey at 144,000 cycles (other strain and displacement)

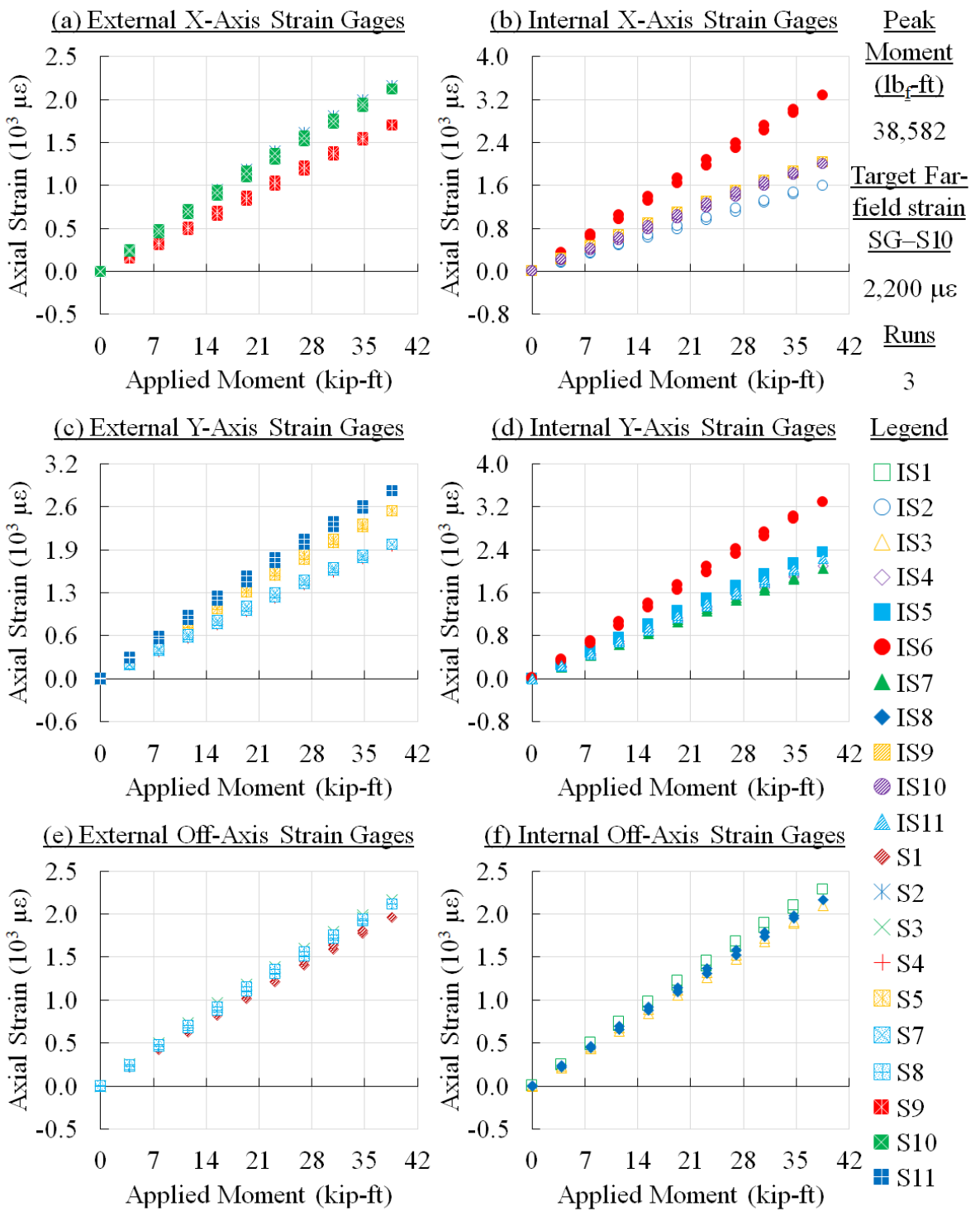


Figure B 57. Panel 5 (additional fatigue at SL strain level): strain survey at 165,000 cycles (axial strain)

**CFRP Panel 5 – Partial (Half)-Depth Scarf 2, Step 4: 165,000 Cycles – Strain Survey Results**

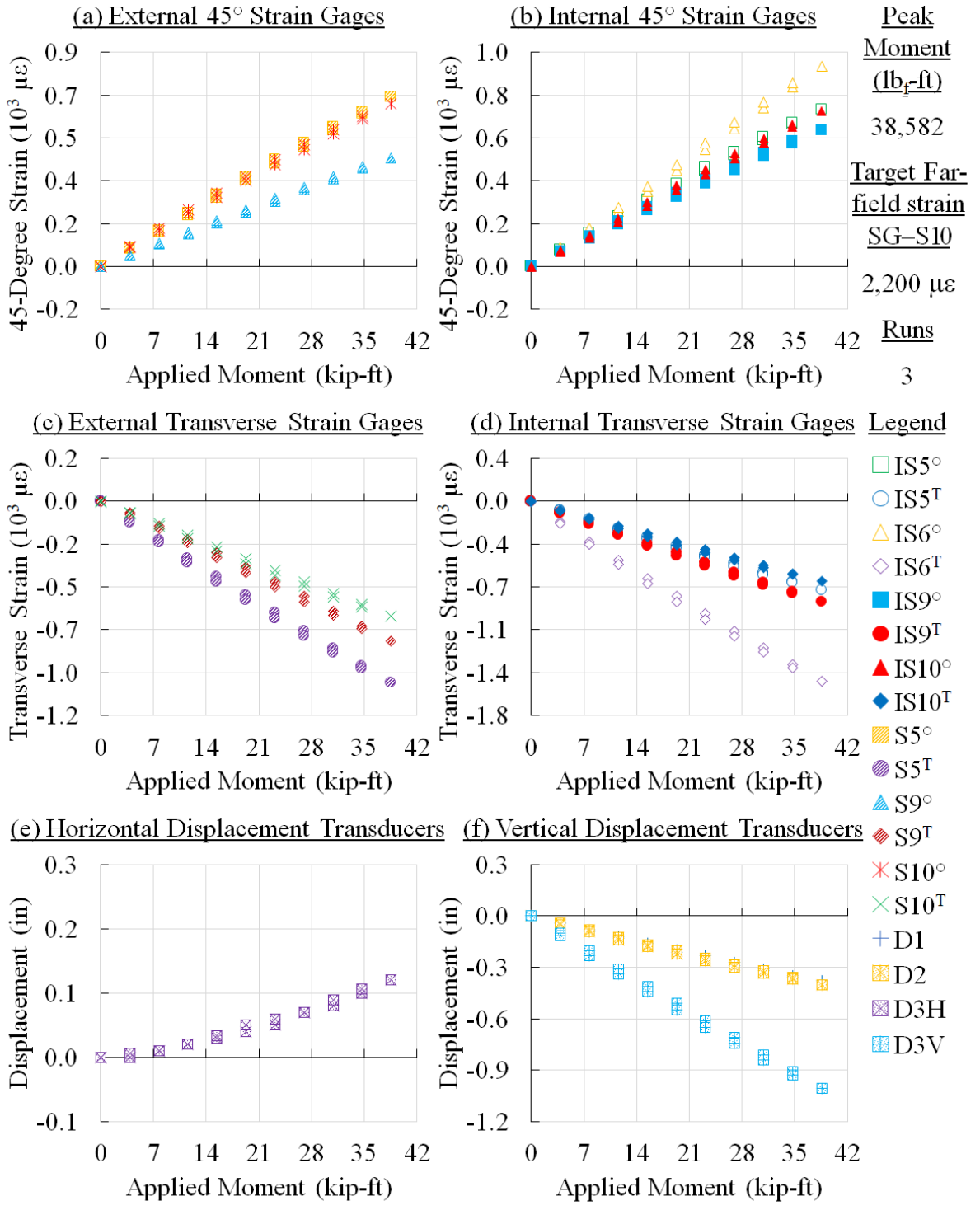


Figure B 58. Panel 5 (additional fatigue at SL strain level): strain survey at 165,000 cycles (other strain and displacement)

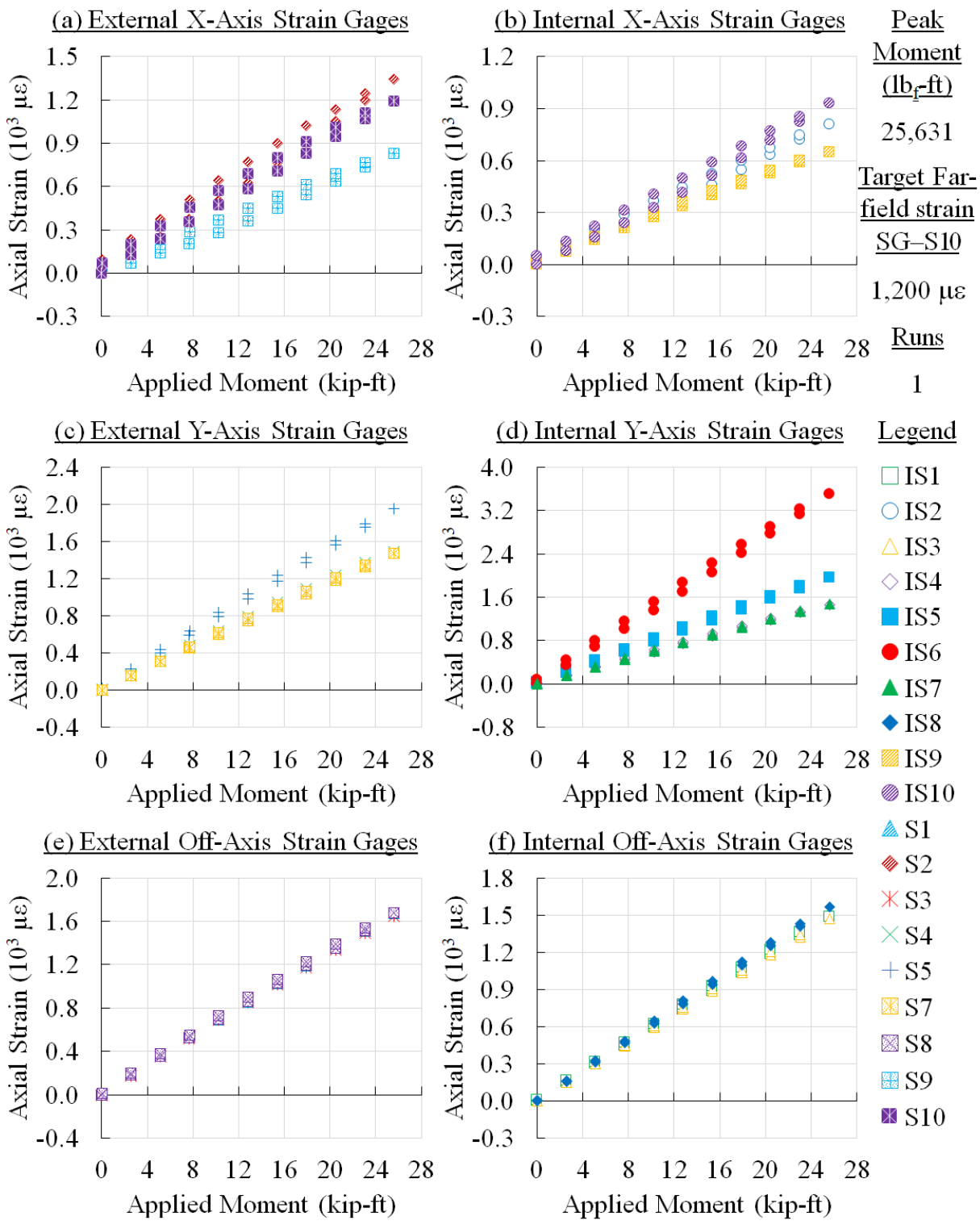


Figure B 59. Panel 4: baseline strain survey (axial strain)

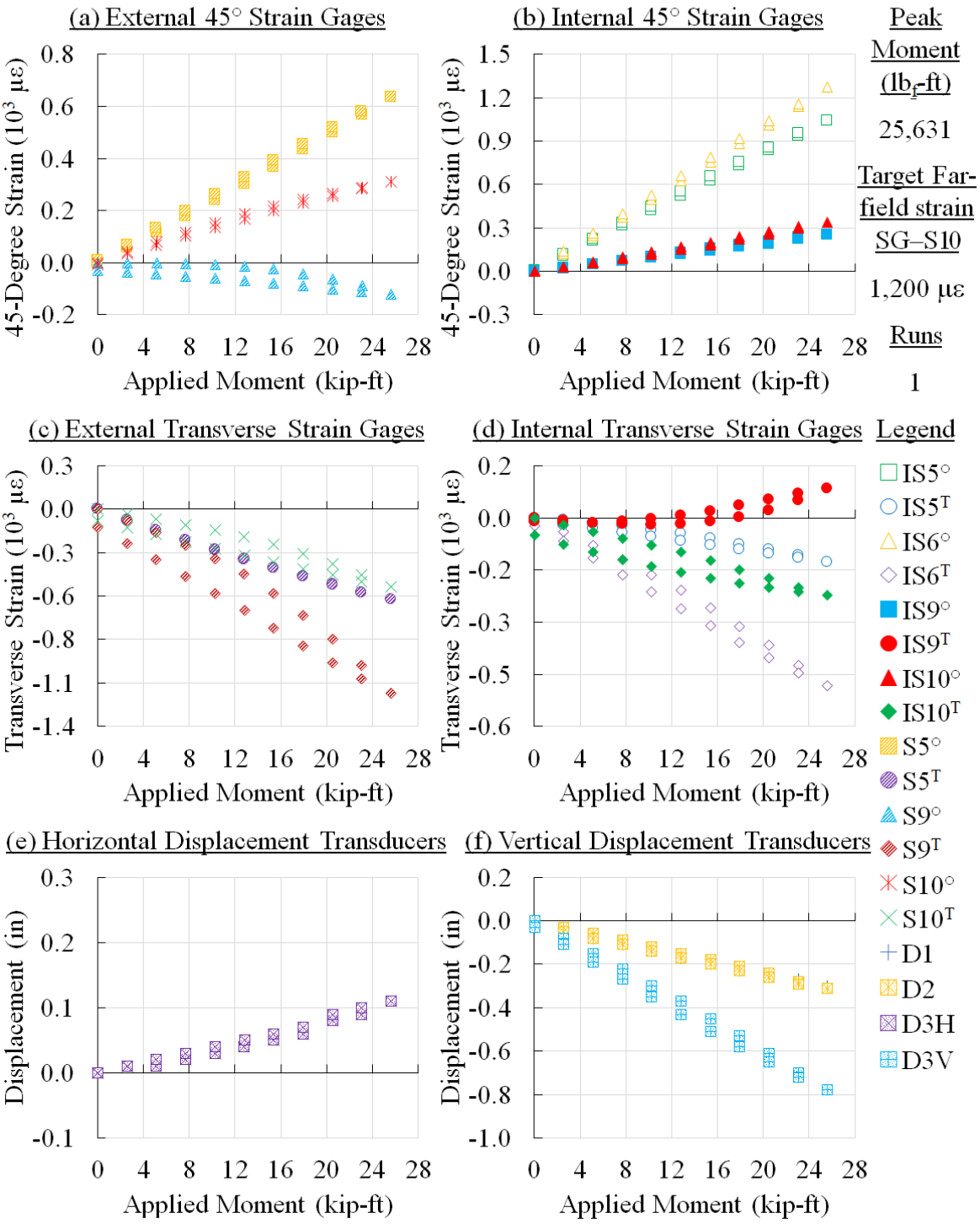


Figure B 60. Panel 4: baseline strain survey (other strain and displacement)

**CFRP Panel 6 – Full-Depth Scarf 2, Step 1: Baseline Strain Survey Results**

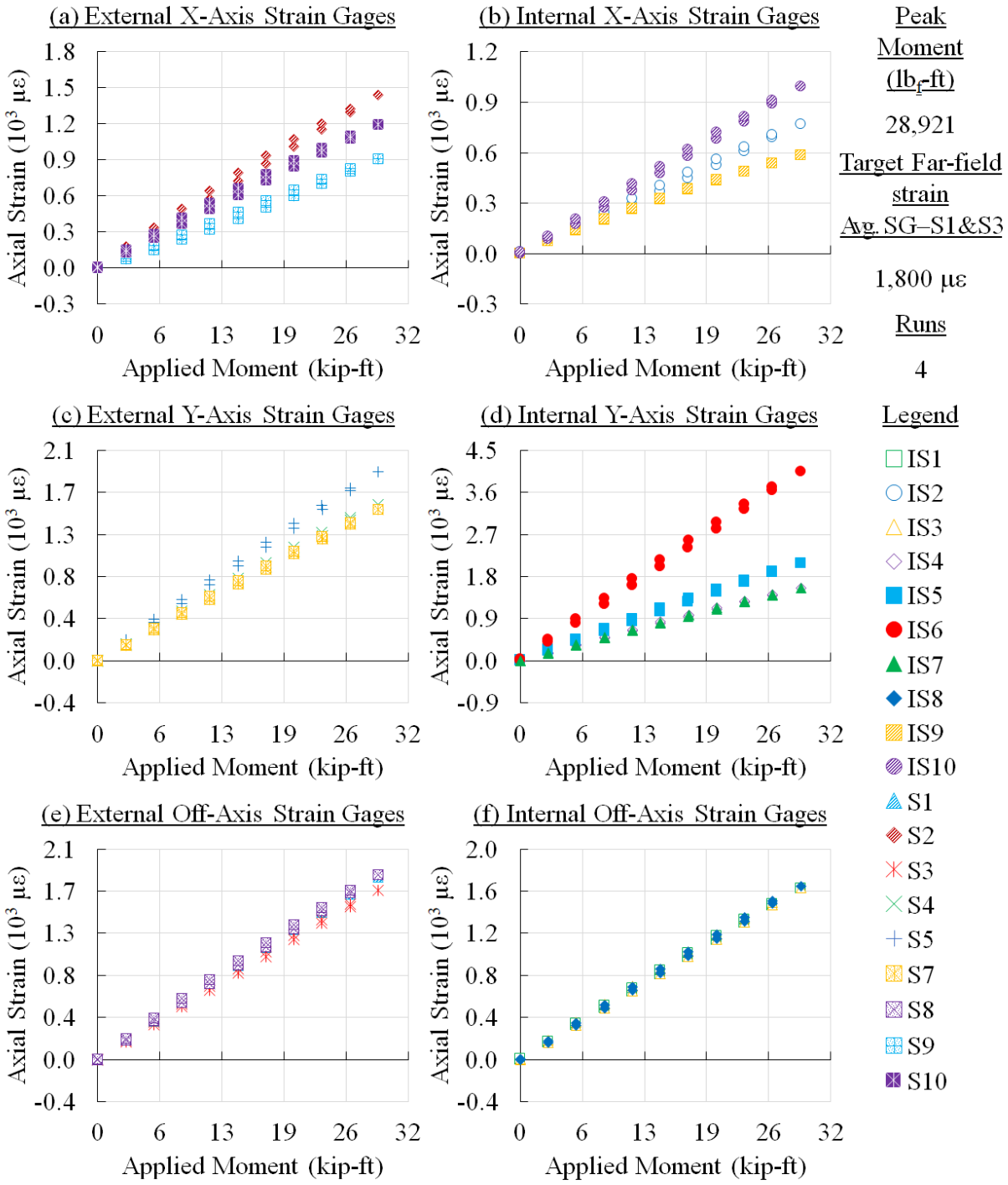


Figure B 61. Panel 6: baseline strain survey (axial strain)

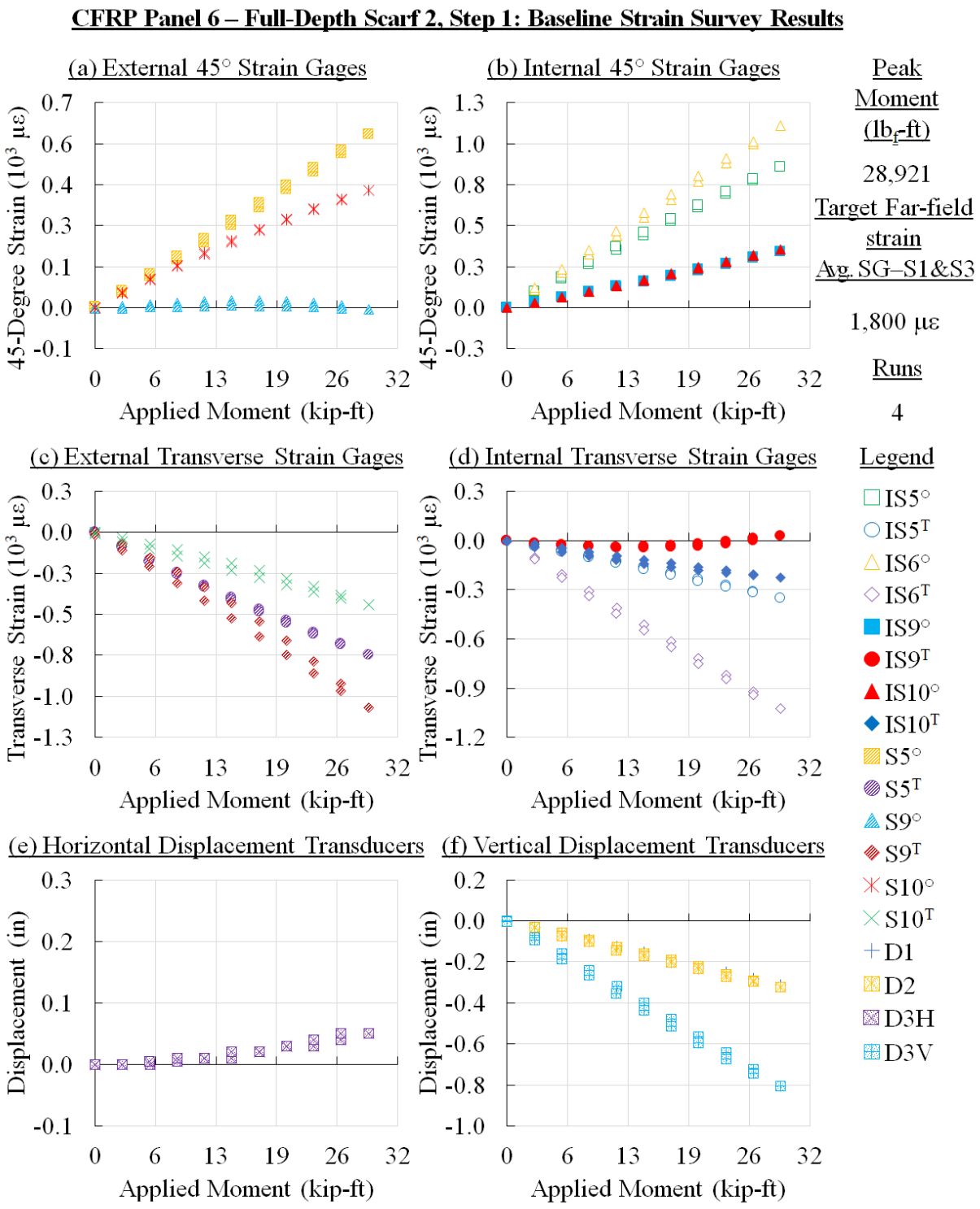


Figure B 62. Panel 6: baseline strain survey (other strain and displacement)

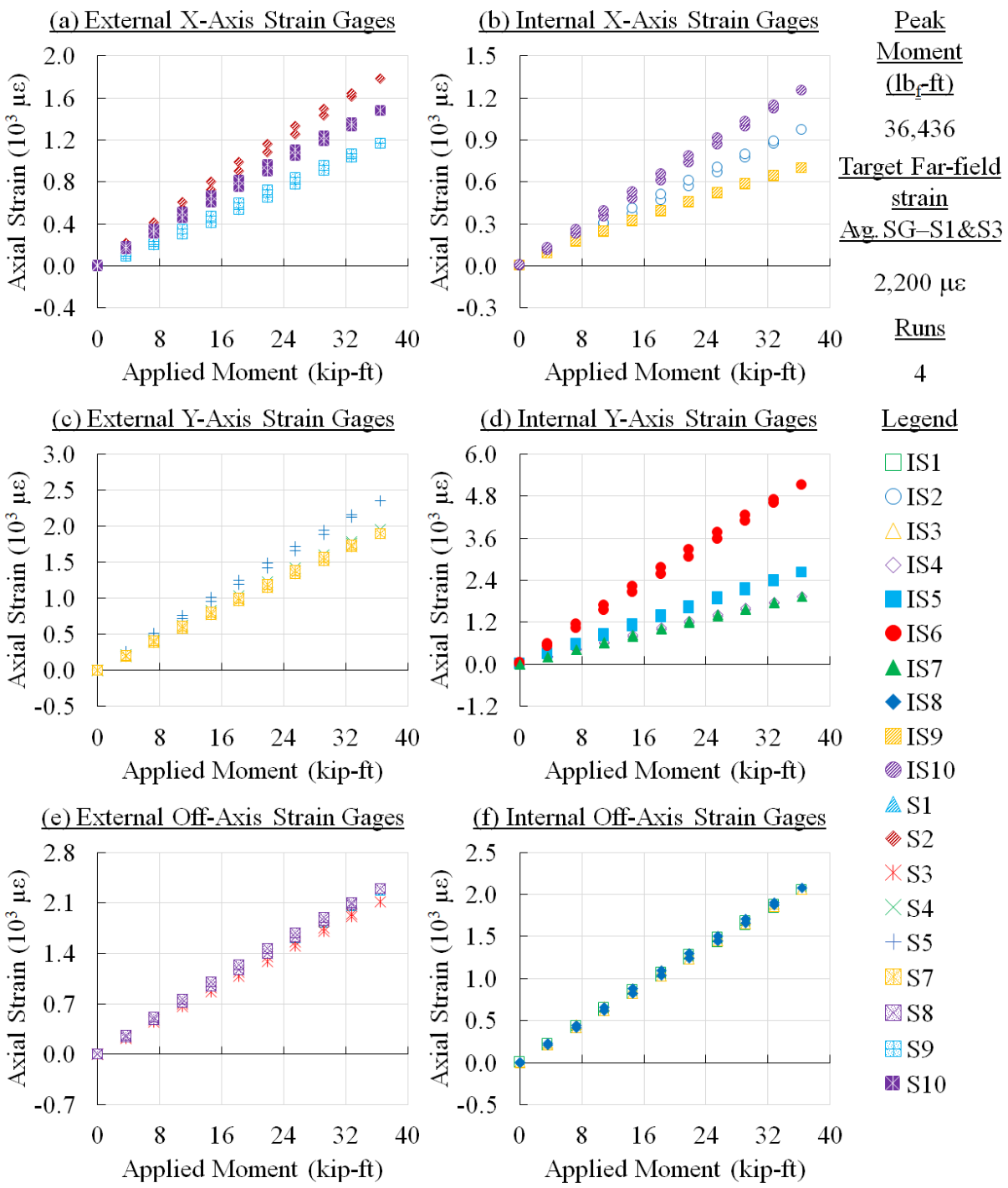


Figure B 63. Panel 6 (fatigue at SL strain level): strain survey results at 0 cycles (axial strain)

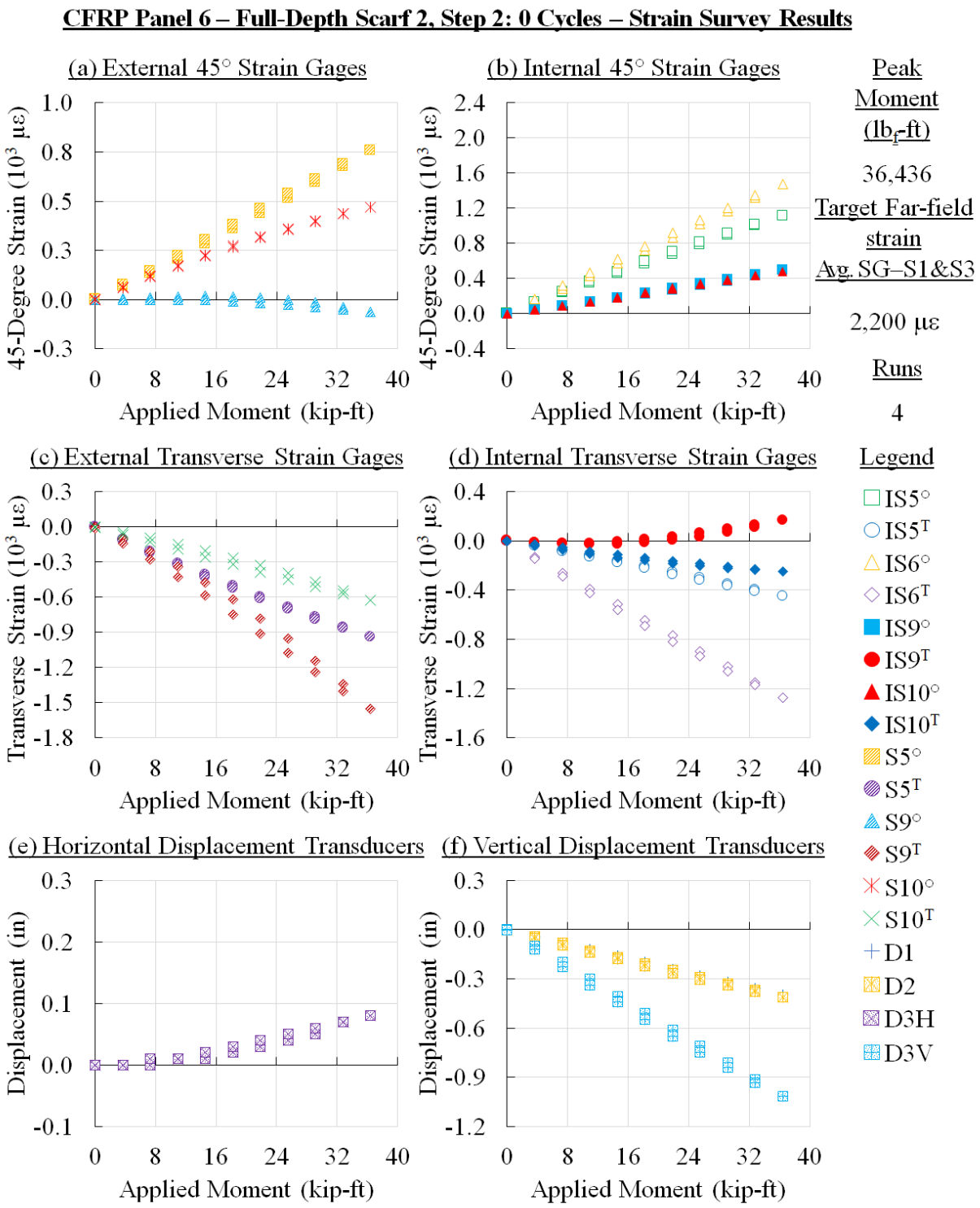


Figure B 64. Panel 6 (fatigue at SL strain level): strain survey at 0 cycles (other strain and displacement)

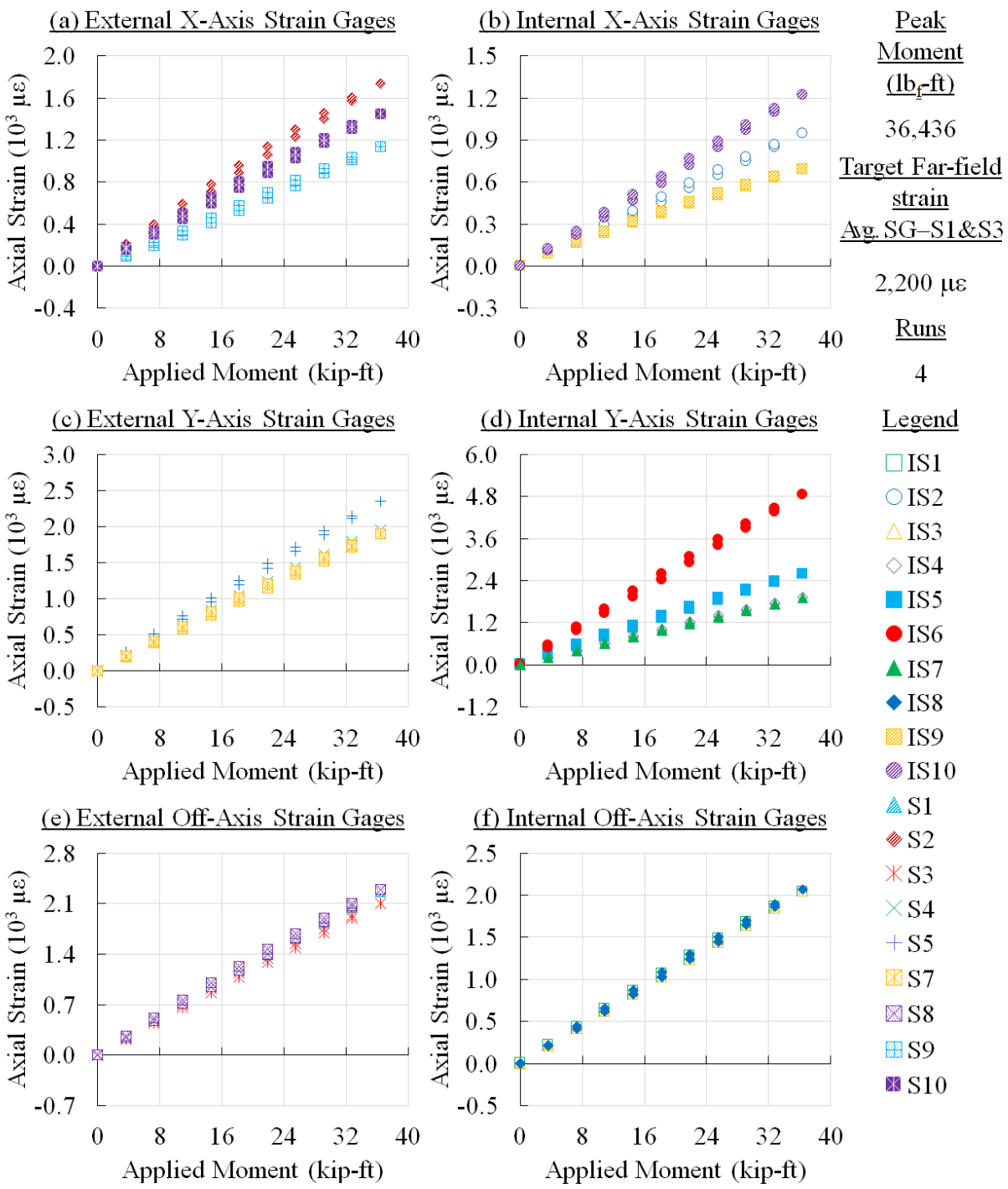


Figure B 65. Panel 6 (fatigue at SL strain level): strain survey at 12,000 cycles (axial strain)

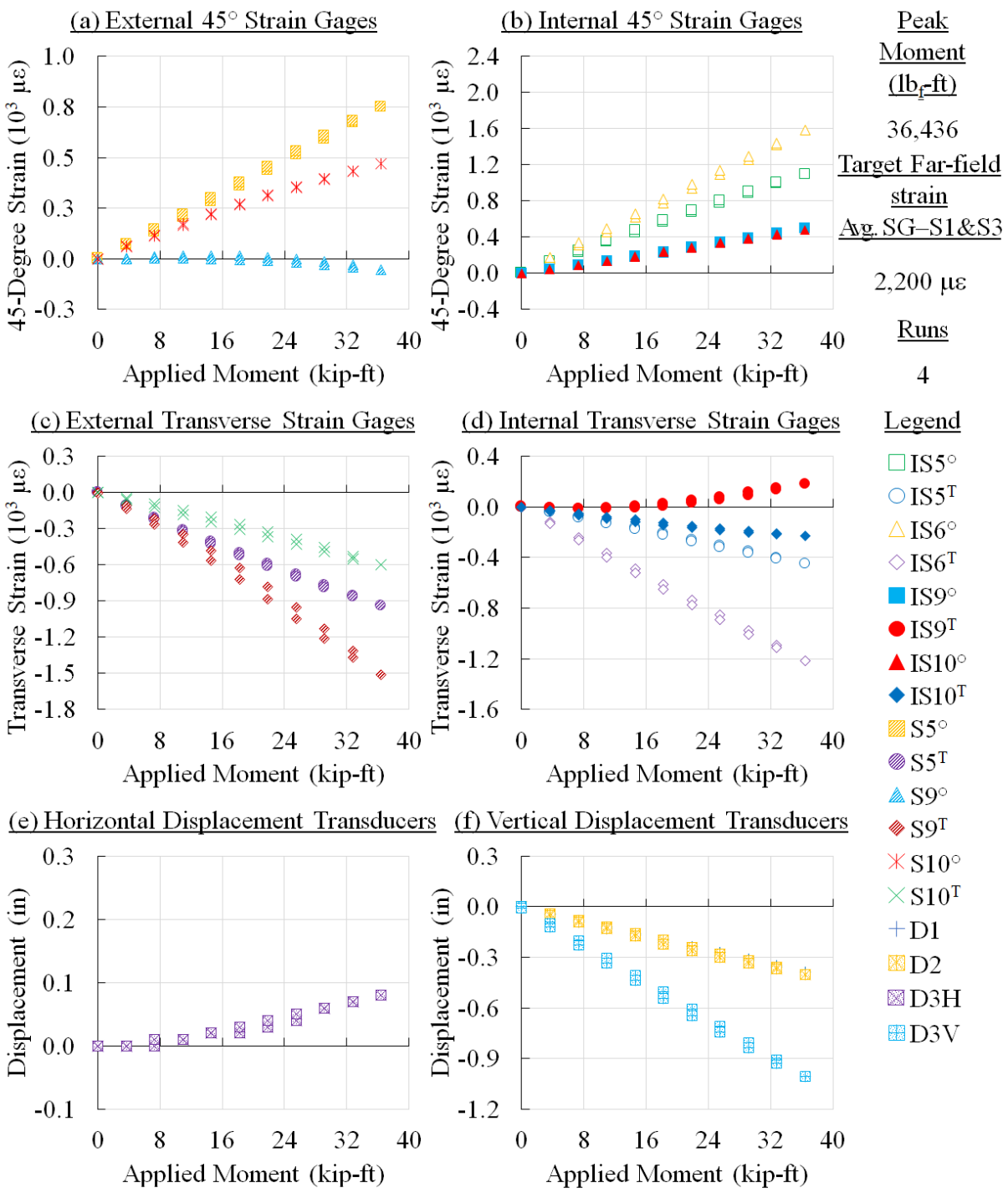


Figure B 66. Panel 6 (fatigue at SL strain level): strain survey at 12,000 cycles (other strain and displacement)

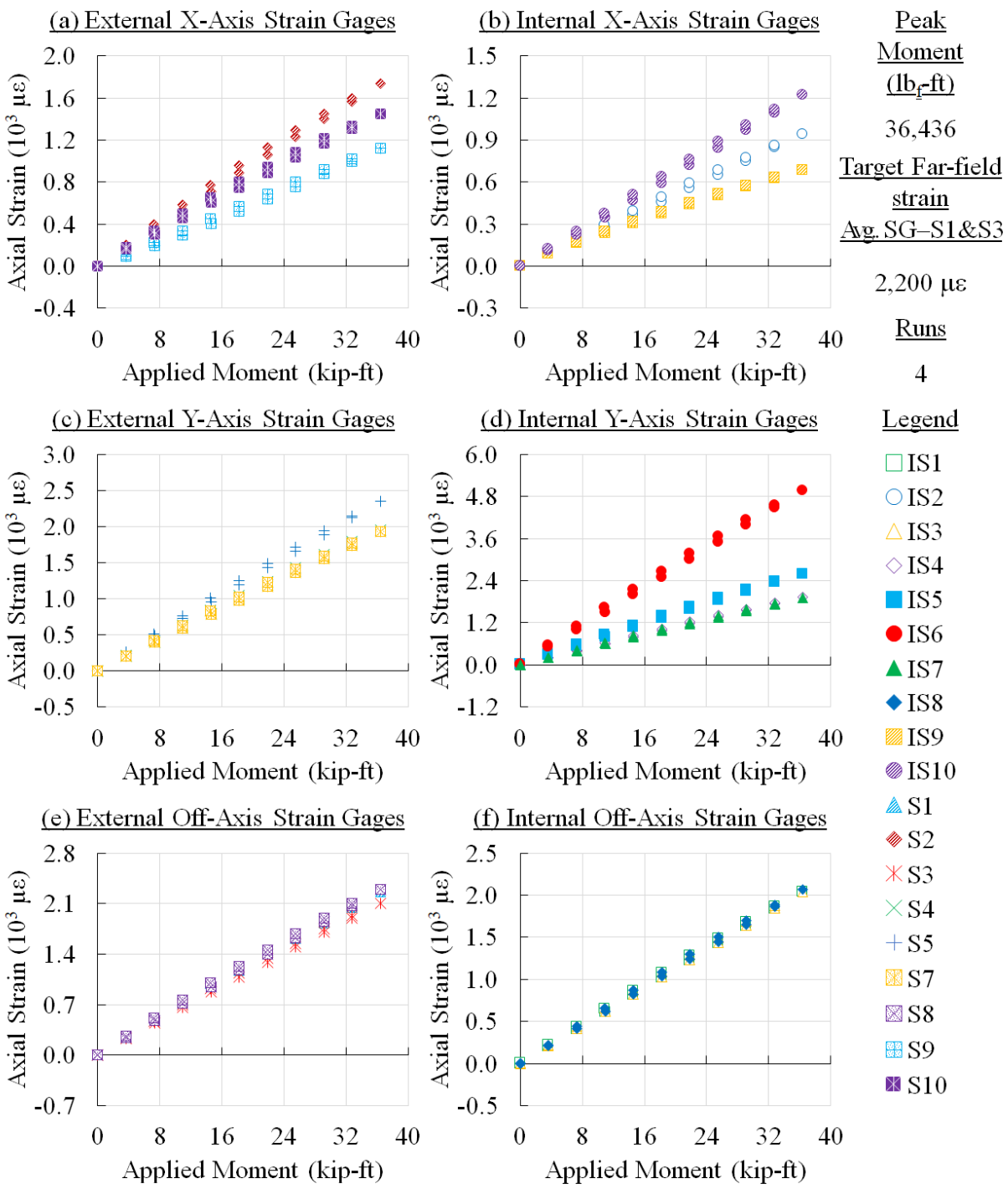


Figure B 67. Panel 6 (fatigue at SL strain level): strain survey at 24,000 cycles (axial strain)

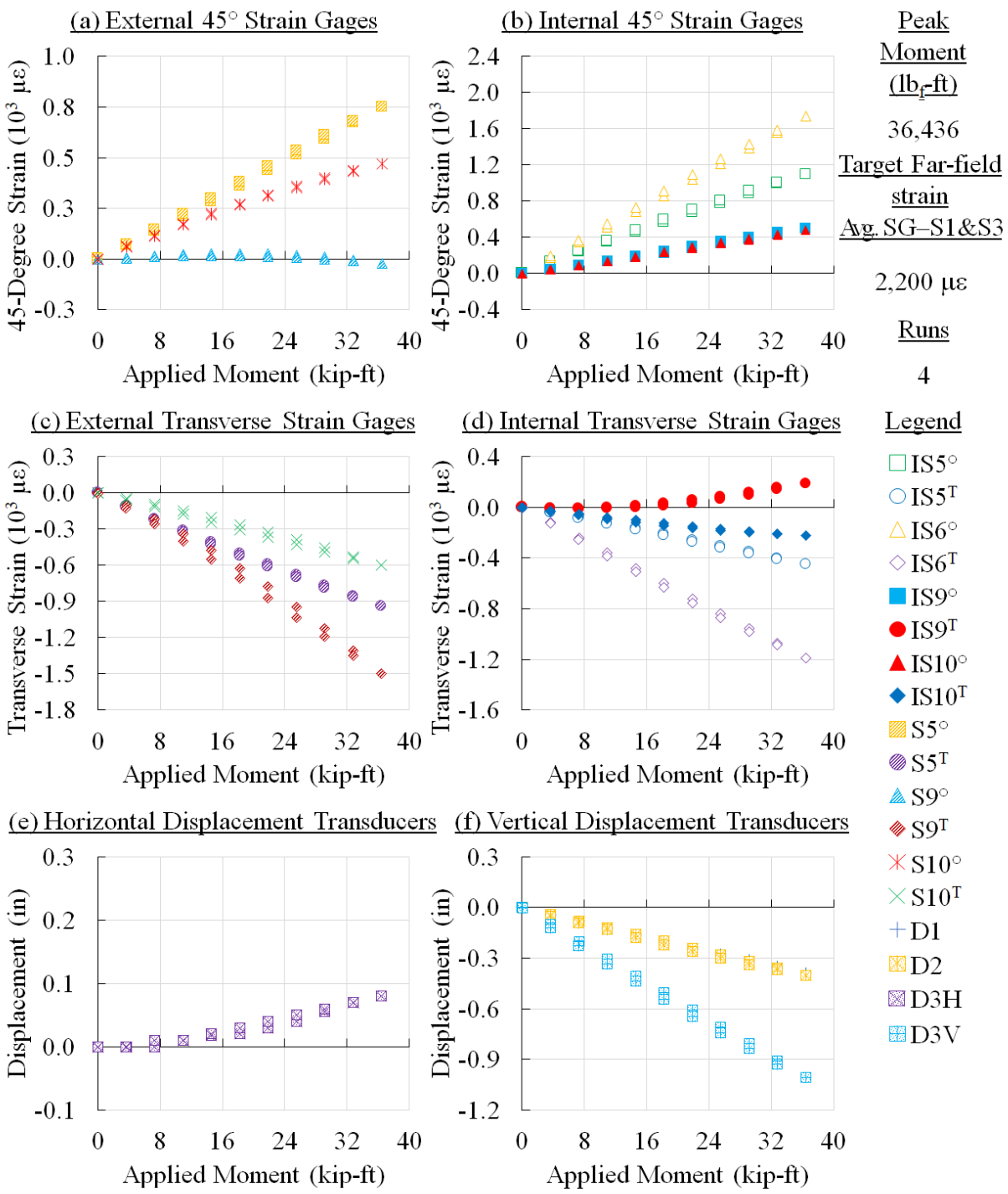


Figure B 68. Panel 6 (fatigue at SL strain level): strain survey at 24,000 cycles (other strain and displacement)

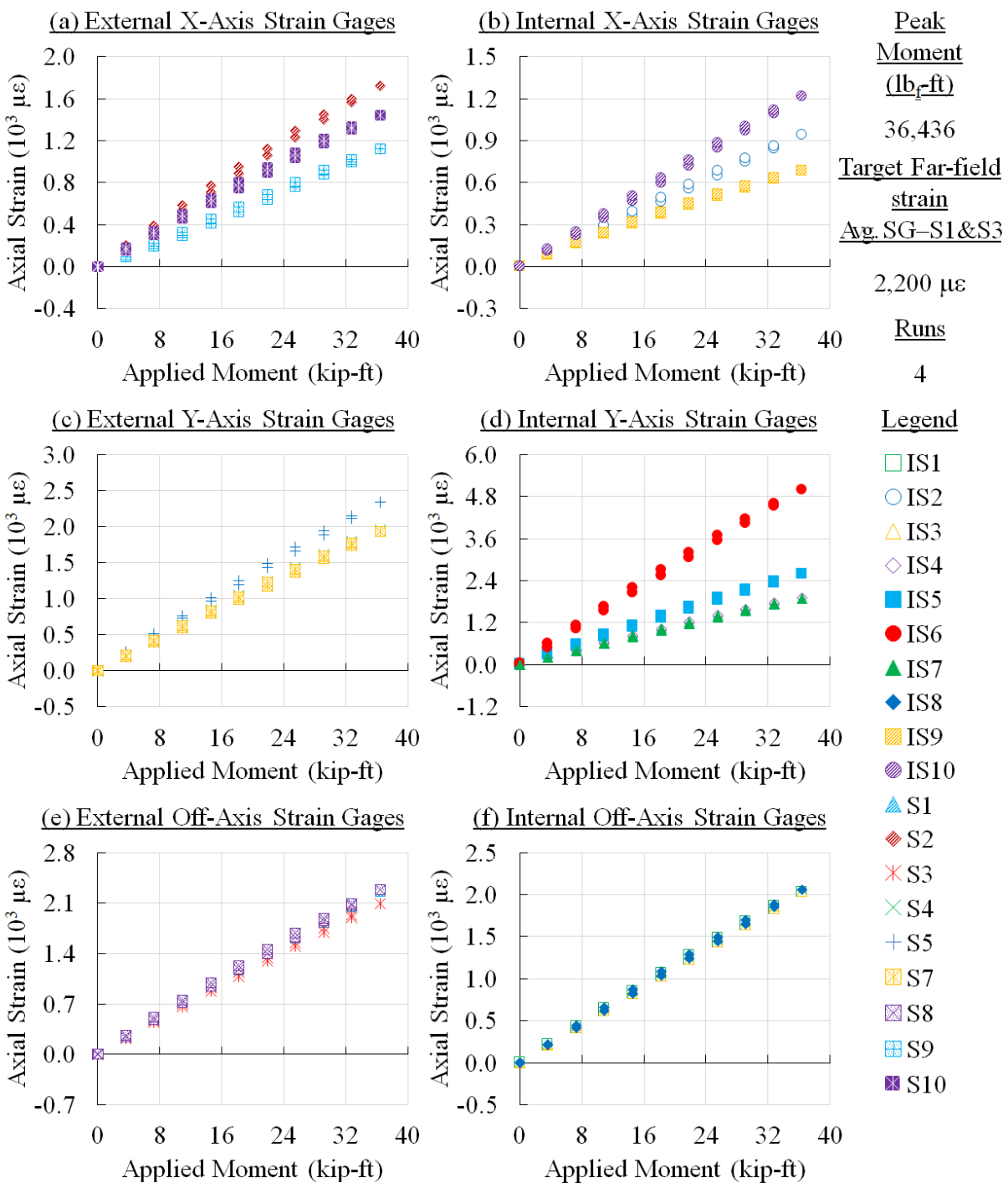


Figure B 69. Panel 6 (fatigue at SL strain level): strain survey at 36,000 cycles (axial strain)

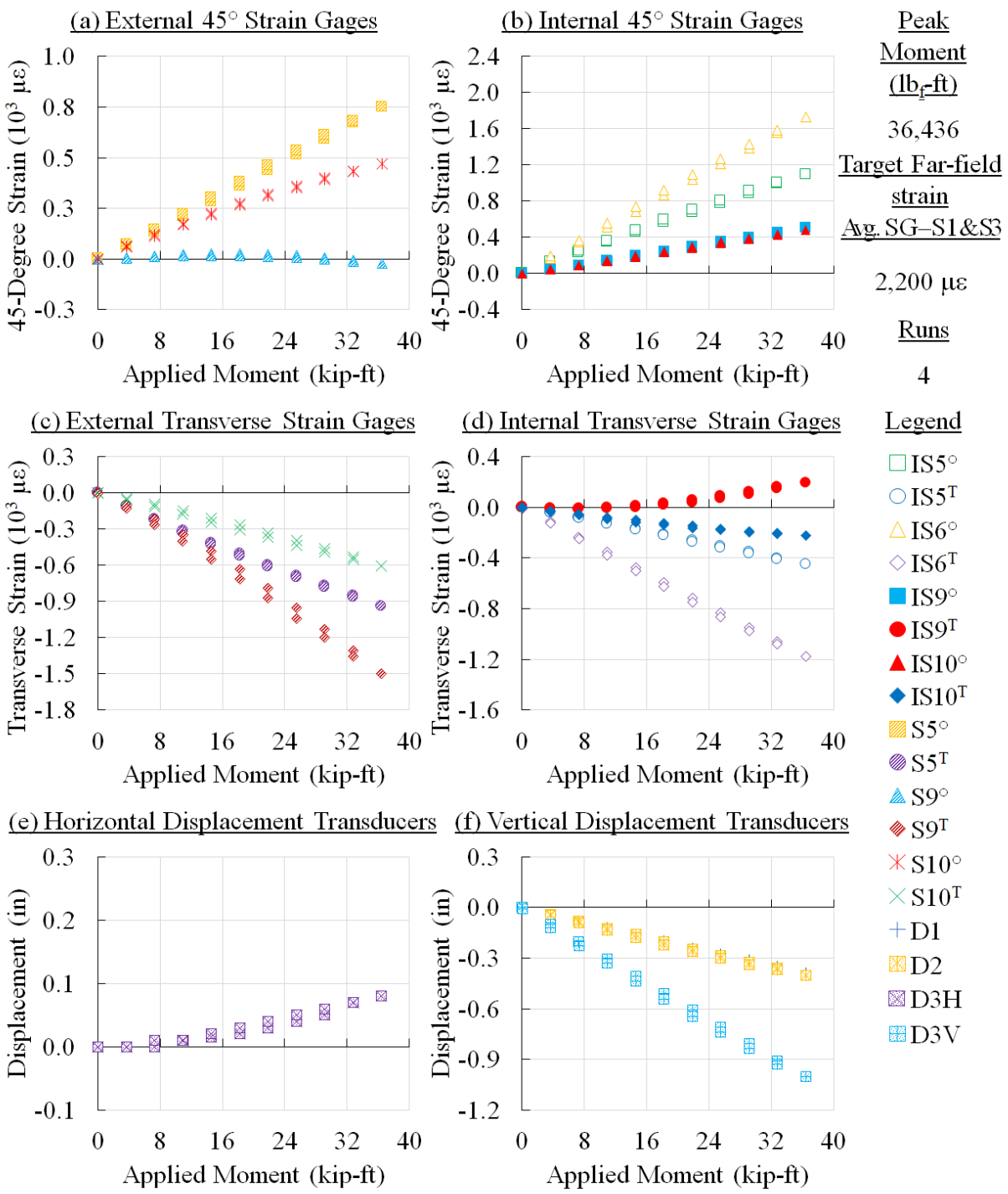


Figure B 70. Panel 6 (fatigue at SL strain level): strain survey at 36,000 cycles (other strain and displacement)

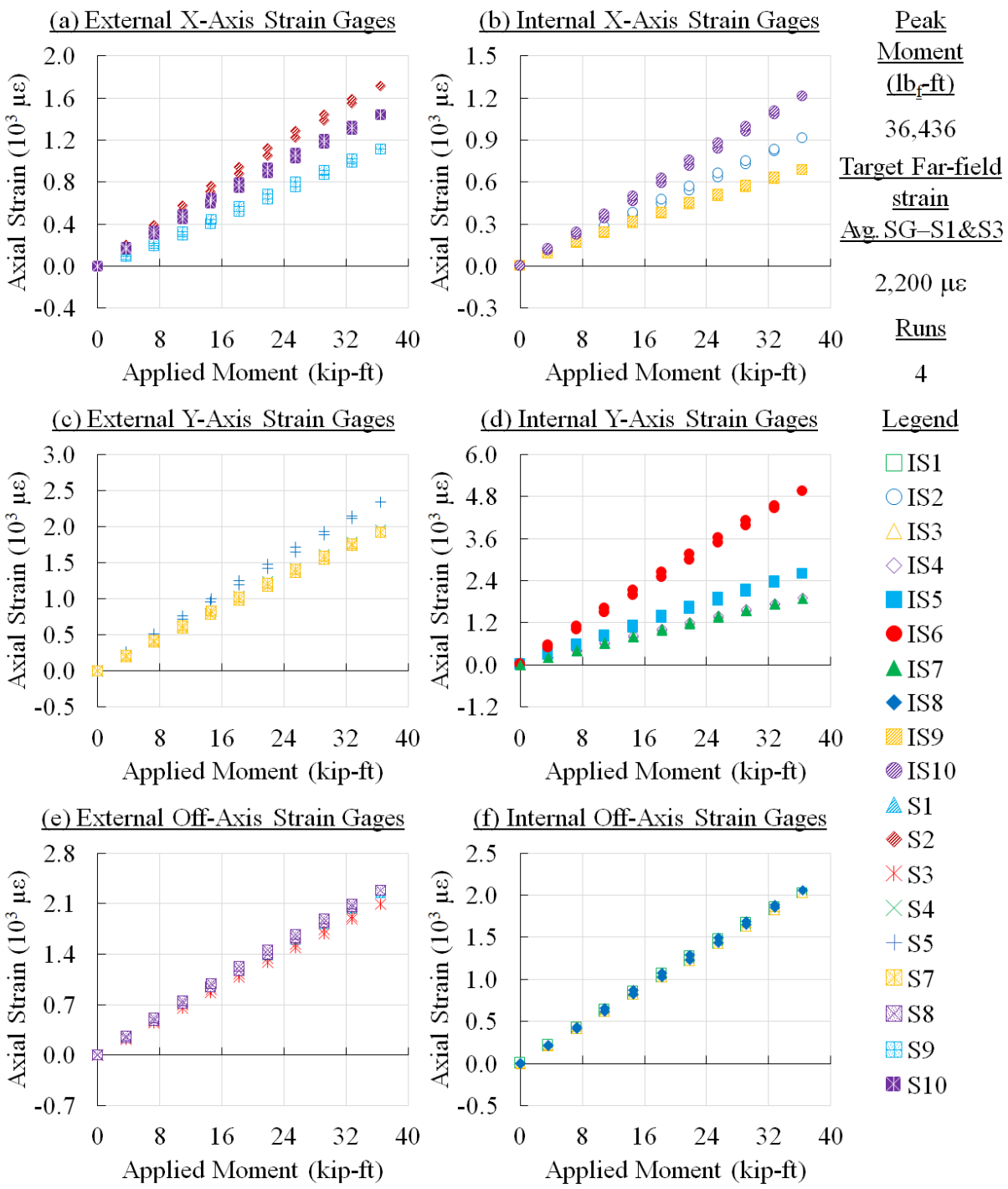


Figure B 71. Panel 6 (fatigue at SL strain level): strain survey at 48,000 cycles (axial strain)

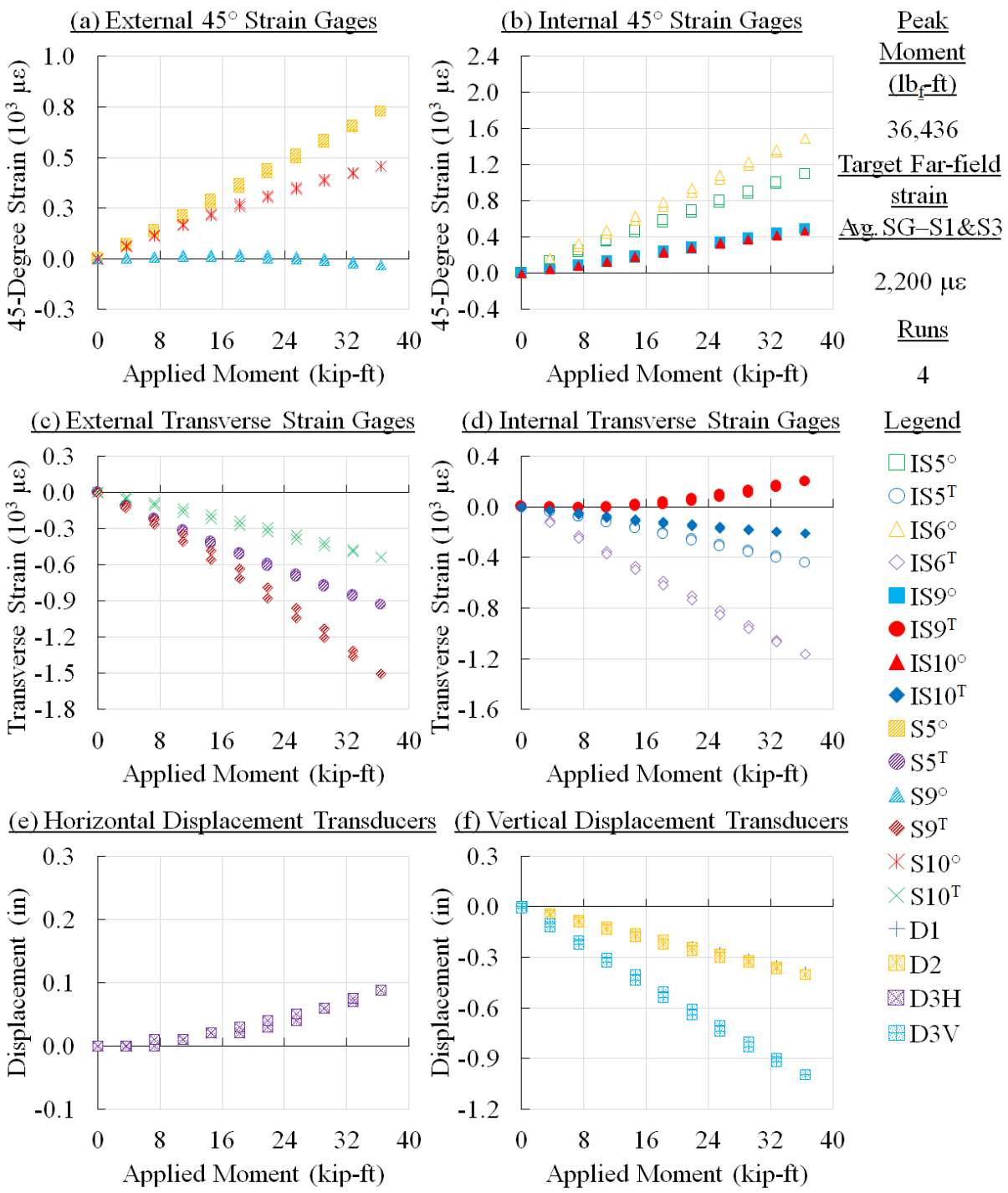


Figure B 72. Panel 6 (fatigue at SL strain level): strain survey at 48,000 cycles (other strain and displacement)

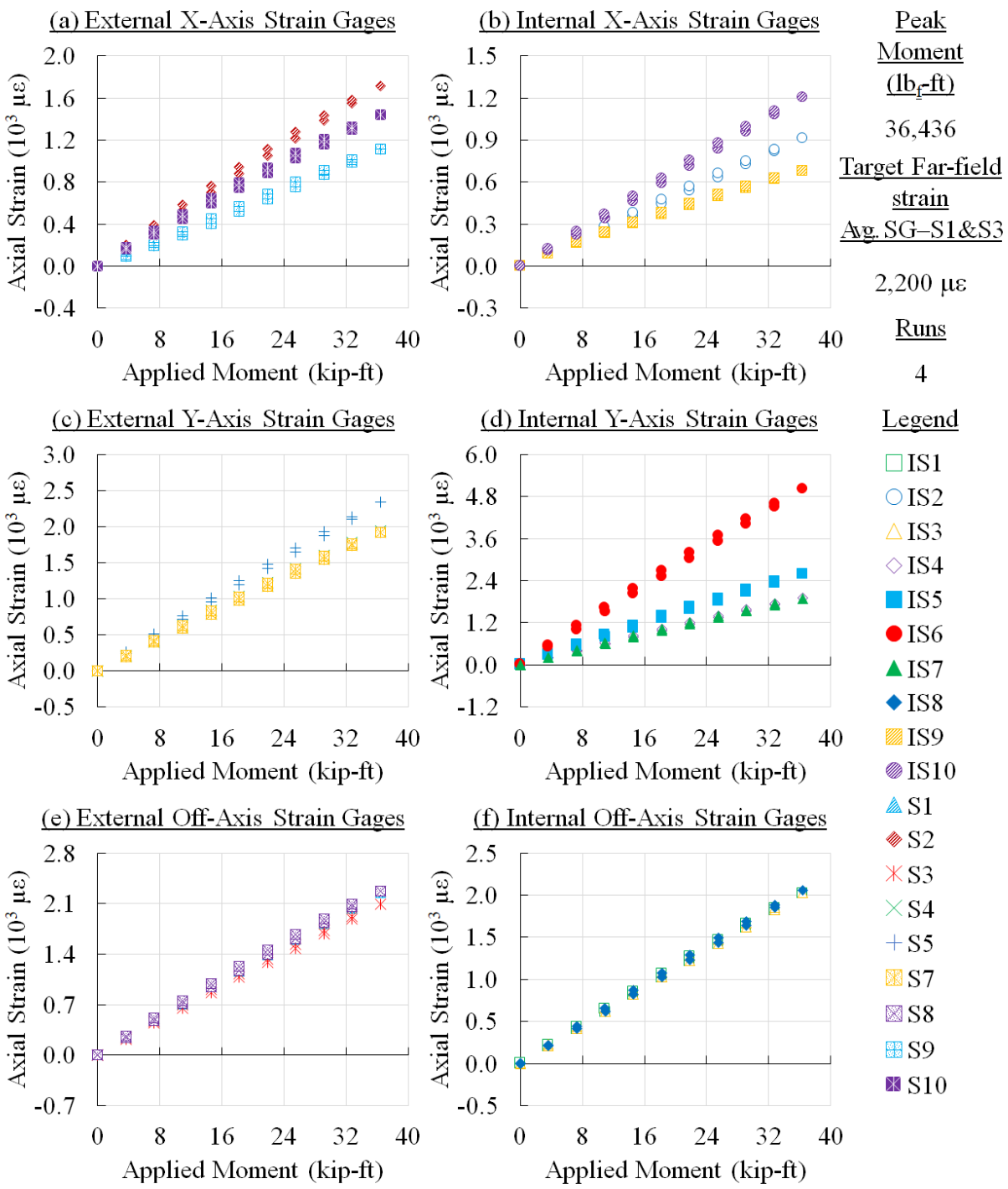


Figure B 73. Panel 6 (fatigue at SL strain level): strain survey at 60,000 cycles (axial strain)

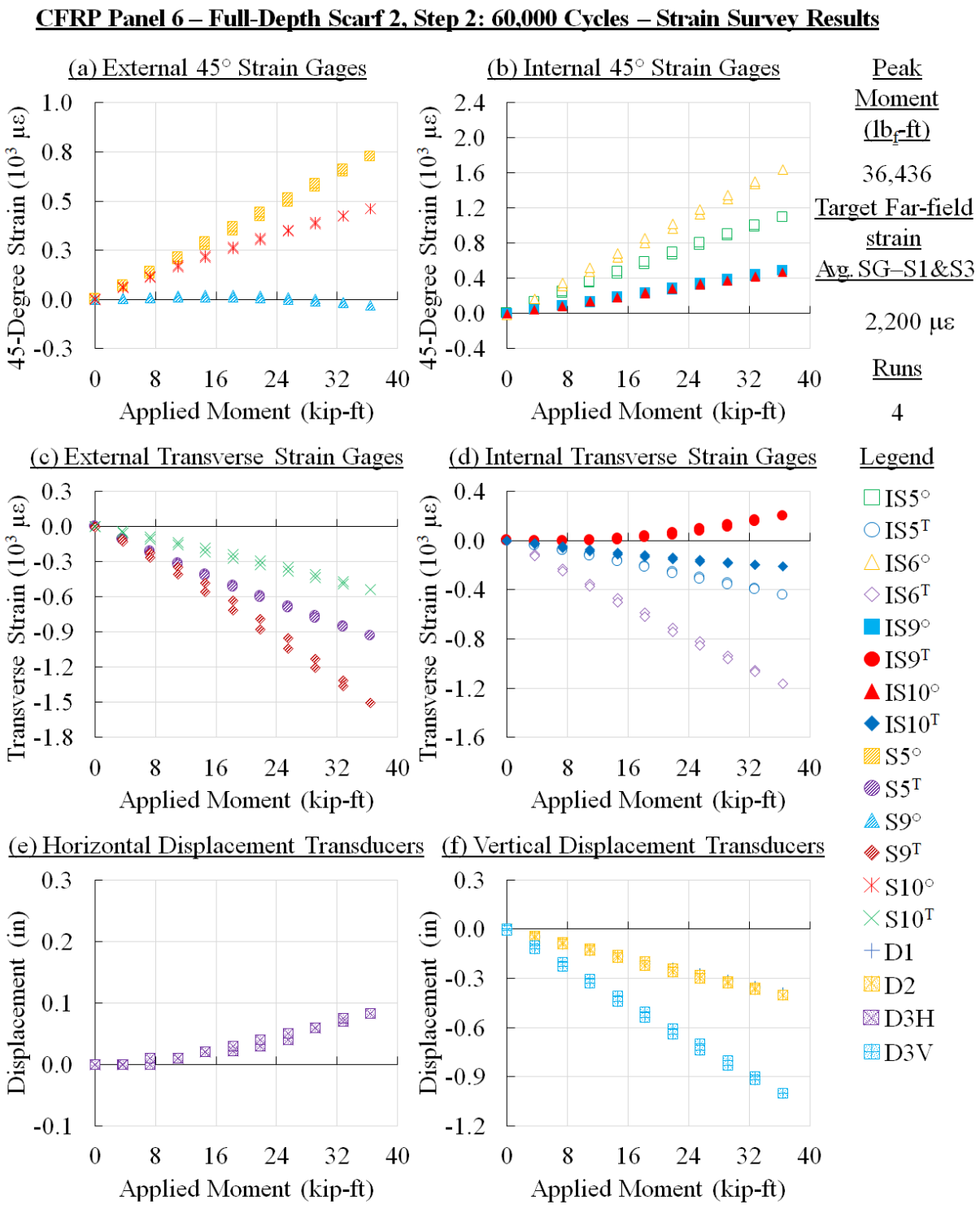


Figure B 74. Panel 6 (fatigue at SL strain level): strain survey at 60,000 cycles (other strain and displacement)

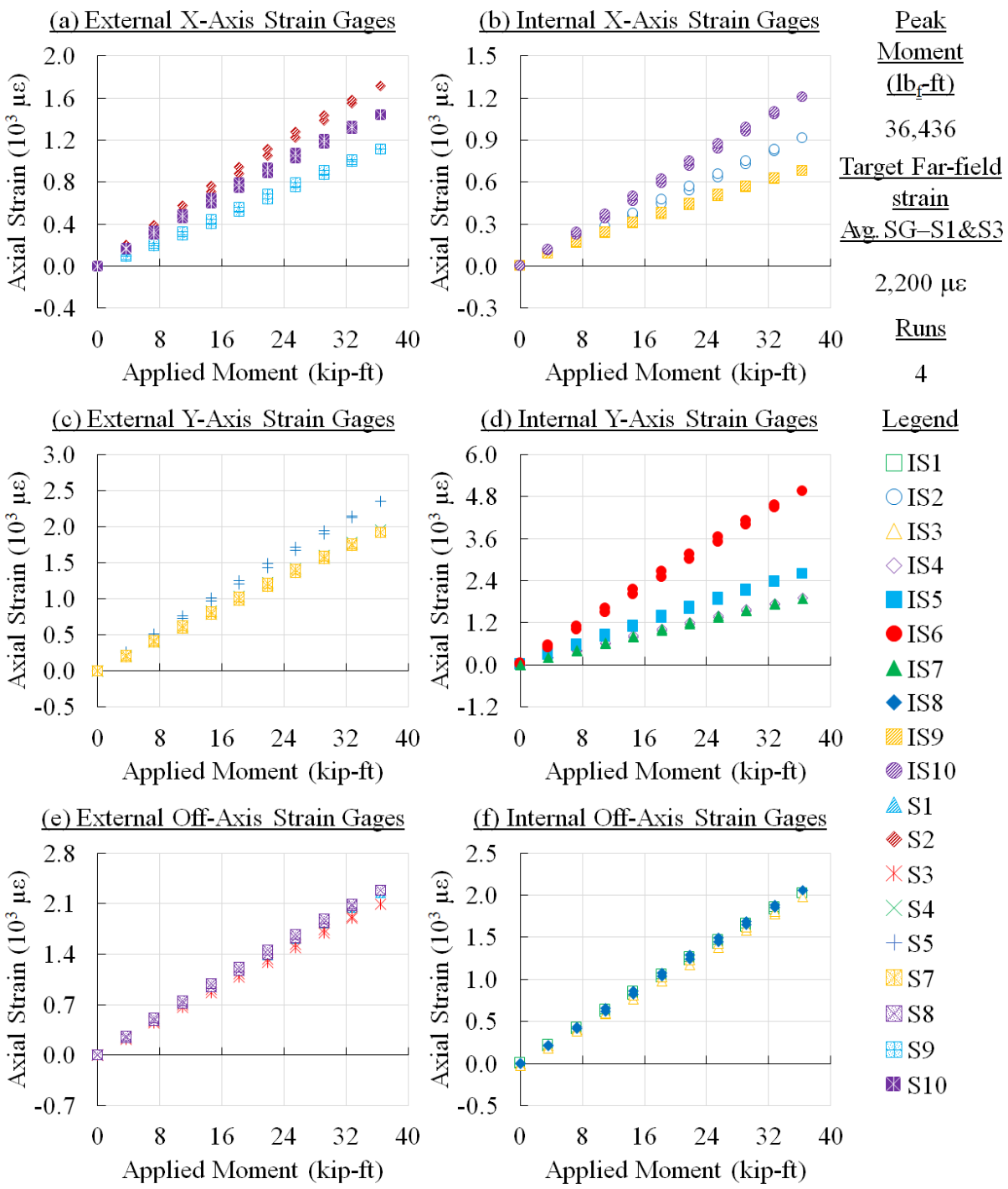


Figure B 75. Panel 6 (fatigue at SL strain level): strain survey at 72,000 cycles (axial strain)

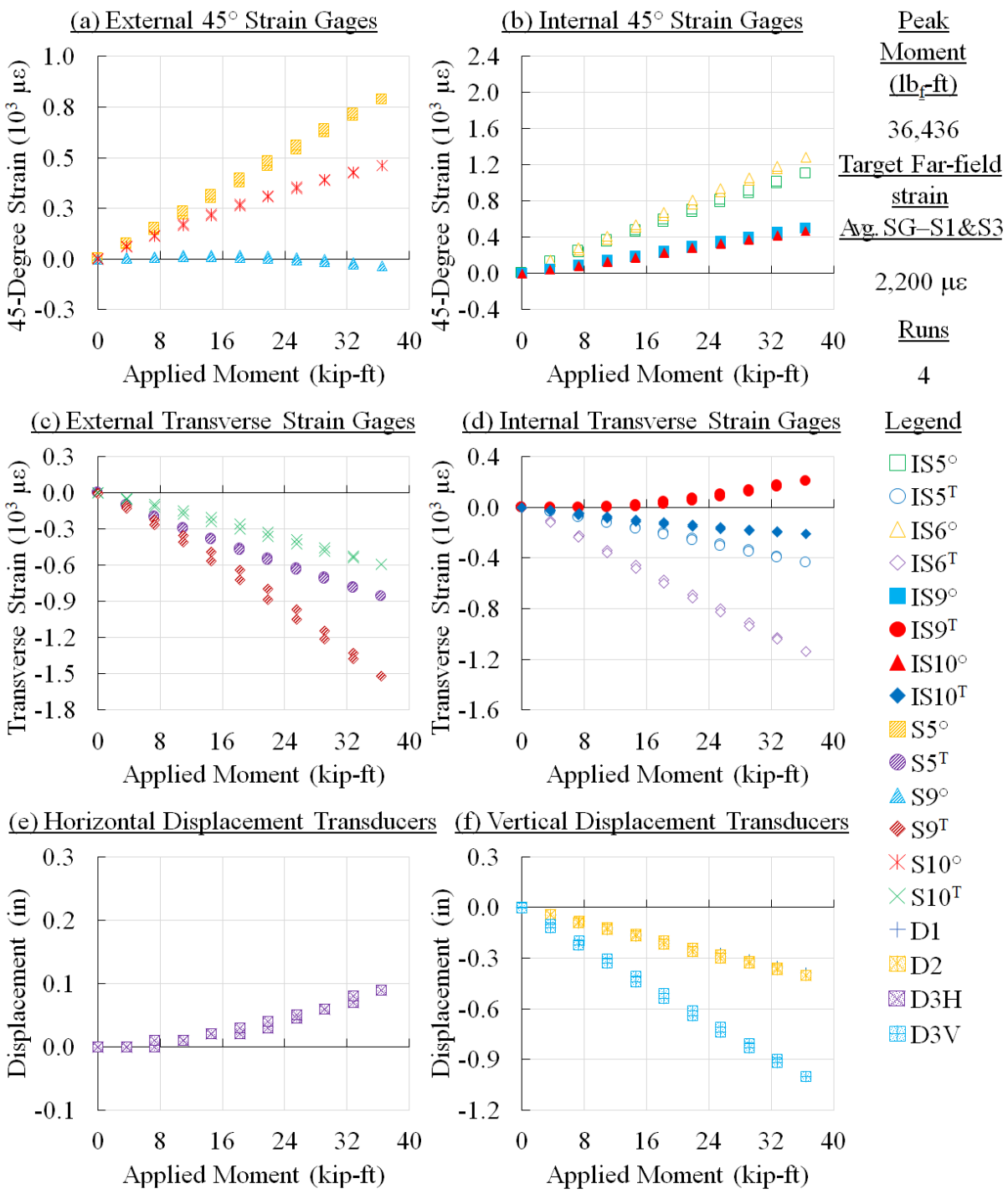


Figure B 76. Panel 6 (fatigue at SL strain level): strain survey at 72,000 cycles (other strain and displacement)

**CFRP Panel 6 – Full-Depth Scarf 2, Step 2: 84,000 Cycles – Strain Survey Results**

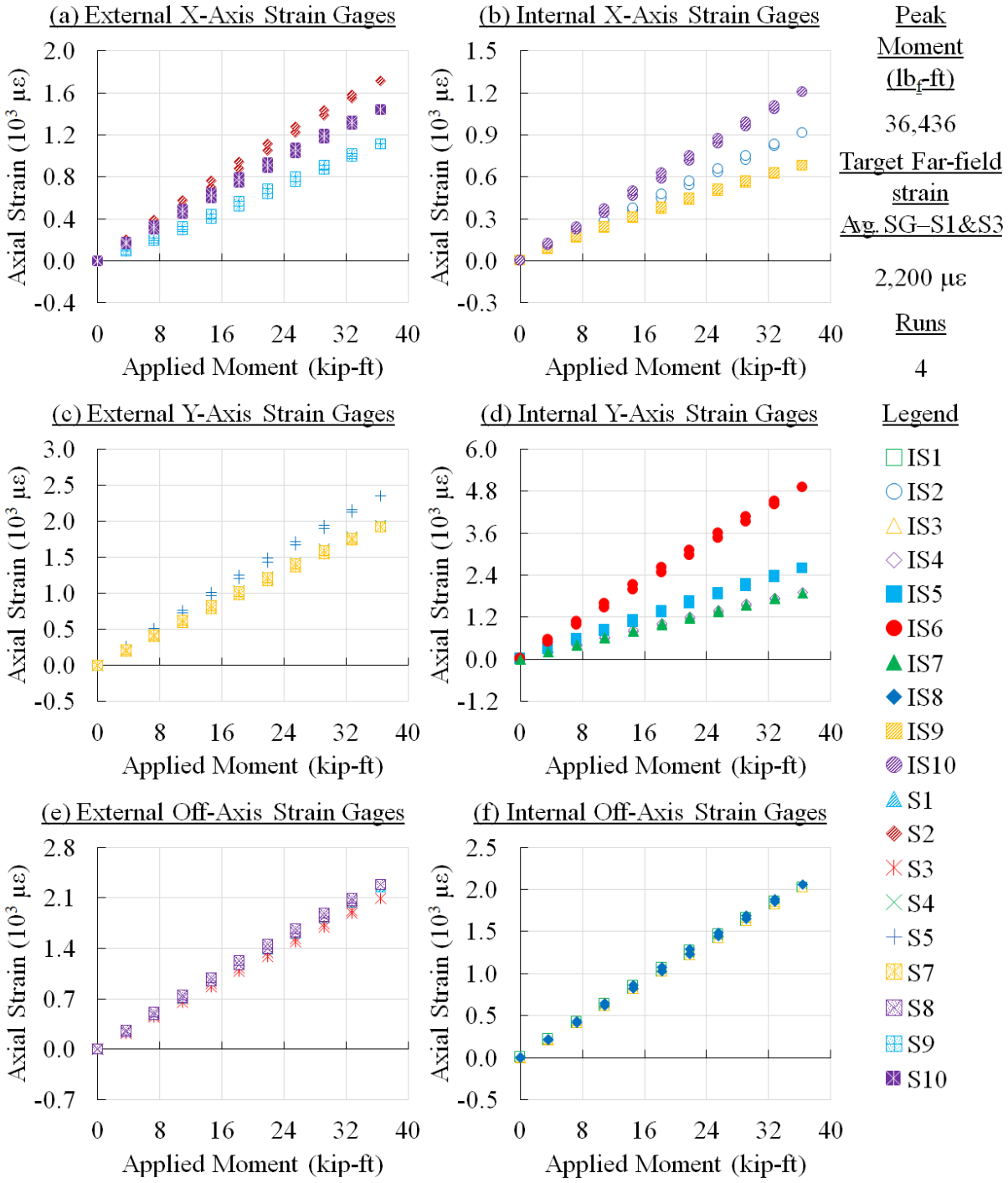


Figure B 77. Panel 6 (fatigue at SL strain level): strain survey at 84,000 cycles (axial strain)

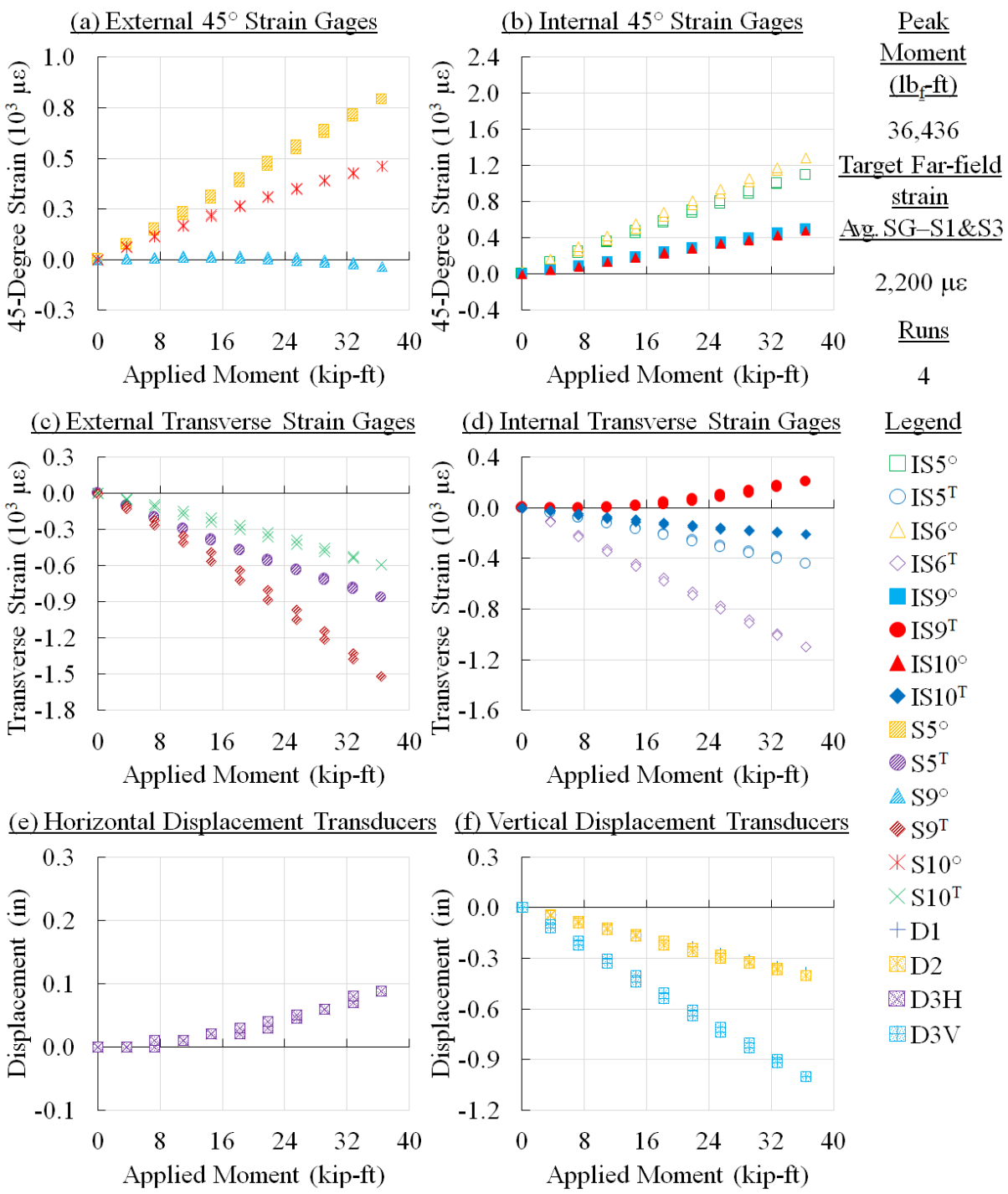


Figure B 78. Panel 6 (fatigue at SL strain level): strain survey at 84,000 cycles (other strain and displacement)

**CFRP Panel 6 – Full-Depth Scarf 2, Step 2: 96,000 Cycles – Strain Survey Results**

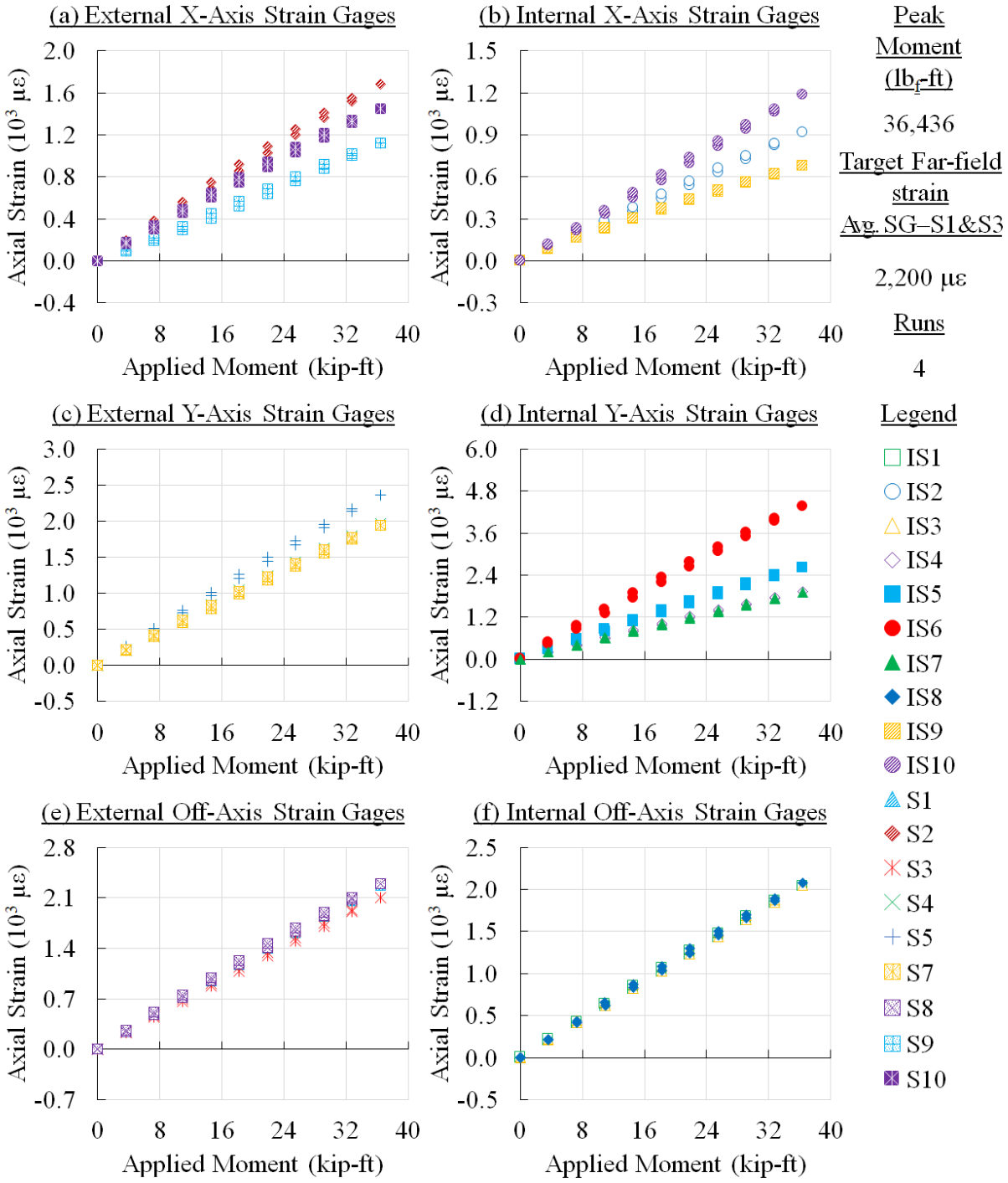


Figure B 79. Panel 6 (fatigue at SL strain level): strain survey at 96,000 cycles (axial strain)

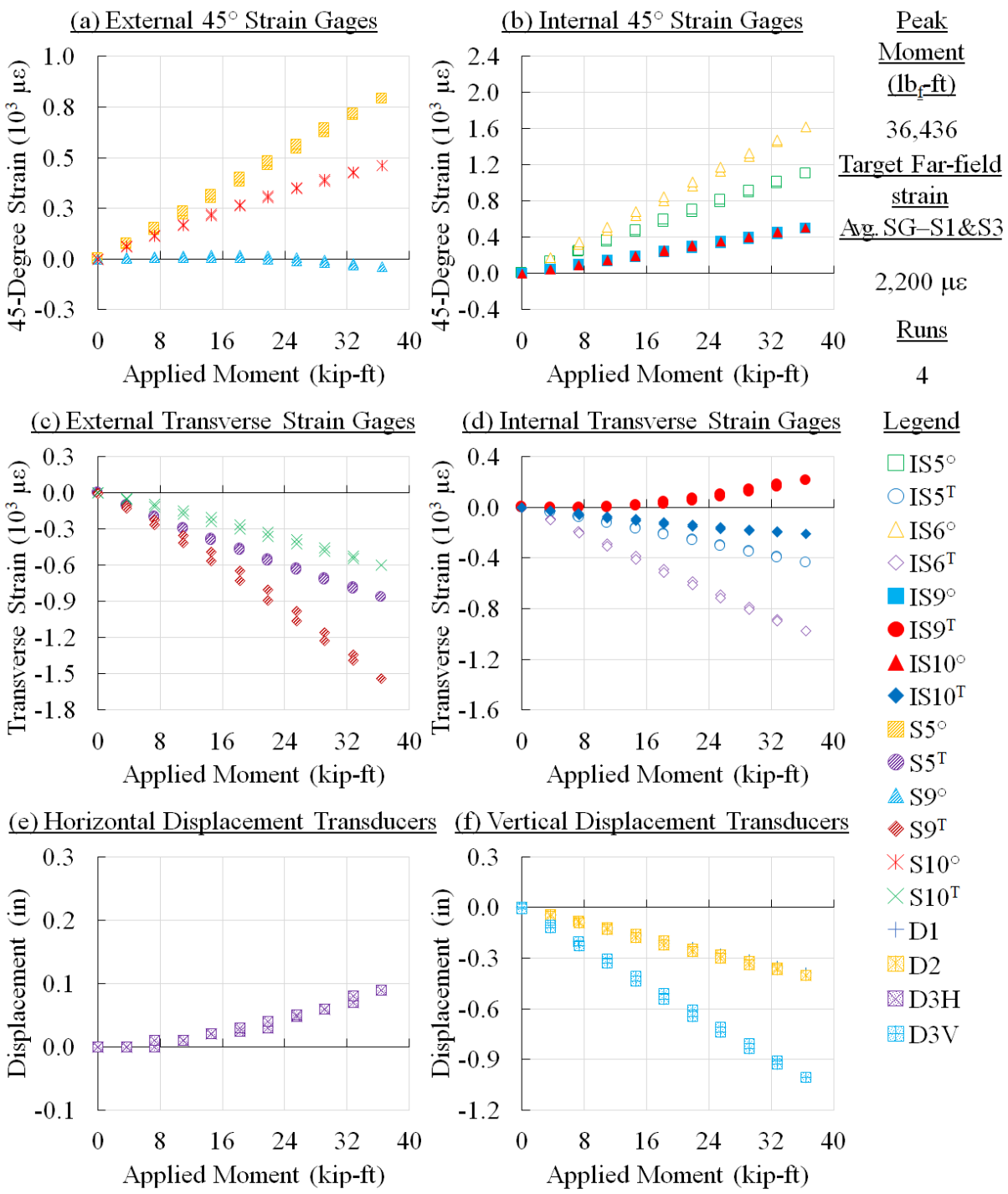


Figure B 80. Panel 6 (fatigue at SL strain level): strain survey at 96,000 cycles (other strain and displacement)

**CFRP Panel 6 – Full-Depth Scarf 2, Step 2: 108,000 Cycles – Strain Survey Results**

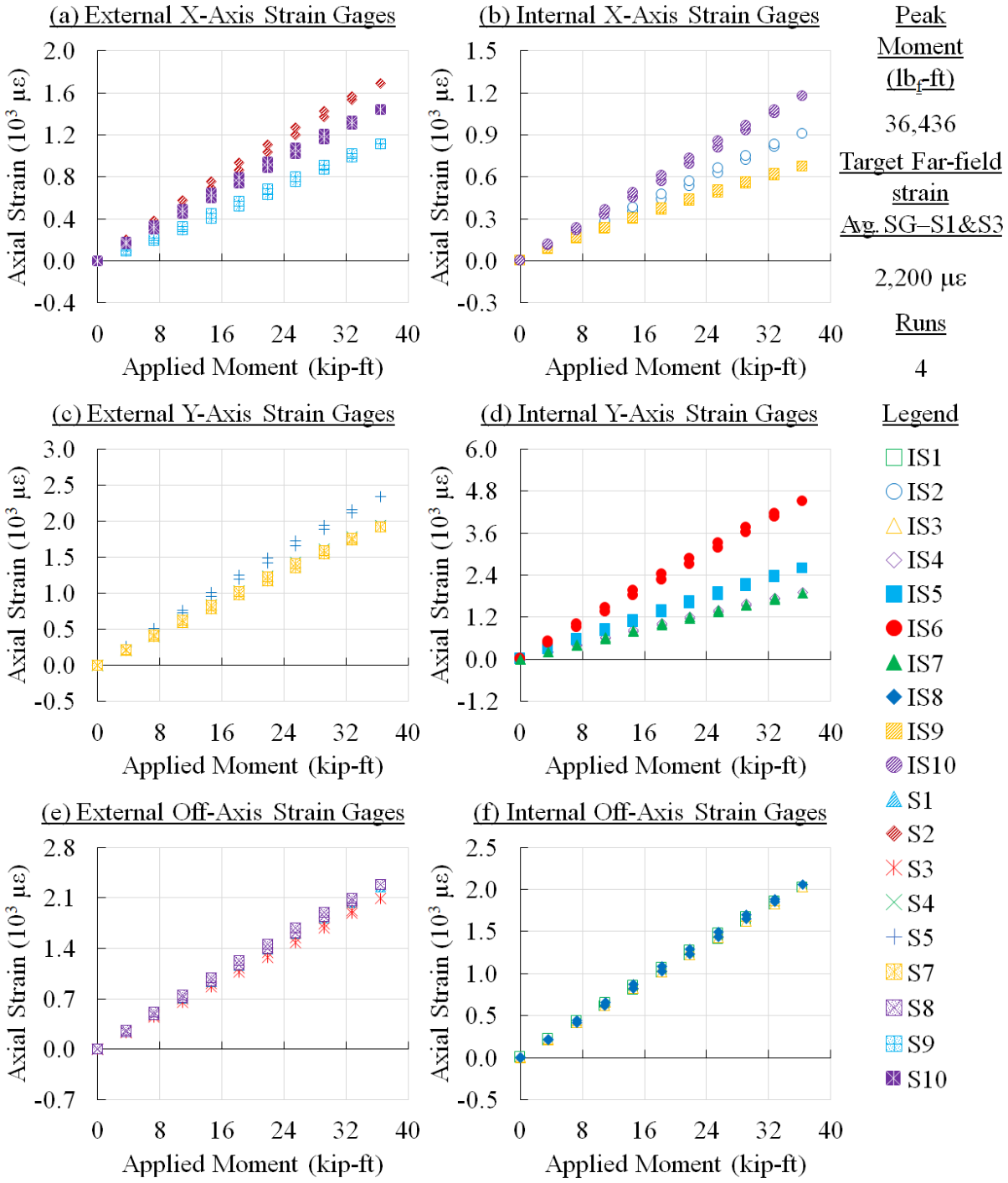


Figure B 81. Panel 6 (fatigue at SL strain level): strain survey at 108,000 cycles (axial strain)

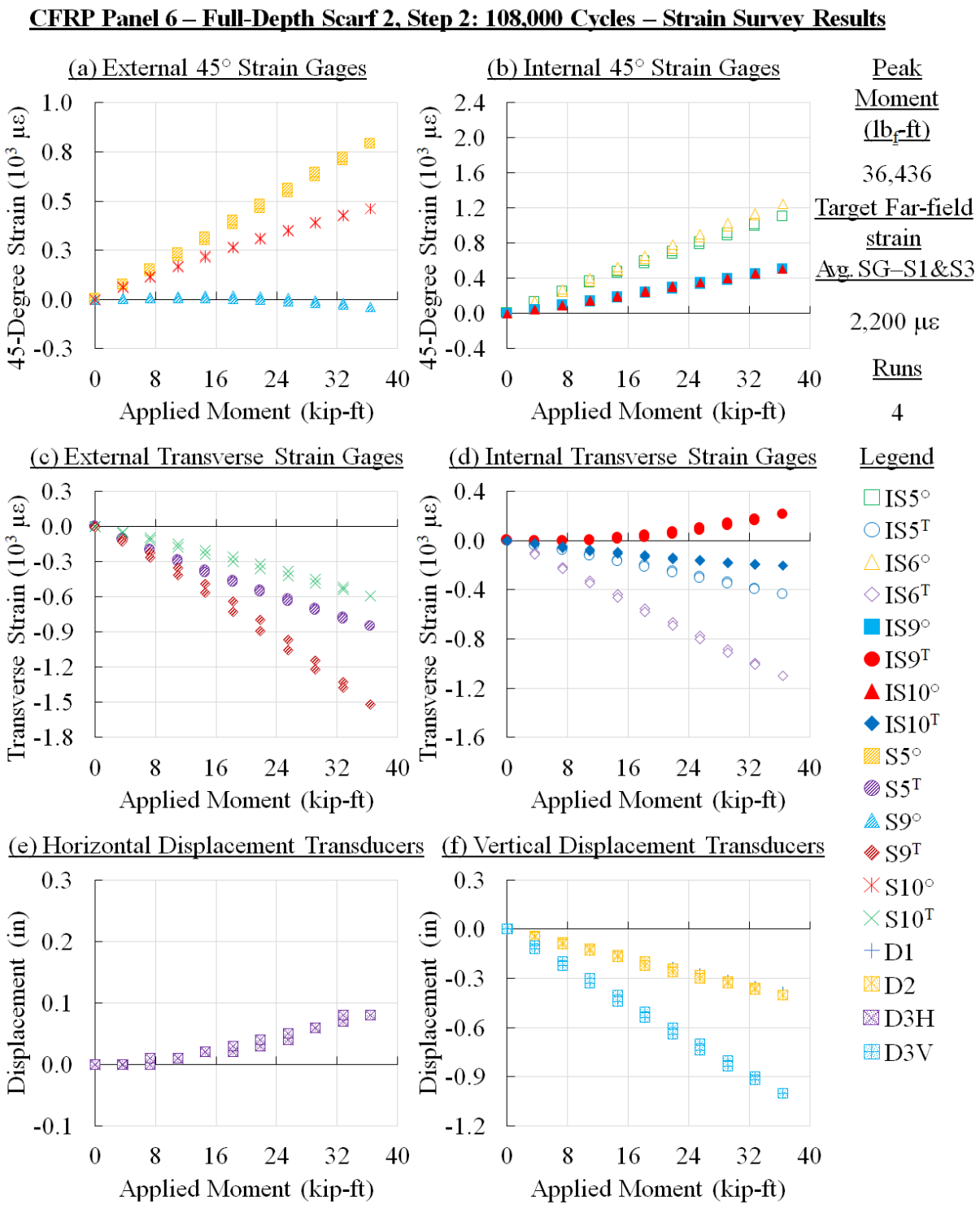


Figure B 82. Panel 6 (fatigue at SL strain level): strain survey at 108,000 cycles (other strain and displacement)

**CFRP Panel 6 – Full-Depth Scarf 2, Step 2: 120,000 Cycles – Strain Survey Results**

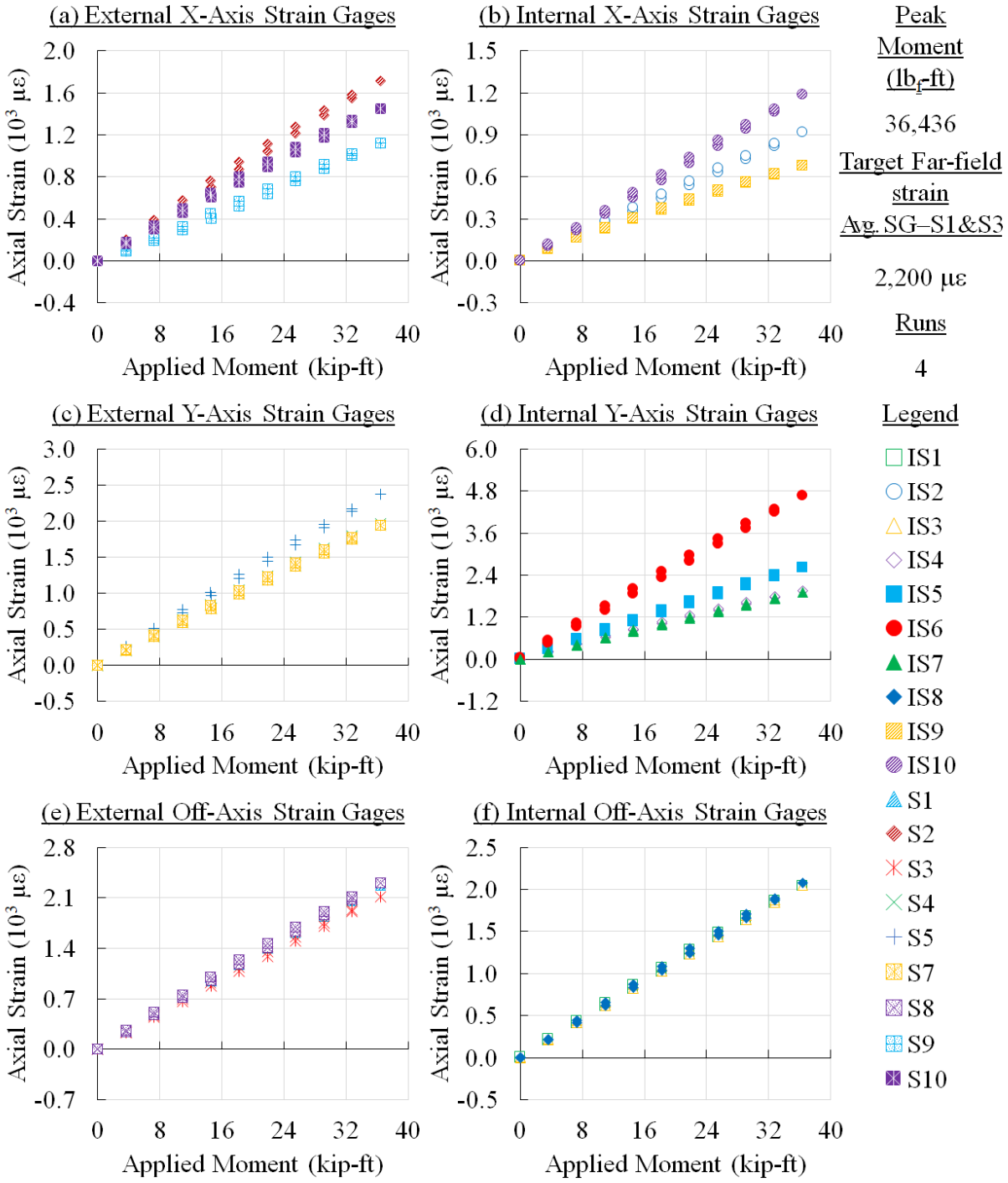


Figure B 83. Panel 6 (fatigue at SL strain level): strain survey at 120,000 cycles (axial strain)

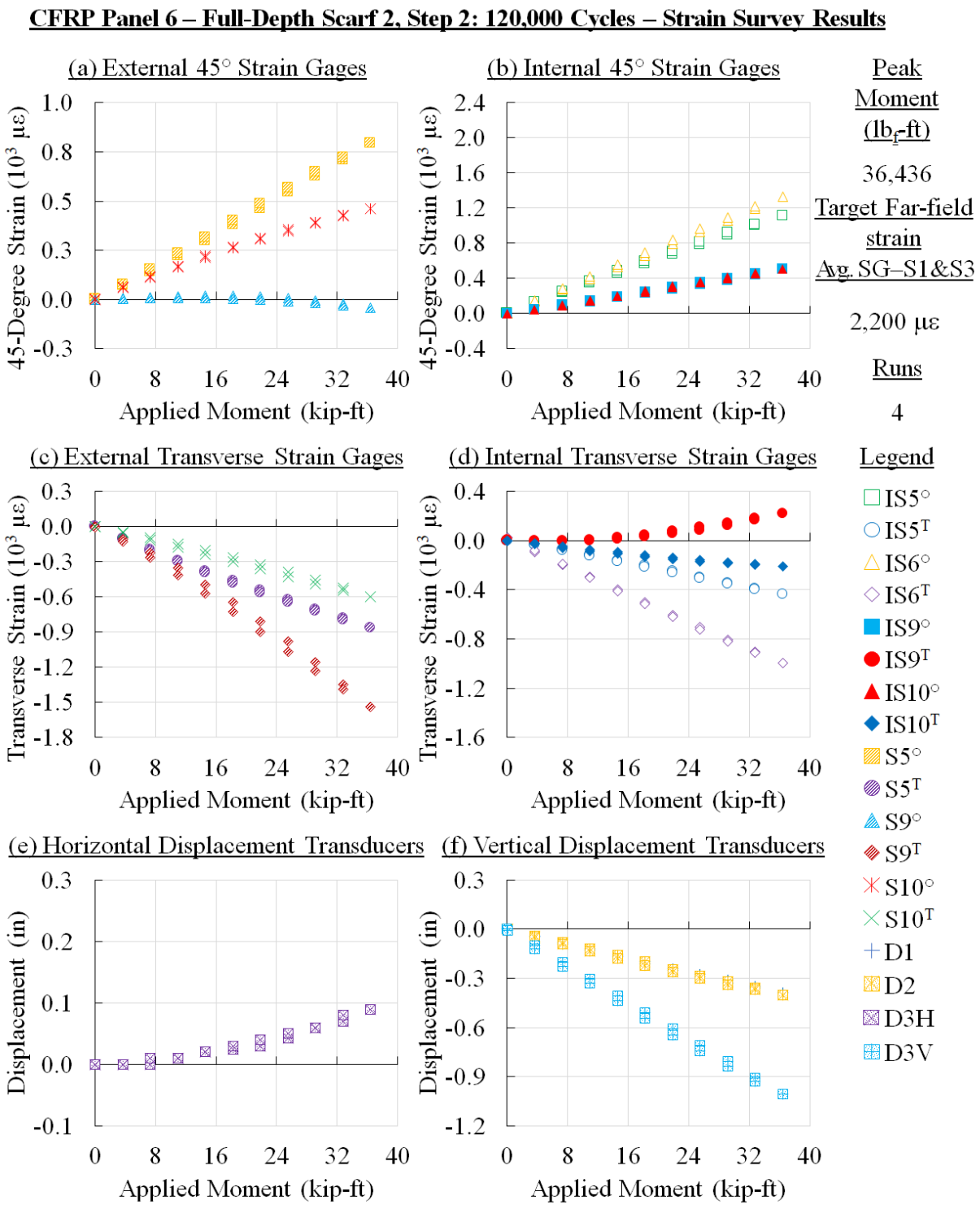


Figure B 84. Panel 6 (fatigue at SL strain level): strain survey at 120,000 cycles (other strain and displacement)

**CFRP Panel 6 – Full-Depth Scarf 2, Step 2: 132,000 Cycles – Strain Survey Results**

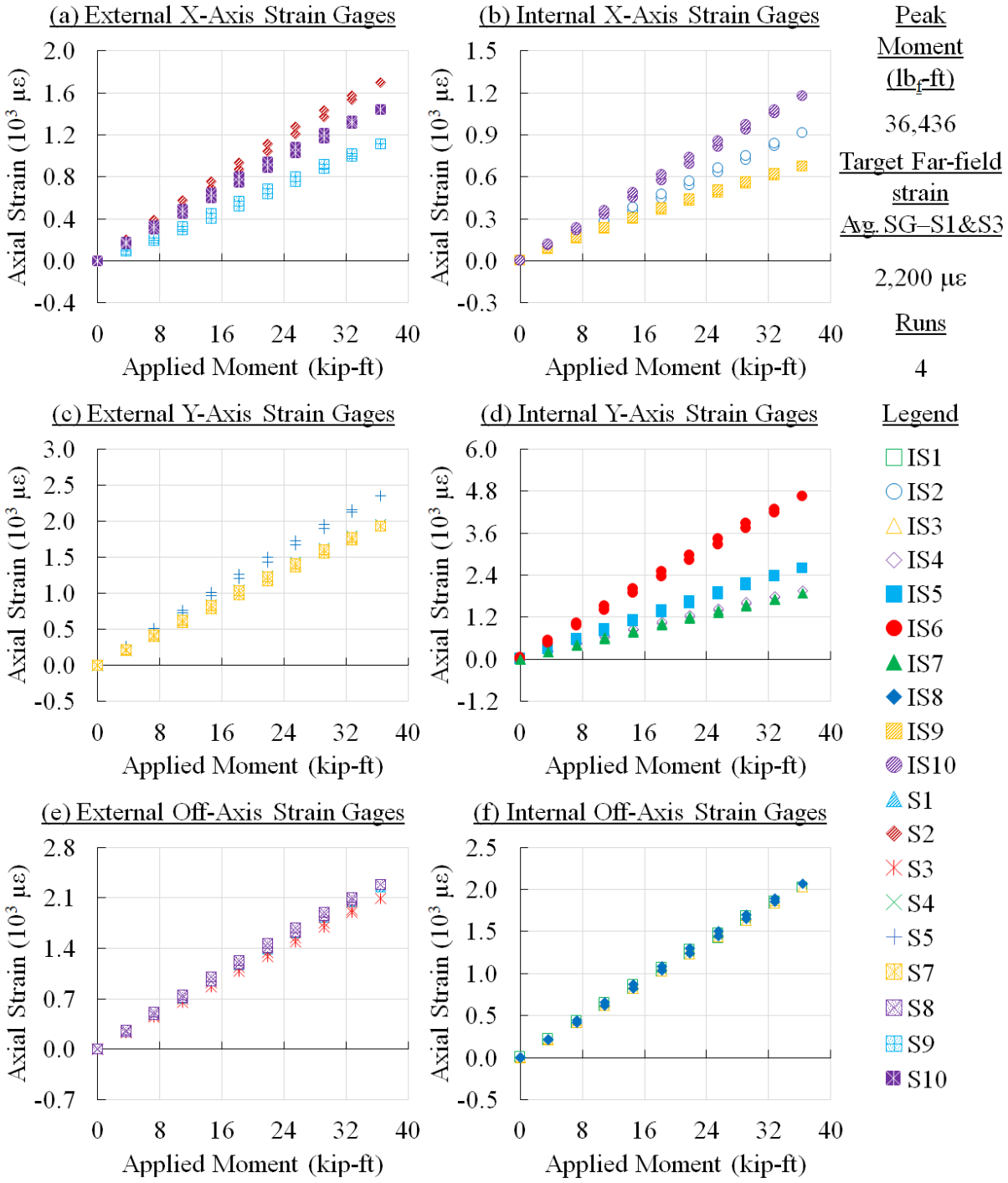


Figure B 85. Panel 6 (fatigue at SL strain level): strain survey at 132,000 cycles (axial strain)

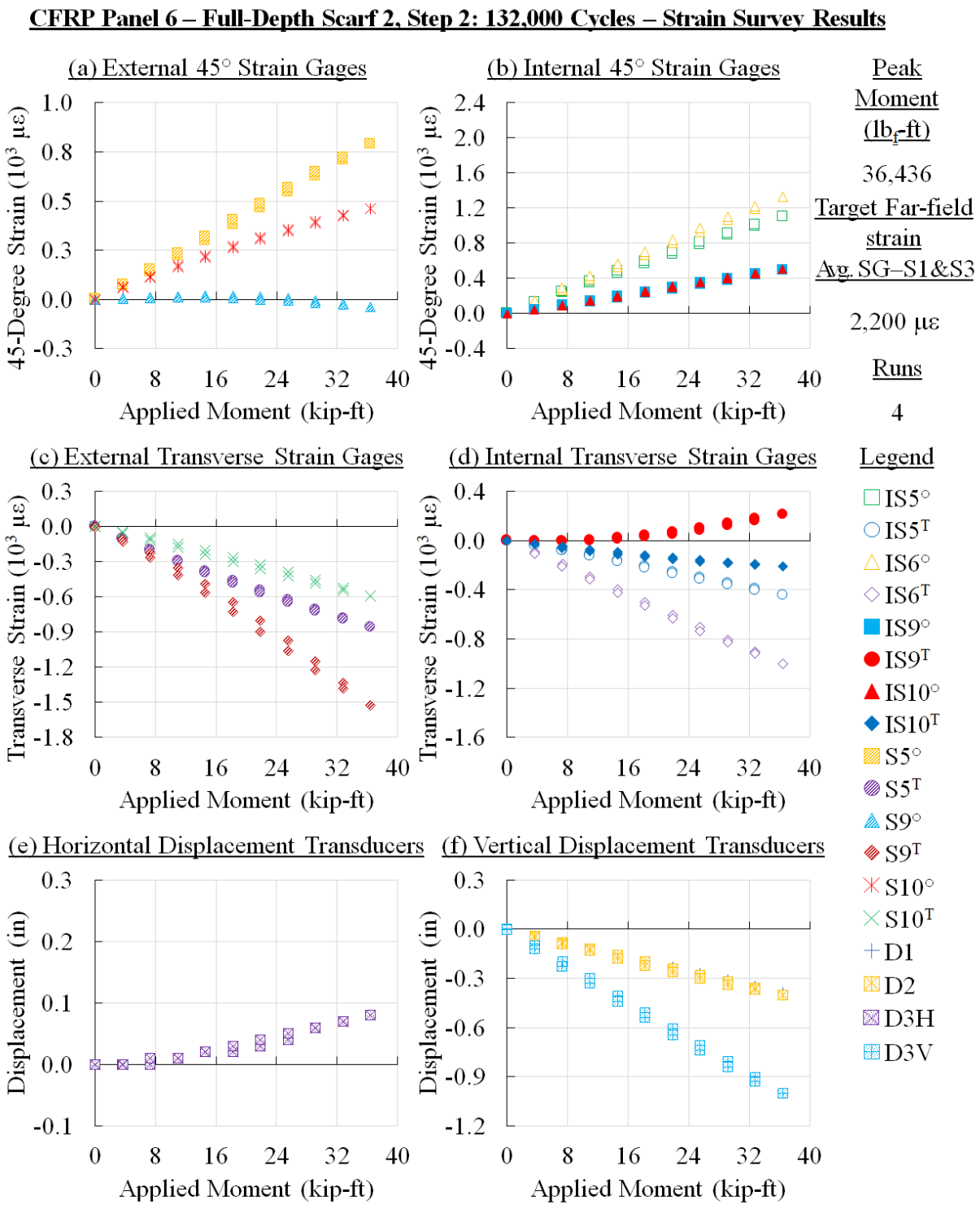


Figure B 86. Panel 6 (fatigue at SL strain level): strain survey at 132,000 cycles (other strain and displacement)

**CFRP Panel 6 – Full-Depth Scarf 2, Step 2: 144,000 Cycles – Strain Survey Results**

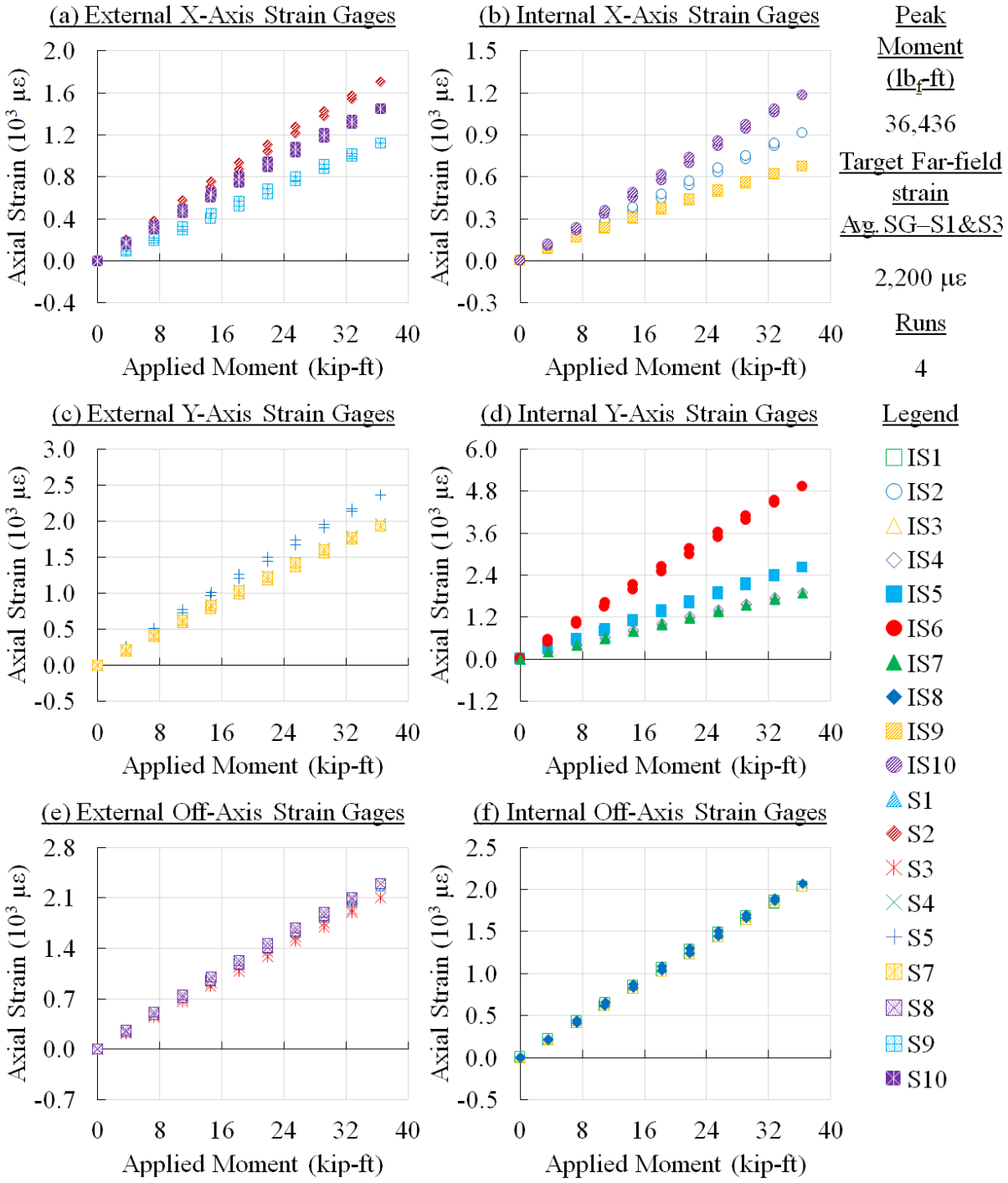


Figure B 87. Panel 6 (fatigue at SL strain level): strain survey at 144,000 cycles (axial strain)

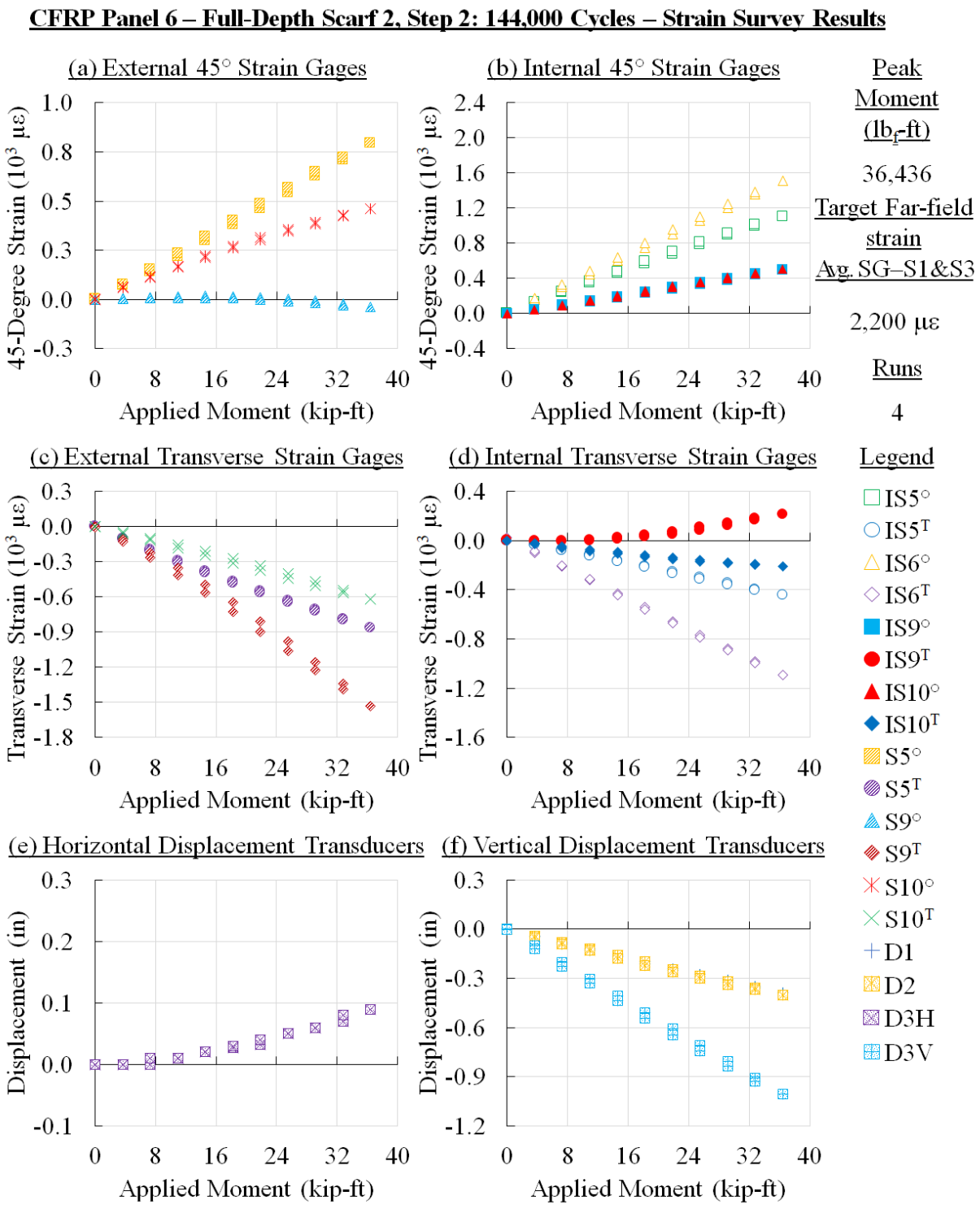


Figure B 88. Panel 6 (fatigue at SL strain level): strain survey at 144,000 cycles (other strain and displacement)

**CFRP Panel 6 – Full-Depth Scarf 2, Step 2: 156,000 Cycles – Strain Survey Results**

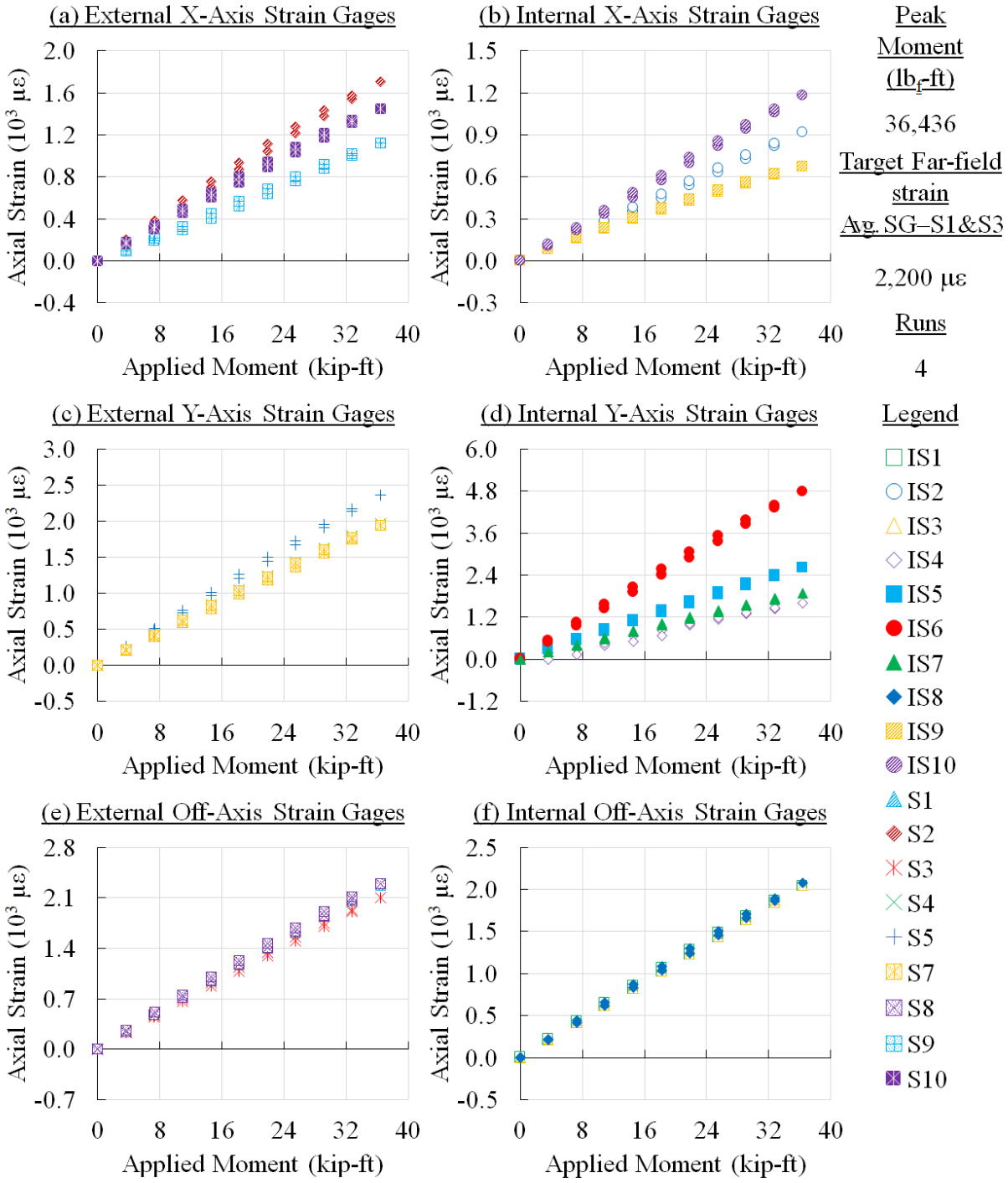


Figure B 89. Panel 6 (fatigue at SL strain level): strain survey at 156,000 cycles (axial strain)

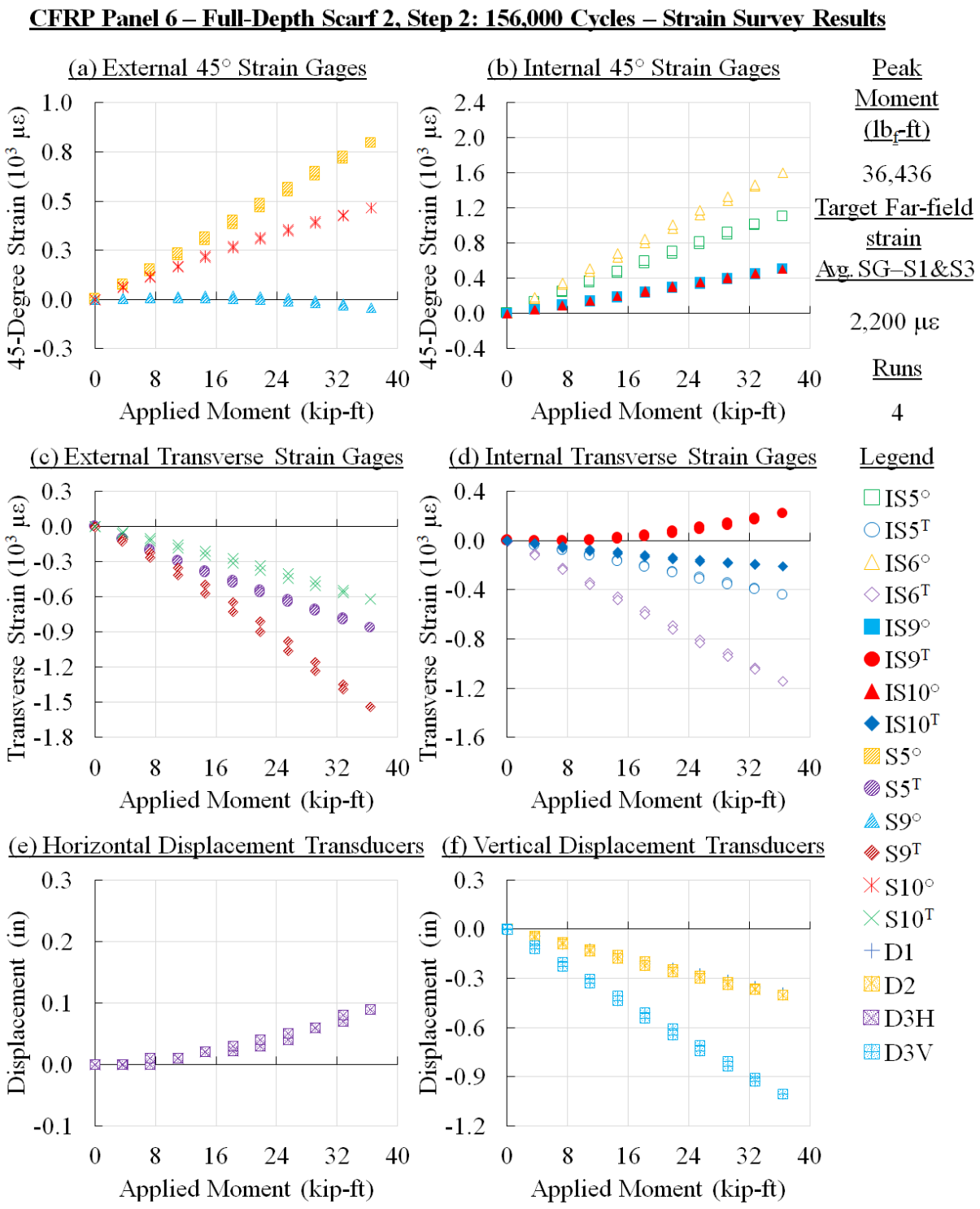


Figure B 90. Panel 6 (fatigue at SL strain level): strain survey at 156,000 cycles (other strain and displacement)

**CFRP Panel 6 – Full-Depth Scarf 2, Step 2: 165,000 Cycles – Strain Survey Results**

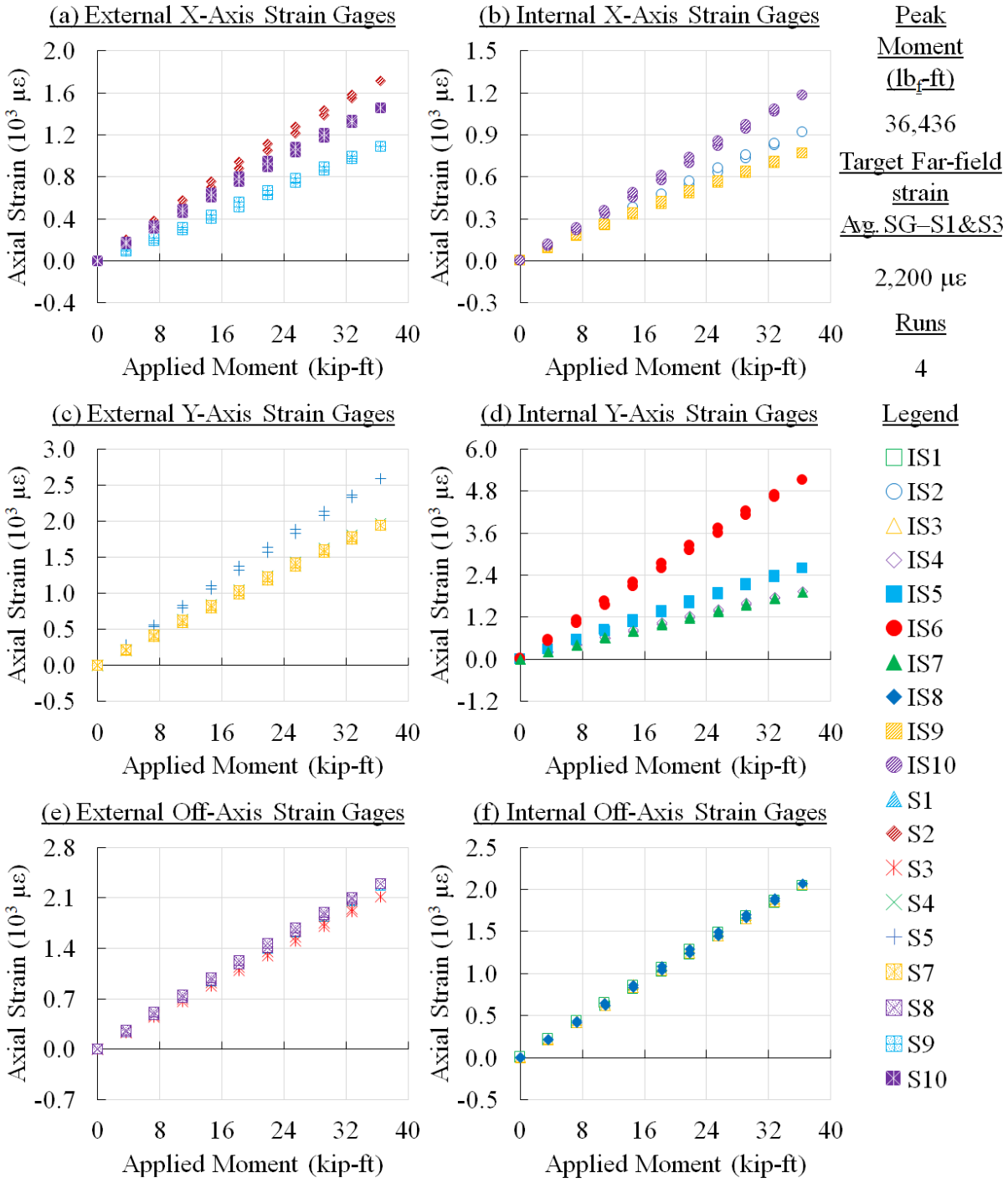


Figure B 91. Panel 6 (fatigue at SL strain level): strain survey at 165,000 cycles (axial strain)

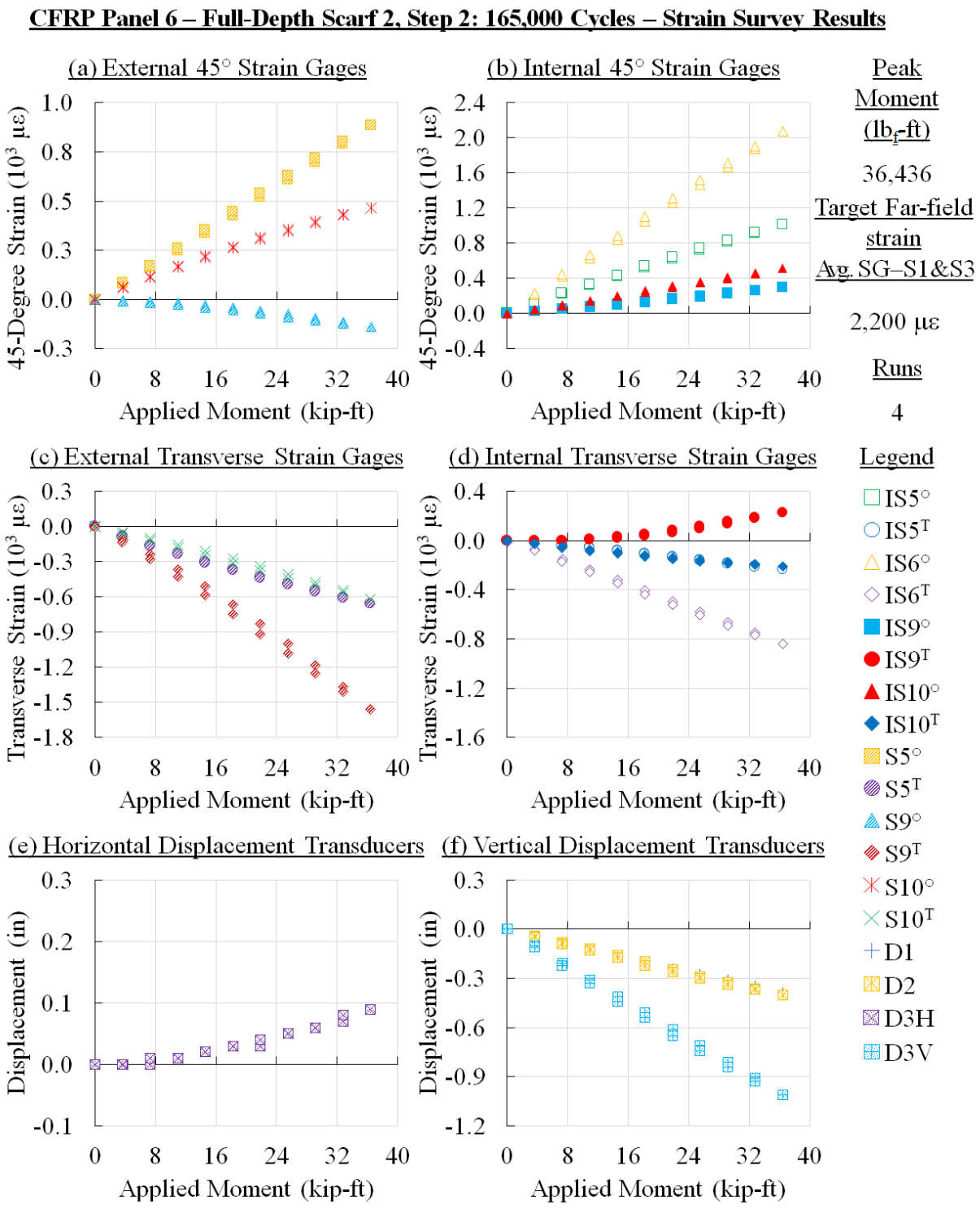


Figure B 92. Panel 6 (fatigue at SL strain level): strain survey at 165,000 cycles (other strain and displacement)

# C Strain and displacement during residual strength test

This appendix presents the results of the strain gages and displacement transducers captured during residual strength loading of the partial- and full-depth scarf panels. Residual strength tests load increments for all four panels are shown in Figure C 1. These load increments were defined based on the predicted critical load (PCL) level, which was considered the 100% load level. The figure also shows the predicted critical load and actual failure load bending moments for each panel. Panel 3, partial-depth scarf residual strength test results are provided in Figure C 2–Figure C 25. For panel 5, partial-depth scarf post-fatigue residual strength test results are shown in Figure C 26–Figure C 61. Panel 4, full-depth scarf and panel 5, full-depth scarf results are provided in Figure C 62–Figure C 97 and Figure C 98–Figure C 133, respectively.

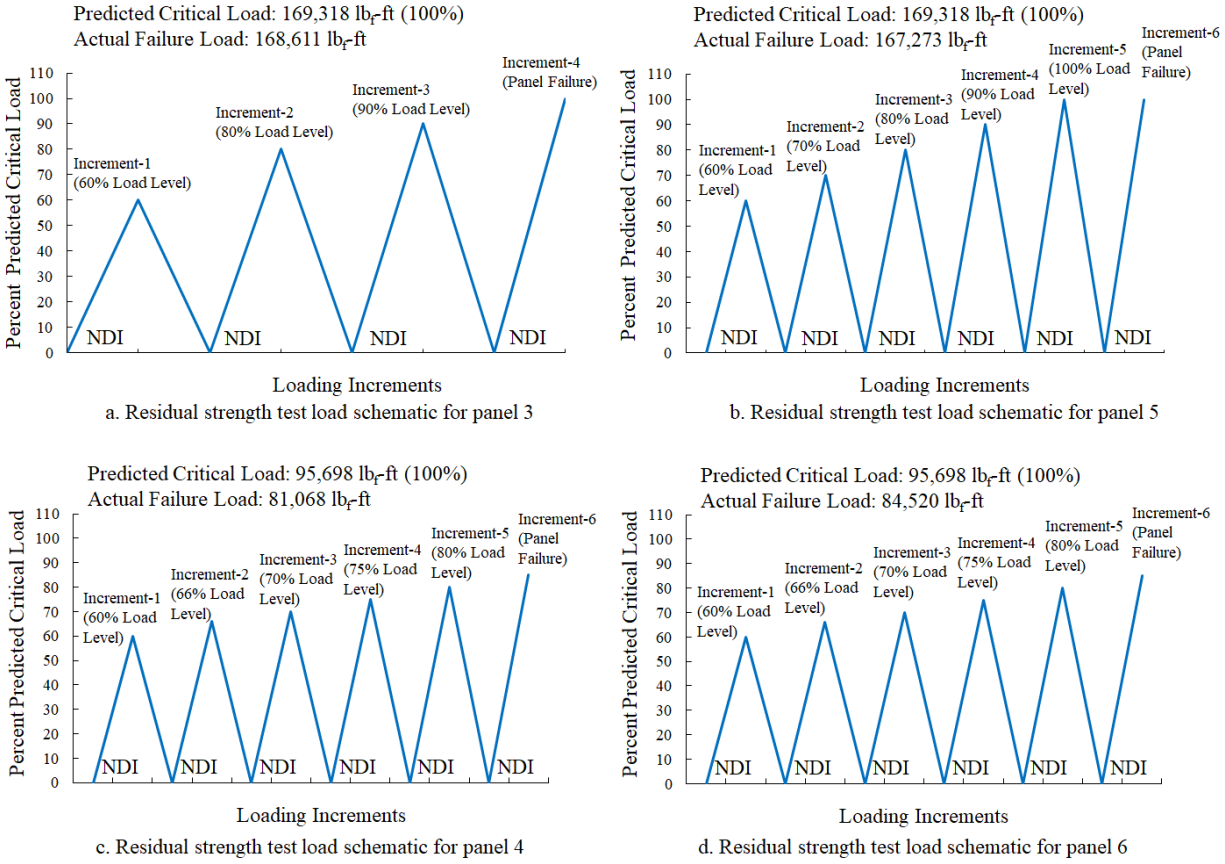


a. Residual strength test load schematic for panel 3

b. Residual strength test load schematic for panel 5

c. Residual strength test load schematic for panel 4

d. Residual strength test load schematic for panel 6

Figure C 1. Residual strength test load results for panels 3–6

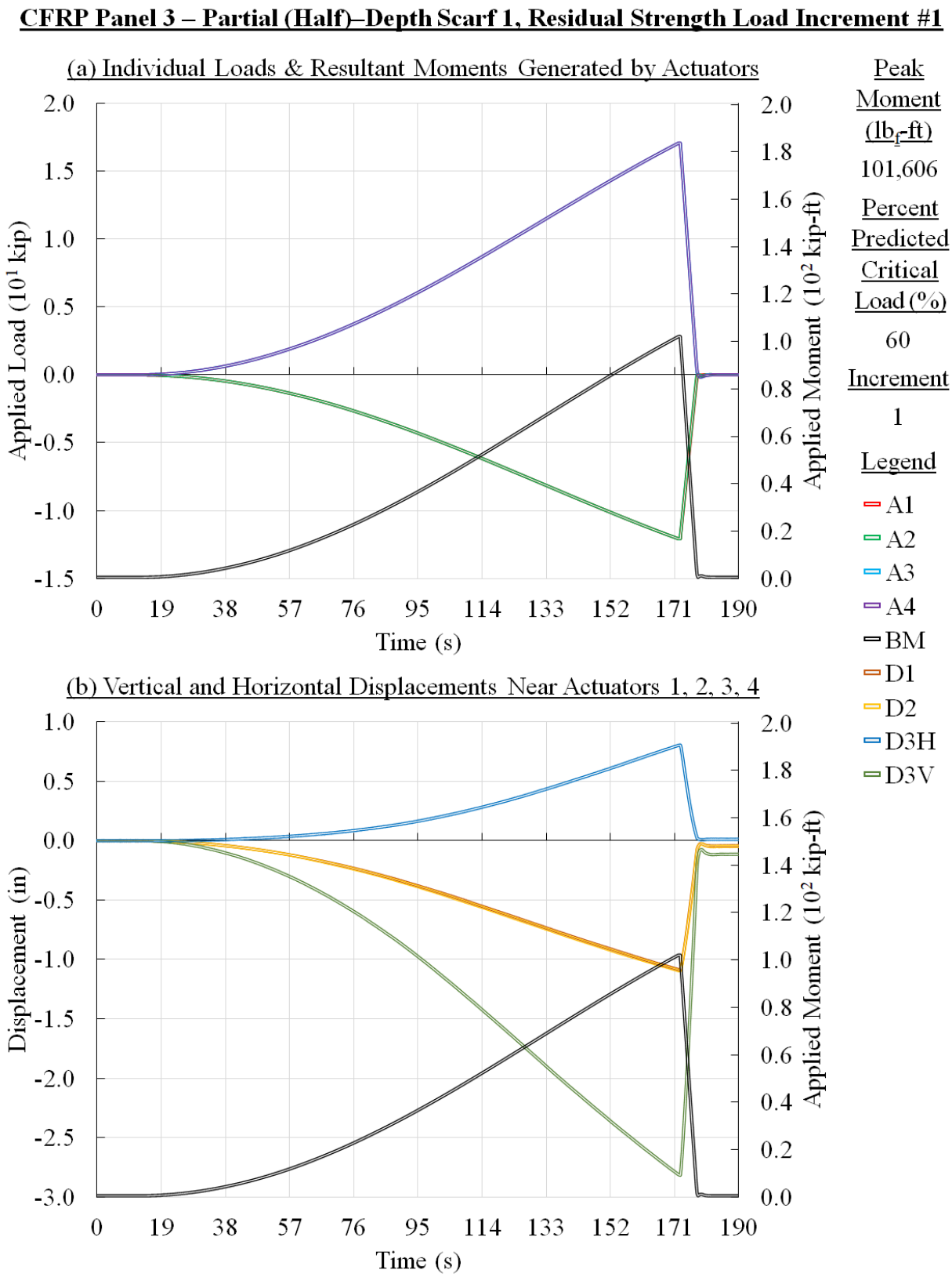


Figure C 2. Panel 3 load increment 1 (60% load level), load and displacement

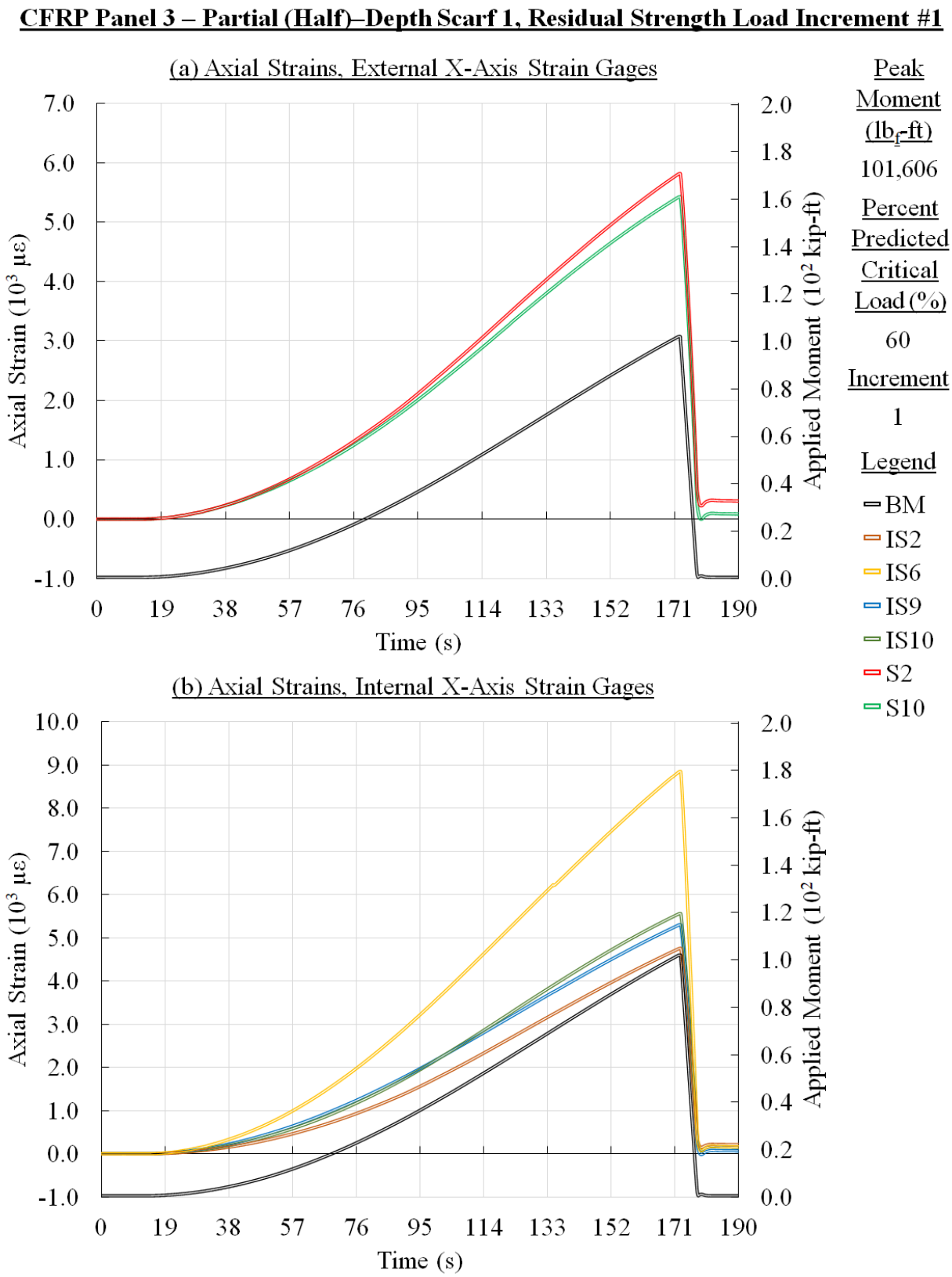


Figure C 3. Panel 3 load increment 1 (60% load level), axial strain along the X-axis strain gages

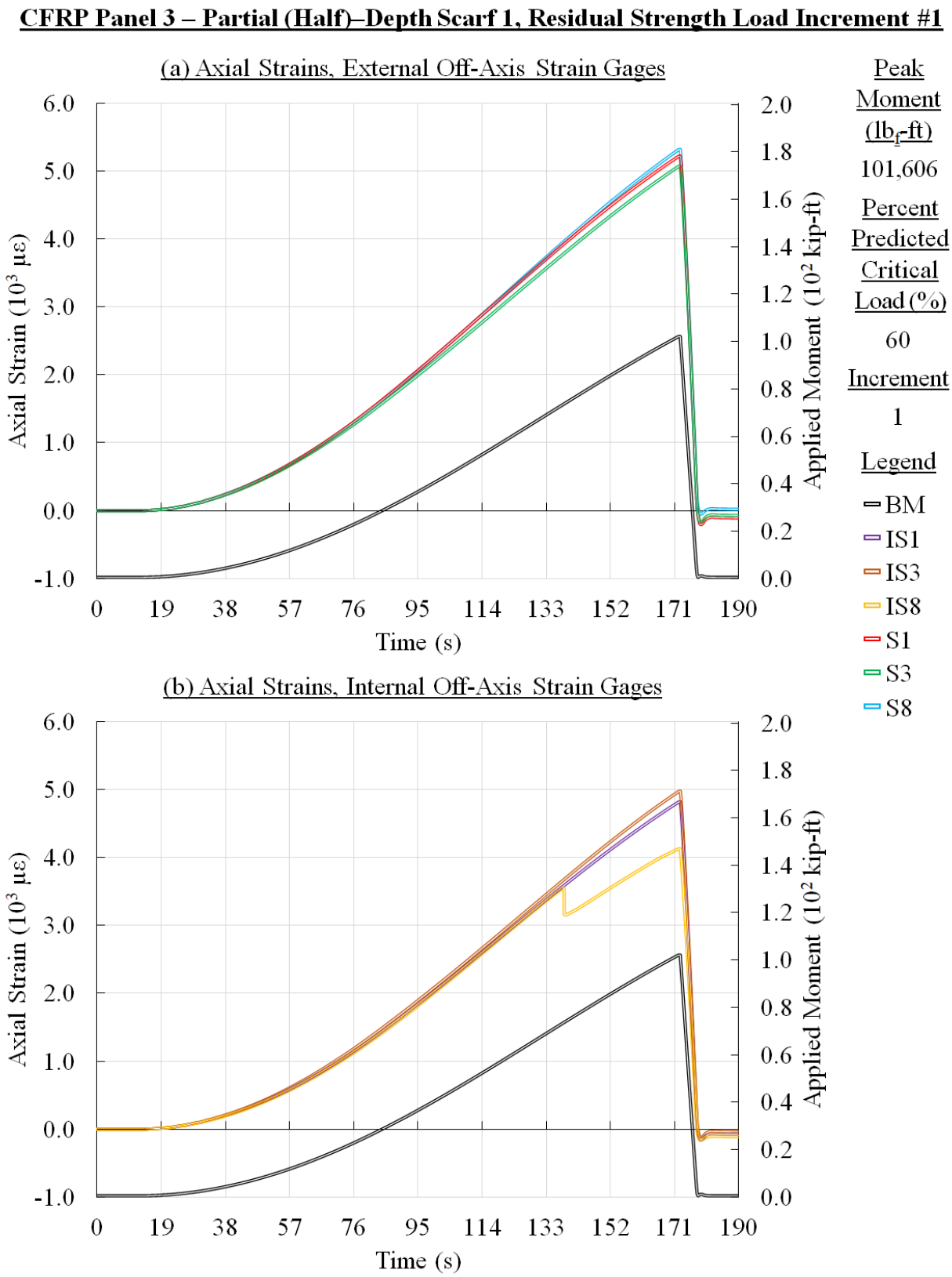


Figure C 5. Panel 3 load increment 1 (60% load level), axial strain along the off-axis strain gages

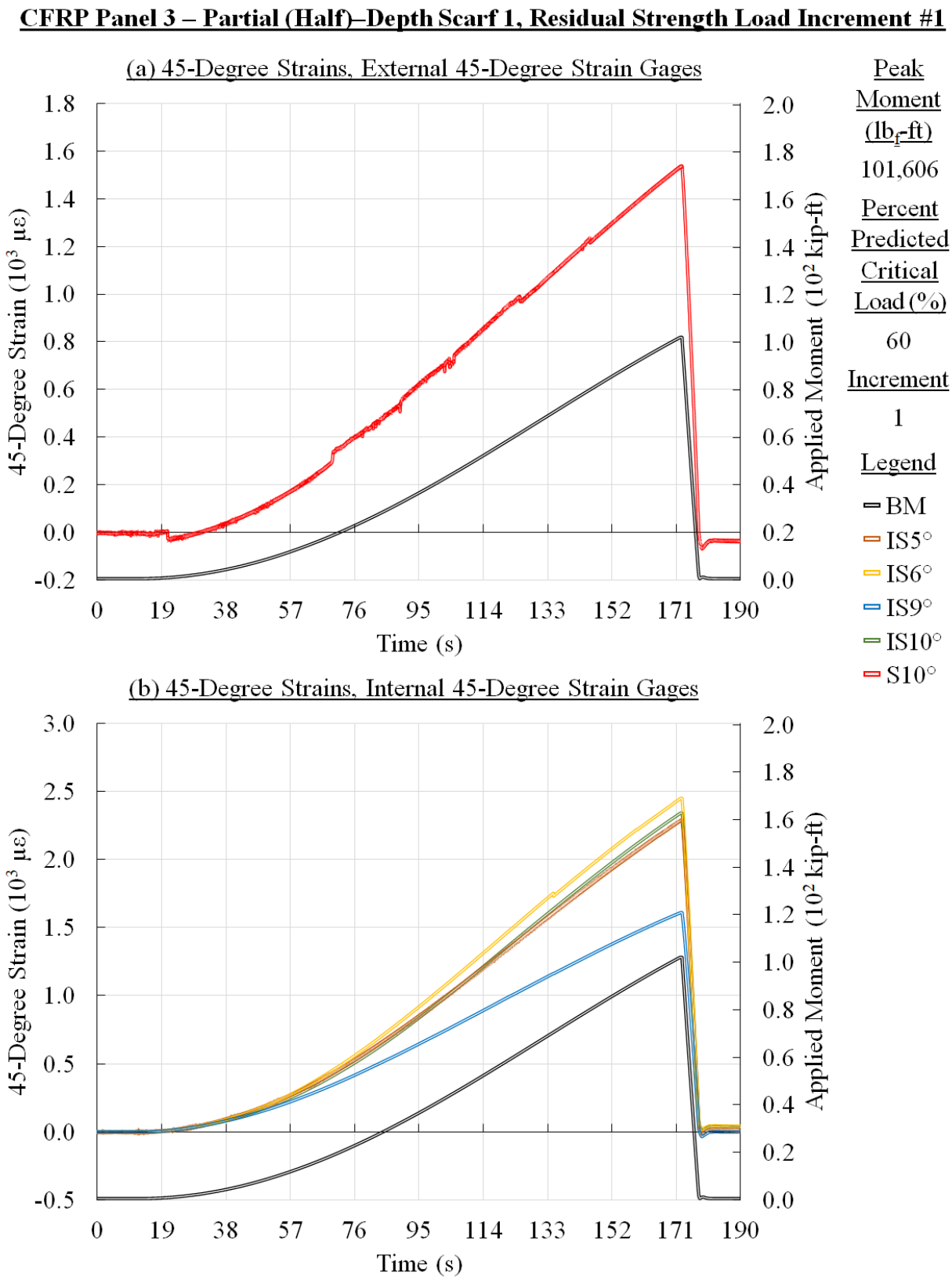


Figure C 6. Panel 3 load increment 1 (60% load level), 45 degree strain

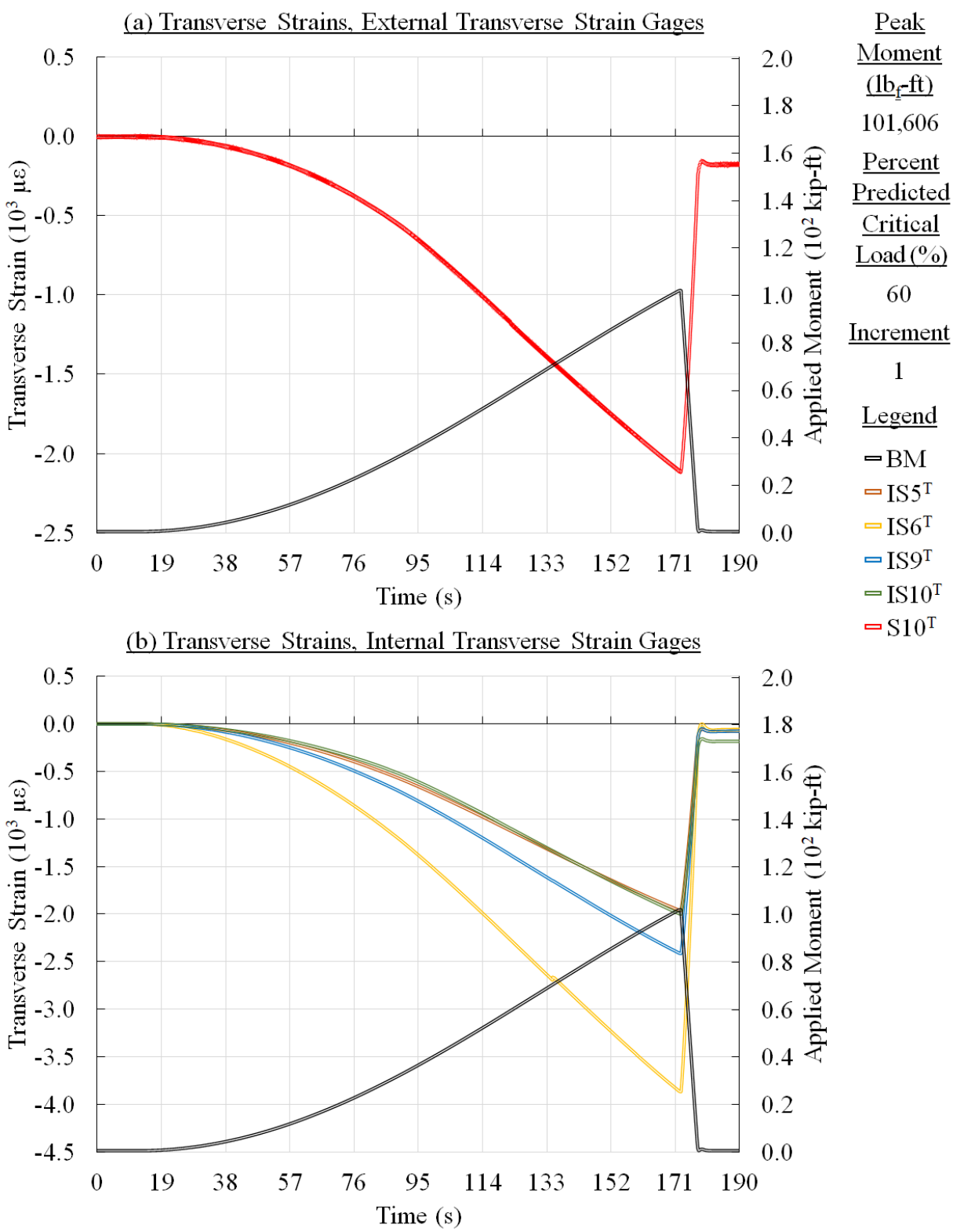


Figure C 7. Panel 3 load increment 1 (60% load level), transverse strain

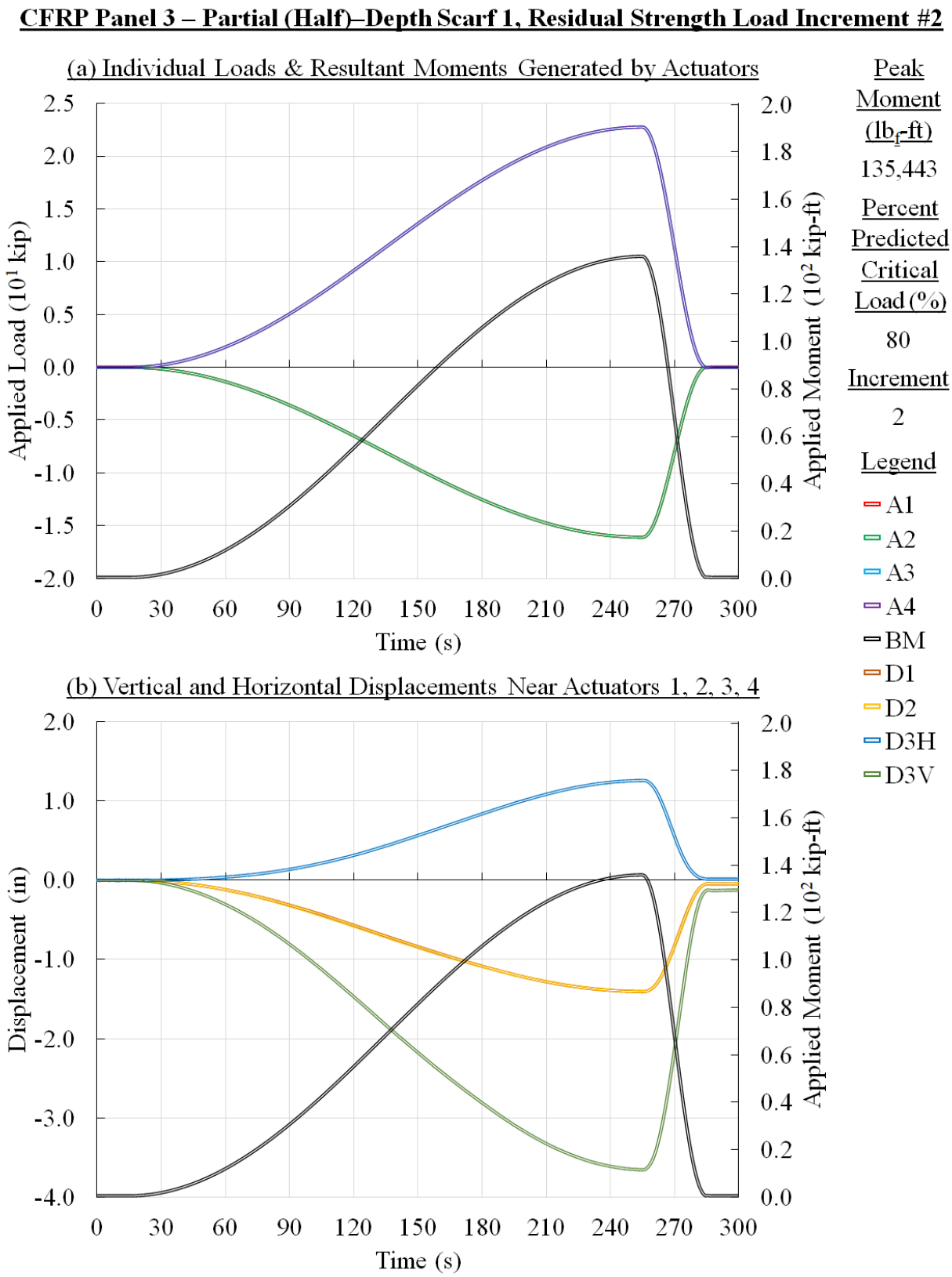


Figure C 8. Panel 3 load increment 2 (80% load level), load and displacement

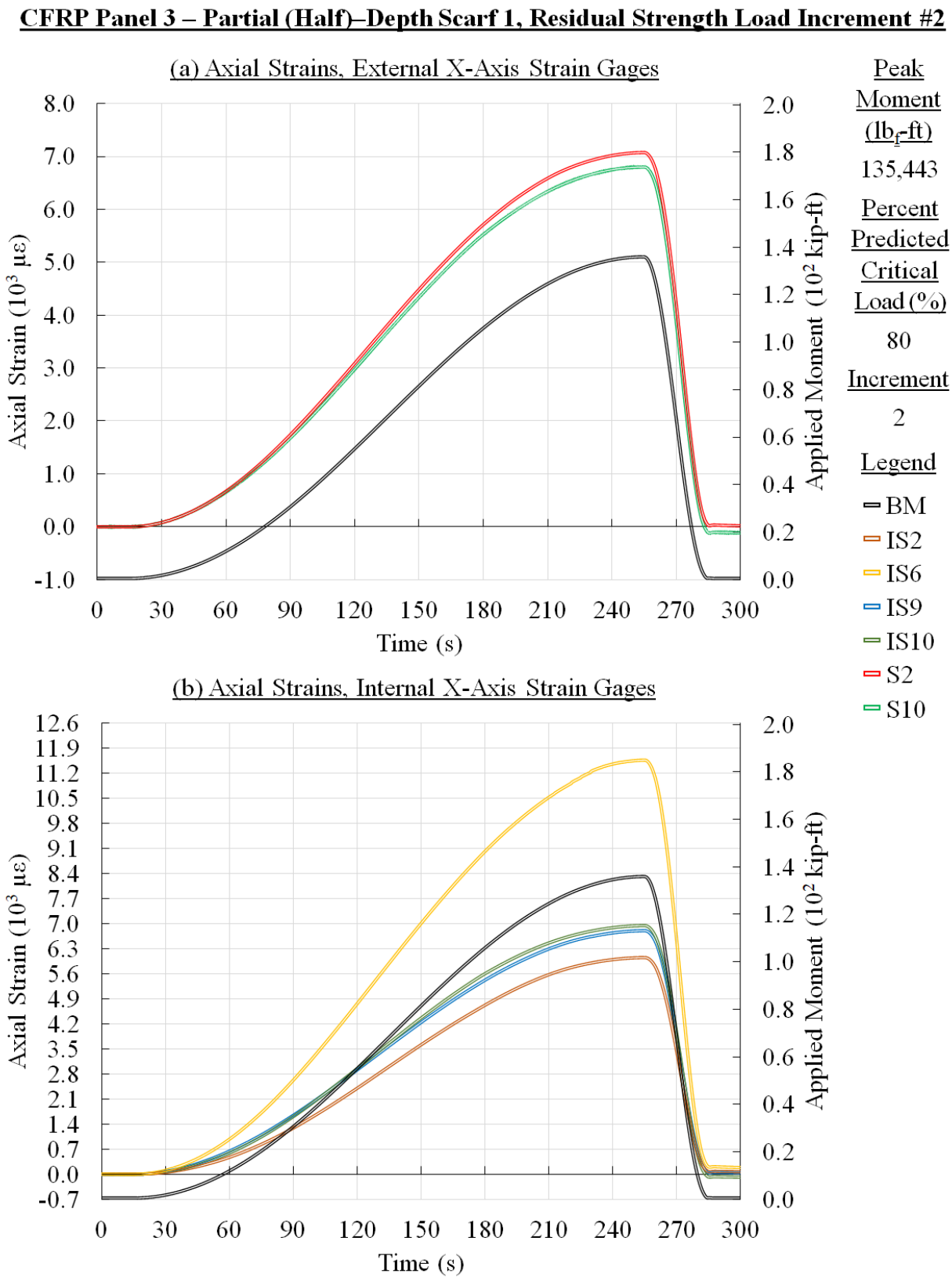


Figure C 9. Panel 3 load increment 2 (80% load level), axial strain along the X-axis strain gages

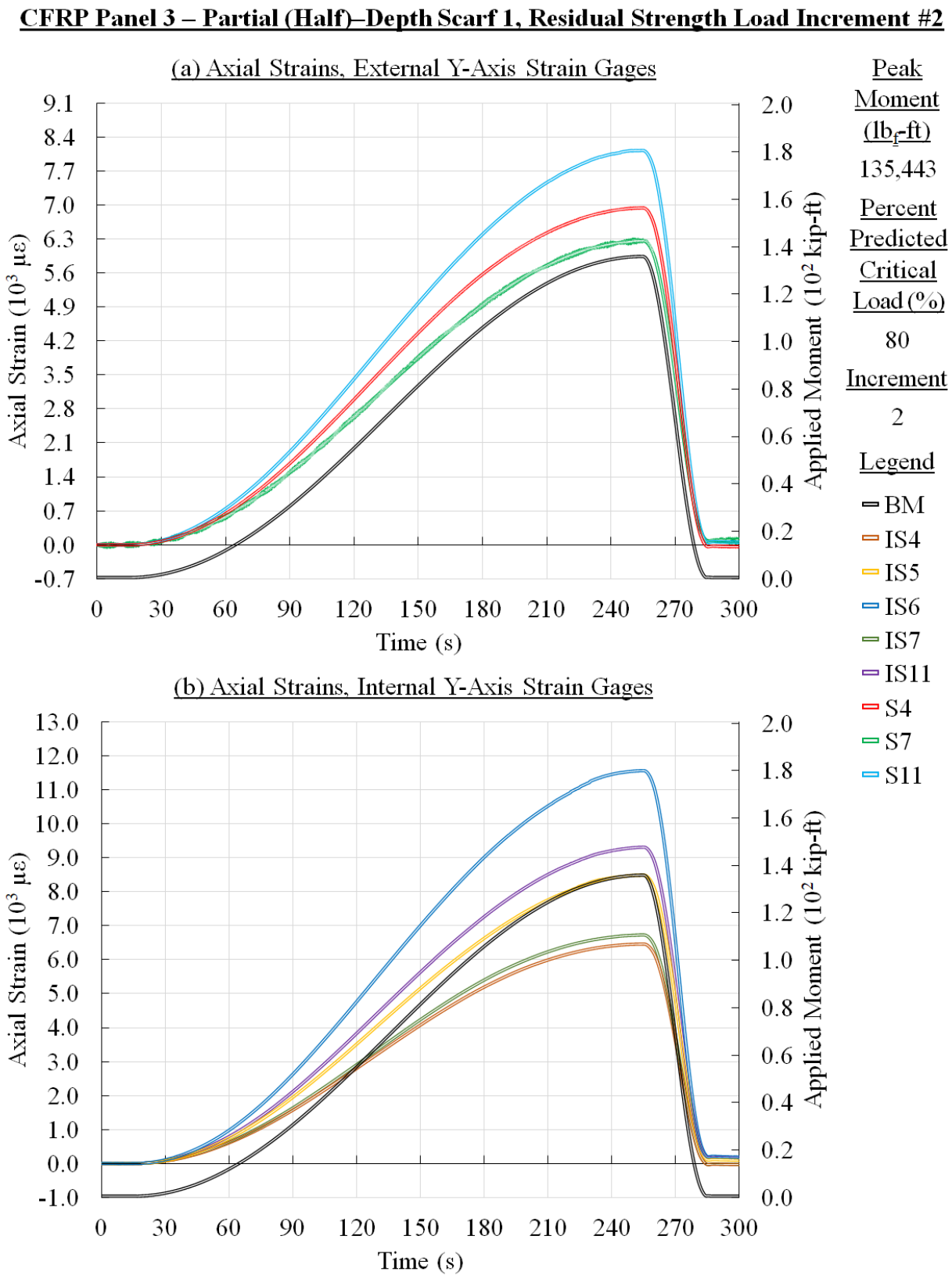


Figure C 10. Panel 3 load increment 2 (80% load level), axial strain along the Y-axis strain gages

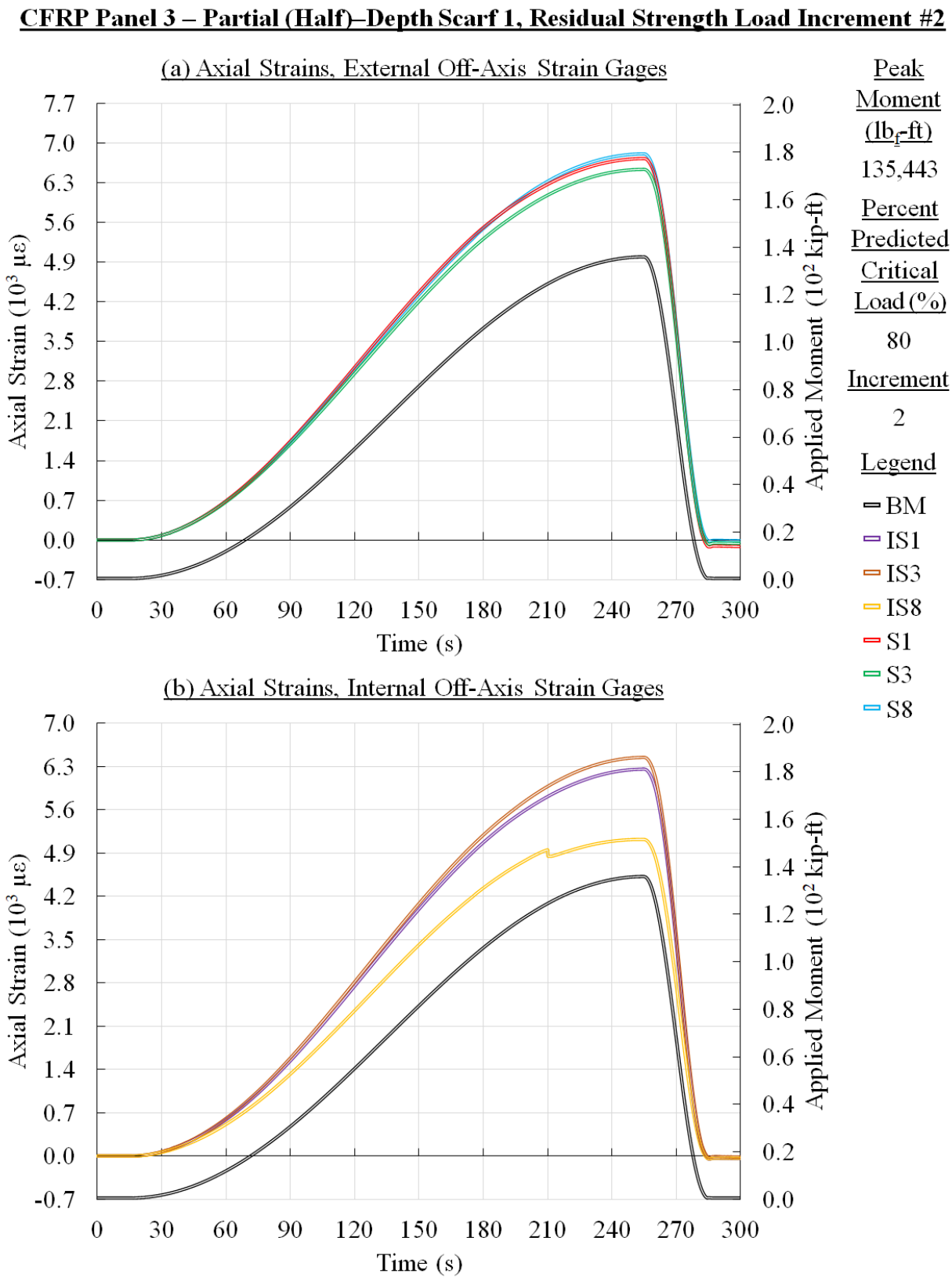


Figure C 11. Panel 3 load increment 2 (80% load level), axial strain along the off-axis strain gages

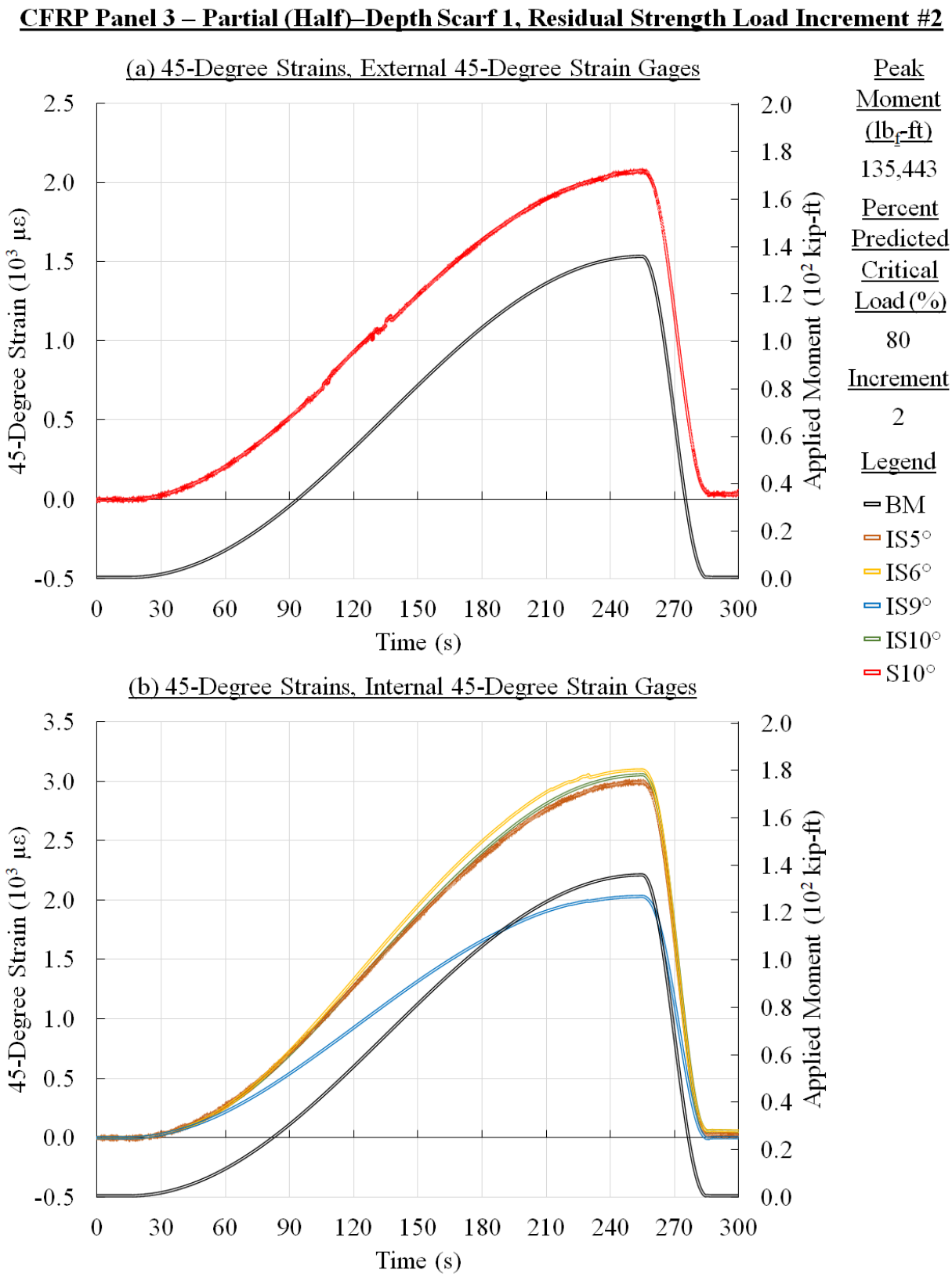


Figure C 12. Panel 3 load increment 2 (80% load level), 45 degree strain

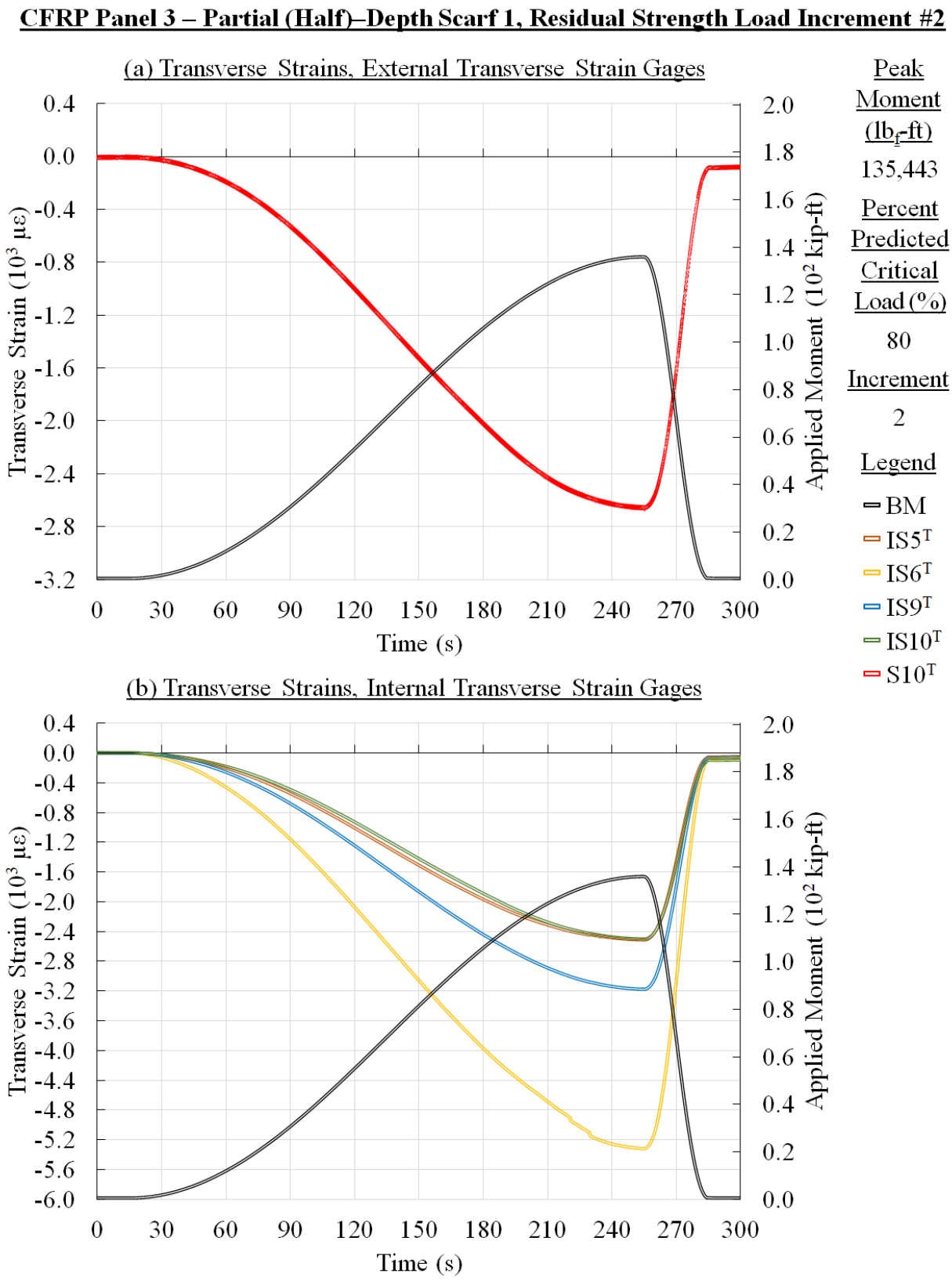


Figure C 13. Panel 3 load increment 2 (80% load level), transverse strain

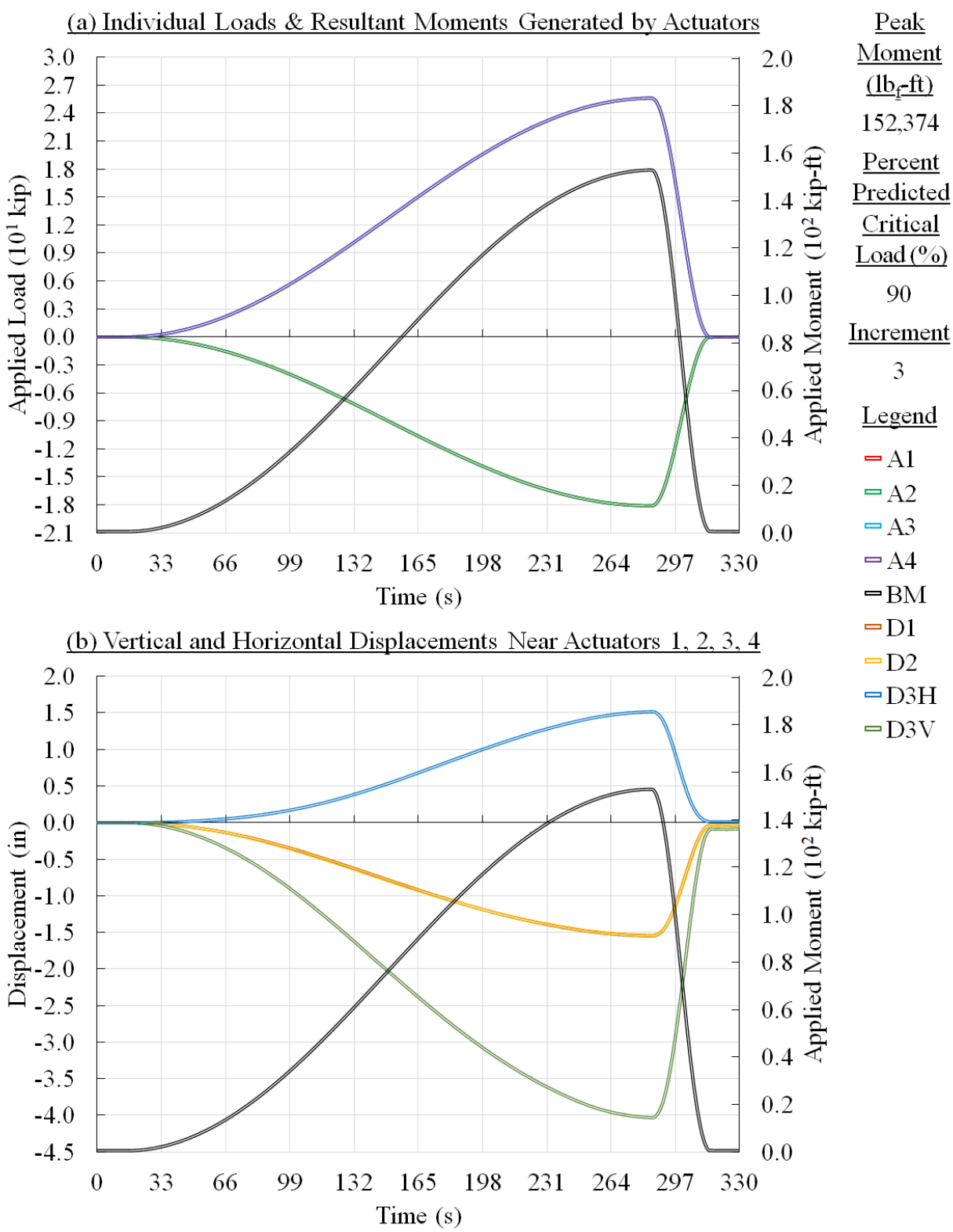


Figure C 14. Panel 3 load increment 3 (90% load level), load and displacement

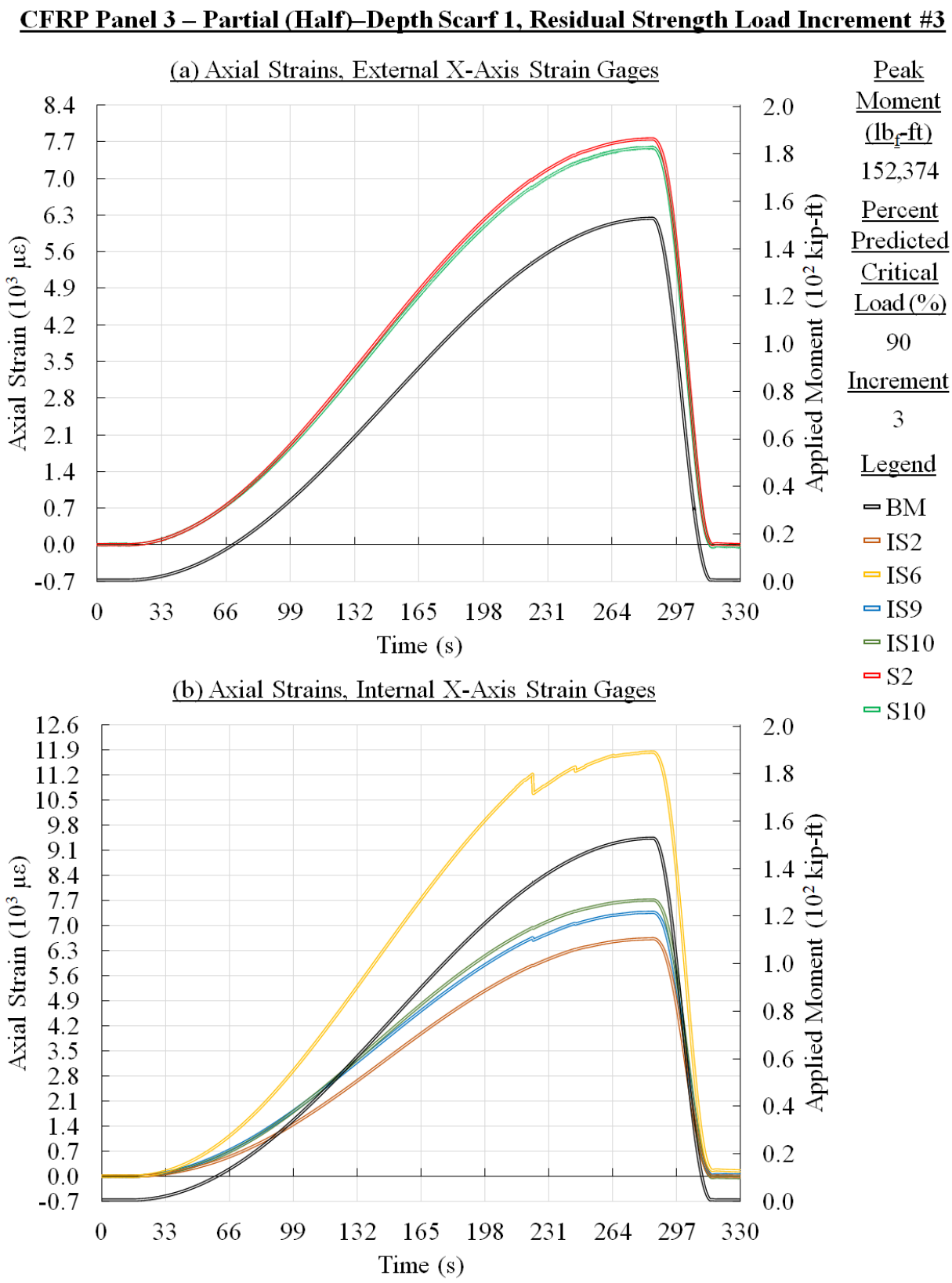


Figure C 15. Panel 3 load increment 3 (90% load level), axial strain along the X-axis strain gages

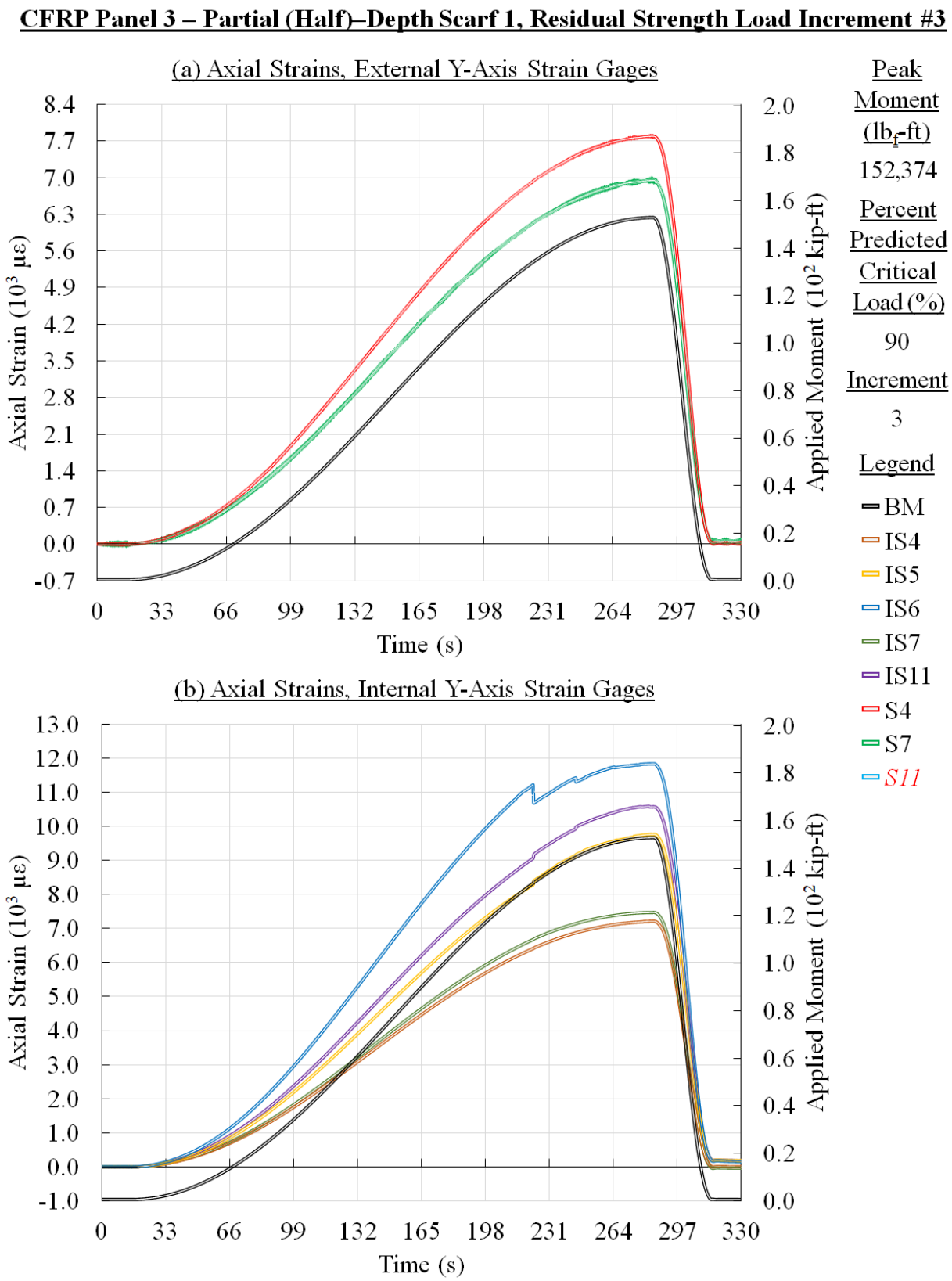


Figure C 16. Panel 3 load increment 3 (90% load level), axial strain along the Y-axis strain gages

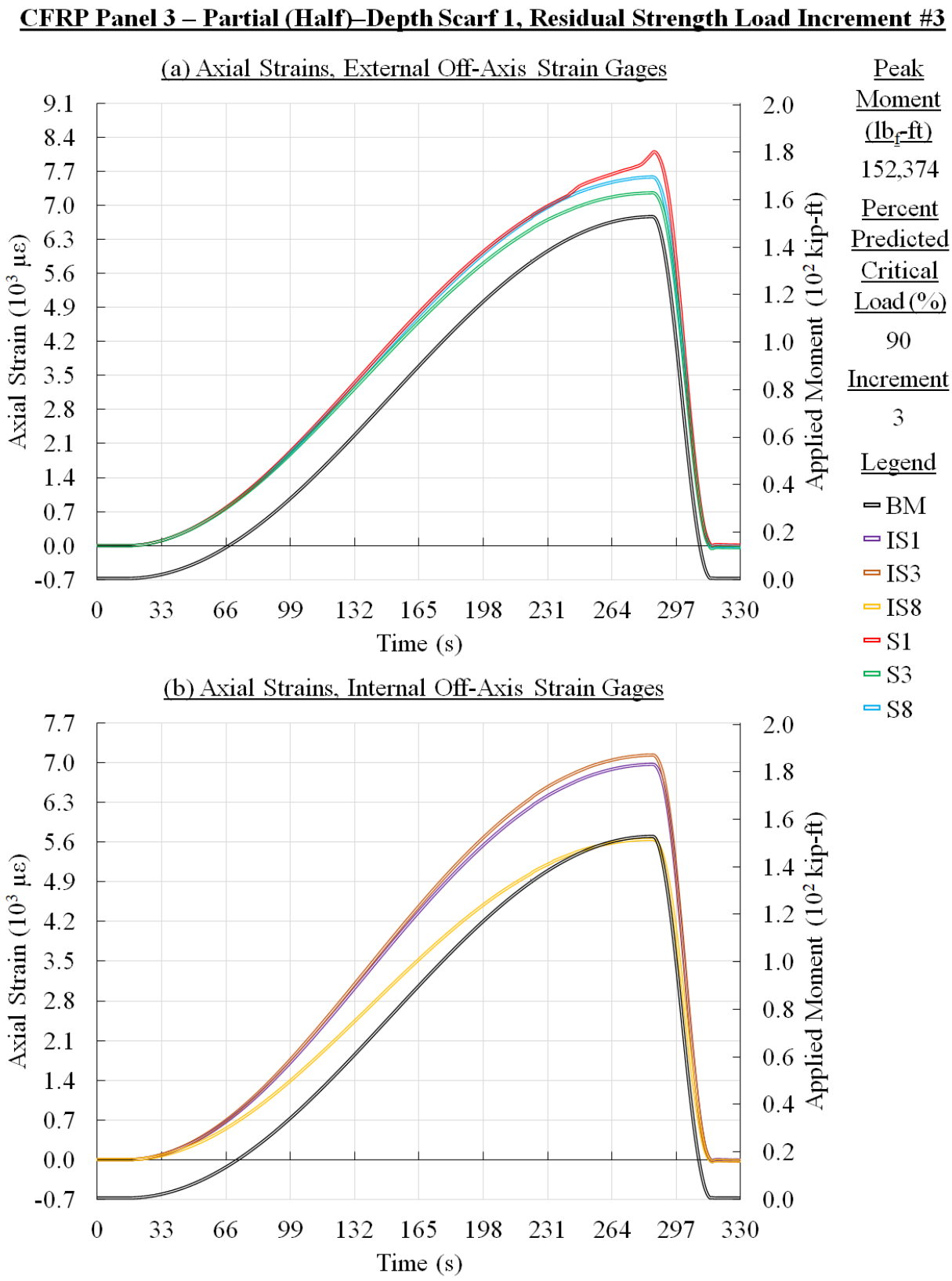


Figure C 17. Panel 3 load increment 3 (90% load level), axial strain along the off-axis strain gages

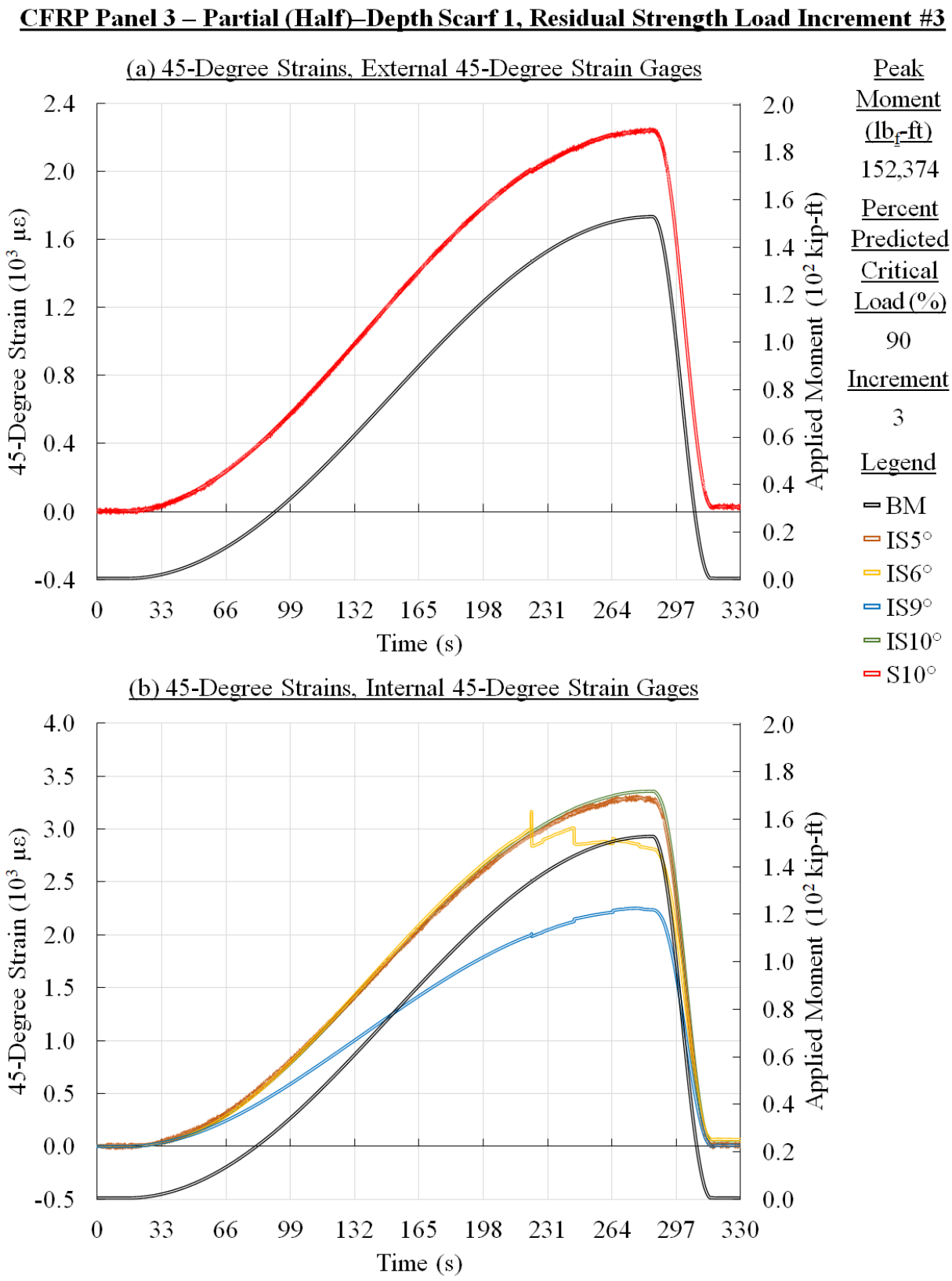


Figure C 18. Panel 3 load increment 3 (90% load level), 45 degree strain

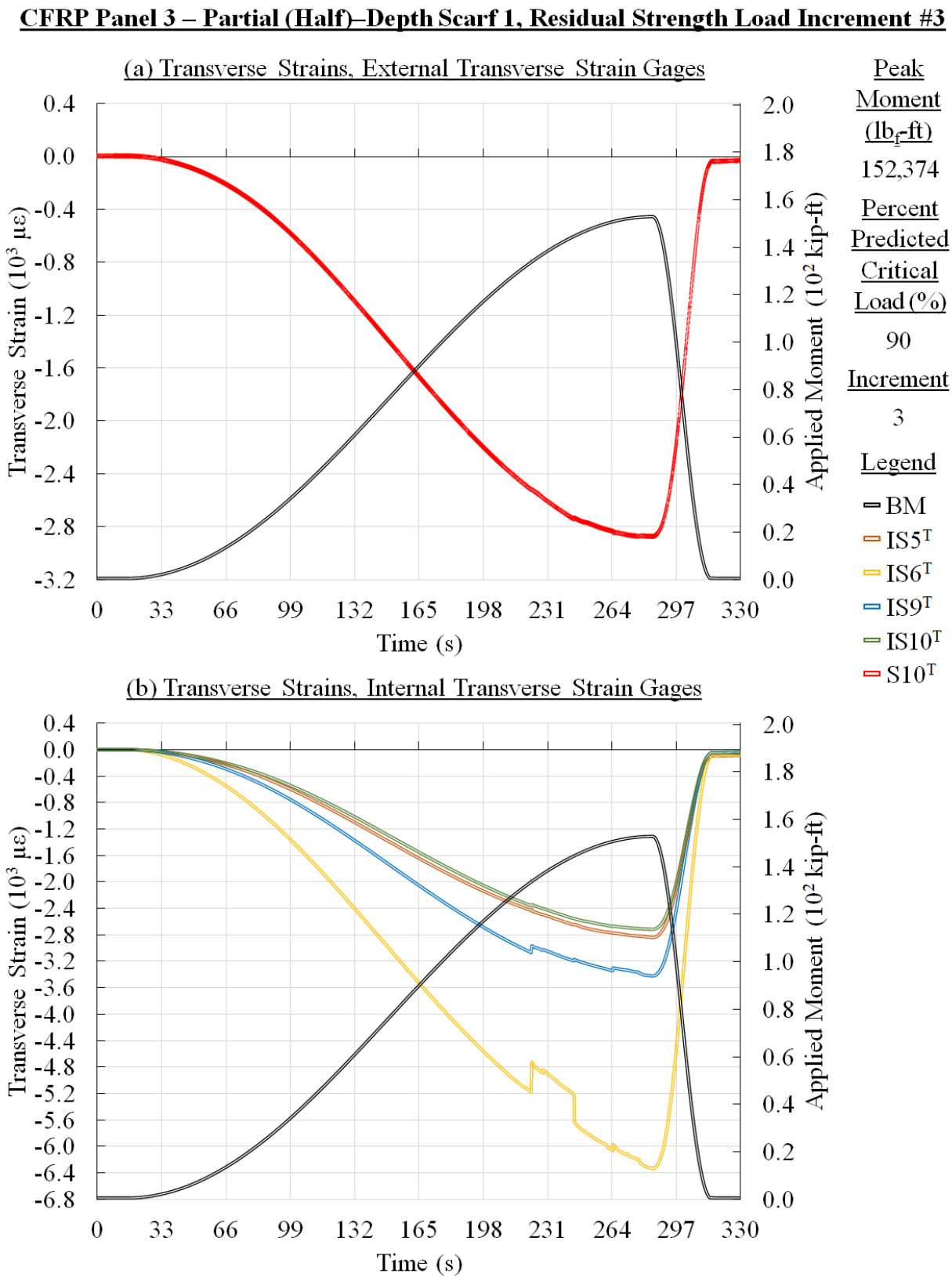


Figure C 19. Panel 3 load increment 3 (90% load level), transverse strain

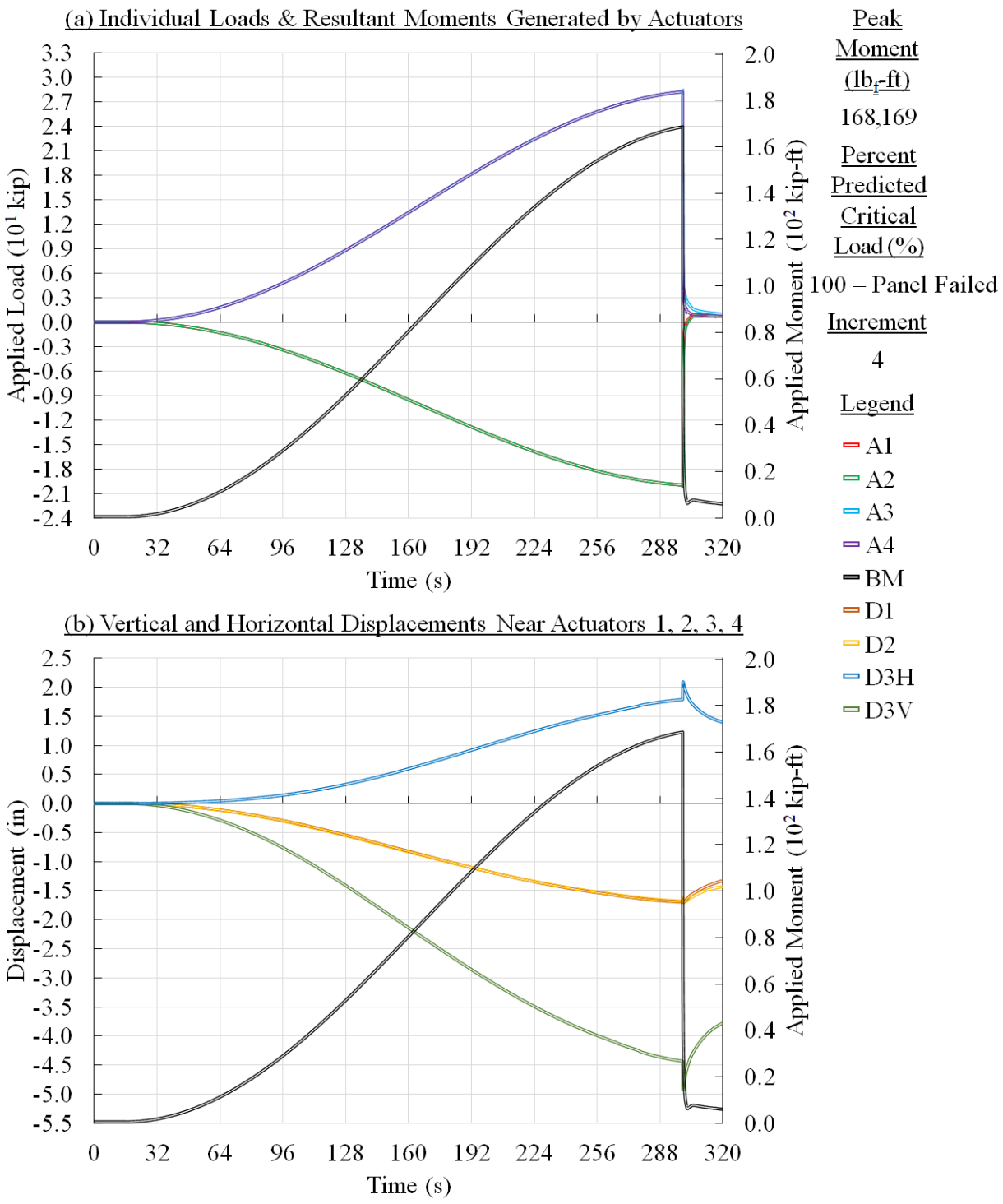


Figure C 20. Panel 3 load increment 4 (panel failure), load and displacement

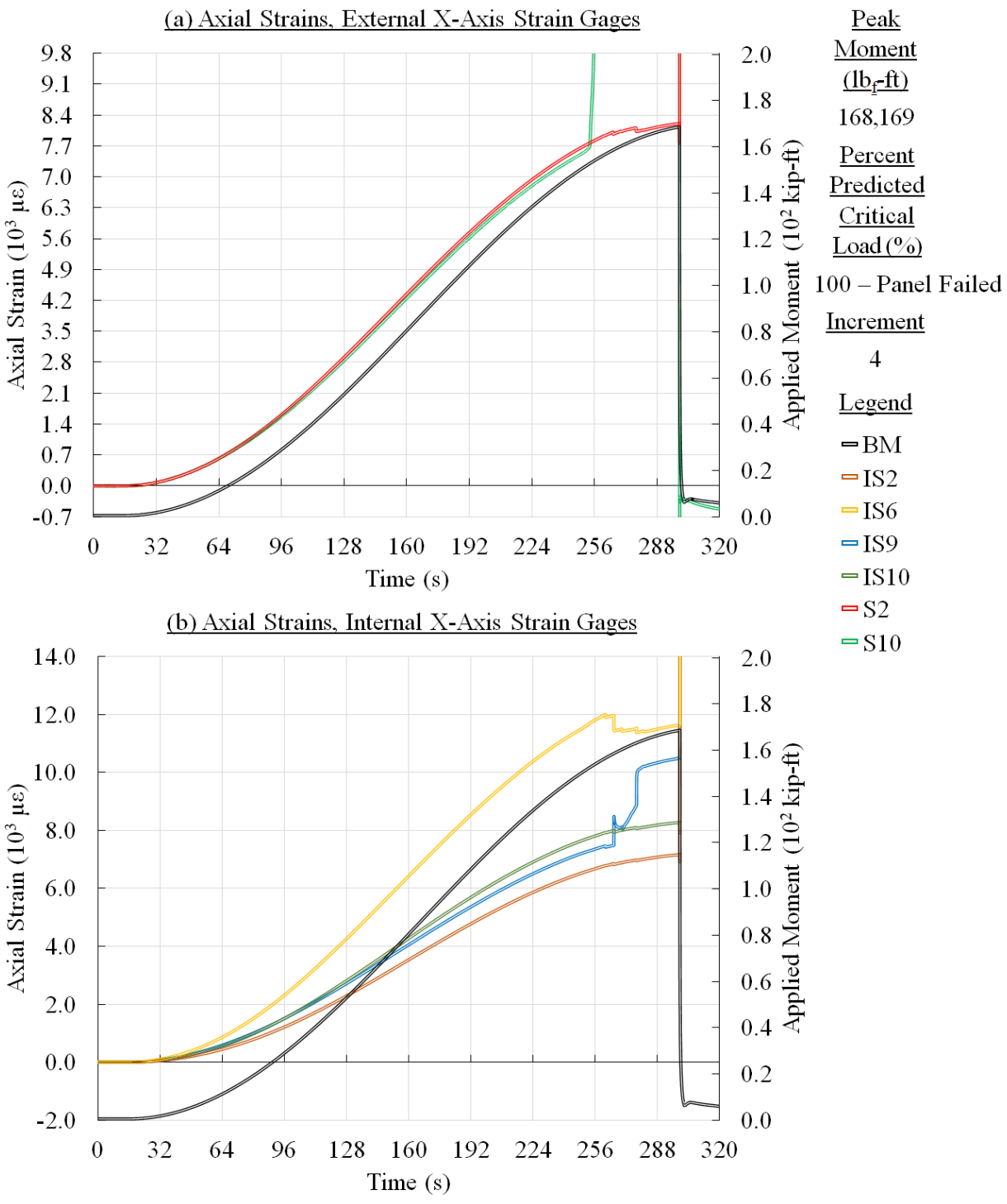


Figure C 21. Panel 3 load increment 4 (panel failure), axial strain along the X-axis strain gages

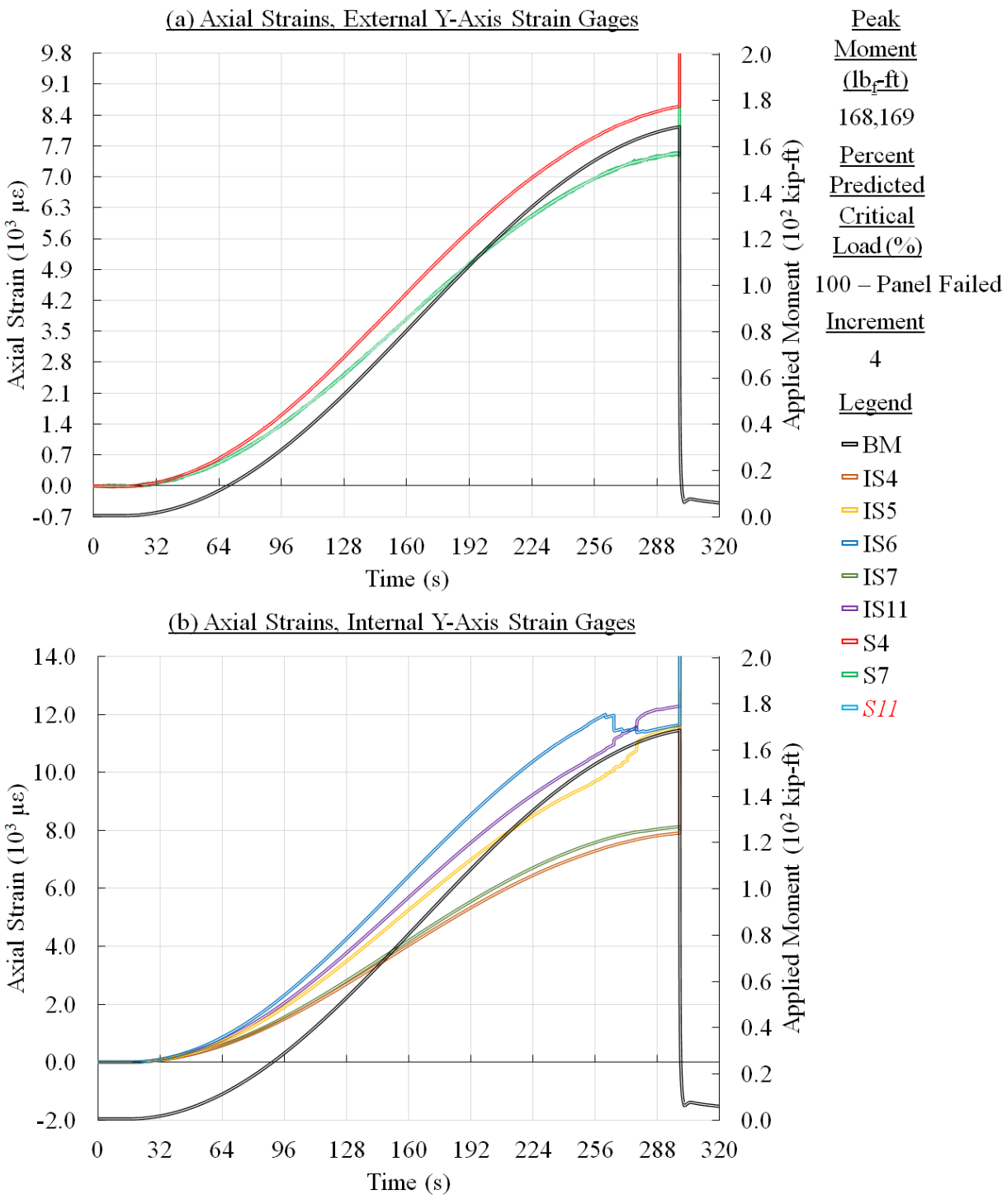


Figure C 22. Panel 3 load increment 4 (panel failure), axial strain along the Y-axis strain gages

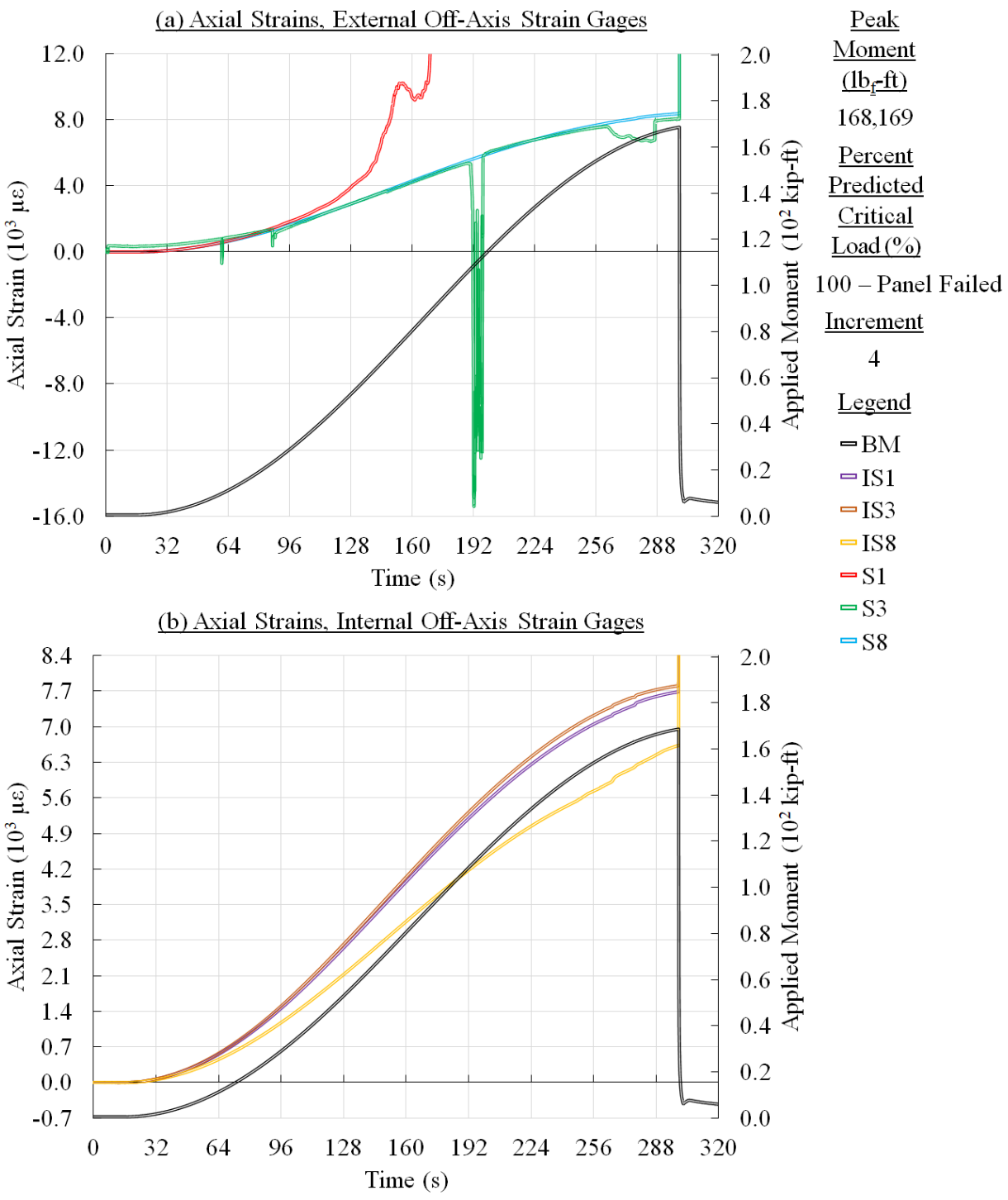


Figure C 23. Panel 3 load increment 4 (panel failure), axial strain along the off-axis strain gages

**CFRP Panel 3 – Partial (Half)–Depth Scarf 1, Residual Strength Load Increment #4**

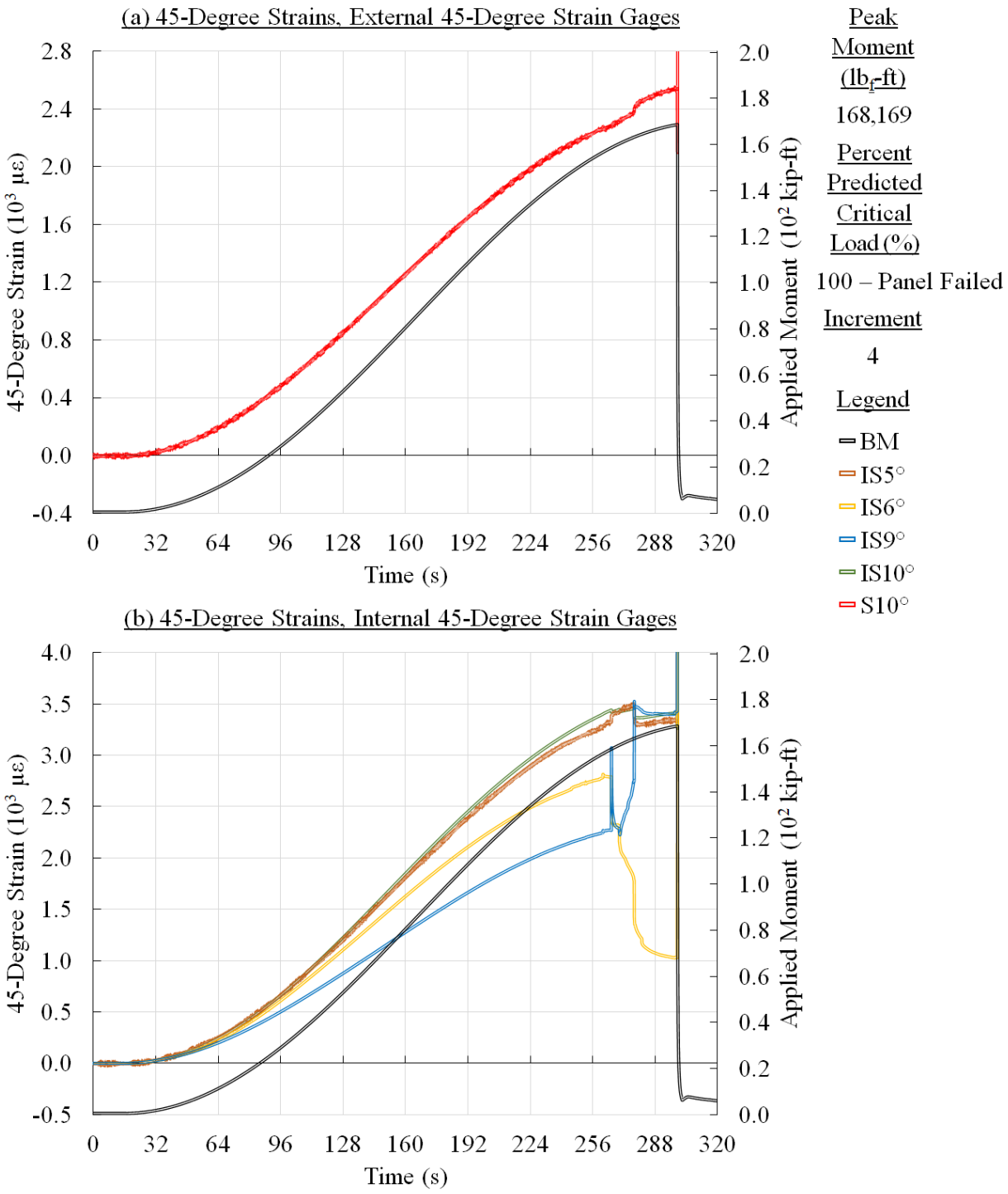


Figure C 24. Panel 3 load increment 4 (panel failure), 45 degree strain

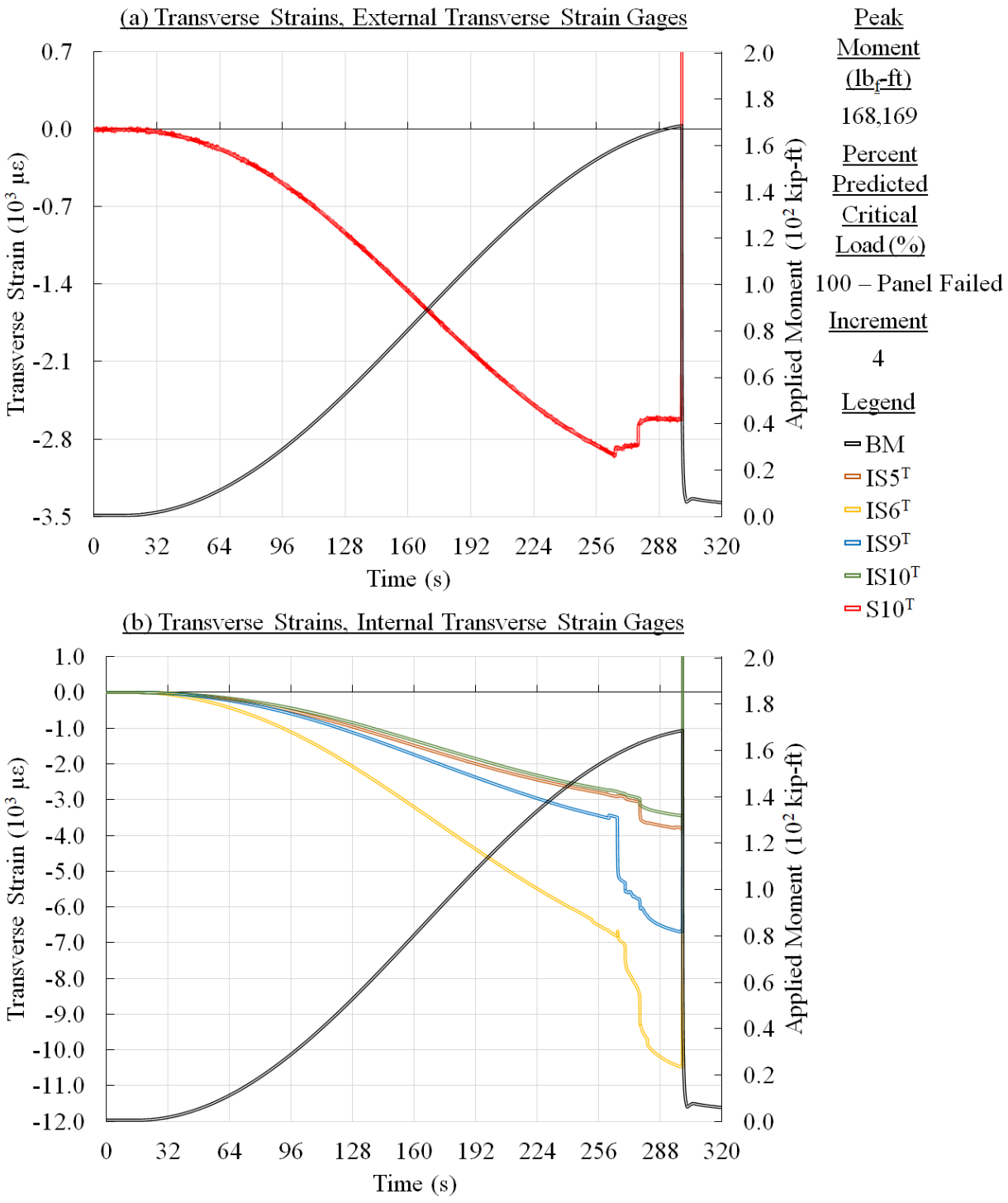


Figure C 25. Panel 3 load increment 4 (panel failure), transverse strain

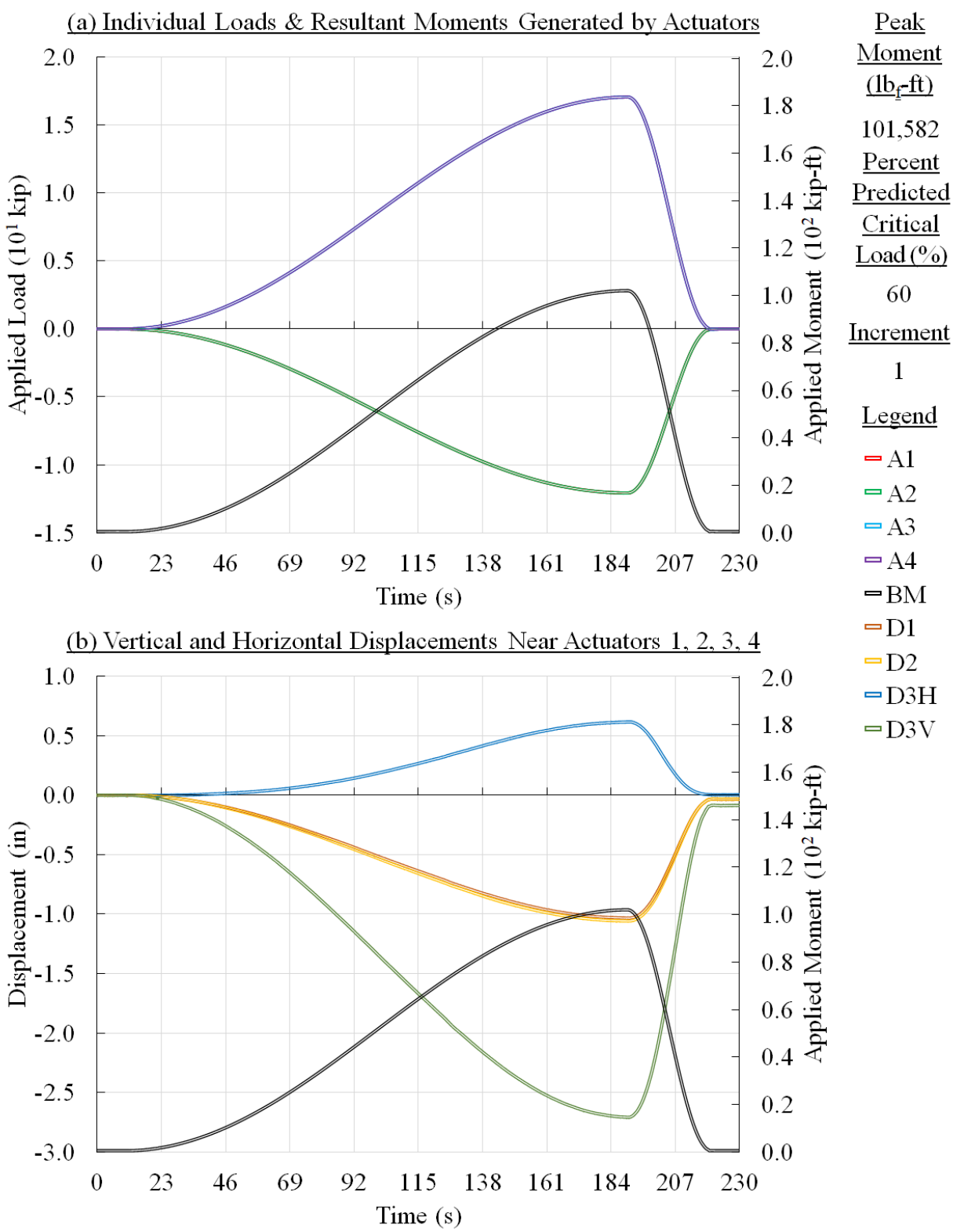


Figure C 26. Panel 5 load increment 1 (60% load level), load and displacement

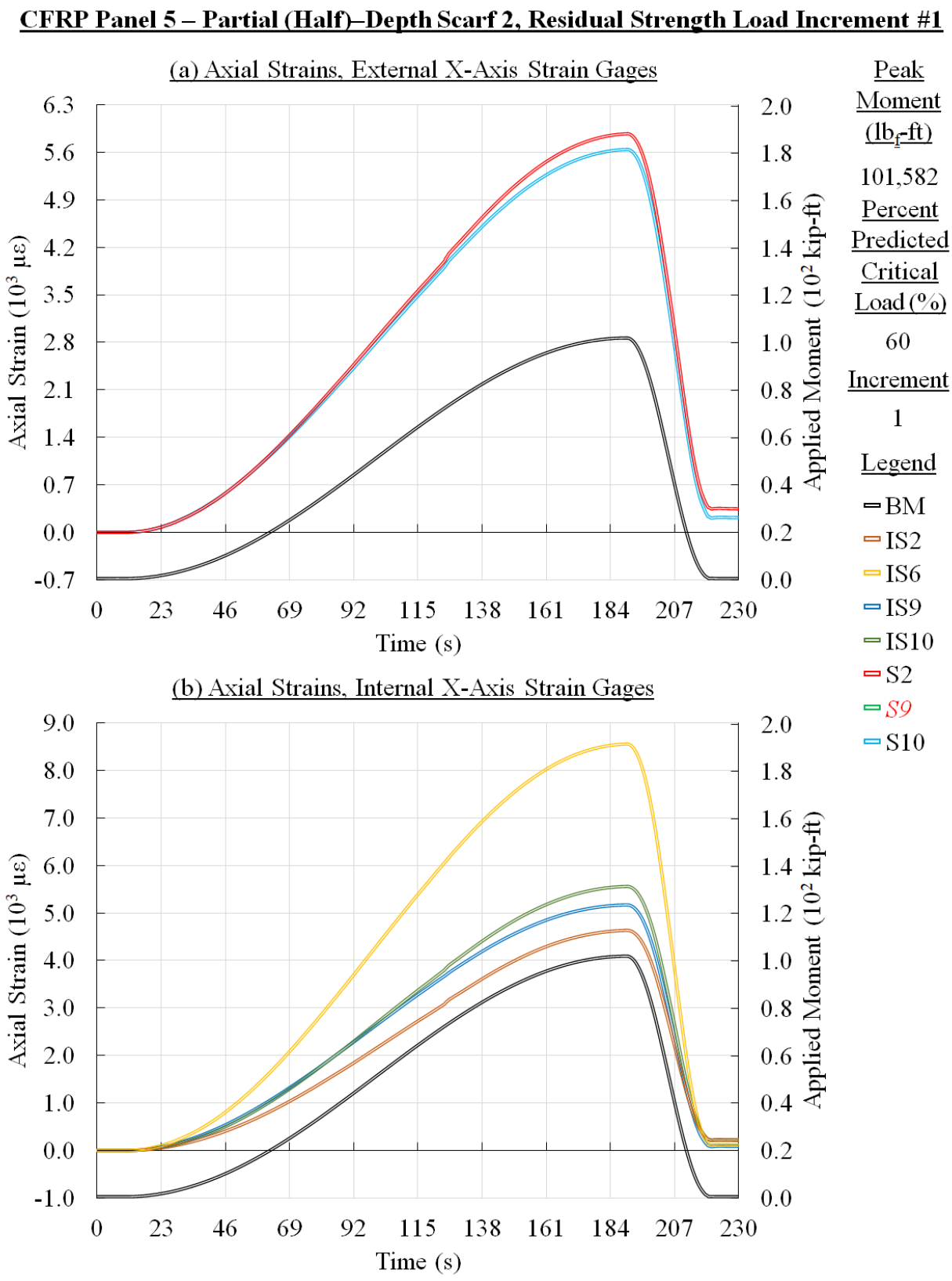


Figure C 27. Panel 5 load increment 1 (60% load level), axial strain along the X-axis strain gages

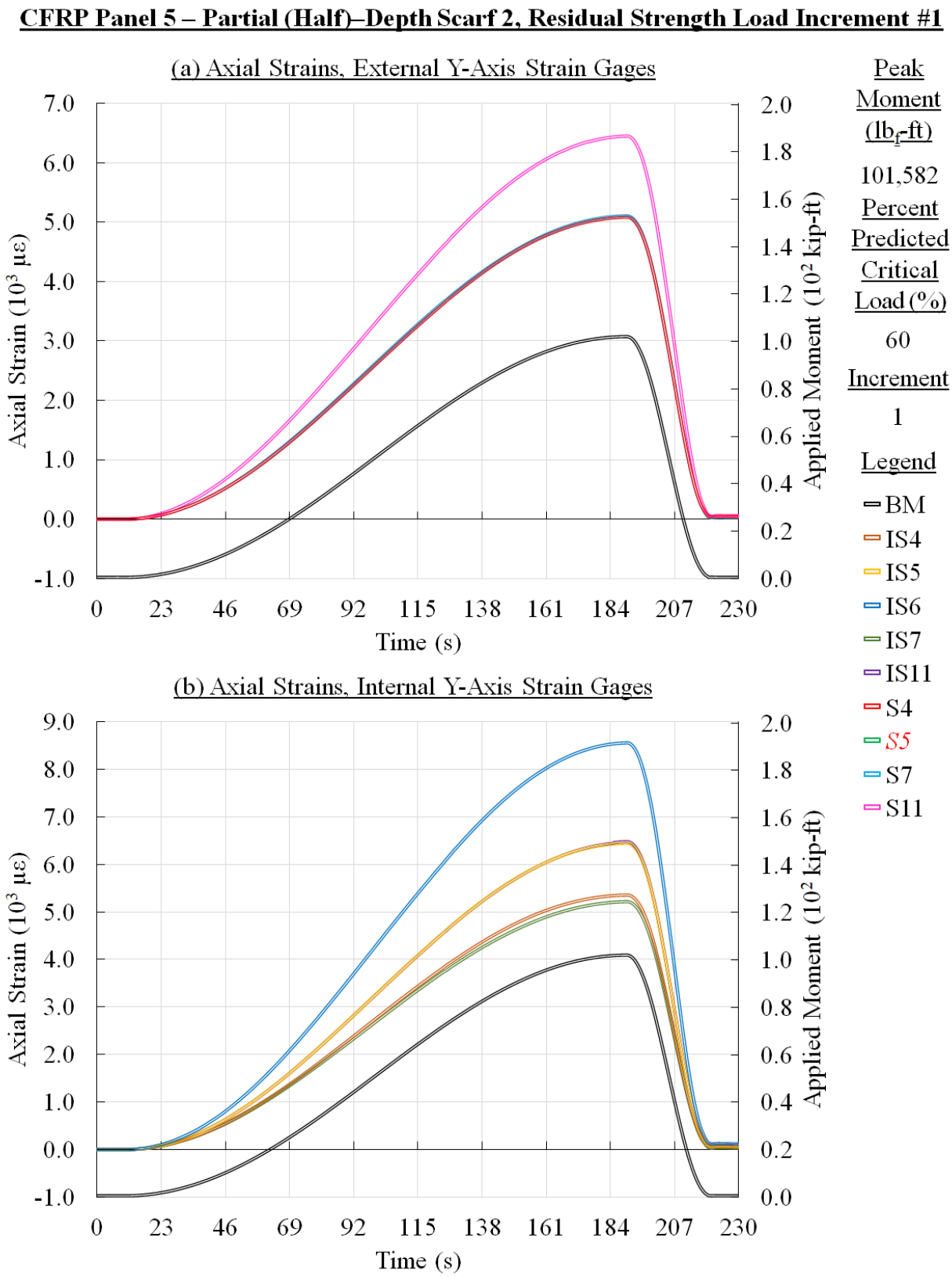


Figure C 28. Panel 5 load increment 1 (60% load level), axial strain along the Y-axis strain gages

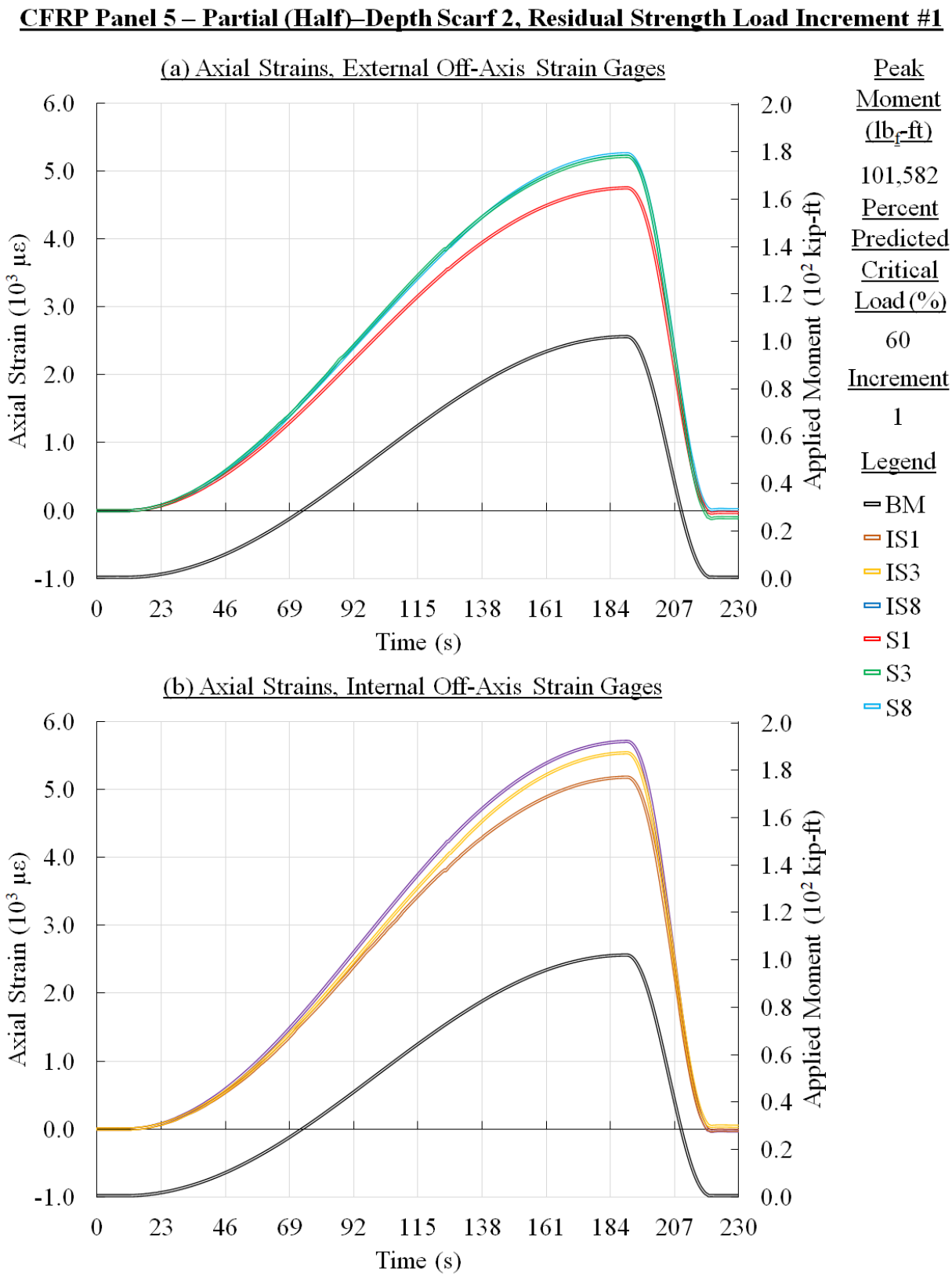


Figure C 29. Panel 5 load increment 1 (60% load level), axial strain along the off-axis strain gages

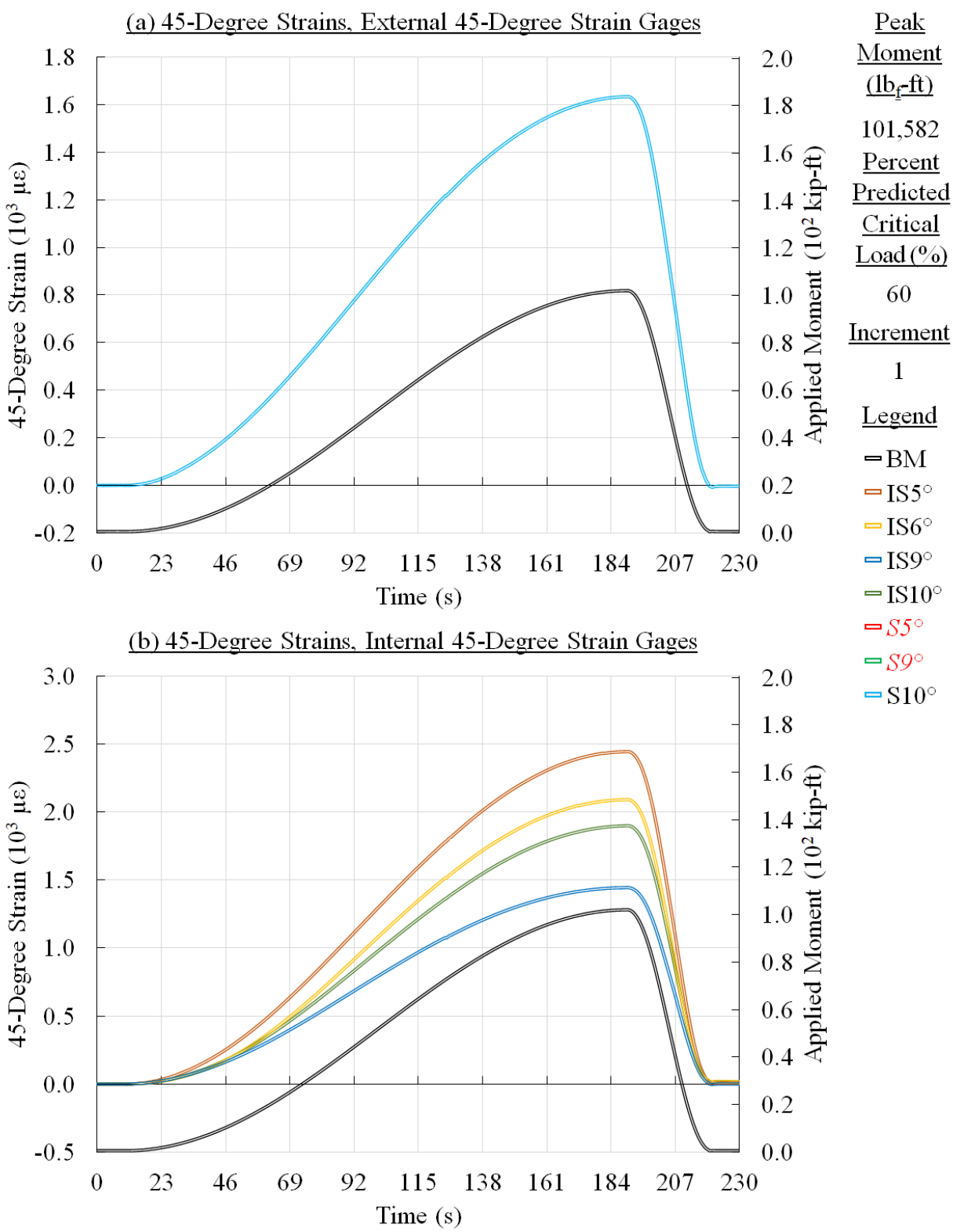


Figure C 30. Panel 5 load increment 1 (60% load level), 45 degree strain

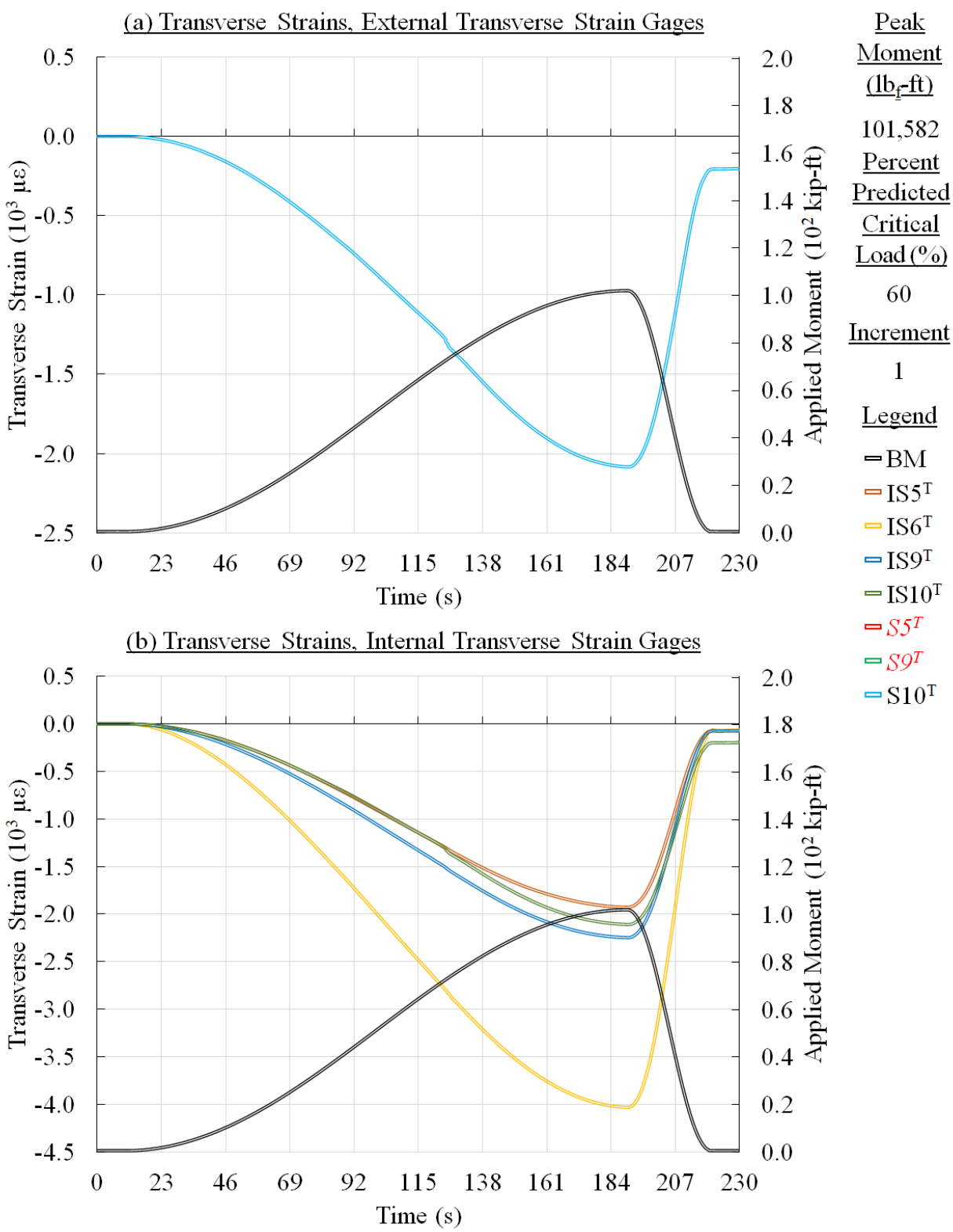


Figure C 31. Panel 5 load increment 1 (60% load level), transverse strain

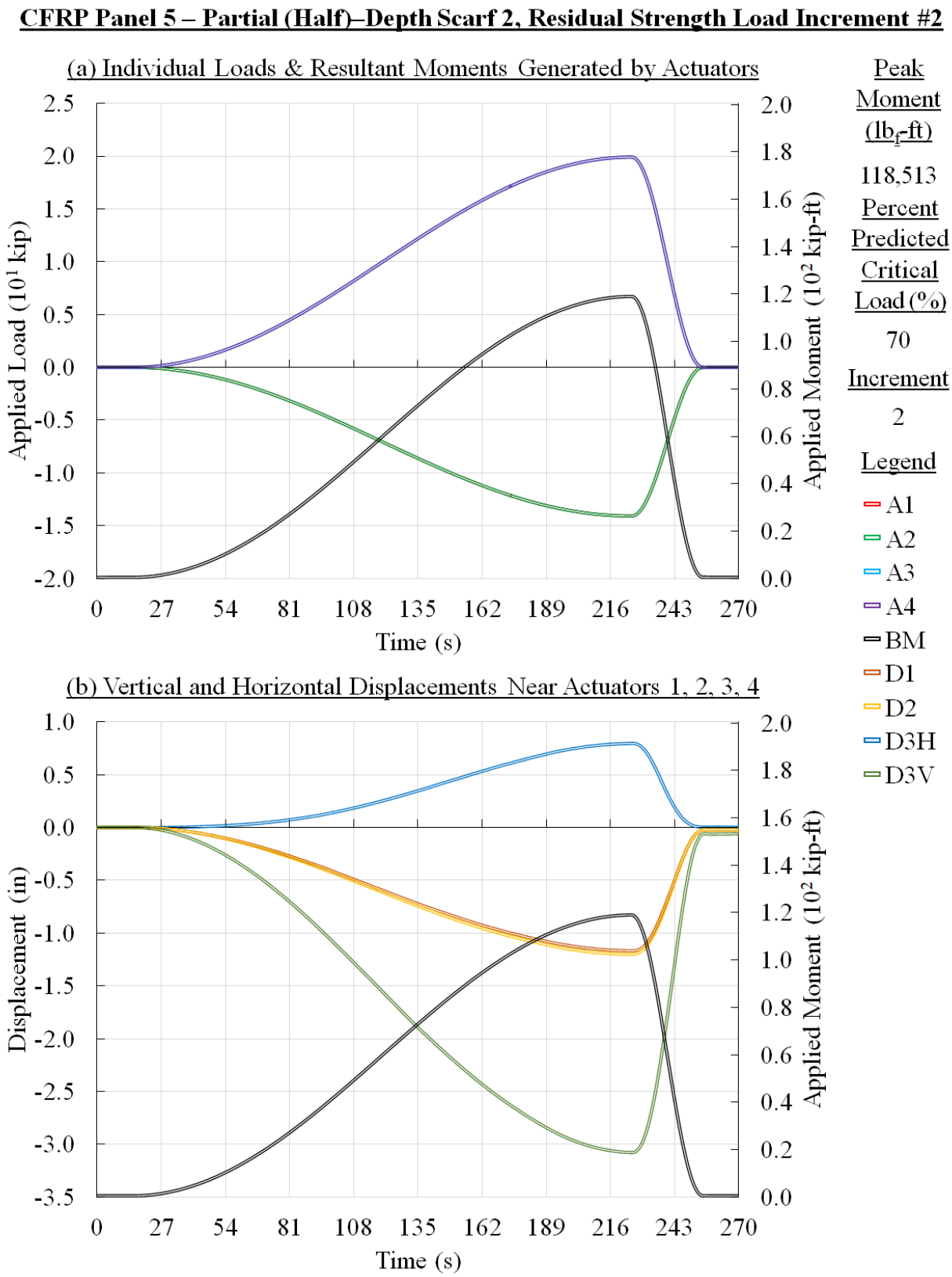


Figure C 32. Panel 5 load increment 2 (70% load level), load and displacement

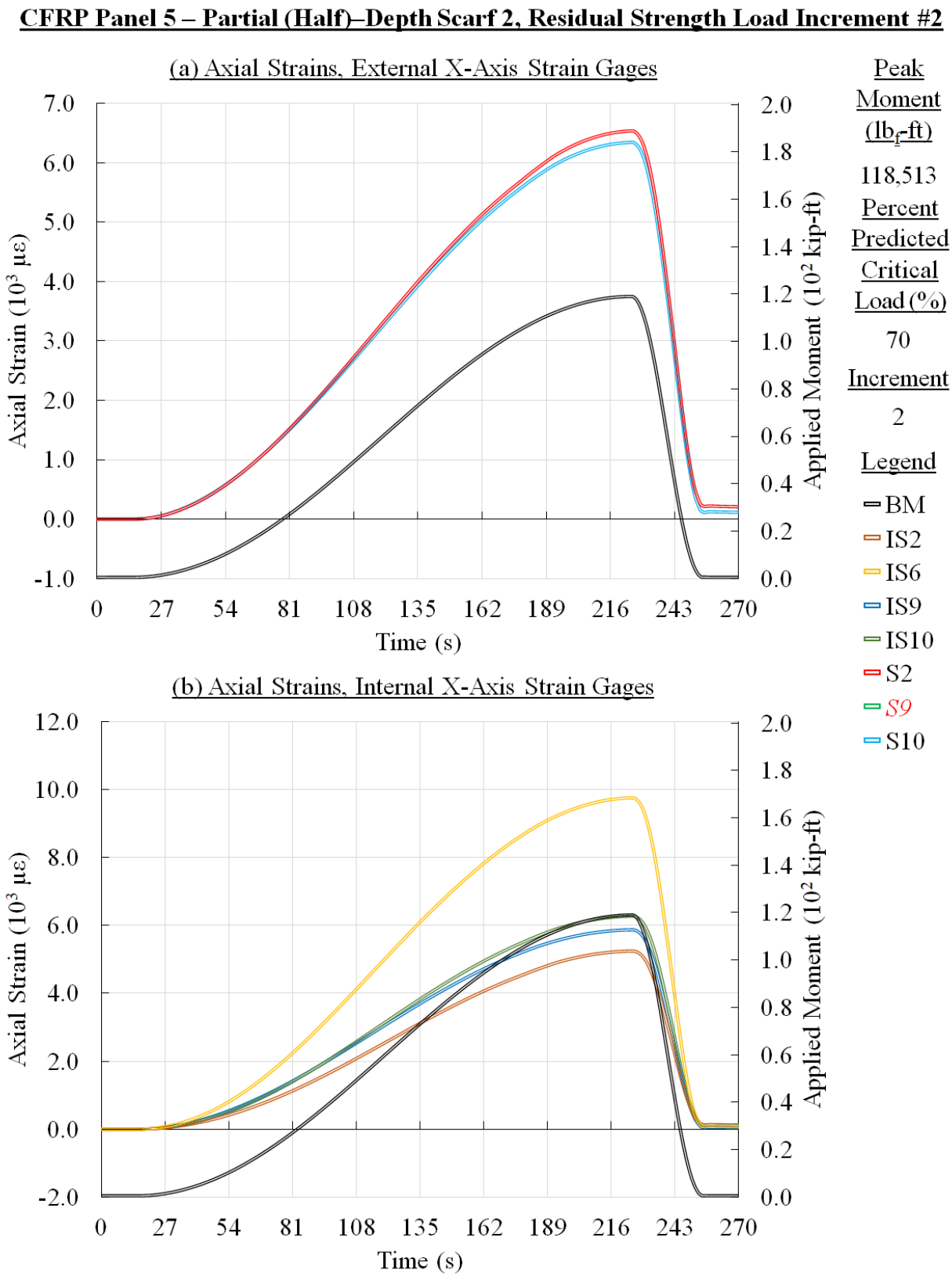


Figure C 33. Panel 5 load increment 2 (70% load level), axial strain along the X-axis strain gages

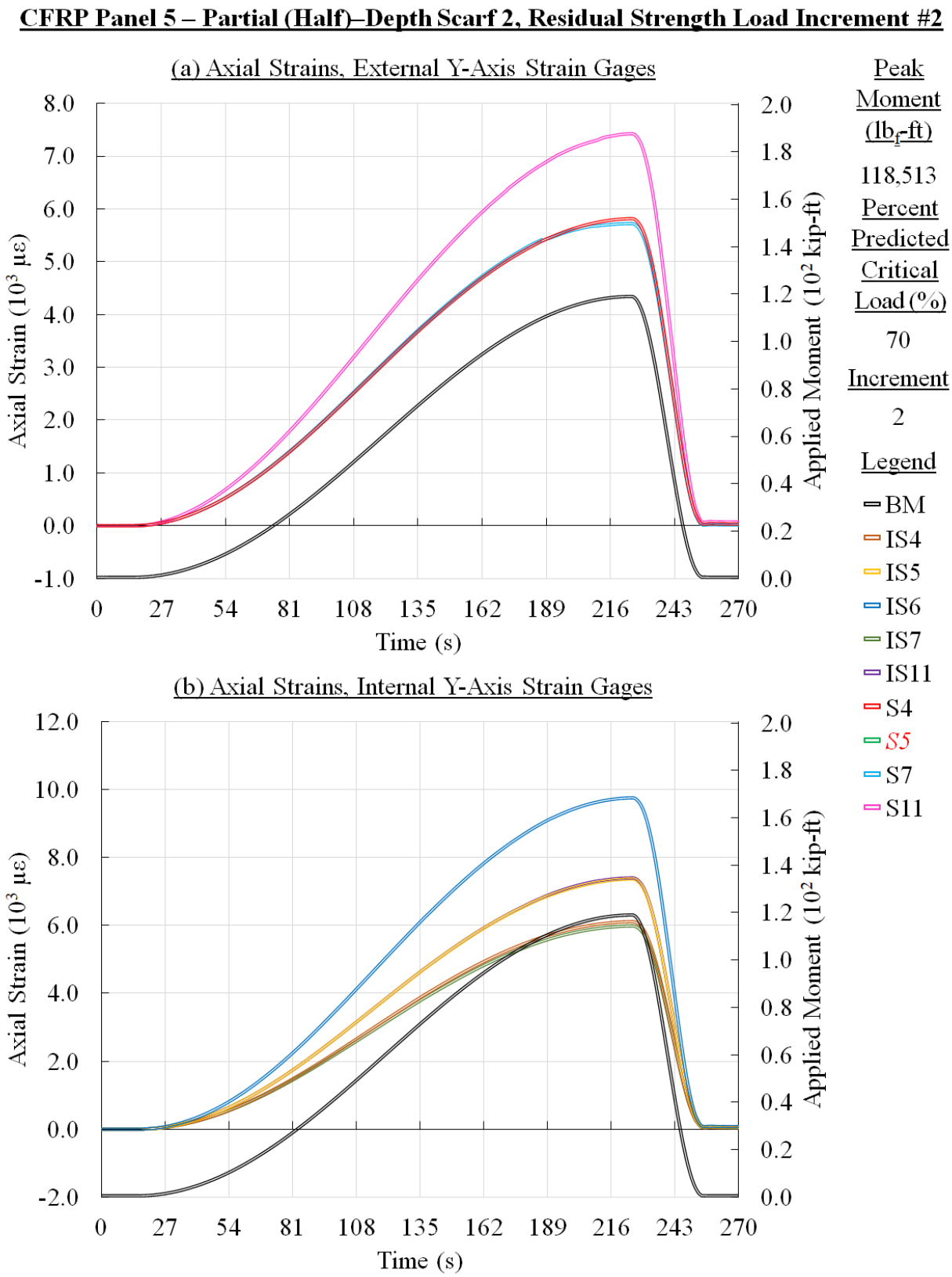


Figure C 34. Panel 5 load increment 2 (70% load level), axial strain along the Y-axis strain gages

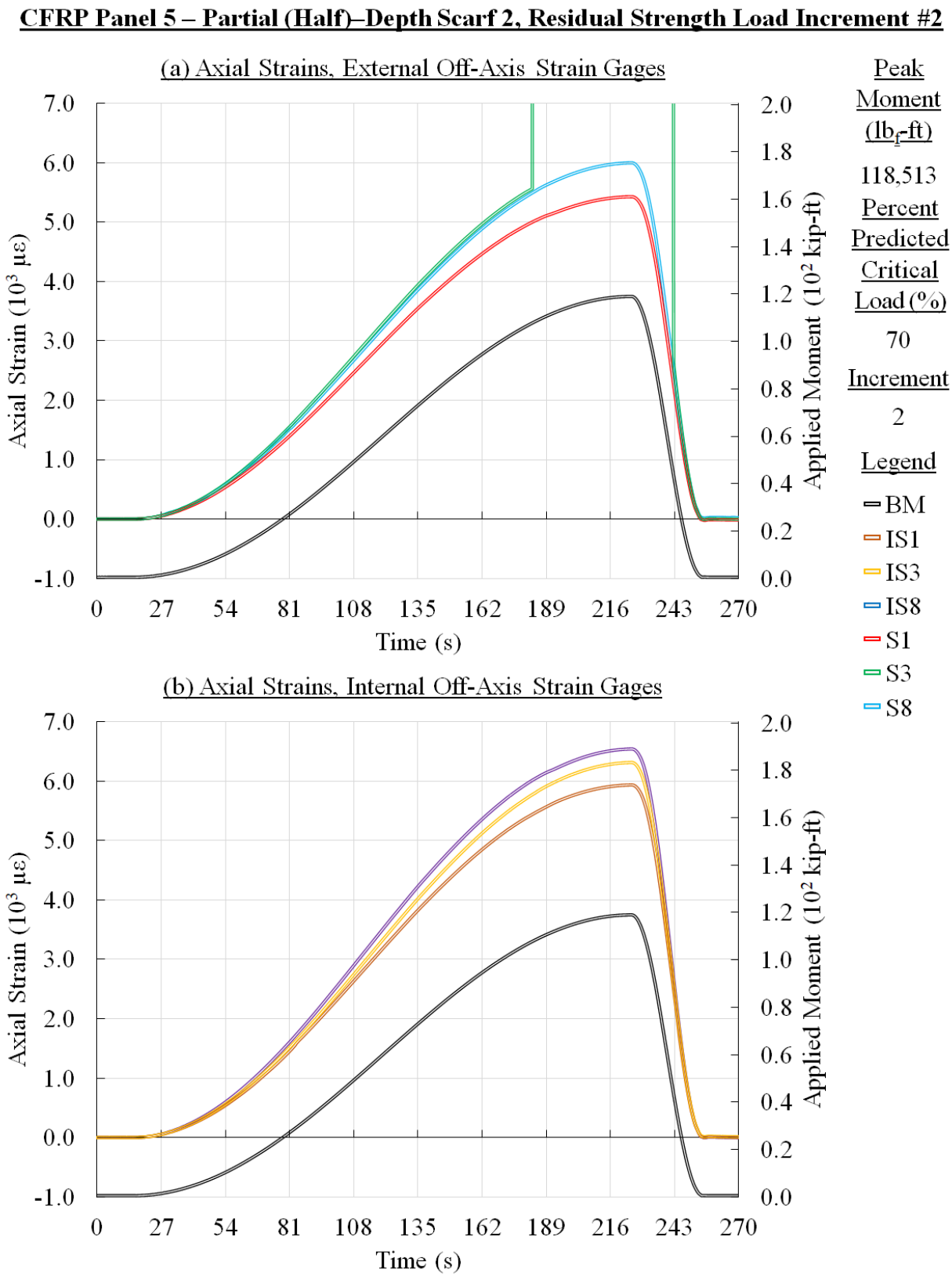


Figure C 35. Panel 5 load increment 2 (70% load level), axial strain along the off-axis strain gages

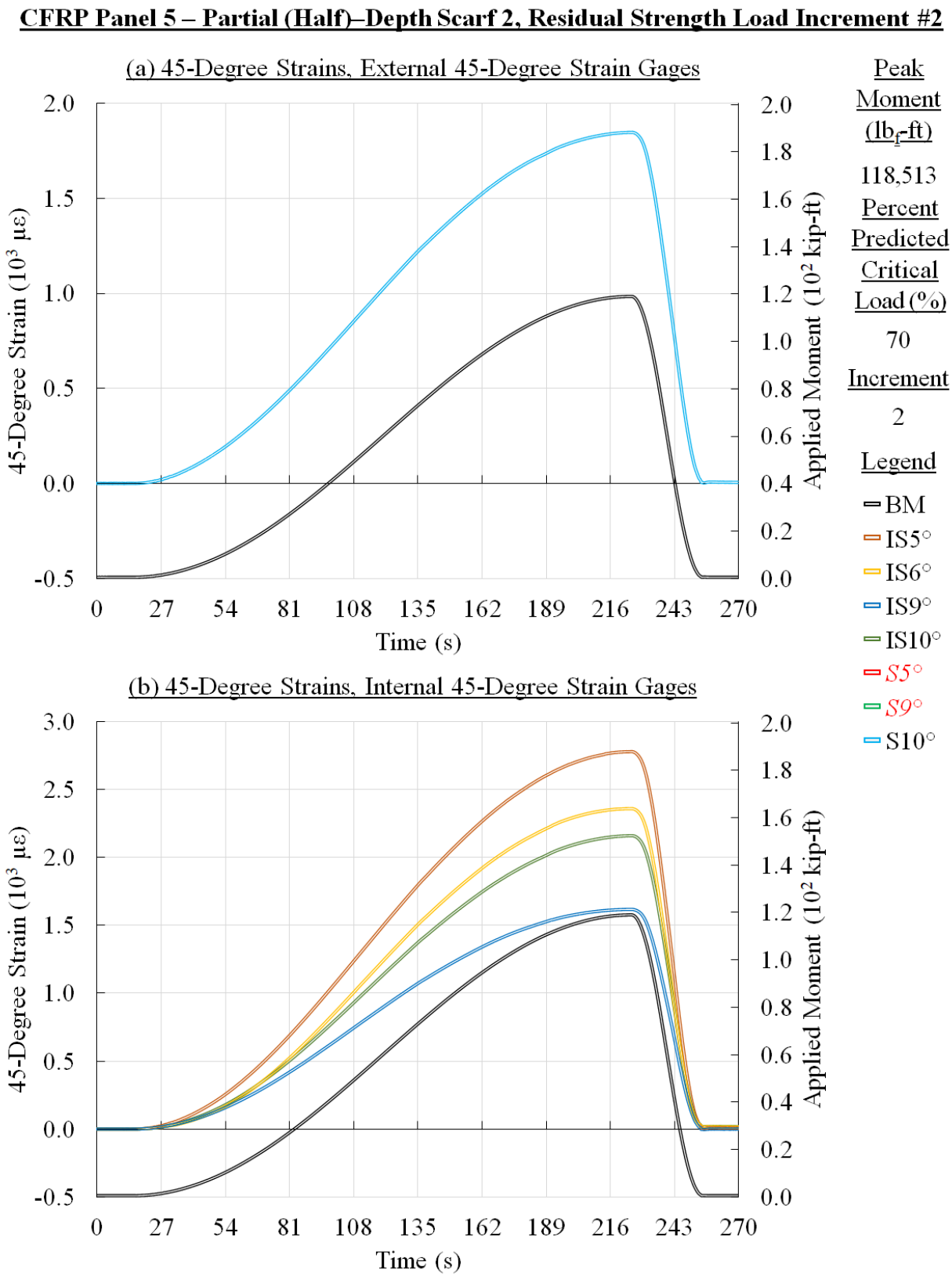


Figure C 36. Panel 5 load increment 2 (70% load level), 45 degree strain

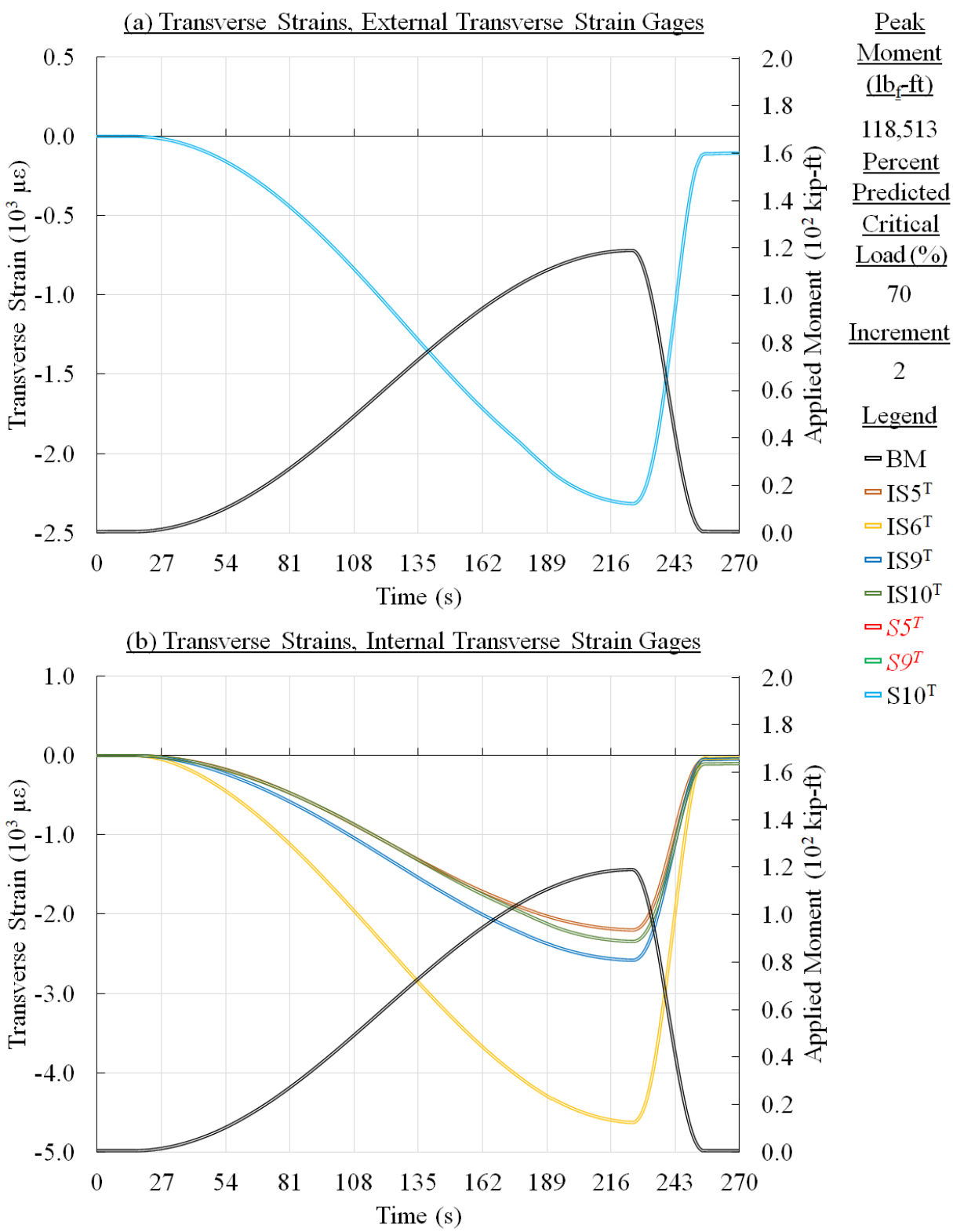


Figure C 37. Panel 5 load increment 2 (70% load level), transverse strain

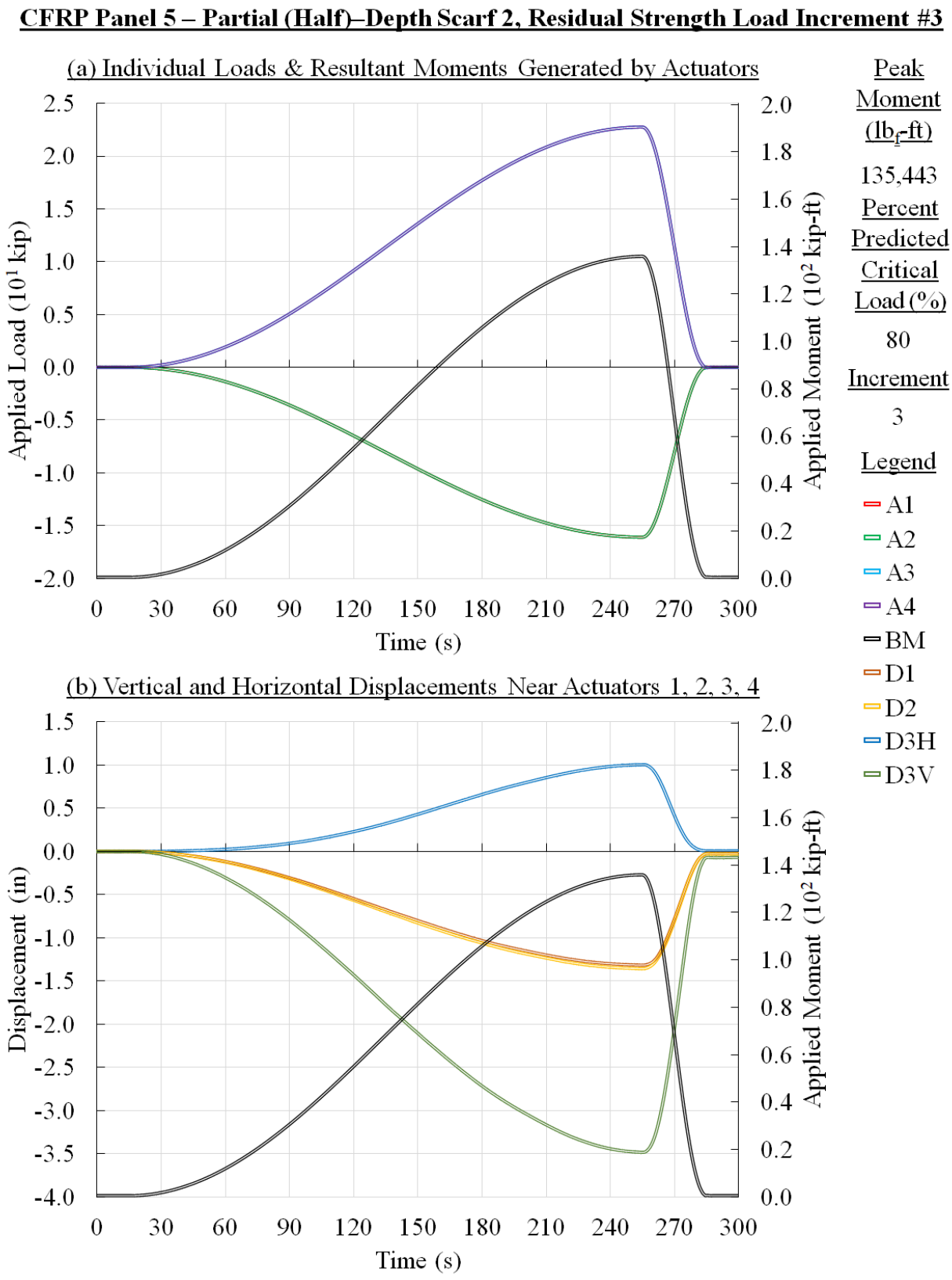


Figure C 38. Panel 5 load increment 3 (80% load level), load and displacement

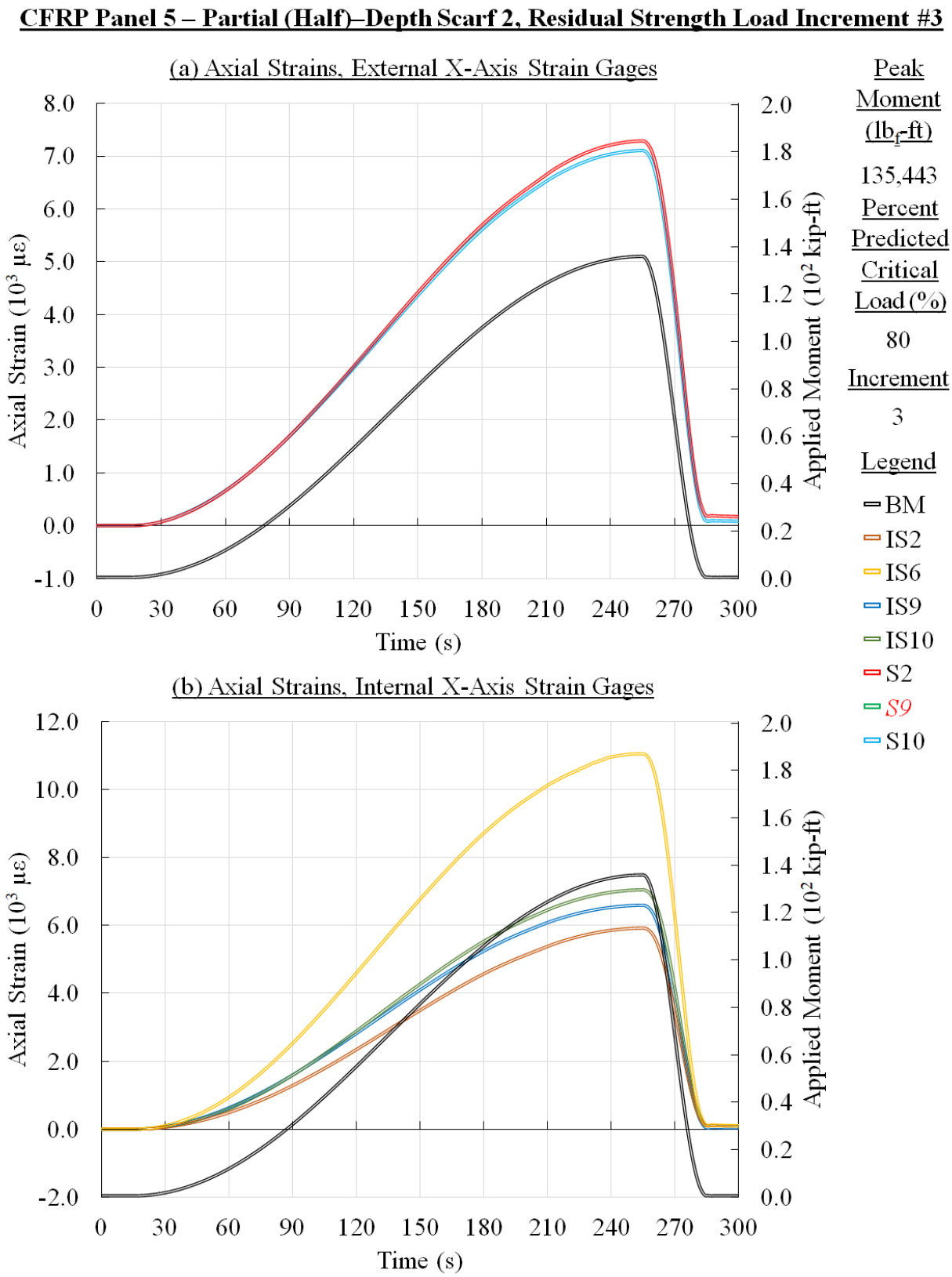


Figure C 39. Panel 5 load increment 3 (80% load level), axial strain along the X-axis strain gages

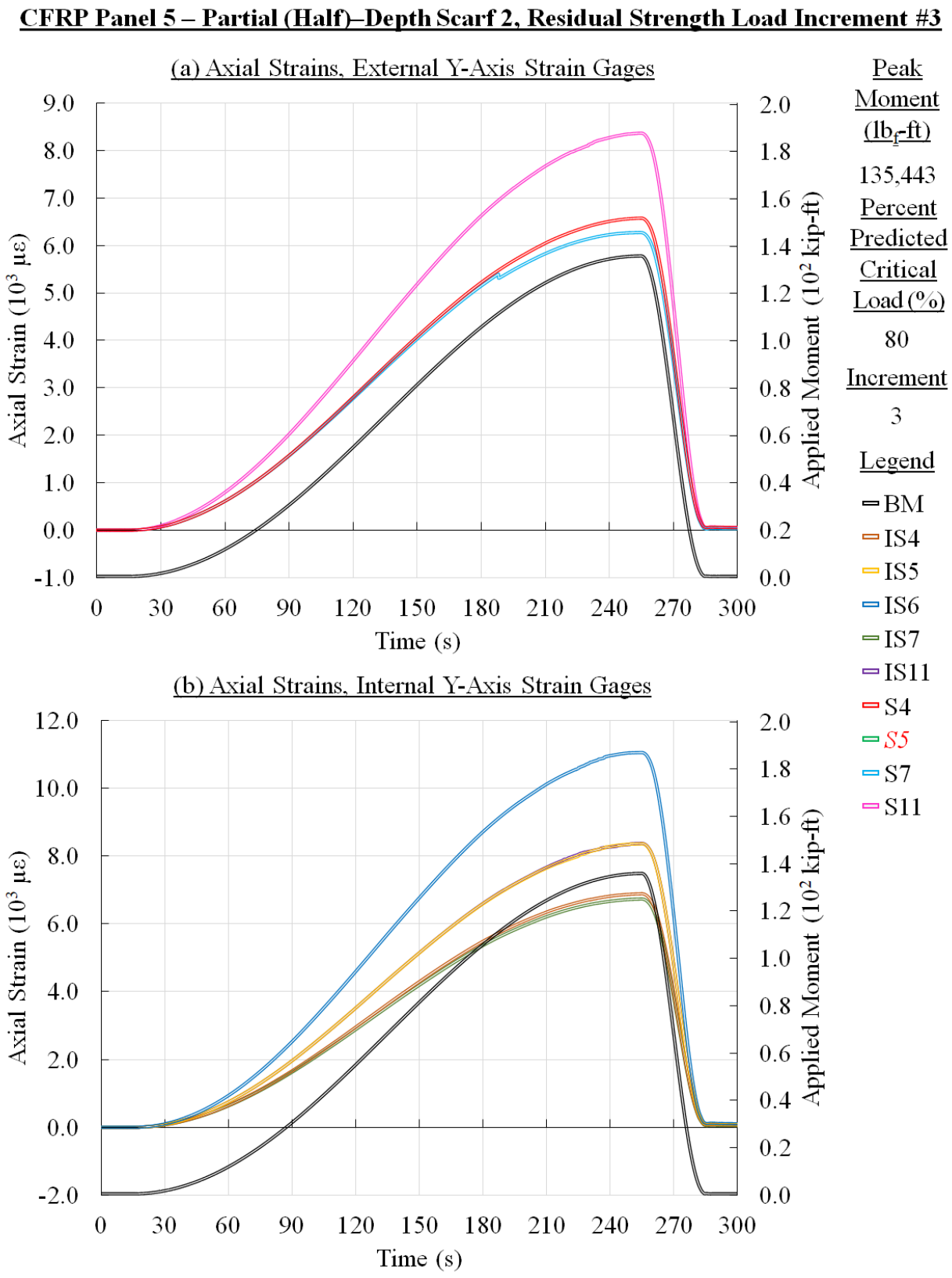


Figure C 40. Panel 5 load increment 3 (80% load level), axial strain along the Y-axis strain gages

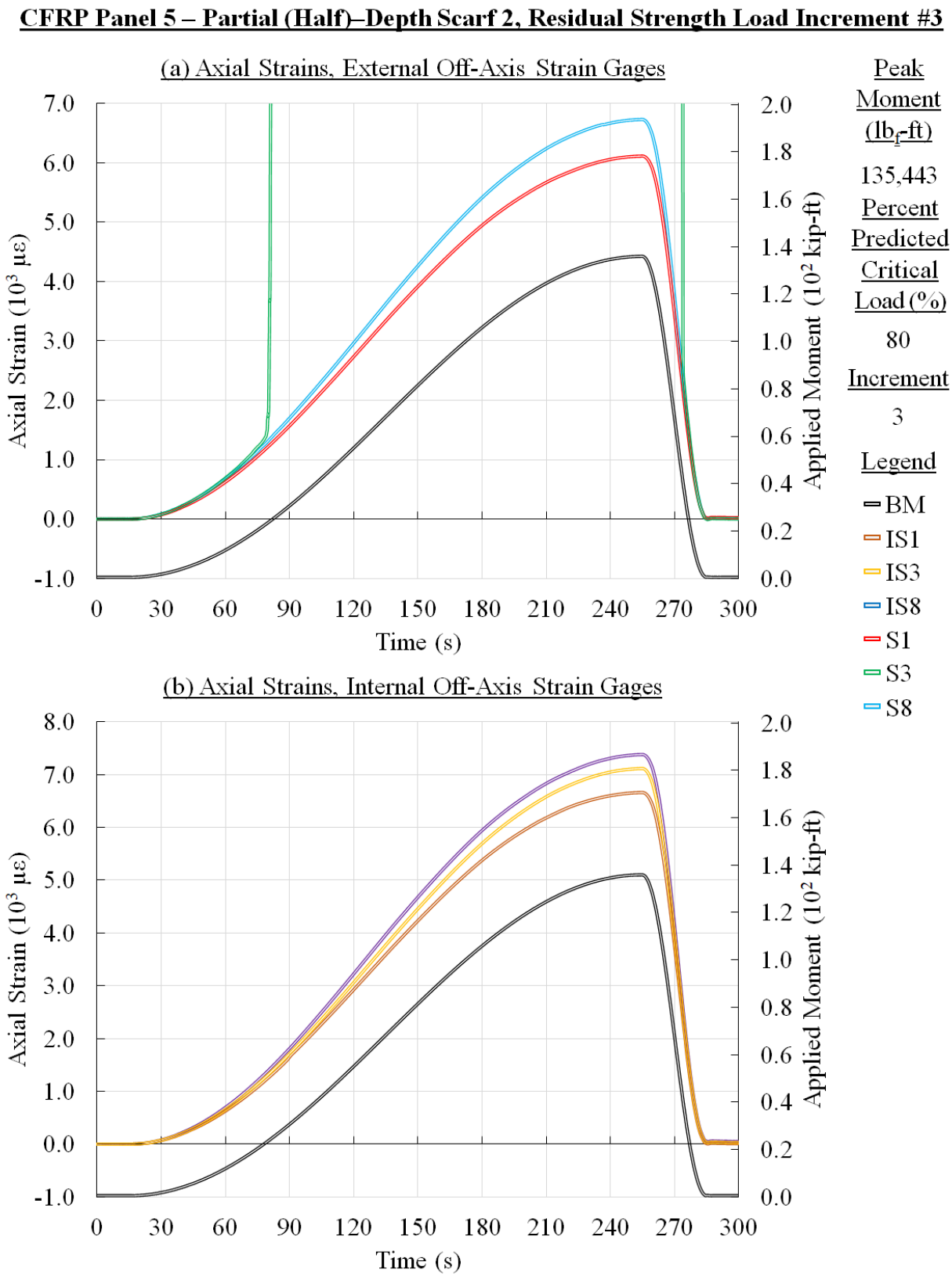


Figure C 41. Panel 5 load increment 3 (80% load level), axial strain along the off-axis strain gages

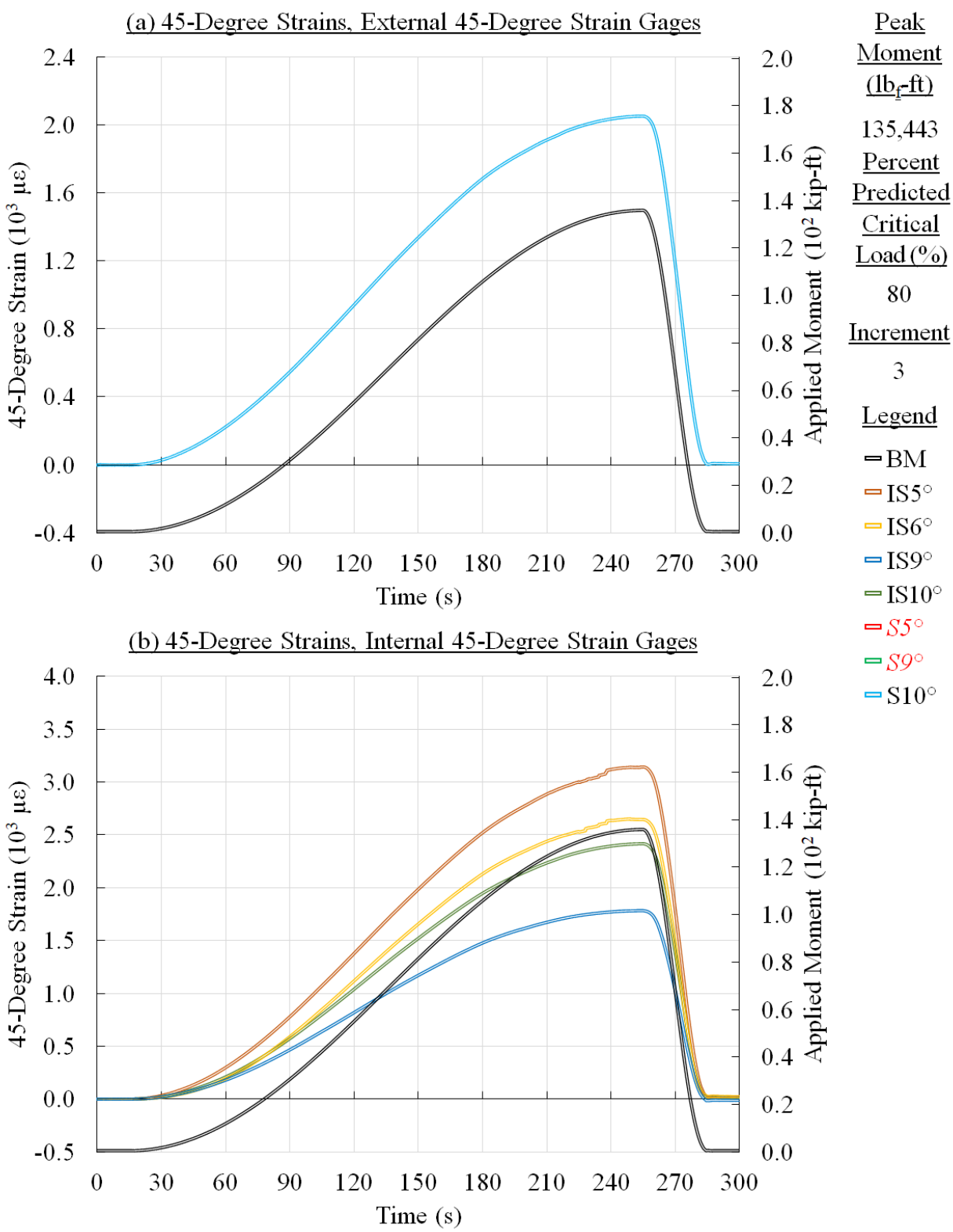


Figure C 42. Panel 5 load increment 3 (80% load level), 45 degree strain

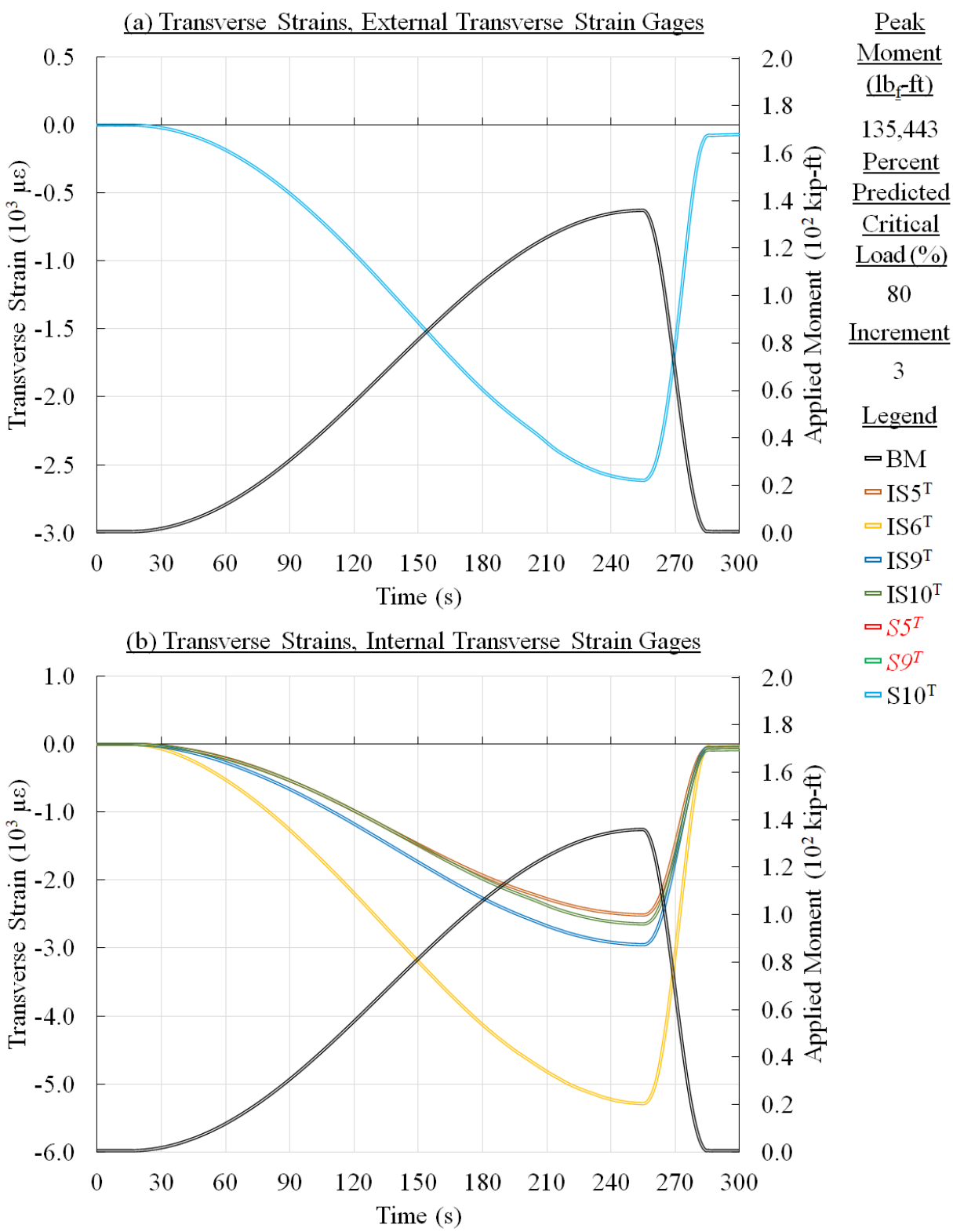


Figure C 43. Panel 5 load increment 3 (80% load level), transverse strain

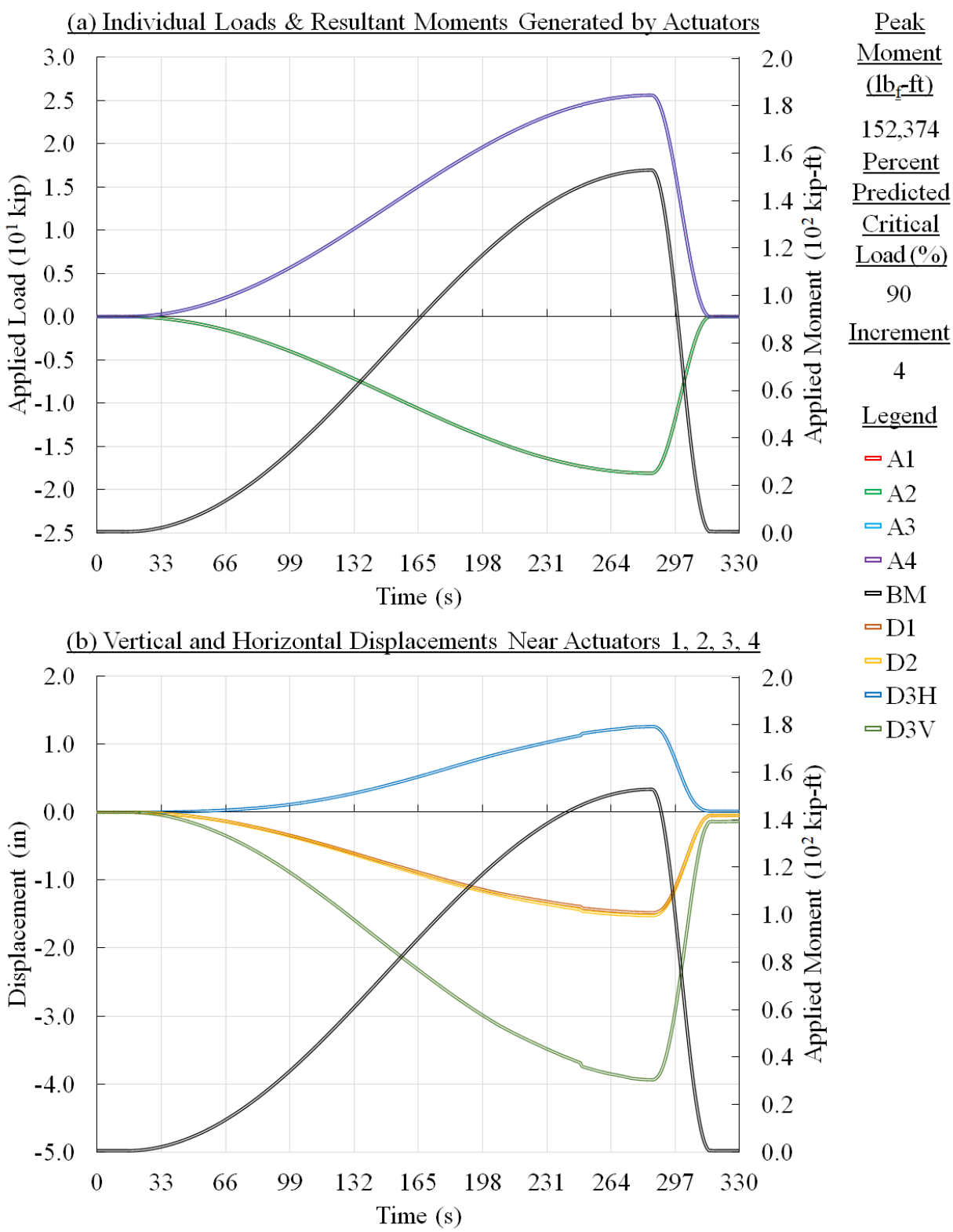


Figure C 44. Panel 5 load increment 4 (90% load level), load and displacement

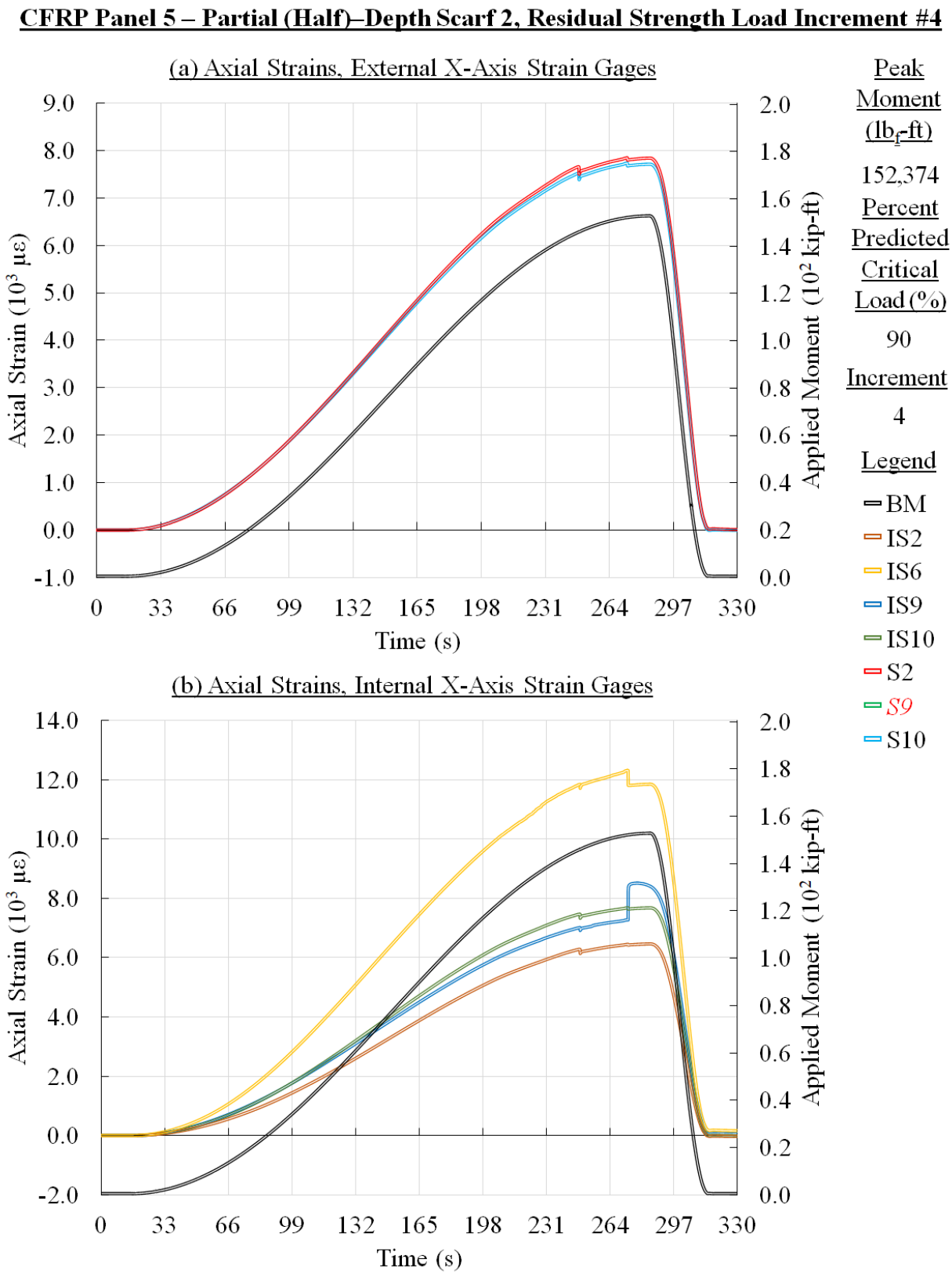


Figure C 45. Panel 5 load increment 4 (90% load level), axial strain along the X-axis strain gages

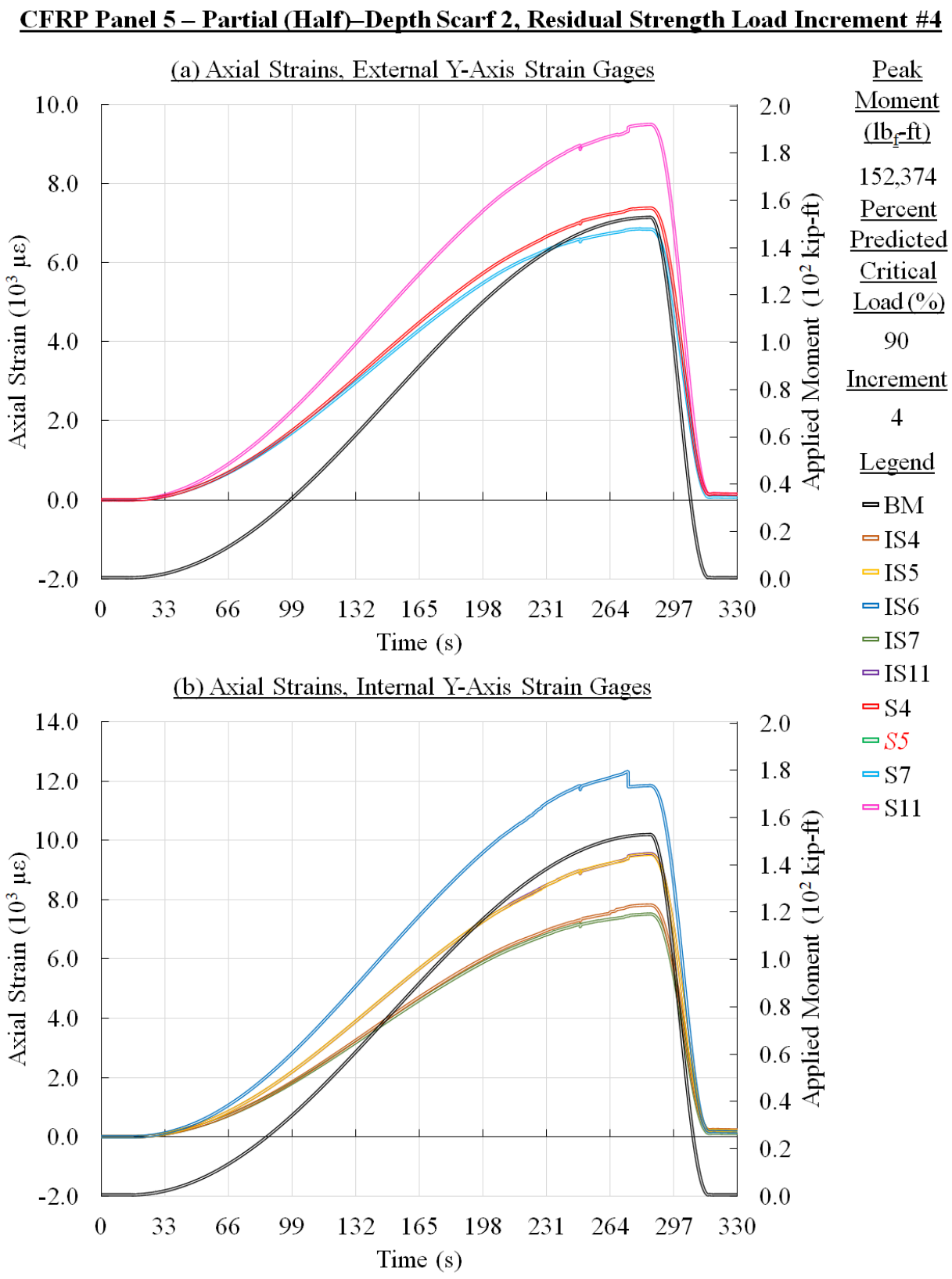


Figure C 46. Panel 5 load increment 4 (90% load level), axial strain along the Y-axis strain gages

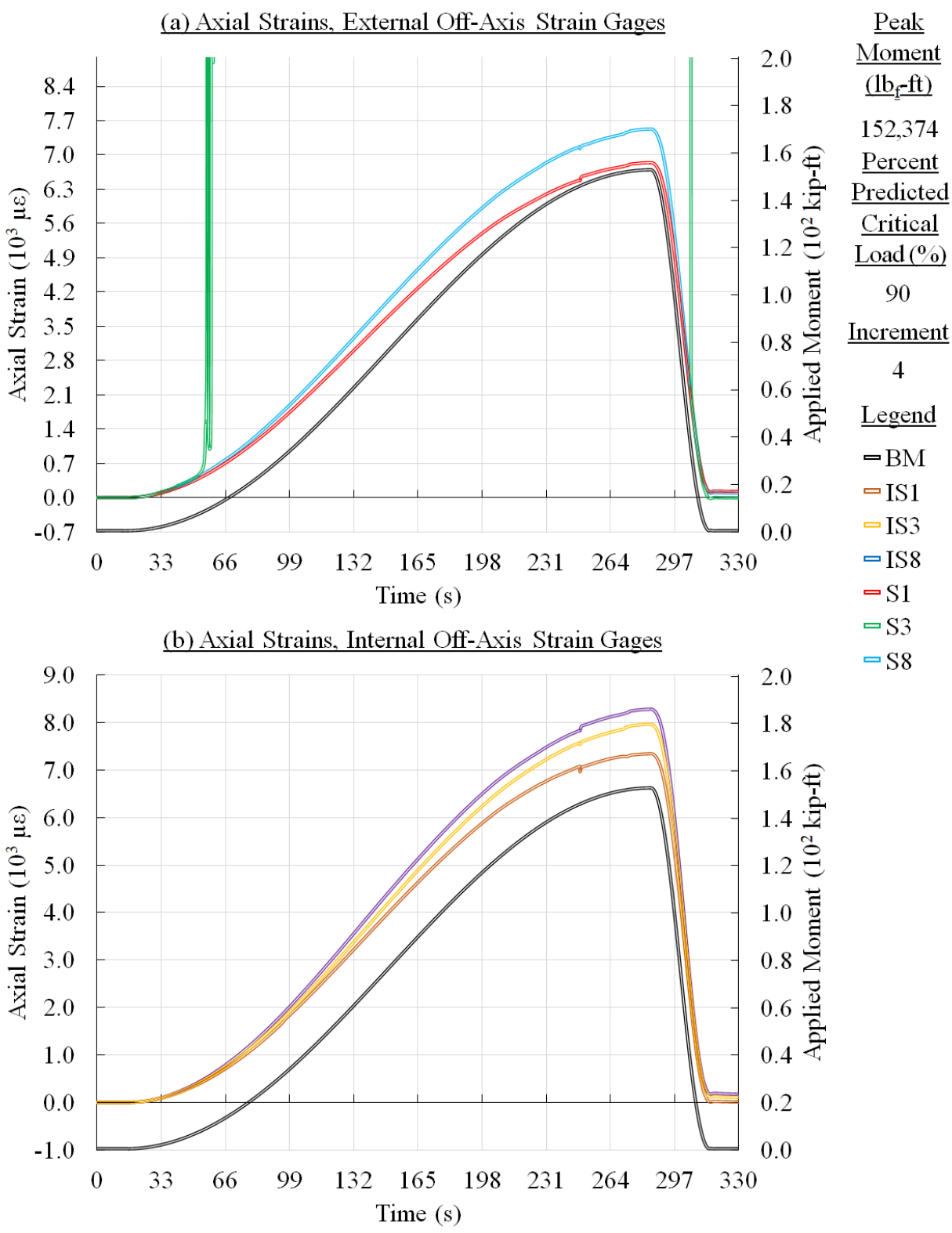


Figure C 47. Panel 5 load increment 4 (90% load level), axial strain along the off-axis strain gages

**CFRP Panel 5 – Partial (Half)–Depth Scarf 2, Residual Strength Load Increment #4**

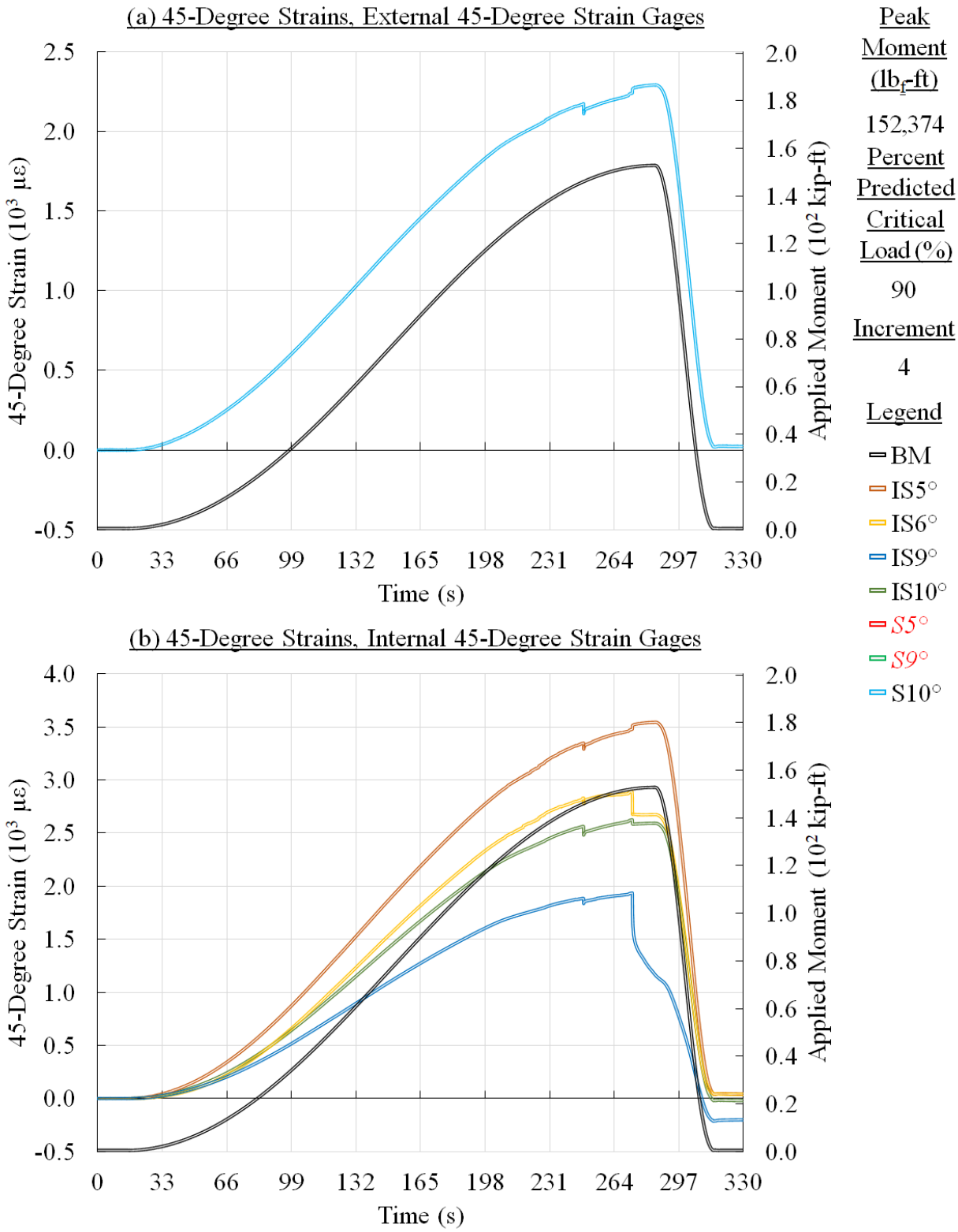


Figure C 48. Panel 5 load increment 4 (90% load level), 45 degree strain

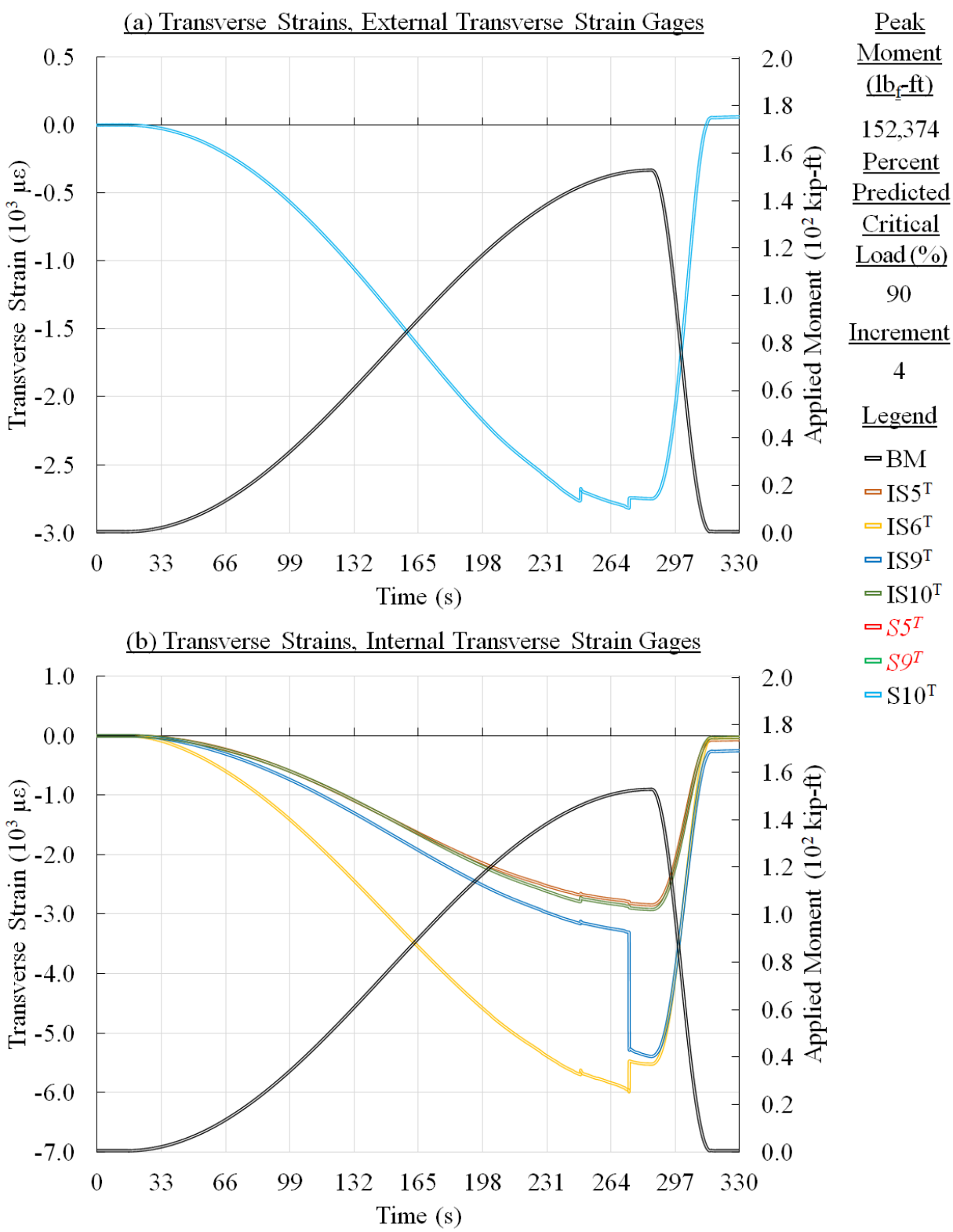


Figure C 49. Panel 5 load increment 4 (90% load level), transverse strain

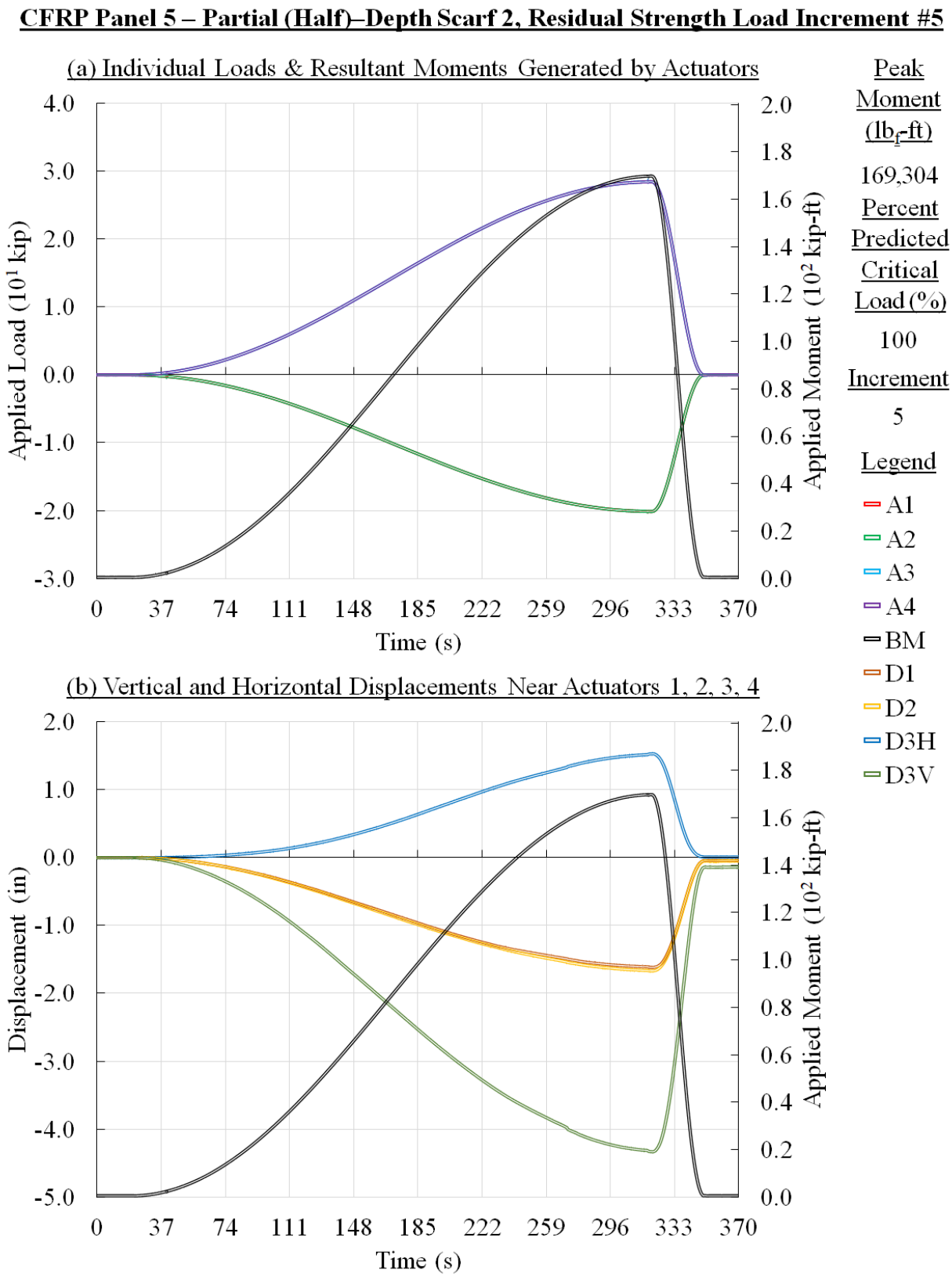


Figure C 50. Panel 5 load increment 5 (100% load level), load and displacement

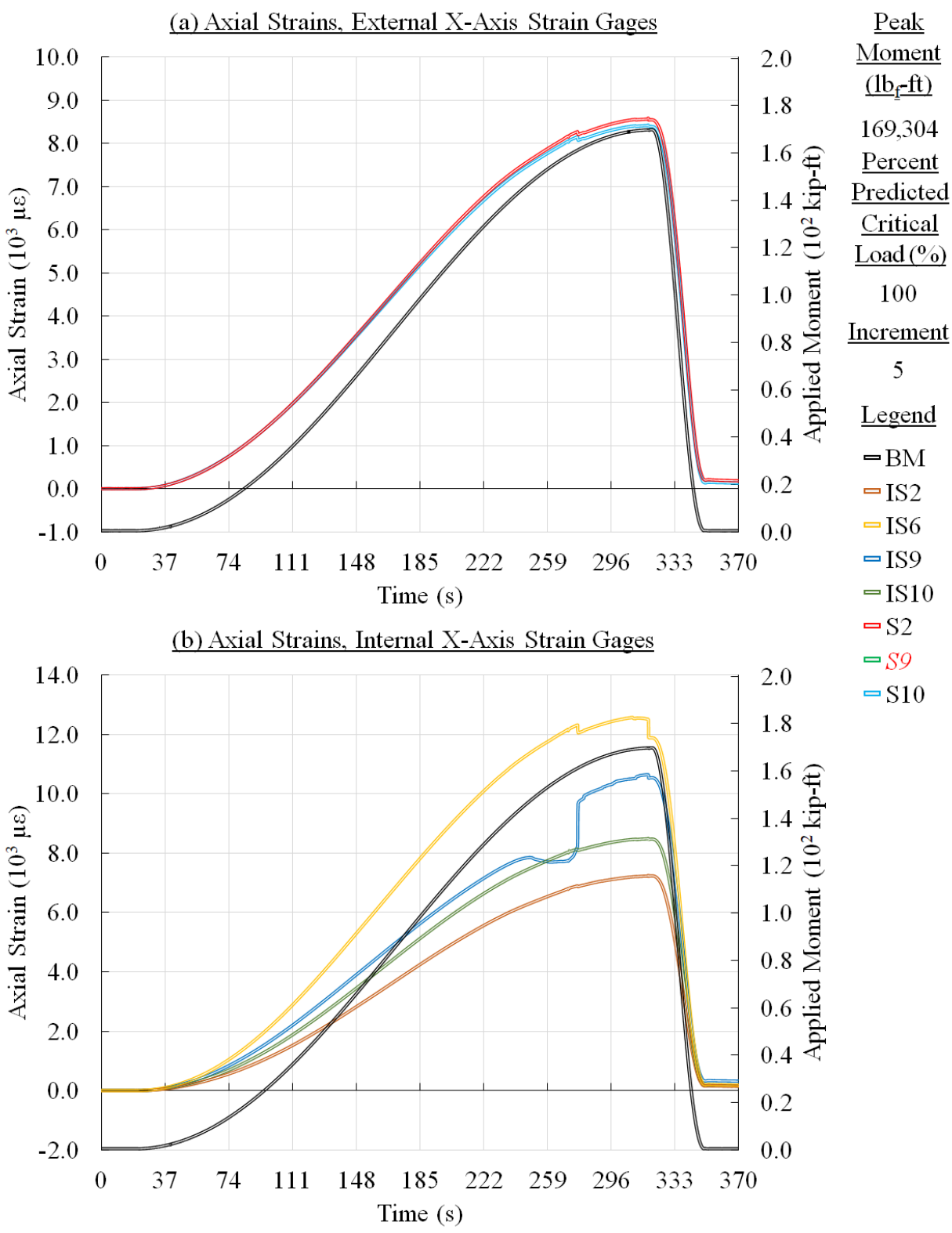


Figure C 51. Panel 5 load increment 5 (100% load level), axial strain along the X-axis strain gages

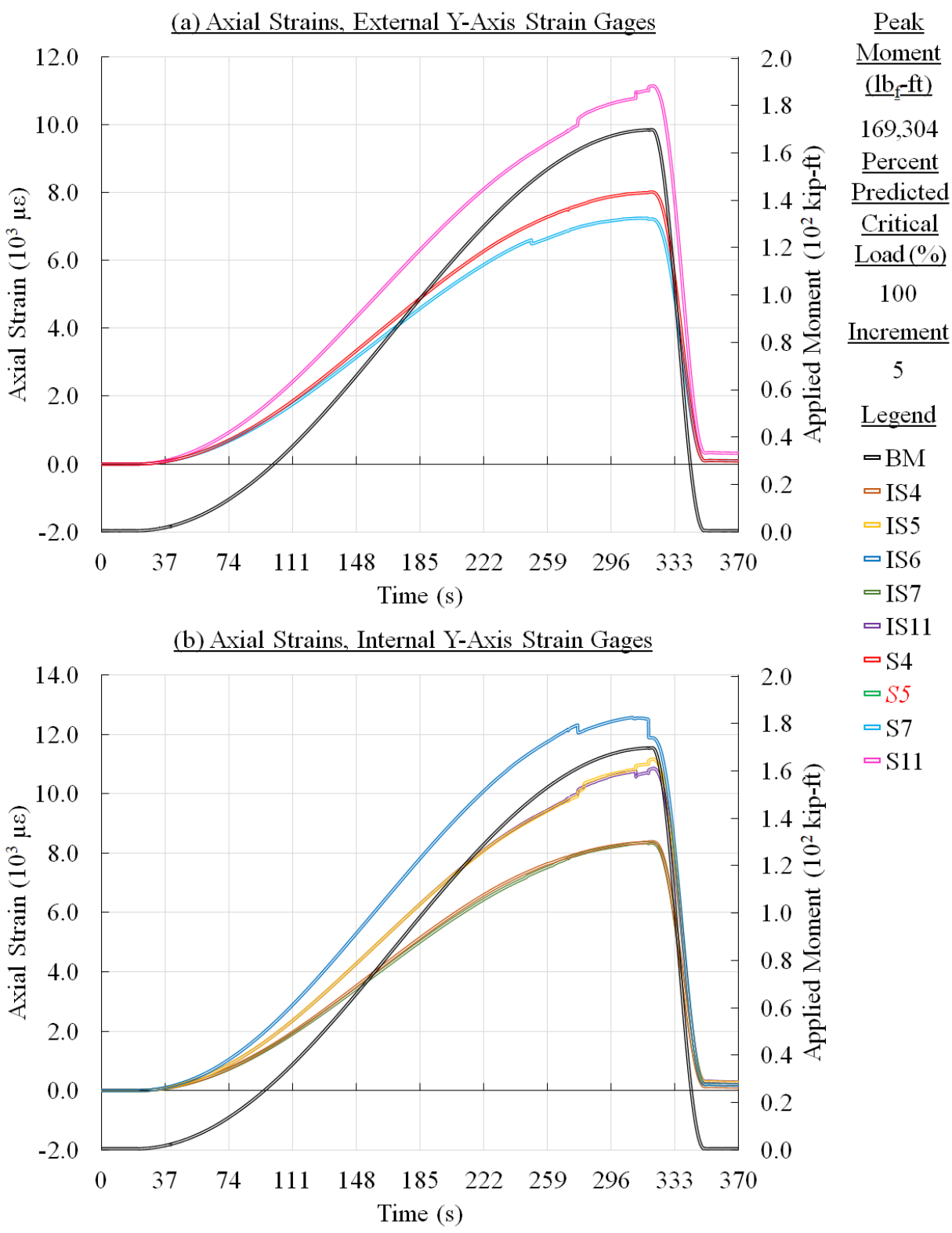


Figure C 52. Panel 5 load increment 5 (100% load level), axial strain along the Y-axis strain gages

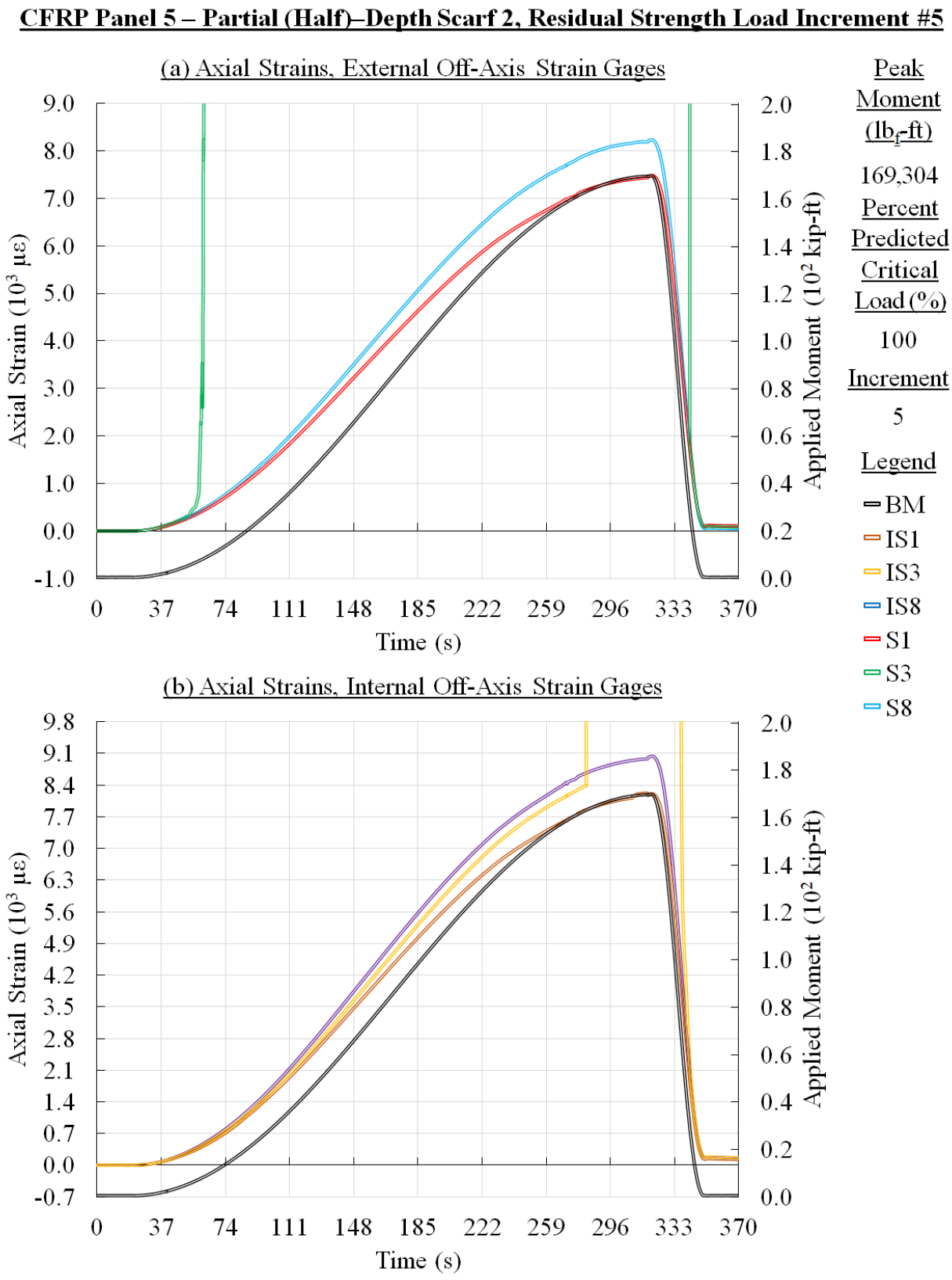


Figure C 53. Panel 5 load increment 5 (100% load level), axial strain along the off-axis strain gages

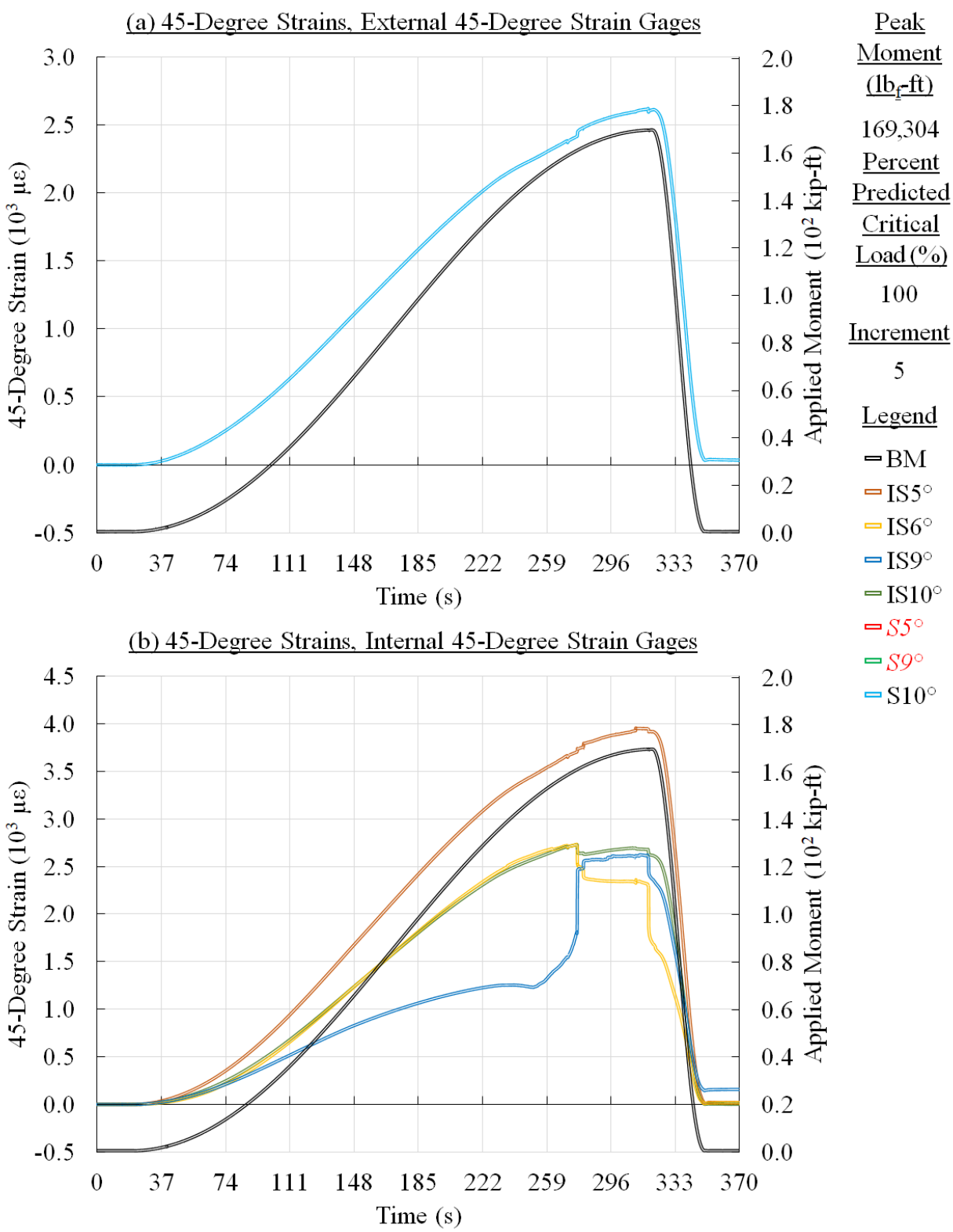


Figure C 54. Panel 5 load increment 5 (100% load level), 45 degree strain

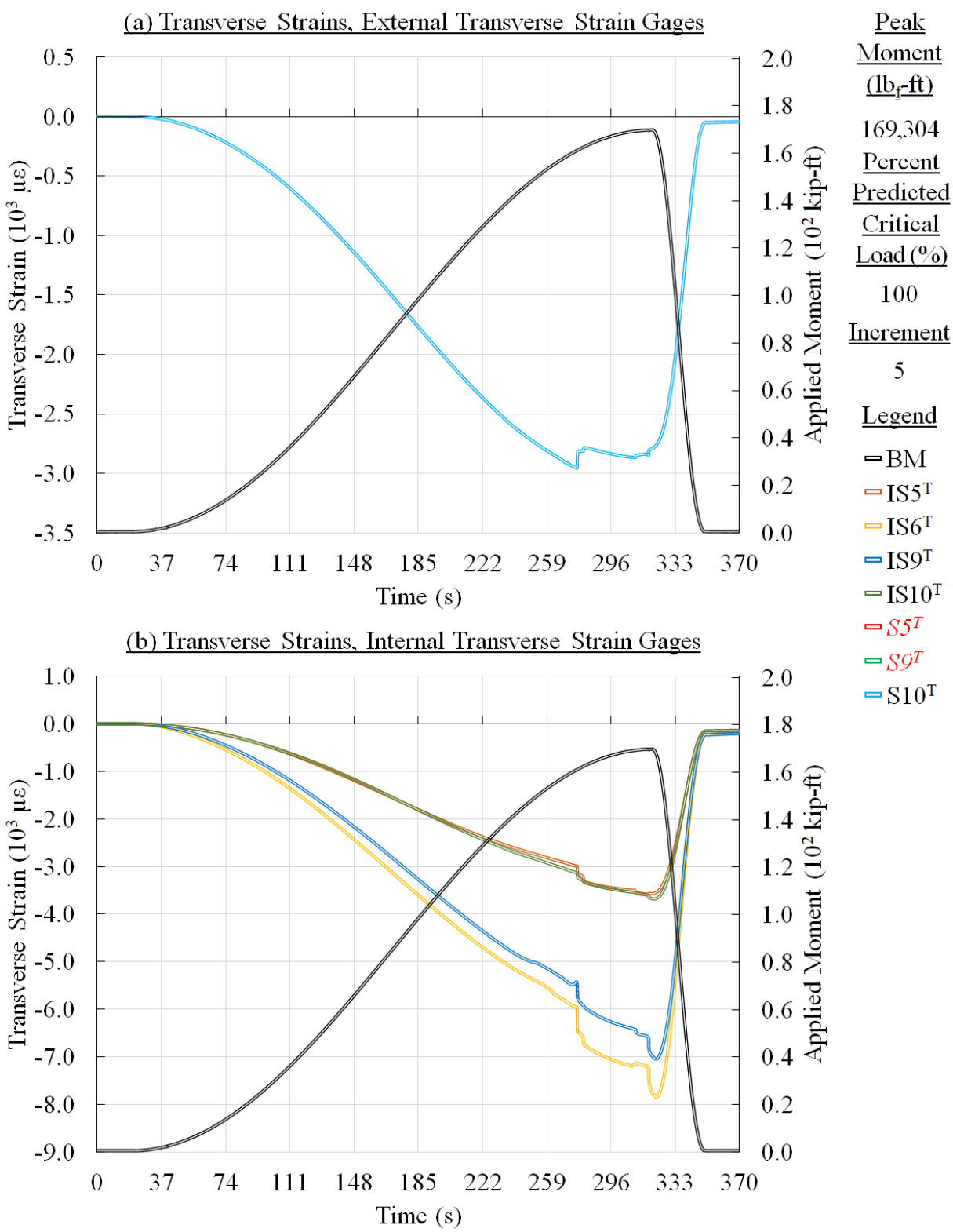


Figure C 55. Panel 5 load increment 5 (100% load level), transverse strain

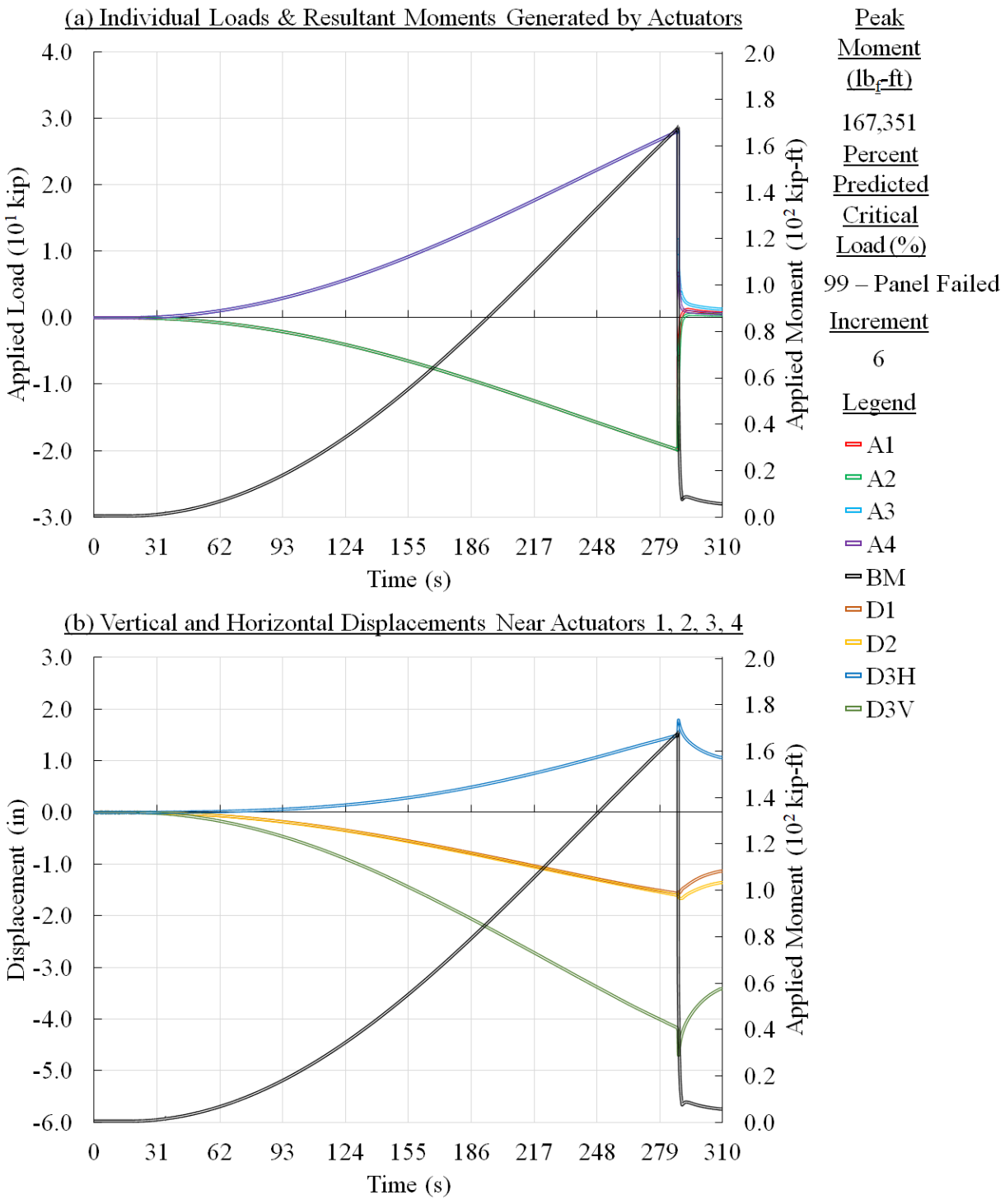


Figure C 56. Panel 5 load increment 6 (panel failure), load and displacement

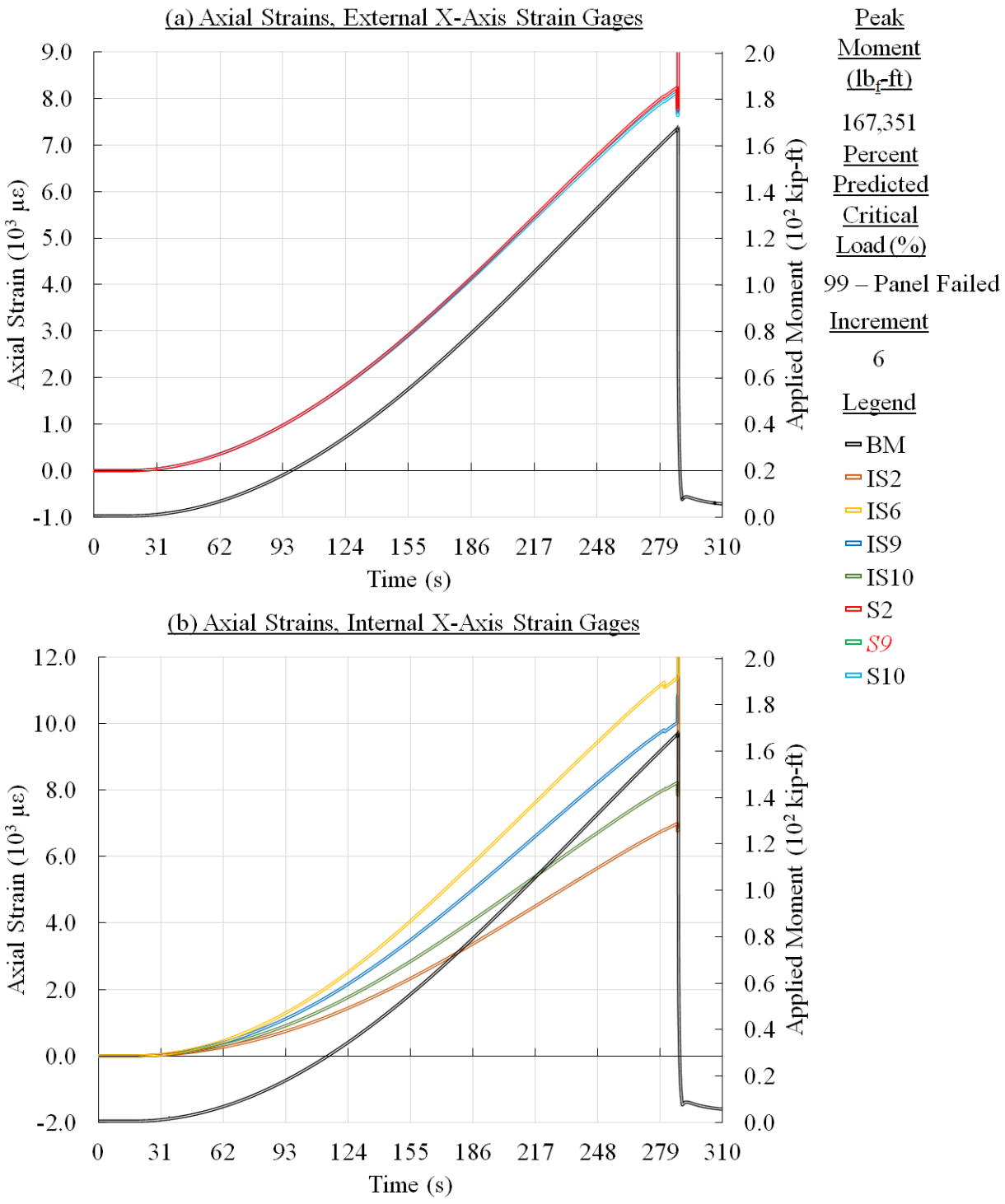


Figure C 57. Panel 5 load increment 6 (panel failure), axial strain along the X-axis strain gages

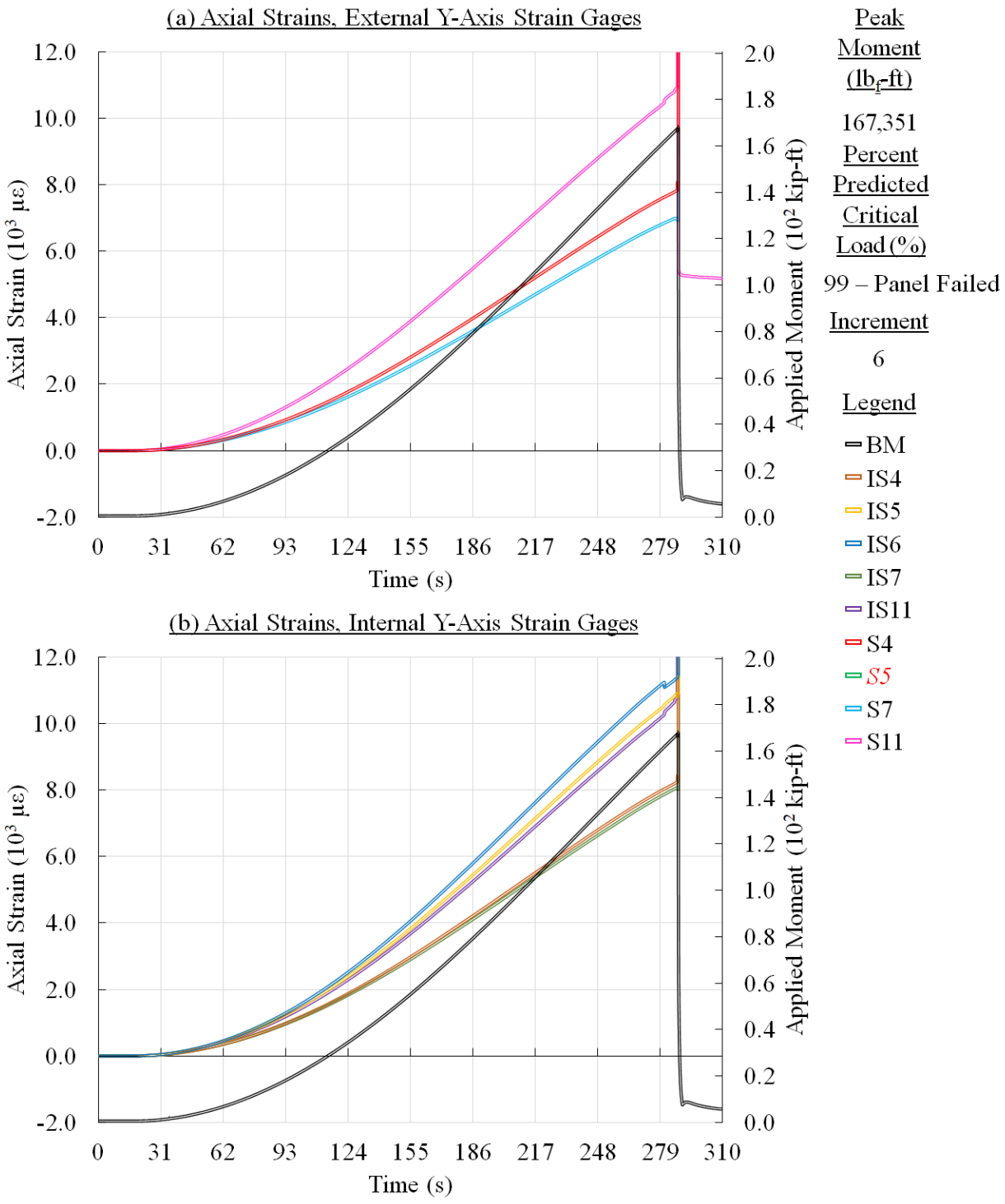


Figure C 58. Panel 5 load increment 6 (panel failure), axial strain along the Y-axis strain gages

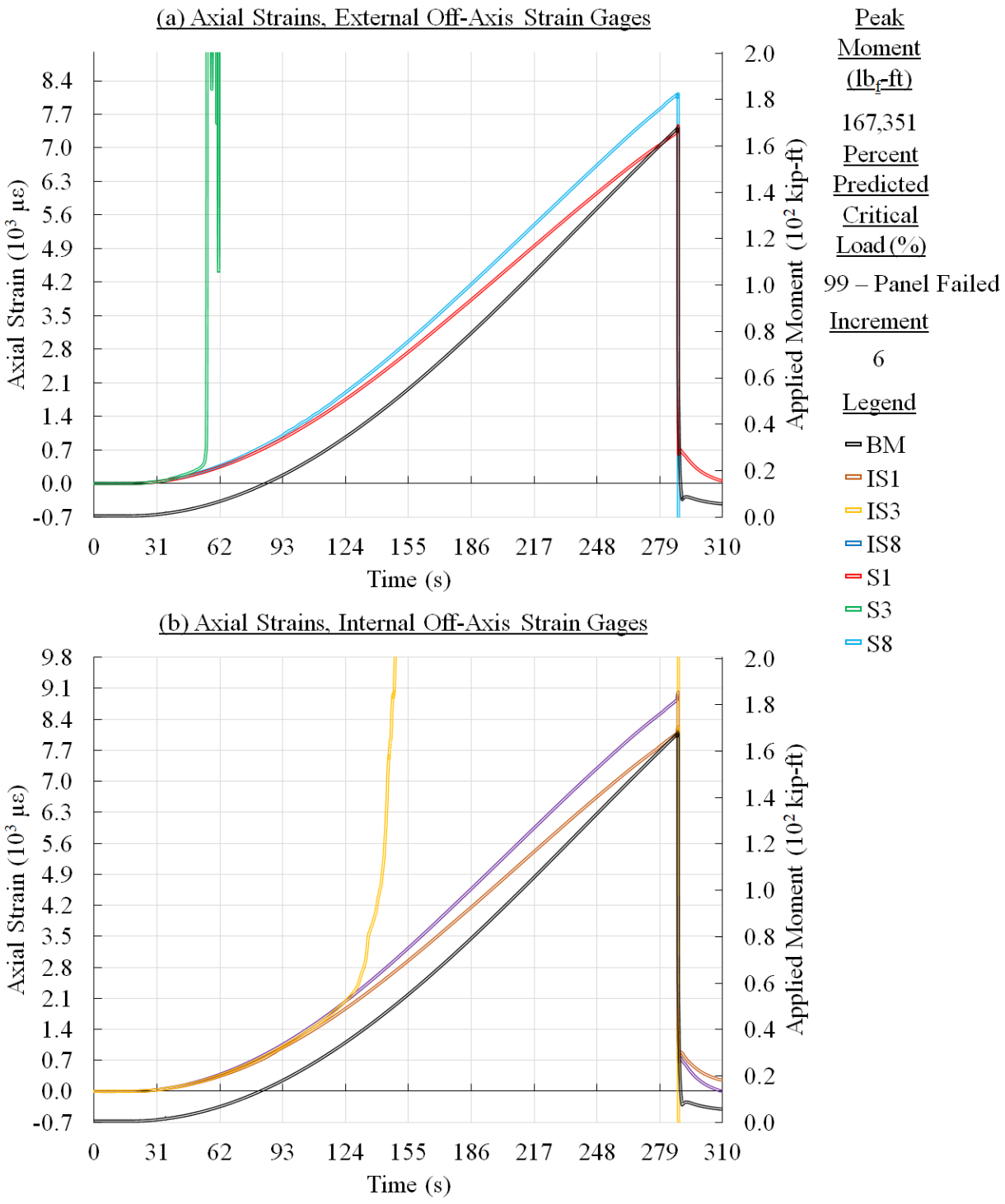


Figure C 59. Panel 5 load increment 6 (panel failure), axial strain along the off-axis strain gages

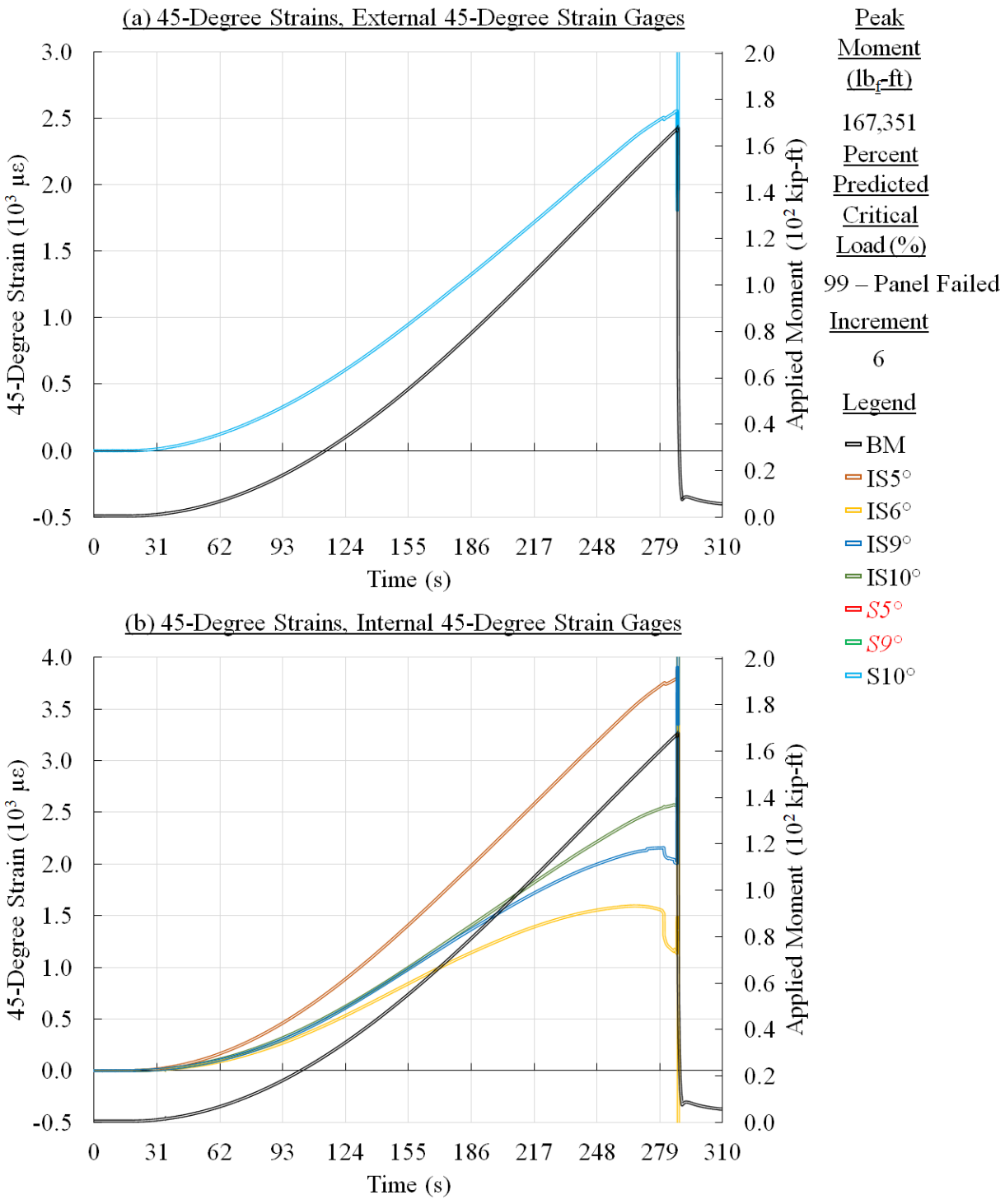


Figure C 60. Panel 5 load increment 6 (panel failure), 45 degree strain

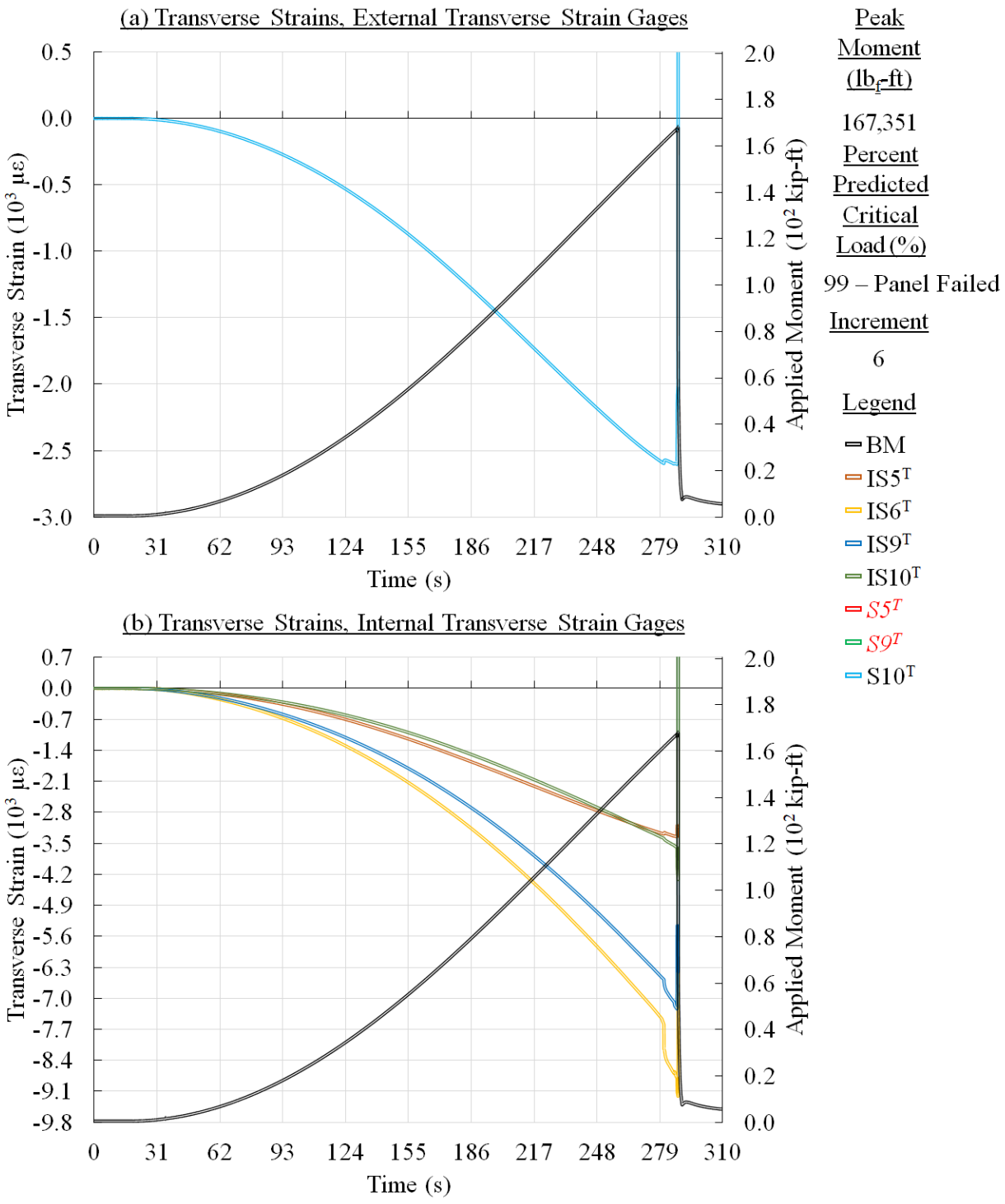


Figure C 61. Panel 5 load increment 6 (panel failure), transverse strain

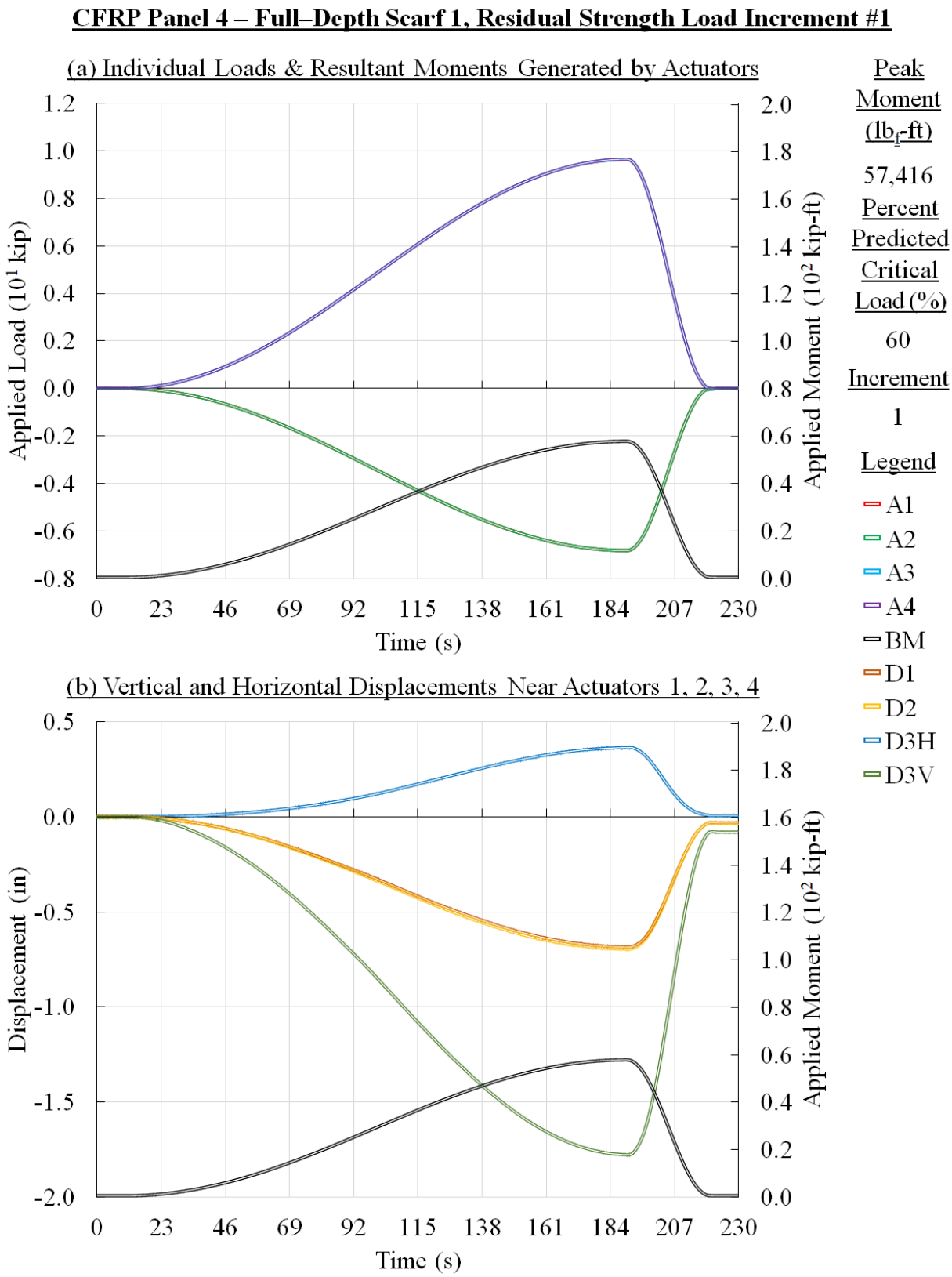


Figure C 62. Panel 4 load increment 1 (60% load level), load and displacement

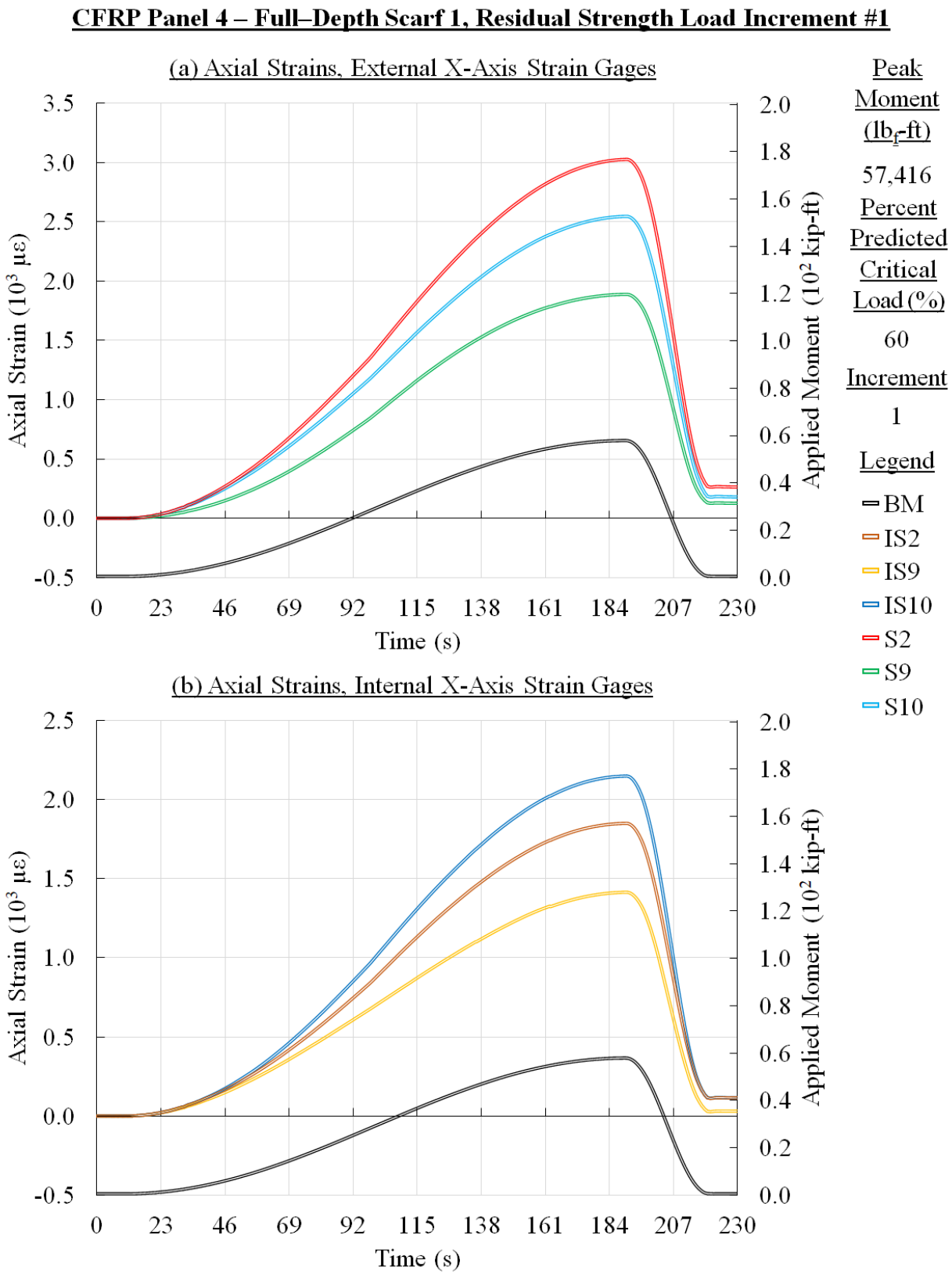


Figure C 63. Panel 4 load increment 1 (60% load level), axial strain along the X-axis strain gages

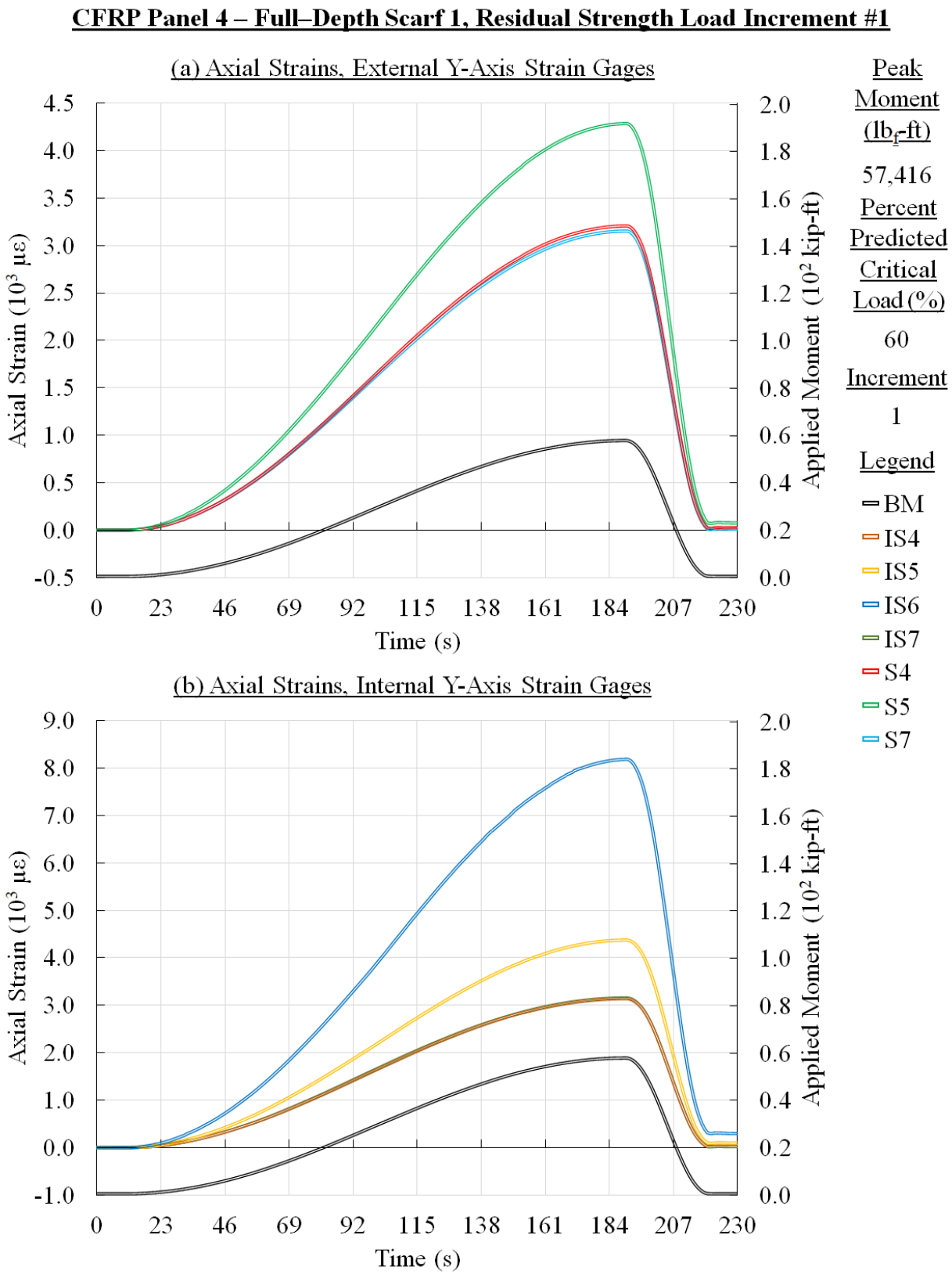


Figure C 64. Panel 4 load increment 1 (60% load level), axial strain along the Y-axis strain gages

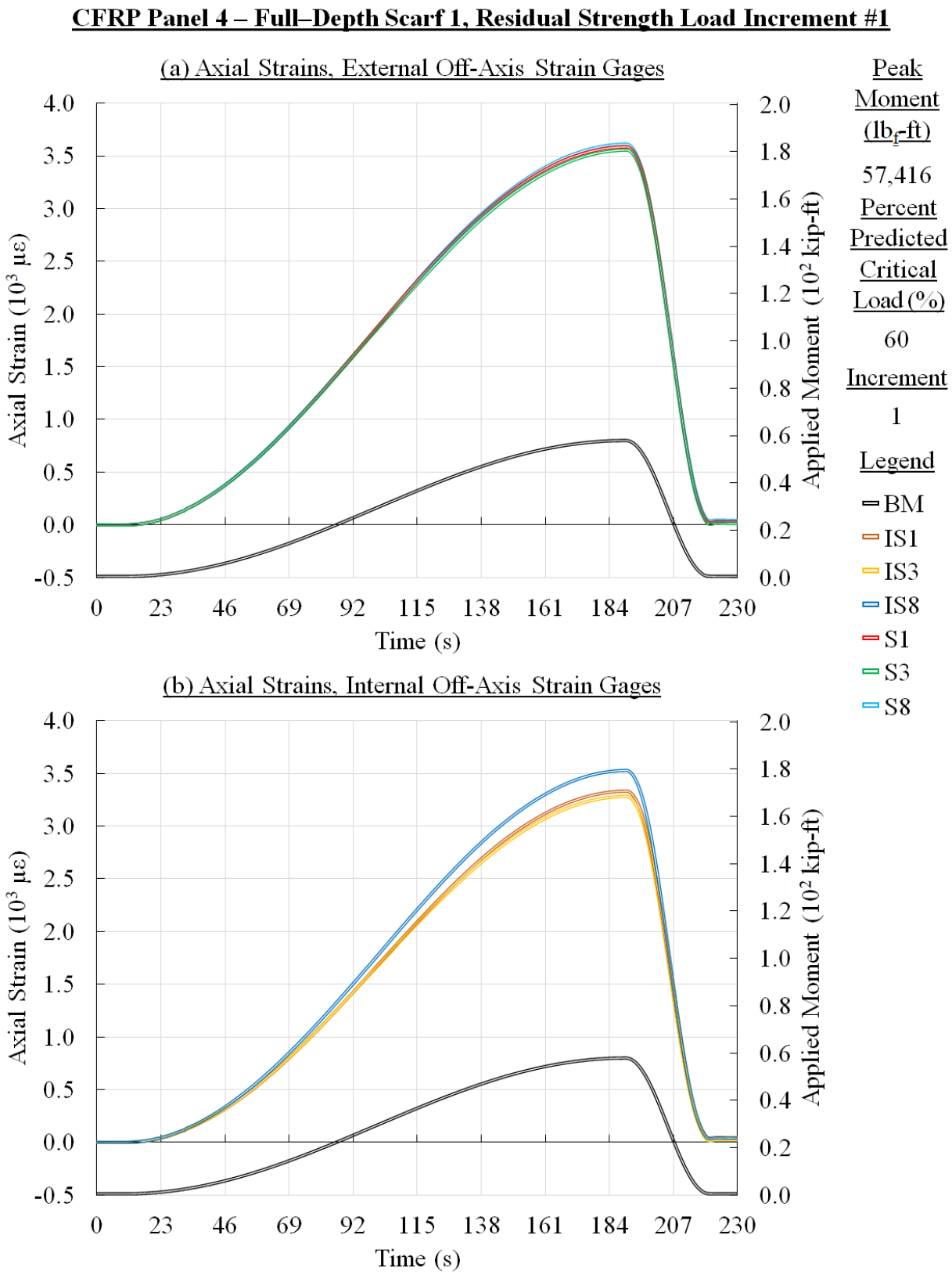


Figure C 65. Panel 4 load increment 1 (60% load level), axial strain along the off-axis strain gages

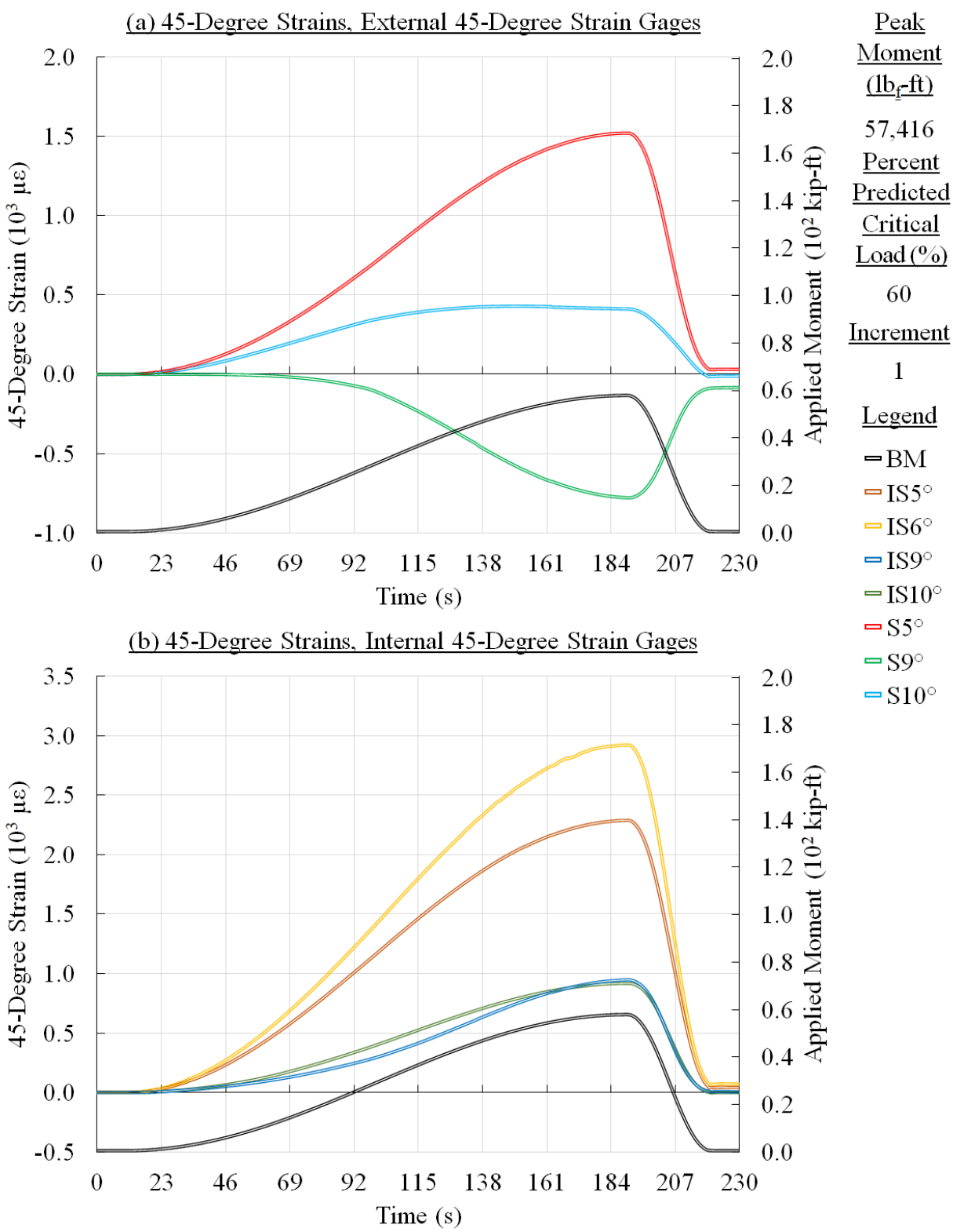


Figure C 66. Panel 4 load increment 1 (60% load level), 45 degree strain

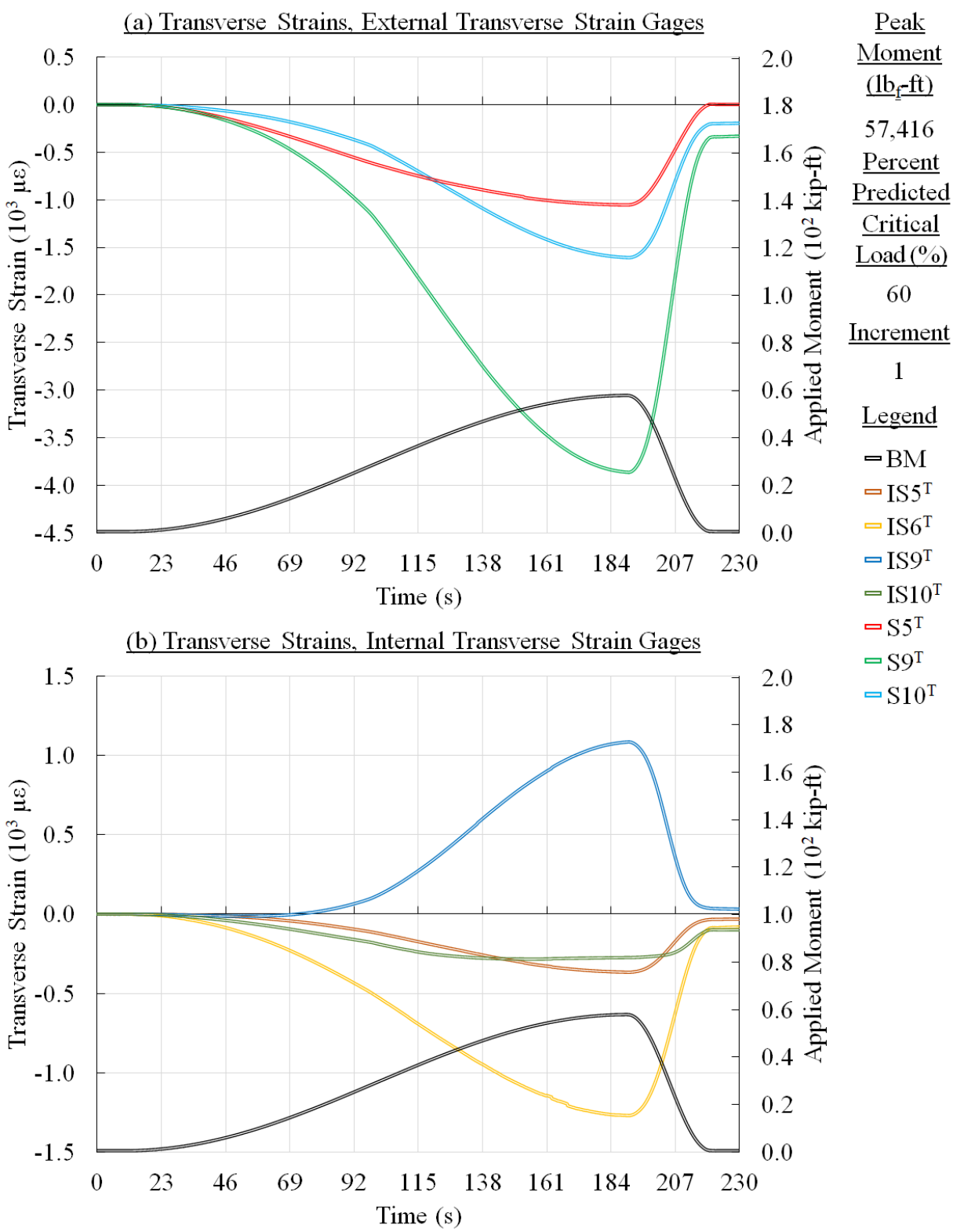


Figure C 67. Panel 4 load increment 1 (60% load level), transverse strain

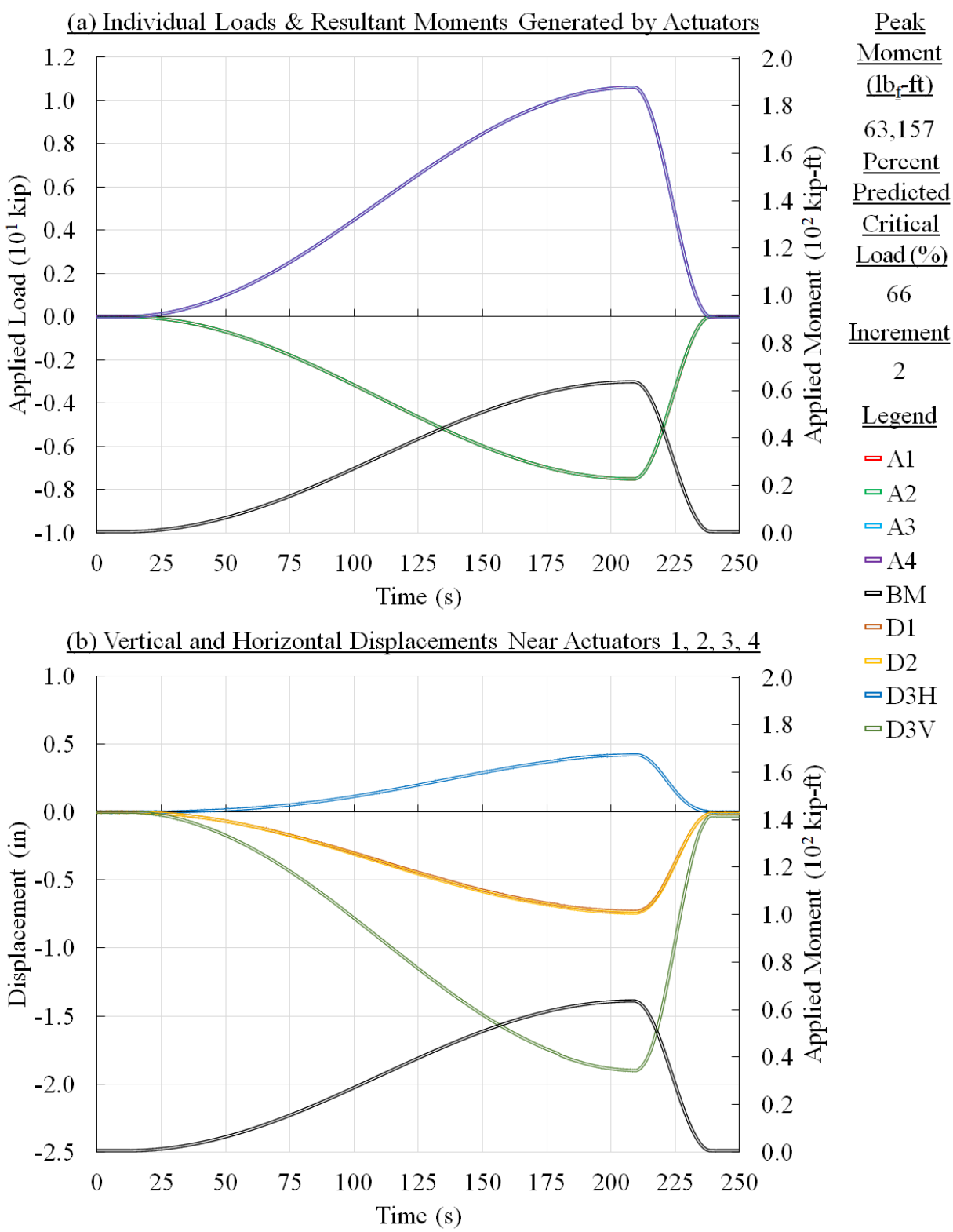


Figure C 68. Panel 4 load increment 2 (66% load level), load and displacement

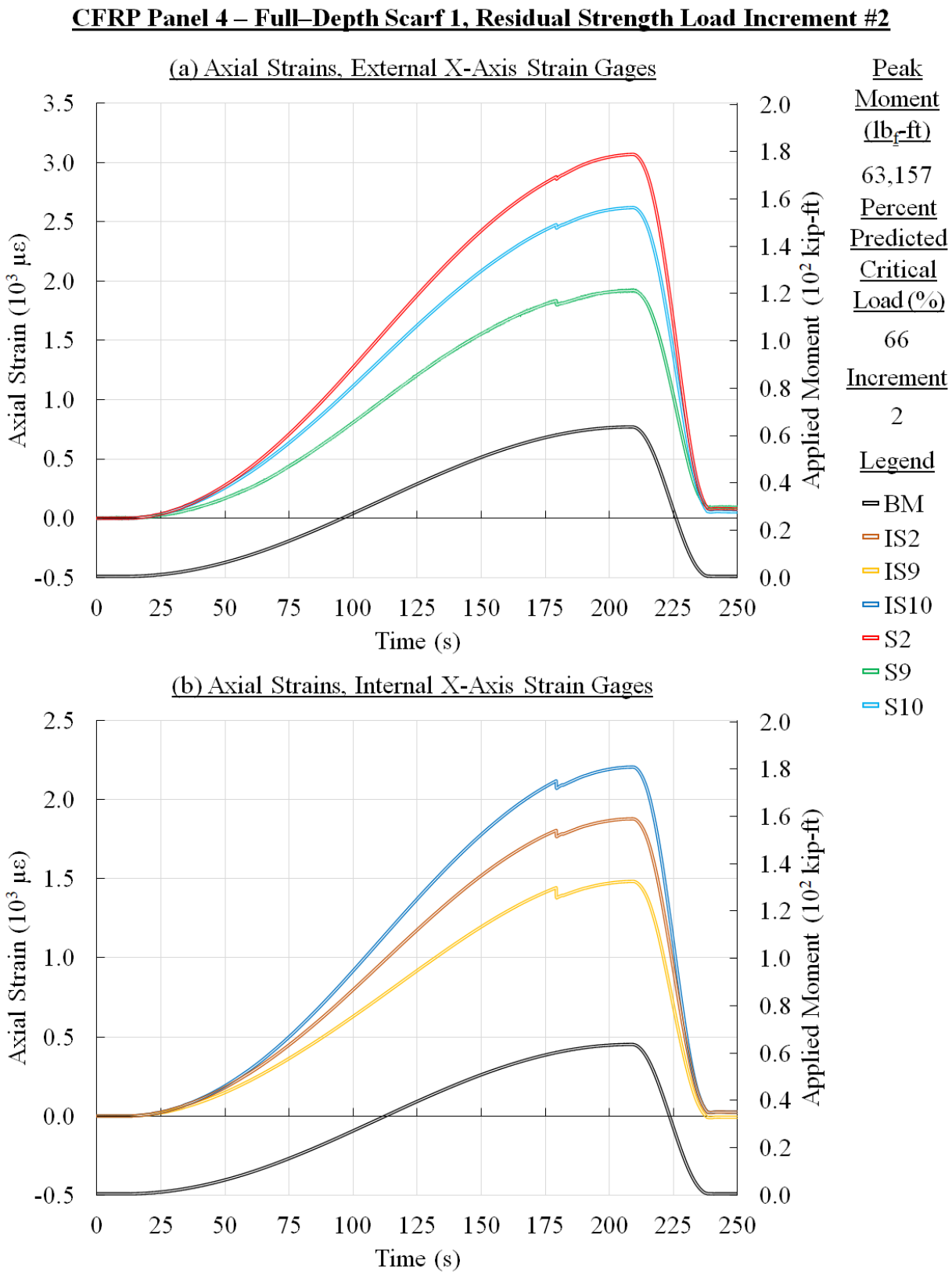


Figure C 69. Panel 4 load increment 2 (66% load level), axial strain along the X-axis strain gages

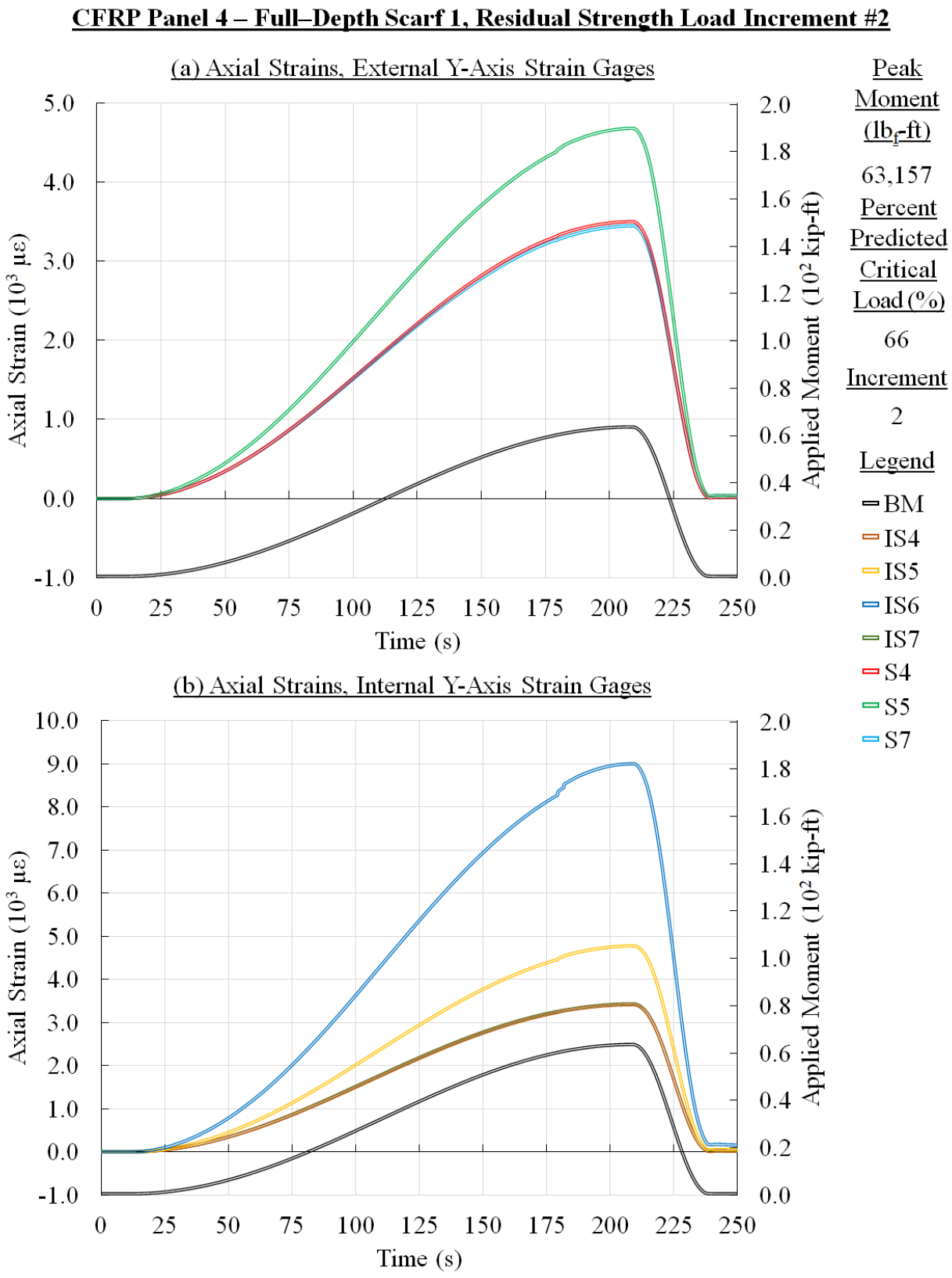


Figure C 70. Panel 4 load increment 2 (66% load level), axial strain along the Y-axis strain gages

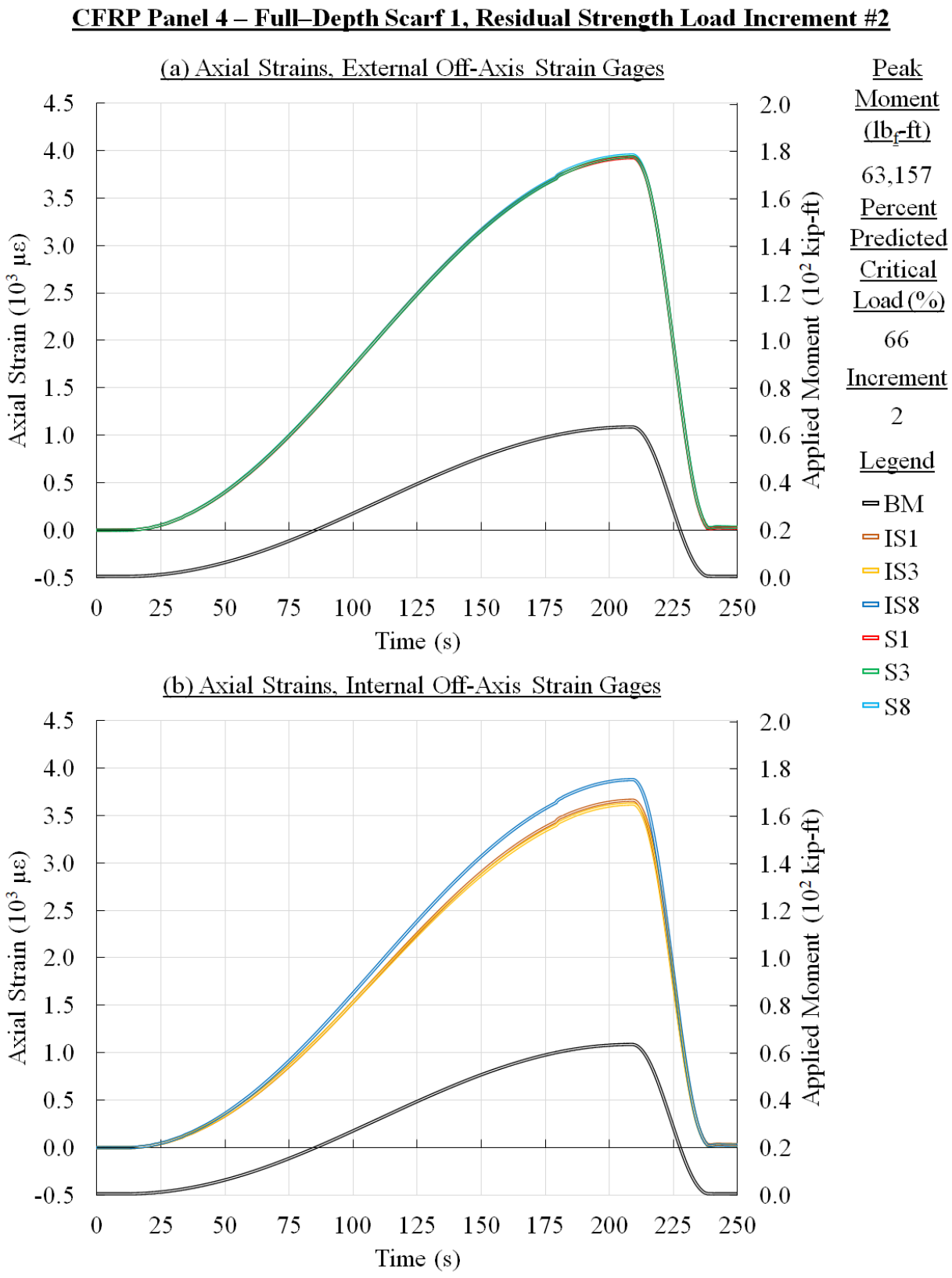


Figure C 71. Panel 4 load increment 2 (66% load level), axial strain along the off-axis strain gages

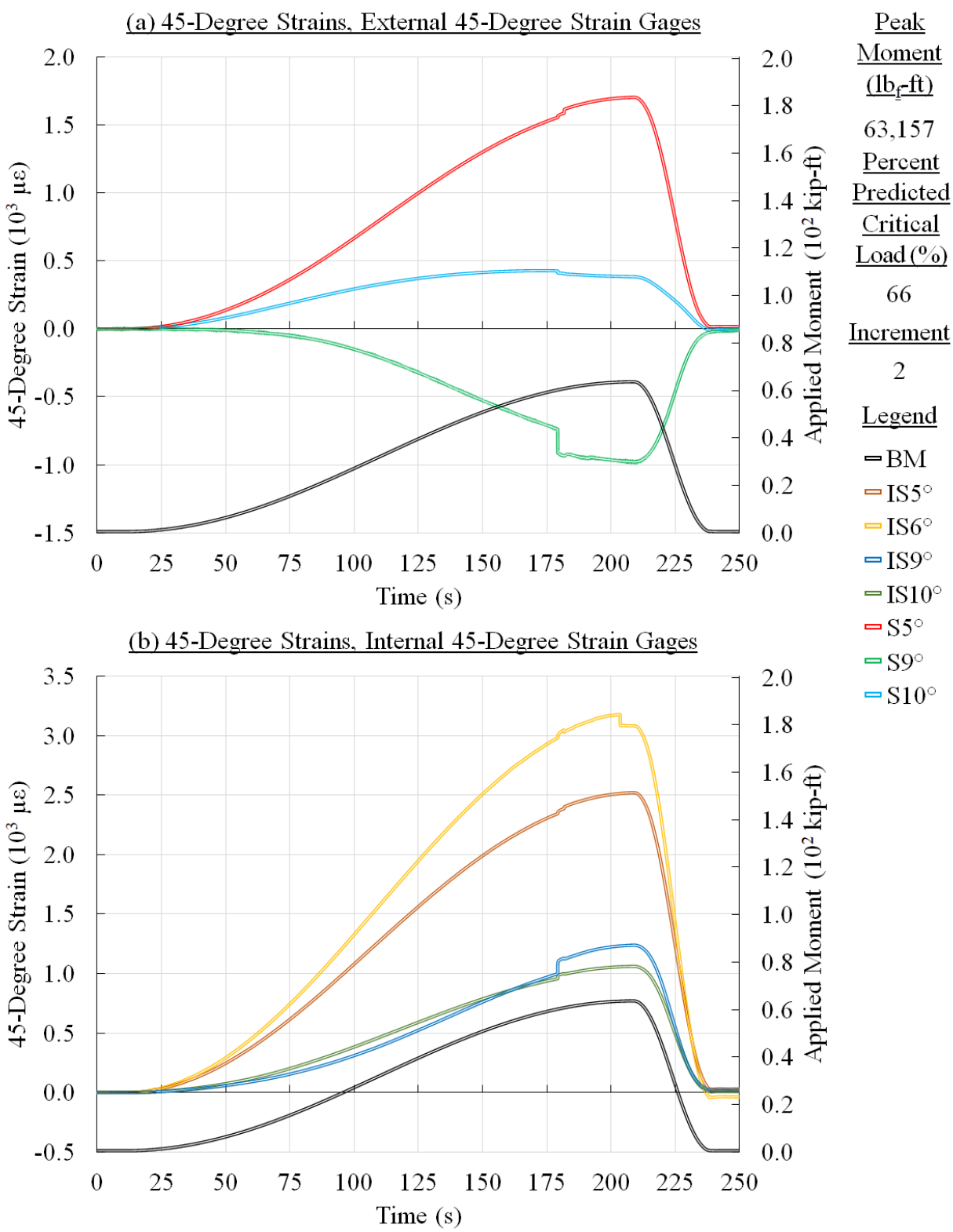


Figure C 72. Panel 4 load increment 2 (66% load level), 45 degree strain

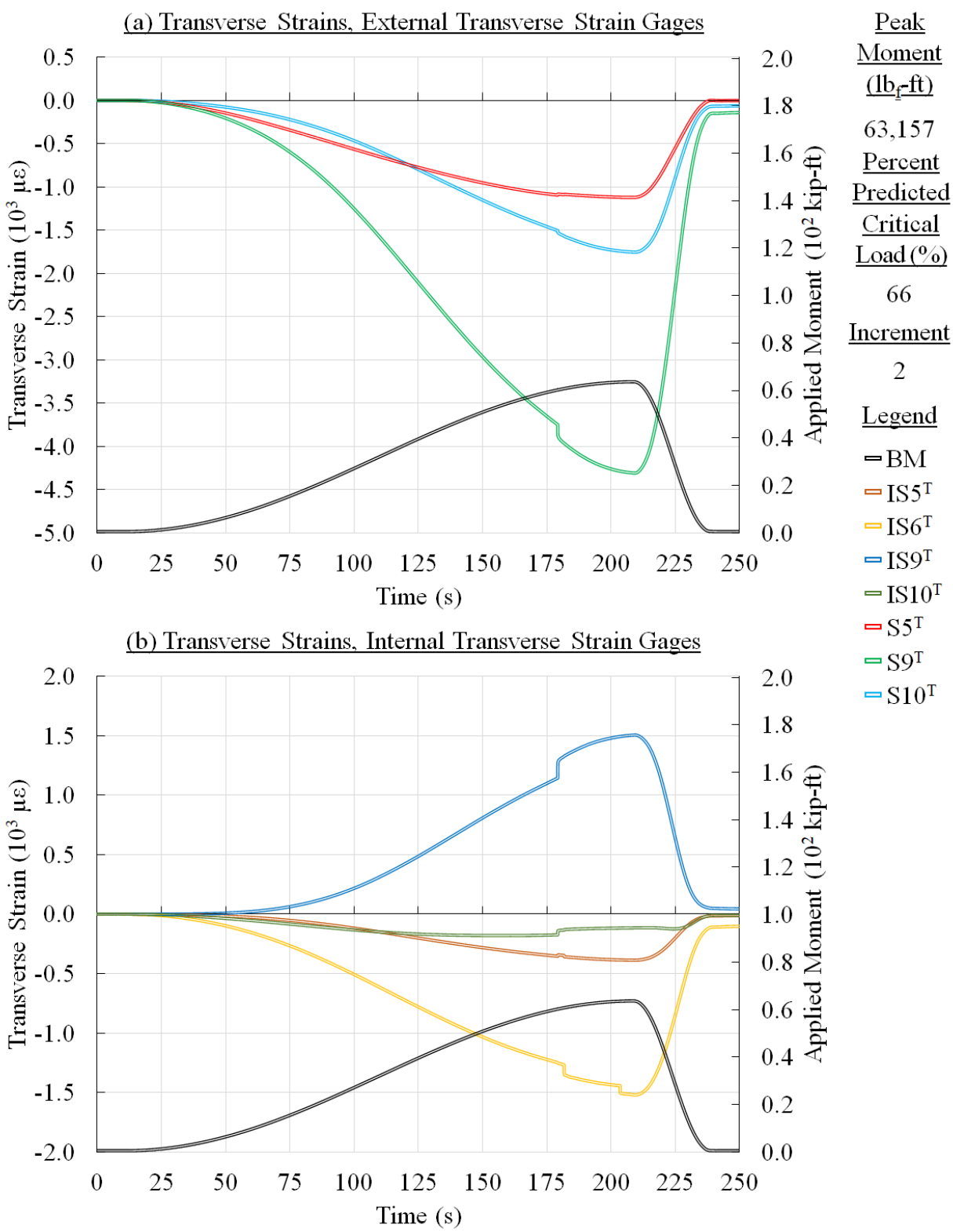


Figure C 73. Panel 4 load increment 2 (66% load level), transverse strain

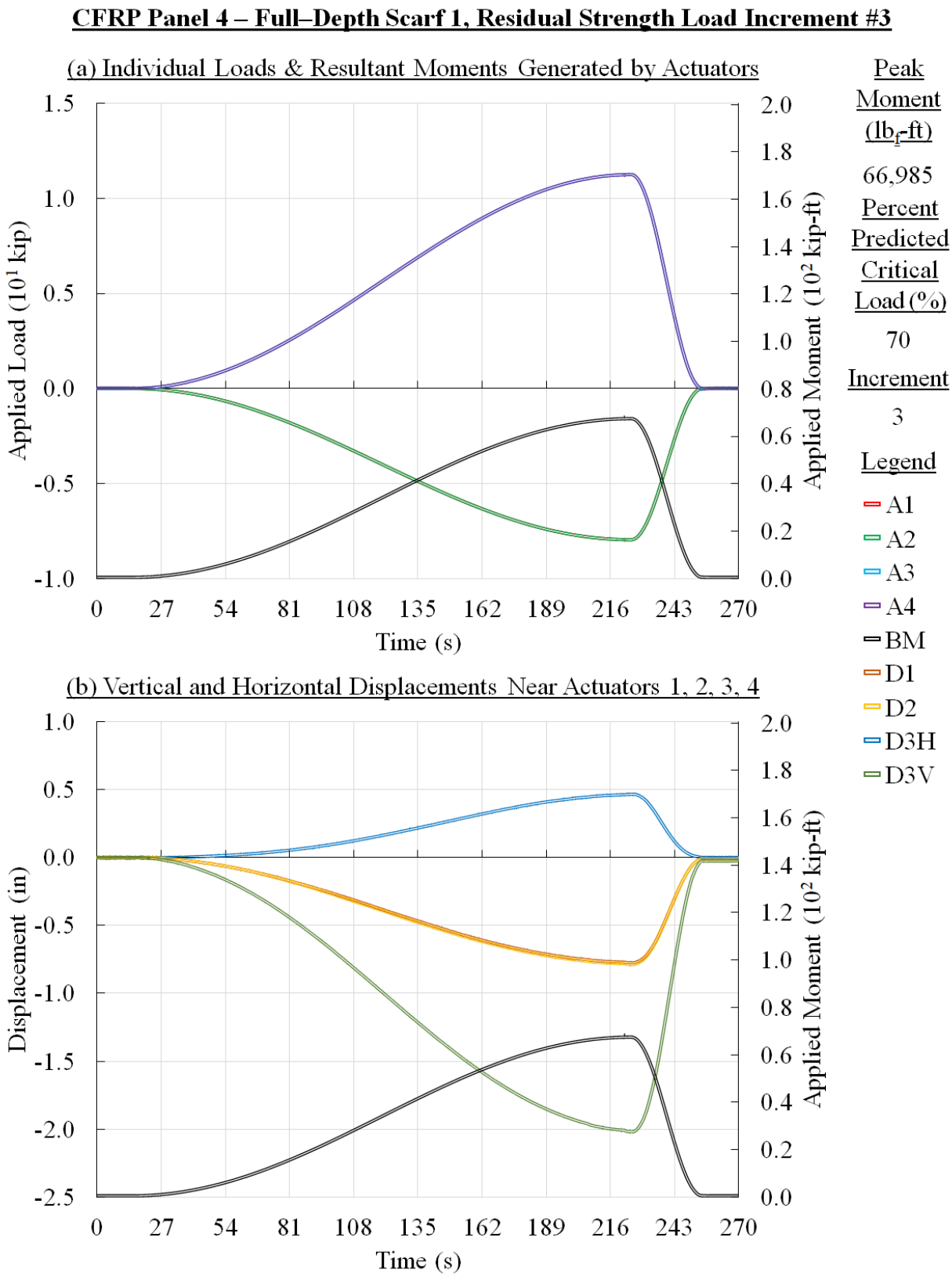


Figure C 74. Panel 4 load increment 3 (70% load level), load and displacement

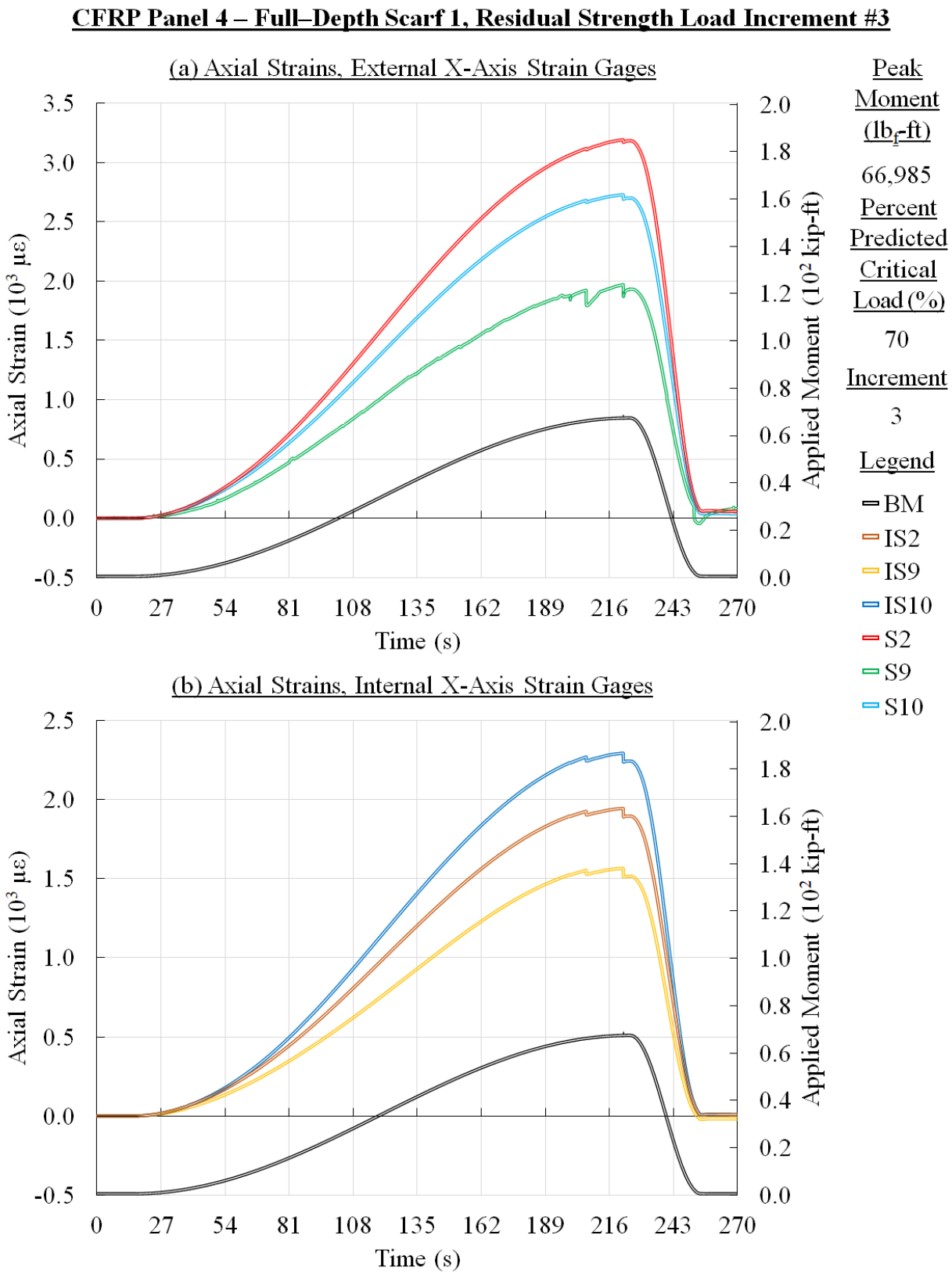


Figure C 75. Panel 4 load increment 3 (70% load level), axial strain along the X-axis strain gages

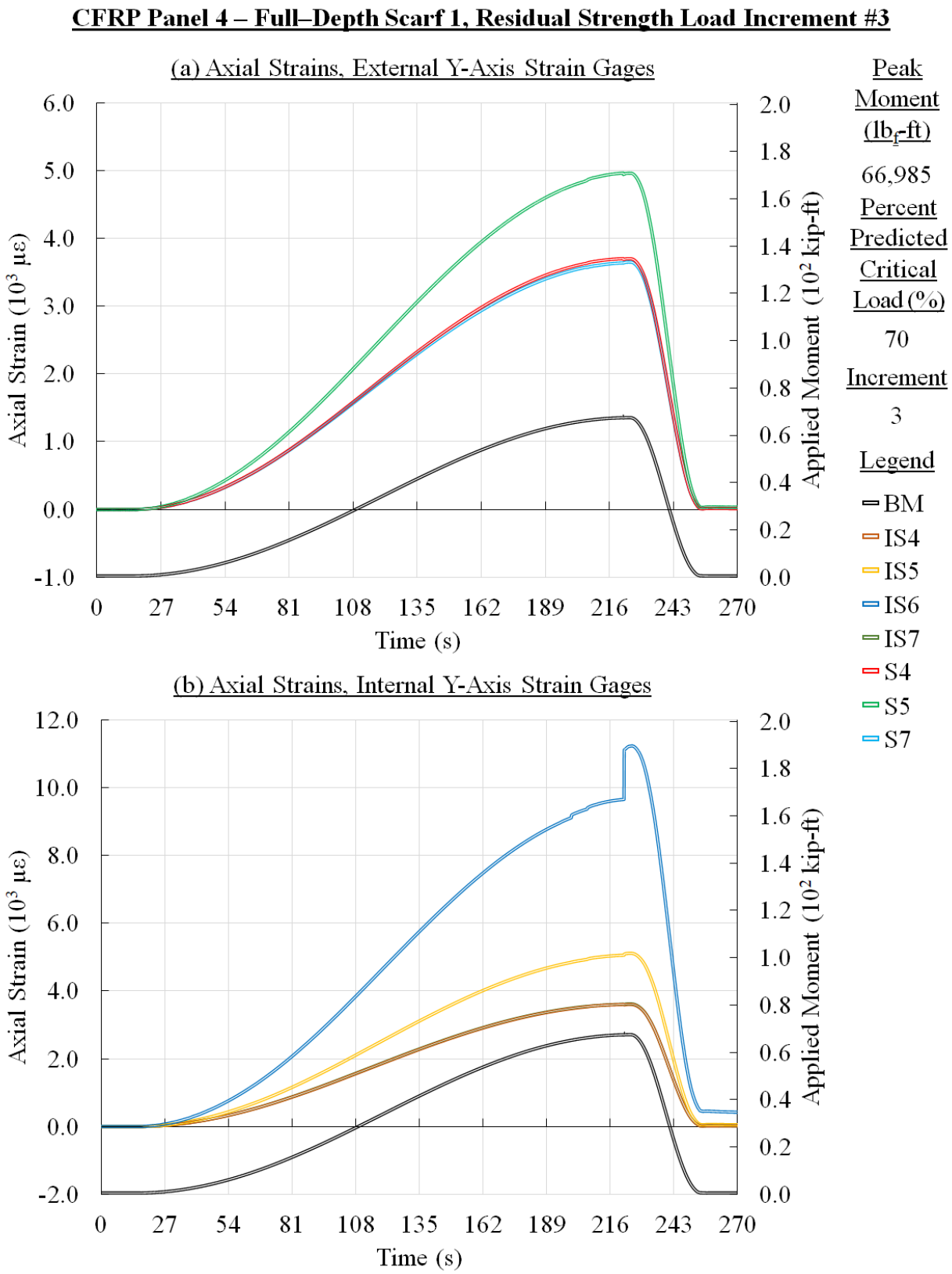


Figure C 76. Panel 4 load increment 3 (70% load level), axial strain along the Y-axis strain gages

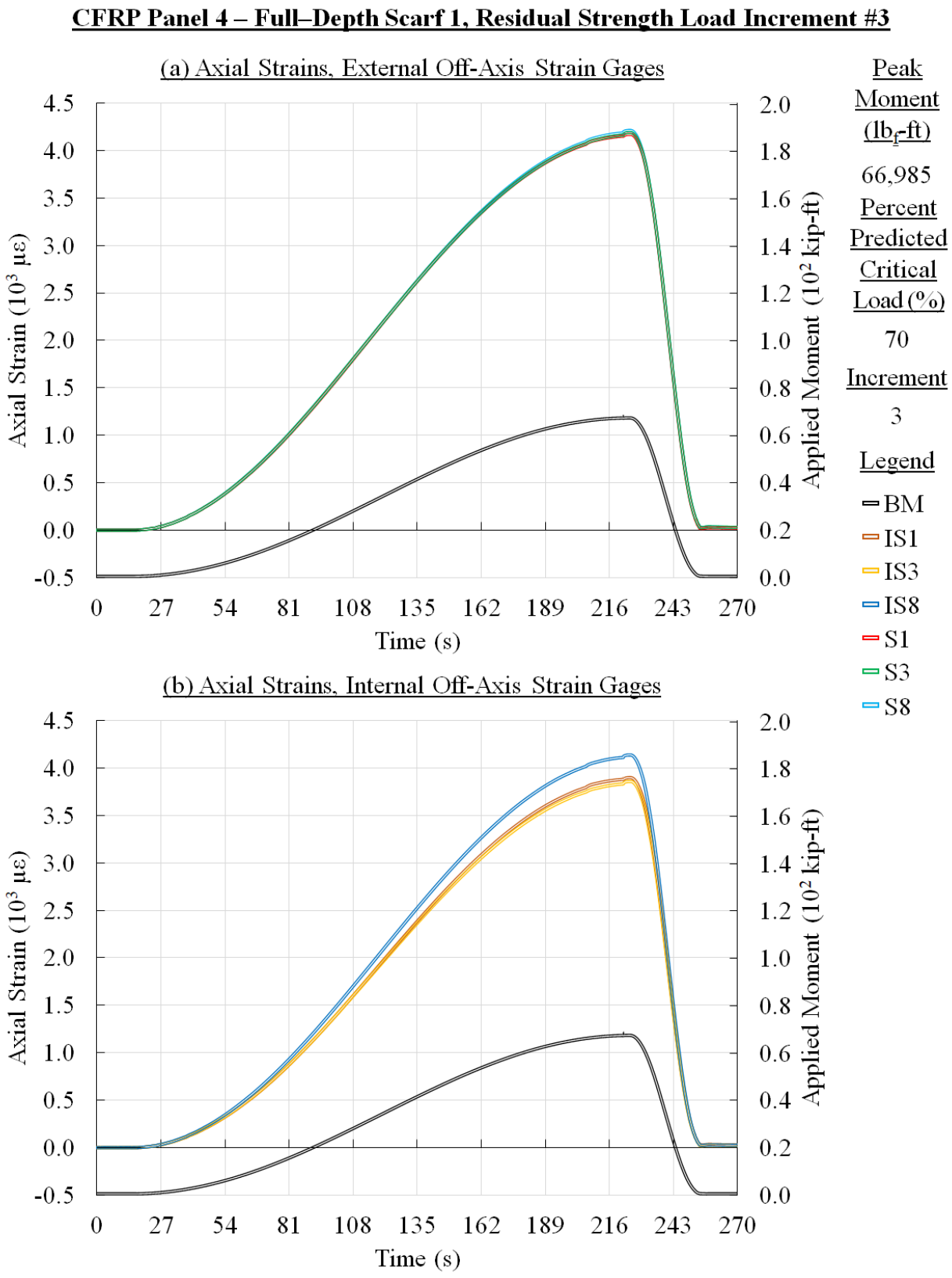


Figure C 77. Panel 4 load increment 3 (70% load level), axial strain along the off-axis strain gages

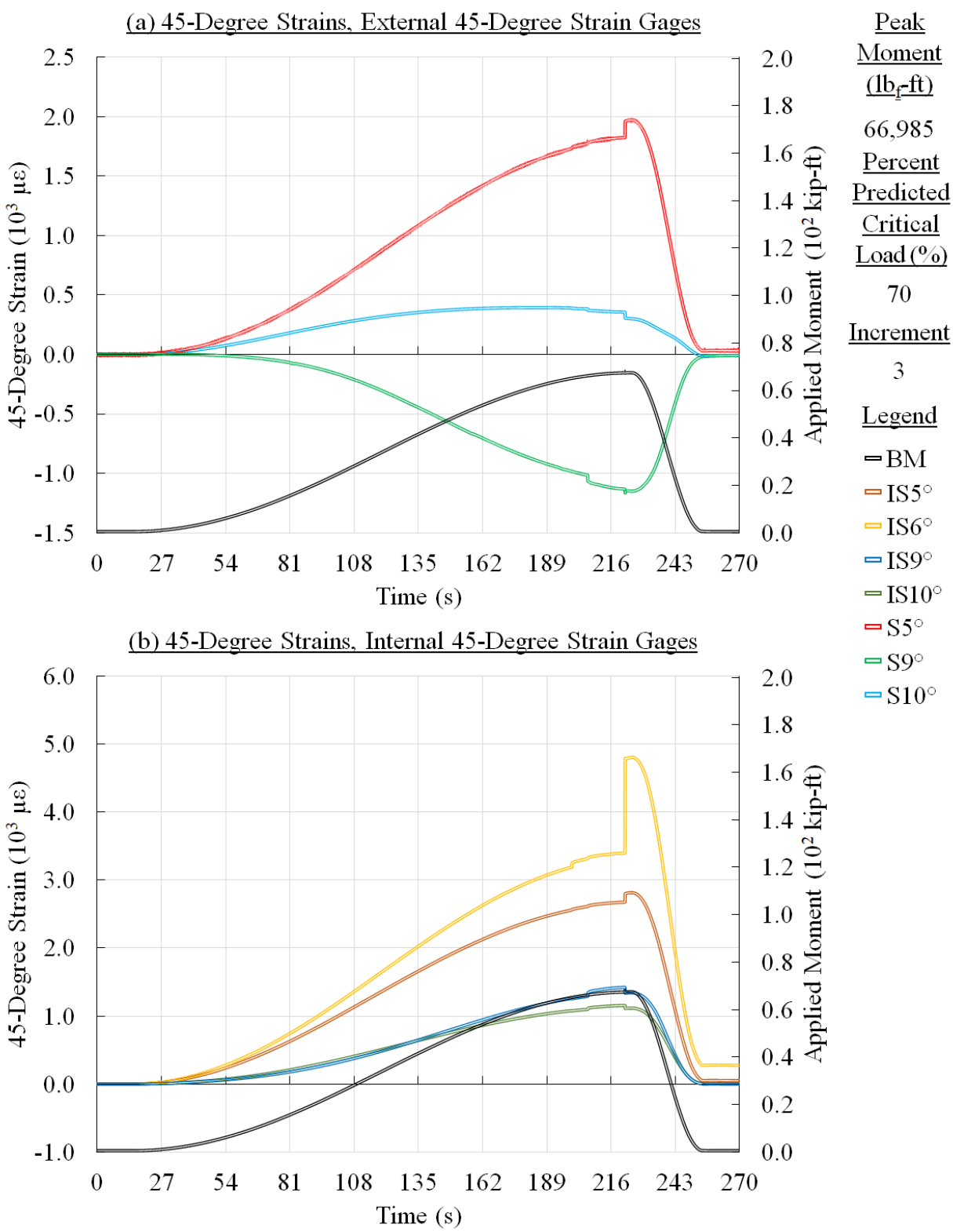


Figure C 78. Panel 4 load increment 3 (70% load level), 45 degree strain

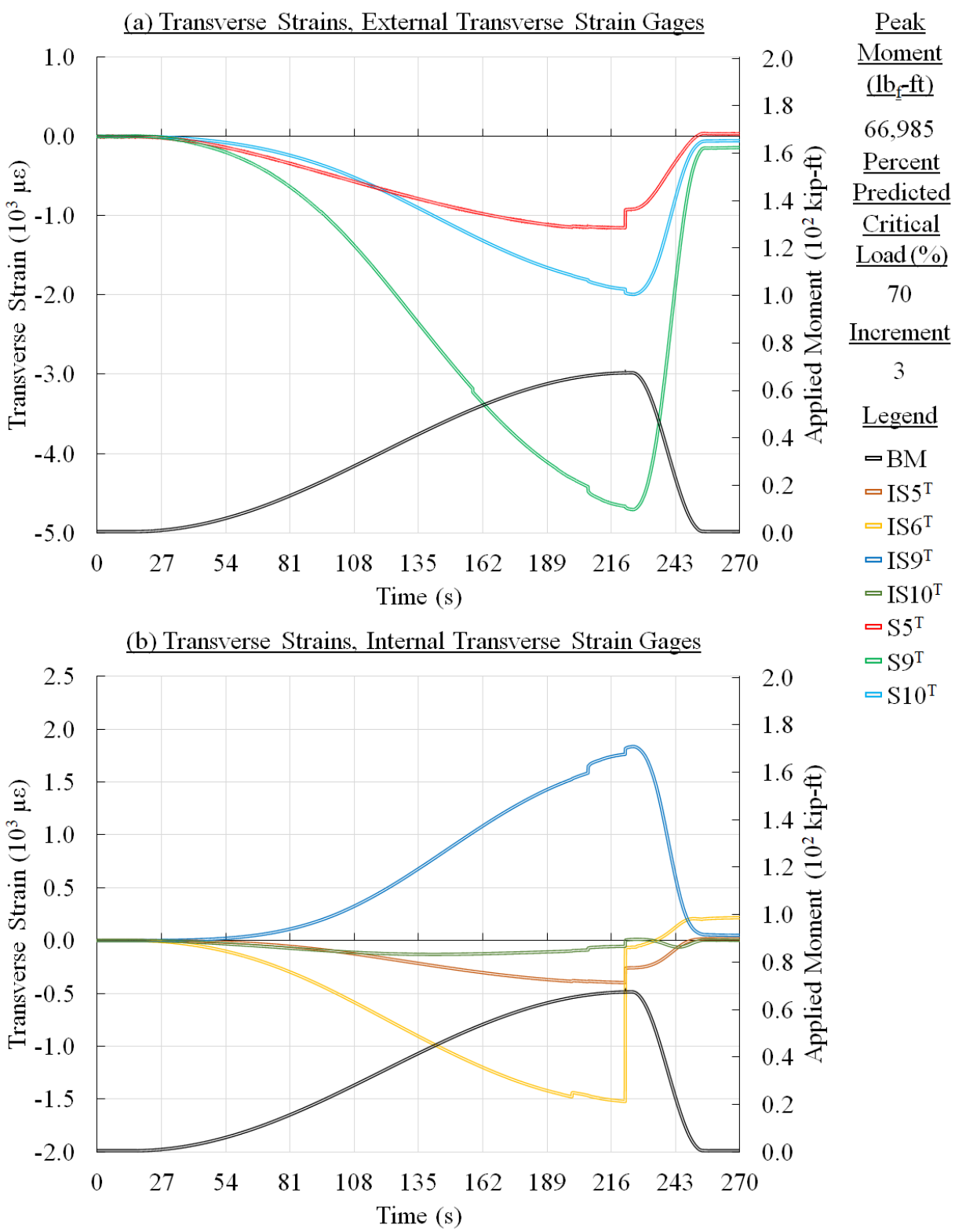


Figure C 79. Panel 4 load increment 3 (70% load level), transverse strain

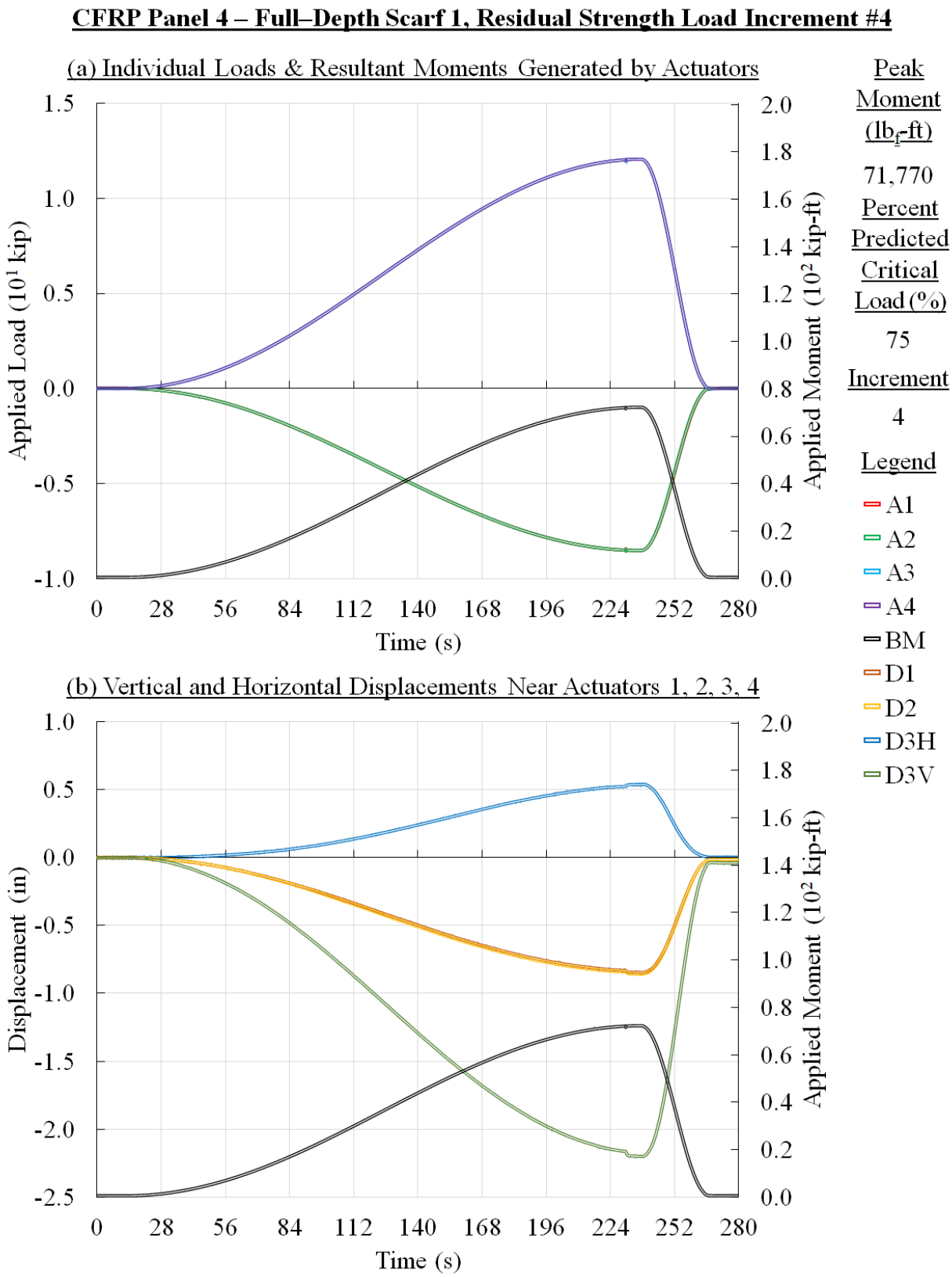


Figure C 80. Panel 4 load increment 4 (75% load level), load and displacement

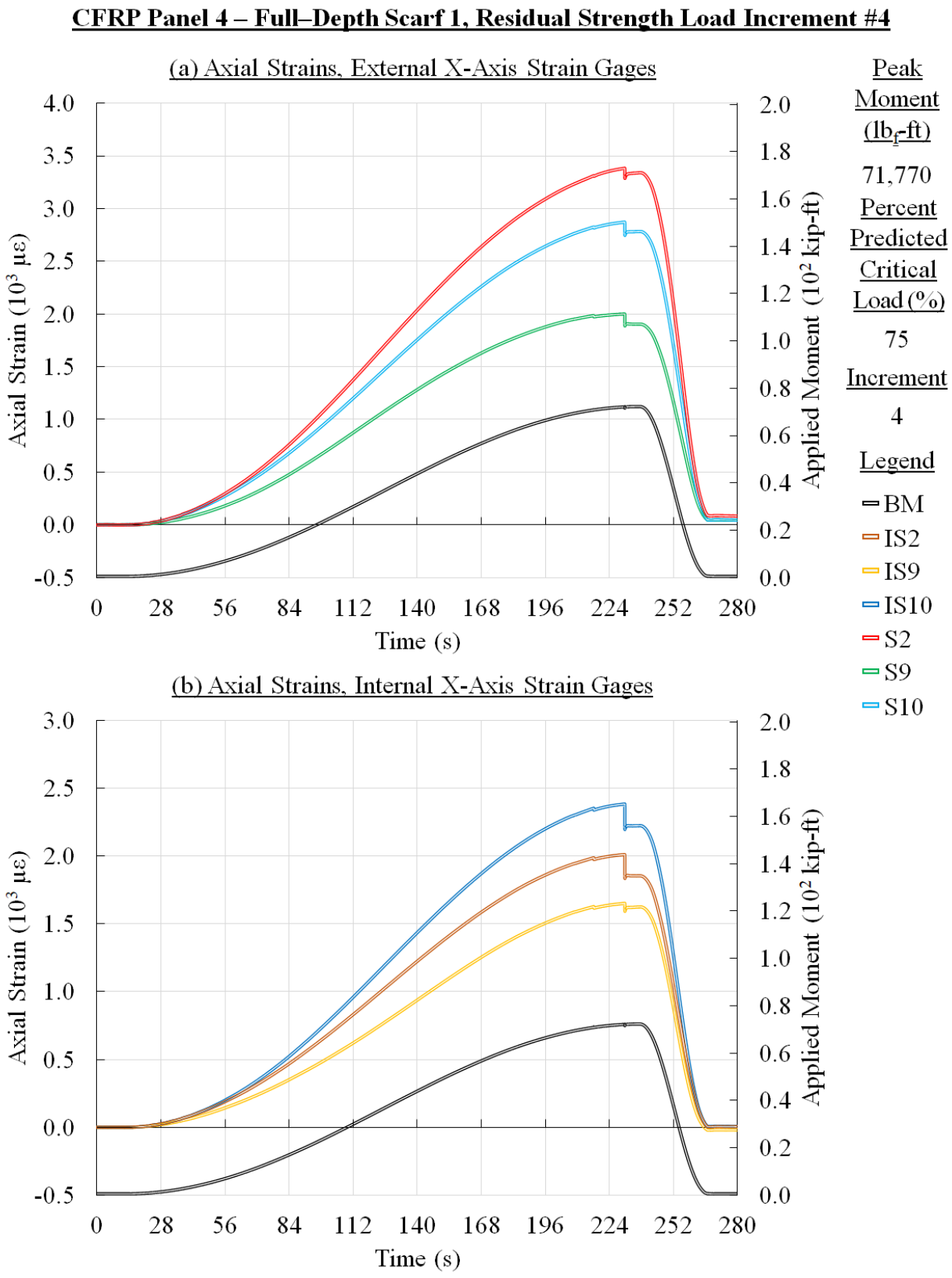


Figure C 81. Panel 4 load increment 4 (75% load level), axial strain along the X-axis strain gages

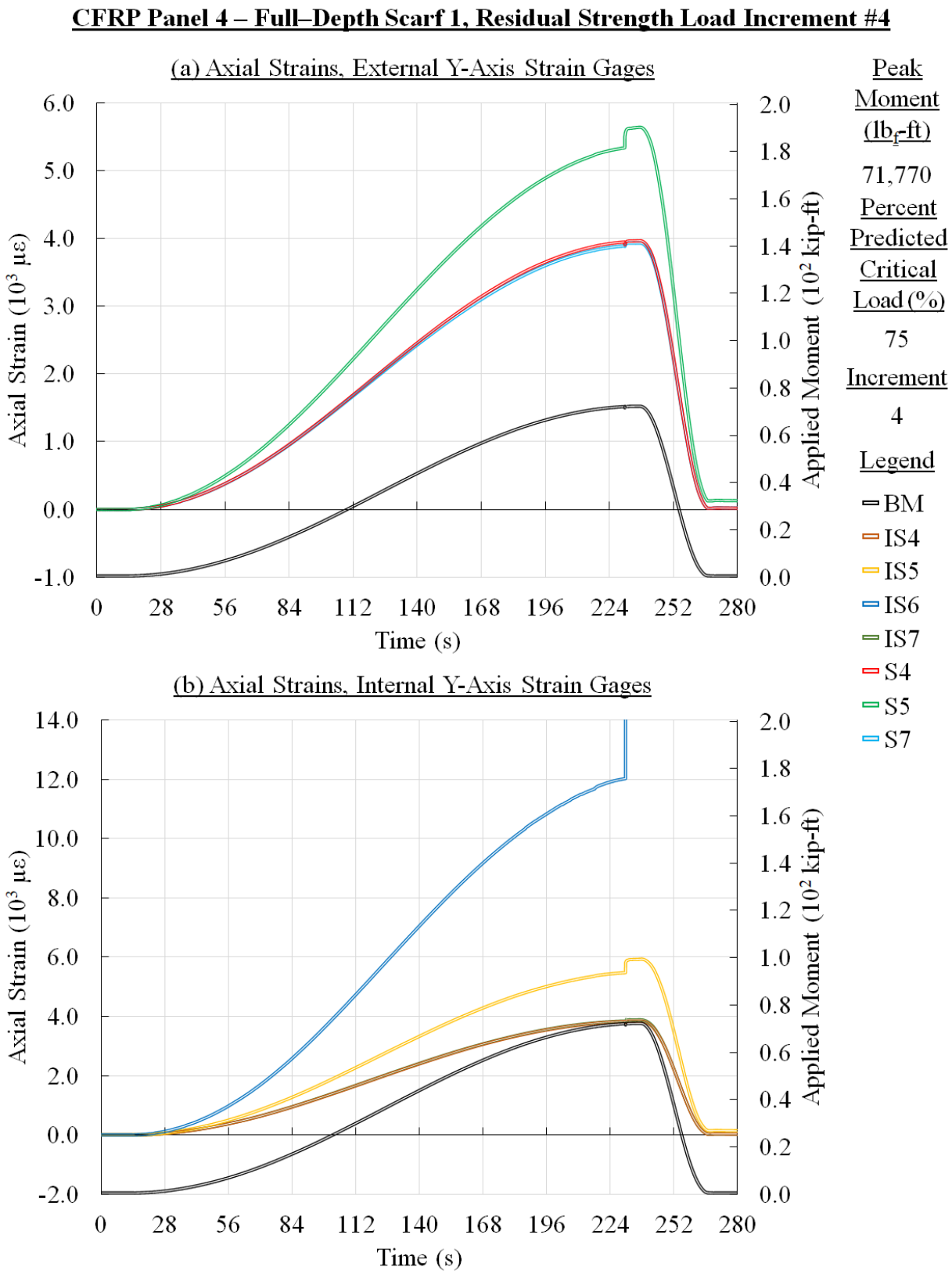


Figure C 82. Panel 4 load increment 4 (75% load level), axial strain along the Y-axis strain gages

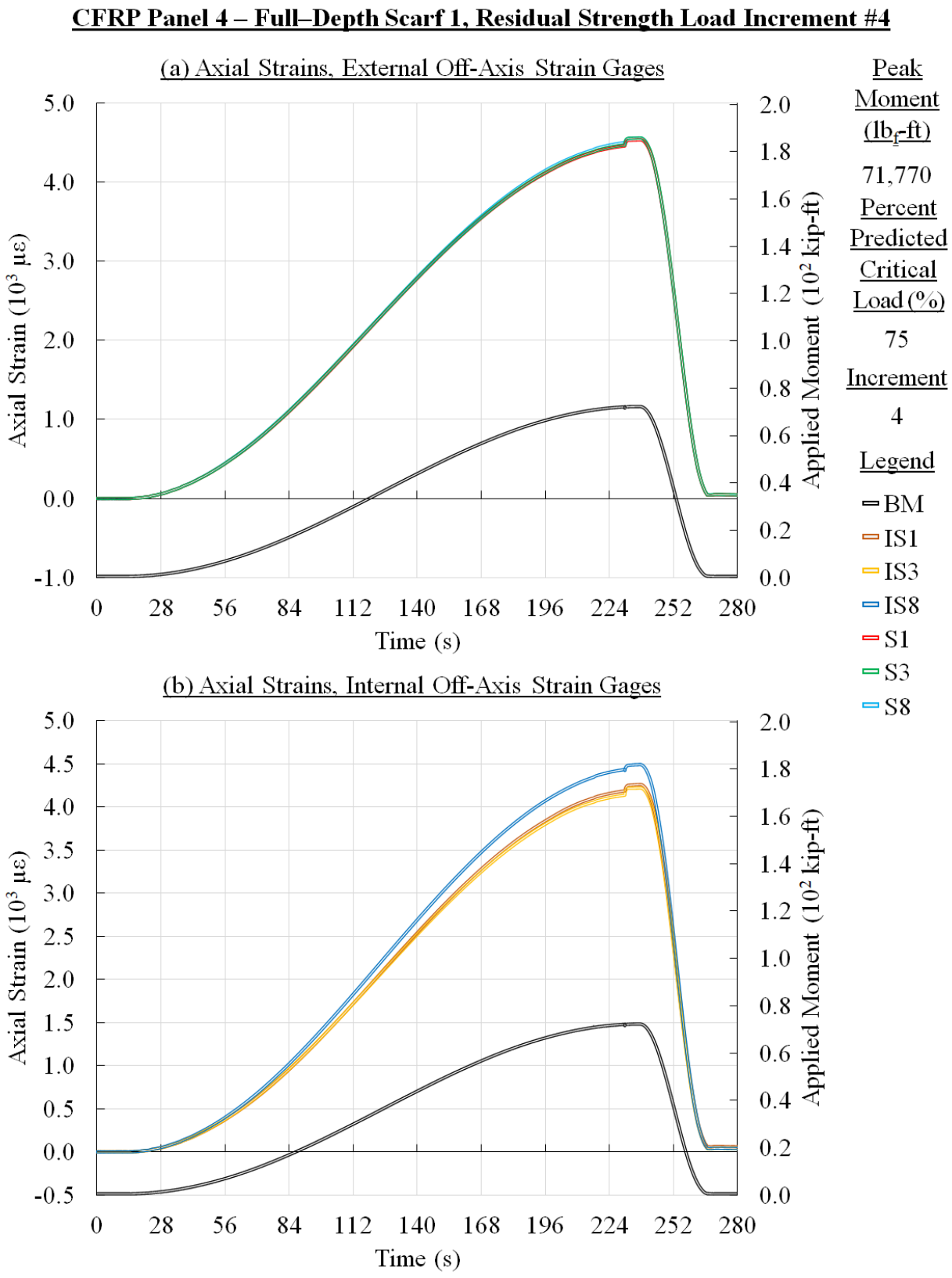


Figure C 83. Panel 4 load increment 4 (75% load level), axial strain along the off-axis strain gages

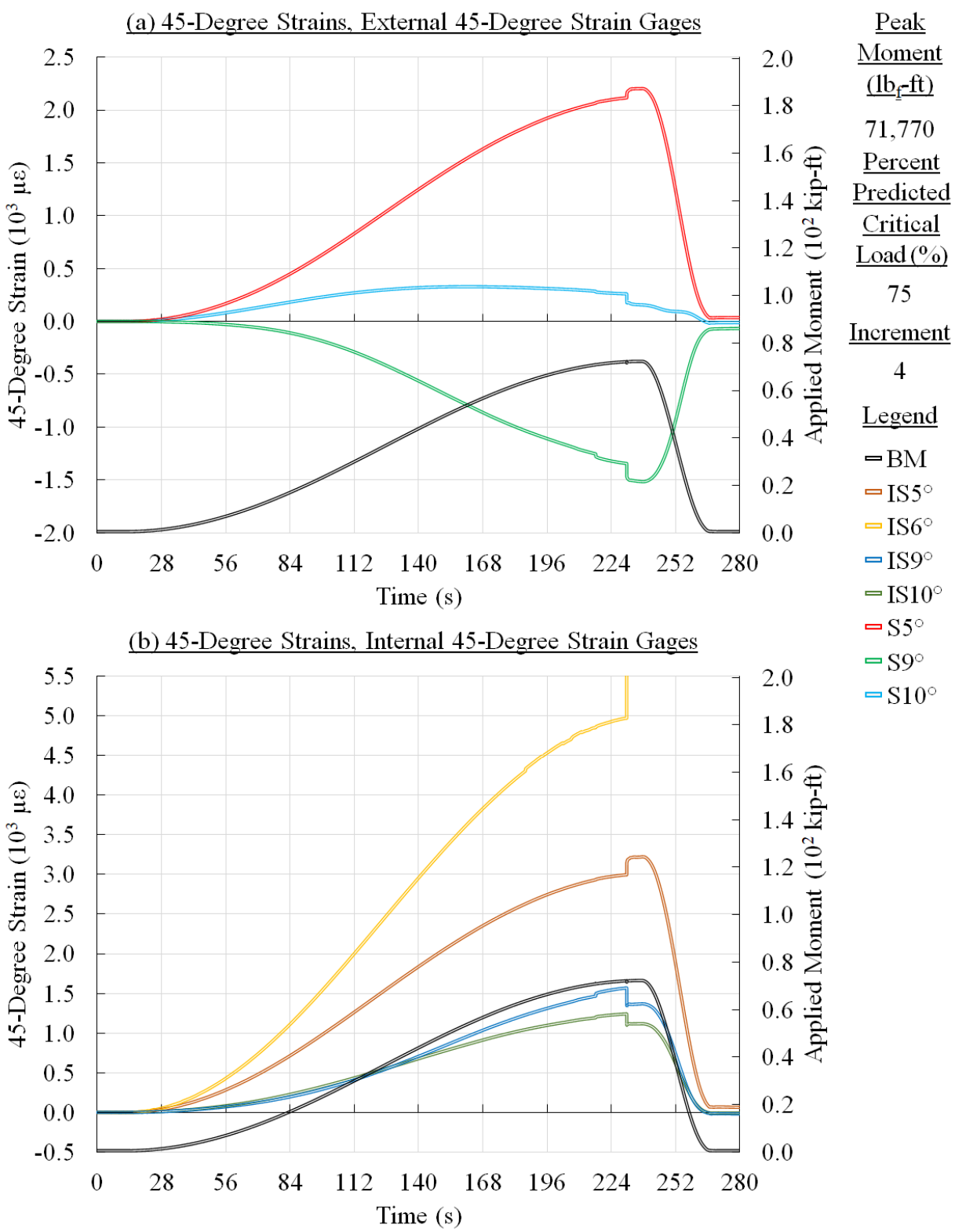


Figure C 84. Panel 4 load increment 4 (75% load level), 45 degree strain

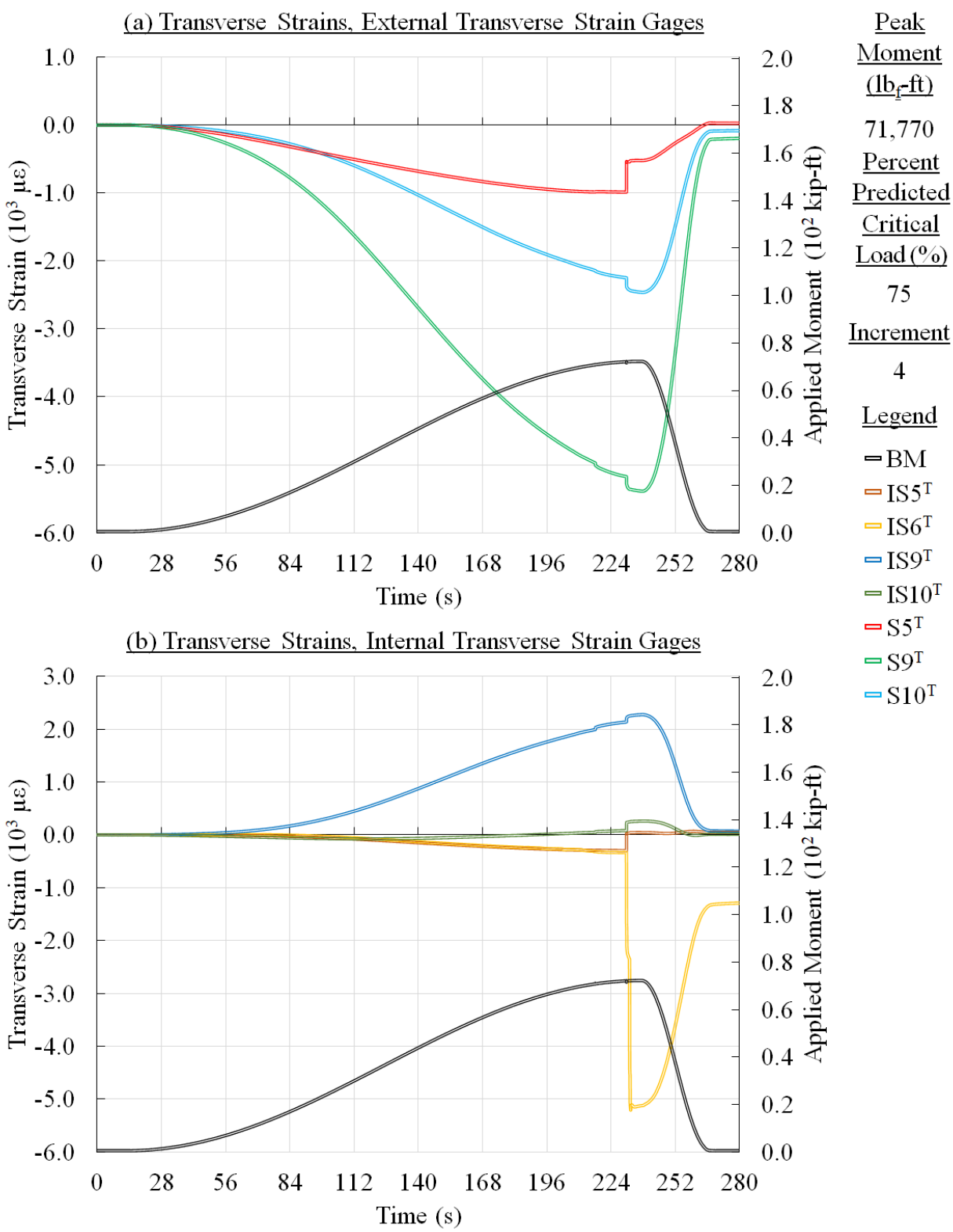


Figure C 85. Panel 4 load increment 4 (75% load level), transverse strain

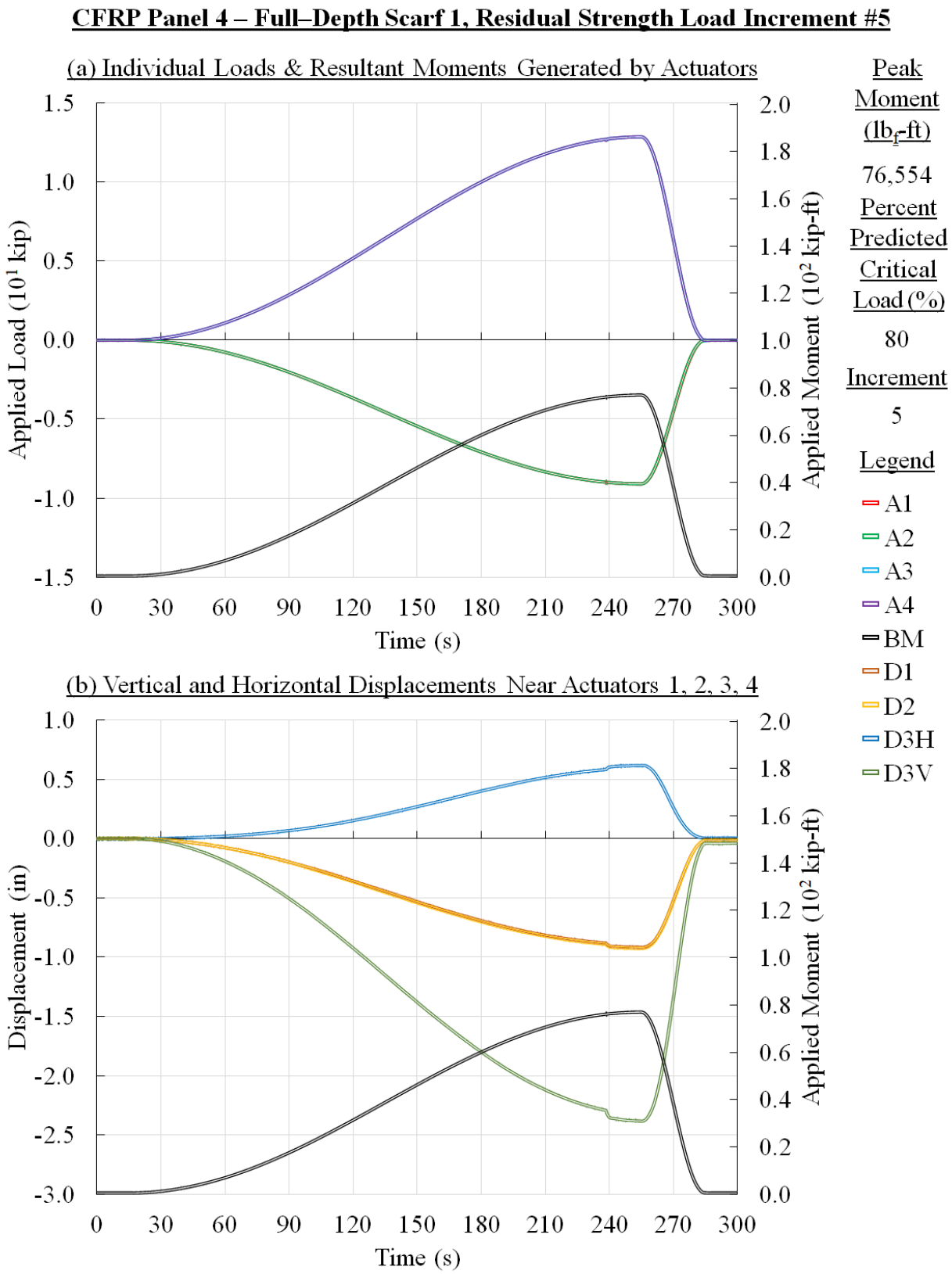


Figure C 86. Panel 4 load increment 5 (80% load level), load and displacement

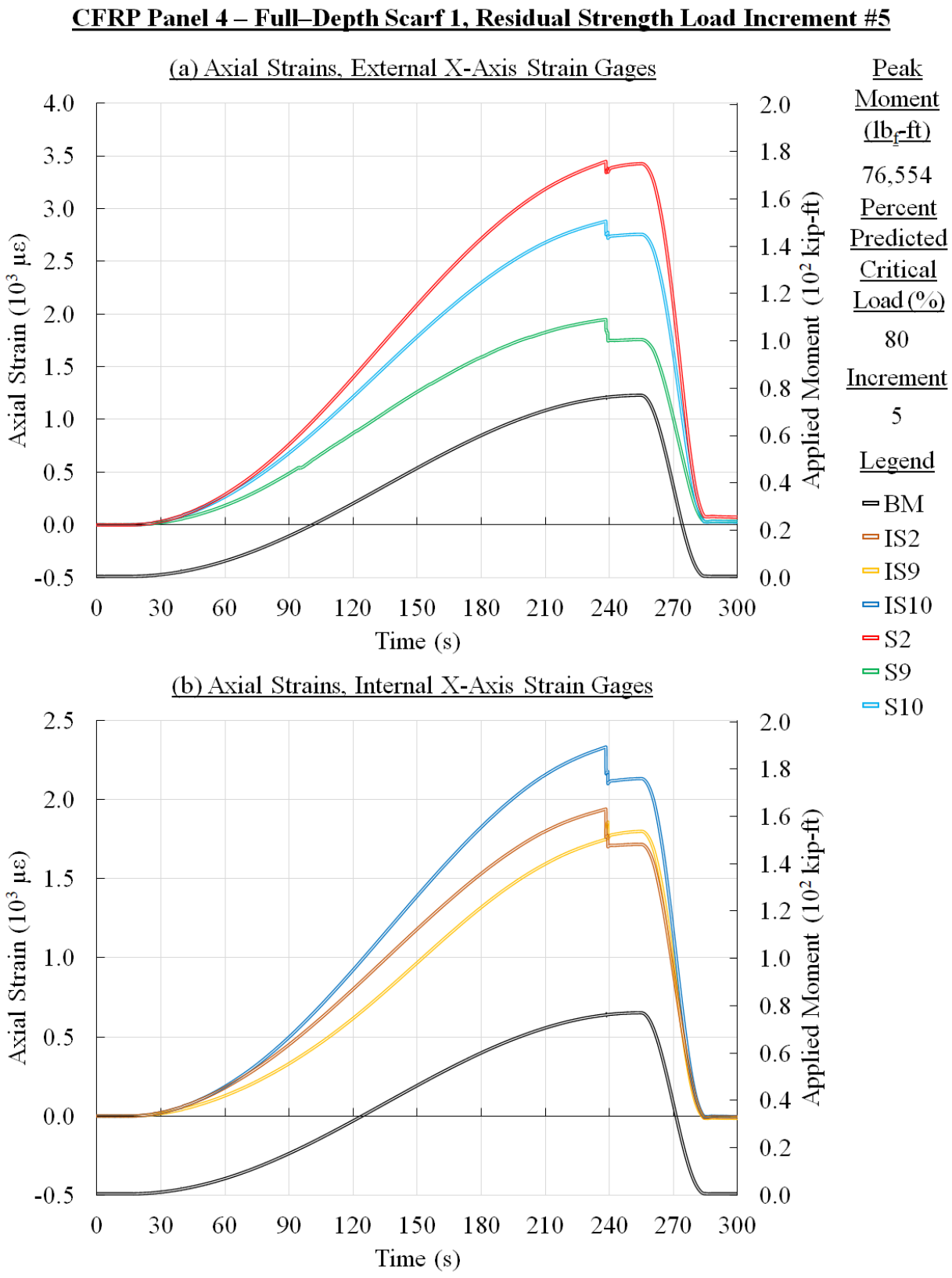


Figure C 87. Panel 4 load increment 5 (80% load level), axial strain along the X-axis strain gages

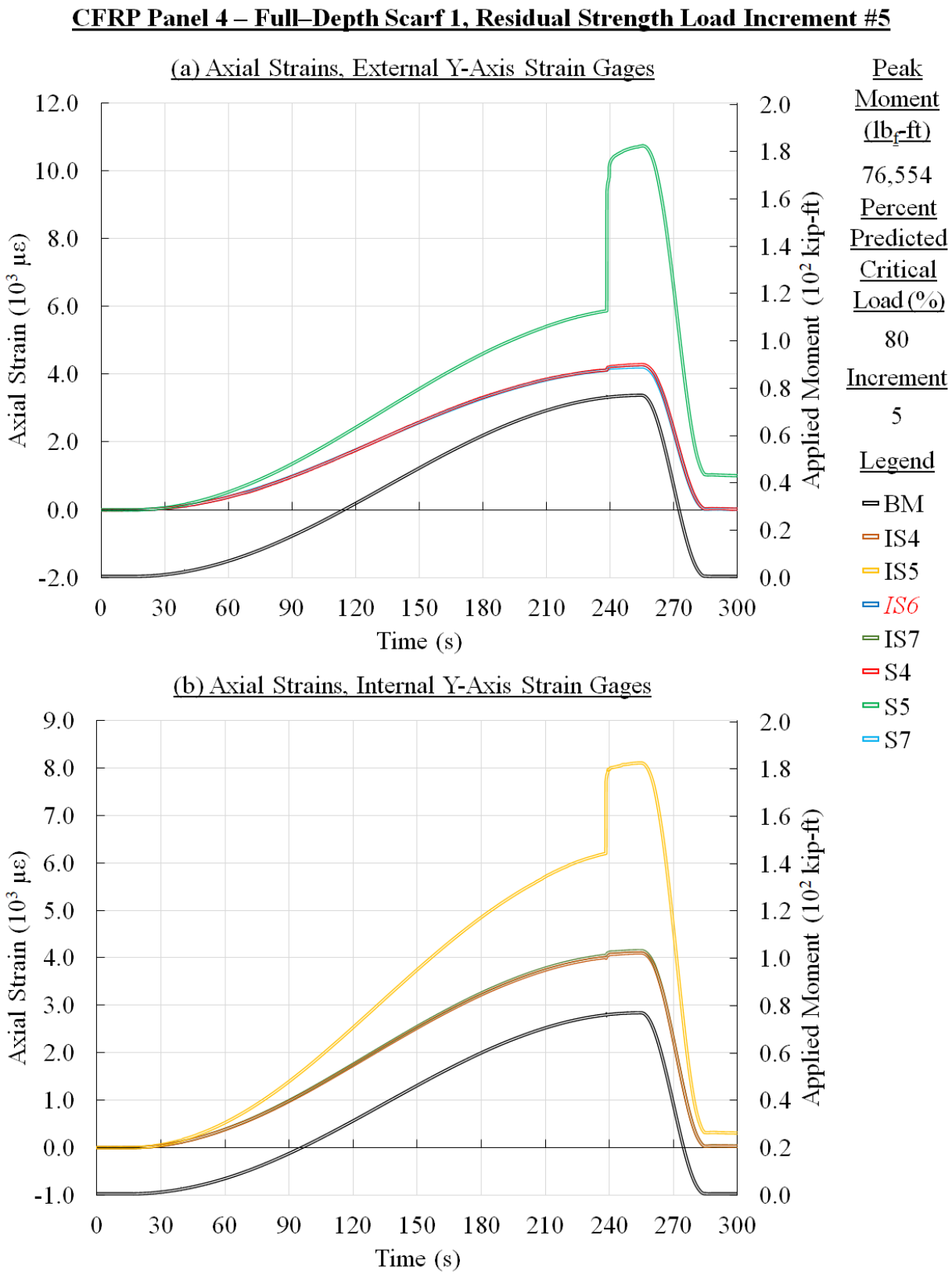


Figure C 88. Panel 4 load increment 5 (80% load level), axial strain along the Y-axis strain gages

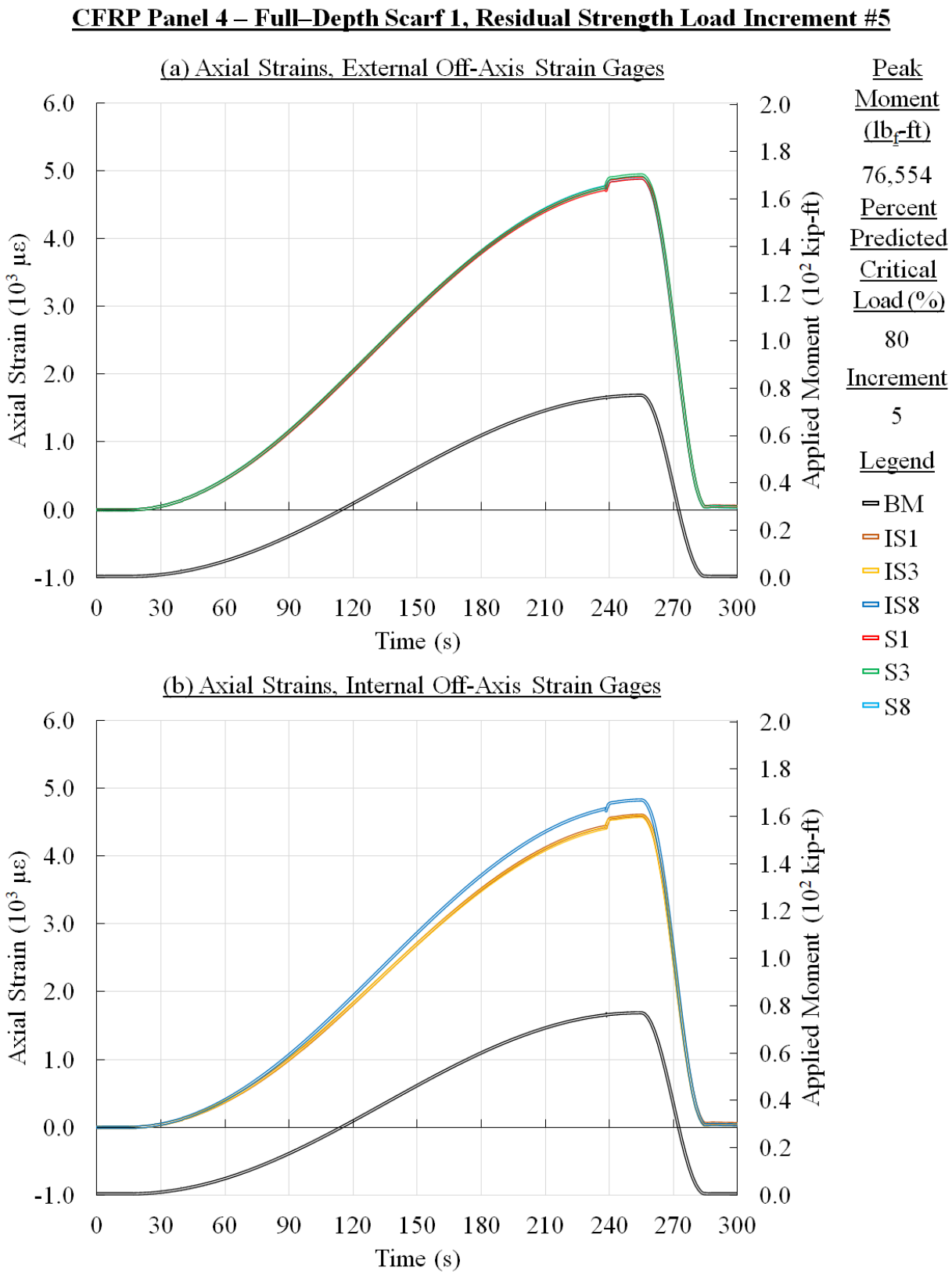


Figure C 89. Panel 4 load increment 5 (80% load level), axial strain along the off-axis strain gages

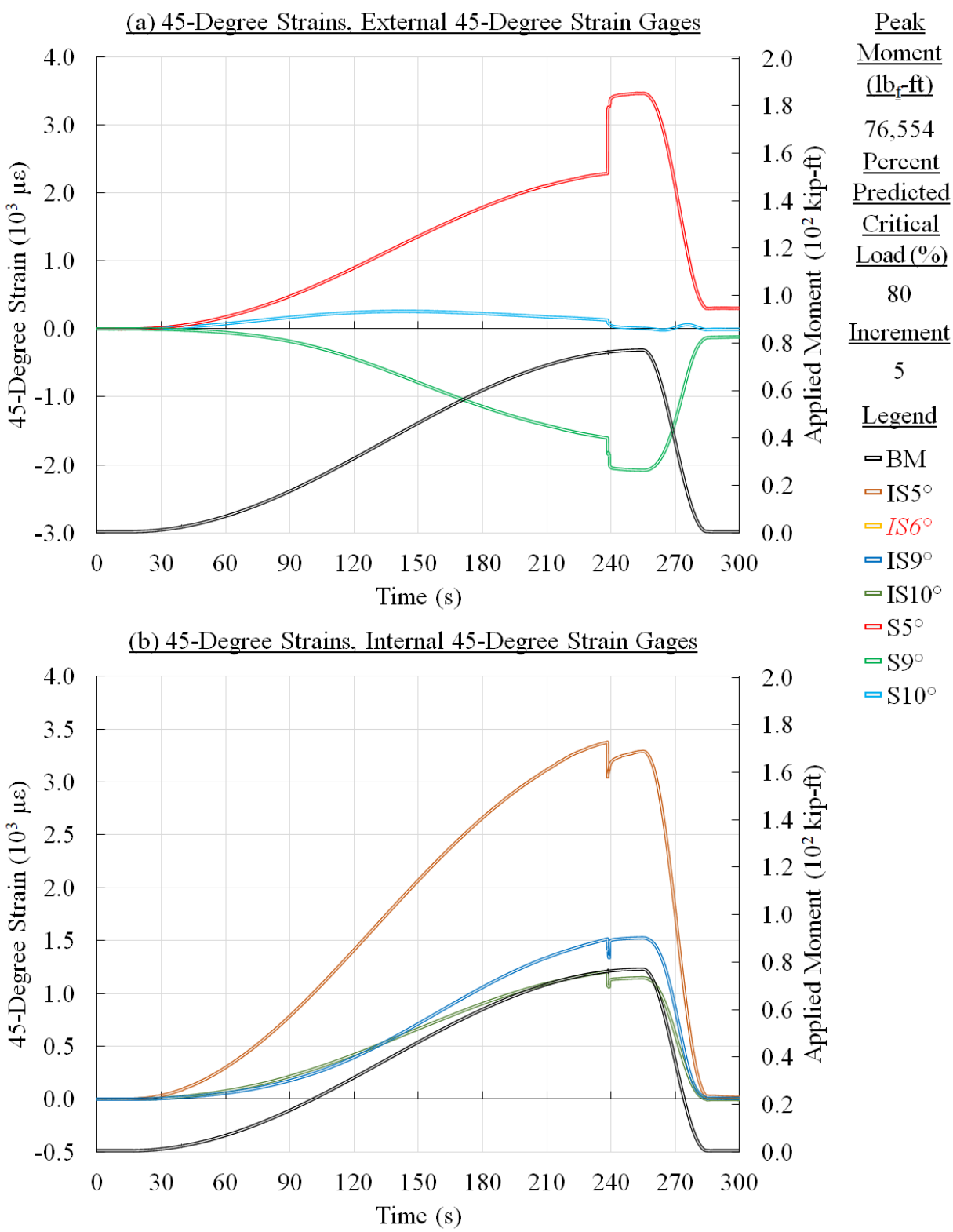


Figure C 90. Panel 4 load increment 5 (80% load level), 45 degree strain

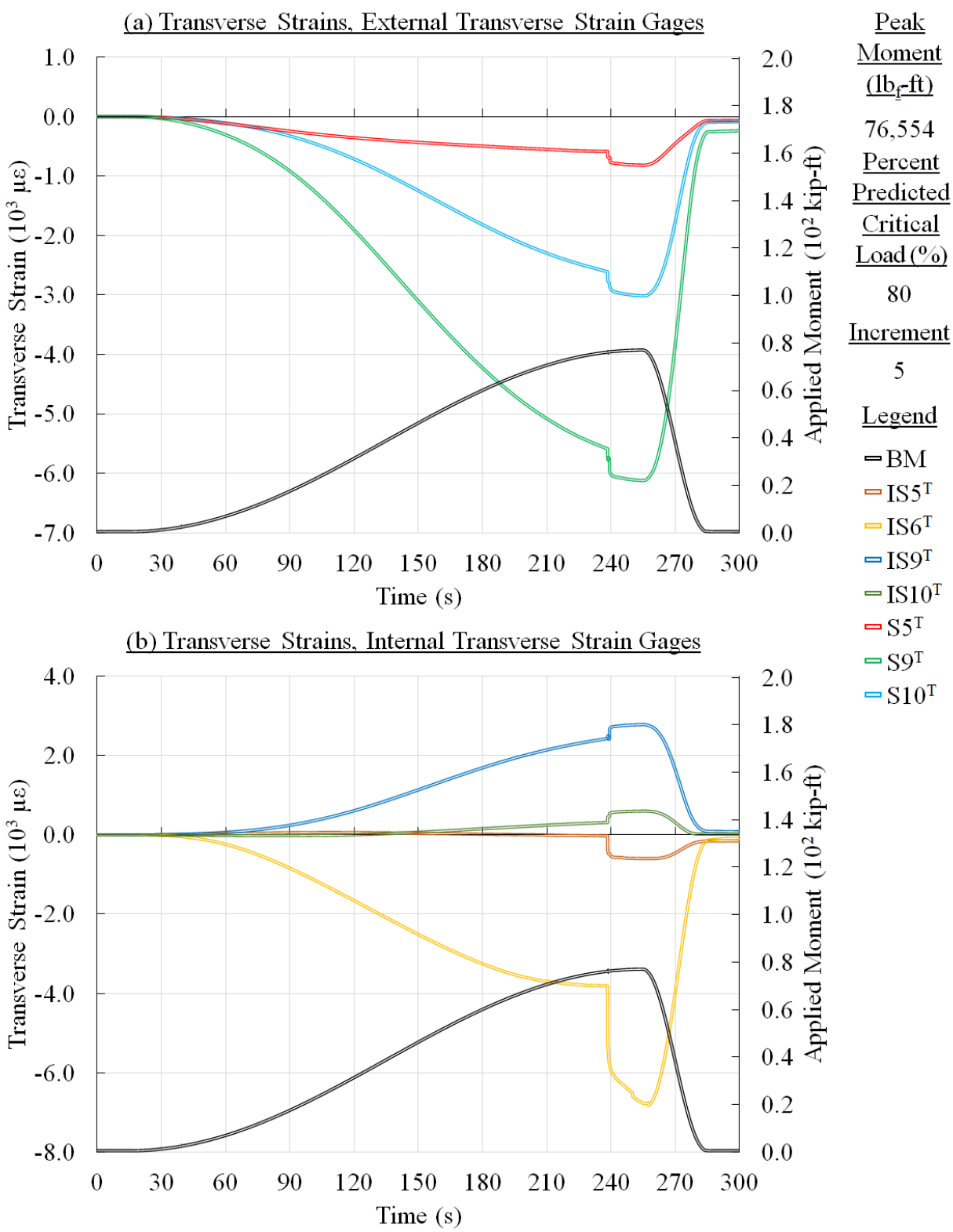


Figure C 91. Panel 4 load increment 5 (80% load level), transverse strain

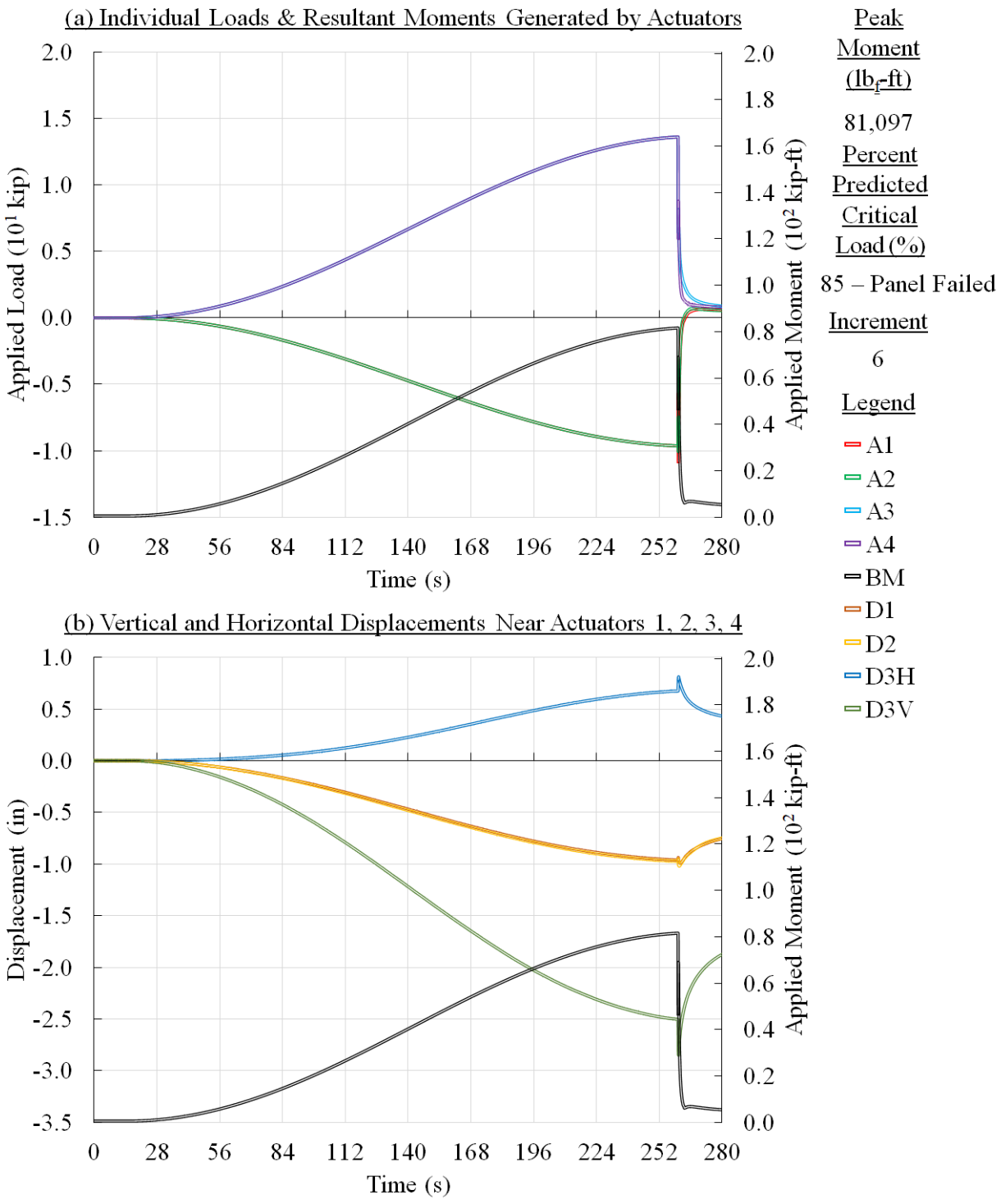


Figure C 92. Panel 4 load increment 6 (panel failure), load and displacement

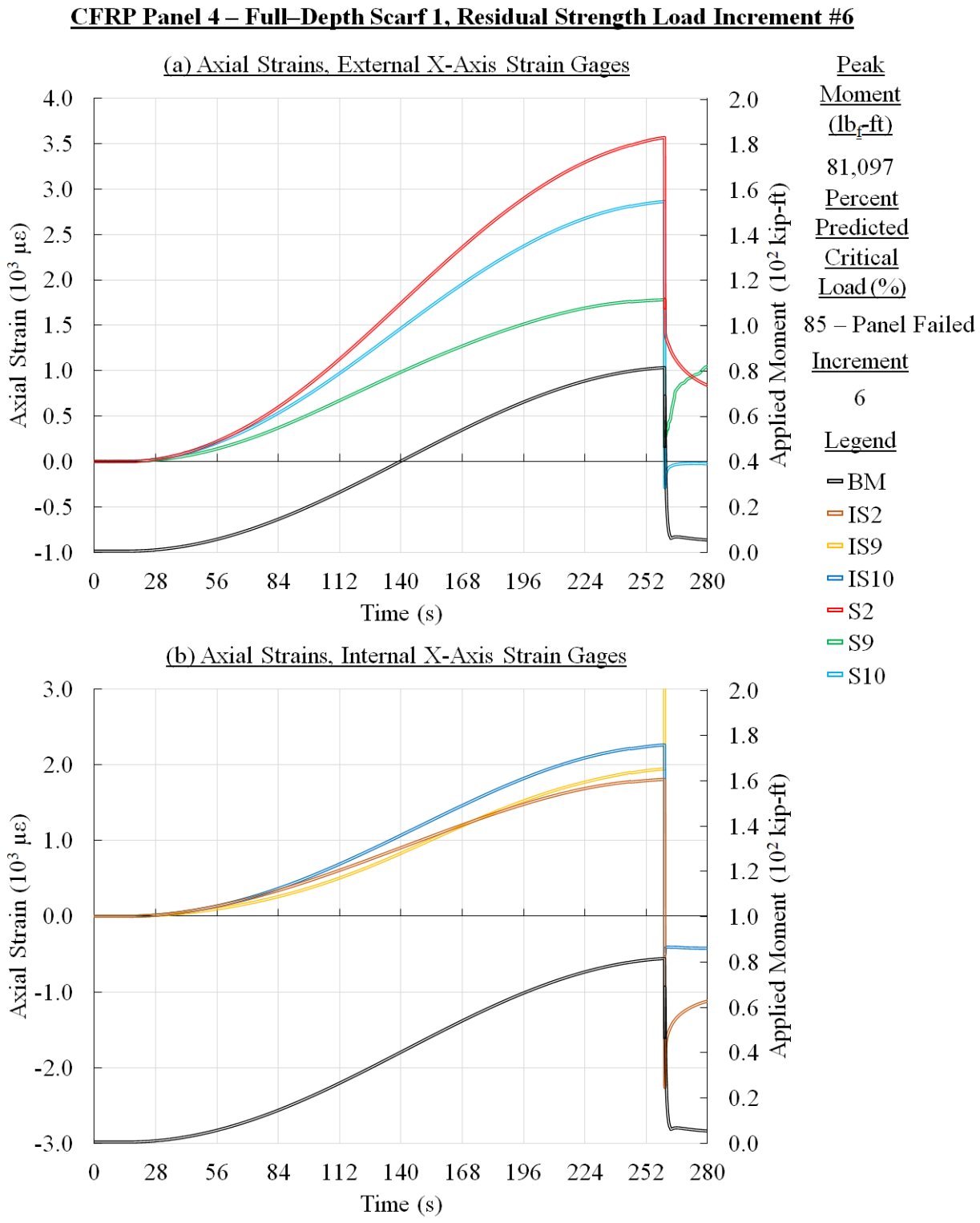


Figure C 93. Panel 4 load increment 6 (panel failure), axial strain along the X-axis strain gages

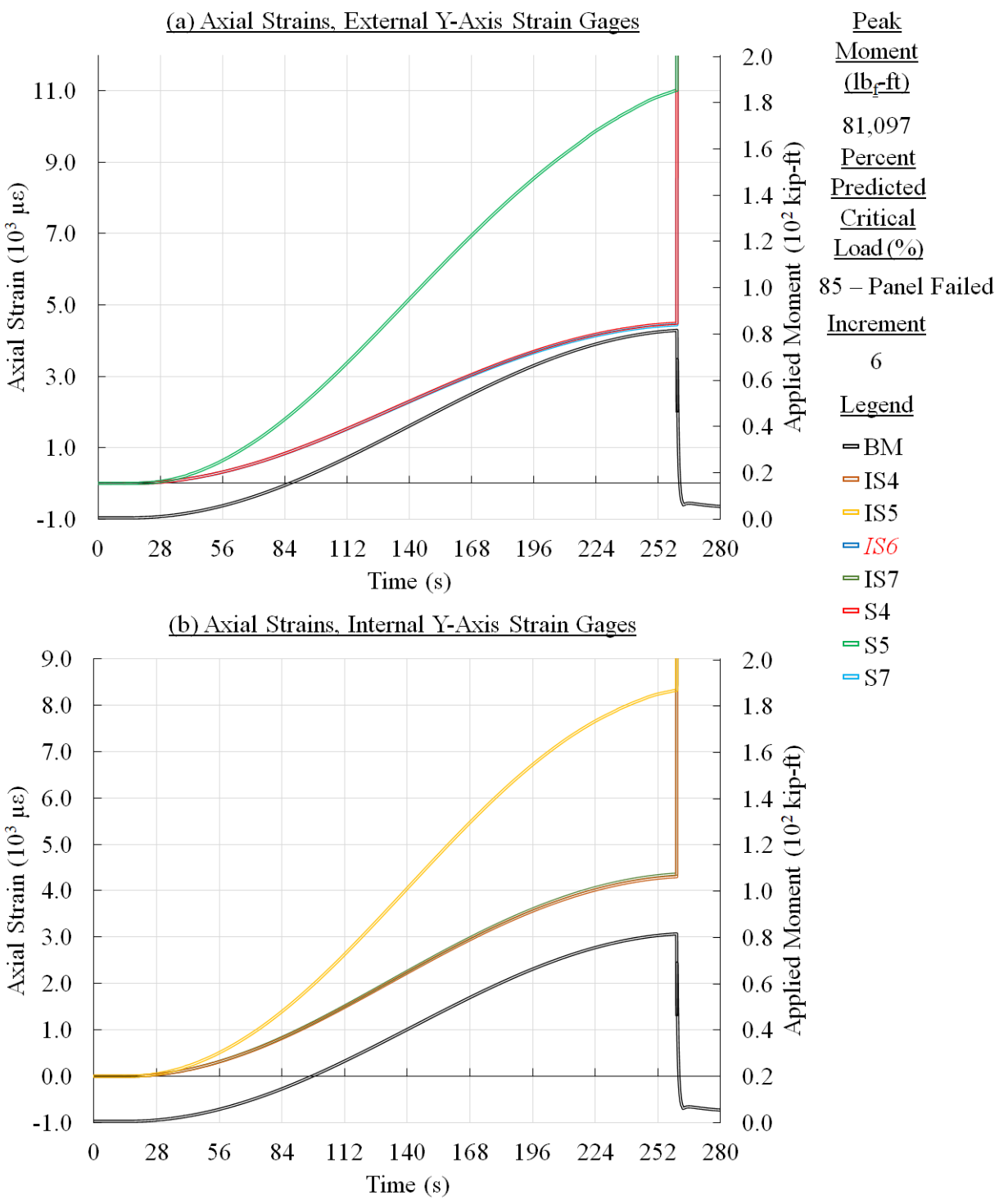


Figure C 94. Panel 4 load increment 6 (panel failure), axial strain along the Y-axis strain gages

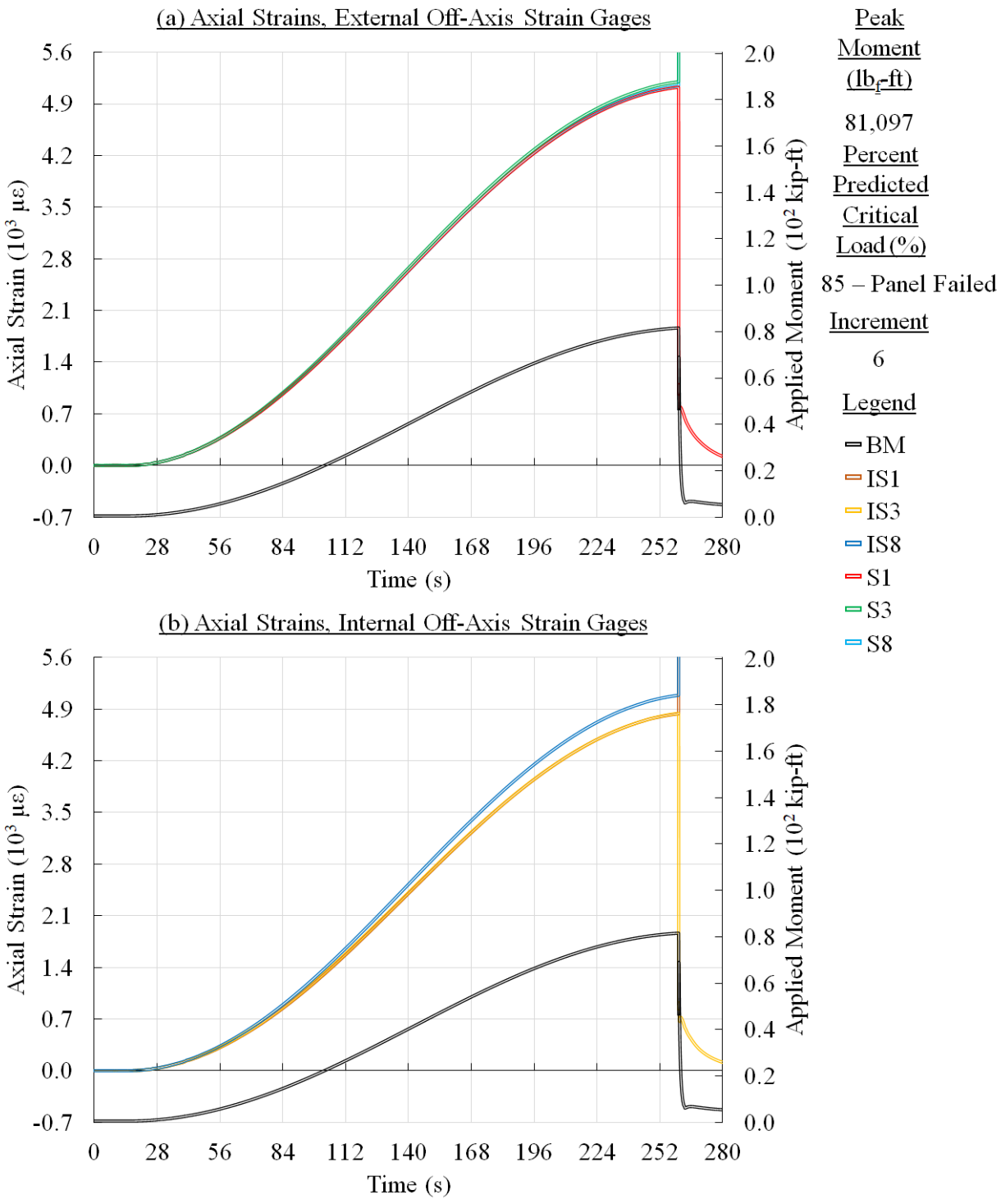


Figure C 95. Panel 4 load increment 6 (panel failure), axial strain along the off-axis strain gages

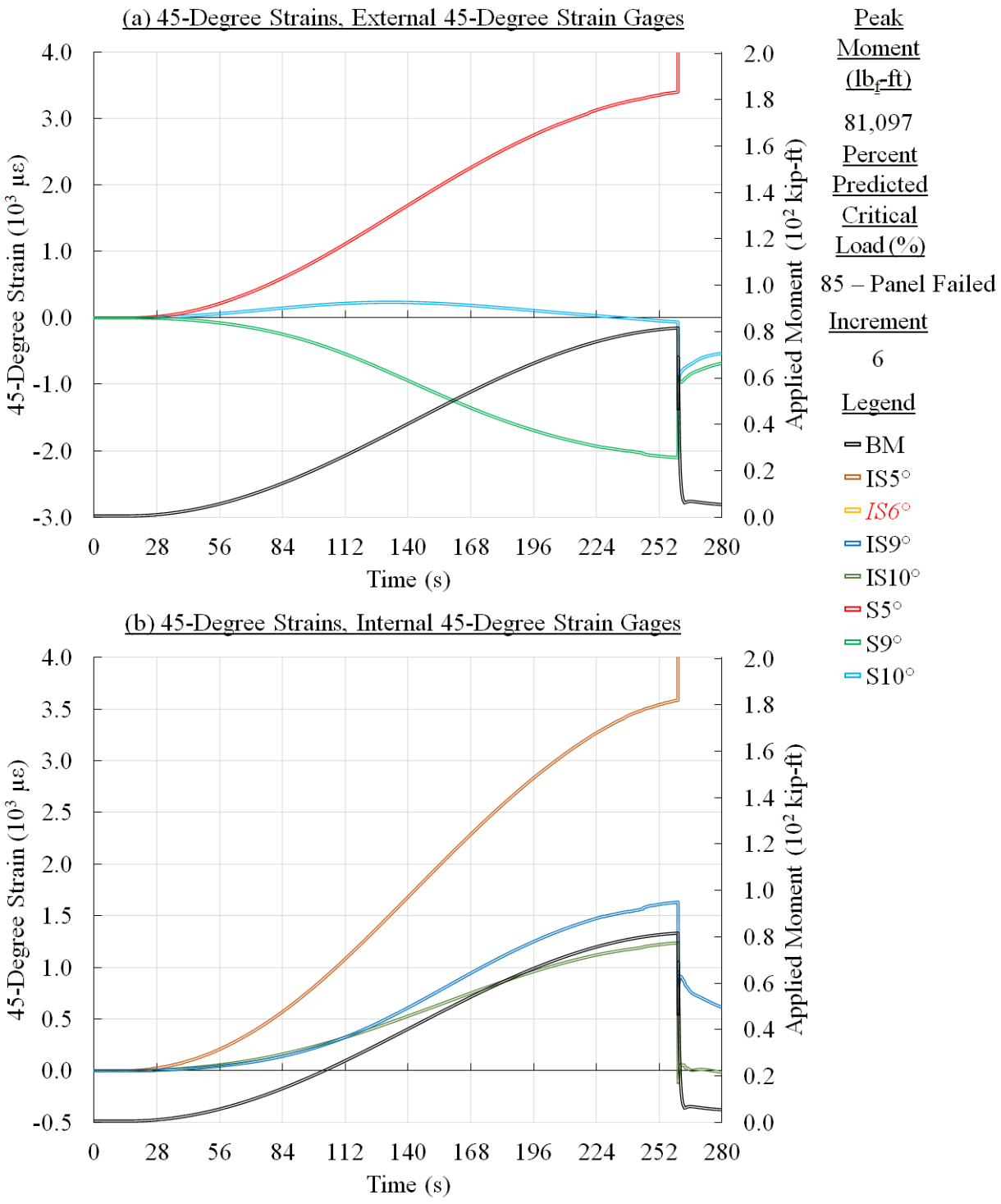


Figure C 96. Panel 4 load increment 6 (panel failure), 45 degree strain

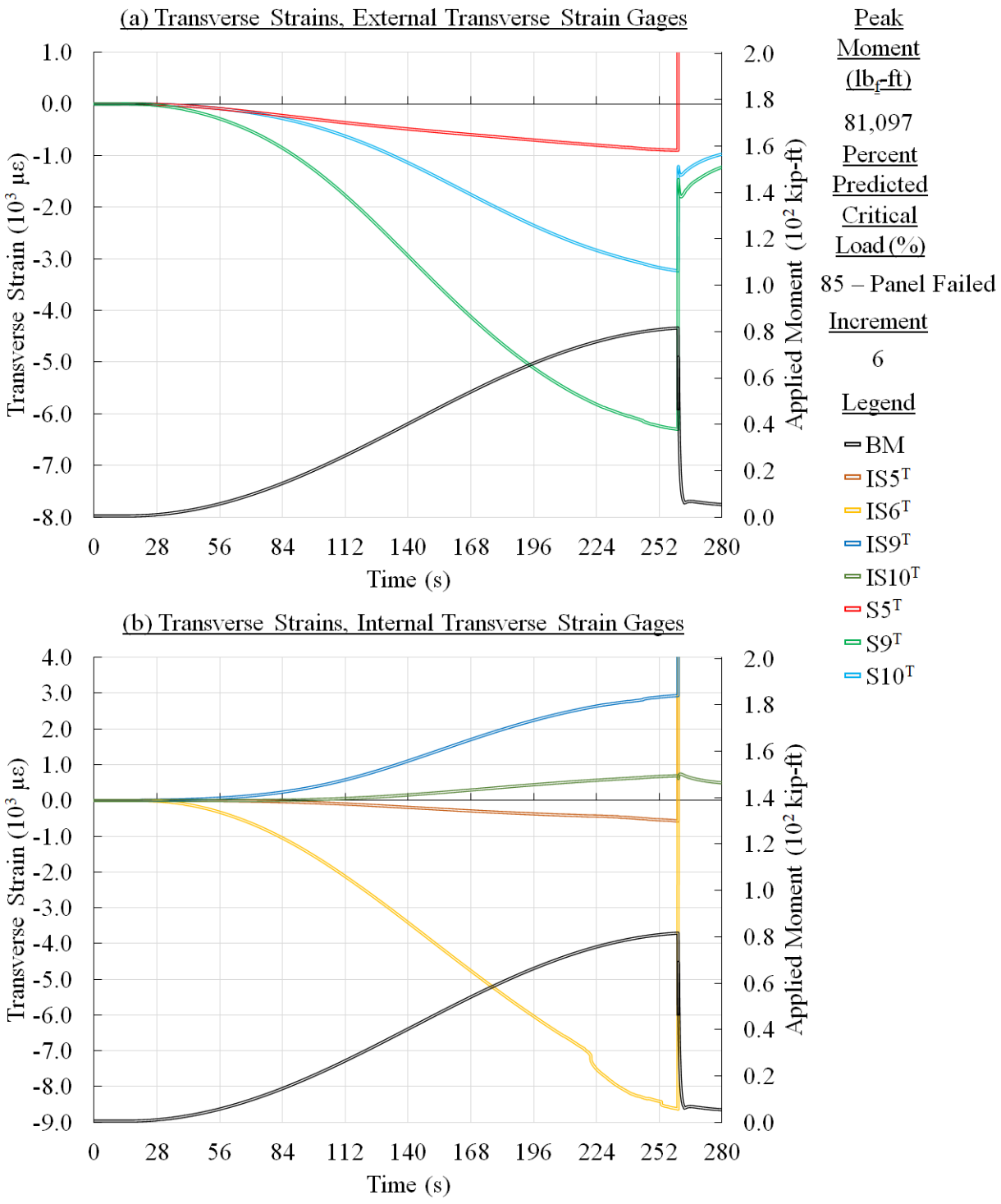


Figure C 97. Panel 4 load increment 6 (panel failure), transverse strain

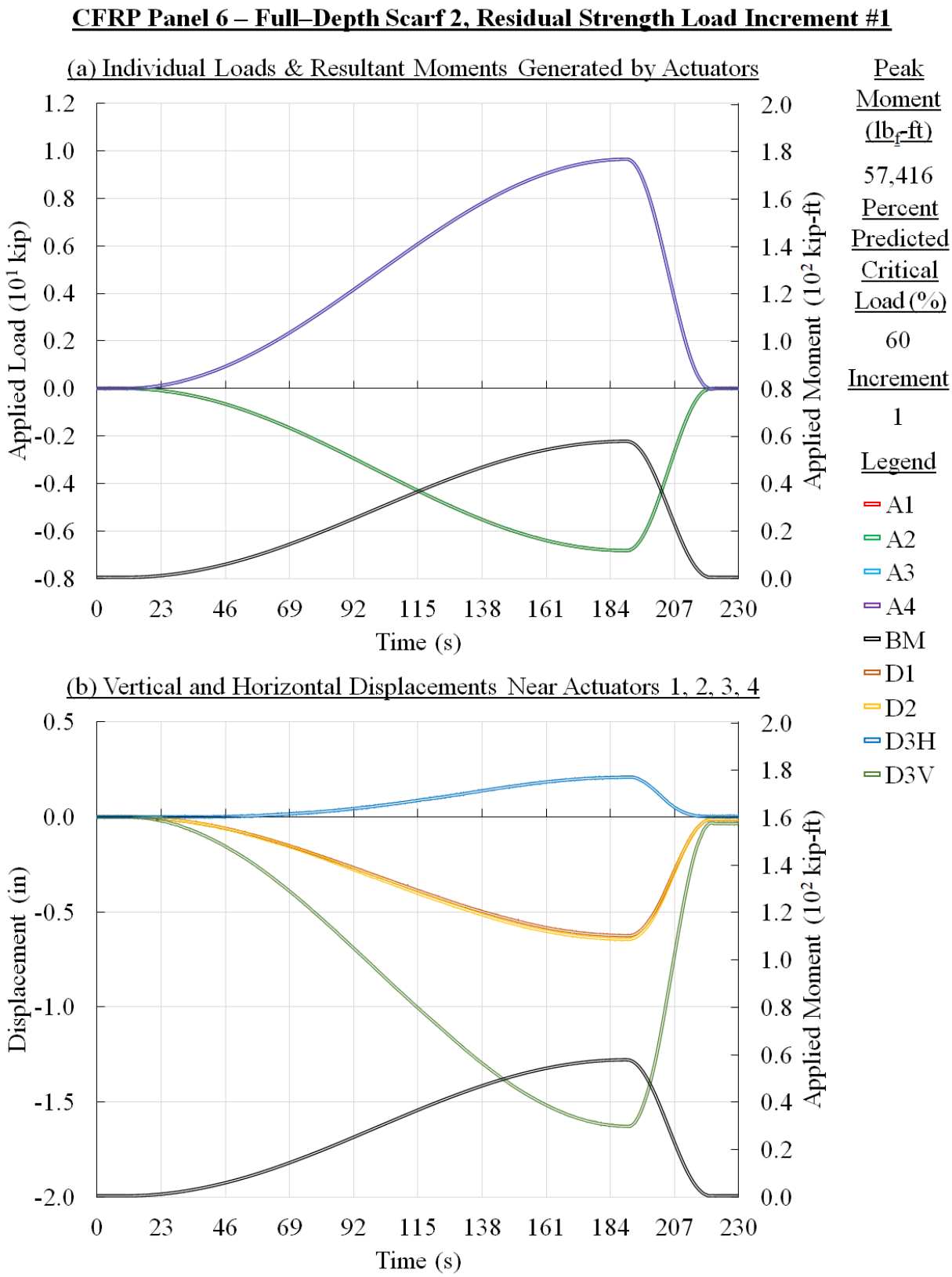


Figure C 98. Panel 6 load increment 1 (60% load level), load and displacement

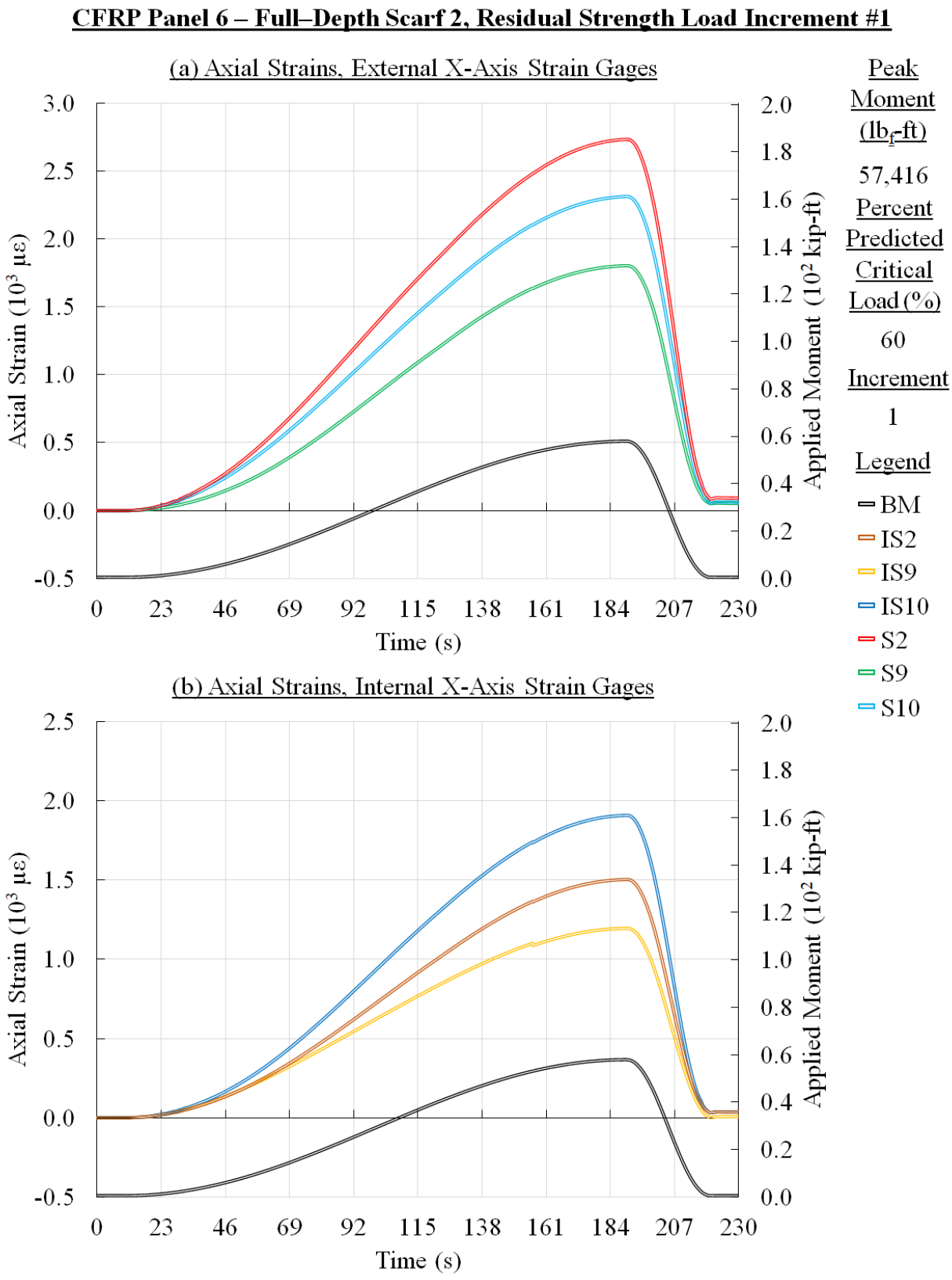


Figure C 99. Panel 6 load increment 1 (60% load level), axial strain along the X-axis strain gages

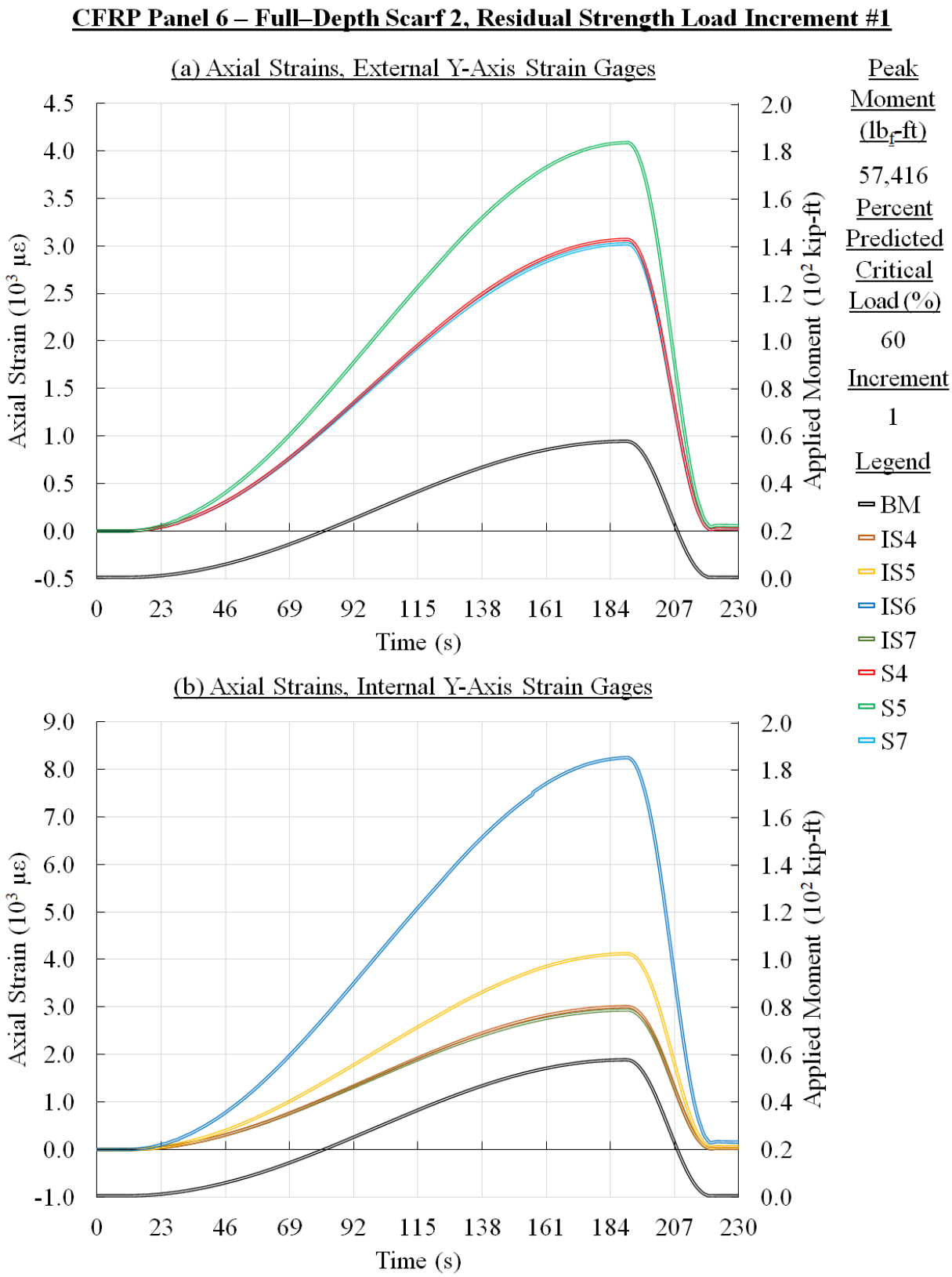


Figure C 100. Panel 6 load increment 1 (60% load level), axial strain along the Y-axis strain gages

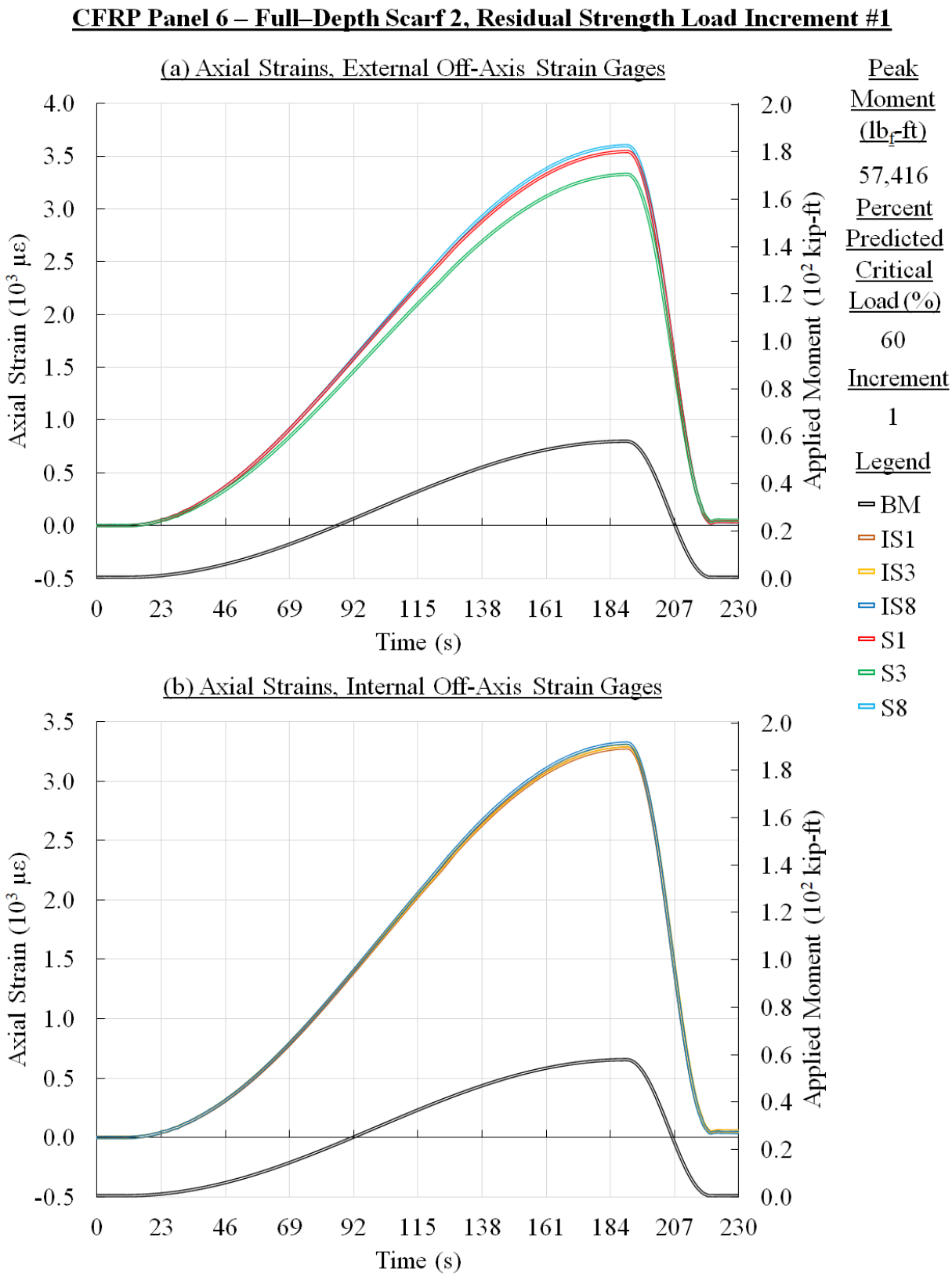


Figure C 101. Panel 6 load increment 1 (60% load level), axial strain along the off-axis strain gages

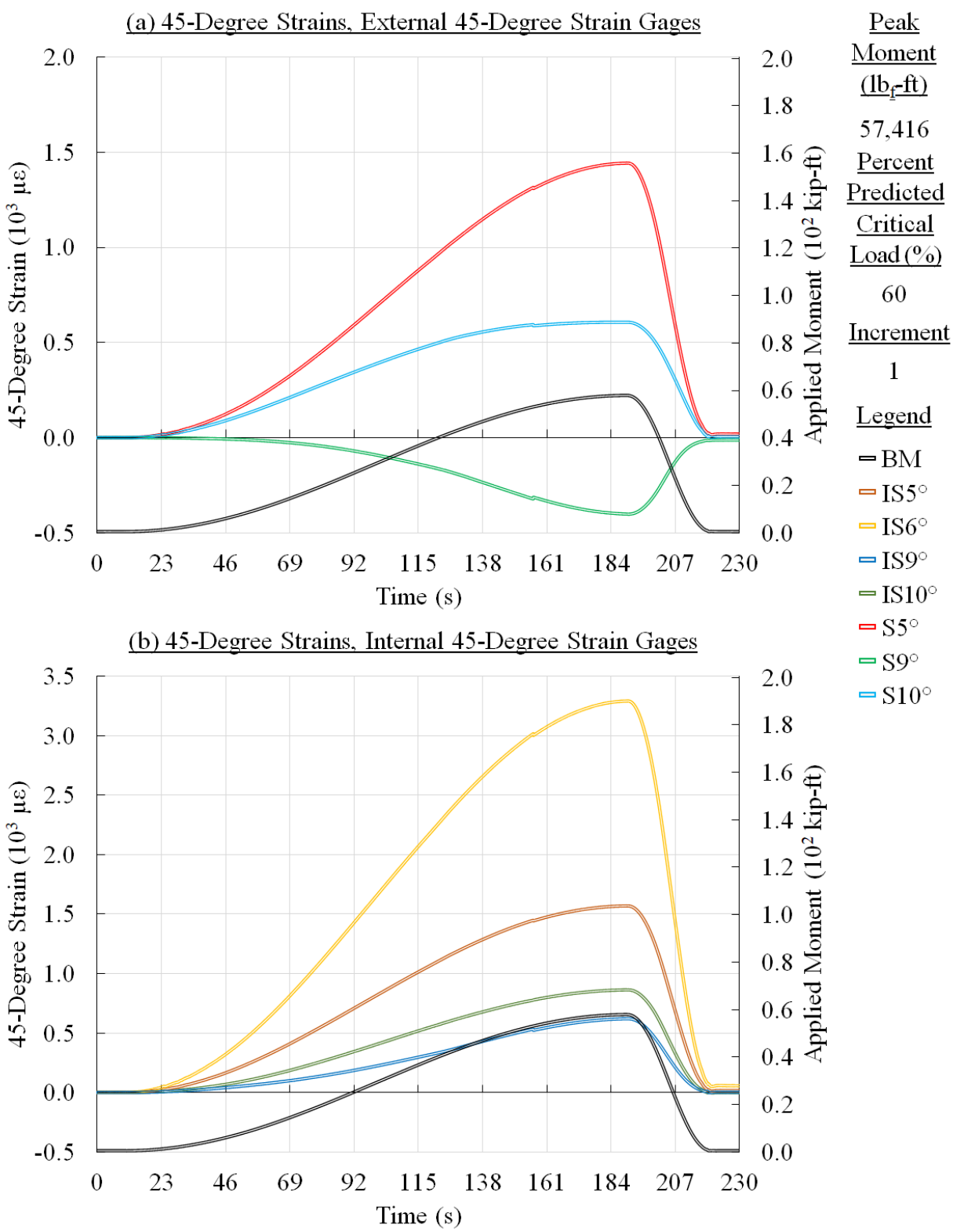


Figure C 102. Panel 6 load increment 1 (60% load level), 45 degree strain

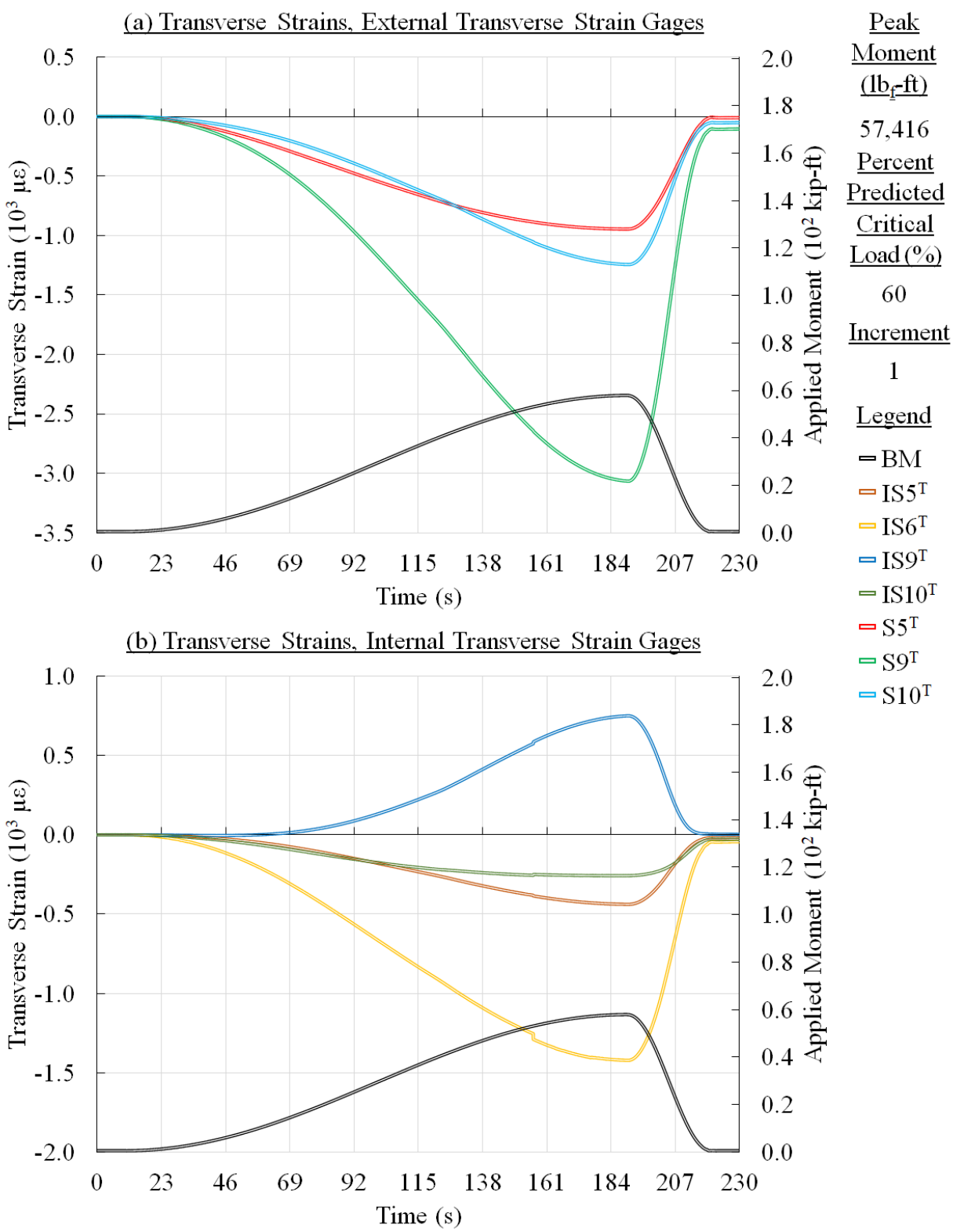


Figure C 103. Panel 6 load increment 1 (60% load level), transverse strain

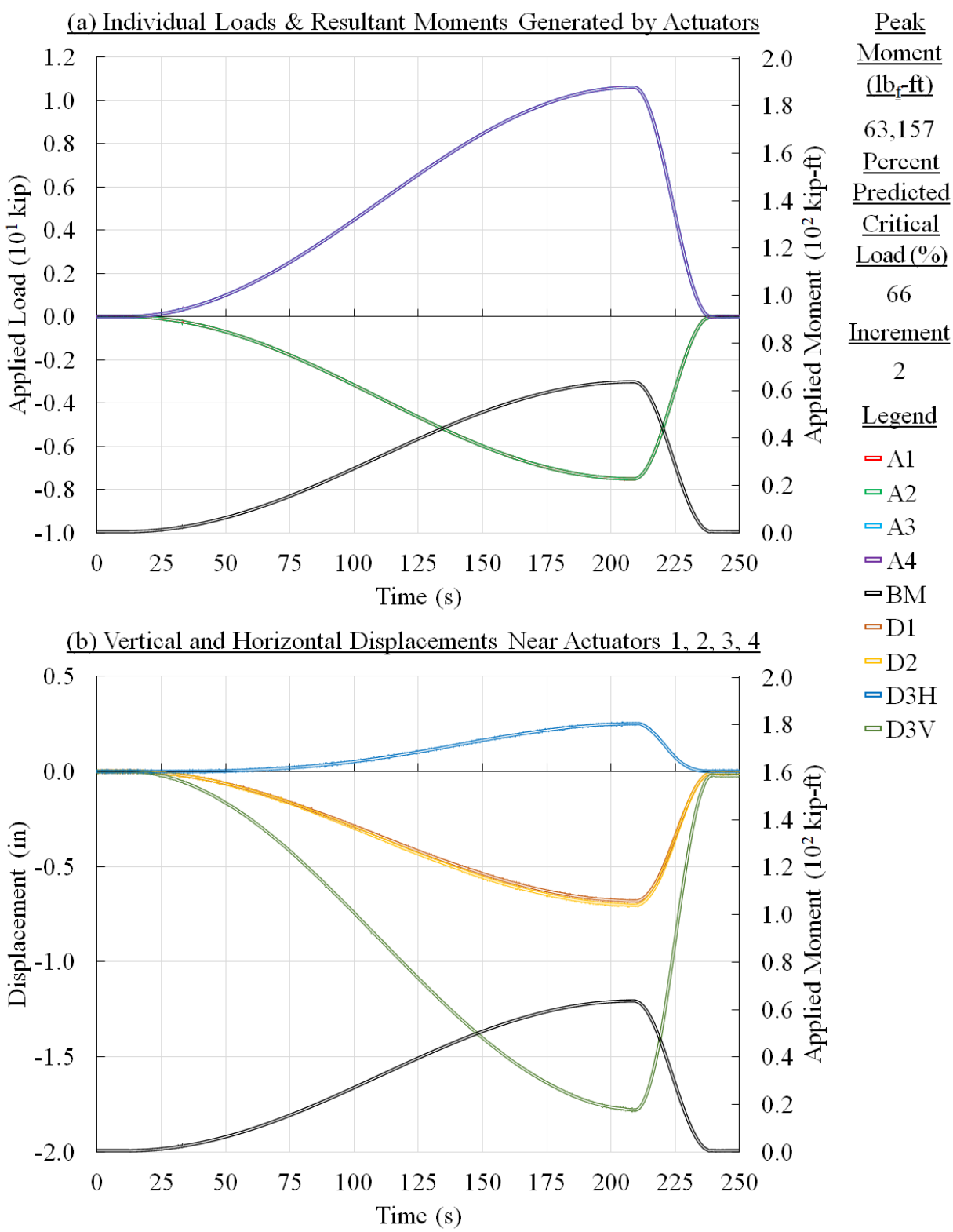


Figure C 104. Panel 6 load increment 2 (66% load level), load and displacement

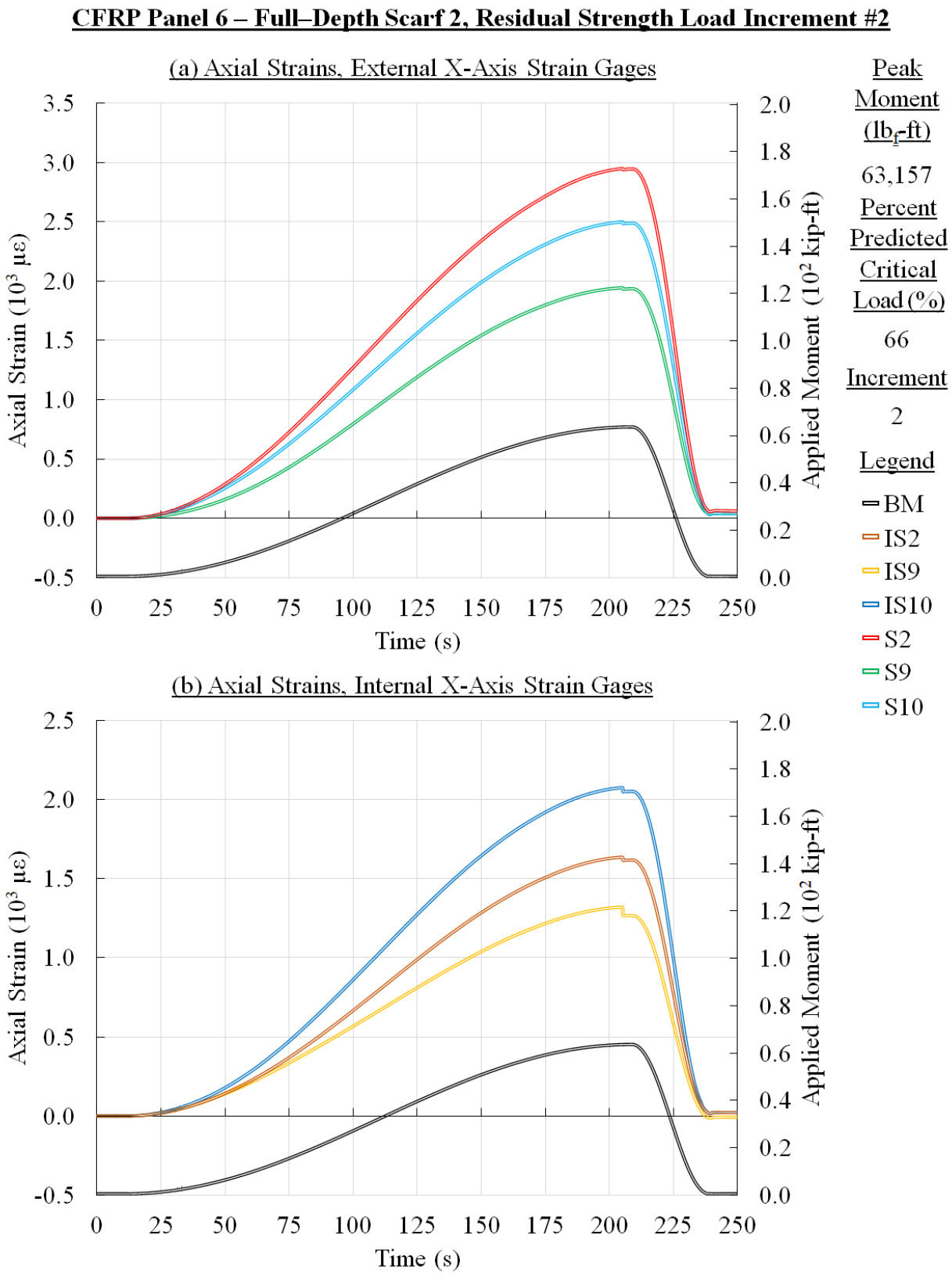


Figure C 105. Panel 6 load increment 2 (66% load level), axial strain along the X-axis strain gages

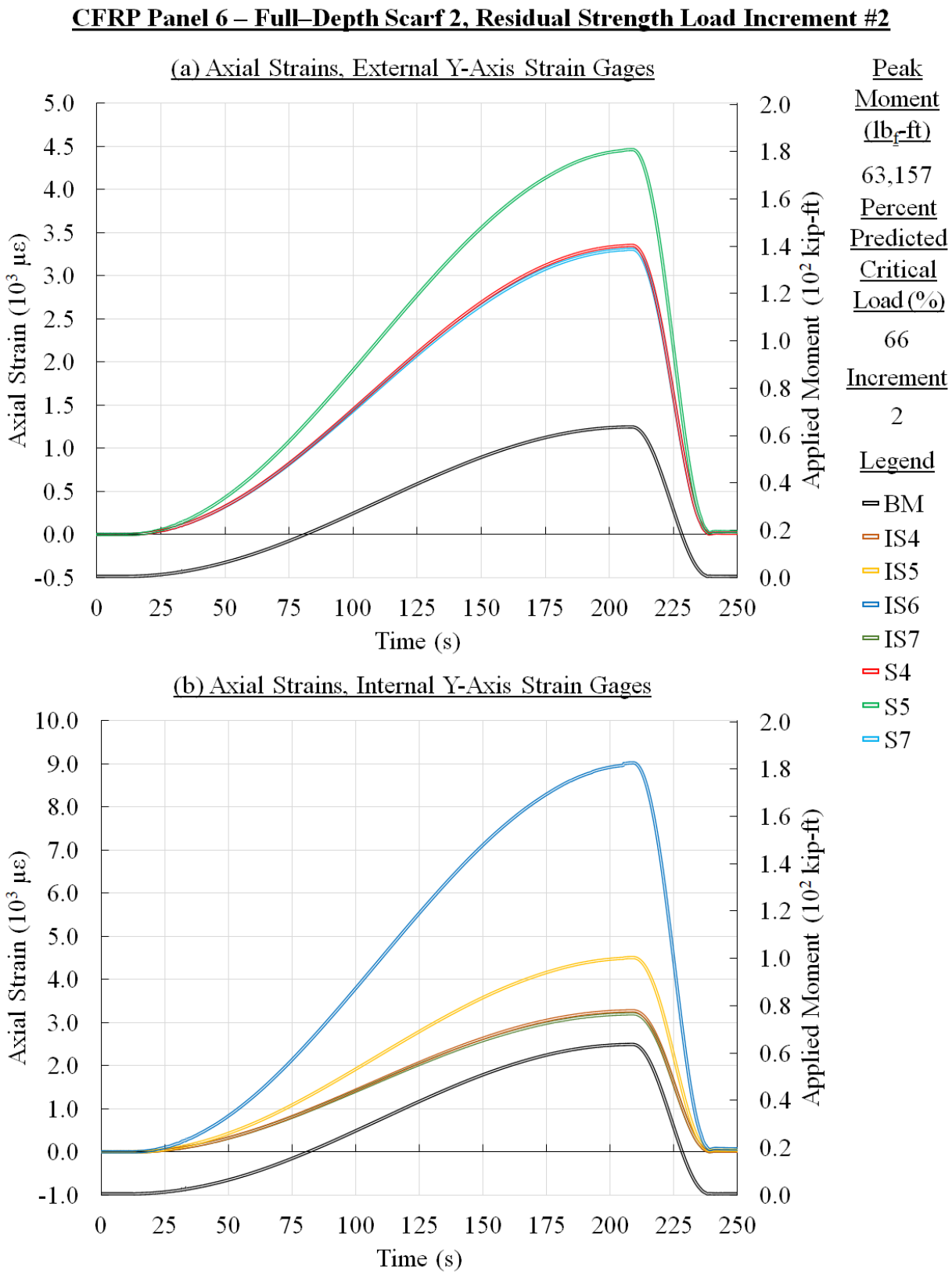


Figure C 106. Panel 6 load increment 2 (66% load level), axial strain along the Y-axis strain gages

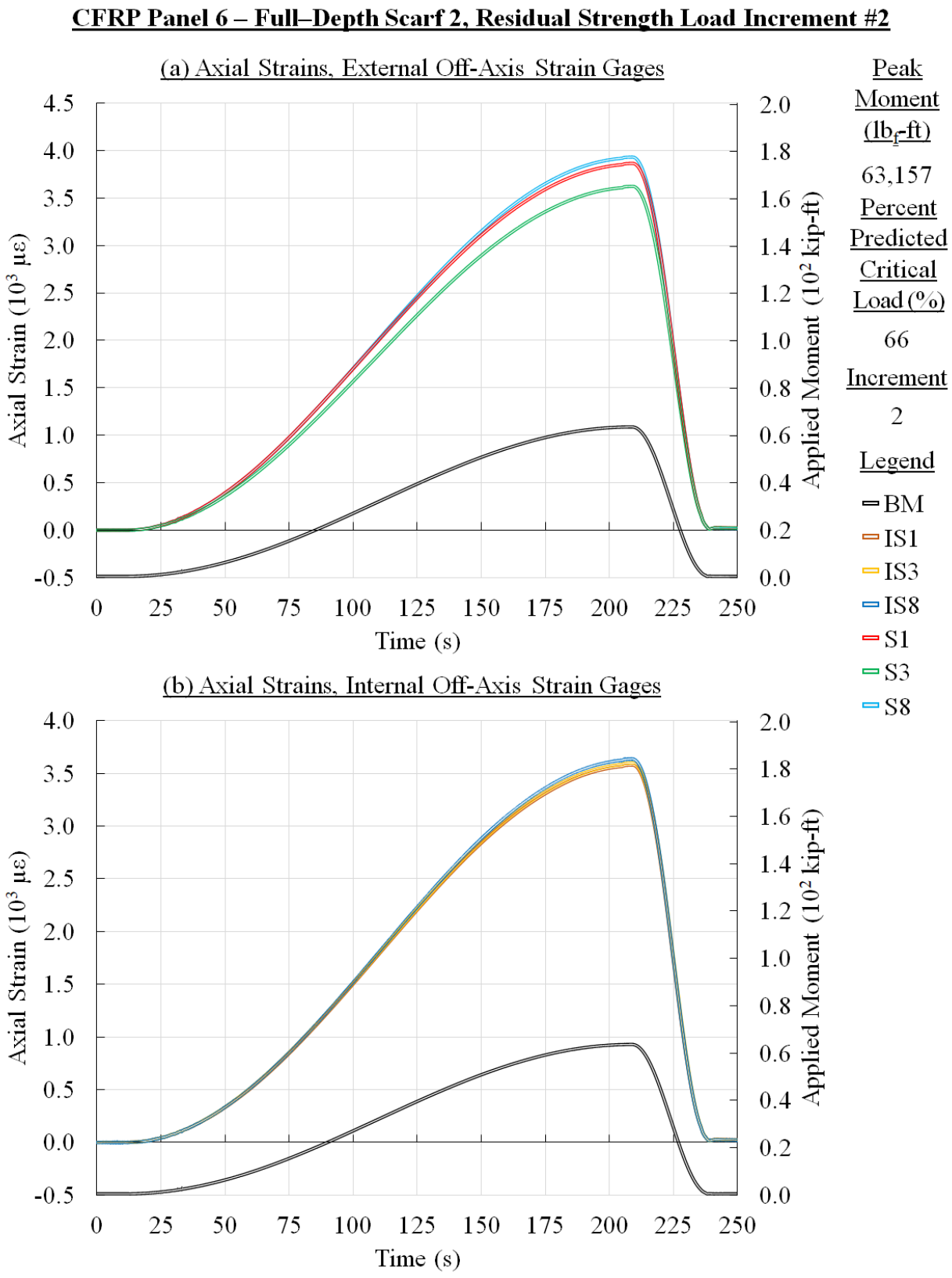


Figure C 107. Panel 6 load increment 2 (66% load level), axial strain along the off-axis strain gages

**CFRP Panel 6 – Full–Depth Scarf 2, Residual Strength Load Increment #2**

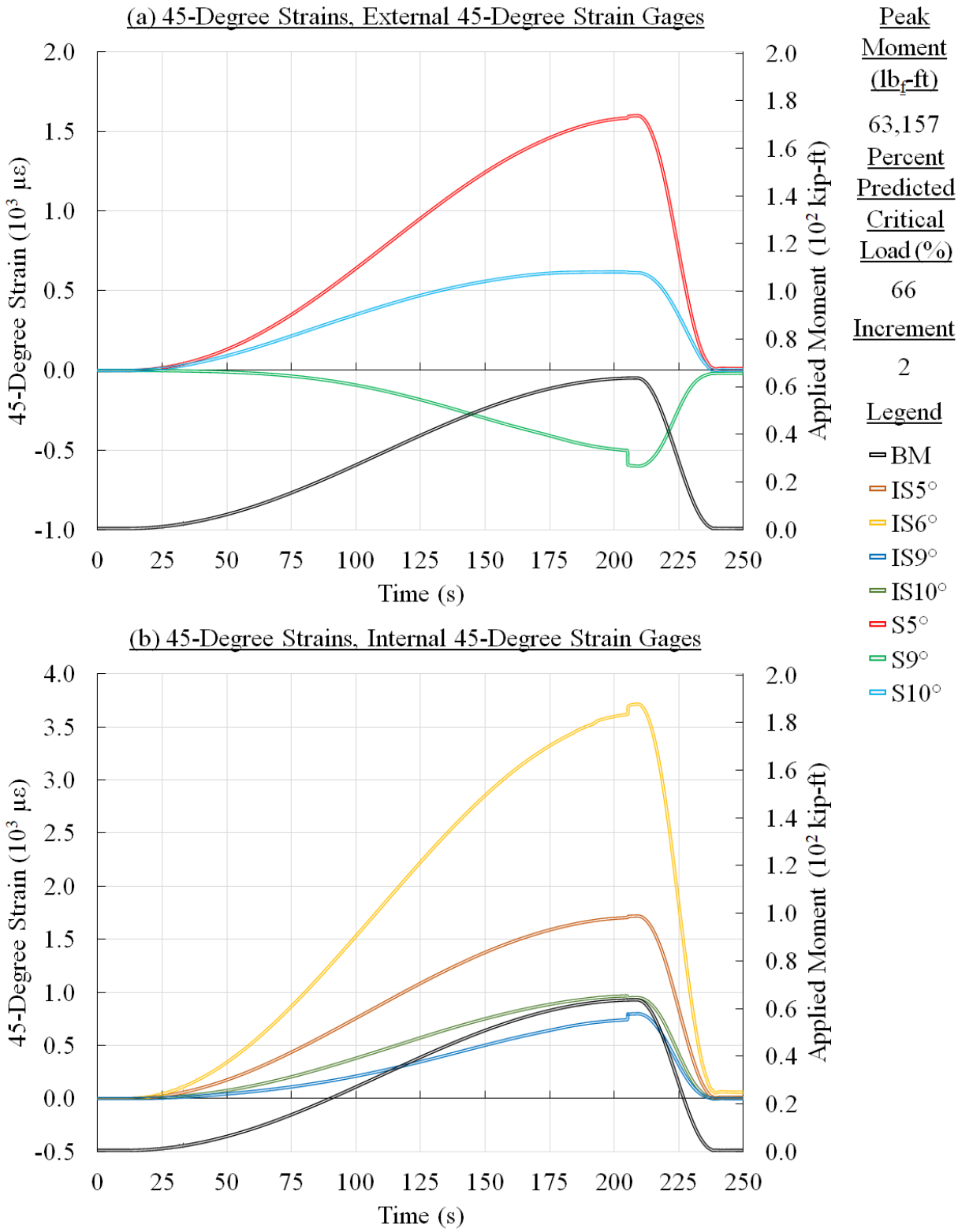


Figure C 108. Panel 6 load increment 2 (66% load level), 45 degree strain

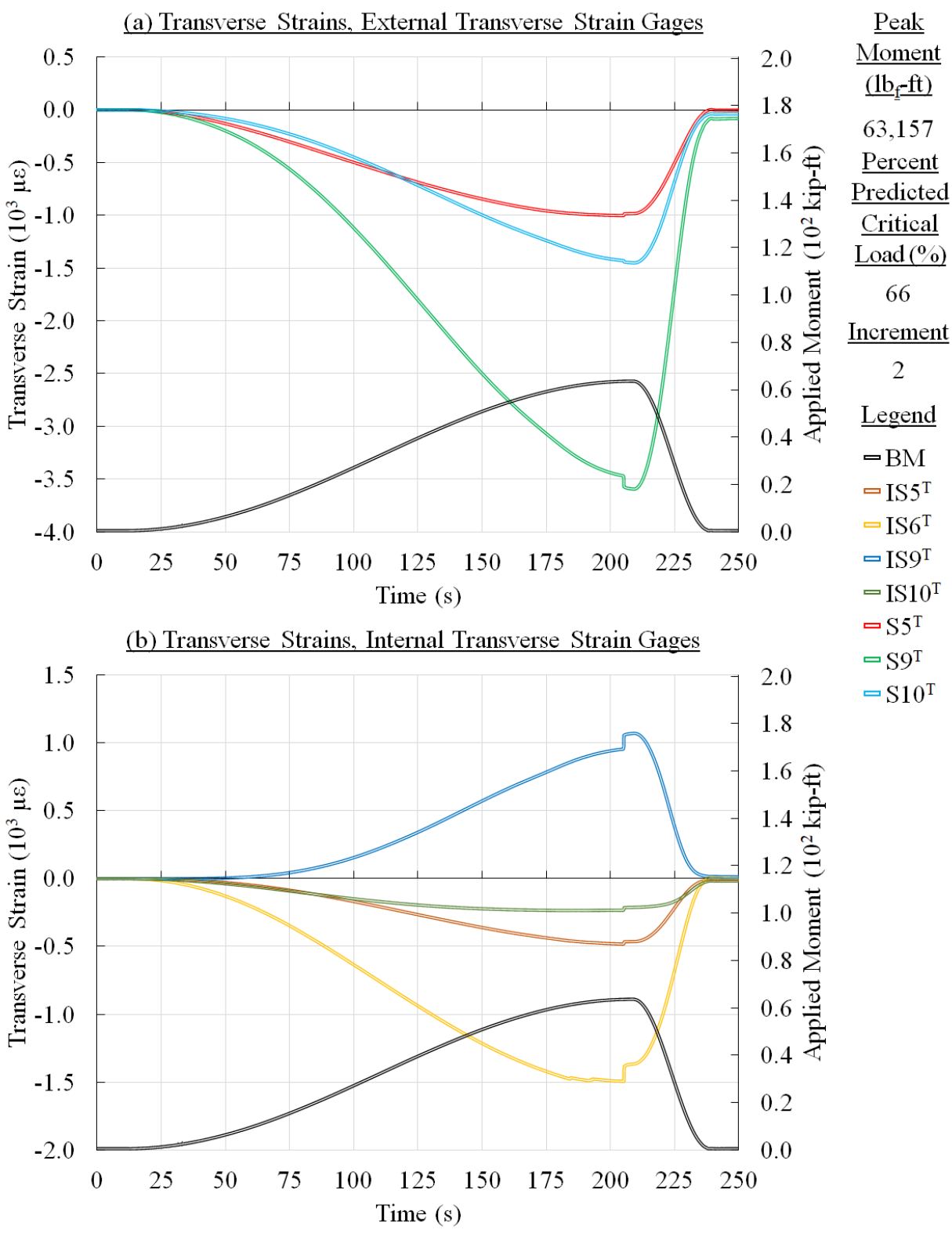


Figure C 109. Panel 6 load increment 2 (66% load level), transverse strain

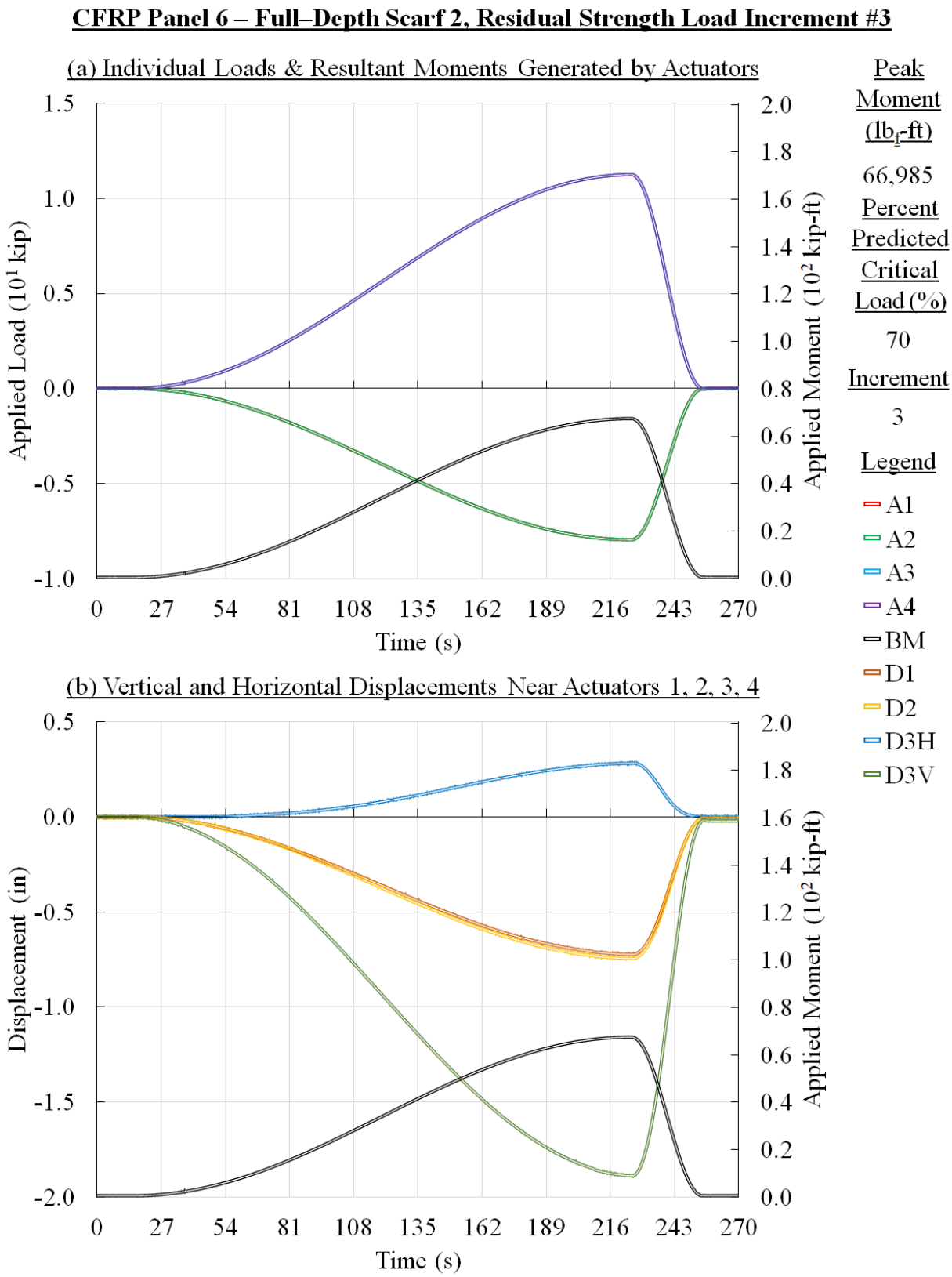


Figure C 110. Panel 6 load increment 3 (70% load level), load and displacement

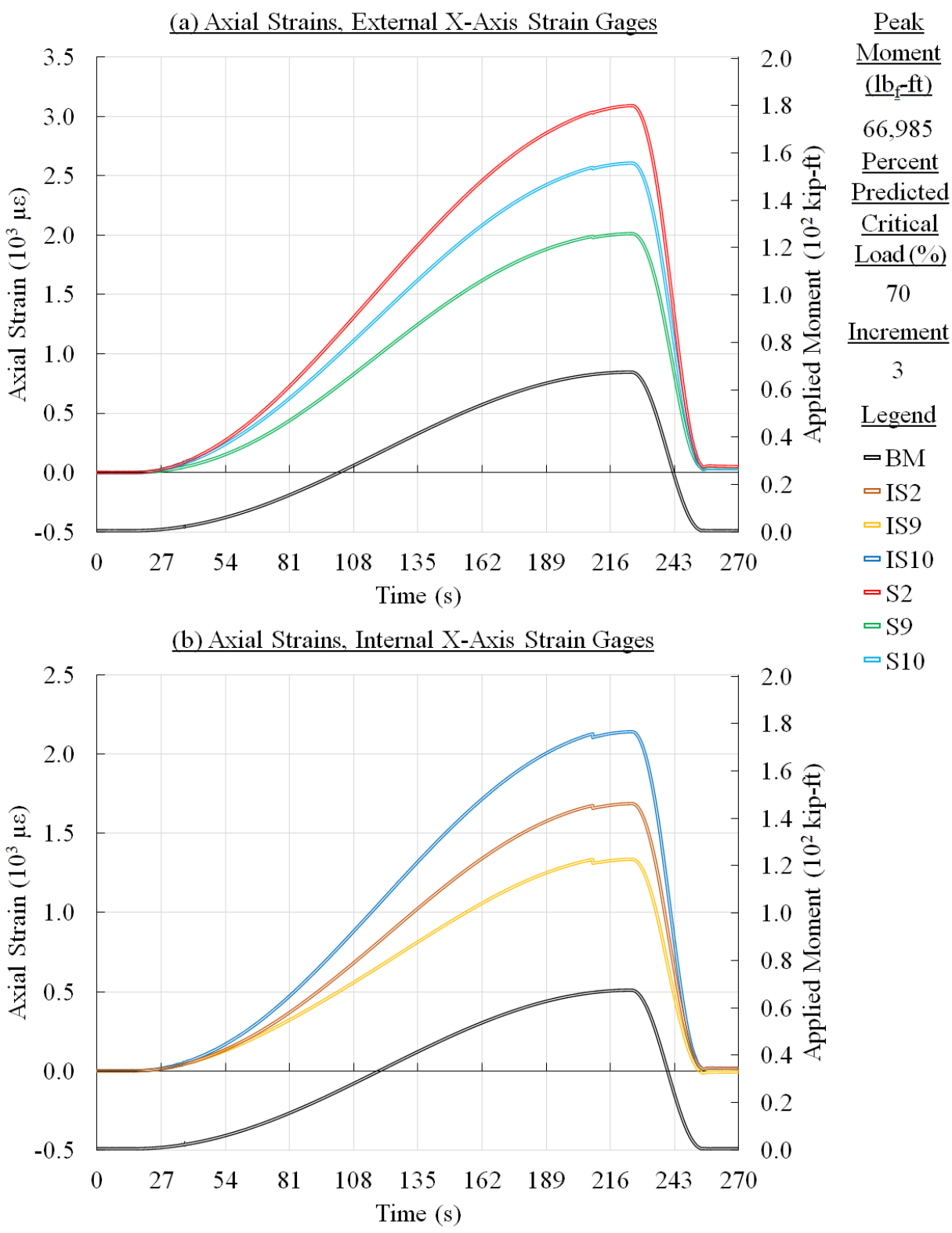


Figure C 111. Panel 6 load increment 3 (70% load level), axial strain along the X-axis strain gages

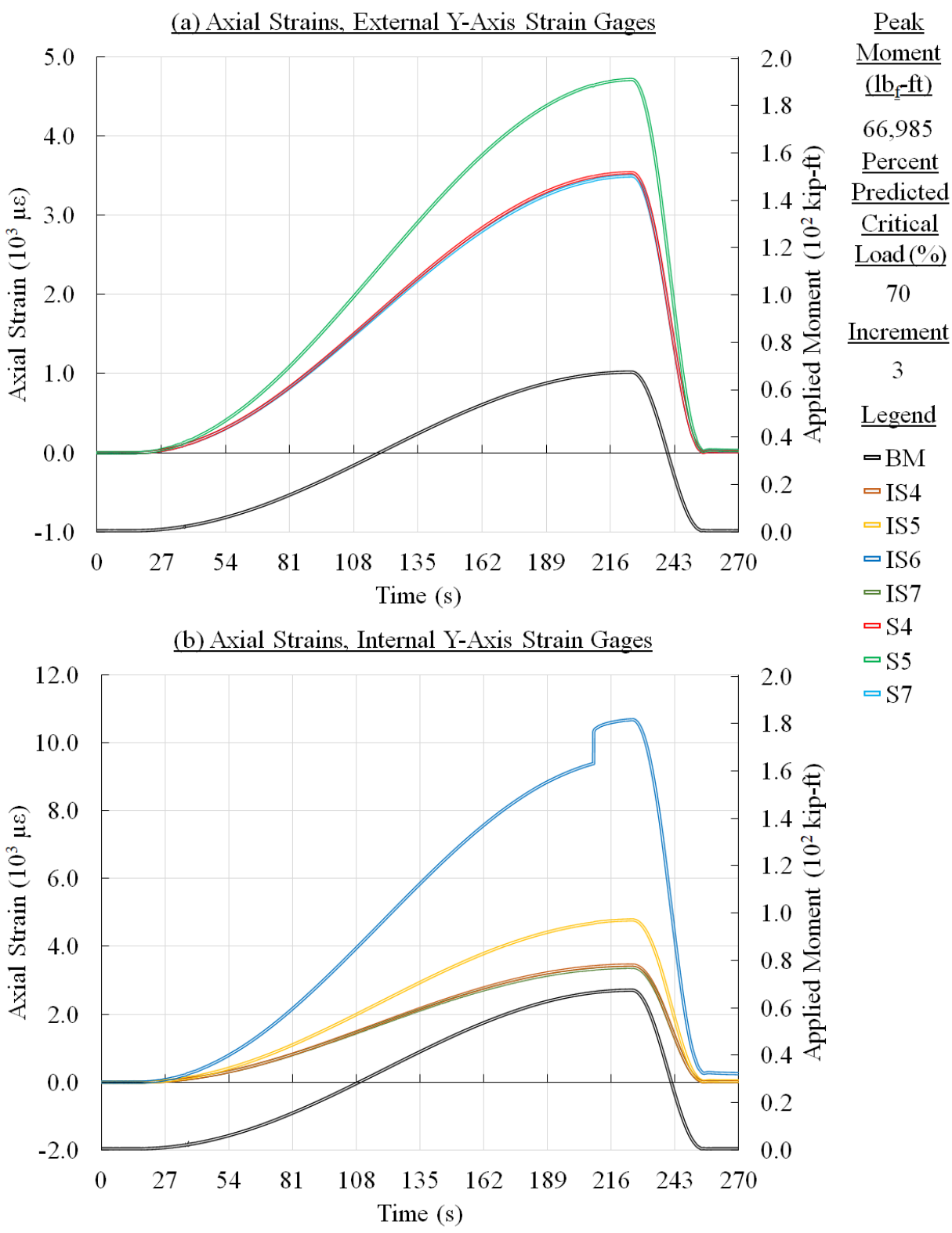


Figure C 112. Panel 6 load increment 3 (70% load level), axial strain along the Y-axis strain gages

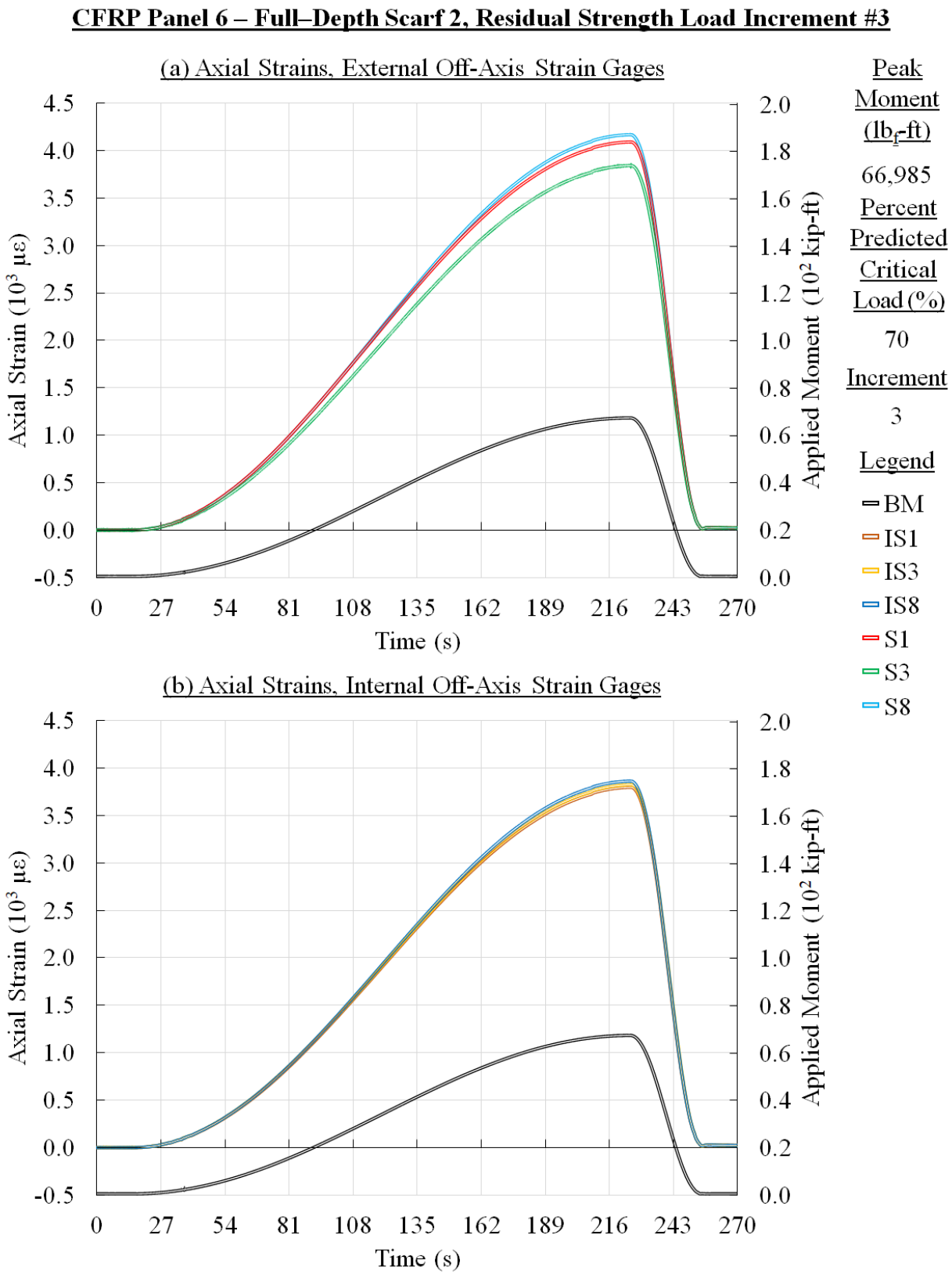


Figure C 113. Panel 6 load increment 3 (70% load level), axial strain along the off-axis strain gages

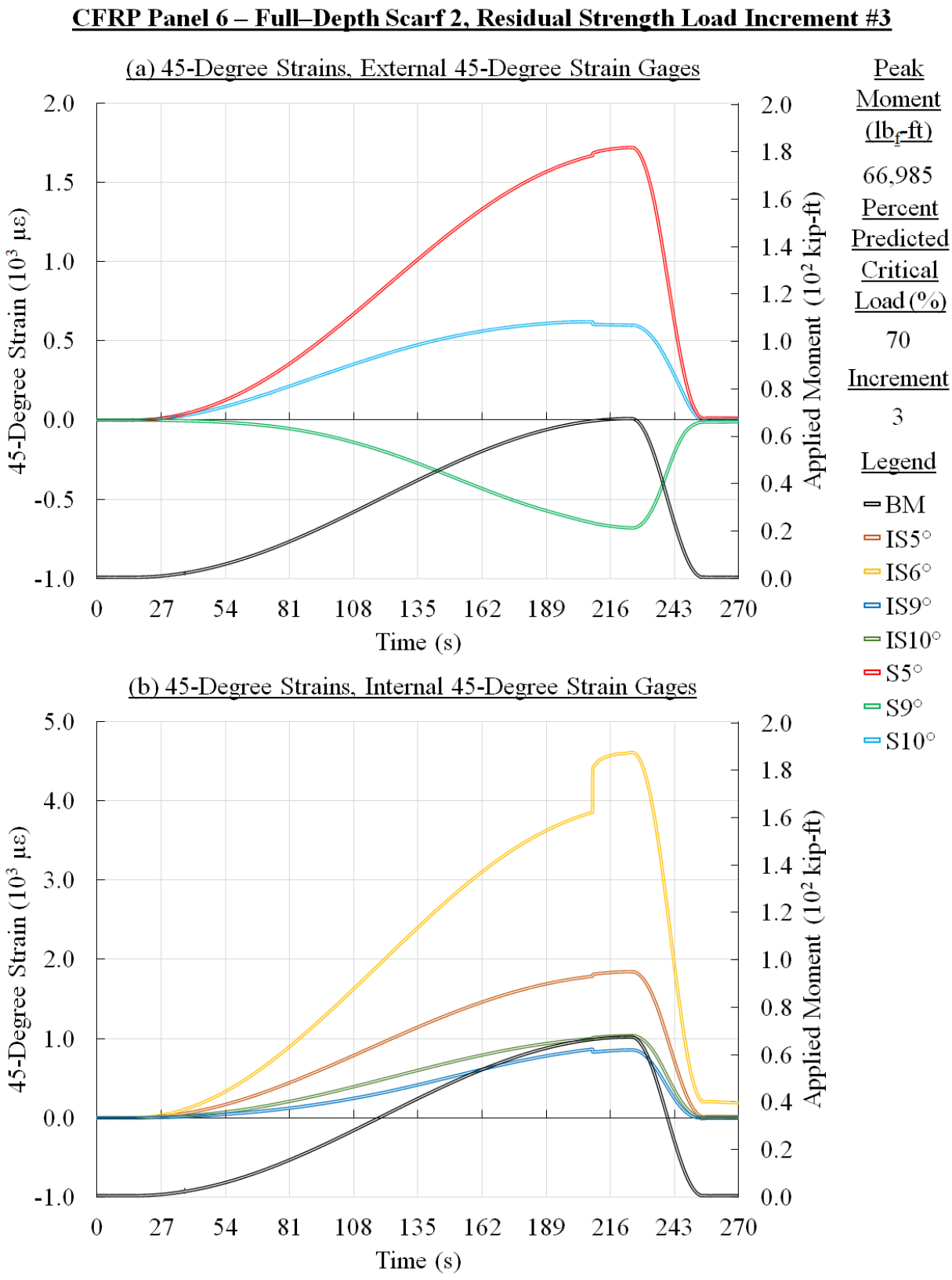


Figure C 114. Panel 6 load increment 3 (70% load level), 45 degree strain

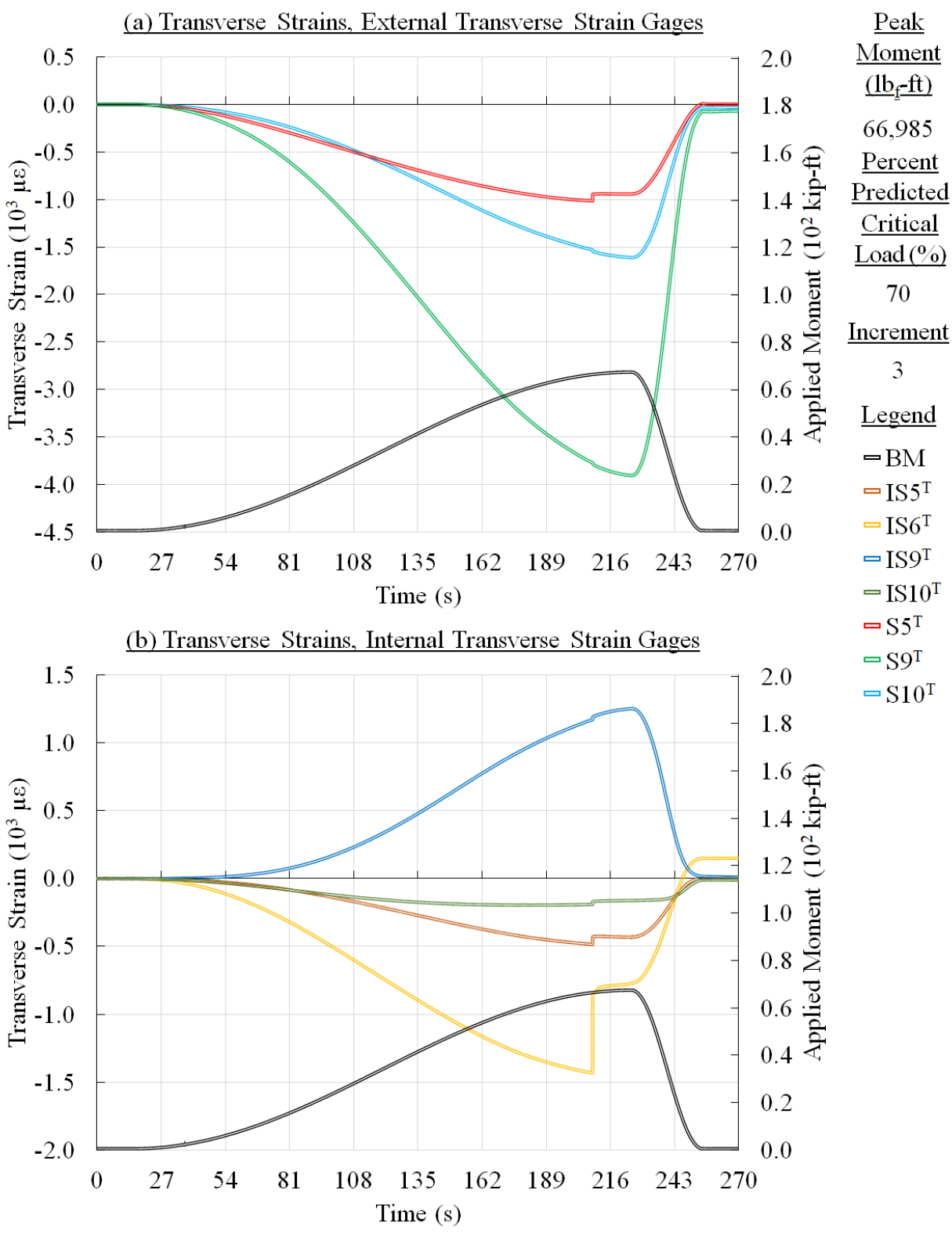


Figure C 115. Panel 6 load increment 3 (70% load level), transverse strain

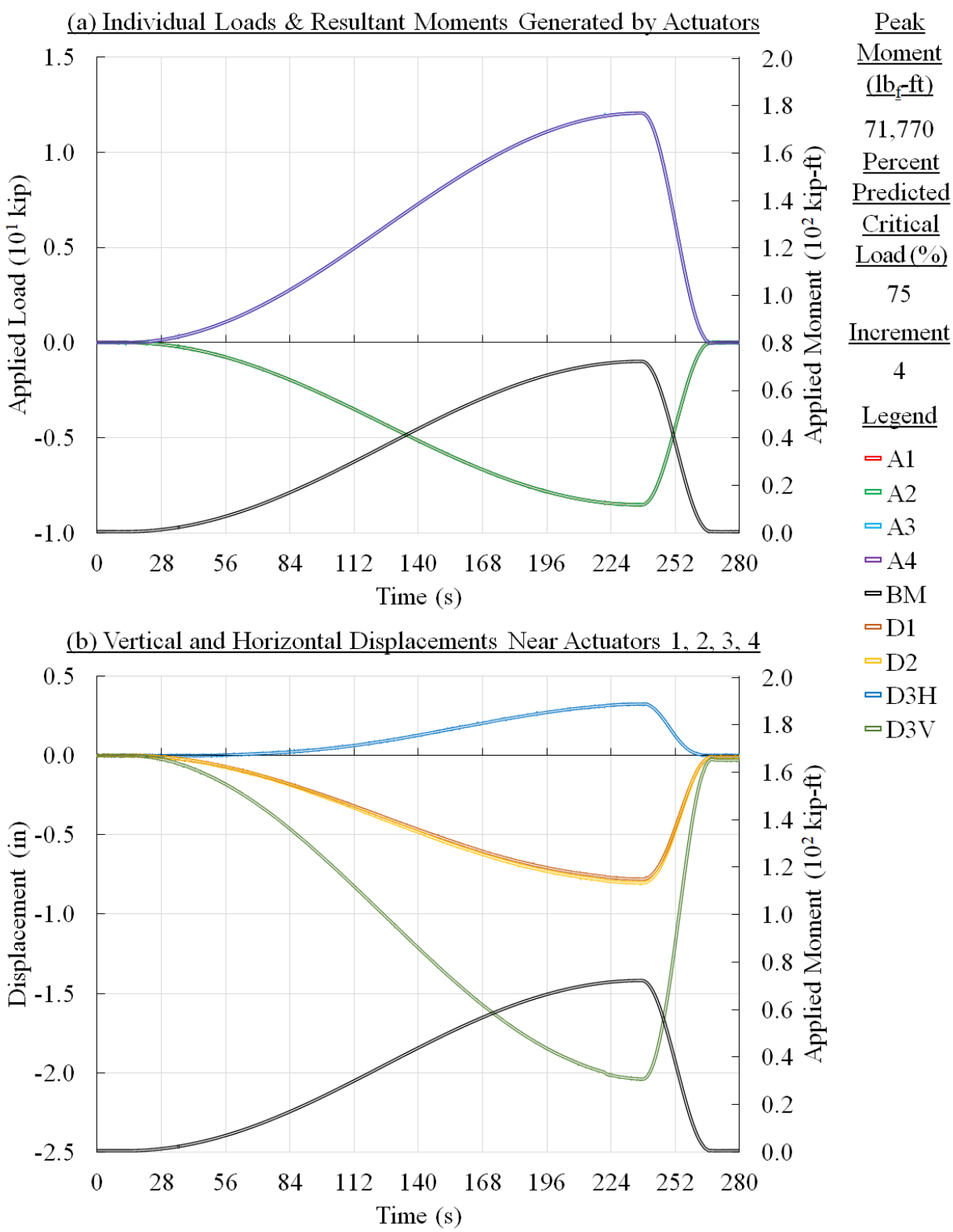


Figure C 116. Panel 6 load increment 4 (75% load level), load and displacement

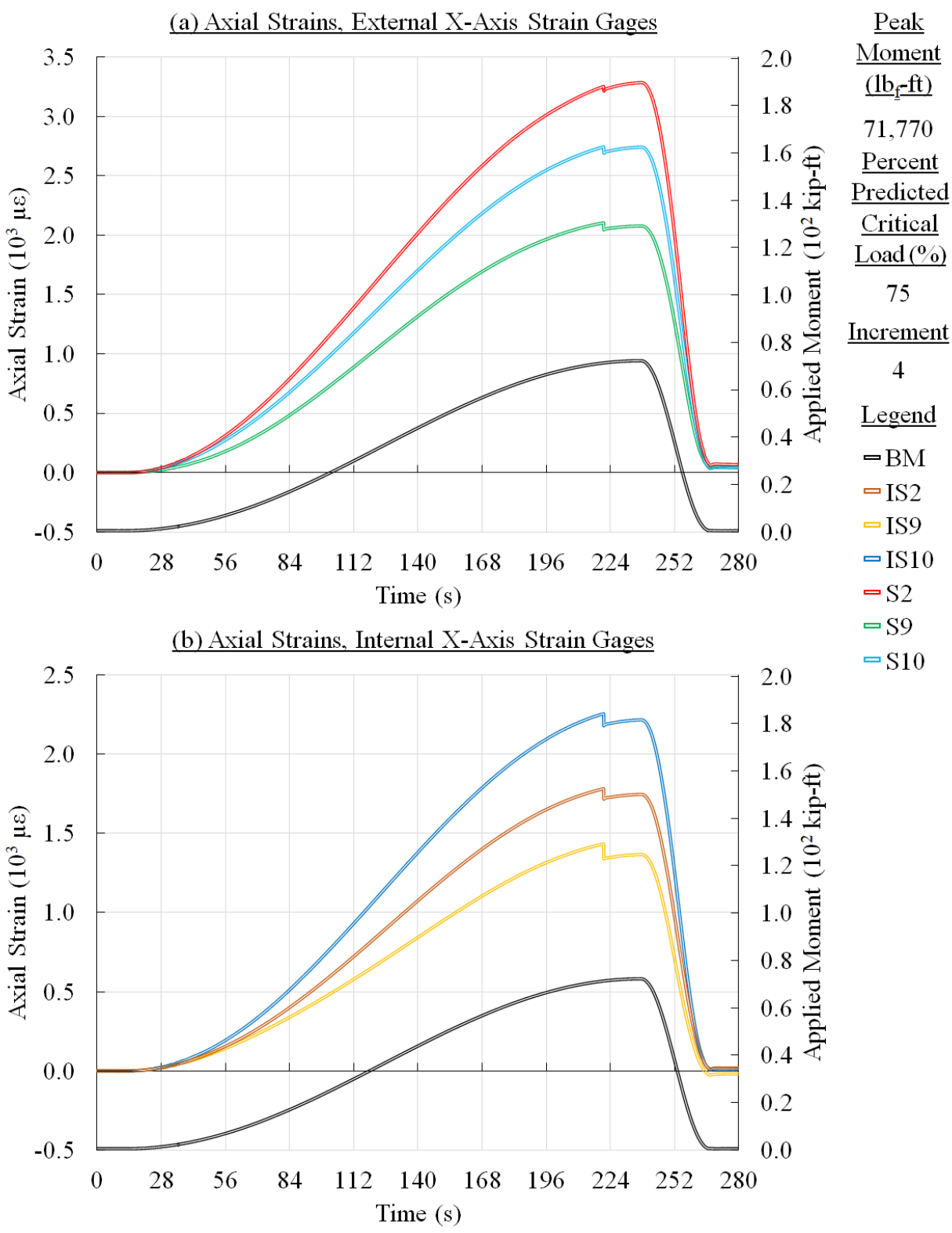


Figure C 117. Panel 6 load increment 4 (75% load level), axial strain along the X-axis strain gages

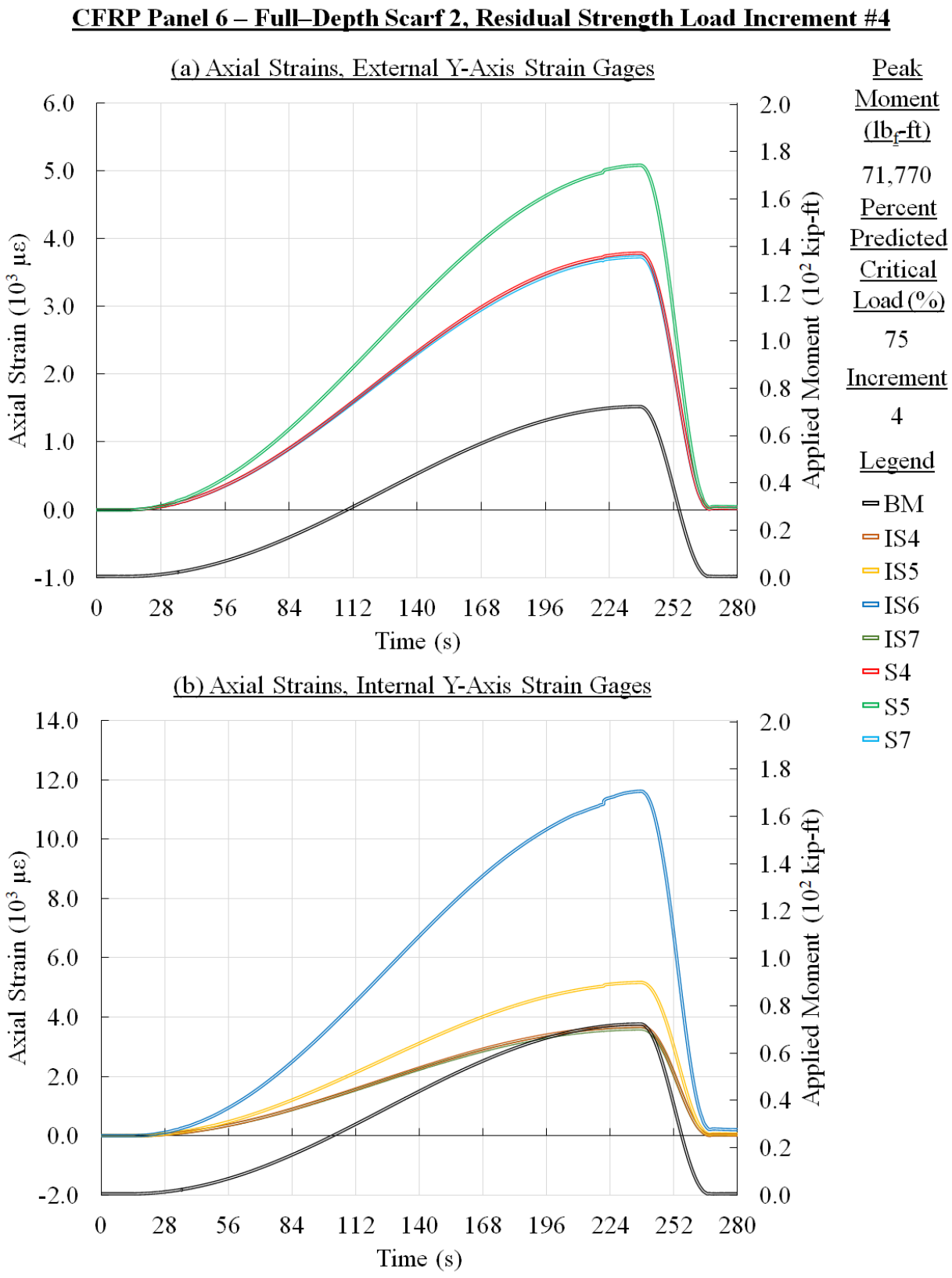


Figure C 118. Panel 6 load increment 4 (75% load level), axial strain along the Y-axis strain gages

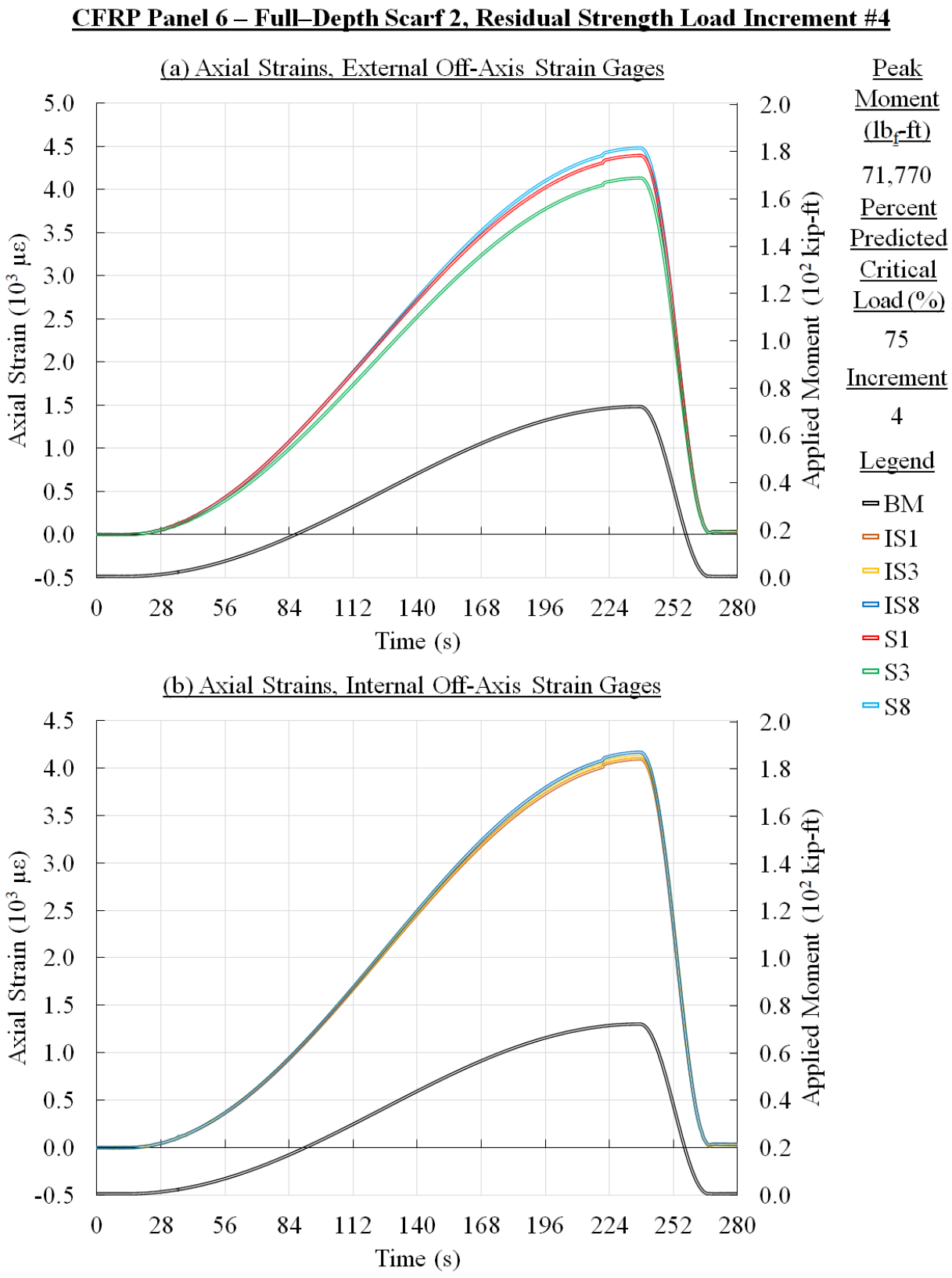


Figure C 119. Panel 6 load increment 4 (75% load level), axial strain along the off-axis strain gages

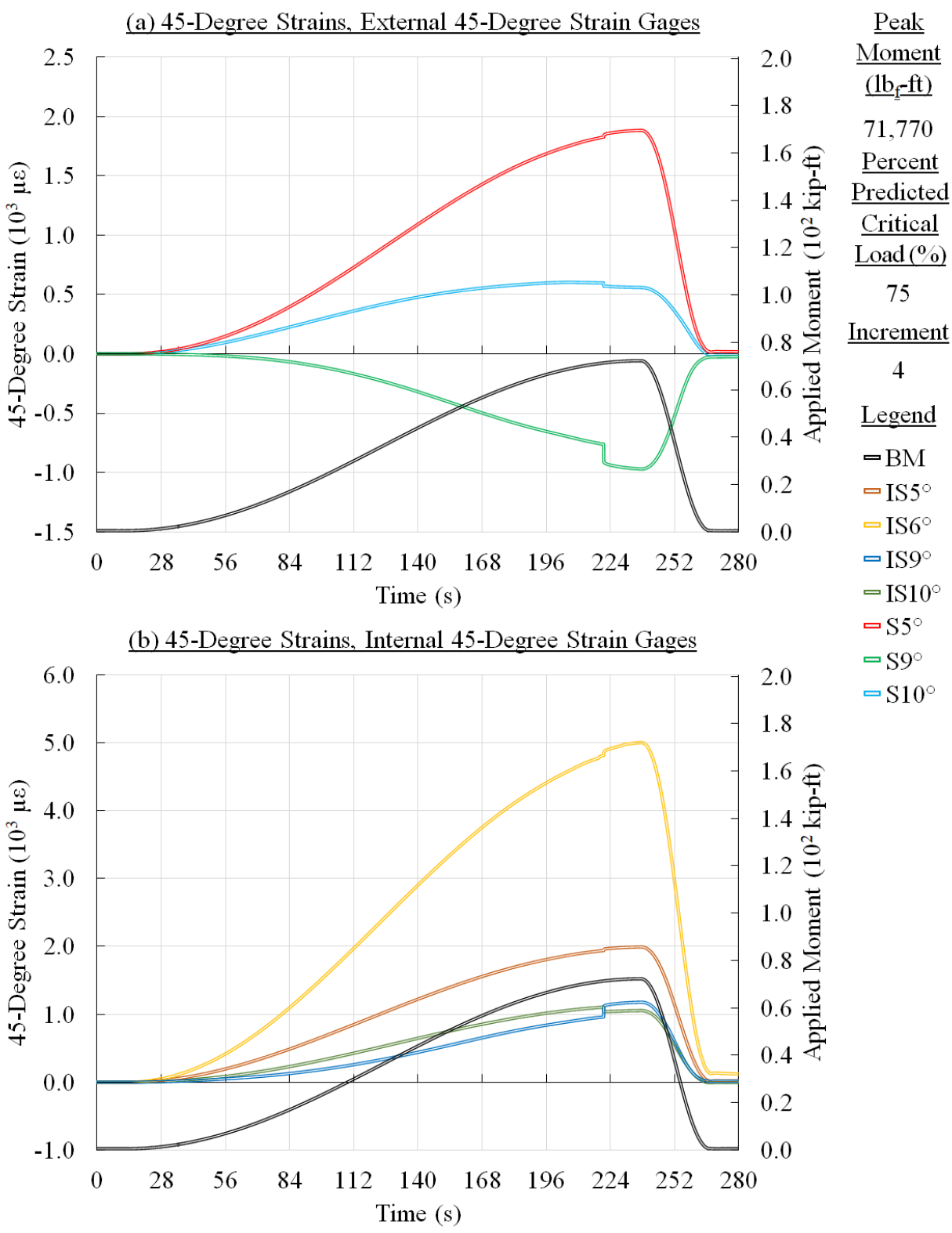


Figure C 120. Panel 6 load increment 4 (75% load level), 45 degree strain

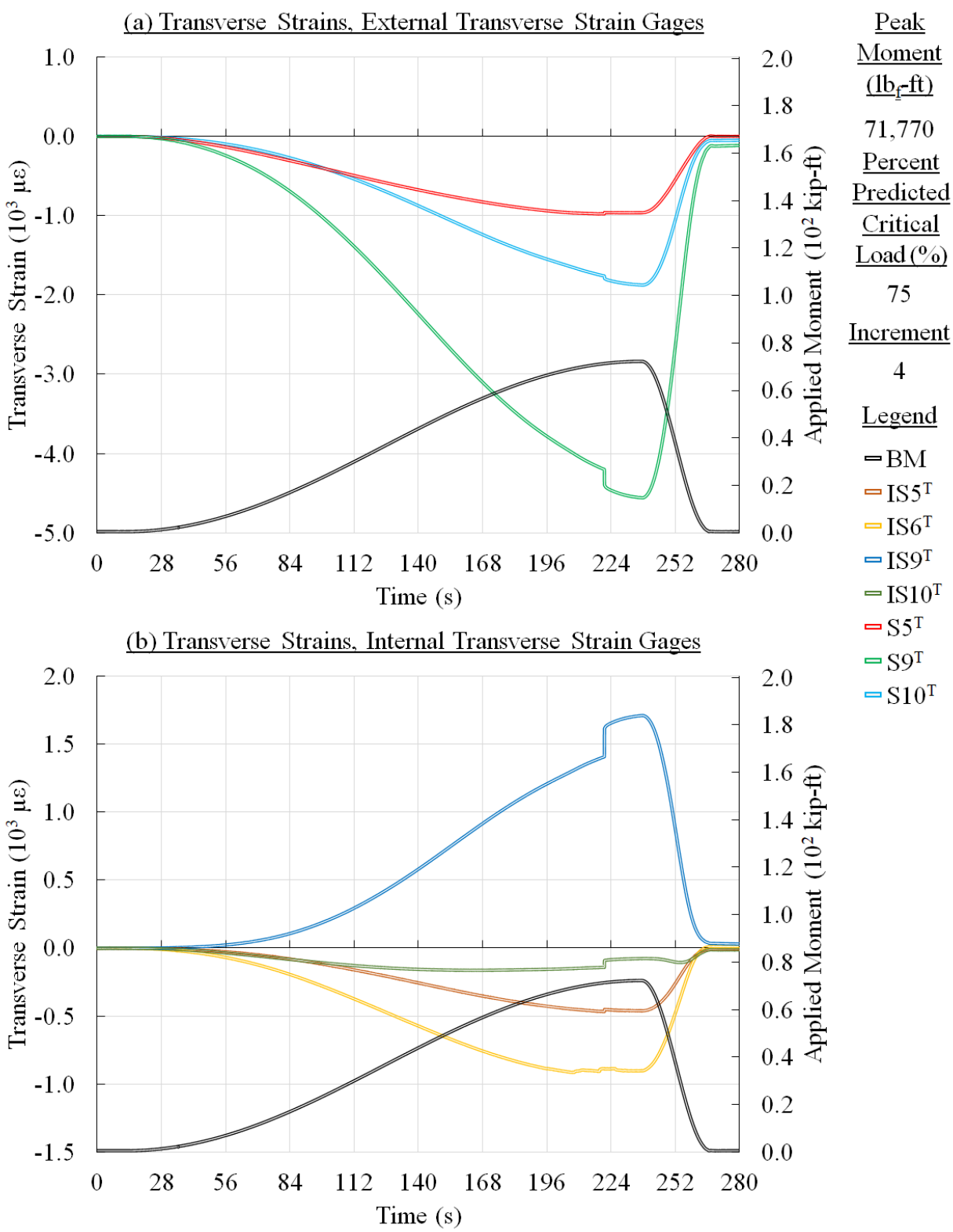


Figure C 121. Panel 6 load increment 4 (75% load level), transverse strain

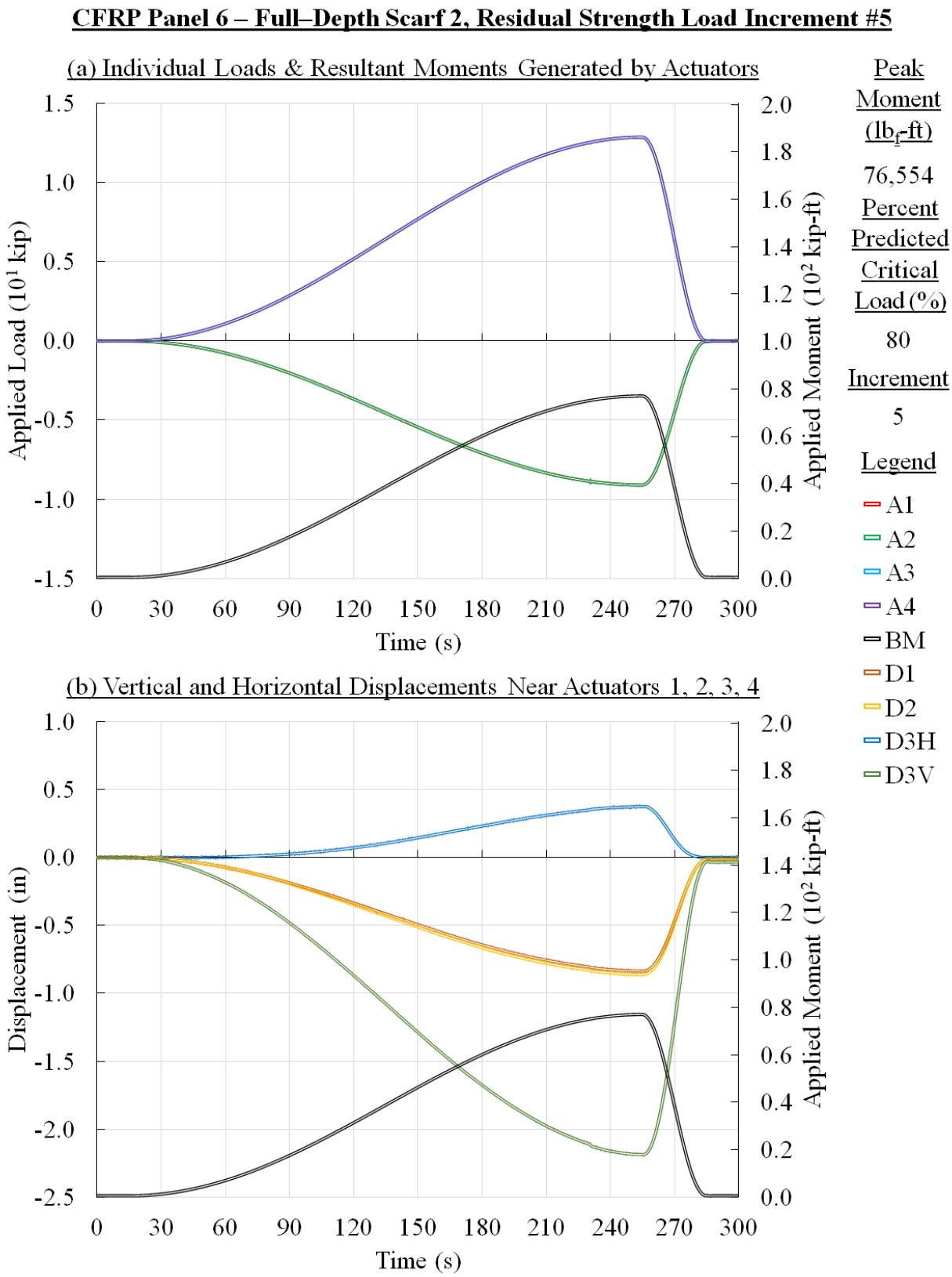


Figure C 122. Panel 6 load increment 5 (80% load level), load and displacement

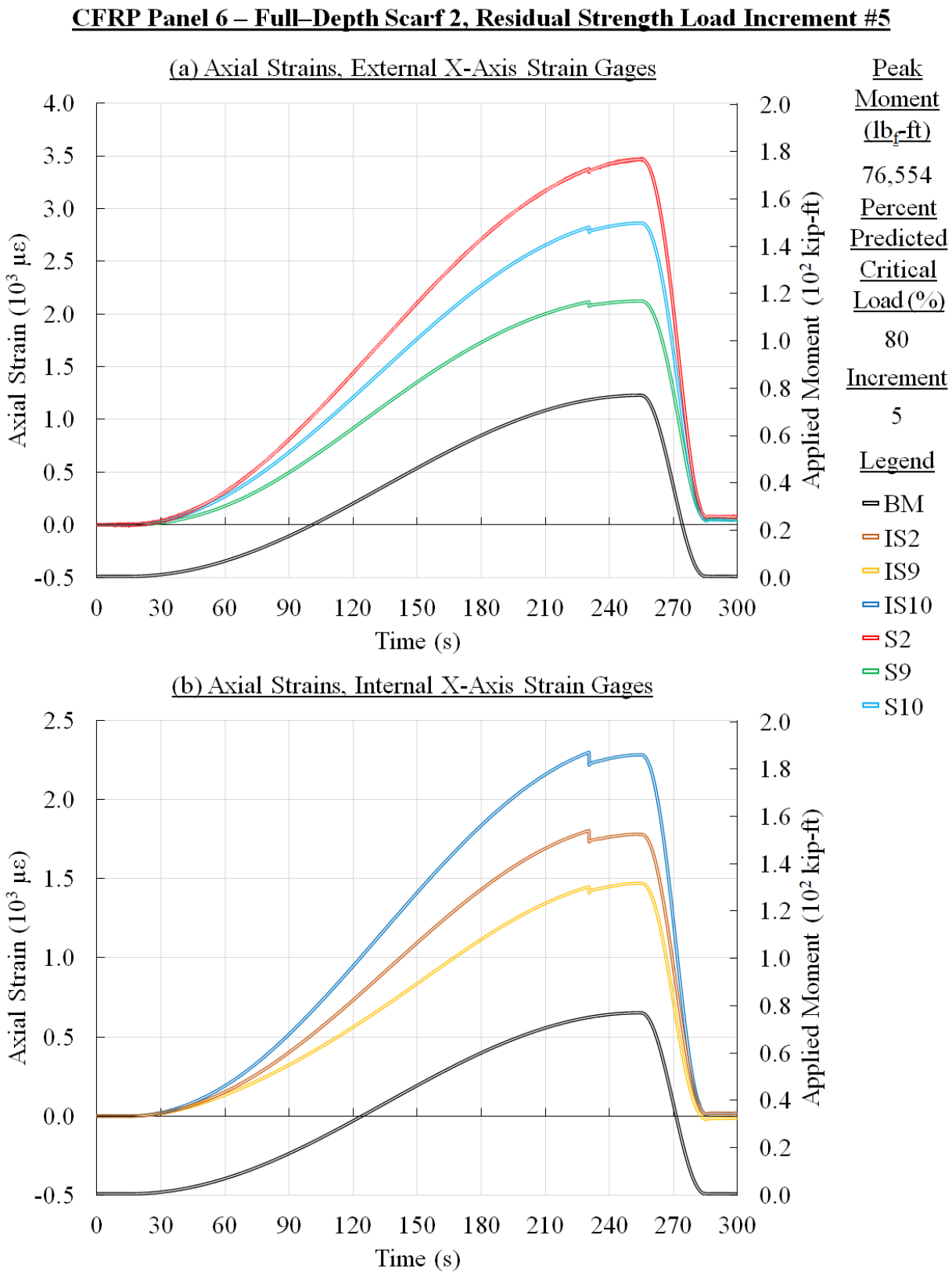


Figure C 123. Panel 6 load increment 5 (80% load level), axial strain along the X-axis strain gages

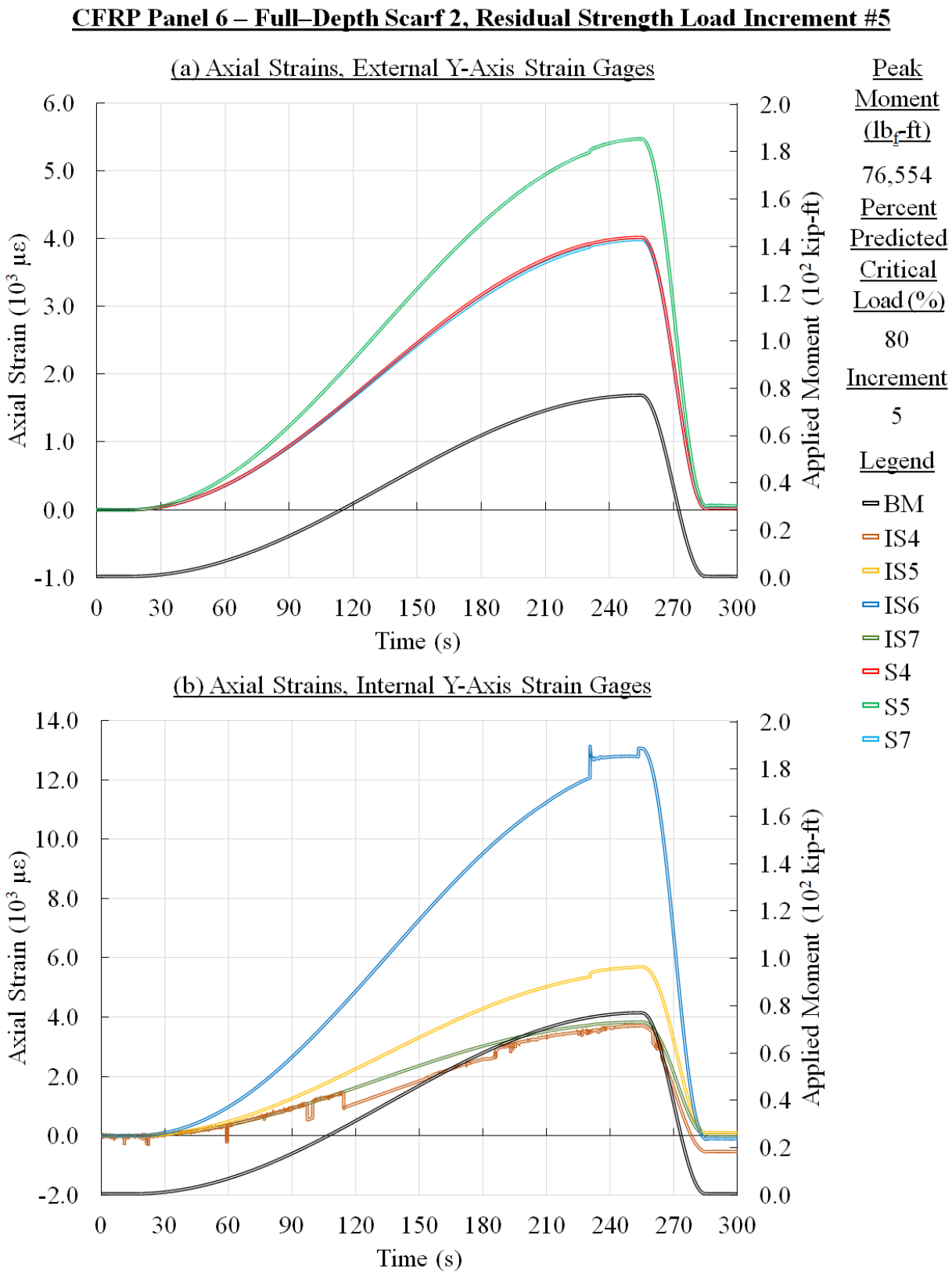


Figure C 124. Panel 6 load increment 5 (80% load level), axial strain along the Y-axis strain gages

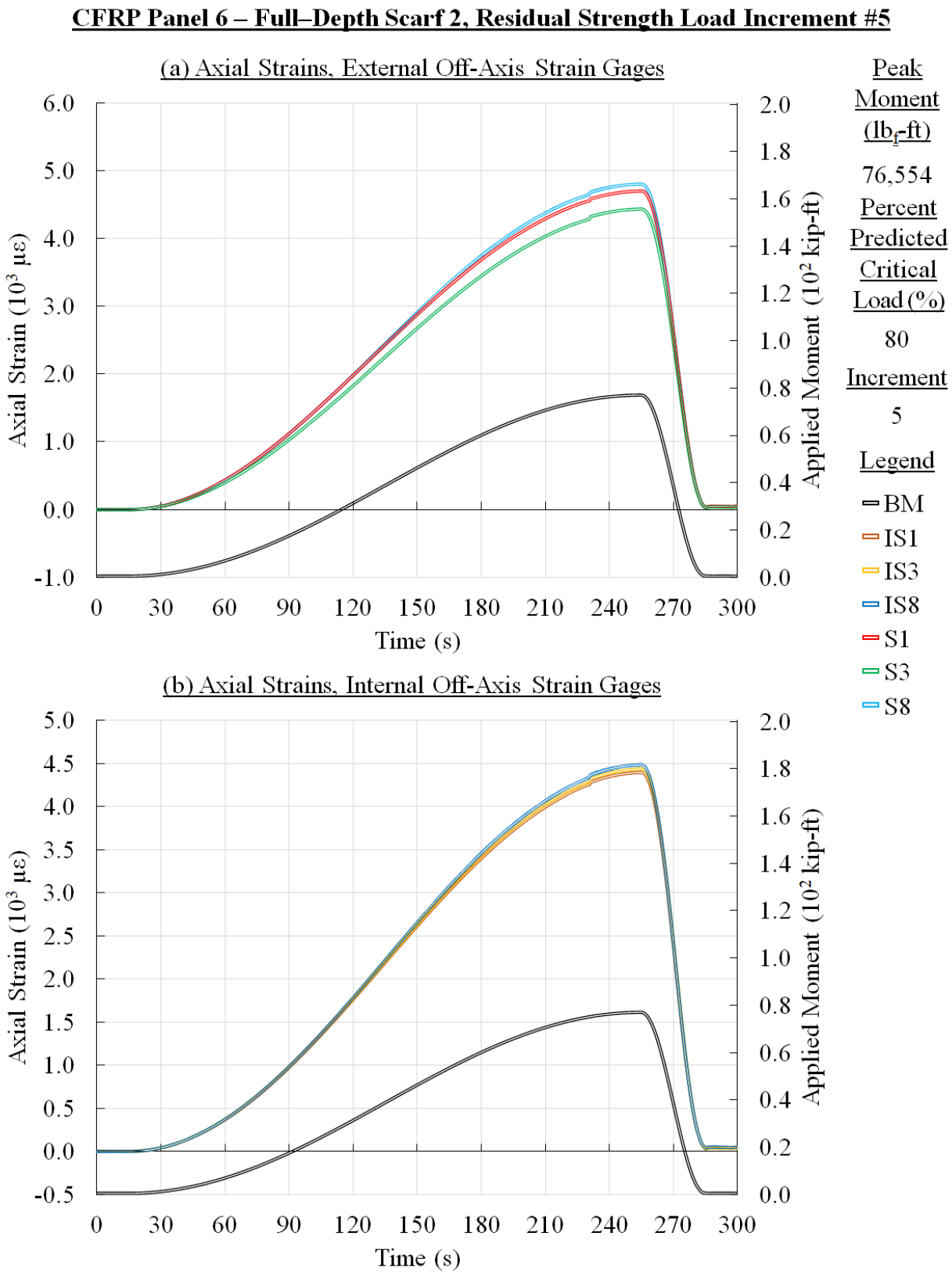


Figure C 125. Panel 6 load increment 5 (80% load level), axial strain along the off-axis strain gages

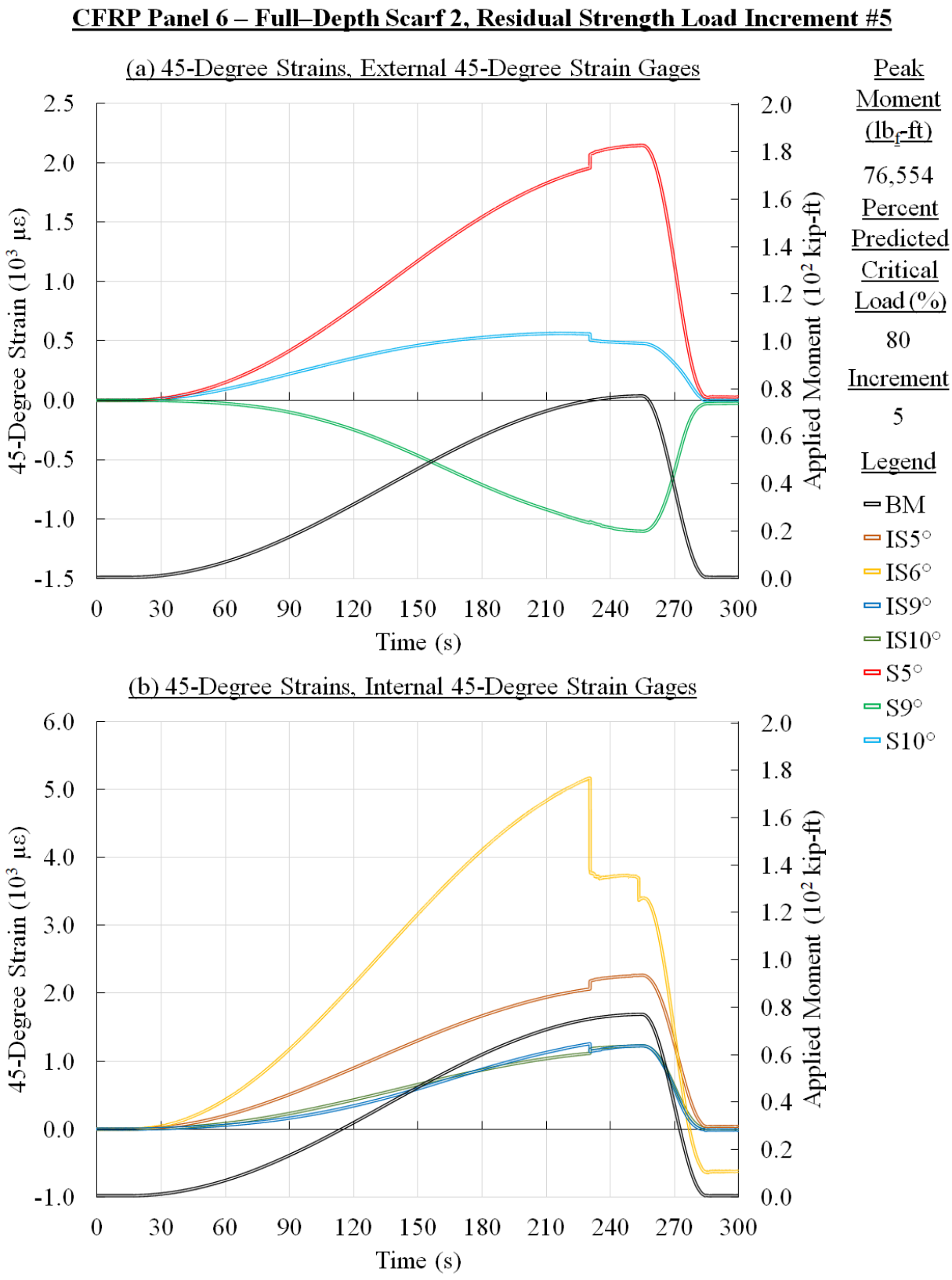


Figure C 126. Panel 6 load increment 5 (80% load level), 45 degree strain

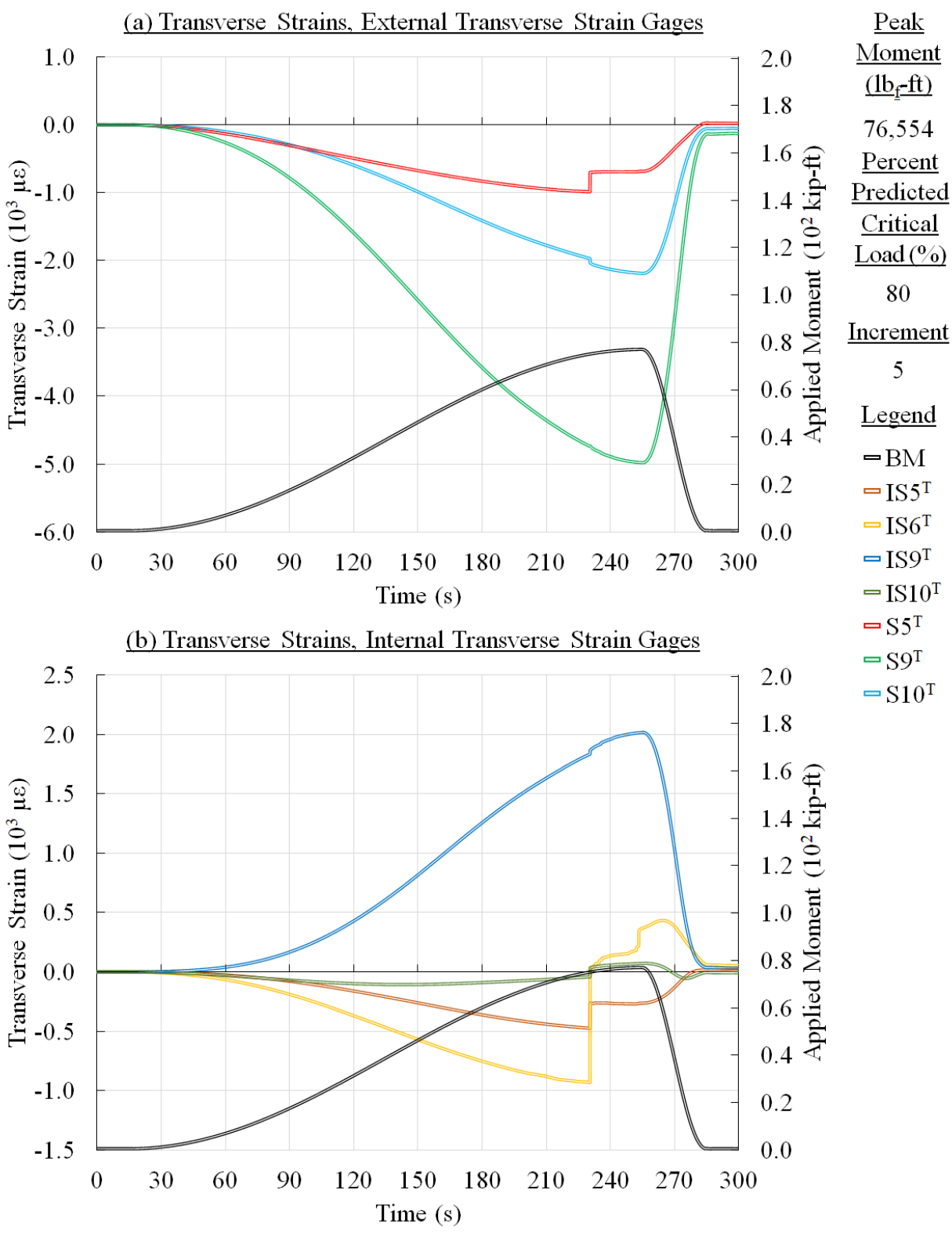


Figure C 127. Panel 6 load increment 5 (80% load level), transverse strain

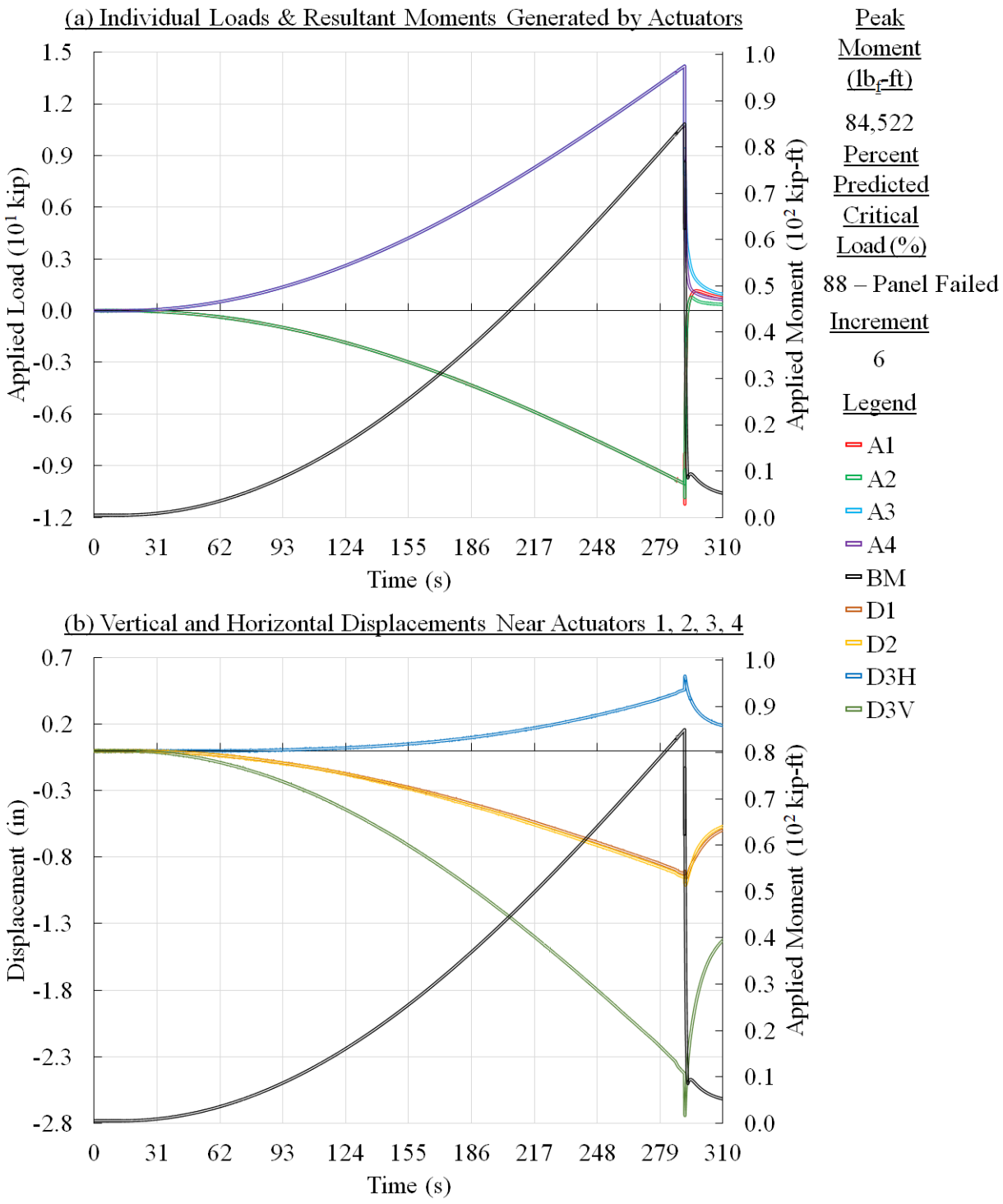


Figure C 128. Panel 6 load increment 6 (panel failure), load and displacement

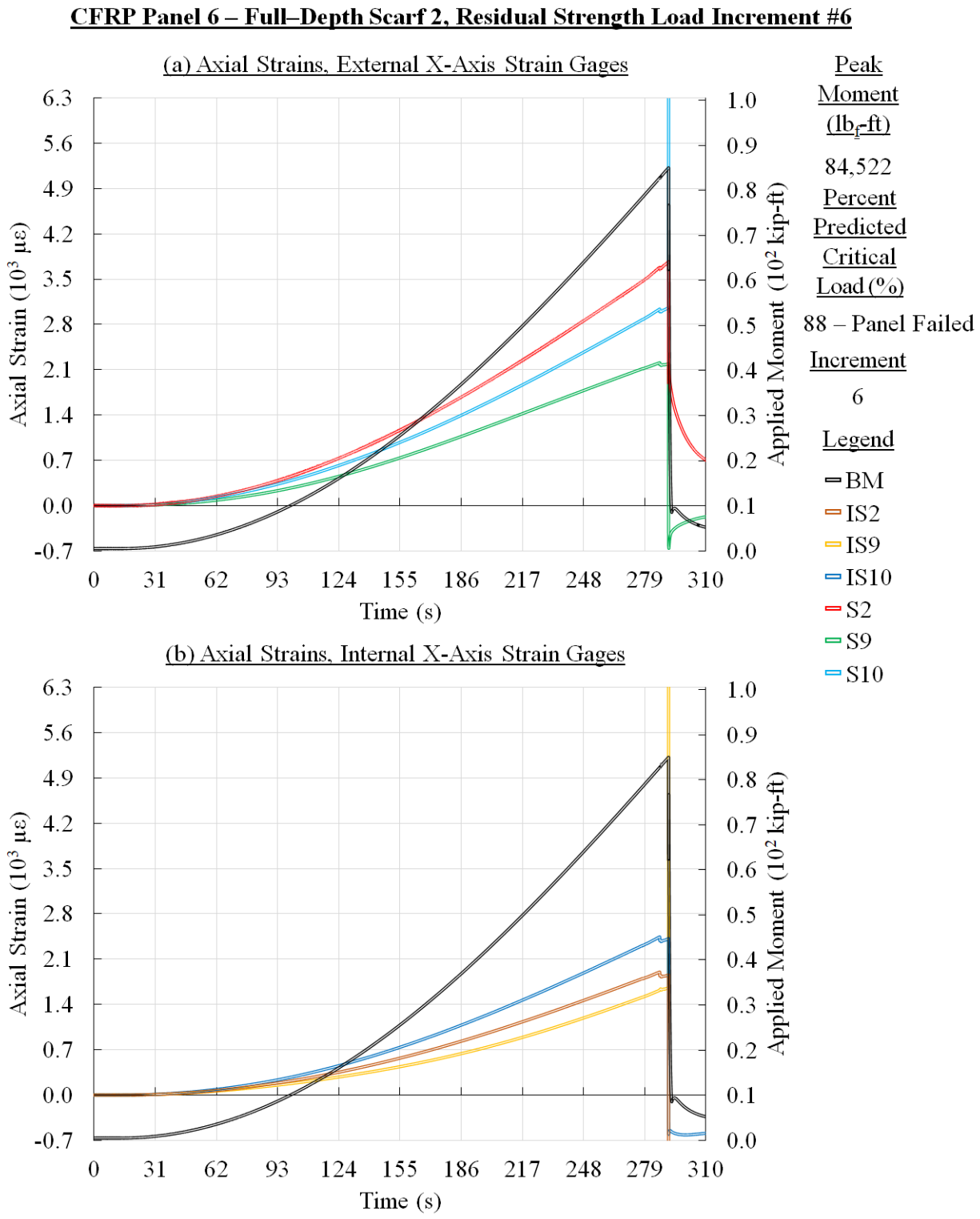


Figure C 129. Panel 6 load increment 6 (panel failure), axial strain along the X-axis strain gages

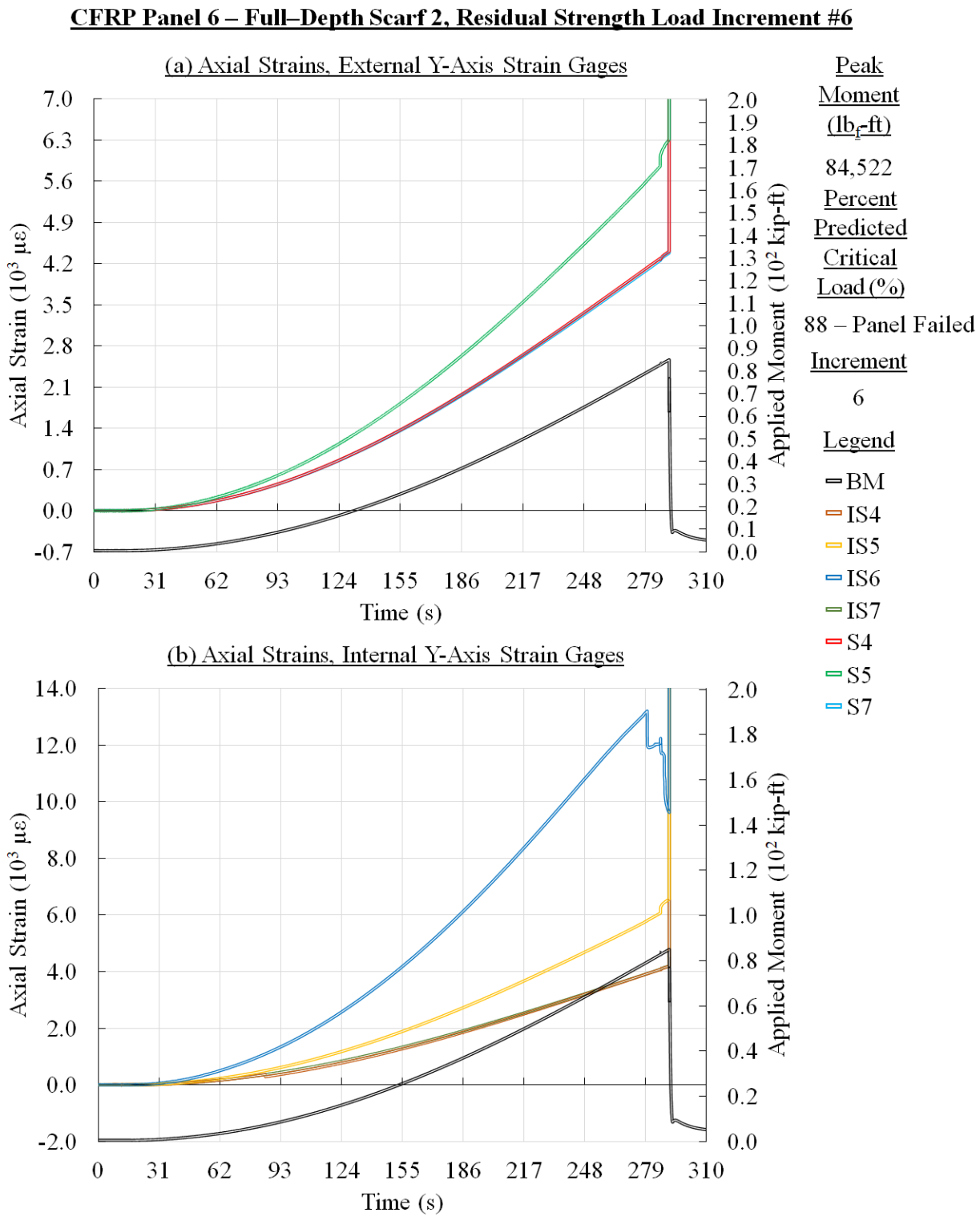


Figure C 130. Panel 6 load increment 6 (panel failure), axial strain along the Y-axis strain gages

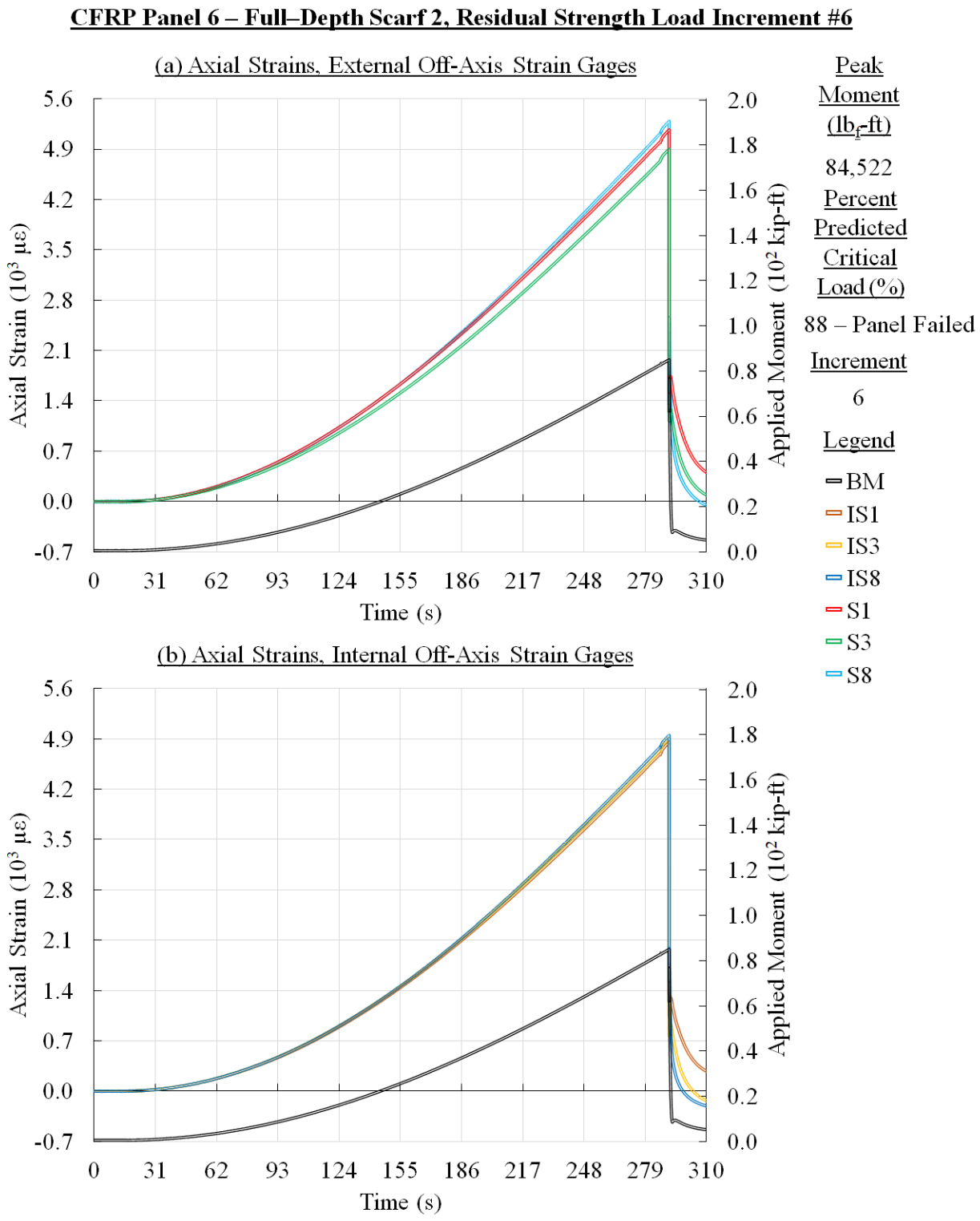


Figure C 131. Panel 6 load increment 6 (panel failure), axial strain along the off-axis strain gages

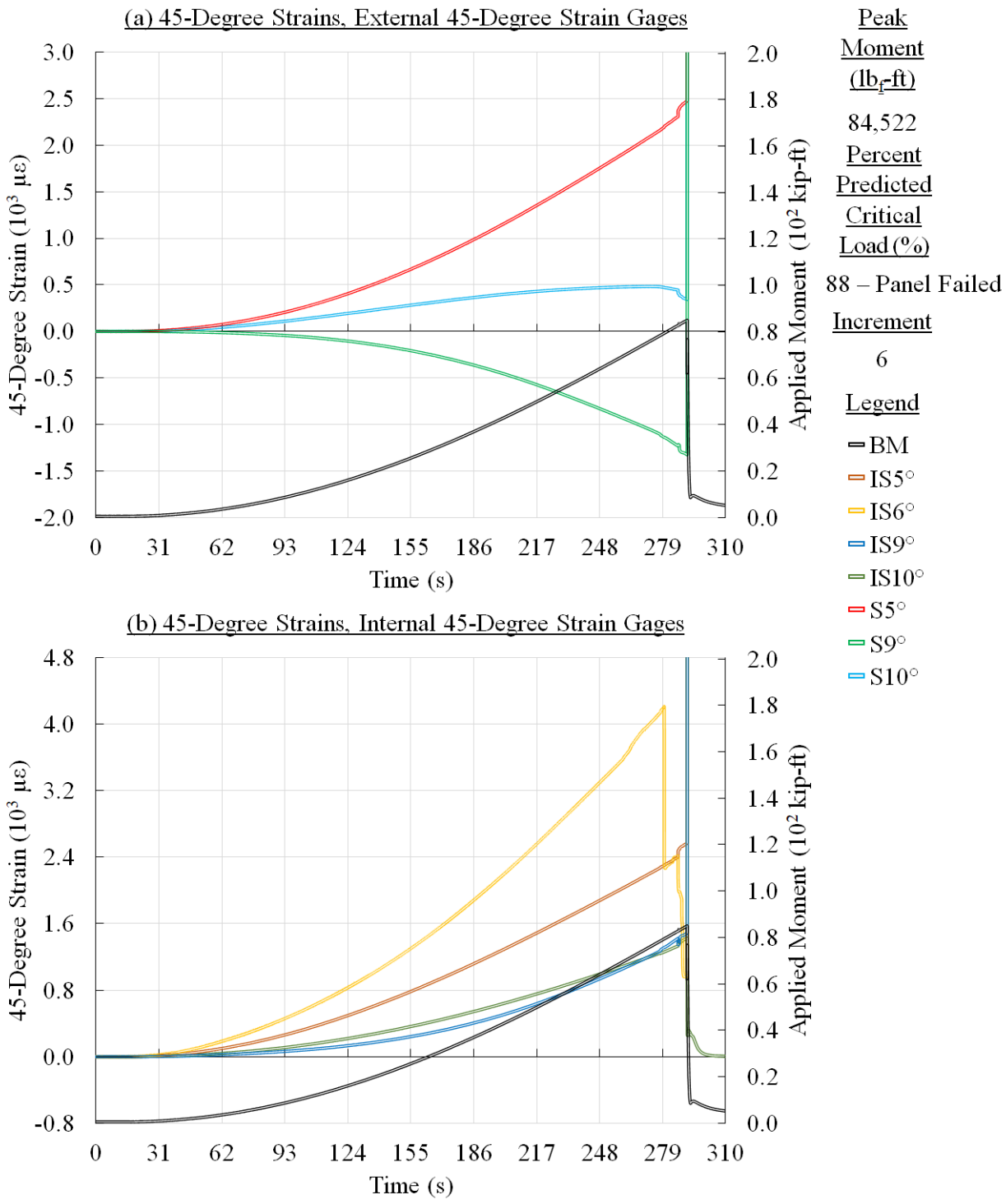


Figure C 132. Panel 6 load increment 6 (panel failure), 45 degree strain

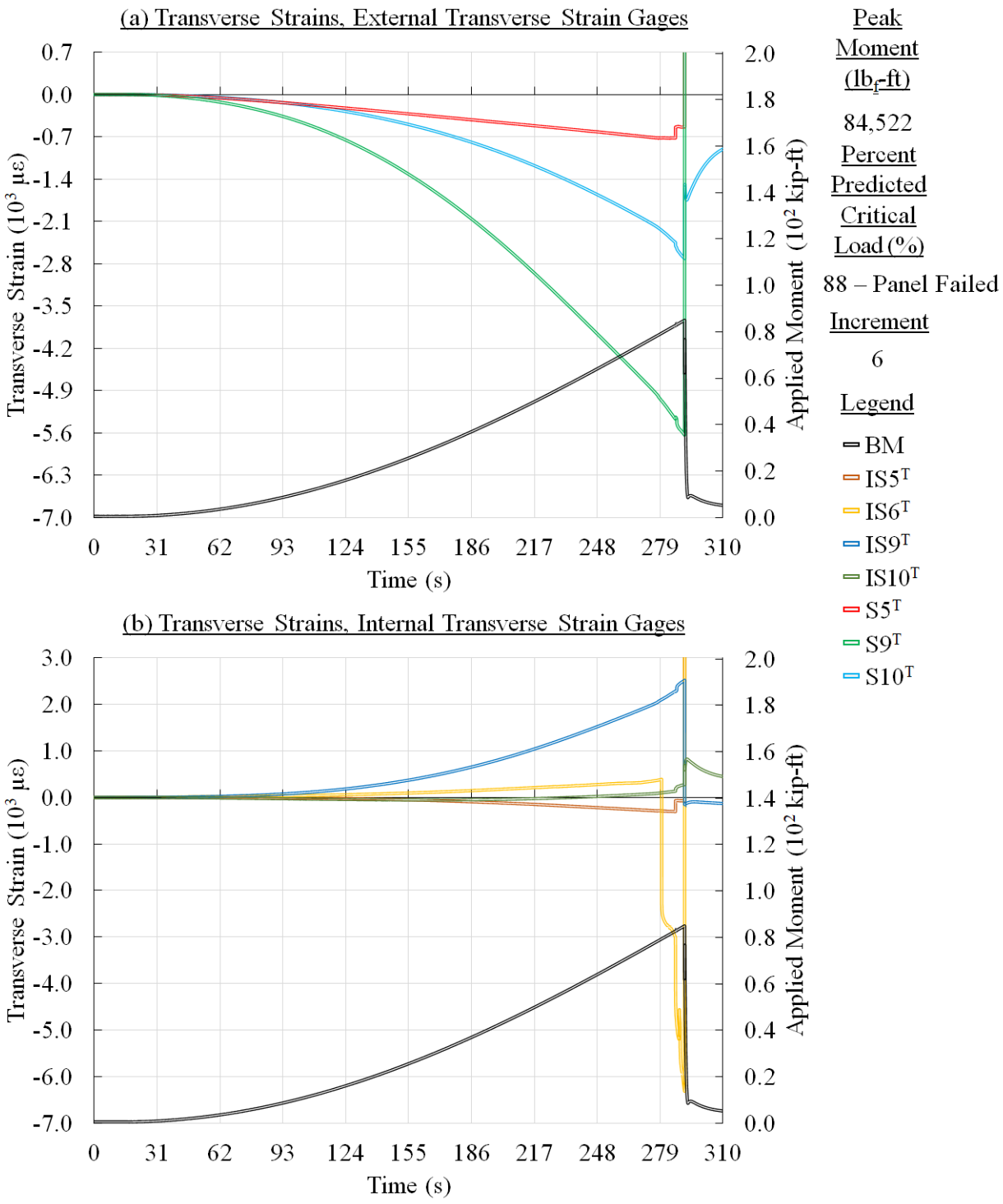


Figure C 133. Panel 6 load increment 6 (panel failure), transverse strain

# D Digital image correlation results

This appendix presents the results of three-dimensional (3D) digital image correlation (DIC) results for the panels during quasi-static strain surveys. 3D DIC is a non-contact, material-independent NDI method capable of utilizing sequential digital images of a specimen subjected to mechanical loading to measure in-plane deformation and strain, and in- and out-of-plane displacements. Throughout the duration of the tests described in this report, 5M ARAMIS 3D DIC systems were used to monitor strains exhibited in the central test sections of the panels during quasi-static strain surveys. Each ARAMIS DIC system consisted of a sensor unit, a sensor controller, a high-performance PC system, and ARAMIS 3D DIC analysis software. The sensor unit, which featured two 5-megapixel cameras with 12-mm (WFOV) and 50-mm (NFOV) focal length lenses, a laser pointer, and two adjustable LED spotlights mounted on a circular support bar.

Panel 3 axial strains and von Mises strains measured in the vicinity of the scarf during residual strength test are shown in Figure D 1 and Figure D 2, respectively. For panel 5, axial strain distributions during fatigue at SL strain level, fatigue at elevated load strain level and additional fatigue at SL strain level are shown in Figure D 3, Figure D 4, and Figure D 5, respectively, and von Mises strains for the same increments are shown in Figure D 6–Figure D 8. The axial strains and von Mises strains measured during post-fatigue residual strength tests for panel 5 are shown in Figure D 9 and Figure D 10. Panel 4 axial strains and von Mises strains measured in the vicinity of the scarf during residual strength test are shown in Figure D 11 and Figure D 12, respectively. The axial strain and von Mises strains collected during fatigue at SL strain level for panel 6 are shown in Figure D 13 and Figure D 14. Similarly, axial strains and von Mises strains during post-fatigue residual strength tests are shown in Figure D 16 and Figure D 15, respectively.

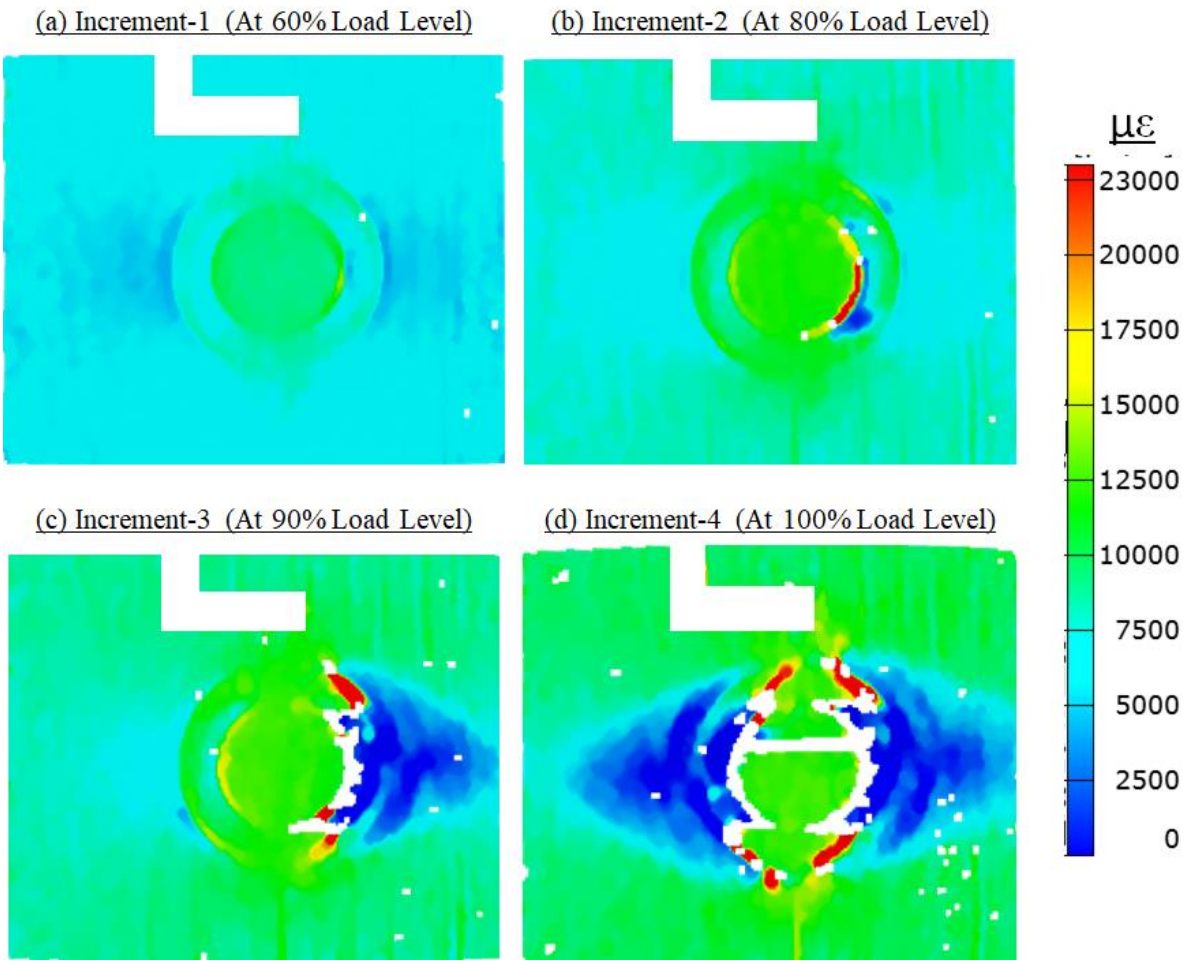


Figure D 1. Panel 3 DIC results (axial strains) during residual strength test

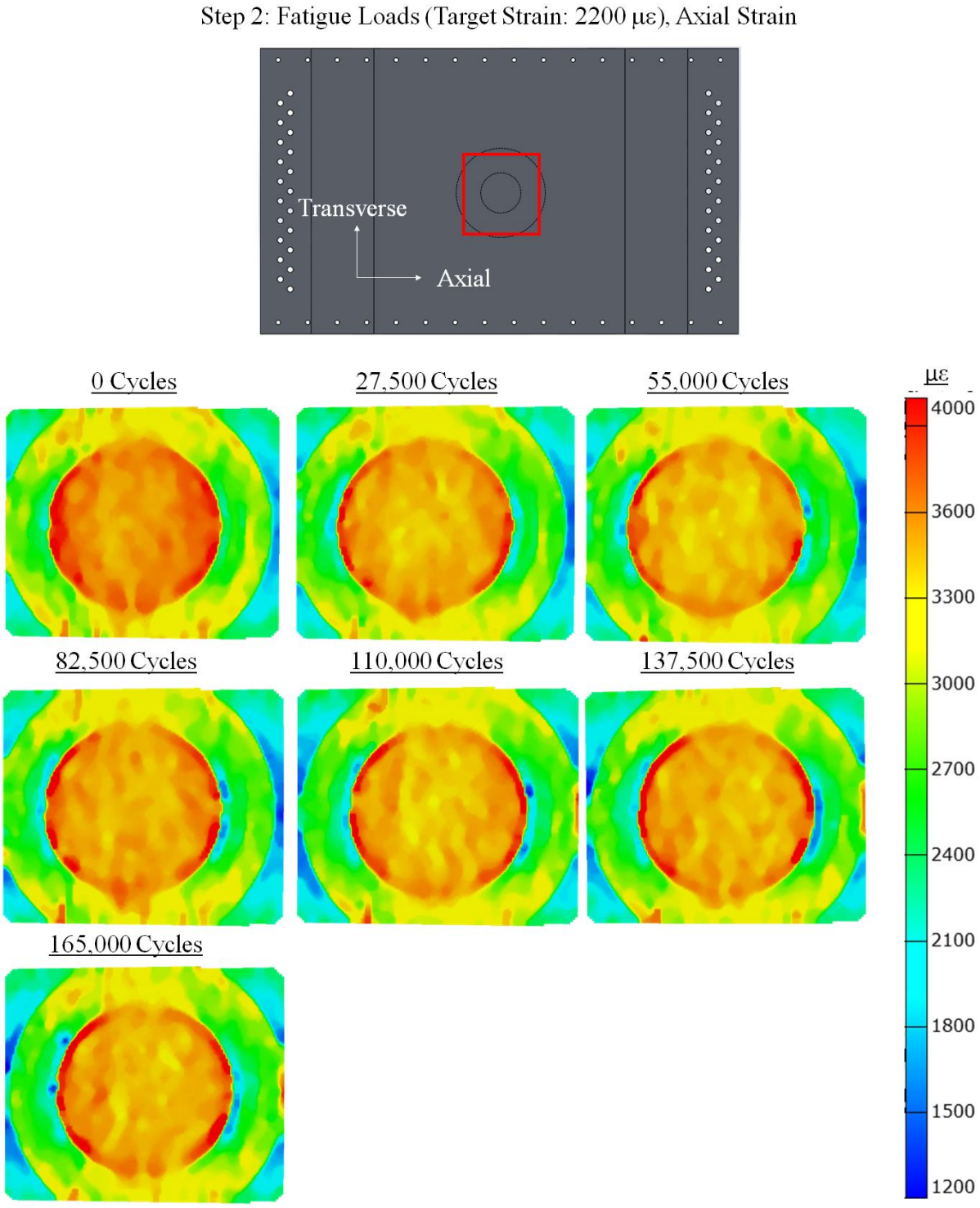


Figure D 3. Panel 5 DIC results (axial strains) during fatigue at SL strain level

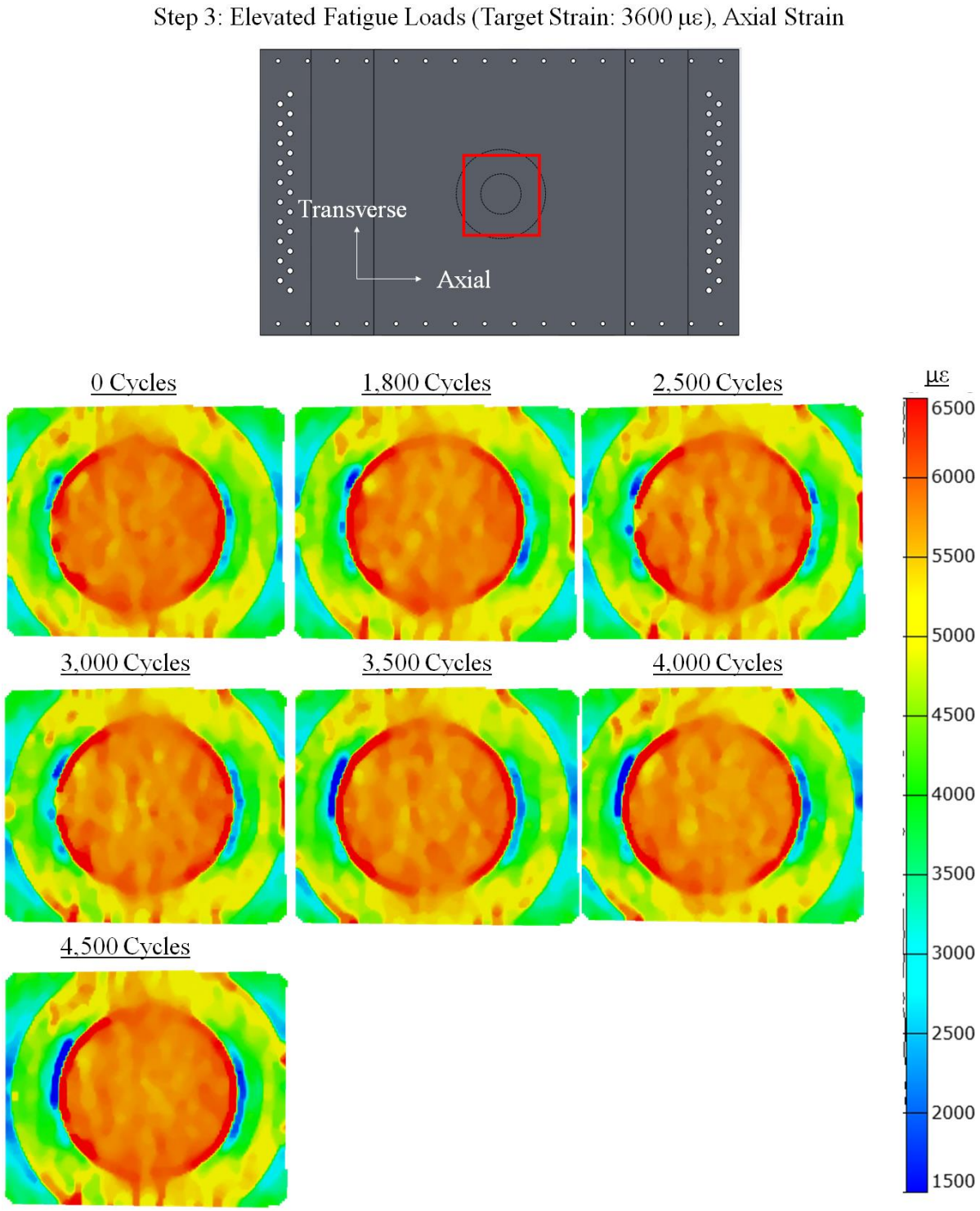


Figure D 4. Panel 5 DIC results (axial strains) during fatigue at elevated load strain level

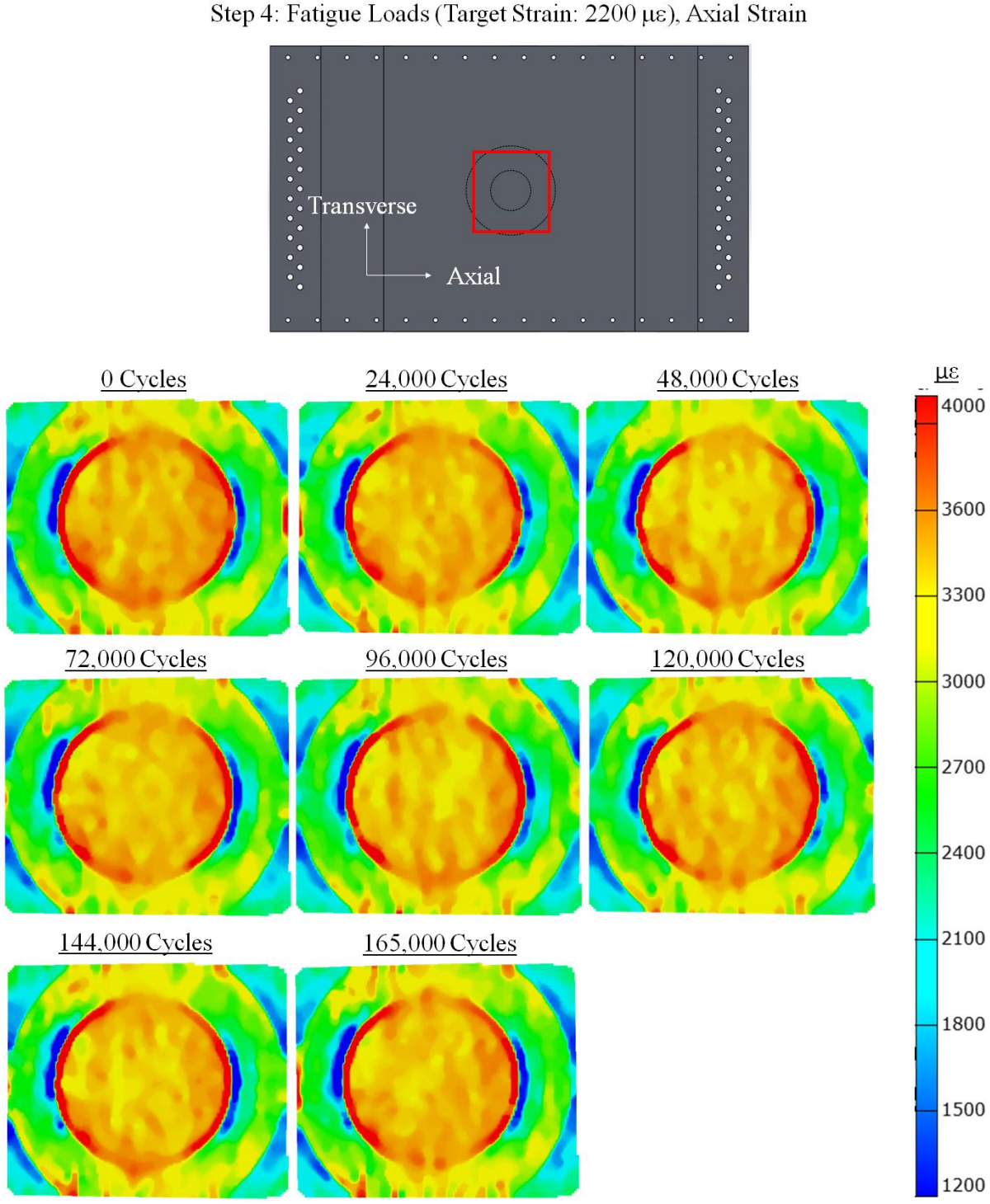


Figure D 5. Panel 5 DIC results (axial strains) during additional fatigue at SL strain level

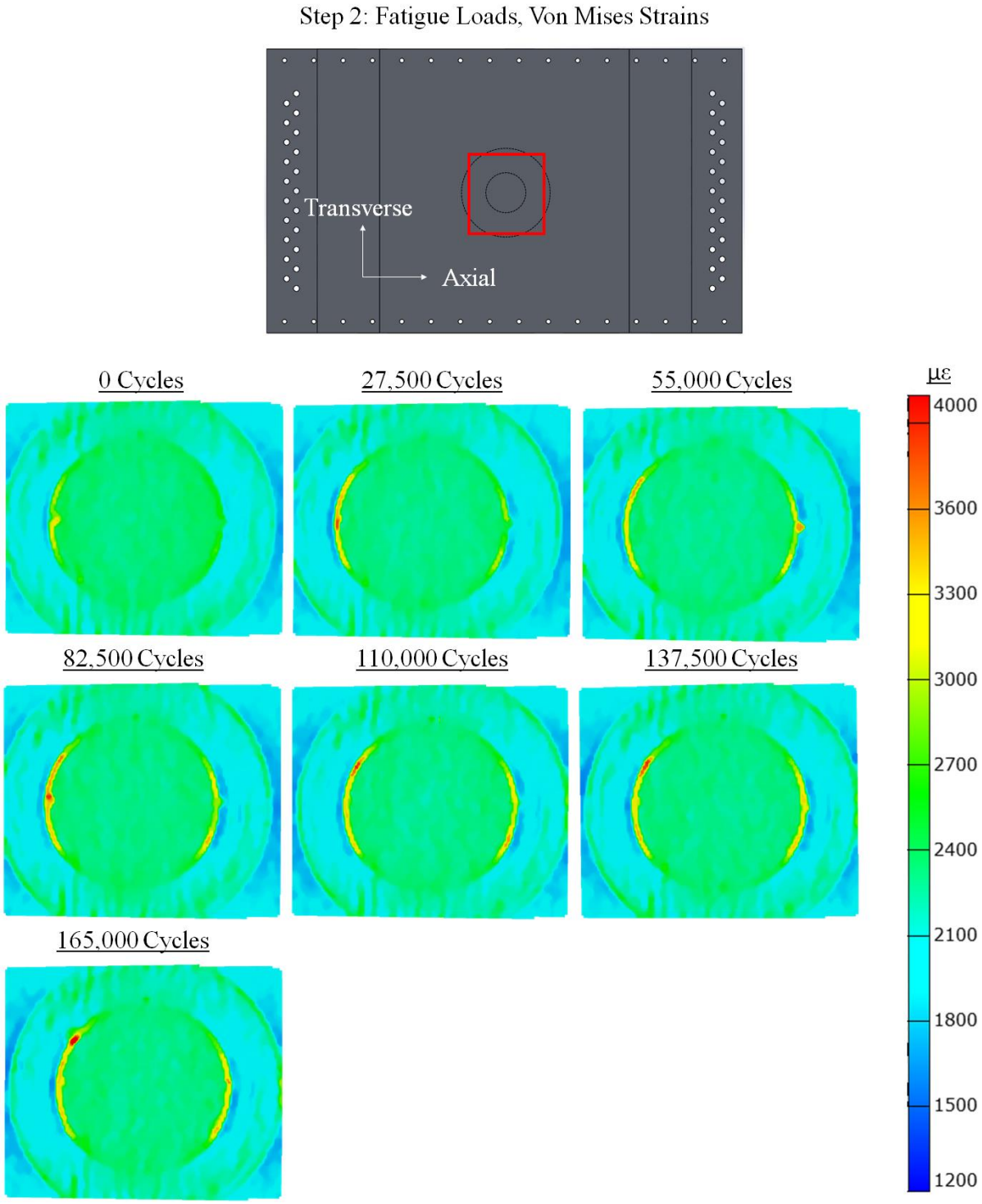


Figure D 6. Panel 5 DIC results (von Mises strains) during fatigue at SL strain level

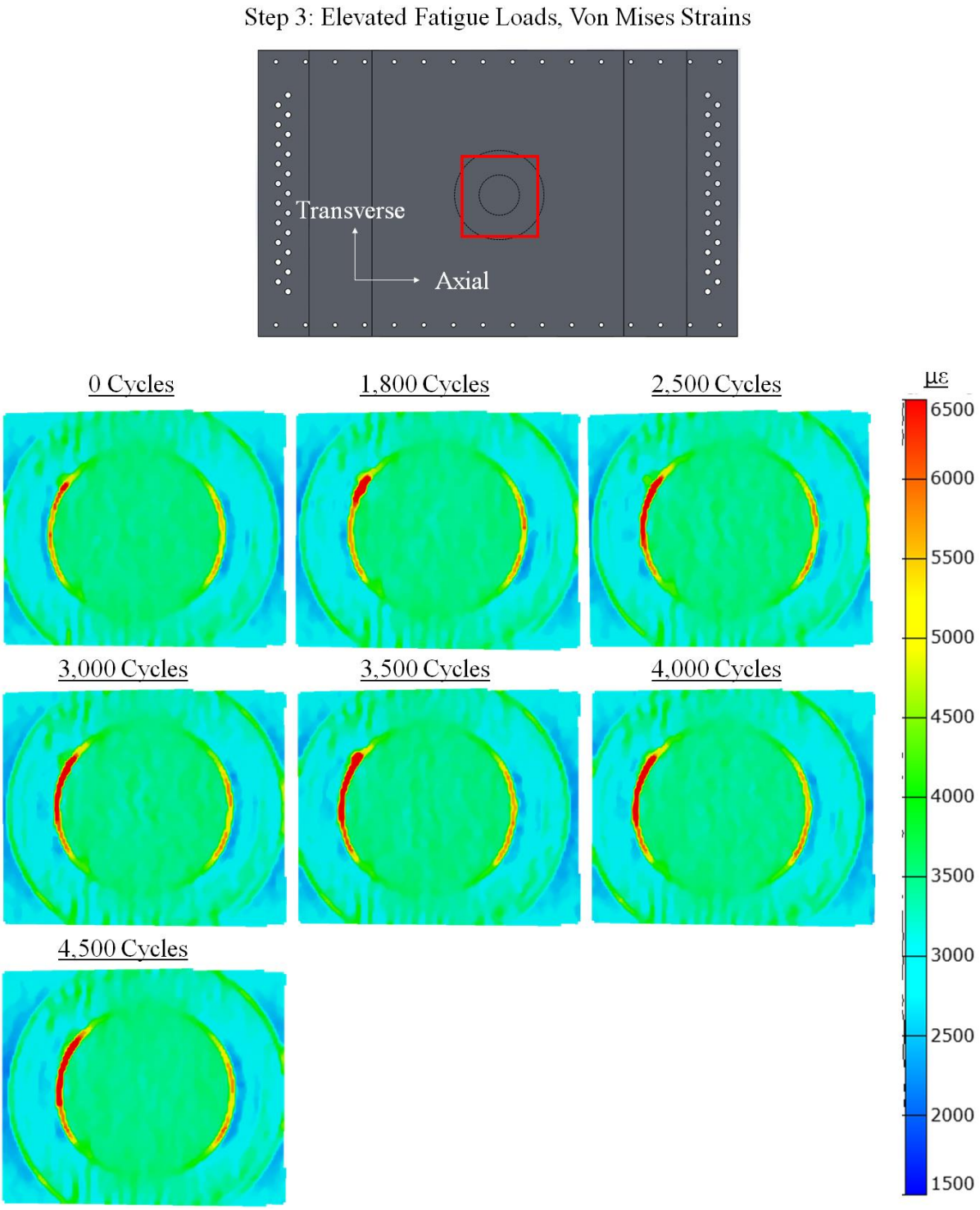


Figure D 7. Panel 5 DIC results (von Mises strains) during fatigue at elevated load strain level

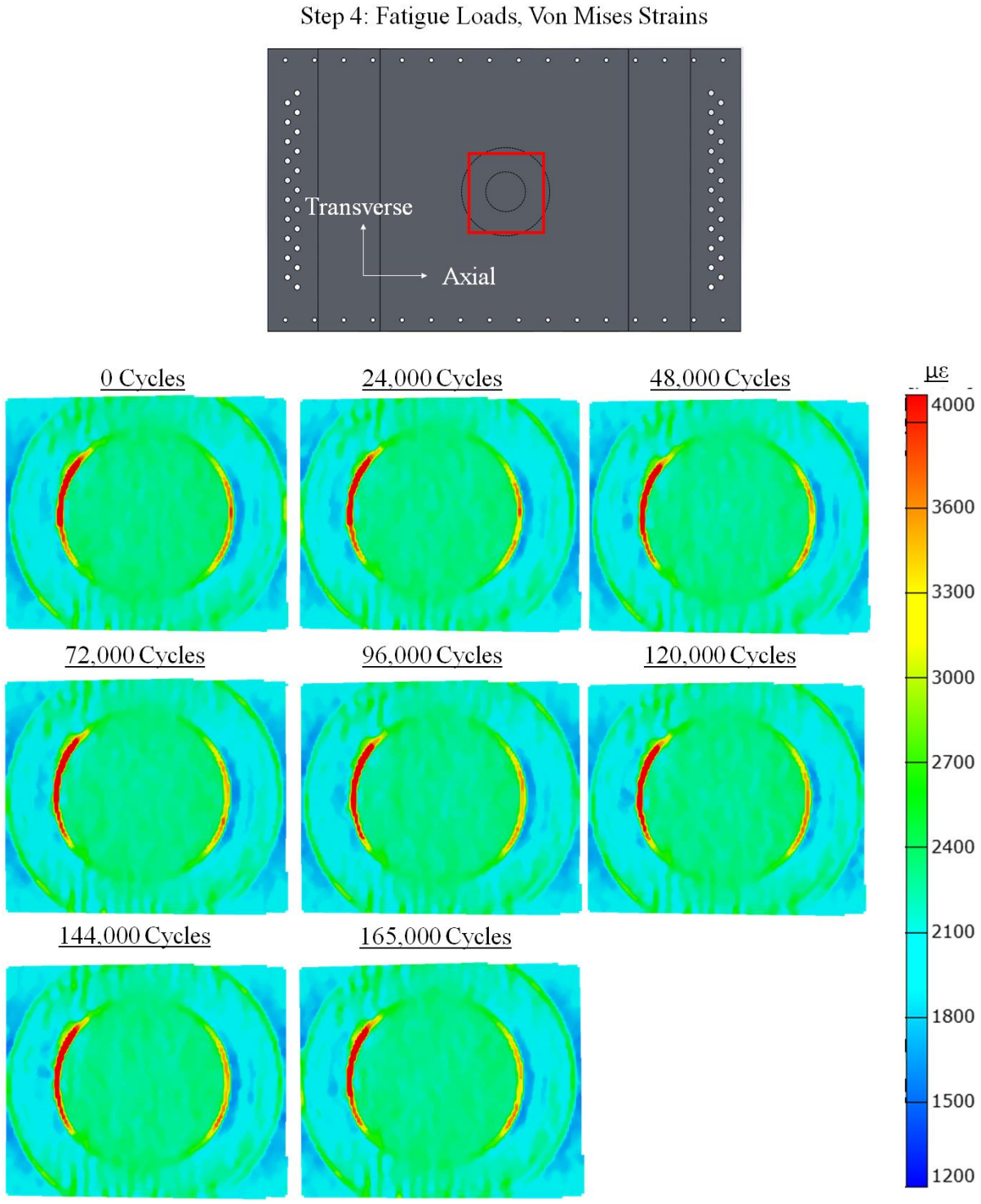


Figure D 8. Panel 5 DIC results (von Mises strains) during additional fatigue at SL strain level

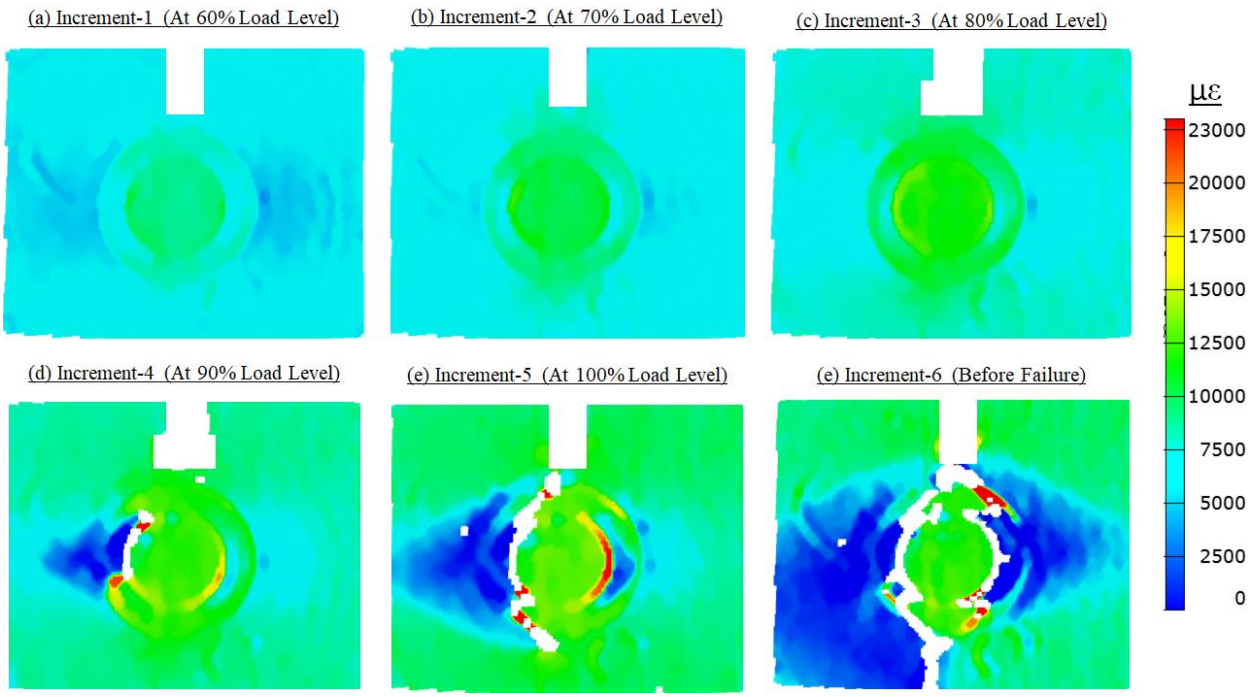


Figure D 10. Panel 5 DIC results (axial strains) during post-fatigue residual strength test

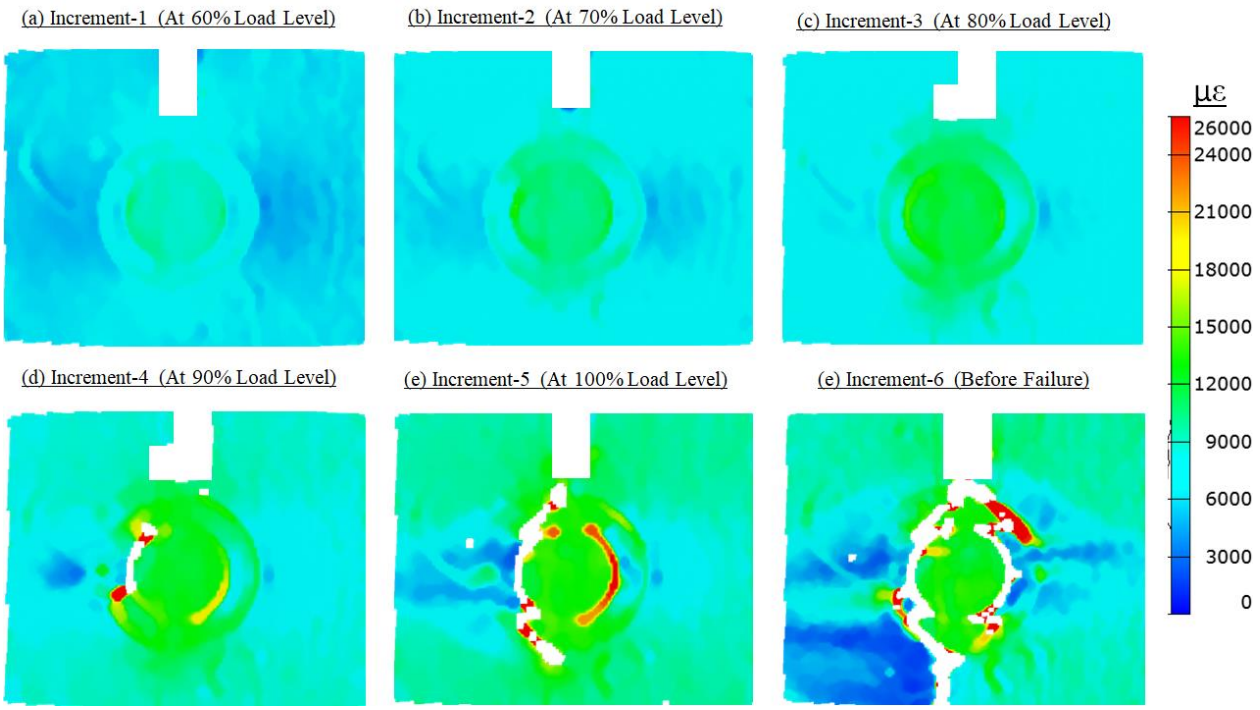


Figure D 9. Panel 5 DIC results (von Mises strains) during post-fatigue residual strength test

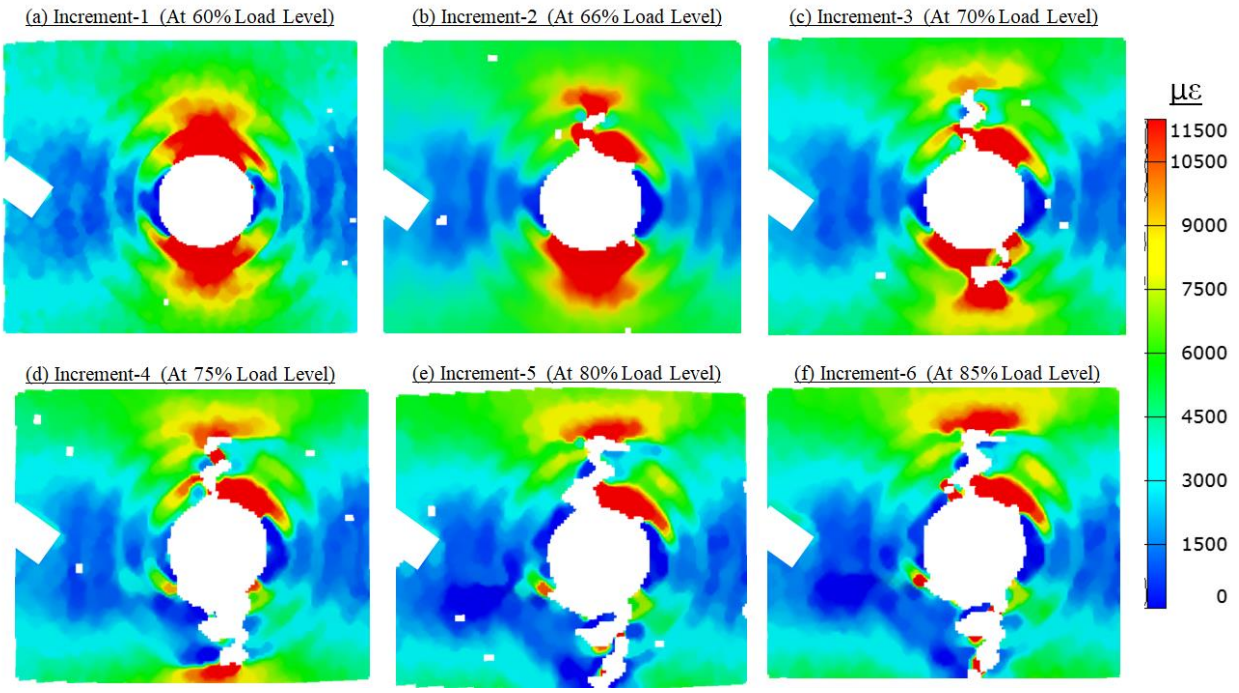


Figure D 12. Panel 4 DIC results (axial strains) during residual strength test

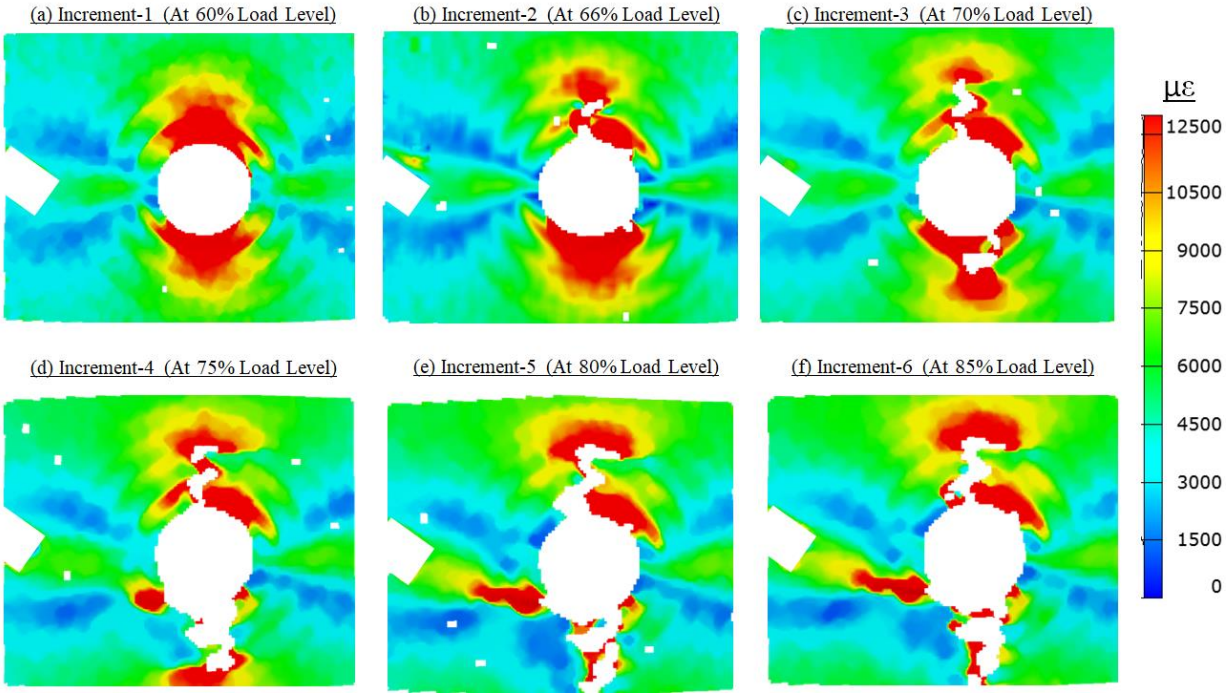


Figure D 11. Panel 4 DIC results (von Mises strains) during residual strength test

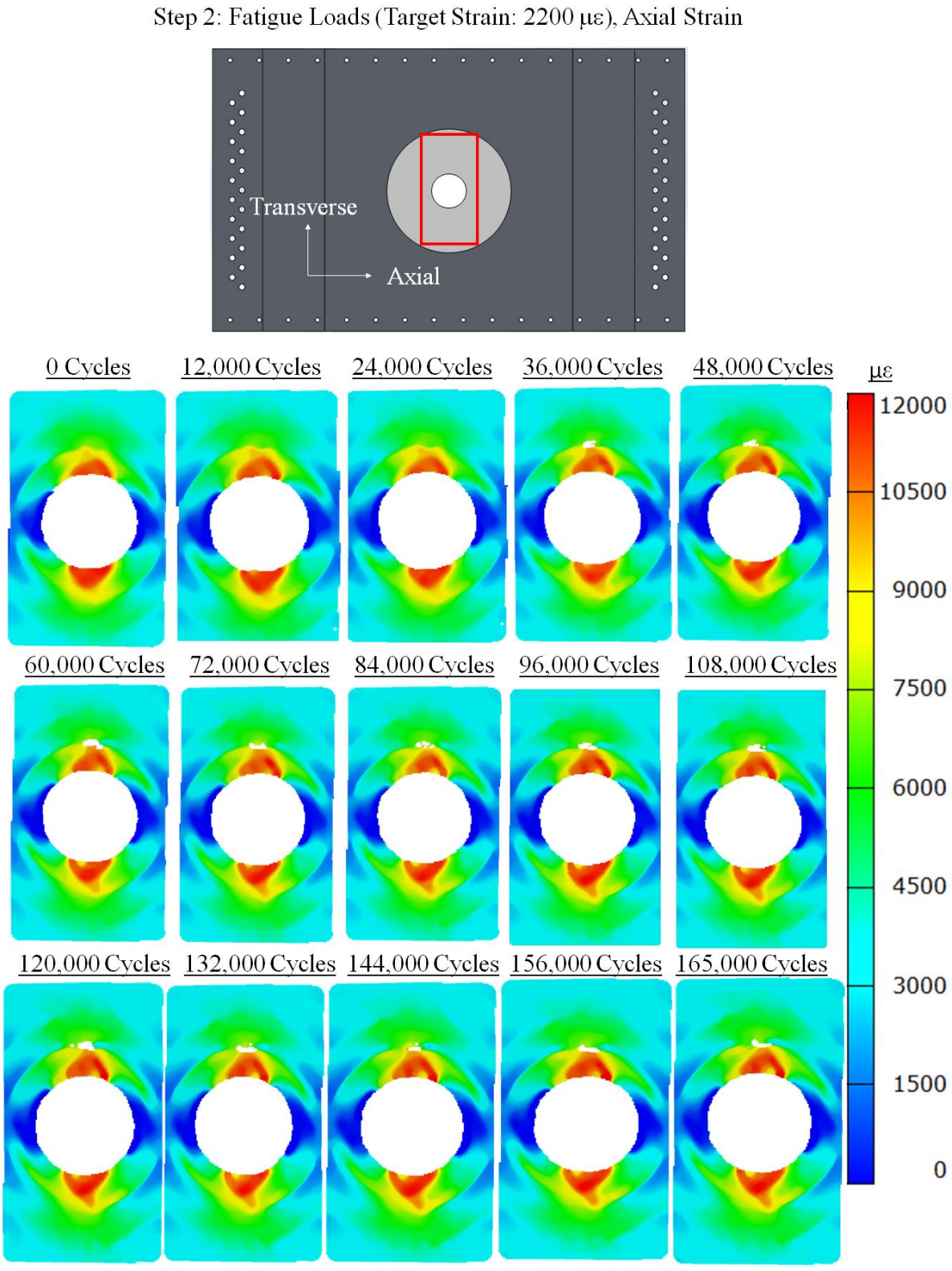


Figure D 13. Panel 6 DIC results (axial strains) during fatigue at SL strain level

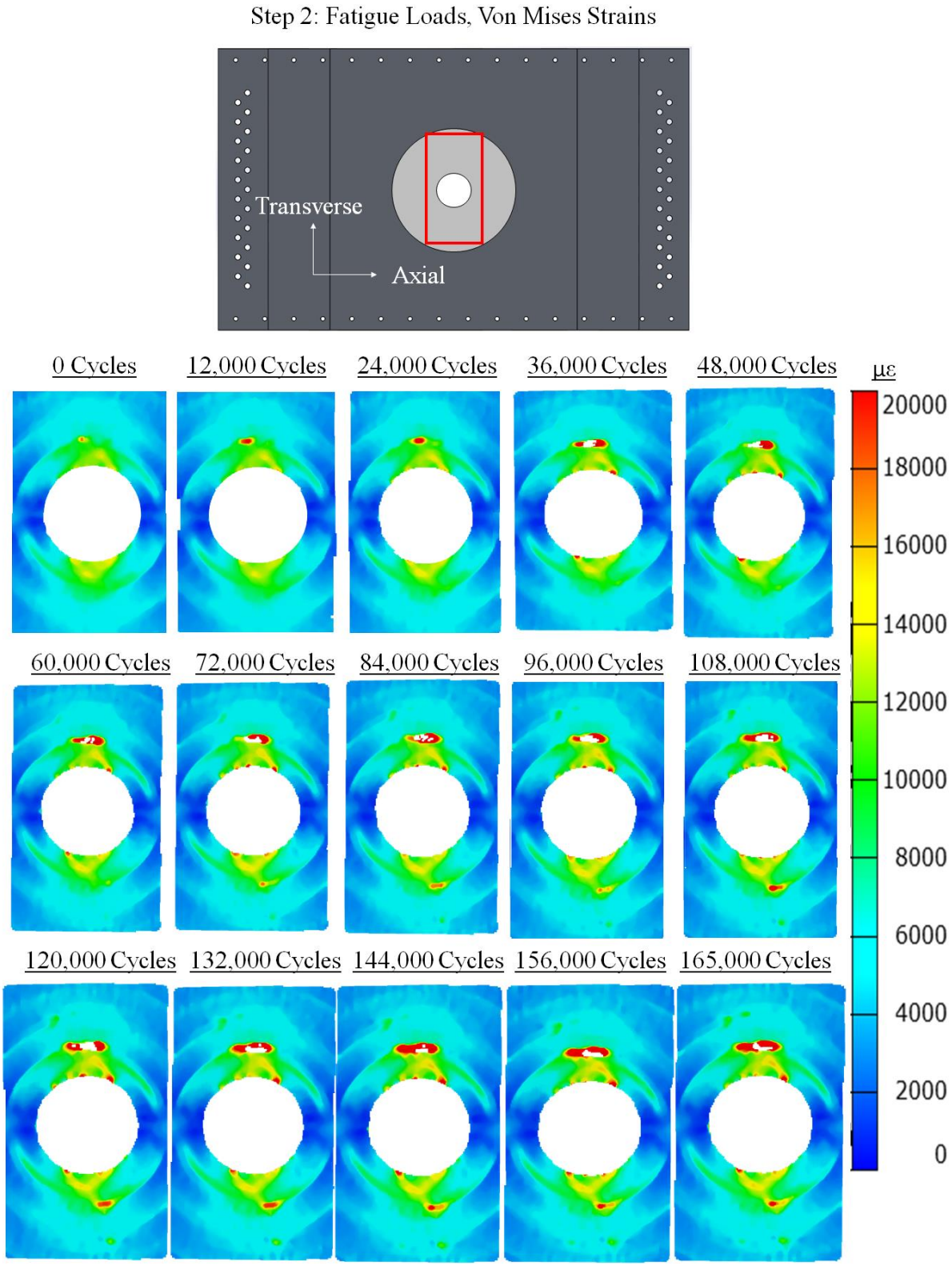


Figure D 14. Panel 6 DIC results (von Mises strains) during fatigue at SL strain level

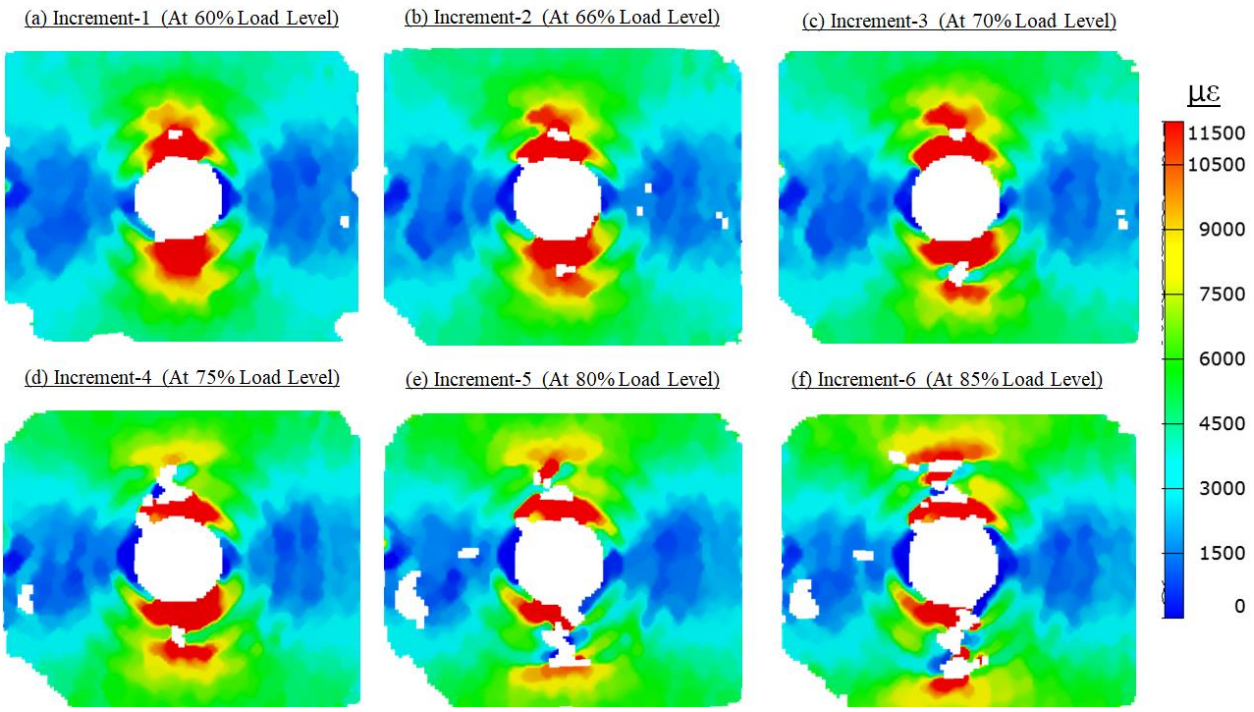


Figure D 16. Panel 6 DIC results (axial strains) during post-fatigue residual strength test

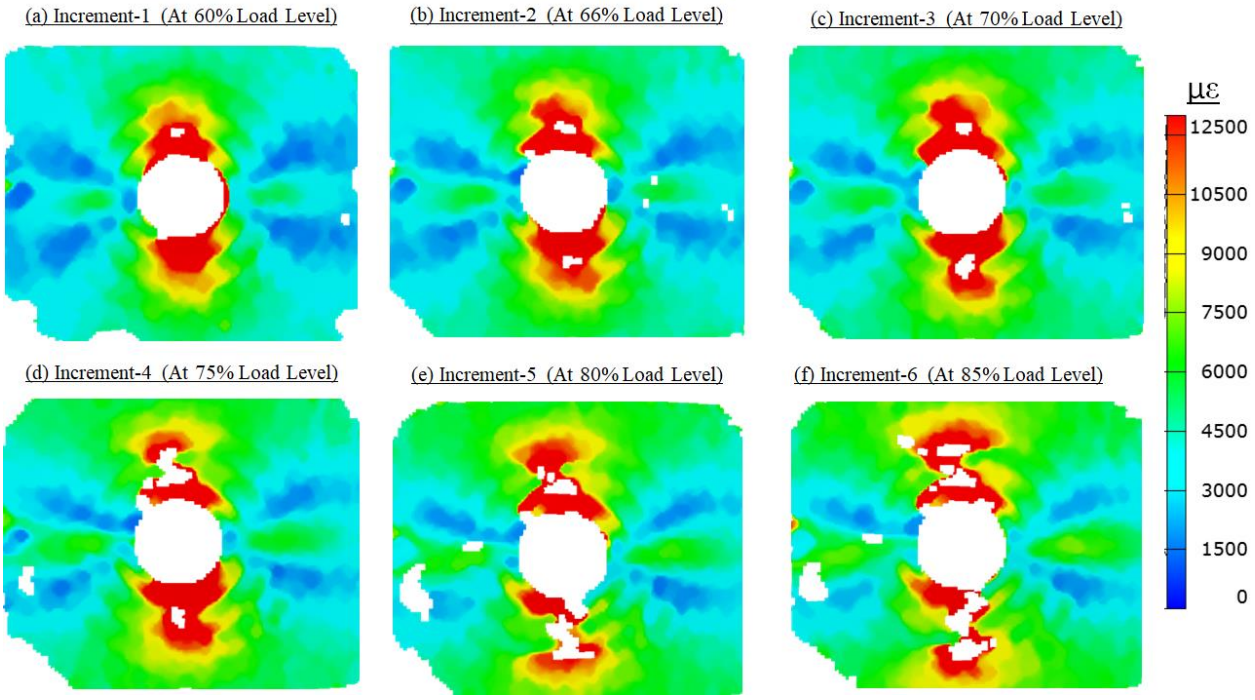


Figure D 15. Panel 6 DIC results (von Mises strains) during post-fatigue residual strength test

# E Visual results

This appendix provides the visual results captured throughout fatigue, residual strength loading and post panels failure of the two partial-depth scarf panels (panels 3 and 5) and two full-depth scarf panels (panels 4 and 6).

Images captured for panel 3 during the residual strength test and after failure are shown in Figure E 1–Figure E 2 and Figure E 3–Figure E 4, respectively. Images captured for panel 5 during fatigue are provided in Figure E 5–Figure E 7. The images captured during post-fatigue residual strength test for panel 5 are provided in Figure E 8 and Figure E 9 and after failure in Figure E 10 and Figure E 11. Images captured for panel 4 during residual strength are shown in Figure E 12 and Figure E 13 and after failure in Figure E 14 and Figure E 15. Panel 6 images during fatigue, post-fatigue residual strength loading, and after failure are shown in Figure E 16, Figure E 17–Figure E 18, and Figure E 19–Figure E 20, respectively.


Figure E 1. Panel 3 visual results using WFOV camera during residual strength test

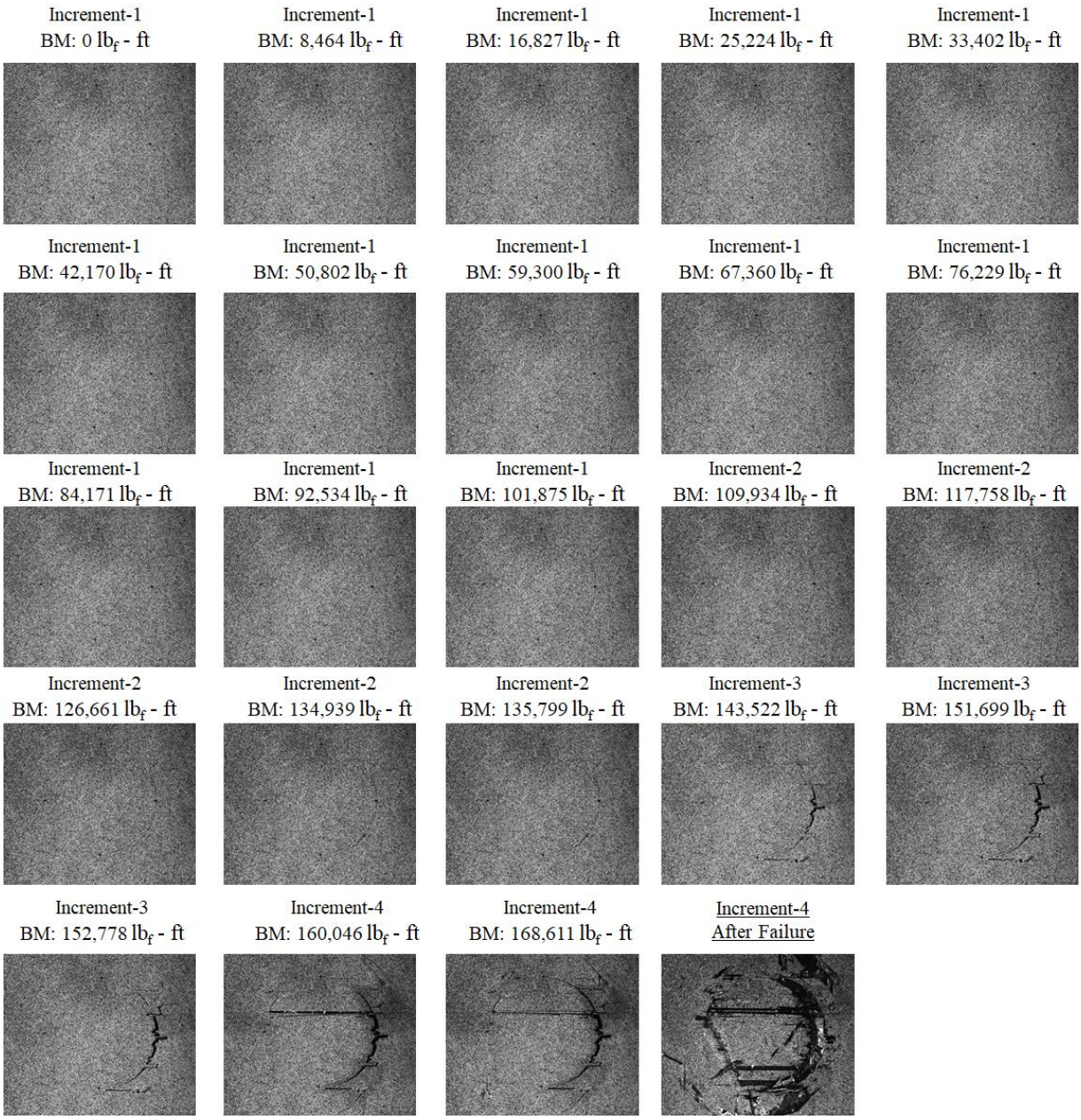


Figure E 2. Panel 3 visual results using NFOV camera during residual strength test

**CFRP Panel 3 - Partial (Half)-Depth Scarf 1 – Post-Failure Visual Inspection Results**

Top View of Wingbox Structure

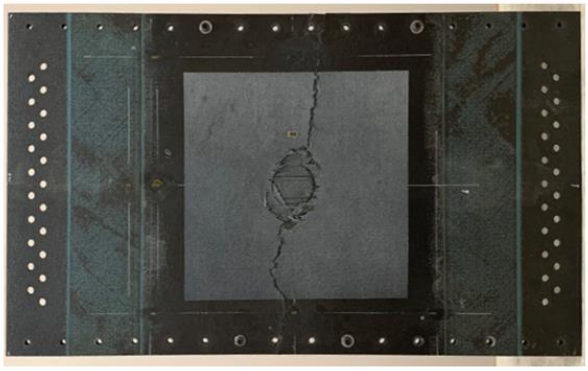

Bottom View of Wingbox Structure

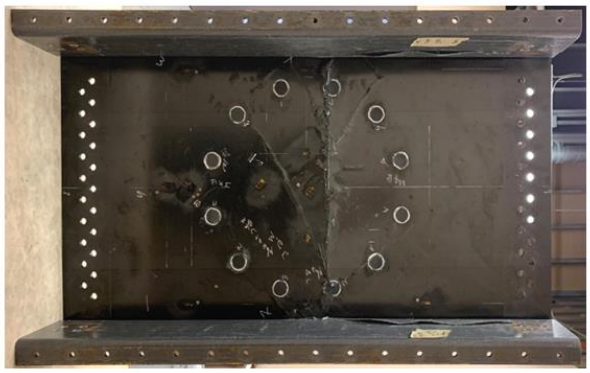

Direct and Perspective Views of the Positive Transverse Side of the Wingbox Structure

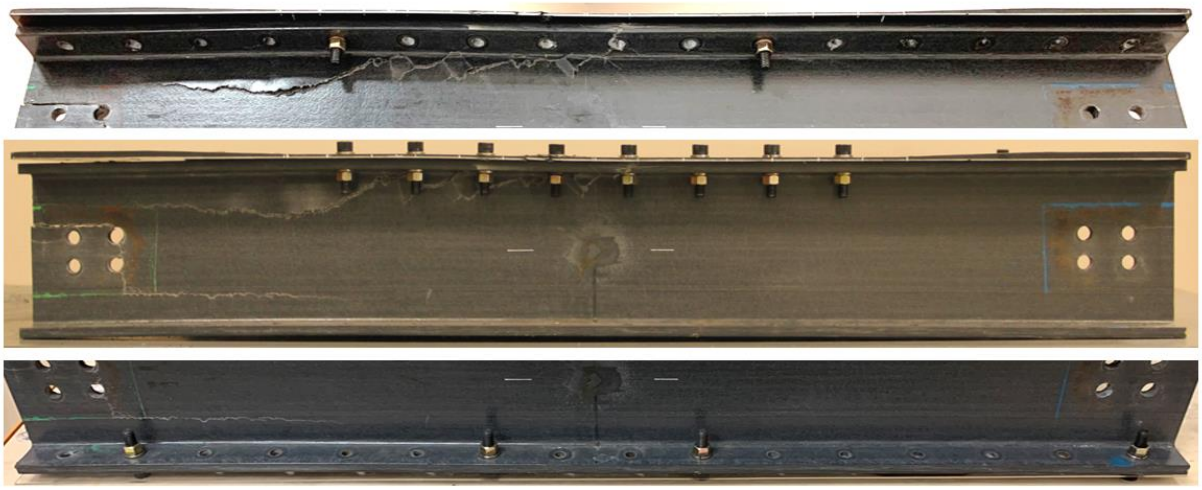

Direct and Perspective Views of the Negative Transverse Side of the Wingbox Structure

Figure E 3. Post-failure images of panel 3 and side-channels

**CFRP Panel 3 - Partial (Half)-Depth Scarf 1 – Post-Failure Visual Inspection Results**

Top View of Wingbox Structure

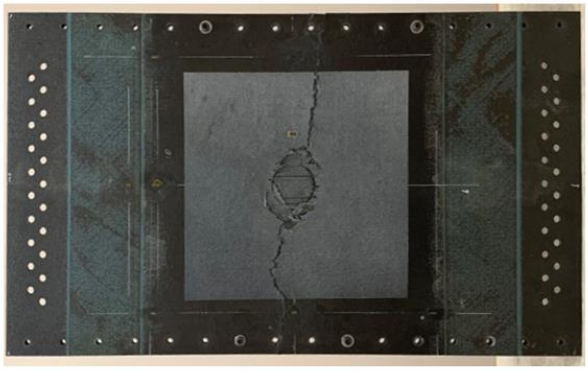

Bottom View of Wingbox Structure

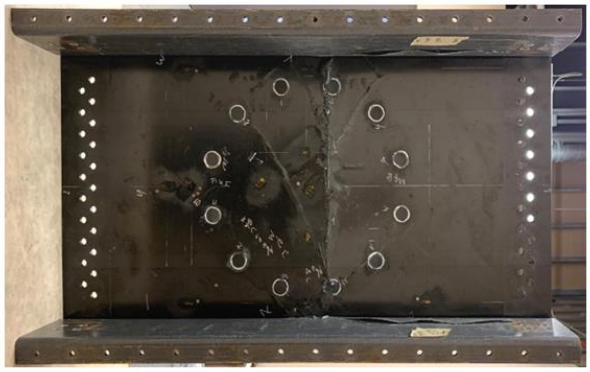

Test Section, Top Surface of Panel

Test Section, Bottom Surface of Panel

Figure E 4. Post-failure images of panel 3

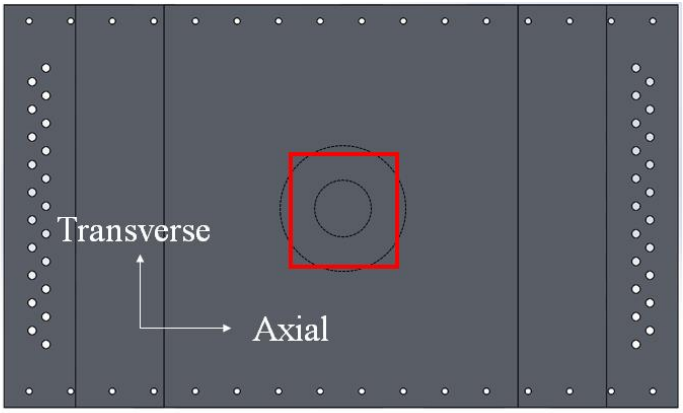


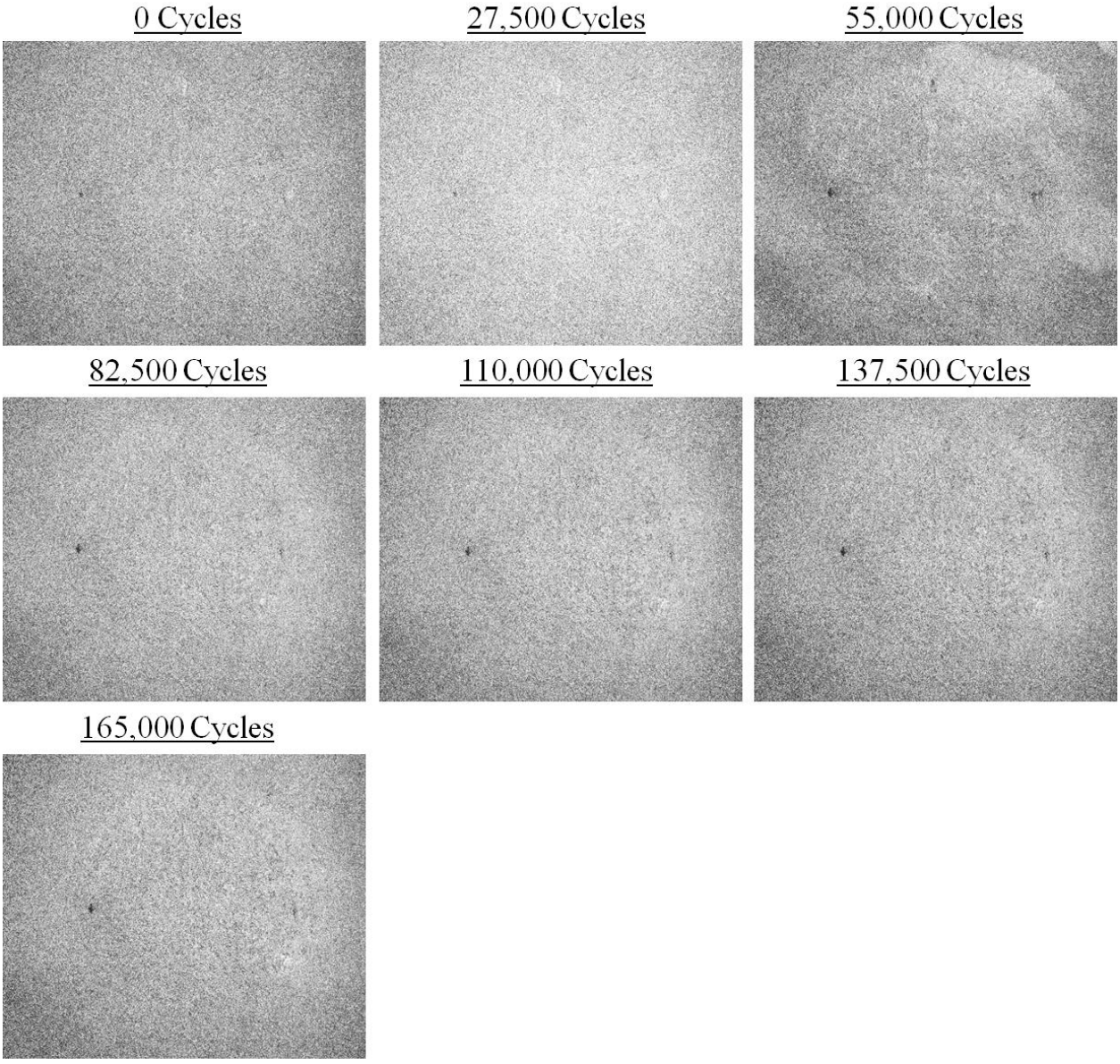


Figure E 5. Images of panel 5 scarf region captured during fatigue at SL strain level

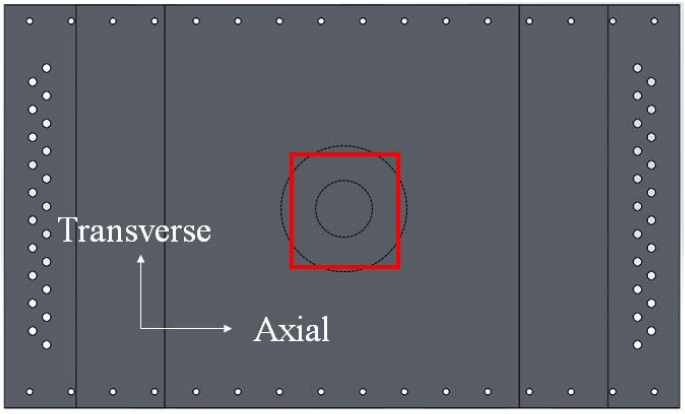


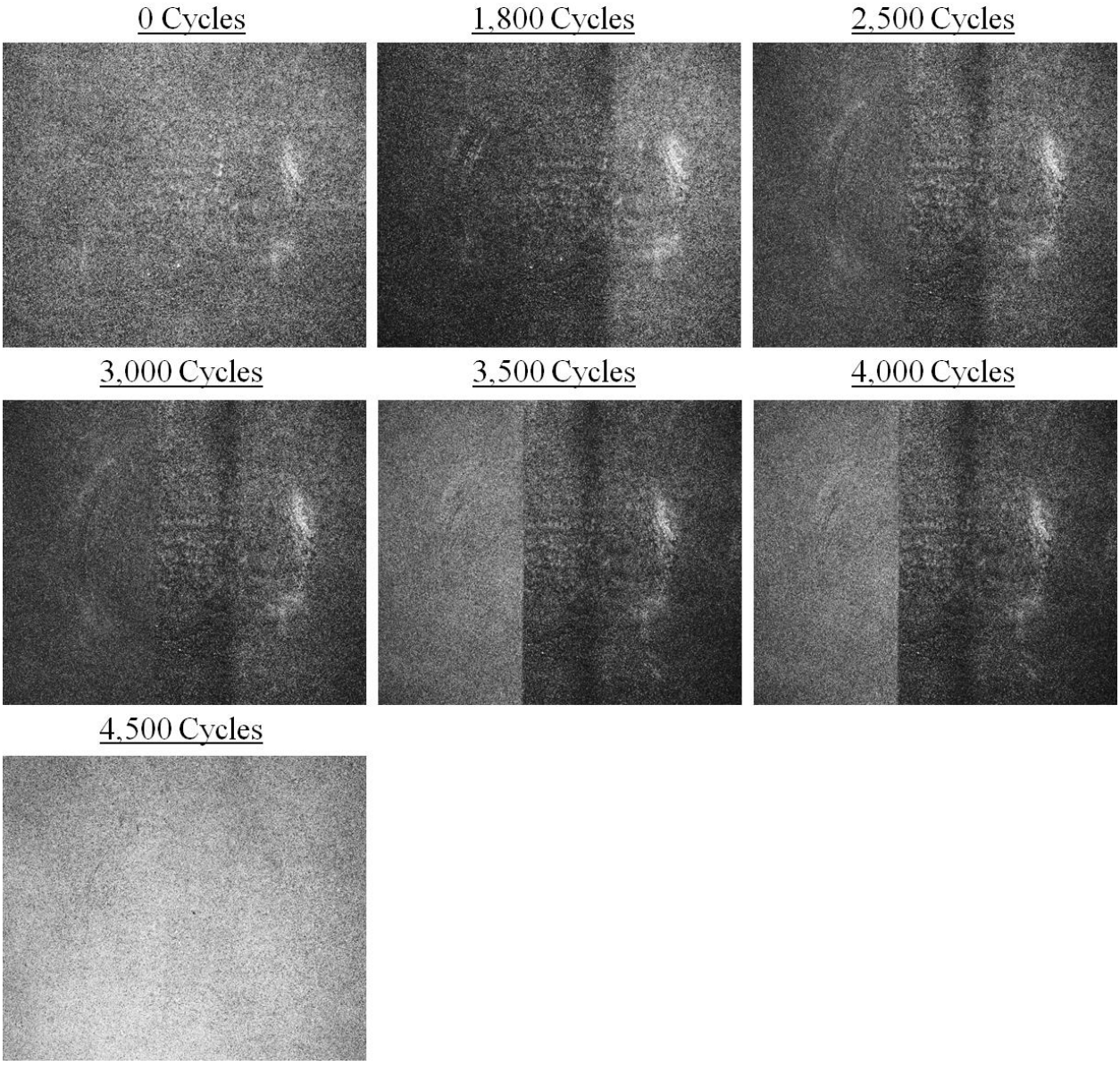


Figure E 6. Images of panel 5 scarf region captured during fatigue at elevated load strain level

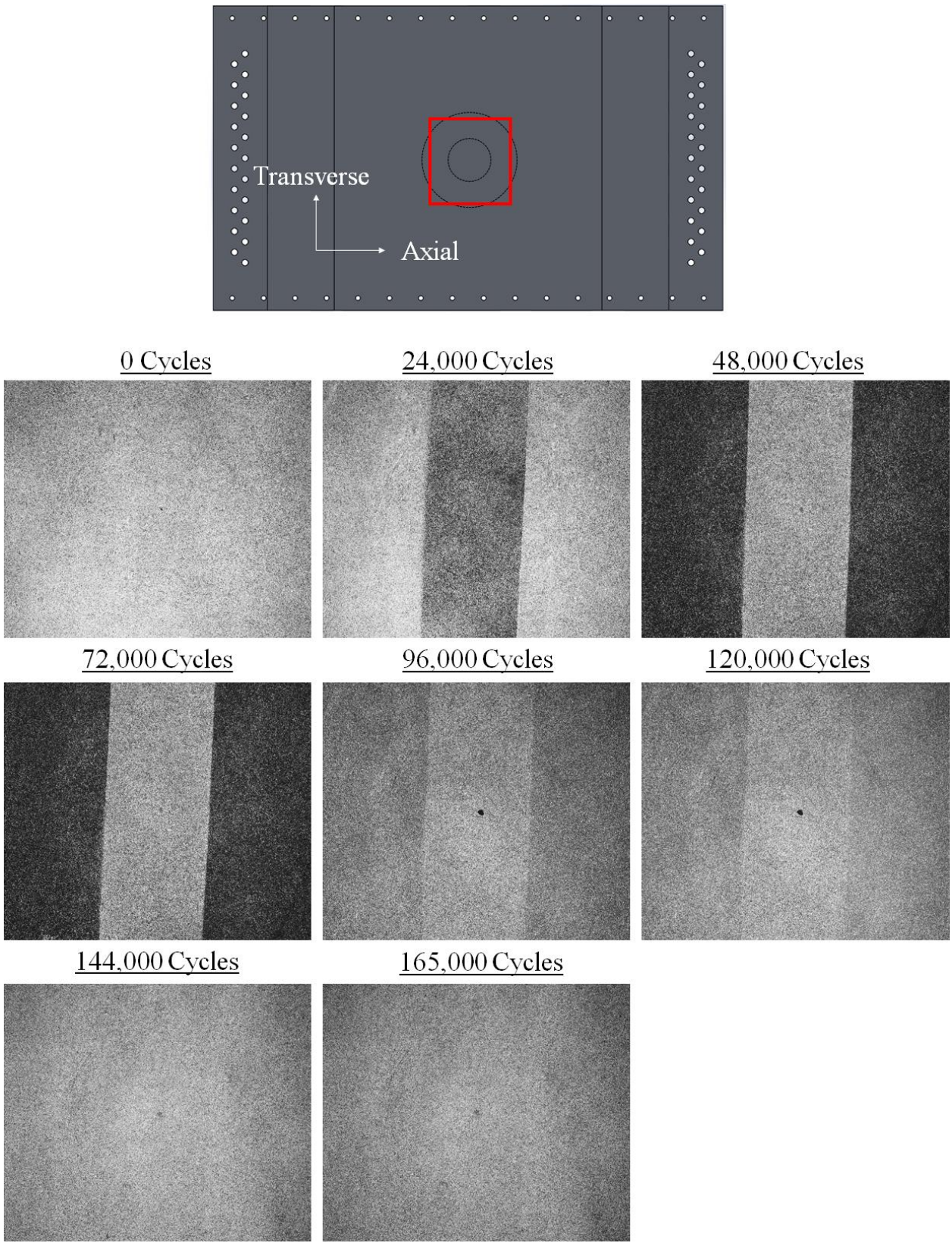


Figure E 7. Images of panel 5 scarf region captured during additional fatigue at SL strain level

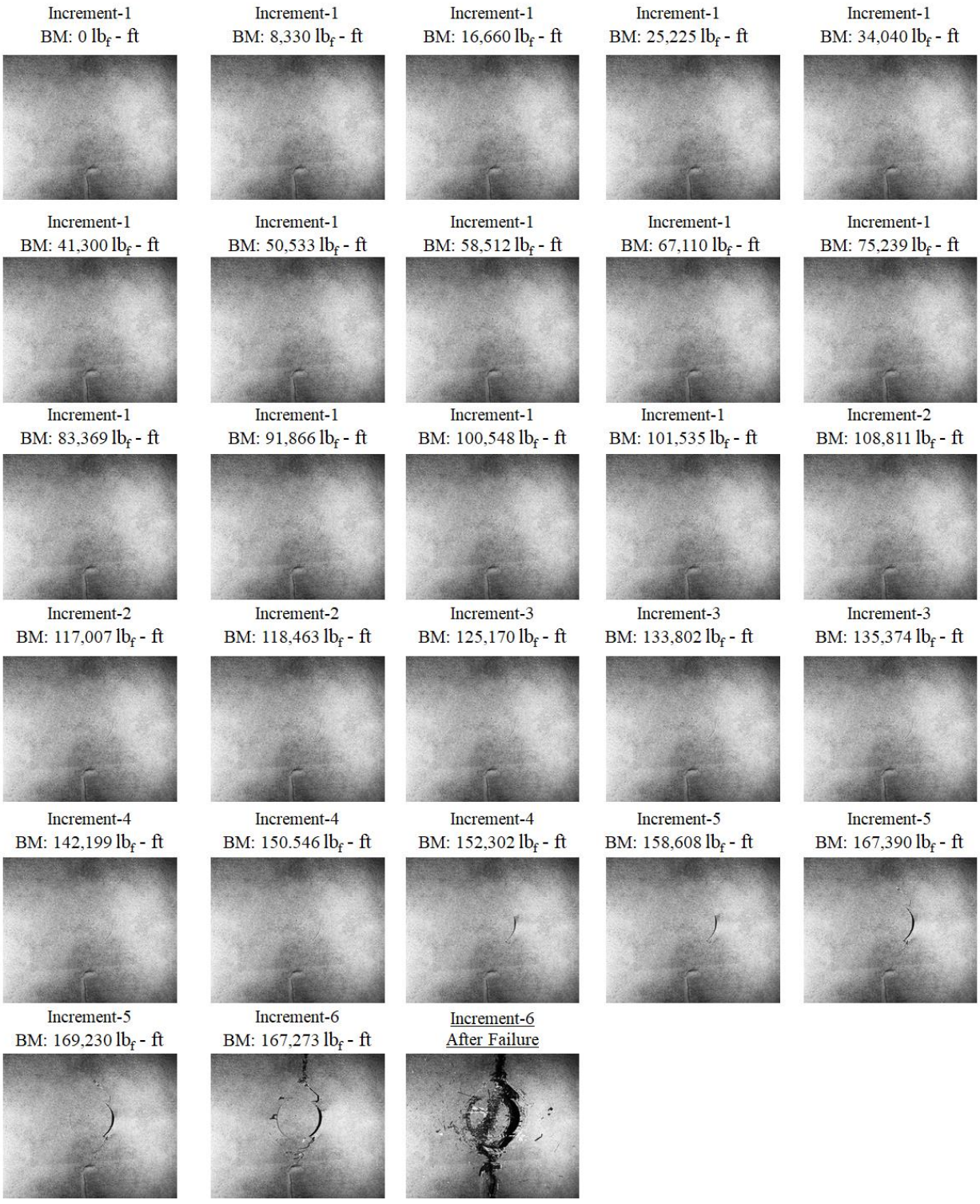


Figure E 8. Panel 5 visual results using WFOV camera during post-fatigue residual strength test

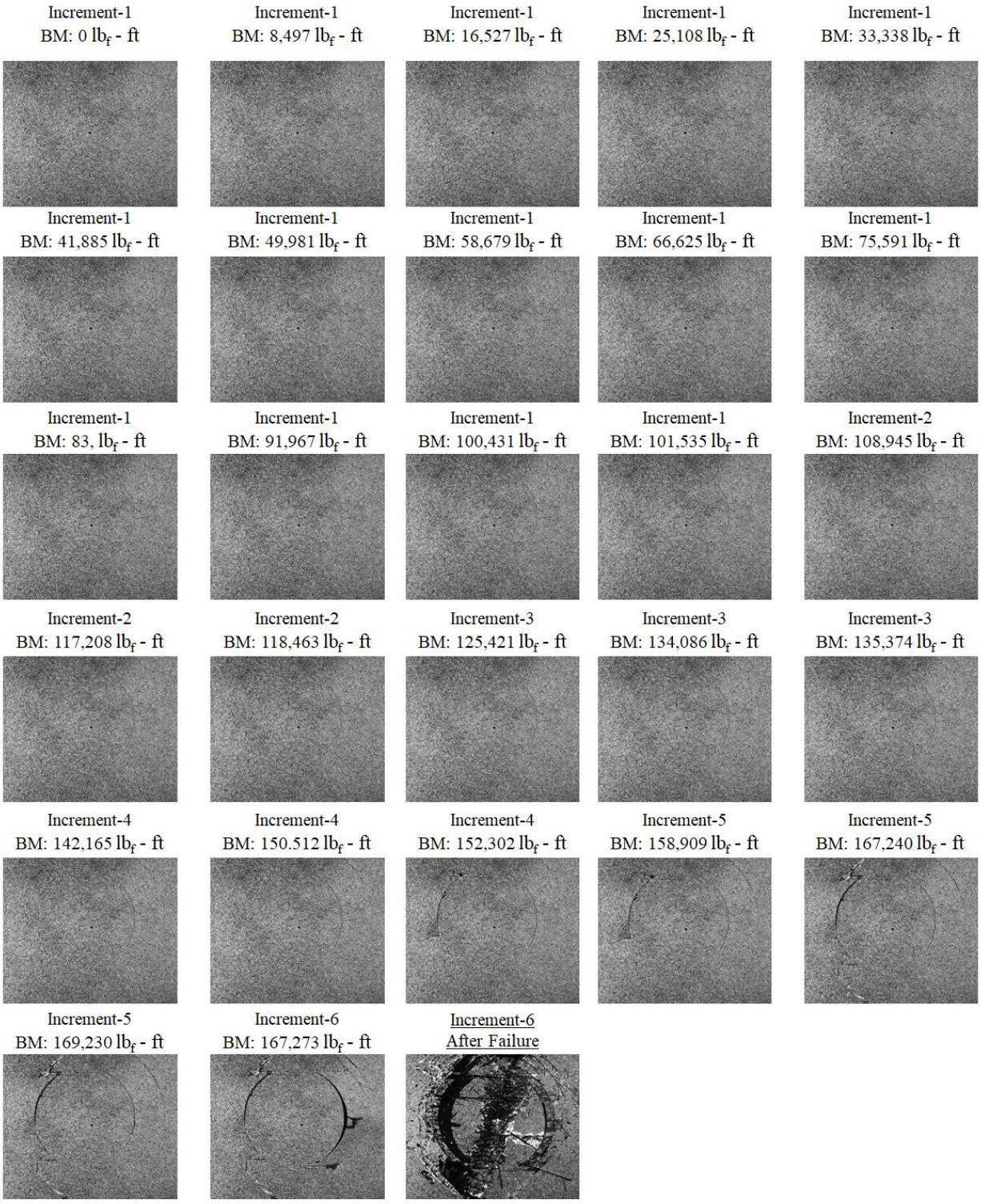


Figure E 9. Panel 5 visual results using NFOV camera during post-fatigue residual strength test

**CFRP Panel 5 - Partial (Half)-Depth Scarf 2 – Post-Failure Visual Inspection Results**

Top View of Wingbox Structure

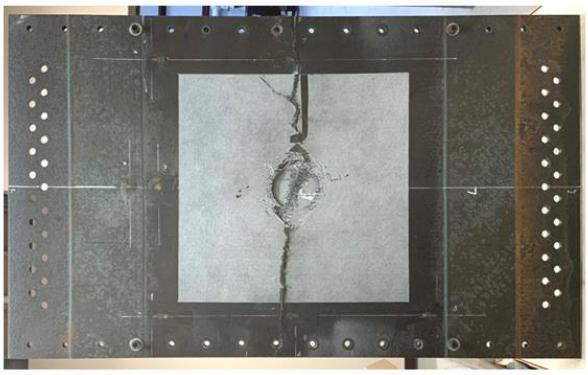

Bottom View of Wingbox Structure

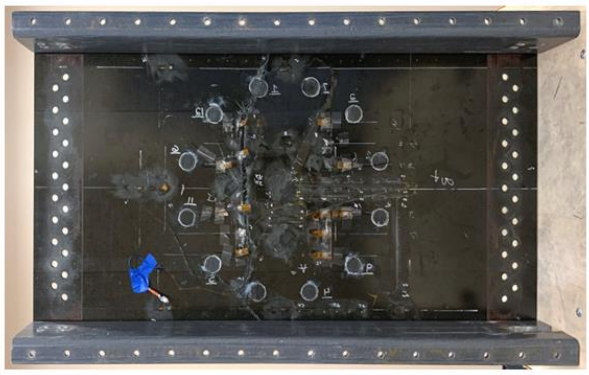

Direct and Perspective Views of the Positive Transverse Side of the Wingbox Structure

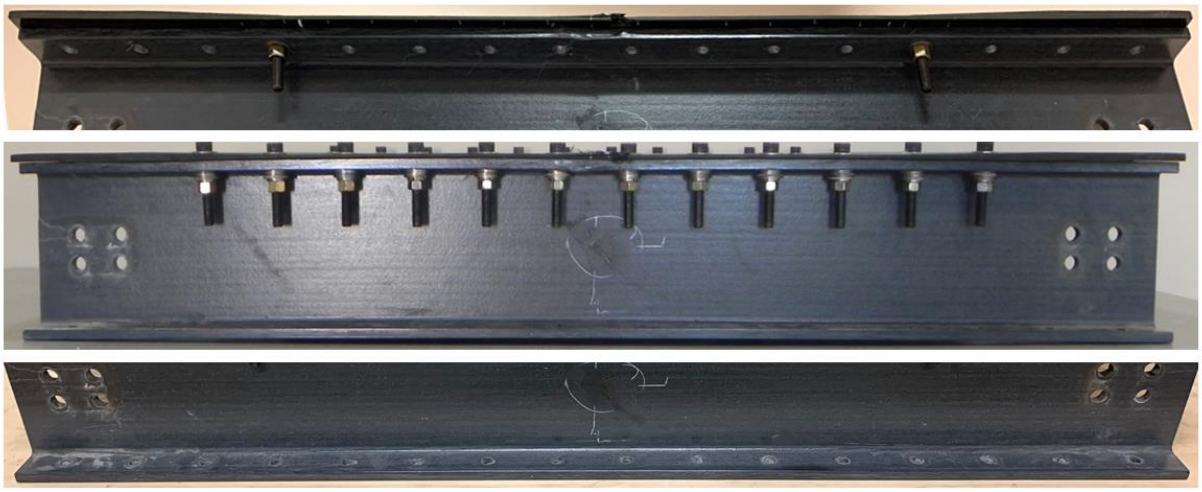

Direct and Perspective Views of the Negative Transverse Side of the Wingbox Structure

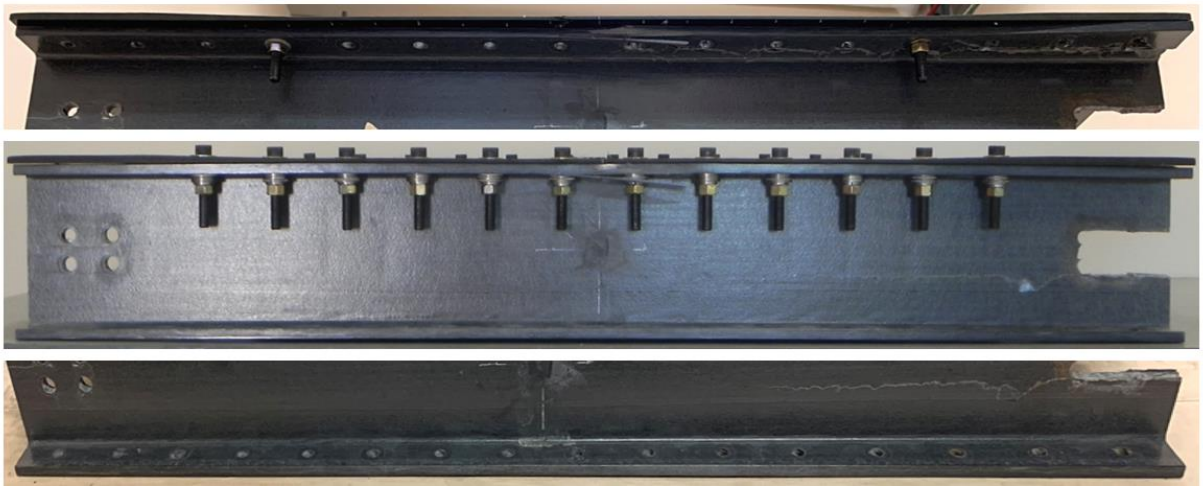

Figure E 10. Post-failure images of panel 5 and side channels

**CFRP Panel 5 - Partial (Half)-Depth Scarf 2 – Post-Failure Visual Inspection Results**

Top View of Wingbox Structure

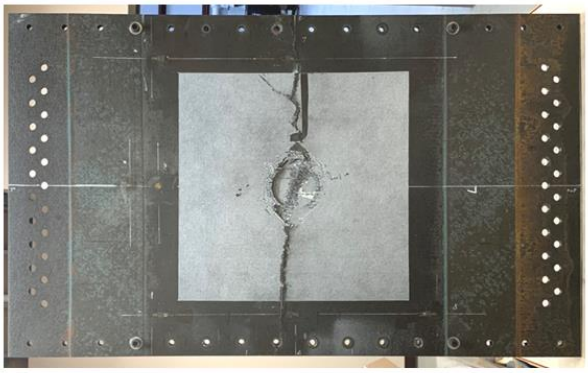

Bottom View of Wingbox Structure

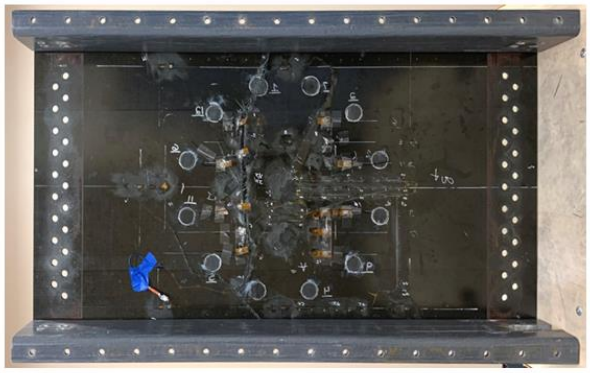

Test Section, Top Surface of Panel

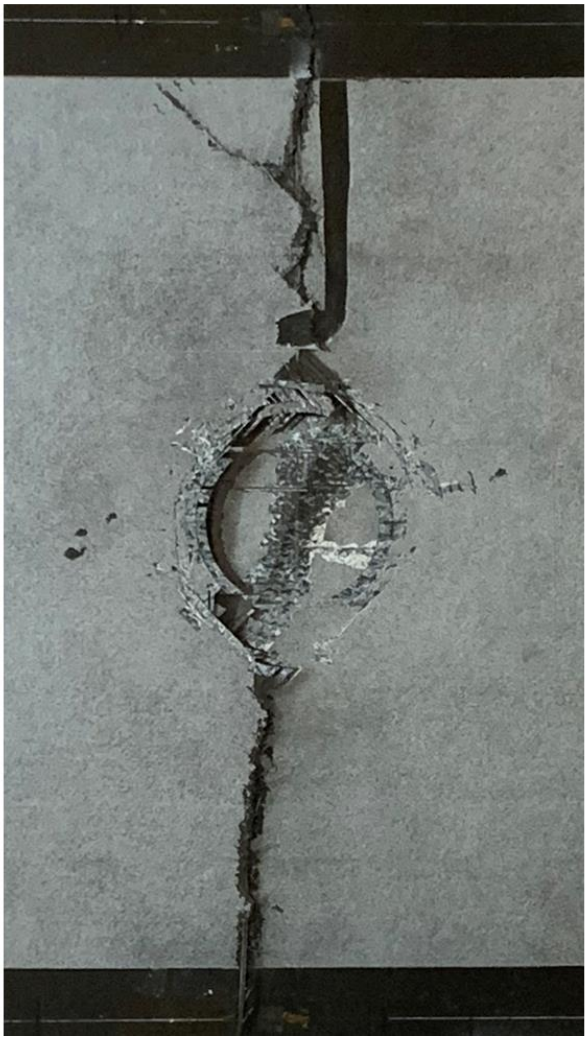

Test Section, Bottom Surface of Panel

Figure E 11. Post-failure images of panel 5

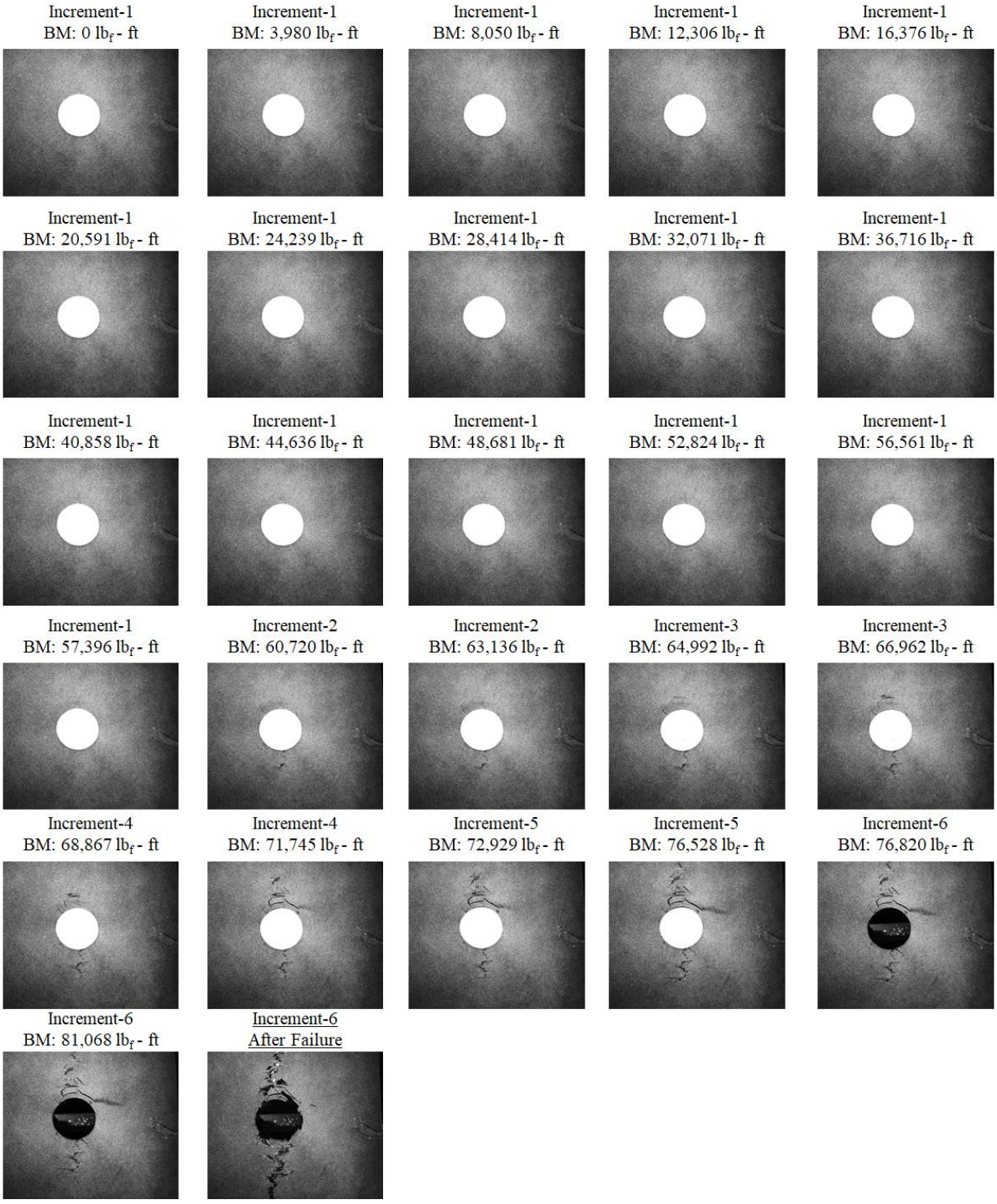


Figure E 12. Panel 4 visual results using WFOV camera during residual strength test


Figure E 13. Panel 4 visual results using NFOV camera during residual strength test

**CFRP Panel 4 - Full-Depth Scarf 1 – Post-Failure Visual Inspection Results**

Top View of Wingbox Structure

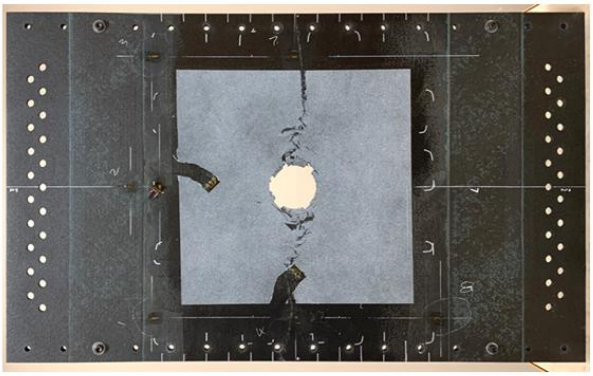

Bottom View of Wingbox Structure

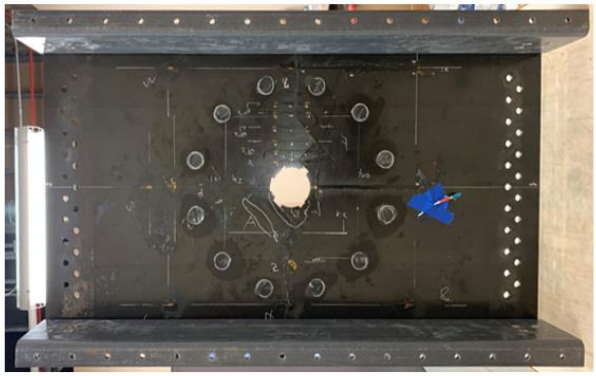

Direct and Perspective Views of the Positive Transverse Side of the Wingbox Structure

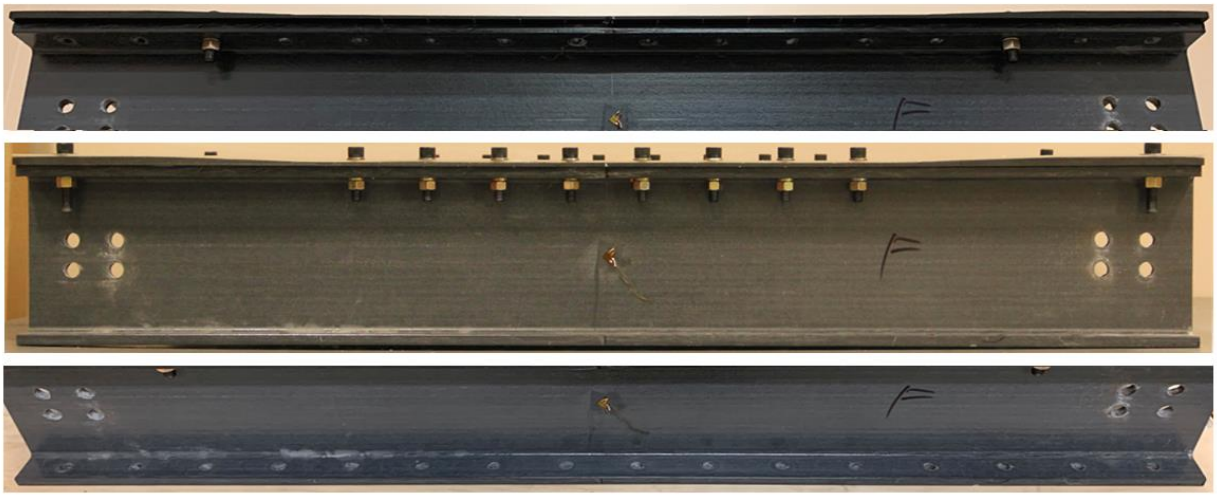

Direct and Perspective Views of the Negative Transverse Side of the Wingbox Structure

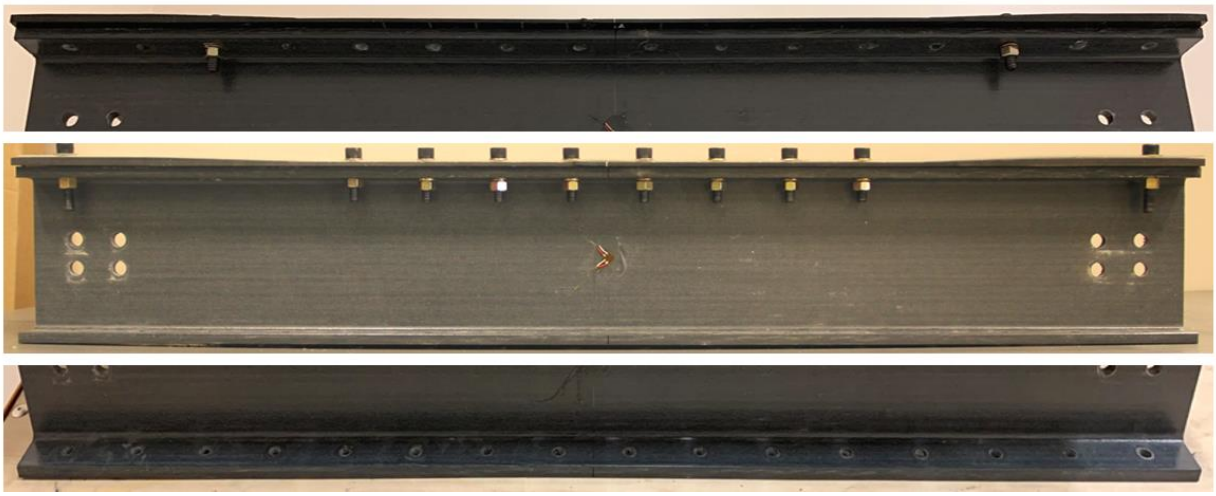

Figure E 14. Post-failure images of panel 4 and side channels

**CFRP Panel 4 - Full-Depth Scarf 1 – Post-Failure Visual Inspection Results**

Top View of Wingbox Structure

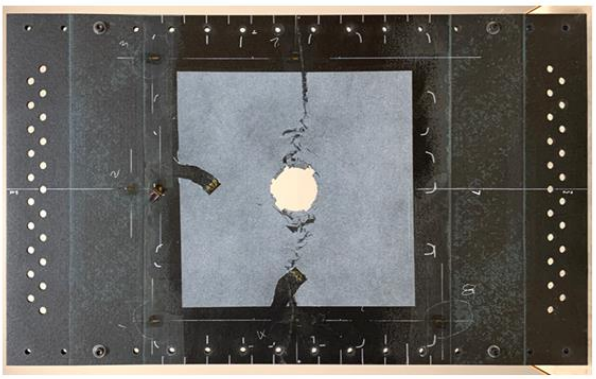

Bottom View of Wingbox Structure

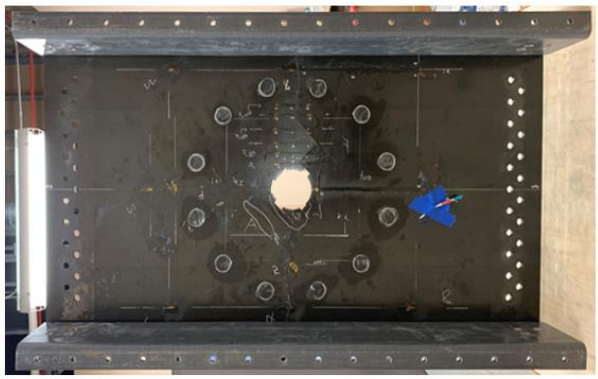

Test Section, Top Surface of Panel

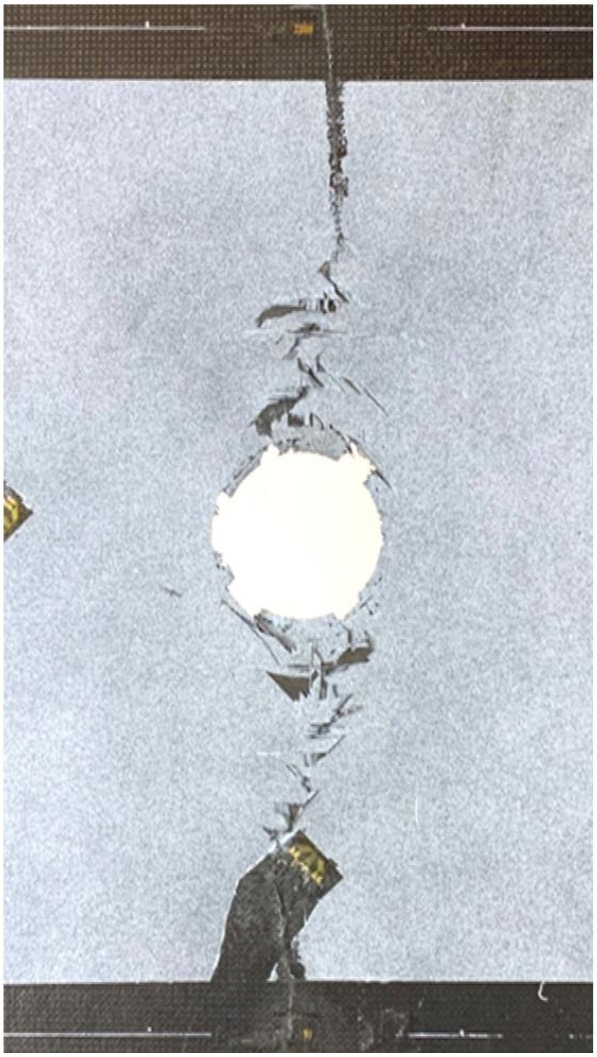

Test Section, Bottom Surface of Panel

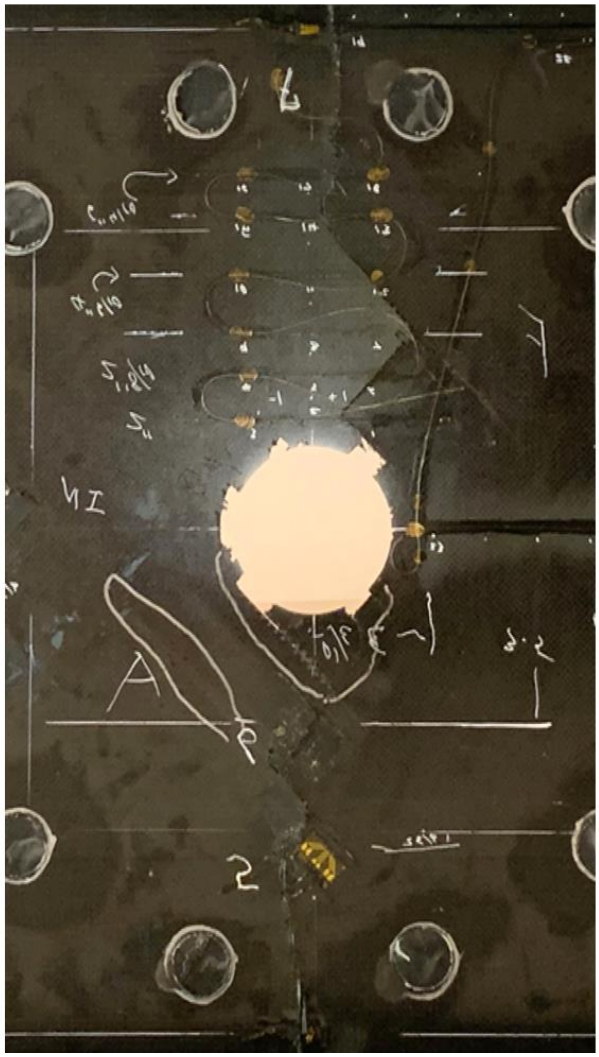

Figure E 15. Post-failure images of panel 4

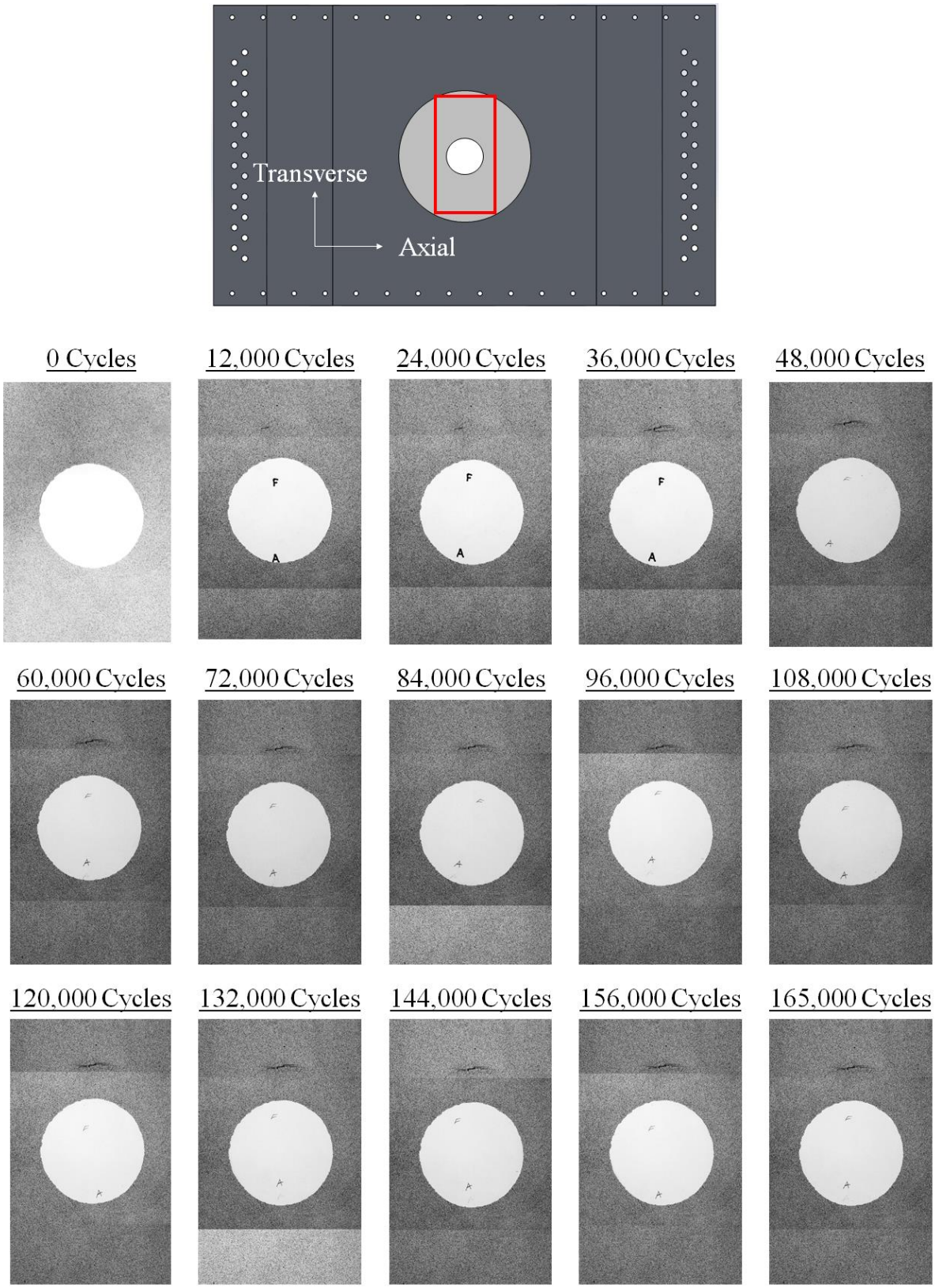


Figure E 16. Images of panel 6 scarf region captured during fatigue at SL strain level

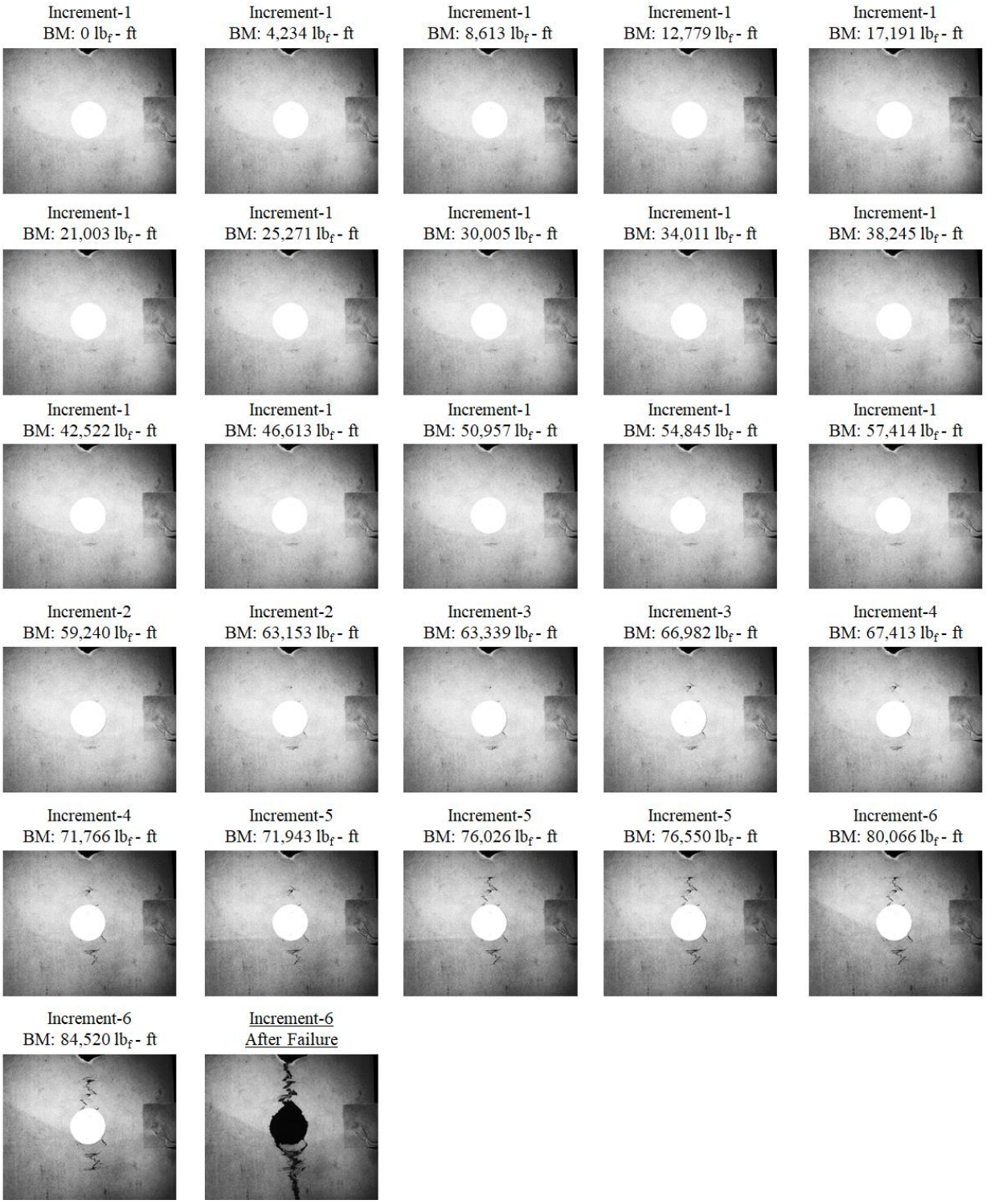


Figure E 17. Panel 6 visual results using WFOV camera during post-fatigue residual strength test


Figure E 18. Panel 6 visual results using NFOV camera during post-fatigue residual strength test

**CFRP Panel 6 - Full-Depth Scarf 2 – Post-Failure Visual Inspection Results**

Top View of Wingbox Structure

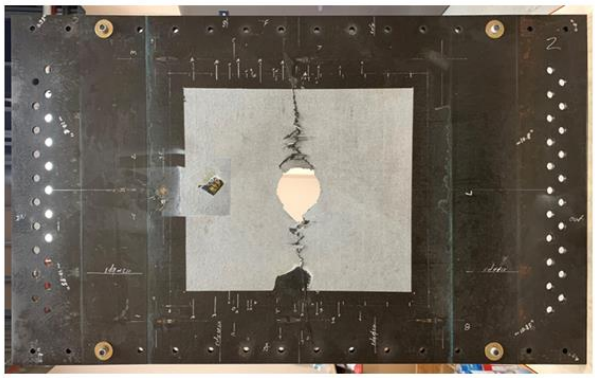

Bottom View of Wingbox Structure

Direct and Perspective Views of the Positive Transverse Side of the Wingbox Structure

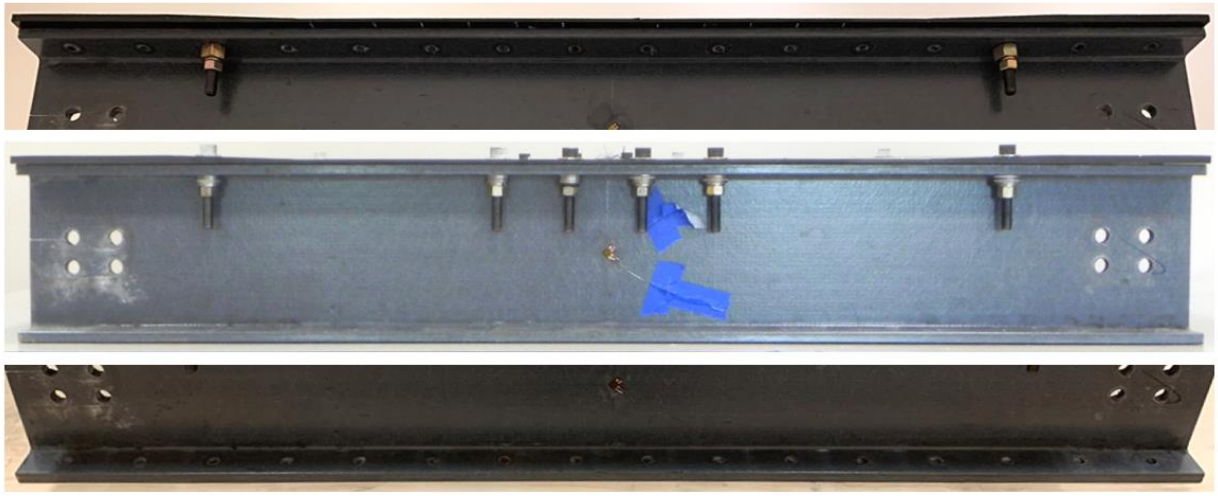

Direct and Perspective Views of the Negative Transverse Side of the Wingbox Structure

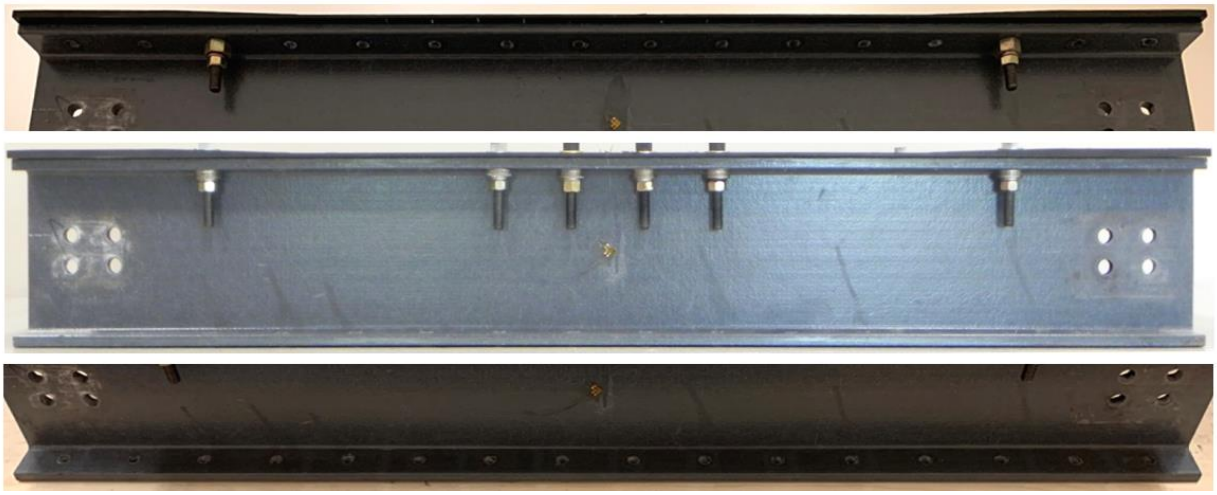

Figure E 19. Post-failure images of panel 6 and side channels

**CFRP Panel 6 - Full-Depth Scarf 2 – Post-Failure Visual Inspection Results**

Top View of Wingbox Structure

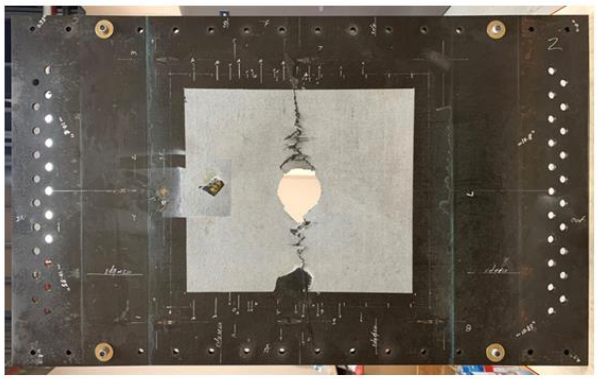

Bottom View of Wingbox Structure

Test Section, Top Surface of Panel

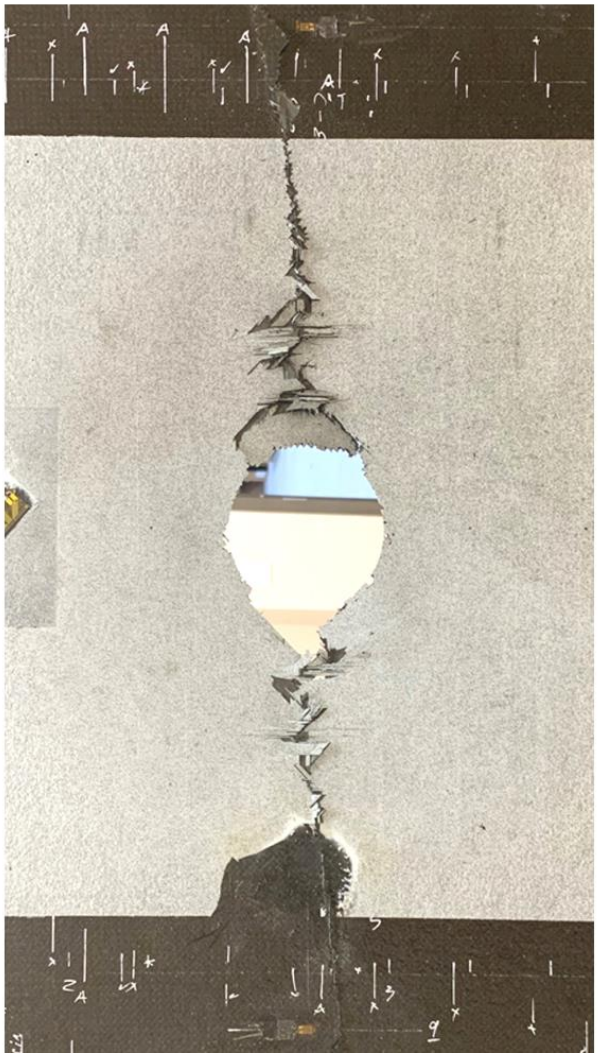

Test Section, Bottom Surface of Panel

Figure E 20. Post-failure images of panel 6

# F Flash thermography results

This appendix provides the flash thermography results captured throughout residual strength loading of panels 3 and 4, and fatigue and residual strength loading of panels 5 and 6.

Results captured during residual strength loading for panel 3 is shown in Figure F 1. Figure F 2, Figure F 3, Figure F 4, and Figure F 6 show results during fatigue at SL strain level, fatigue at elevated load strain level, additional fatigue at SL strain level, and post-fatigue residual strength test for panel 5. For panel 4, residual strength loading results are shown in Figure F 5. For panel 6, Figure F 7–Figure F 9 shows thermography results collected during fatigue at SL strain level, and Figure F 10 shows the results during post-fatigue residual strength tests.

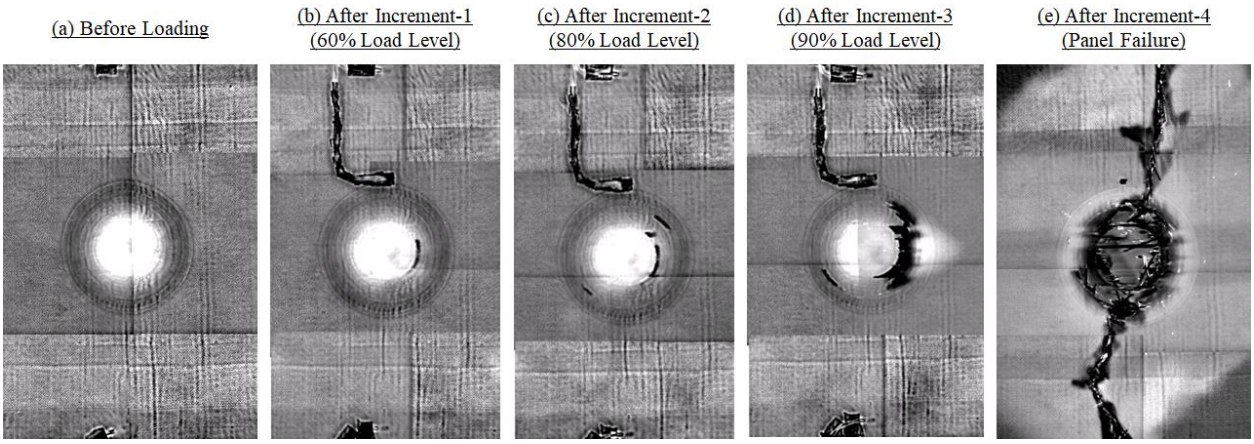


Figure F 1. Panel 3 flash thermography results during residual strength test

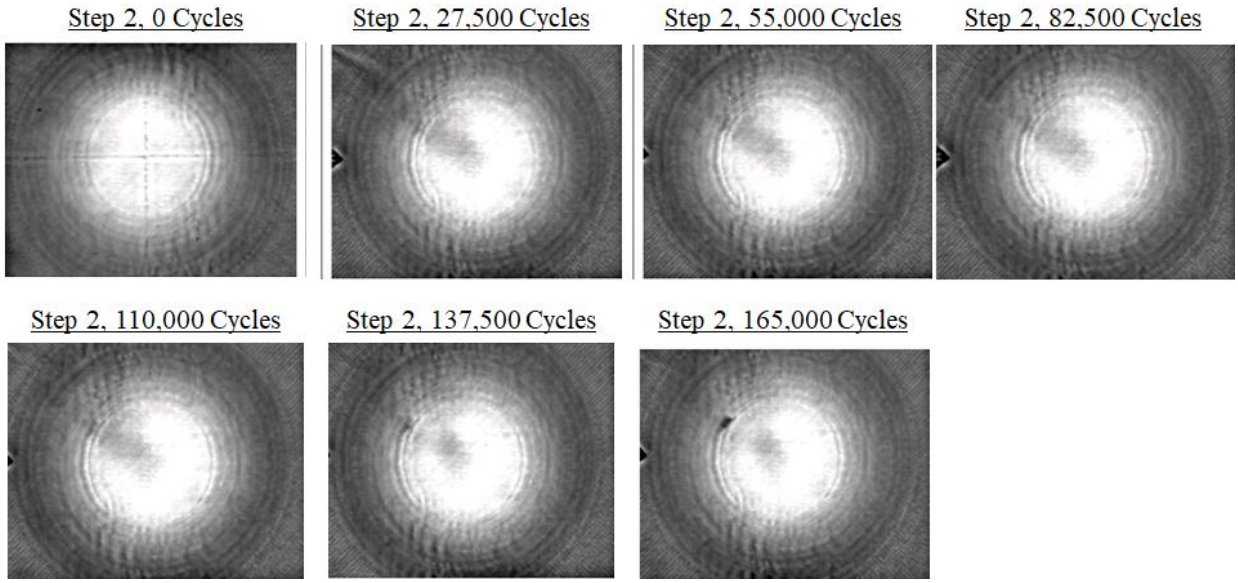


Figure F 2. Panel 5 flash thermography results during fatigue at SL strain level

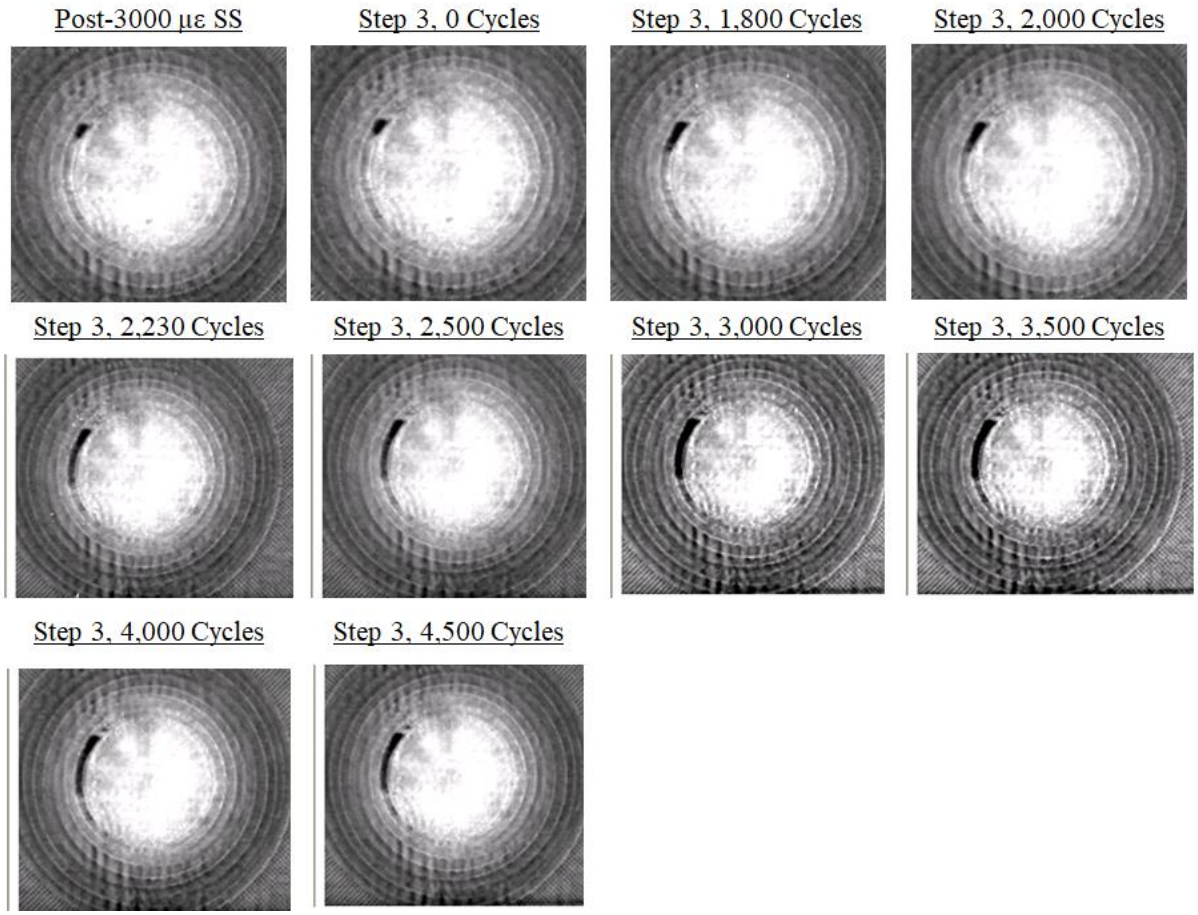


Figure F 3. Panel 5 flash thermography results during fatigue at elevated load strain level

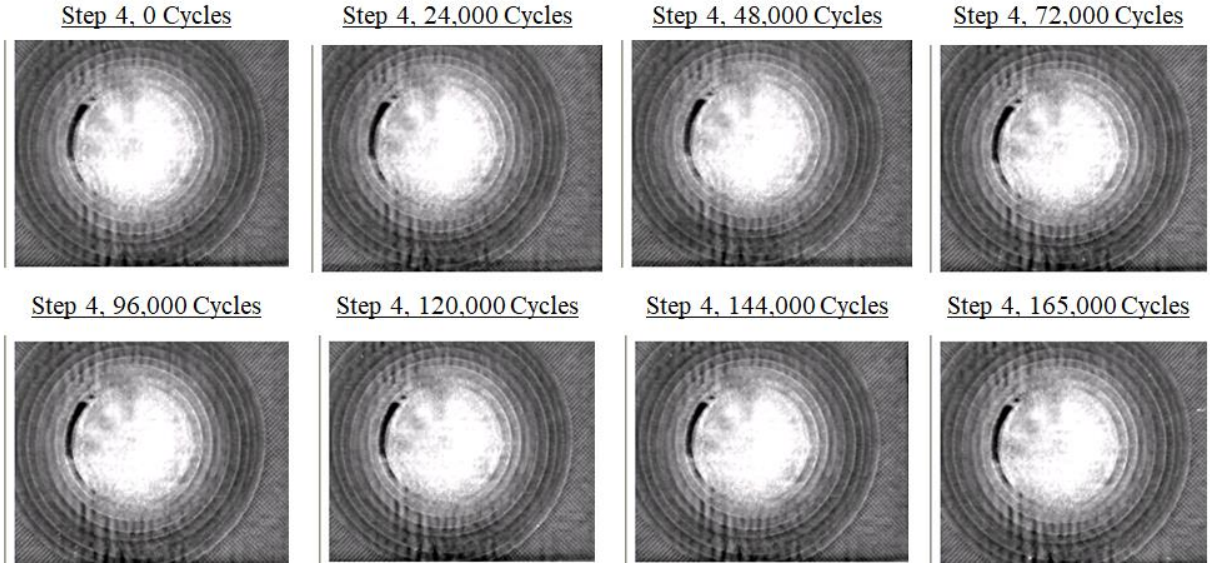


Figure F 4. Panel 5 flash thermography results during additional fatigue at SL strain level

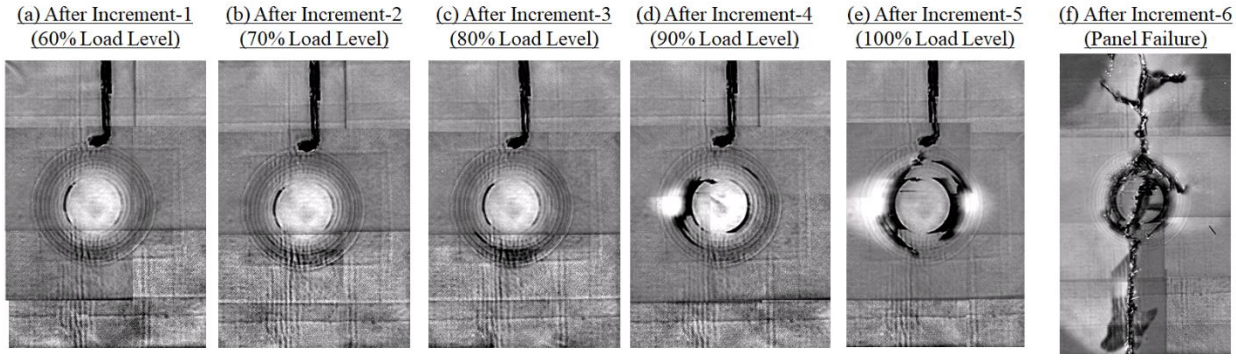


Figure F 5. Panel 5 flash thermography results during post-fatigue residual strength test

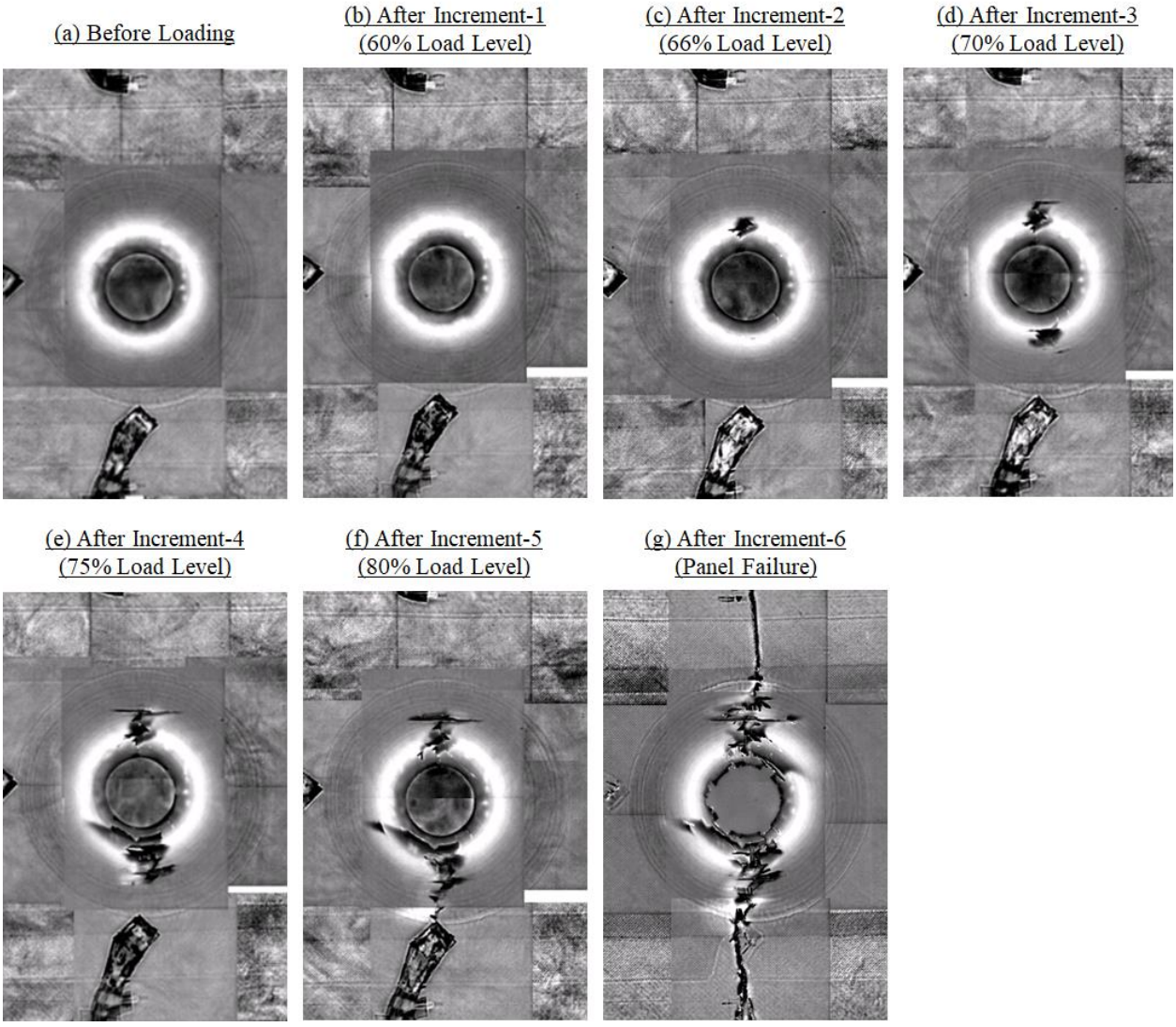


Figure F 6. Panel 4 flash thermography results during residual strength test

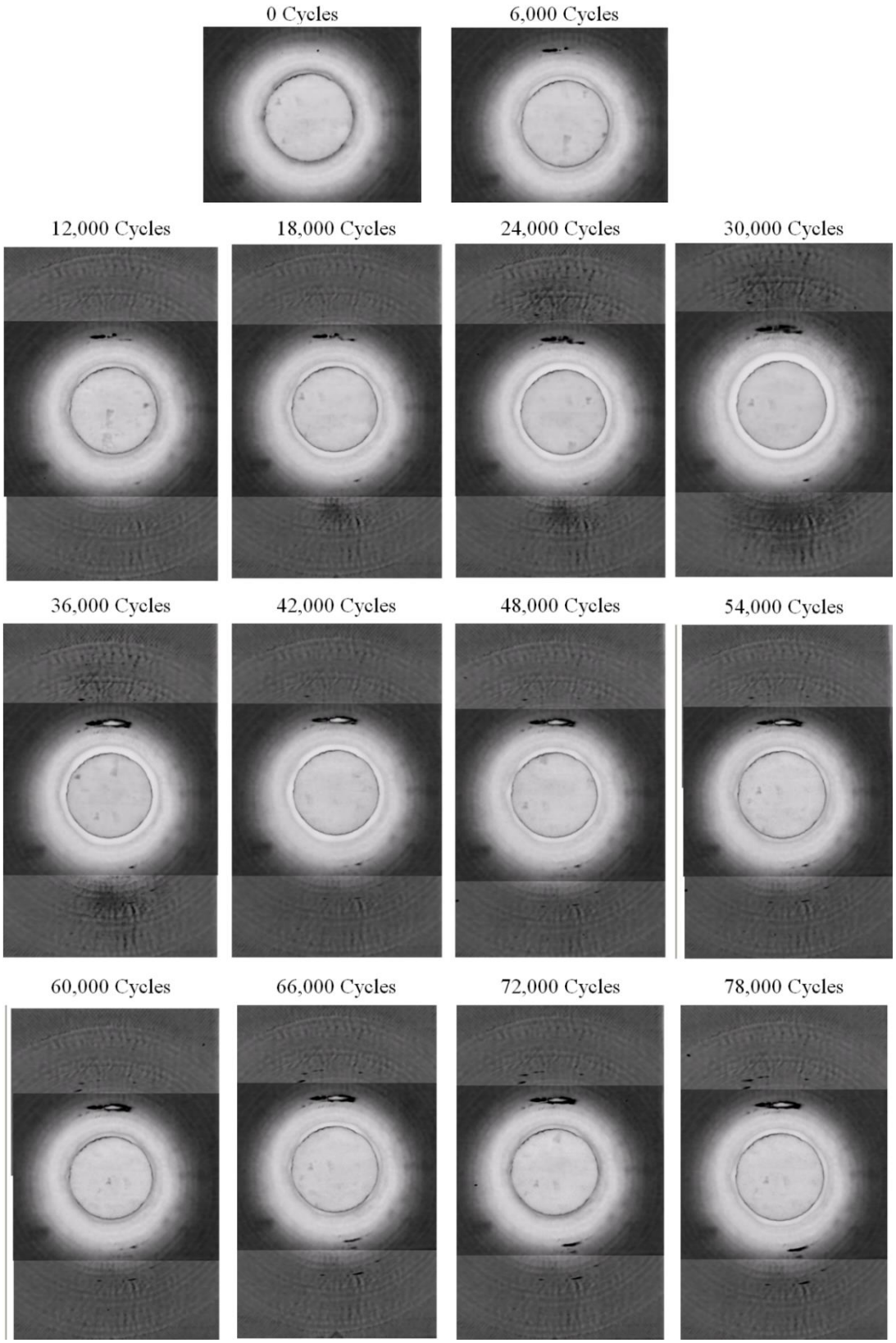


Figure F 7. Panel 6 flash thermography results during fatigue at SL strain level

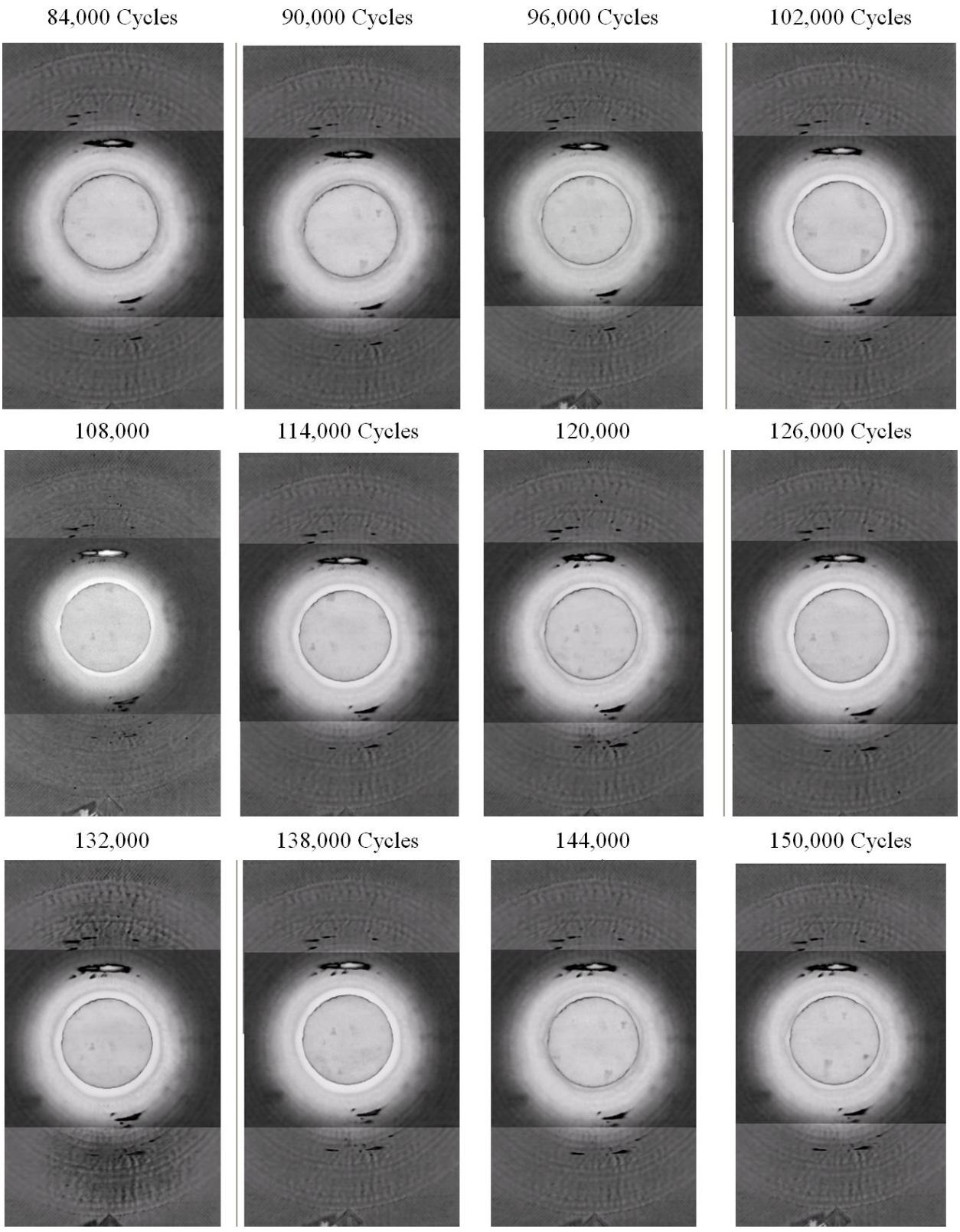


Figure F 8. Panel 6 flash thermography results during fatigue at SL strain level

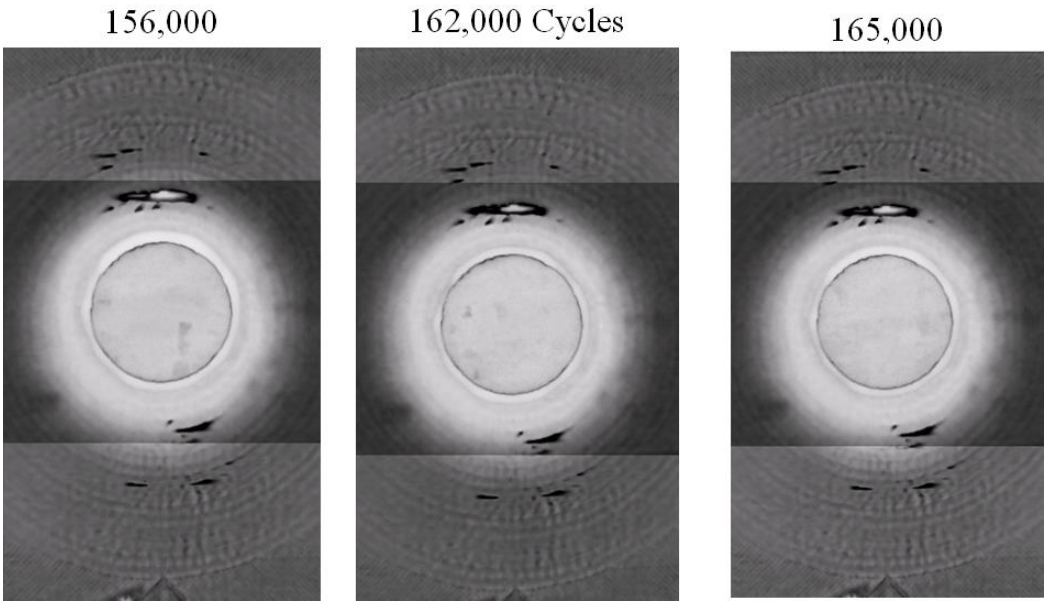

Figure F 9. Panel 6 flash thermography results during fatigue at SL strain level

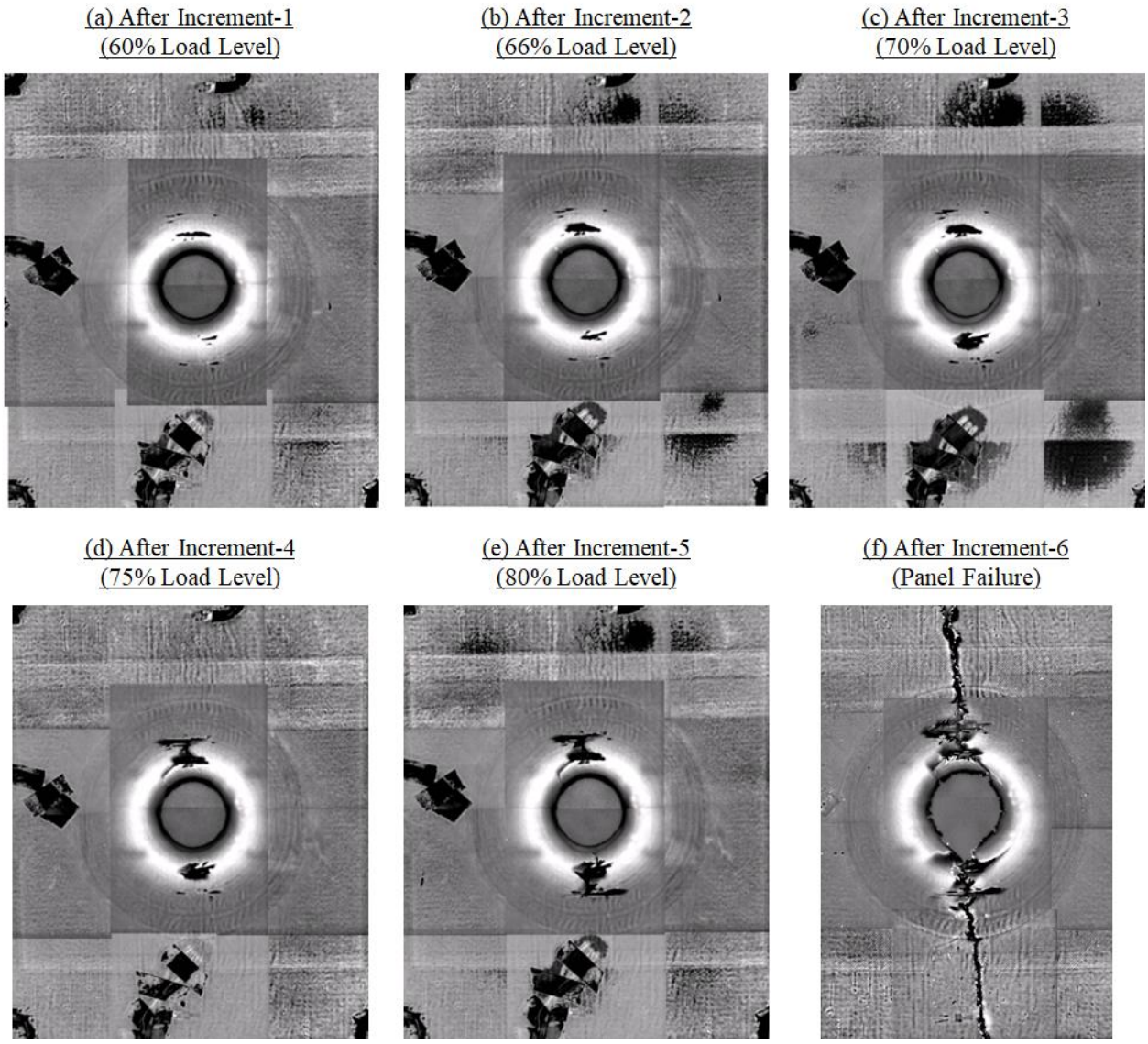


Figure F 10. Panel 6 flash thermography results during post-fatigue residual strength test

# G Phased array ultrasonic results

This appendix presents the phased array ultrasonic results captured throughout testing for panels 3–5.

Phased array results captured for panel 3 during residual strength loading are shown in Figure G 1 and Figure G 2. For panel 5, results captured during three steps of fatigue are shown in Figure G 3 and Figure G 4. For panel 4, residual strength loading, the results are provided in Figure G 6 and Figure G 5.

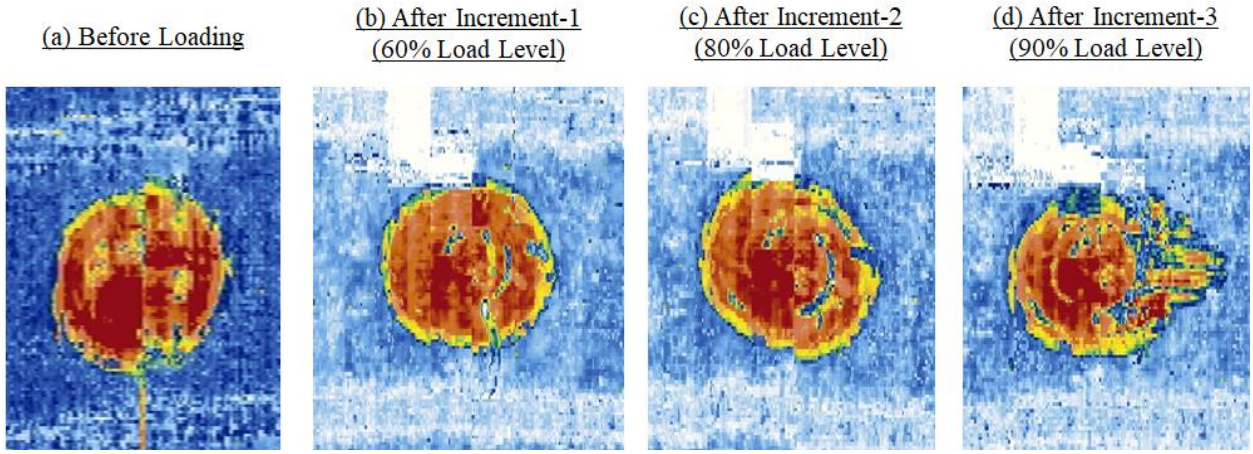


Figure G 1. Panel 3 phased array results (amplitude) during residual strength test

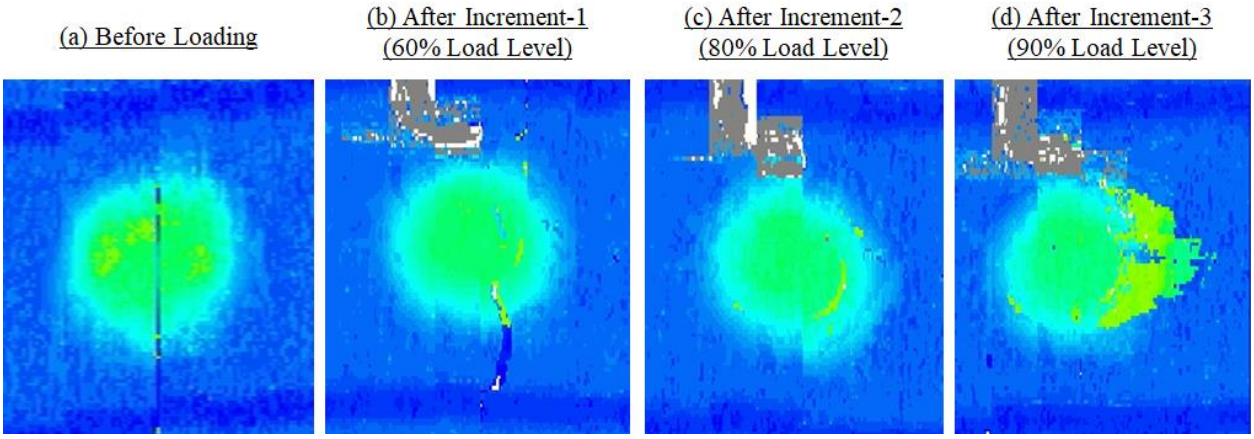


Figure G 2. Panel 3 phased array results (time of flight) during residual strength test

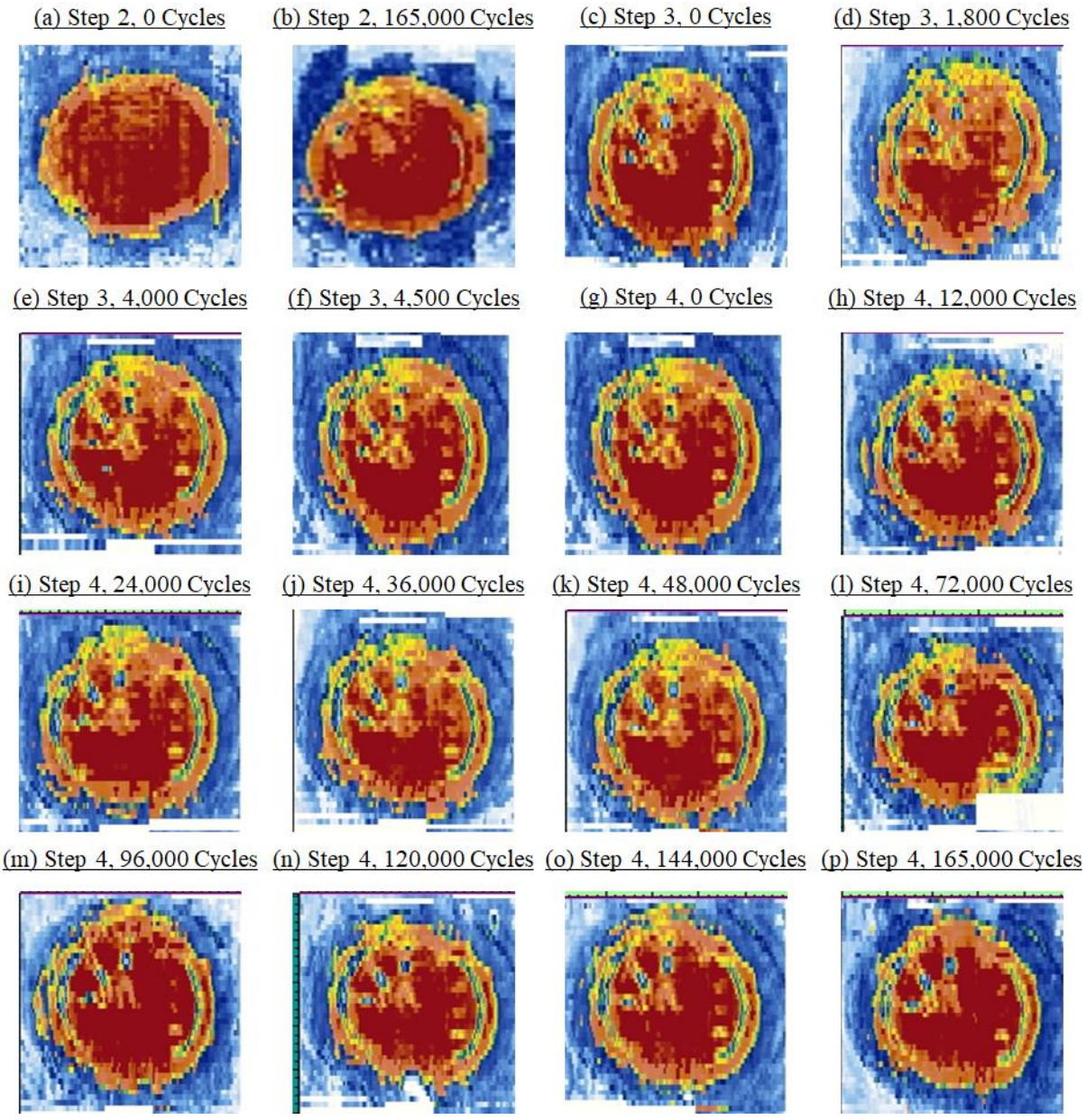


Figure G 3. Panel 5 phased array results (amplitude) during fatigue at SL strain level

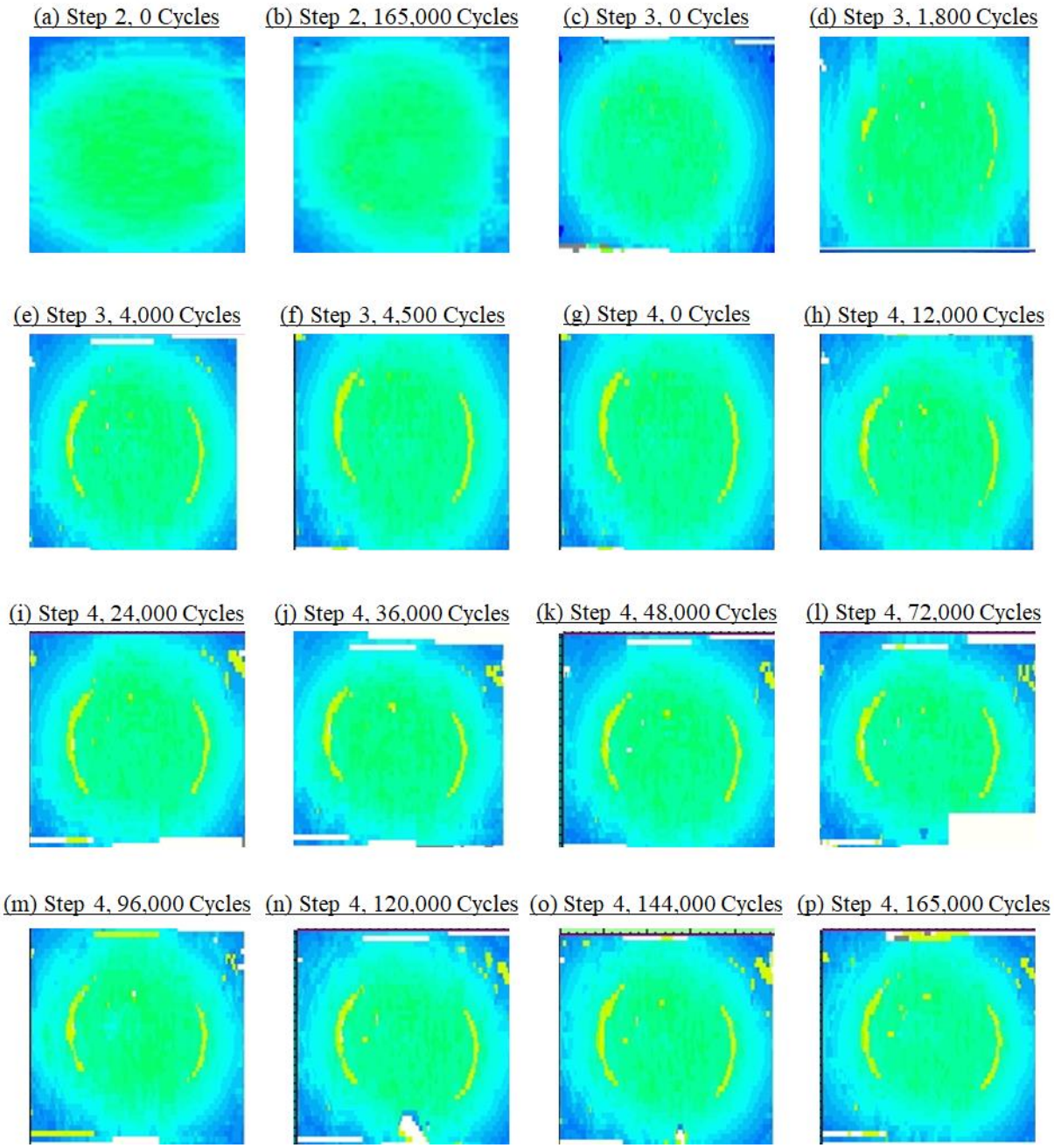


Figure G 4. Panel 5 phased array results (time of flight) during fatigue at SL strain level

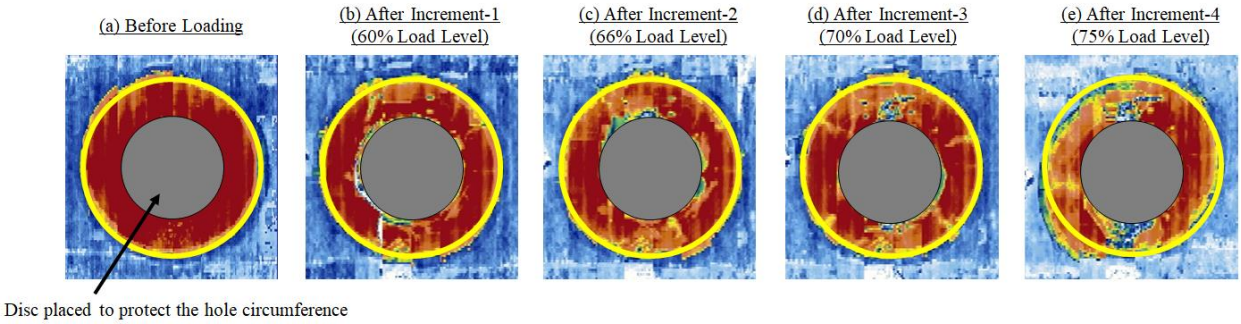


Figure G 6. Panel 4 phased array results (amplitude) during residual strength test

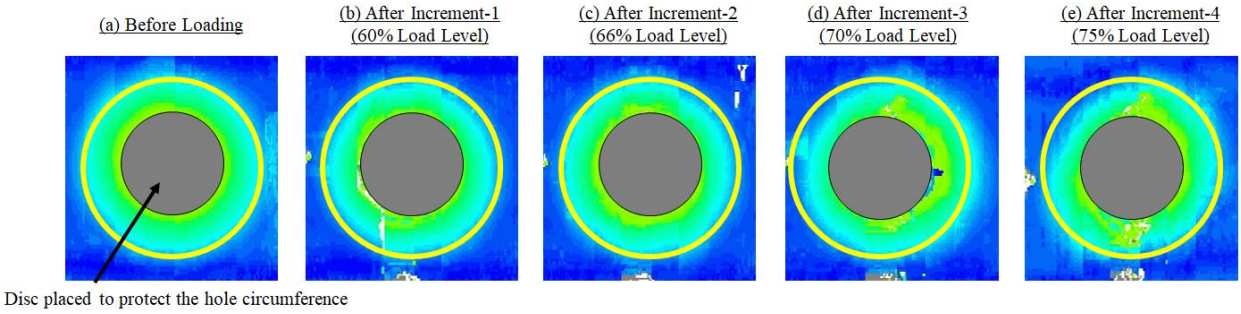


Figure G 5. Panel 4 phased array results (time of flight) during residual strength test

# H Pulse-echo ultrasonic results

This appendix presents the pulse-echo ultrasonic results for the second partial-depth scarf panel captured throughout fatigue loading.

Pulse-echo inspection results for panel 5 during fatigue at SL strain level, fatigue at elevated load strain level and additional fatigue at SL strain level are provided in Figure H 1, Figure H 2, and Figure H 3, respectively.

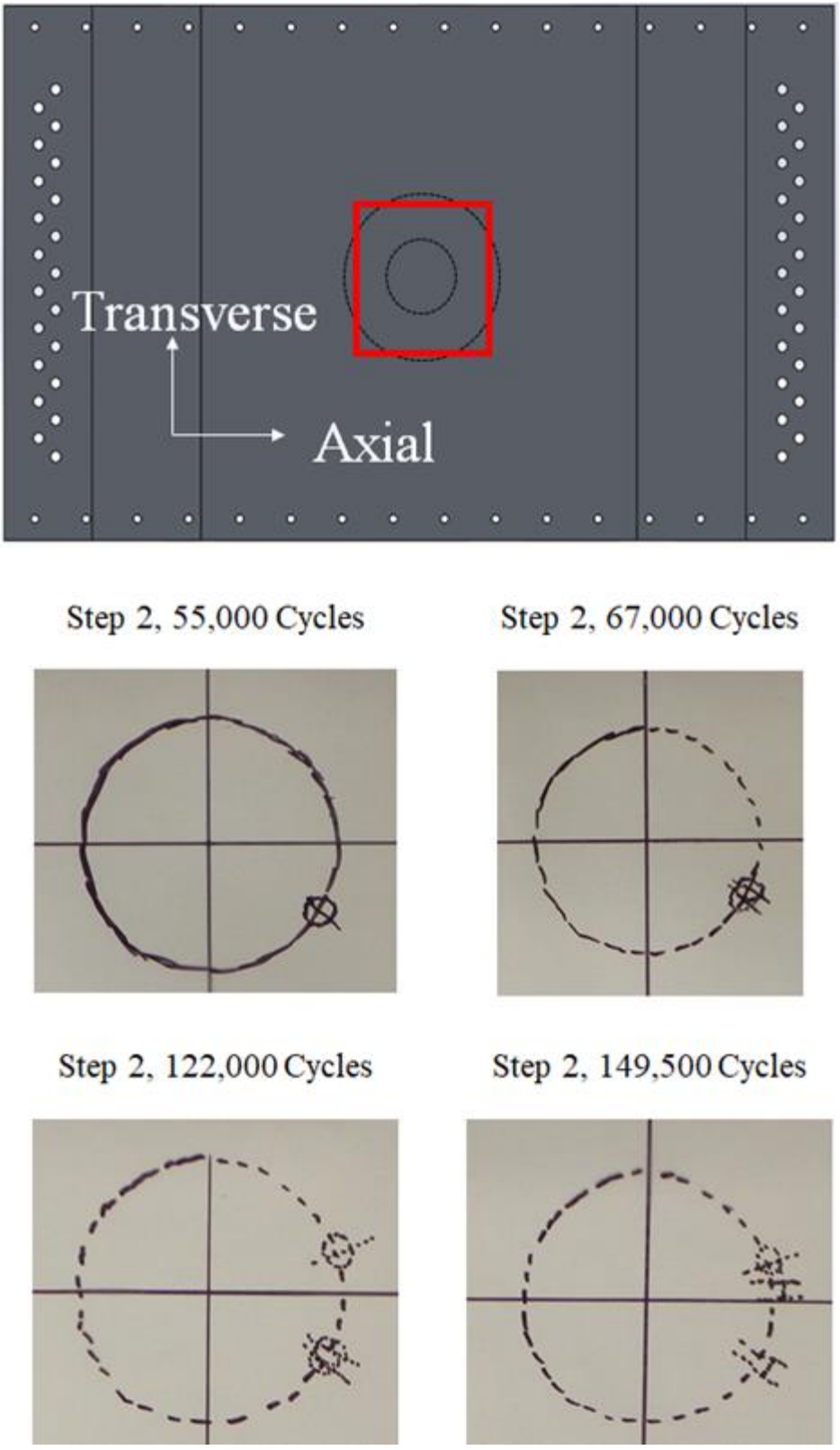


Figure H 1. Panel 5 pulse-echo results during fatigue at SL strain level

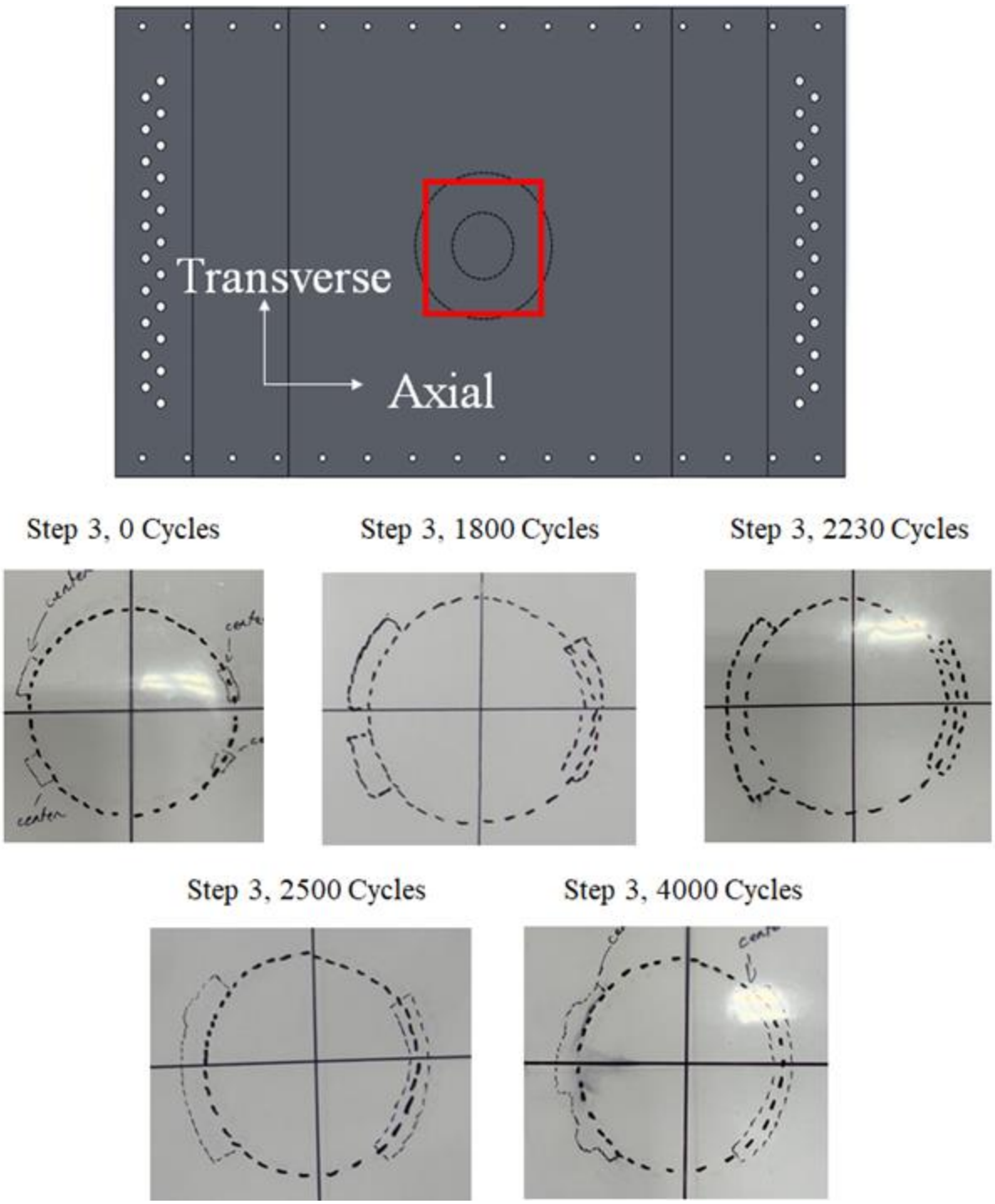


Figure H 2. Panel 5 pulse-echo results during fatigue at elevated load strain level

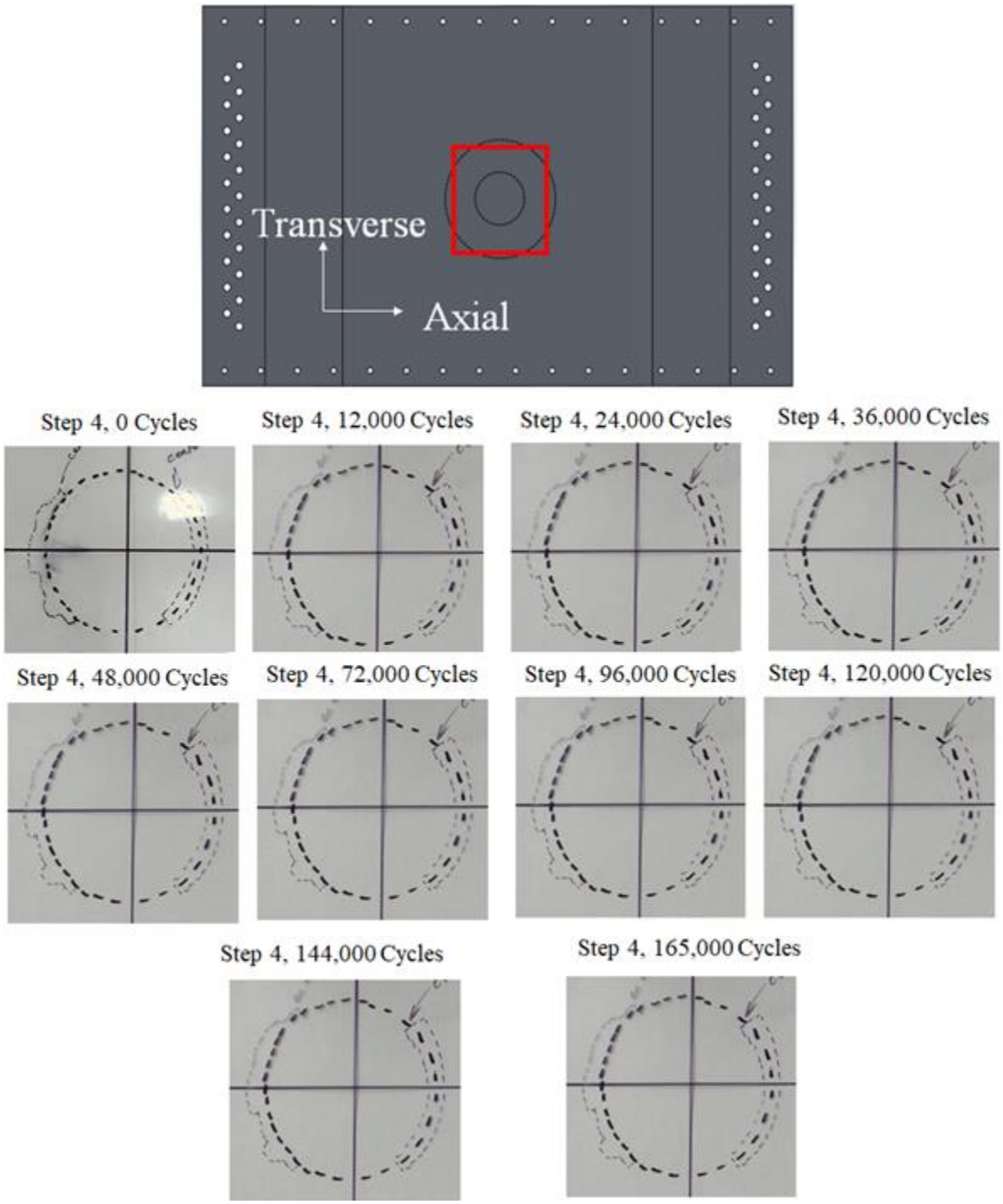


Figure H 3. Panel 5 pulse-echo results during additional fatigue at SL strain level